RL.2.1990-593

ERCB Report 90-B
Volume 1

CANADIANA

DEC - 7 1990

ERCB

Field Measurement Program

Atmospheric Dispersion Tracer Study Under Stable Conditions and Meteorological Study

October 1990

Digitized by the Internet Archive
in 2016

https://archive.org/details/fieldmeasurement04albe_0

ERCB

Field Measurement Program

Atmospheric Dispersion Tracer Study Under Stable Conditions and Meteorological Study

FIELD MEASUREMENT PROGRAM

Atmospheric Dispersion Tracer Study Under Stable Conditions and Meteorological Study

Volume 1

There are three other volumes:

FIELD MEASUREMENT PROGRAM - Volume 2
Appendices to Volume 1 - Appendix A

FIELD MEASUREMENT PROGRAM - Volume 3
Appendices to Volume 1 - Appendices B through D

FIELD MEASUREMENT PROGRAM - Volume 4
GASCON2 Evaluation

October 1990

Published by:

Energy Resources Conservation Board
640 Fifth Avenue S.W.
Calgary, Alberta
T2P 3G4

Telephone: (403) 297-3642

APPENDICES TO VOLUME 1

Table of Contents

Page

Volume 2

TRACER DATA

A1 Traverse Plume Catalogue A-1
A2 C/Q Sorted Index for Traverses A-567

Volume 3

TRACER DATA

B Stationary Plume Catalogue B-1

SOURCE DATA

C1 Summary of Fan Calibration C-1
C2 Reduction in Jet Momentum by Obstacle Drag C-5
C3 Slide Analysis for Plume Rise Estimations From Smoke Tests C-9
C4 Source Mass Flow Rate Plots C-19

METEOROLOGICAL DATA

D1 Tethersonde Data Manipulation and Plots D-1
D2 Acoustic Sounder Manipulation and Plots D-63
D3 Three-Dimensional Persistence Plots D-101
D4 Calgary International Airport Data D-115
D5 ADRP Crossfield 1-Hour Data D-123

Table of Contents

Appendices .... *i*
Table of Contents .... *ii*
List of Figures .... *vi*
List of Tables .... *xii*
Table of Photos .... *xiv*
Acknowledgements *1*
Field Measurement Program Summary *E-1*

1 INTRODUCTION 1-1
- 1.1 Background 1-1
- 1.2 Field Measurement Program Administration 1-3
  - 1.2.1 Organization 1-3
  - 1.2.2 Program Contributions 1-5
- 1.3 Field Measurement Program Approach 1-5
- 1.4 Field Measurement Program Objectives 1-7
  - 1.4.1 Tracer Objectives 1-7
  - 1.4.2 Meteorological Objectives 1-8
- 1.5 Project Schedule 1-8
- 1.6 Project Reports 1-9

2 SITE DESCRIPTION 2-1
- 2.1 Site Selection Process 2-1
- 2.2 Site Layout 2-1

3 TRACER GAS RELEASE 3-1
- 3.1 Background 3-1
- 3.2 Approach 3-1
  - 3.2.1 Tracer Gas 3-1
  - 3.2.2 Methodology 3-2
- 3.3 Source Equipment 3-3
  - 3.3.1 Flow Measurement Hardware 3-3
  - 3.3.2 Ground Source Hardware 3-7
  - 3.3.3 Elevated Source Hardware 3-7
  - 3.3.4 Meteorological Hardware 3-12
  - 3.3.5 Field Set-Up Procedure 3-13
- 3.4 Plume Rise for Elevated Source 3-14
  - 3.4.1 Observed Plume Rise 3-14
  - 3.4.2 Predicted Plume Rise 3-15
  - 3.4.3 Comparison Between Observed and Predicted Plume Rise 3-16
- 3.5 Data Reduction and Results 3-16
  - 3.5.1 SF_6 Release Rate 3-20
  - 3.5.2 Elevated Source Exit Velocity 3-24

4 TRACER GAS SAMPLING 4-1
- 4.1 Introduction 4-1
- 4.2 Hardware and System Design 4-1
  - 4.2.1 Analyser System 4-1
  - 4.2.2 Inlet Manifold System 4-3
  - 4.2.3 Supply Gas System 4-3
  - 4.2.4 Data Acquisition System 4-3
  - 4.2.5 Power Generation System 4-4
- 4.3 Analyser Performance and Operation 4-4
  - 4.3.1 Calibration 4-4

4.4 Monitoring Procedures 4-5
4.4.1 Sampling Arcs 4-5
4.4.2 Mobile Analyser Operations 4-5
4.4.3 Stationary Analyser Operations 4-6
4.5 Data Reduction 4-7
4.5.1 Data Handling and Back-Up 4-7
4.5.2 Baseline Calculations 4-7
4.5.3 Concentration Calculations 4-7
4.5.4 Distance Calculations 4-8
4.6 DART Program 4-8
4.6.1 Parameters Calculated From Traverse Data 4-8
4.6.2 Parameters Calculated From Stationary Monitoring Data 4-12

5 METEOROLOGICAL DATA 5-1
5.1 On-site Data Collection 5-1
5.1.1 Location 5-1
5.1.2 Station Overview 5-4
5.1.3 Sonic Anemometer System 5-4
5.1.4 Conventional Sensor System 5-9
5.1.5 Acoustic Sounder System 5-14
5.1.6 Tethersonde 5-14
5.2 Off-Site Data Collection 5-18
5.2.1 Calgary International Airport 5-18
5.2.2 East Crossfield 5-20
5.2.3 Plant Air Quality Monitoring Data 5-20
5.3 Meteorological Data Organization and Reduction 5-21
5.3.1 Quality-Controlled Sonic Anemometer Data 5-21
5.3.2 Quality-Controlled Conventional Meteorological Data 5-23
5.3.3 Sonic Temperature Correction 5-26
5.3.4 Working-level Three-minute Average Data 5-28
5.3.5 Working-level 30-minute Average Data 5-34
5.3.6 Quality-Controlled High-Frequency Sonic Anemometer Data 5-35
5.4 Data Recovery 5-35
5.5 Surface Roughness Z_o 5-35

6 DATA INTEGRATION 6-1
6.1 Traverse Data 6-1
6.2 Stationary Data 6-2
6.3 Traverse Data Summary 6-8
6.3.1 Worst Case Meteorological Conditions 6-9
6.3.2 Individual Field Test Summary 6-14

7 TRACER GAS ASSESSMENT 7-1
7.1 Traverse Data 7-1
7.1.1 Gaussian Plume Approximation 7-2
7.1.2 Alternate Plume Spread Calculation Methods 7-5
7.1.3 Concurrent Meteorology 7-8
7.1.3.1 Wind Speed 7-9
7.1.3.2 Temperature Gradient 7-10
7.1.3.3 Vertical Turbulence (σ_ϕ) 7-10
7.1.3.4 Horizontal Turbulence (σ_θ) 7-13
7.1.3.5 Heat Flux (H_o) 7-15
7.1.3.6 Friction Velocity (U^*) 7-15
7.1.3.7 Monin-Obukhov Stability Parameter (Z/L) 7-15
7.1.3.8 Meteorology Summary 7-17

7.1.4 Instantaneous Plume Spreads 7-18
7.1.4.1 Observed Instantaneous Values 7-18
7.1.4.2 Theoretical Considerations 7-28
7.1.4.3 Comparison to Observed Values 7-30
7.1.5 Time-Averaged Plume Spreads 7-40
7.1.5.1 Theoretical Considerations 7-40
7.1.5.2 Observed Values 7-42
7.1.5.3 Comparison to Observed Values 7-45
7.2 Stationary Data 7-52
7.3 Predicted SF_6 Centreline Concentrations 7-53
7.3.1 Gaussian Model Formulations 7-53
7.3.2 Model Comparison Input Opotions 7-56
7.3.3 Model Performance Measures 7-57
7.3.4 Model Performance - Paired Data 7-60
7.3.5 Model Performance - Unpaired Data 7-63
7.3.6 Comments 7-65

8 METEOROLOGICAL DATA ASSESSMENT 8-1
8.1 Meteorology Objectives 8-1
8.2 Field Measurement Site (Kathyrn) Climatology 8-3
8.2.1 Temperature 8-4
8.2.2 Wind Speed 8-9
8.2.3 Lateral Turbulence Intensity 8-14
8.2.4 Vertical Turbulence Intensity 8-19
8.2.5 Heat Flux 8-24
8.2.6 Friction Velocity 8-29
8.2.7 Gradient Richardson Number 8-34
8.2.8 Monin-Obukhov Stability Parameter 8-39
8.2.9 Comments 8-45
8.3 Boundary Layer Parameterization 8-46
8.3.1 Drainage and Non-drainage Winds 8-46
8.3.2 Primary Stable/Unstable Criteria 8-48
8.3.3 Surface Layer Stability Relationships 8-51
8.3.4 Normalized Wind Shear 8-54
8.3.5 Wind Speed Ratios 8-55
8.3.6 Normalized Thermal Stratification 8-61
8.3.7 Variance of Wind Components 8-64
8.3.8 Vertical Profiles of Variance 8-70
8.3.9 Vertical Profiles of Fluxes 8-73
8.3.10 Comments 8-73
8.4 Low Wind, Low Turbulence Statistics 8-76
8.4.1 Low Wind Speed Statistics 8-76
8.4.2 Minimum Turbulence Levels 8-87
8.4.3 Turbulence Level Dependence on Wind Speed 8-98
8.5 Meteorological Preprocessor 8-105
8.5.1 Pasquill - Gifford Stability Class 8-105
8.5.2 Pasquill - Gifford Stability Class Versus Meteorology Parameters 8-107
8.5.3 Stabilty Class Based on σ_θ and σ_ϕ 8-119
8.5.4 Observed Heat Flux 8-121
8.5.5 Predicted Heat Flux 8-129
8.5.6 Comparison of Predicted and Observed Heat Fluxes 8-132
8.5.7 Preprocessor Predictions of U^* and L 8-138
8.5.7.1 Preprocessor Formulations 8-138
8.5.7.2 Comparison Between Predicted and Observed U^* 8-144
8.5.7.3 Comparison Between Predicted and Observed Z/L 8-149

8.6 Spatial Representativeness 8-151
  8.6.1 Pressure 8-153
  8.6.2 Temperature 8-153
  8.6.3 Relative Humidity 8-155
  8.6.4 Wind Speed 8-156
  8.6.5 Wind Direction 8-156
  8.6.6 Comments 8-159
8.7 Averaging Time 8-160
  8.7.1 Field Measurement Program Results 8-161
  8.7.2 Comments 8-163
8.8 Anemometer Comparison 8-167
  8.8.1 Comparison Statistics 8-167
  8.8.2 Wind Speed 8-168
  8.8.3 Wind Direction 8-170
  8.8.4 Standard Deviation of Wind Direction 8-170
  8.8.5 Standard Deviation of Vertical Wind Speed 8-170
  8.8.6 Standard Deviation of Vertical Wind Angle 8-174
  8.8.7 Turbulence Frequency Distribution 8-174
  8.8.8 Comments 8-180
8.9 Mixing Height 8-185

9 Comments 9-1
9.1 Tracer Study Comments 9-1
9.2 Meteorological Study Comments 9-5

10 Bibliography 10-1

11 Symbol Glossary 11-1

List of Figures

PAGE

Figure 1.1 - ERCB Field Measurement Program Organization Chart 1-4

Figure 2.1 - FMP Site in Relation to Major Sour Gas Areas in Alberta. 2-2
Figure 2.2 - Reductions of Figures 2.4 and 2.5 that Include the Location of the Test Site. 2-3
Figure 2.3 - Gas Release Radius Points. 2-4
Figure 2.4 - Topographical Map of Test Site and Surrounding Area. 2-5
Figure 2.5 - Aerial Photo of Test Site and Surrounding Area. 2-6
Figure 2.6 - Perspective Terrain Diagram of Test Site and Surrounding Area. 2-7
Figure 2.7 - Section Terrain of Test Site and Surrounding Area. 2-8

Figure 3.1 - Schematic Showing the SF_6 Flow Measurement and Recording Hardware. 3-4
Figure 3.2 - Mass Flowrate Calibration (g/min) as a Function of Voltage. 3-6
Figure 3.3 - Ground Source for Tracer Gas Release. 3-8
Figure 3.4 - Elevated Source for Tracer Gas Release. 3-8
Figure 3.5 - Elevated Source Port Layout for the Tracer Gas Release. 3-9
Figure 3.6 - Observed Velocity Profile Across the Fan Shroud. 3-11
Figure 3.7 - Exit Velocity Calibration Curve for the Elevated Release. 3-11
Figure 3.8 - Comparison of Predicted and Observed Plume Rises for the Elevated Source Smoke Tests. .... Photo Page 3-8
Figure 3.9 - Location of the SF_6 Source Release Points. 3-17
Figure 3.10 - SF_6 Release Rate for Test 10. 3-23
Figure 3.11 - SF_6 Release Rate for Test 26. 3-23

Figure 4.1 - Analyser Plumbing Schematic. 4-2
Figure 4.2 - Analyser Electrical Schematic. 4-2
Figure 4.3 - 1-Dimensional Plot from DART - T13B25. 4-11
Figure 4.4 - 2-Dimensional Plot from DART - T13B25. 4-11

Figure 5.1 - Schematic of Test Site. 5-2
Figure 5.2 - Overview of Meteorological Station. 5-3
Figure 5.3 - Schematic Showing the Relative Locations of Sensors on the Meteorological Tower. 5-5
Figure 5.4 - Schematic of Signal Processing for Sonic Anemometers. 5-8
Figure 5.5 - Schematic of Signal Processing for Conventional Meteorological Instruments. 5-12
Figure 5.6 - Example Plot of Acoustic Sounder Data. 5-15
Figure 5.7 - Example Plot of Tethersonde Data. 5-17
Figure 5.8 - Location of Off-site Meteorological Stations. 5-19
Figure 5.9 - Correction Angle for the Sonic Anemometers. 5-24
Figure 5.10 - The Median Difference Between the Uncorrected $(\overline{W'T'_s})$ and the True $(\overline{W'T'})$ Heat Flux Term as a Function of Wind Speed. 5-27
Figure 5.11 - The Median Difference Between the Corrected $(\overline{W'T'_s})$ and the True $(\overline{W'T'})$ Heat Flux Term as a Function of Wind Speed. 5-29
Figure 5.12 - Mean Estimated Values for the Aerodynamic Surface Roughness as a Function of Time of Year. 5-40

List of Figures

PAGE

Figure 7.1 - Selected Examples of the Crosswind SF_6 Concentration Profiles. 7-3
Figure 7.2 - Selected Examples of Crosswind SF_6 Concentration Profiles Illustrating Positive Skewness, Negative Skewness, Kurtosis > 3.0 and Kurtosis < 3.0. 7-4
Figure 7.3 - Histogram of Skewness Coefficients for the 846 Crosswind Traverses. 7-6
Figure 7.4 - Histogram of Kurtosis Coefficient for the 846 Crosswind Traverses. 7-6
Figure 7.5 - 4 m Level Wind Speed Observed During the Plume Traverses. 7-9
Figure 7.6 - 10 m Level Wind Speed Observed During the Plume Traverses. 7-9
Figure 7.7 - 10 to 2 m Vertical Temperature Gradient Observed During the Plume Traverses. 7-11
Figure 7.8 - 25 to 2 m Vertical Temperature Gradient Observed During the Plume Traverses. 7-11
Figure 7.9 - 4 m Level σ_ϕ Observed During the Plume Traverses. 7-12
Figure 7.10 - 10 m Level σ_ϕ Observed During the Plume Traverses. 7-12
Figure 7.11 - 4 m Level σ_θ Observed During the Plume Traverses. 7-14
Figure 7.12 - 10 m Level σ_θ Observed During the Plume Traverses. 7-14
Figure 7.13 - Heat Flux (W/m^2) Observed During the Plume Traverses. 7-16
Figure 7.14 - U* (m/s) Observed During the Plume Traverses. 7-16
Figure 7.15 - Monin-Obukhov Stability Parameter (Z/L) Observed During the Plume Traverses. 7-17
Figure 7.16 - Plume Spread Frequency Distribution for Elevated and Ground Releases and Downwind Distances of 700, 1400 and 2100 m. 7-19
Figure 7.17 - Median Values of σ_y as a Function of Pasquill-Gifford Stability Class. 7-25
Figure 7.18 - Frequency Distribution of σ_{z_i} for Neutral (PG Class D) and Stable (PG Classes E and F) Conditions for 700 and 1400 m. 7-27
Figure 7.19 - Median Value of σ_{z_i} as a Function of Pasquill-Gifford Stability Class. 7-29
Figure 7.20 - Frequency Distribution of Wind Direction Difference (α) Over the 4 and 10 m Level, and σ_W/σ_V during the Times of the Traverses. 7-31
Figure 7.21 - Frequency Distribution of Wind Shear Enhancement Factor (*WDE*) to the Crosswind Plume Spread. 7-33
Figure 7.22 - Comparison of Instantaneous Predicted and Observed Plume Spreads (σ_{y_i}) for All Source Types (Elevated and Ground) and all Sampling Arcs (700, 1400 and 2100 m). 7-34
Figure 7.23 - Comparison of Instantaneous Predicted and Observed Plume Spreads (σ_{y_i}) for Ground Source, 700 m Data. 7-36
Figure 7.24 - Comparison of Instantaneous Predicted and Observed Plume Spreads (σ_{y_i}) for Elevated Source, 700 m Data. 7-37
Figure 7.25 - Comparison of Instantaneous Predicted and Observed Plume Spreads (σ_{y_i}) for Elevated Source, 1400 m Data. 7-39
Figure 7.26 - Histogram of Composite Plume Spread (σ_{y_c}) to Relative Dispersion (σ_{y_i}) Ratio for One-half Hour and One-hour Averaging Periods (All Stability Classes). 7-45

List of Figures

PAGE

Figure 7.27 - Median Value of Ratio *M* as a Function of Wind Speed for One-half Hour and One-hour Averaging Periods. 7-46
Figure 7.28 - Median Value of Ratio *M* as a Function of *Z/L* for One-half Hour and One-hour Average Periods. 7-47
Figure 7.29 - Comparison of Predicted and Observed 1/2 Hour Average Plume Spreads (σ_{y_c}) for All Source Types (Elevated and Ground) and all Sampling Arcs (700, 1400 and 2100 m). 7-49
Figure 7.30 - Comparison of Predicted and Observed 1/2 Hour Average Plume Spreads (σ_{y_c}) for Ground Source, 700 m Data. 7-49
Figure 7.31 - Comparison of Predicted and Observed 1/2 Hour Average Plume Spreads (σ_{y_c}) for Elevated Source, 700 m Data. 7-51
Figure 7.32 - Comparison of Predicted and Observed 1/2 Hour Average Plume Spreads (σ_{y_c}) for Elevated Source, 1400 m Data. 7-51
Figure 7.33 - Frequency Distribution of the Instantaneous Peak SF_6 Concentration to the 30 Minute Mean SF_6 Concentration. 7-54
Figure 7.34 - Frequency Distribution of the 99% Peak SF_6 Concentration to the 30 Minute Mean SF_6 Concentration. 7-54
Figure 7.35 - Frequency Distribution of the Instantaneous Peak SF_6 Concentration to the 3 Minute Mean SF_6 Concentration. 7-55
Figure 7.36 - Cumulative Frequency Distributions of Observed and Predicted Normalized SF_6 Concentration [ppt(g/min)] for Surface Releases. 7-64
Figure 7.37 - Cumulative Frequency Distributions of Observed and Predicted Normalized SF_6 Concentration [ppt(g/min)] for Elevated Releases. 7-66

Figure 8.1 - Monthly Frequency Distributions of 2 m Level Temperature. 8-5
Figure 8.2 - Median 2 m Level Temperature as a Function of Time of Day and Month. 8-7
Figure 8.3 - Monthly Frequency Distributions of 4, 10, 16 and 25 m Level Windspeeds. 8-10
Figure 8.4 - Median 4, 10, 16 and 25 m Level Windspeeds as a Function of Time of Day and Month. 8-12
Figure 8.5 - Monthly Frequency Distributions of 4, 10, 16 and 25 m Level Lateral Turbulence Intensities (σ_θ). 8-15
Figure 8.6 - Median 4, 10, 16 and 25 m Level Lateral Turbulence Intensities (σ_θ) as a Function of Time of Day and Month. 8-17
Figure 8.7 - Frequency Distributions of 4, 10, 16 and 25 m Level Vertical Turbulence Intensities (σ_ϕ). 8-20
Figure 8.8 - Median 4, 10, 16 and 25 m Level Vertical Turbulence Intensities (σ_ϕ) as a Function of Time of Day and Month. 8-22
Figure 8.9 - Monthly Frequency Distributions of 4, 10, 16 and 25 m Heat Fluxes. 8-25
Figure 8.10 - Median 4, 10, 16 and 25 m Level Heat Fluxes as a Function of Time of Day and Month. 8-27
Figure 8.11 - Monthly Frequency Distributions of 4, 10, 16 and 25 m Level Friction Velocities (*U**). 8-30
Figure 8.12 - Median 4, 10, 16 and 25 m Level Friction Velocity (*U**) as a Function of Time of Day and Month. 8-32

List of Figures

PAGE

Figure 8.13 - Monthly Frequency Distributions of 4, 10, 16 and 25 m Level Richardson Gradient Number. 8-35
Figure 8.14 - Median 4, 10, 16 and 25 m Level Richardson Gradient Number as a Function of Time of Day and Month. 8-37
Figure 8.15 - Monthly Frequency Distributions of 4, 10, 16 and 25 m Level Monin-Obukhov Stability Parameter (Z/L). 8-40
Figure 8.16 - Median 4, 10, 16 and 25 m Level Monin-Obukhov Stability Parameter (Z/L) as a Function of Month. 8-43
Figure 8.17 - Selected Non-drainage and Drainage Flow Wind Speed and Direction Profiles. 8-47
Figure 8.18 - Comparison of Predicted and Observed Interrelationships among R_g, R_f and Z/L. 8-52
Figure 8.19 - Comparison of Predicted and Observed Normalized Wind Shear ϕ_m as a Function of Z/L and R_g. 8-56
Figure 8.20 - Predicted and Observed Wind Speed Ratios as a Function of $1/L$. 8-59
Figure 8.21 - Comparison of Predicted and Observed Normalized Thermal Stratification ϕ_h as a Function of Z/L and R_g. 8-62
Figure 8.22 - Normalized Standardized Deviations (σ_U/U^*, σ_V/U^*, σ_W/U^*) as a Function of Z/L. 8-65
Figure 8.23 - Normalized Standardized Deviations (σ_U/U^*, σ_V/U^*, σ_W/U^*) as a Function of R_g. 8-68
Figure 8.24 - Longer Averaging Time Analysis - Kathyrn. Wind Speed frequencies for Averaging Times from 1/2 to 8 Hours. 0 to 3 m/s Scale. 8-79
Figure 8.25 - Longer Averaging Time Analysis - Kathyrn. Wind Speed frequencies for Averaging Times from 1/2 to 8 Hours. Full Scale. 8-80
Figure 8.26 - Short Averaging Time Analysis. Wind Persistence Contours as a Function of Wind Speed. 8-86
Figure 8.27 - Observed 10 m Level Frequency Distribution for σ_U, σ_V and σ_W. 8-89
Figure 8.28 - Observed 10 m Level Frequency Distribution for Small σ_U, σ_V and σ_W. 8-91
Figure 8.29 - Frequency Distributions of 3 and 30 Minute Sigma Theta (σ_θ) and Sigma Phi (σ_ϕ). 8-94
Figure 8.30 - Frequency Distributions of 3 and 30 Minute Sigma Theta (σ_θ) and Sigma Phi (σ_ϕ). 8-96
Figure 8.31 - 6 Month Averaged, 3 and 30 Minute σ_U, σ_V and σ_W as a Function of Wind Speed. 8-99
Figure 8.32 - 6 Month Averaged, 3 and 30 Minute σ_θ and σ_ϕ as a Function of Wind Speed. 8-102
Figure 8.33 - Frequency Distribution of Predicted PG Classes Using Calgary Airport and Field Measurement Program Data. 8-106
Figure 8.34 - Cumulative Frequency Distribution of U, $\partial T/\partial Z$, Q_{in} and H_o as a Function of the PG Stability Class. 8-109
Figure 8.35 - Cumulative Frequency Distribution of σ_V,σ_W, σ_θ, σ_ϕ as a Function of the PG Stability Class. 8-113
Figure 8.36 - Cumulative Frequency Distribution of R_g, R_b, Z/L and KM as a Function of the PG Stability Class. 8-116

List of Figures

PAGE

Figure 8.37 - Cumulative Frequency Distribution of R_g, Z/L and KM for Selected σ_θ Classes. 8-120
Figure 8.38 - Cumulative Frequency Distribution of R_g, Z/L and KM for Selected σ_ϕ Classes. 8-122
Figure 8.39 - Median Observed Net Radiation (Q_{net}) Soil Heat Flux (G) and Calculated Latent Heat Flux (LE) for Wet Grass ($\alpha = 1.0$) and Dry Grass ($\alpha = 0.5$). 8-125
Figure 8.40 - Comparison of the Sensible Heat Flux (H_o) Calculated from the Eddy Correlation and the Energy Budget Methods. 8-126
Figure 8.41 - Comparison of the Heat Fluxes Predicted Using the Eddy Correlation and the Budget Methods. 8-128
Figure 8.42 - Selected Scatterplots Comparing the Energy Budget and Eddy Correlation Methods for Estimating Heat Flux. 8-130
Figure 8.43 - Selected Scatterplots Comparing the Energy Budget and Eddy Correlation Methods for Estimating Heat Flux. 8-131
Figure 8.44 - Heat Flux Frequency Distributions. 8-136
Figure 8.45 - Scatter Plot of Predicted and Observed Heat Fluxes Where the Observed is Based on the Eddy Correlation Method. 8-139
Figure 8.46 - Scatter Plot of Predicted and Observed Heat Fluxes Where the Observed is Based on the Energy Budget Method. 8-140
Figure 8.47 - Comparison of Median Observed and Neutral Predicted U^* Values. 8-145
Figure 8.48 - Comparison of Median Observed and Extremely Stable Predicted U^* Values. 8-147
Figure 8.49 - Comparison of Selected Predicted Values of U^* with Those Observed (Predicted Values Assume Z_o - 10 cm). 8-148
Figure 8.50 - Comparison of Selected Predicted Values of Z/L with Those Observed (Predicted Values Assume Z_o - 10 cm). 8-150
Figure 8.51 - Location of Meteorological Data Stations in the Northeast Calgary Area. 8-152
Figure 8.52 - Frequency Distribution of Pressure Observed at the Kathyrn Site and Calgary Airport. 8-154

Figure 8.53 - Frequency Distribution of Temperature Observed at the Kathyrn Site and Calgary Airport. 8-154
Figure 8.54 - Frequency Distribution of Relative Humidity Observed at the Kathyrn Site and Calgary Airport. 8-155
Figure 8.55 - Frequency Distributions of Wind Speed Observed Concurrent With the Field Measurement Program. 8-157
Figure 8.56 - Frequency Distributions of Wind Direction Observed Concurrent With the Field Measurement Program. 8-158
Figure 8.57 - Median Values of the Exponent p for t_i values. 8-164
Figure 8.58 - Median Values of the Power Exponent for the Vertical Wind Variation σ_ϕ (short and long term) as a Function of Atmospheric Turbulence σ_ϕ. 8-165
Figure 8.59 - Median Values of the Power Exponent for the Horizontal Wind Variation σ_θ (short and long term) as a Function of Atmospheric Turbulence σ_ϕ. 8-166
Figure 8.60 - Wind Speed Plots of Bias, Absolute Precision and Relative Precision for 10 and 25 m levels. 8-169

Figure 8.61 - Wind Direction Plots of Bias and Absolute Precision for 10 and 25 m Levels. 8-171
Figure 8.62 - Sigma Theta Plots of Bias, Absolute Precision and Relative Precision for 10 and 25 m levels. 8-172
Figure 8.63 - Sigma W Plots of Bias, Absolute Precision and Relative Precision for 10 and 25 m levels. 8-173
Figure 8.64 - Sigma Phi Plots of Bias, Absolute Precision and Relative Precision for 10 and 25 m levels. 8-175
Figure 8.65 - Comparison of the σ_W Frequency Distributions for the 10 m Kaijo-Denki Sonic and Gill UVW Anemometers. 8-177
Figure 8.66 - Comparison of the σ_ϕ Frequency Distributions for the 10 m Kaijo-Denki Sonic and Gill UVW Anemometers. 8-178
Figure 8.67 - Comparison of the σ_θ Frequency Distributions for the 10 m Kaijo-Denki Sonic and Gill UVW Anemometers. 8-179
Figure 8.68 - Comparison of Median σ_W Values for the 10 m Kaijo-Denki Sonic and Gill UVW Anemometers Versus Wind Speed. 8-181
Figure 8.69 - Comparison of Median σ_ϕ Values for the 10 m Kaijo-Denki Sonic and Gill UVW Anemometers Versus Wind Speed. 8-182
Figure 8.70 - Comparison of Median σ_θ Values for the 10 m Kaijo-Denki Sonic and Gill UVW Anemometers Versus Wind Speed. 8-183
Figure 8.71 - Median Observed and Predicted Mixing Heights as a Function of Time of Day, Wind Speed and Stability Indicator. 8-187

Figure 9.1 Median Value of the Product ($U \sigma_\theta \sigma_\phi$) as a Function of Wind Speed. 9-9
m

List of Tables

PAGE

Table 1.1 - Organizations Contributing to the Project 1-6

Table 3.1 - Volumetric and Mass Flow Rate Calibration for the Source Flow Meter System. 3-5
Table 3.2 - Summary of Field Measurement Program Source Data. 3-18
Table 3.3 - Summary of SF6 Release Rates for Each Test. 3-21
Table 3.4 - Summary of Mean Momentum Velocity From the Elevated Source. 3-25

Table 4.1 - Angle Coverage for each Arc. 4-5

Table 5.1 - Details Concerning the Placement of Meteorological Sensors on the 25 m Tower. 5-6
Table 5.2 - Sonic Anemometer Specifications. 5-7
Table 5.3 - Input Channels of the 21X and CR-21 Dataloggers. 5-13
Table 5.4 - Record of Tethersonde Releases. 5-16
Table 5.5 - Quality-Controlled Sonic Anemometer Data File Format (three-minute average). 5-22
Table 5.6 - Quality-Controlled Conventional Meteorological Data File Format (three-minute average). 5-25
Table 5.7 - Working Level Meteorological Data File Format (3-minute and 30-minute average). 5-30
Table 5.8 - Data Recovery Efficiency. 5-37
Table 5.9 - Surface Roughness Z_o (cm) as a Function of Month and Height. .. 5-39

Table 6.1 - Number of Time Blocks Which Meteorological Data Were Averaged Over to Reflect the Transport Time. 6-3
Table 6.2 - Integrated Traverse Data File Format. 6-4
Table 6.3 - Integrated Stationary Data File Format. 6-6
Table 6.4 - Summary of the 20 Largest χ/Q Values Observed at 700 m and Associated with Elevated Releases. 6-10
Table 6.5 - Summary of the 20 Largest χ/Q Values Observed at 1400 m and Associated with Elevated Releases. 6-11
Table 6.6 - Summary of the 20 Largest χ/Q Values Observed at 700 m and Associated with Surface Releases. 6-12
Table 6.7 - Summary of the Range of Values of χ/Q and Wind Speed During the Individual Field Tests for Elevated Releases. 6-15
Table 6.8 - Summary of the Range of Values of χ/Q and Wind Speed During the Individual Field Tests for Surface Releases. 6-16

Table 7.1 - Comparison of the Three Methods for Calculating Plume Spreads (σ_{y_i}). 7-7
Table 7.2 - Comparison of the Three Methods for Calculating the Normalized Peak Concentration. 7-7

List of Tables (Continued) PAGE

Table 7.3 - Summary of 700 m Traverses Where the σ_{y_i} Values are Less Than 10 m. 7-21
Table 7.4 - Summary of 1400 m Traverses Where the σ_{y_i} Values are Less Than 20 m. 7-22
Table 7.5 - Comparison of Model Performance Statistics. 7-61
Table 7.6 - Comparison of Model Performance Statistics for Low Wind Speed Stable Conditons. 7-62

Table 8.1 - Comparison of Normalized Variance From the Field Measurement Program with Those Reported by Others for Neutral Conditions. 8-64
Table 8.2 - Median Wind Standard Deviations σ_U, σ_V and σ_W (m/s) and σ_θ and σ_ϕ (degrees) as a Function of Height and Stability. 8-71
Table 8.3 - Median H_O, U^* and L as a Function of Height and Atmospheric Stability. 8-74
Table 8.4 - Wind Speed Frequencies for Averaging Times From 1/2 Hour to 8 Hours. 8-78
Table 8.5 - FMP Duration Analysis for the Period October 1988 to March 1989. 8-84
Table 8.6 - Occurrence of Wind Speed Duration for Selected Wind Speed Classes (Normalized for an 8760 Hour Year). 8-85
Table 8.7 - Sonic Anemometer Zero Air Test Results. 8-88
Table 8.8 - Cumulative Frequency Distribution Values of Observed 10 m Level Wind Standard Deviations (m/s). 8-98
Table 8.9 - Comparison of Stability Classes Determined by Various Methods (Frequency in %). 8-107
Table 8.10 - Method of Determining Latent Heat Flux. 8-124
Table 8.11 - Calculation of Solar Related Parameters. 8-133
Table 8.12 - The Determination of Hourly Snow Cover. 8-134
Table 8.13 - Comparison of Observed and Predicted Heat Fluxes. 8-135
Table 8.14 - Solution of L and U^* for Stable Conditions. 8-142
Table 8.15 - Solution of L and U^* for Unstable Conditions. 8-144
Table 8.16 - Averaging Periods Used to Evaluate the Power Law Exponent p. 8-161
Table 8.17 - Averaging Values of the Power Law Exponent (p) Based Upon 10 Hz 10 and 25 m Wind Data. 8-162
Table 8.18 - Comparison of Predicted and Observed Mixing Height Values. ... 8-188

Table of Photos

PAGE

The Landowners with Members of the Field Measurement Program Project Team. .... Photo Page A-1

Contributions such as the Field Offices and Signs made the Project Possible. .... Photo Page A-1
Management Committee. .... Photo Page A-2
Technical Committee and Project Staff. .... Photo Page A-2
Communication Plans Included Newsletters to the Local Area as Well as Residents on the NE Calgary Mailing List. .... Photo Page E-1

Photo 2.1 - Members of the Technical Committee Were at the Site to Ensure it was Appropriate. .... Photo Page 2-1
Photo 2.2 - Members of the Technical Committee Were at the Site to Ensure it was Appropriate. .... Photo Page 2-1
Photo 2.3 - Stations Along the Arc were Marked with Stakes. .... Photo Page 2-2
Photo 2.4 - Stations Along the Arc were Marked with Stakes. .... Photo Page 2-2

Photo 3.1 - Ground Source for Tracer Gas Release. .... Photo Page 3-1
Photo 3.2 - Elevated Source for Tracer Gas Release. .... Photo Page 3-1
Photo 3.3 - Fan Calibration Prior to Start of Field Tests. .... Photo Page 3-2
Photo 3.4 - Source Anemometer and Large Fan Used for Elevated Releases. .... Photo Page 3-2
Photo 3.5 - Flow Rate Instrumentation for the Source. .... Photo Page 3-3
Photo 3.6 - The SF_6 Cylinder and Tubing Connectors. .... Photo Page 3-3
Photo 3.7 - Example of Smoke Generation Equipment Tried for the Elevated Release Fan But Not Found Suitable. .... Photo Page 3-4
Photo 3.8 - Example of Smoke Generation Equipment Tried for the Ground Release Fan But Not Found Suitable. .... Photo Page 3-4
Photo 3.9 - Smoke Plume Visualization With Elevated Release Fan Off. .... Photo Page 3-5
Photo 3.10 - Smoke Plume Visualization With Elevated Release Fan On. ... Photo Page 3-5
Photo 3.11 - Smoke Plume Visualization With Elevated Release Fan On. Side View. .... Photo Page 3-6
Photo 3.12 - Smoke Plume Visualization With Elevated Release Fan On. Rear View. .... Photo Page 3-6
Photo 3.13 - Smoke Plume Visualization With Ground Release Fan On. Side View. .... Photo Page 3-7
Photo 3.14 - Smoke Plume Visualization With Ground Release Fan On. Rear View. .... Photo Page 3-7

Photo 4.1 - The Pick-up Box of One of the Tracer Trucks Containing Gas Cylinders and Generator. .... Photo Page 4-1
Photo 4.2 - The Three Identical Continuous Tracer Monitoring Trucks. .... Photo Page 4-1
Photo 4.3 - Full Range Calibrations Before and After the Tests Were Required. .... Photo Page 4-2
Photo 4.4 - Side View of Probe and Tubing Leading Into Analyser. .... Photo Page 4-2
Photo 4.5 - Inside View of Analyser and Portable Computer. .... Photo Page 4-2

Table of Photos

PAGE

Photo 5.1 - A View of the Meteorological Trailer, Tower, Acoustic Sounder Enclosure and Tethersonde Tent. .... Photo Page 5-1
Photo 5.2 - A View of the Inside of the Meteorological Trailer. .... Photo Page 5-1
Photo 5.3 - The Meteorological Tower Showing All the Instrumentation on it. .... Photo Page 5-2
Photo 5.4 - 16 and 25 m Level Anemometer Sensors. .... Photo Page 5-3
Photo 5.5 - 10 m Level Kaijo-Denke Anemometer. .... Photo Page 5-3
Photo 5.6 - 4 m Level Applied Technologies Anemometer. .... Photo Page 5-3
Photo 5.7 - As Mentioned in Section 3.3.4, A Mast-Mounted Anemometer was Located at the Source. .... Photo Page 5-4

Acknowledgements

The ERCB managed the Field Measurement Program which was a joint effort receiving significant financial, equipment and manpower support from government and industry. These contributions are identified specifically in Section 1.2.2. Photos of the landowners, contributions, management and technical committees and communication efforts are shown on the following page. Additionally, there were other contributions made to the program which made it a success and the ERCB would like to express its appreciation for those special efforts to:

- The landowners, Harold and Marion Randall, who offered their property, generous support and a warm welcome to all project staff. They hosted a media tour and a wind-up barbecue. Their neighbourly attitude proved to be a valuable asset to the smooth sailing of the program.

- The local people from the Kathyrn area who provided enthusiasm and support:

  Judith Barry (sign/poster painting and newsletter distribution)
  Ernie Harrison (monitoring truck driver)
  Max Nichols (monitoring truck driver)
  Stewart Randall (monitoring truck driver)
  Ian Willdig (monitoring truck driver)
  Warren Wise (mechanic)

- The Management Committee members who offered encouragement and kept the program on track by overseeing all aspects:

  Frank Mink
  Ted Brown
  Ed McMaster

- The Technical Committee members, who defined the scope and provided feedback during the course of the program, are gratefully acknowledged. There were many technical meetings as well as lengthy phone calls and many hours spent on the review of data as it was generated. In particular, Randy Angle, Sven Djurfors, Keith Hage and David Wilson spent many hours on data review. Without this input, progress would have been difficult. The expertise among the members provided the necessary direction to the project:

  Randy Angle
  Hugh Brown
  Sven Djurfors
  Ed Fox
  Keith Hage
  Lynda Holizki
  Jim Swiss
  David Wilson

- The Program Co-ordinator, Lynda Holizki of the ERCB, provided the link to all aspects of the project. She was the Senior Environmental Engineer responsible for technical direction, data analysis, report writing, budget reviews, technical meetings and some aspects of public communication. Lynda was involved in authoring and reviewing all four volumes of the Field Measurement Program.

- The Field Project Manager, Vic Bohme, who provided strong leadership and motivation and provided the needed encouragement to operate from dusk to dawn.

- The Principal Investigator, Mervyn Davies of Concord Environmental Corporation, whose expertise in field work, meteorology and computer applications made him a key individual during the design and implementation of the field program and during the analyses and interpretation of the data. Mervyn was the primary author of Volume 1.

- Touche Howard of Indaco Air Quality Services was responsible for many technical aspects of the tracer analysis. He was also the primary author of the model evaluation report, Volume 4.

- The ERCB Communications Department, in particular Jack Bales and George Kupfer, who spent time with the public, the media and newsletter production. They developed the communication plans throughout the program.

- The project staff who worked many more hours than were originally anticipated. There were a total of 26 people whom we mention here, however, other staff in these organizations assisted:

ERCB Technical Staff	Paul Angrave	Concord Environmental Corporation Staff	Mike Brennand
	Ken Bahadur		Mervyn Davies
	Jim Davis		Ann Jamieson
	Arnold Dick		Judy Smith
	Ian Dowsett		
	Brian Fleck	Indaco	Alex Guenther
	Lynda Holizki		Touche Howard
	Joseph Mathews		Brian Lamb
	Ross Purvis		
	Brad Simm	Promet	David Chadder
	Stephen Skarstol		Steward Bonner
	John Sutherland		Bill Murray
	Dean Webster		Craig Schneider
	Richard Wright		
		Others	Roberta Hicklin

- Peter Slawson, a special technical adviser, provided advice on atmospheric dispersion field programs when the program was in the conceptual design stage.

- The support staff from the ERCB in purchasing, drafting, proofreading, printing, core research storage, shipping and data processing who were a big help. In particular, Paul Angrave who assisted at the meteorological station and took numerous documentary photos, most of which appear in the text of this report.

- The Environment Protection Department staff who have helped with both moral and technical support. Richard Wright was responsible for the production and technical editing of the report and he was assisted by Ann Elahee, Susan Foulds and Janet Shortridge who typed most of this document on the personal computer.

The combined efforts and support of the above personnel made this ambitious effort a reality.

Harold Randall **Vic Bohme** **George Kupfer** **Lynda Holizki** **Marion Randall**

The Landowners with Members of the Field Measurement Program Project Team.

RESEARCH PROJECT FIELD OFFICE
ERCB Energy Resources Conservation Board
AIR MONITORING VEHICLES WILL OPERATE SOUTH OF HERE FROM SEPT-DEC
PLEASE DO NOT DISTURB THE RESEARCHERS DURING THEIR WORK
INFORMATION

Contributions such as the Field Offices and Signs made the Project Possible.

Management Committee

(T. Brown, F. Mink (Chairman), E. McMaster)

Technical Committee and Project Staff

Technical Committee seated: E. Fox, V. Bohme, D. Wilson, K. Hage, S. Djurfors, R. Angle, H. Brown, (L. Holizki standing)
Project staff standing: T. Howard, J. Sutherland, R. Purvis, I. Dowsett, J. Davis, R. Wright, L. Holizki, D. Webster, M. Davies, M. Brennand, S. Skarstol. Missing: J. Swiss, K. Bahadur, P. Angrave, B. Fleck, A. Dick.

Field Measurement Program Summary

Introduction

The ERCB has strongly enforced policies regarding sour gas emergency planning zones and appropriate setback distances between sour gas facilities and residents, which include wells, pipelines and processing plants. Over the many years of sour gas production, there have been improvements in the handling of sour gas, qualitatively reducing the risk to workers and members of the public. However, public concern regarding sour gas has grown, particularly because of the 1982 Lodgepole sour gas well blowout and increased sour gas development near populated areas.

These public concerns prompted the ERCB to commission Concord Scientific Corporation (now Concord Environmental Corporation) to independently develop hazard and risk assessment models (GASCON and GASRISK respectively) in 1986. A Scientific Advisory Board was established to oversee the work.

The draft GASCON model results were released in June 1987 and were followed by a recommendation to do a model evaluation with actual field testing, prior to completion of both the GASCON and GASRISK work. All sectors including the public, government and industry supported the recommendation for such a field program.

The ERCB assumed primary responsibility for management of the Field Measurement Program and obtained co-operation and support from the public, government and industry. The significant funding in the order of $500 000 came from industry with additional financing, equipment, and manpower support from government and the ERCB. A Management Committee and Technical Committee, both chaired by the ERCB were established in late 1987 to provide direction and technical support. Details of the program's contributions and administration are contained in Section 1.2, Volume 1. More specifically, the Technical Committee was appointed to determine the technical scope and design of the program and provide feedback on results as they were generated.

Prior to the field testing, the Technical Committee reviewed the GASCON and simple Gaussian model results, and confirmed that low turbulence atmospheric conditions warranted the most attention when predicting the behaviour of an accidental release of hydrogen sulphide. GASCON was a more rigorous model than the simple Gaussian model and could predict both hydrogen sulphide and sulphur dioxide concentrations under various scenarios. However, the highest hydrogen sulphide concentrations predicted were for stable conditions when the wind speeds were less than 1 m/s.

In June 1988, once the Technical Committee had determined the scope, tender invitations were requested. In August 1988, a contract for key aspects of the program was awarded to Concord Environmental Corporation with Promet Environmental Group and Indaco Air Quality Services acting as subconsultants. A number of ERCB staff were also involved in the field work.

The Field Measurement Program co-ordinator was Lynda Holizki (ERCB), who was assisted by:

- Vic Bohme, who acted as field program manager,
- Mervyn Davies (Concord) and Touche Howard (Indaco), who acted as primary technical consultants,
- George Kupfer and Jack Bales (ERCB), who acted as communication co-ordinators, and,
- The Technical Committee and many ERCB staff.

The Field Measurement Program started in September 1988 with considerable support from the public, industry and government. Data analysis started in January 1989 and continued until October 1990. All results were documented and are contained in Volumes 1, 2 and 3. A review of the field analysis results indicated that certain GASCON assumptions should be changed. These changes were incorporated into a new model that had integrated the GASCON and GASRISK models. The new model was called GASCON2 as it incorporated the **con**centration and **con**sequence aspects. An evaluation of the passive dispersion module of GASCON2 was then undertaken using the field data. The results of this comparison are presented in Volume 4.

The risk work was referred to as a risk approach rather than a model and that approach was documented in Volume 6. To complete the risk examples, a review of historical failure and toxicological data was required. These statistics and accompanying support information on toxic load are found in Volume 7. There are also three other related documents. Volume 8 is the GASCON2 User's Guide, Volume 9 is the Scientific Advisory Board Commentary and Volume 10 is a summary document. The ERCB packaged the 10-volume set and released all volumes in October, 1990.

Program Approach

The Technical Committee's design was based on having a generic program consisting of two parts, a tracer and meteorological study. The decision to complete generic testing was made to ensure that any atmospheric dispersion model could be evaluated against the data.

Tracer Study

During an intensive study period, a sulphur hexafluoride (SF_6) tracer gas was released into the atmosphere. This tracer gas was released during low wind speed, stable atmospheric conditions. Downwind SF_6 concentrations were measured at several downwind locations using SF_6 continuous analysers. Cross-wind SF_6 concentration profiles were collected to establish the behaviours and patterns associated with plume dispersion. Meteorological data, concurrent with each tracer release, were obtained to aid in the interpretation of the tracer gas results.

Meteorological Study

The Field Measurement Program was conducted on reasonably flat terrain approximately 20 km from the City of Calgary. The tracer release and sampling occurred during the months of October, November and December 1988. The diffusion meteorological station commenced operation in October 1988 and continued to operate until a 12-month set of data was collected. The meteorological study involved the collection of atmospheric turbulence and wind profile data to obtain meteorological information on the frequency and persistence of low wind speed and low turbulence atmospheric conditions.

Program Overview

Tracer Gas Release and Sampling

On 33 evenings between October and December 1988 when suitable dispersion conditions prevailed, SF_6 was released, with the aid of a fan, to simulate a release of gas escaping from a well or from a ruptured pipeline. A large fan was used for elevated releases and a smaller fan was used for ground level releases. In-plume SF_6 concentrations were then measured by continuous SF_6 analysers mounted in trucks.

A combination of mobile and stationary monitoring was conducted to obtain plume concentration profiles at 700, 1 400 and 2 100 m downwind of the release point. Mobile monitoring provided nearly instantaneous plume profiles, while the stationary monitoring provided plume intermittency information.

For the tracer release, SF_6 was injected into a fan to ensure complete mixing of SF_6 into the simulated plume. Smoke was also injected into this source fan to provide a visible reference from which plume rise information could be obtained. A dozen smoke plume visualization/plume rise tests were conducted prior to sunset using photographic techniques to determine plume heights. During the night when SF_6 was released, smoke was not injected into the fan.

Meteorological Station

A 25 m tower adjacent to the tracer release and sampling sites served as a platform for meteorological sensors. Three axis sonic anemometers at four levels (4, 10, 16 and 25 m) were used to measure mean winds, their variance and fluxes of heat and momentum. A nominal sampling rate of the four sonic anemometers was 10 Hz.

Additional sensors on the tower included backup propeller anemometers (10 and 25 m) and aspirated temperature sensors (2, 10, 16 and 25 m). The backup anemometers allowed for comparison to the more sophisticated sonic systems. In addition, measurements of net radiation, relative humidity, barometric pressure and soil heat flux were made. All conventional meteorological sensors were sampled at 1 Hz. Three-minute averages from all sensors were archived on a continuous basis. During the tracer tests, the sonic data were archived from the 10 and 25 m levels at the 10 Hz rate..

Supplementary meteorological data were obtained from tethersonde releases conducted during the tracer release and from a monostatic acoustic sounder. Both data sets were analysed to determine stratification of layers.

Data Reduction and Analysis

Data reduction and analysis were a large aspect of the Field Measurement Program. A total of 700 megabytes of raw data were collected during the testing period with an additional 100 megabytes for the 3-minute meteorological data. A 16-member project team, comprised of meteorologists and engineers, worked on the program objectives for over 20 months to complete the analysis on all 12 months of data. It was the opinion of both the project team and the Technical Committee that a significant data set had been collected.

A large effort was made to collect and analyse concurrent SF_6 source, ambient SF_6 concentrations and meteorological data to describe atmospheric transport and dispersion under low wind speed stable atmospheric conditions. Additional effort was made to gain an understanding and a confidence level in meteorological measurements and atmospheric turbulence processes. Special attention was given to documentation of the data analysis, as it and the data set may prove useful to other investigators.

Program Findings

The initial results of the analysis presented in Volume 1 focussed on reviewing all the data, rather than the review of case studies. This approach had the advantage of providing an overview of the important processes and a degree of understanding of the significant features of those processes.

Tracer Study

- A significant portion of the cross-wind plume concentration profiles could be reasonably approximated by a Gaussian profile. In many cases the observed concentration profiles were virtually indistinguishable from a Gaussian distribution, while in others the observed profiles were skewed or even bimodal. This information is valuable considering that the Gaussian approximation is the basis of most dispersion models.

- On average, the smallest plume spread values were not necessarily associated with the lowest wind speed conditions, the smallest vertical or horizontal turbulence or with the strongest temperature gradients. This finding was contrary to the expectation that the smallest plume spreads would be associated with the lowest wind speed and turbulence conditions.

- Furthermore, the minimum cross-wind plume spreads were not associated with the largest concentrations. The "worst case" did not appear to occur at the low wind speeds. The largest concentration values were associated with wind speeds of around 3 m/s rather than wind speeds of less than 2 m/s.

- The comparison between the predicted and observed instantaneous plume spreads resulted in considerable scatter. For some source configurations and receptor distances, there was evidence that incorporation of a wind shear enhancement increased this performance, however, the best performance was without the wind shear enhancement. Additionally, the time-averaged plume spread observations and predictions tended to have better agreement, without the wind shear enhancement term.

- Comparisons of observed SF_6 concentration to values predicted by a simple Gaussian model showed that the simple model was performing well, within a factor of two for paired data, 50% of the time. This was considered to be good, considering the amount of scatter and variability in the atmosphere under stable conditions.

- A review of the stationary data indicated that instantaneous peak to 30-minute mean concentration ratios were in the 3 to 7 range and instantaneous peak to 3-minute ratios were in the 1 to 3 range. A further assessment of the stationary data, which is not part of this review, will evaluate concentration fluctuation statistics.

- Further case studies may be able to isolate selected behaviour characteristics and explain any disagreements between predictions and observations.

Meteorological Study

- The objective of the program was to collect tracer data during low wind speed, stable conditions. During the tracer tests, wind speeds were less than 2 m/s for 16% of the time and stable atmospheres occurred 70 to 80% of the time. The collection of tracer data under other atmospheric conditions was also beneficial to the program.

- In addition to the Field Measurement Program data, other data sets were available to evaluate the frequency and duration of low wind speeds under stable conditions. These included the Calgary International Airport and the Acid Deposition Research Program data sets. All three data sets indicated that low wind speeds (less than 2 m/s) occurred around 20% of the time, and if further subdivided into both low winds speeds **and** stable conditions, the frequency drops to around 10% of the time. During that time, the low wind speeds typically persist for approximately one hour, and rarely persist for more than three hours (only 1% of the time). Due to normal diurnal variations in meteorological conditions, it is not surprising that the conditions do not frequently persist for more than three hours.

  Substantiating this meteorological assumption provides valuable information for model application purposes since concentrations predicted downwind often assume that steady-state conditions will persist for 5 to 10 hours. If the model predicts a large concentration a great distance away, such that it takes longer than three hours to get there, it would seem unlikely for that to happen. Model predictions based on steady-state assumptions have to account for persistence.

- With regard to the minimum turbulence issue, it was found that turbulence measurements of σ_θ and σ_ϕ increased with decreasing wind speeds. The product of $\sigma_\theta \sigma_\phi U$ indicates the magnitude of dilution. Small values are associated with smaller turbulence. For this specific data set, the product tends to take on a minimal winter value in the wind speed range of 3 to 4 m/s. This was a significant finding, one of the unknowns prior to the Field Measurement Program.

- To determine the effectiveness of various stability classification schemes, an evaluation of the STAR (Airport) and other meteorological preprocessors was done. The Pasquill-Gifford (PG) stability class scheme for classifying turbulence in the atmosphere was evaluated using the STAR approach with airport data and another approach using on-site data. The two approaches agreed on the PG class about 50% of the time and were within one PG class about 90% of the time. An alternate meteorological preprocessor based on heat flux was also evaluated. The evaluation indicated that there were difficulties in measuring the heat flux under low turbulence, stable conditions.

- An empirical power law relationship is frequently used to convert atmospheric turbulence measurements and concentrations from one averaging time to another. The evaluation indicated that the power law relationship generally held for averaging periods less than three minutes. Prior to the program, this was uncertain. The value for the exponent ranged from about 0.2 to 0.3. This was consistent with the 0.2 value assumed by Alberta Environment.

- The comparison of sonic anemometer data to the conventional propeller anemometer data indicated that the propeller anemometer had limitations in measuring the vertical turbulence under low wind speed conditions.

- A general observation was that care should be taken in the extrapolation of meteorological wind data from one location to another due to site-to-site variations.

Application to GASCON2

- The formulations in the meteorological preprocessor be reviewed to allow latent heat flux to be incorporated and for heat flux values to be less than the current minimum.

- An alternate vertical profile for stable conditions was proposed which provides better agreement with the field data than currently incorporated into GASCON2.

- Care should be taken when specifying on-site lateral and vertical turbulence values, as these values can vary with height and stability.

- Previous model predictions were estimating the "worst case" at wind speeds less than 1 m/s. This should be reviewed in light of the Field Measurement Program's "worst case" occurring at 3 to 4 m/s.

- A review of the uncertainties, with instantaneous versus time-averaged plume cross-wind speeds, indicated that predictions were typically within a factor of two anywhere from 60 to 75% of the time. This same level of performance is the maximum that GASCON2 would be expected to predict.

The findings of the program have provided a level of confidence in atmospheric behaviour that was not present at the onset of the program. There were many findings that supported the current model work as well as other interesting surprises. The quality of data collection and analysis is high and will provide useful research material for atmospheric scientists in the future. All data files and documentation were made available to the public in October 1990.

Communication of Results

The list of acknowledgements indicates that the support of many made this ambitious effort a reality. This support would not have been there without a great deal of communication. As soon as there was an awareness of the plan, many individuals and organizations volunteered time and resources. An early commitment to release all results to the public was made and was undertaken in October 1990. Communication efforts also included newsletters and a trip to the site for the media where landowners Harold and Marion Randall acted as excellent hosts. In fact, they offered a warm welcome to many visitors at the site. (The photos on the next page show some of the newsletters and the media trip.)

In addition to communicating the findings in the local area and Alberta, the ERCB plans to have the scientific information reach other scientists by way of technical papers and presentations at conferences. In October of 1989, a presentation was made to the World Clean Air Congress in Holland outlining the type of study that was undertaken. Plans currently include presentations at conferences and workshops in North America.

ERCB

Energy Resources
Conservation Board
640 Fifth Avenue SW
Calgary, Alta T2P 3G4

FIELD MEASUREMENT PROGRAM February 1989

An Update for Residents of the Kathyrn & Keoma Area

As you know, a team of scientists have been working in your area since September 1988. They have been measuring the dispersion of a harmless tracer gas under "worst case" dispersion conditions; when the atmosphere is stable, with little or no wind. Chinook winds during the fall of '88 caused our testing to continue into December. However, the field portion of this measurement program now is complete and we would like to take this opportunity to let you know what has been accomplished so far.

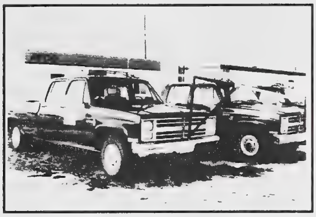

The air sampling tube running over the top of the truck and down inside the back window is part of the plume monitoring equipment.

Outside air was drawn into the analyzer and the data collected. A portable generator was used to power this equipment.

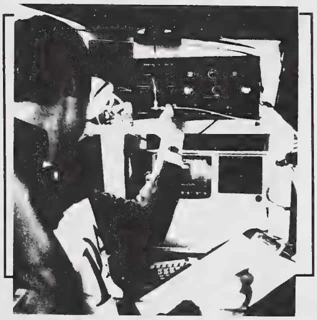

The Measurement Tests

There were 33 evenings between October and mid-December of 1988 when suitable dispersion conditions prevailed. On these evenings, a harmless tracer gas was released with the aid of a large fan, to simulate the dispersion (or plume) created by gas escaping from a well, or from a ruptured pipeline. Plume measurements were then taken by monitoring devices mounted on trucks. Sometimes, these measurements were taken with a stationary unit parked directly in the tracer gas cloud, while other units were passing through the cloud. At other times, three units were parked in positions such that at least one unit would always be in the gas cloud as it moved back and forth. To aid our record-keeping, a number of photographs were taken, as well as a video tape at various stages of the project.

ERCB

FIELD MEASUREMENT PROGRAM

September 1988

An Update for Residents of the Kathyrn & Keoma Area

of scientists will be working
rea (on the farm of Harold
om late September
er. Under contract
ll be measuring
r gas under
hen the

described to you in previous newsletters. Most of the necessary equipment now is in place. ERCB's contractors—**Concord** Scientific Corporation (prime contractor), **Promet** Environment Group and **Indaco** Air Quality Services—will be ready to begin the actual measurements around the end of September.

As we prepare to launch this important program, perhaps it would be helpful if we told you again of the scientific work which will be going on in
ur area. Beginning early in October, the scien-
will be **releasing small amounts of a**
s tracer gas—up to 20 times in all—
racing the gas as it spreads out
ay from the release site. As the
sed, a large fan will force it
site, thus simulating a re-
ptured pipeline. What
ing is what happens
, when the gas is
mosphere and
gas using
crew
orth

AUGUST 1988

KEOMA AREA

nent program
nths. The
nsible for all
is the
gas (gas

Communication Plans Included Newsletters to the Local Area as Well as Residents on the NE Calgary Mailing List.

1 INTRODUCTION

1.1 Background

The Energy Resources Conservation Board (ERCB) is responsible for approving applications for new energy projects and for regulating the operation of existing energy facilities in the Province of Alberta. In assuming this role, the ERCB is also responsible for providing advice and information on Alberta energy-related issues to industry, government and the public.

Natural gas is an extremely important energy resource for the Province of Alberta. Somewhat more than half of this natural gas is derived from sour gas reserves which contain hydrogen sulphide (H_2S). The H_2S content of commercial sour gas reserves in the Province of Alberta can vary from a few parts per million (ppm) to more than 50 per cent. As a consequence, sour gas has to be treated with respect since high concentrations of H_2S are extremely toxic (~ 600 to 1 000 ppm by volume) and low concentrations (20 to 50 ppm by volume) can be irritating to the lungs, nose, throat and eyes (Barr 1988).

For this reason, the ERCB has strongly enforced policies regarding sour gas emergency planning zones and the establishment of appropriate setback distances for sour gas facilities which include wells, pipelines and processing plants. Safeguard guidelines have been established using a combination of predicted atmospheric dispersion behaviour, risk assessment methods, judgement based on sour gas releases from blowouts and pipeline ruptures, and the results of field simulations of sour gas releases (APIGEC 1974, 1978, 1979 and Atwell 1979). The provincial subdivision approving authorities have adopted the same setback distances as the ERCB through the Subdivision Regulations pursuant to the Planning Act (ERCB ID 79-2, ID 81-3, ID 87-2, IL 88-9 and IL 88-9 Amendment, ERCB Enerfax 6 and 7, Alberta Municipal Affairs 1986, Alberta Public Safety Services 1985, Canadian Petroleum Association 1987).

Drilling for, producing, transporting and treating sour gas has always presented a number of difficulties including: fouling and coagulation of drilling fluids, rapid stress corrosion cracking of metals and, if released into the atmosphere, extreme toxicity to humans and animals through inhalation. Over the years, improved design of drilling equipment and procedures, improved H_2S resistant pipelines, improved process plant metallurgy, special emergency alarms and shut-down and control procedures have been implemented. These improvements in the handling of sour gas have qualitatively reduced the risks to industry workers and members of the public by reducing the incidences and occurrences of sour gas releases.

Despite these achievements, public concern regarding sour gas has grown, particularly because of the 1982 Lodgepole sour well blowout and increased sour gas developments near populated areas (Sage 1985). The Lodgepole blowout vented 2 800 x 10^3 m^3/d of sour gas containing 25% H_2S and was out of control for 60 days. H_2S concentrations of 10 ppm were recorded on monitors 22 kilometres from the well. H_2S odours were observed in the cities of Edmonton (140 km) and Calgary (240 km) (ERCB D 84-9).

Public concerns over the Lodgepole blowout and other proposed sour gas development in populated areas prompted the ERCB to commission Concord Scientific Corporation, in 1986, to develop a dispersion model and risk approach specific to sour gas releases. Originally this was to result in two models, GASCON and GASRISK. Model development methodology and results were subject to scientific peer review and public scrutiny. The scientific peer review group was called the Scientific Advisory Board. A communications plan was established to ensure the study and the views of the Scientific Advisory Board would become public knowledge (ERCB Newsletters 1986 to 1987). The draft GASCON model results were presented to the public in June 1987 (Alp *et al* 1987). Meanwhile the risk work carried on, developing an approach to incorporate the results of GASCON.

The GASCON computer model was specifically designed to simulate the initial behaviour and dispersion of sour gas plumes. The model addressed releases from either a well blowout or a pipeline rupture and from either an ignited or unignited plume. The GASCON model handled a range of source configurations, such as horizontal or vertical jets. For typical Alberta conditions, the GASCON model predicted large H_2S concentrations under low turbulence conditions.

Scientists reviewing the Concord Scientific 1987 results held differing views on the predicted H_2S concentrations. Some thought the GASCON model predictions would have been smaller, thus posing less public risk if dispersion based on site-specific turbulence observations were used; others thought that the concentrations would be larger if very quiescent "worst case" atmospheric conditions could be simulated by the model.

To resolve this conflict of opinion, a proposal was submitted to the ERCB recommending that risk work be delayed until a field measurement program could be completed to more fully evaluate and verify the GASCON model. The ERCB took this proposal to all the involved parties, including the public, government and industry, and found that all were in favour of the field program. The ERCB, in response to the favourable comments, initiated a field measurement program to evaluate low wind speed, stable atmospheric conditions. The public was advised of the program (ERCB Newsletters 1988) and informed that the final GASCON model and risk work would be complete after the results of the Field Measurement Program could be incorporated.

The Field Measurement Program started in 1988 and was completed by 1990. Details of the Field Measurement Program are contained in this Volume 1 along with an analysis of the results. The appendices for Volume 1 are presented as Volumes 2 and 3. A review of the field analysis results indicated that certain GASCON assumptions should be changed. These changes were incorporated into a GASCON2 model so that an evaluation of the passive dispersion portion of GASCON2 could be undertaken using the field data. Those model evaluation results are in Volume 4.

Additionally, the GASCON and GASRISK models were integrated into the single GASCON2 model. The enhanced GASCON2 model can now predict **con**centrations and **con**sequences and is referred to as GASCON2 (Alp *et al* 1990 - Volume 5). The risk approach that was being developed by Concord Environmental Corporation over the same time period incorporates the results of GASCON2 and is documented in Alp *et al* 1990 - Volume 6 and ERCB - Volume 7.

The first seven volumes that have been mentioned in this section refer to the Field Measurement Program, GASCON2 and the risk approach. There are three other related documents. Volume 8 is the GASCON2 User Guide. Volume 9 is the Scientific Advisory Board Commentary on Volumes 4, 5 and 6. Volume 10 is a Summary of the ERCB and Concord Environmental Volumes. Since all documents, including those of the ERCB, Concord and the Scientific Advisory Board, were to be made public, the ERCB packaged the ten-volume set and released all volumes in October 1990.

1.2 Field Measurement Program Administration

1.2.1 Organization

The Field Measurement Program organization chart is shown in Figure 1.1. Primary responsibility for the management of the program was assumed by the ERCB with co-operation from industry and government.

A Program Management Committee was established in late 1987 to oversee the general coordination, administration and direction of the project. The Management Committee was comprised of three members: an ERCB representative (chairman), a public representative from the City of Calgary and an industry representative from the Canadian Petroleum Association.

A Technical Committee was also appointed by the ERCB in late 1987 to determine the technical scope and conceptual design for the program data collection, reduction and analysis portion. The eight-member Technical Committee was comprised of representatives from the ERCB (chairman), University of Alberta, Alberta Environment, the community and industry members representing the Canadian Petroleum Association, the Independent Petroleum Association of Canada and the Small Explorers and Producers Association of Canada. The selected conceptual Field Measurement Program design was submitted to and approved by the Management Committee. The Technical Committee was not involved in the design of the model evaluation.

In June 1988, tender invitations from consulting organizations located in Western Canada and the United States were requested to carry out the field program. In August 1988, a contract was awarded to Concord Environmental Corporation (previously Concord Scientific Corporation) with Promet Environmental Group and Indaco Air Quality Services acting as sub-contractors.

The Field Measurement Program co-ordinator was Lynda Holizki (ERCB) who was assisted by:

- Vic Bohme, who acted as field program manager
- Mervyn Davies (Concord) and Touche Howard (Indaco) who acted as primary technical consultants
- George Kupfer and Jack Bales (ERCB), who acted as communication co-ordinators
- The Technical Committee and many ERCB staff

All individuals have been identified in the acknowledgment section.

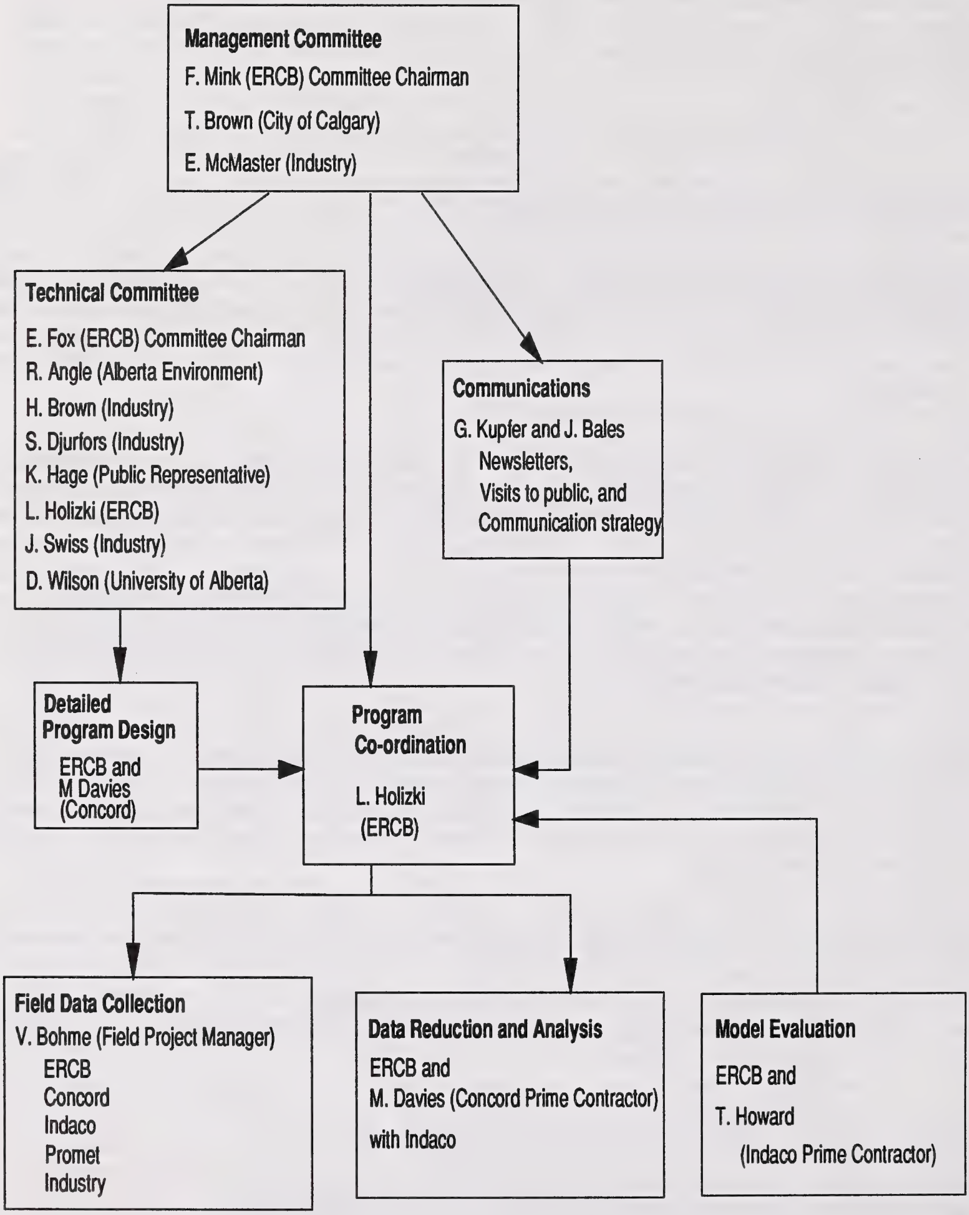

Figure 1.1

ERCB Field Measurement Program Organization Chart.

1.2.2 Program Contributions

To assist with the execution of the Field Measurement Program, the data reduction and data analysis, resources from within the ERCB, Alberta Environment, industry and local public were available. Table 1.1 summarizes the contributions from these sectors. The significant industry contribution provided the essential support. Without it, the project would not have had the initial backing to see it to completion. It is worth noting that the industry contributions came forward on the premise that the field data would be generic in nature, meaning that the data could be used for any model evaluation.

Additionally, work contracts to assist with the field data collection were offered to local residents. For example, local residents acted as drivers for the analyser trucks and a local person painted field and survey signs. It is worth noting that the contributions came forward so that field results would be generic to ensure that a model evaluation could be done.

1.3 Program Data Reduction and Analysis Approach

The Technical Committee reviewed the GASCON report and confirmed that, indeed, the low turbulence atmospheric condition warranted the most attention when predicting the behaviour of an accidental release of H_2S. More specifically, the Technical Committee agreed that most previous research efforts focused upon modelling and monitoring mean concentrations (usually 1-hour averages) downwind of a toxic source for neutral or unstable conditions.

Unfortunately, a mean concentration averaged over minutes or hours is not adequate to estimate the potential damage to a human who may be sensitive to instantaneous, high concentrations. In particular, downwind of a narrow meandering plume, a receptor receives intermittent doses of the pollutant (separated by periods of uncontaminated air) as the plume sweeps back and forth amid large-scale wind direction changes. If the scales of the meandering motions are much larger than the scale of the instantaneous plume, the plume does not impact the receptor very often, and a mean concentration at the receptor is low. On the other hand, the concentrations within the instantaneous plume may be high enough to kill an exposed person. Therefore, plume meander and concentration fluctuation are critically important. The Technical Committee agreed that predicting the short-term peak concentrations under low turbulence conditions was essential and summarized the issue as follows:

- To improve the understanding of meandering plumes, experimental data are required since the process which describes the transport and dispersion of plumes is not clearly understood theoretically. Of the public data in existence, most have been collected in wind tunnel studies where plumes do not meander, and none of the data collected in full-scale studies contain simultaneous concentration and wind measurements.

To address this issue, the Technical Committee and project team designed and implemented a generic field program consisting of two parts:

Table 1.1

Organizations Contributing to the Project

Organization	Contribution
Energy Resources Conservation Board	Management, manpower and office services
Canadian Petroleum Association (CPA), Independent Petroleum Association of Canada (IPAC) and Small Explorers and Producers Association of Canada (SEPAC)	$500 000
TransAlta Utilities Corporation	$10 000
Alberta Power	$5 000
Shell Canada Resources Limited	Office trailers, 4x4 truck, colour photo-copying and radios
Alberta Environment	Equipment and manpower
Canadian Petroleum Association (CPA)	Radios, tents, generators and mechanic
Syncrude Canada Ltd.	Tethersonde and an AC power conditioner
Alberta Public Works, Supply and Services	Vehicle rental
Petro Canada Inc.	Fuel ($5 100)
City of Calgary, Parks and Recreation	Snow-blower fan
Gulf Canada Resources	Video Editing Assistance
Mount Royal College, Department of Chemical and Biological Services	Acoustic sounder
Esso Resources Canada Limited	Surveying (1 week)
Canadian Occidental Petroleum Ltd.	Computers, manpower and meteorological data
Amoco Canada Petroleum Company Ltd.	Meteorological data
Kananaskis Center for Environmental Research, University of Calgary	Meteorological data
Environment Canada, Atmospheric Environment Service	Meteorological data
University of Calgary, Department of Geography	Meteorological data

- Tracer Study

  An intensive period of study, using a sulphur hexafluoride (SF_6) tracer gas, released under low wind speed conditions, with downstream atmospheric monitoring of plume dispersion and concentration behaviours and patterns. During the tracer releases, concurrent meteorological data were obtained to aid in the interpretation of the tracer gas results; and

- Meteorological Study

  Atmospheric turbulence and profile data were collected and used to obtain meteorological information on the frequency and persistence of low turbulence atmospheric conditions.

The Field Measurement Program was conducted over reasonably flat terrain approximately 20 km from the city of Calgary. The tracer release and sampling occurred during the months of October, November and December 1988. Tracer tests were performed whenever low wind speed/stable conditions were expected. The diffusion meteorological station commenced operation in October 1988 and continued to operate until a full 12-month set of meteorological data was collected. The data analysis component of the study was completed in mid 1990. An overview of the program can be found on the following pages.

1.4 Program Data Reduction and Analysis Objectives

1.4.1 Tracer Objectives

The tracer section of the Field Measurement Program involves extraction and analysis of plume concentration data. Data were collected while monitoring under two conditions: traverse (continuous mobile monitoring while travelling through the plume) and stationary (continuous monitoring while stationary in the plume).

Objectives for the tracer component of the study include:

- An assessment of the frequently used Gaussian plume approximation for describing the cross-wind concentration profile in the plume.
- The identification of the conditions which resulted in the smallest cross-wind spreads.
- An evaluation of the instantaneous and time-averaged cross-wind spreads compared with predicted values.
- A determination of peak-to-mean concentration ratios for the stationary concentration data.
- A comparison of predicted and observed plume centreline concentrations using a simple Gaussian plume model.

The analysis of the data focused on all the data collected with a limited review of case studies.

1.4.2 Meteorological Objectives

The meteorological station collected data for a full 12-month period (October 1988 to October 1989). Meteorological objectives identified for the Field Measurement Program include:

- The preparation of a climatological summary of important selected and derived meteorological parameters for the Field Measurement site.
- The evaluation of turbulence-related variables in the atmospheric boundary layer which are responsible for dispersion processes.
- An evaluation of the occurrence and persistence of low wind speed conditions.
- An evaluation of various meteorological preprocessor schemes ranging from those based on the STAR analysis of airport observations to those based on the determination of boundary layer parameters.
- The determination of the spatial representativeness of meteorological observations at various locations in the vicinity of the study area.
- An evaluation of the empirical power laws used to convert turbulence levels from one averaging period to another.
- A comparison of wind and turbulence data collected from sonic anemometers with those collected from conventional propellor anemometers.
- The determination of on-site mixing heights.

For the purposes of analysis, the data were grouped into two 6-month blocks: winter (October 1988 to March 1989) and summer (April 1989 to October 1989). For most of the objectives, the full 12-month data were used while for some, only the winter data were used.

1.5 Field Measurment Program Schedule

The project schedule can be subdivided into pre-field activities, field activities and data reduction activities:

Pre-field Activities

Management Committee appointment	November 1987
Technical Committee appointment	December 1987
Tender invitation	June 1988
Contract award	July 1988

Field Activities

Installation of hardware	August to September 1988
Field tests	October to December 1988
Tracer hardware decommissioning	January 1989
Meteorological hardware decommissioning	October 1989

Data Reduction Activities

Data reduction (tracer)	February to September 1989
Data reduction (meteorology: winter)	February 1989 to March 1990
Data analysis (tracer and meteorology)	September 1989 to March 1990
Data reduction (meteorology: summer)	February to June 1990
Data analysis (meteorology: summer)	June to August 1990
Simple Gaussian model evaluation	January to April 1990
1987 GASCON evaluation/enhancement	January to August 1990
GASCON/GASRISK integration	April to August 1990
GASCON2 model evaluation	August to September 1990

The extended schedule presented project management challenges to ensure continuity and minimize prolonged resource conflicts.

1.6 Field Measurement Program Reports

There are four reports associated with the Field Measurement Program:

Field Measurement Program
Atmospheric Dispersion Tracer Study Under Stable Conditions and Meteorological Study.
Volume 1

Field Measurement Program
Atmospheric Dispersion Tracer Study Under Stable Conditions and Meteorological Study.
Volume 2 - Appendices to **Volume 1**

Field Measurement Program
Atmospheric Dispersion Tracer Study Under Stable Conditions and Meteorological Study.
Volume 3 - Appendices to **Volume 1**

Field Measurement Program
GASCON2 Evaluation.
Volume 4

Volume 1 discusses the design and provides a description of the Field Measurement Program data collection procedures. This is followed by the presentation of the results for the tracer and meteorological components of the program. Volumes 2 and 3 are appendices to Volume 1 and include detailed plots and data for the tracer component of the study. The appendices also provide additional background data on the details of certain aspects of the program. Volume 4, the final volume, provides an assessment of the GASCON2 model based on the Field Measurement Program observations.

2 SITE DESCRIPTION

2.1 Site Selection Process

Major sour gas pools in the province of Alberta tend to fall within the foothills region just east of the Rocky Mountains which define the southwestern Alberta provincial boundary (Figure 2.1). For the most part, these foothills regions are characterized by rolling forested terrain; the density of the tree cover decreases with increasing distance from the mountains. The southern portion of the province, especially in the vicinity of Calgary, tends to be treeless.

Since many of the public concerns raised to the ERCB focus on conflicts between residential and sour gas development in northeast Calgary, it was imperative that the site selected for the Field Measurement Program be as representative as possible of the Calgary area. Specifically, the area northeast of Calgary is characterized by flat, treeless terrain. The land use varies from small residential land-holdings to multi-section farming. Rural residential areas are usually associated with shelter belt tree cover.

The Technical Committee, in conjunction with the ERCB, was responsible for site selection and approval. The committee recommended a four-section site with the tracer source located in the center and sampling arcs radiating from the center. Preference was to be given to sites located in the northeast Calgary area.

The ERCB staff initiated a search for an available four-section study area within a 20-km radius from Calgary (1 section of land = 1.6 km by 1.6 km). Local municipal authorities and existing gas plant staff were contacted. The search was then extended to a 50-km radius. It became evident that finding four sections grouped together which were both unobstructed and flat was difficult, if not impossible.

The Technical Committee was then approached with the concept of a two-section study area using multiple source location sampling arcs. This system would allow for moving the source to the appropriate quadrant depending on wind direction. Although not ideal, it was thought that the source could be transported to different locations in a reasonable amount of time (30 minutes). With agreement on this concept, the ERCB staff were able to approach landowners.

The ERCB staff were able to locate a landowner willing to rent his property during the testing stage and for continued operation of the meteorological station. A site visit by the Technical Committee confirmed that the site would be suitable for the Field Measurement Program (Photos 2.1 and 2.2). The landowners were Harold and Marion Randall. Their property was located 20 km from Calgary at the intersection of Secondary Highways # 566 and # 9 (Figure 2.1). The Randalls were excellent hosts and neighbours. They supported the project, helped out with the media trip to the site and a wind-up barbecue, provided a fully equipped machine shop, a tractor/grader and a front-end loader. They offered a warm welcome to all of the project staff. Figure 2.2 shows the topographic contours and an aerial photograph of the test site. More detailed maps showing a larger area surrounding the test site are presented in Figures 2.4 and 2.5.

2.2 Site Layout

The dimensions of the test site are 1 600 metres (m) (1 mile) by 2 400 m (1.5 miles). Source stations were located on the north, south, east, and west boundaries and at the centre of the test site. Sampling arcs were located 700 and 1 400 m downwind of the source stations. For the south source station, a sampling arc was located 2 100 m to the north. For the centre source station, only the 700-m sampling arc was defined. All the source stations and sampling areas were surveyed (Figure 2.3).

The terrain contours are shown in Figures 2.2 and 2.4. A three dimensional terrain projection is shown in Figure 2.6. Selected east-west terrain cross-sections are shown in Figure 2.7. Over the southern portion of the test site where most of the sampling was done, the terrain rises from east to west with a slope of about 0.015 (about 1 degree). While this site is not completely flat from a meteorological perspective, it is nontheless more representative of conditions in the northeast Calgary area.

The receptor arcs were marked with survey stakes every 20 m for the 700 m distances. For the 1 400 and 2 100-m receptor arcs, the survey stakes were placed 30 and 40 m apart, respectively. Each stake was assigned an alphanumeric designation consisting of a letter and a number, e.g., A1 marked the first stake at every 700-m arc, the next stake was A2 and so on until it reached A0 and then the name changed to B1 and so on (Photos 2.3 and 2.4).

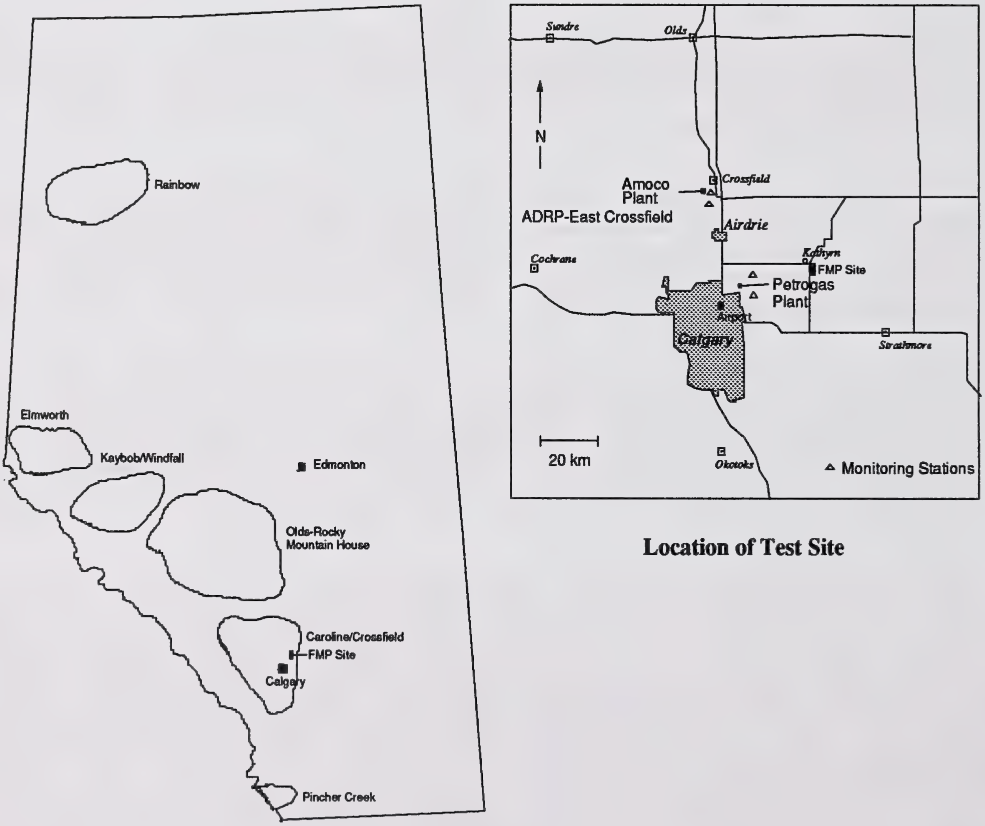

Location of Test Site

Figure 2.1

FMP Site in Relation to Major Sour Gas Areas in Alberta.

Photo 2.1

Members of the Technical Committee Were at the Site to Ensure it was Appropriate.

Photo 2.2

Photo 2.3

Stations Along the Arc were Marked with Stakes.

Photo 2.4

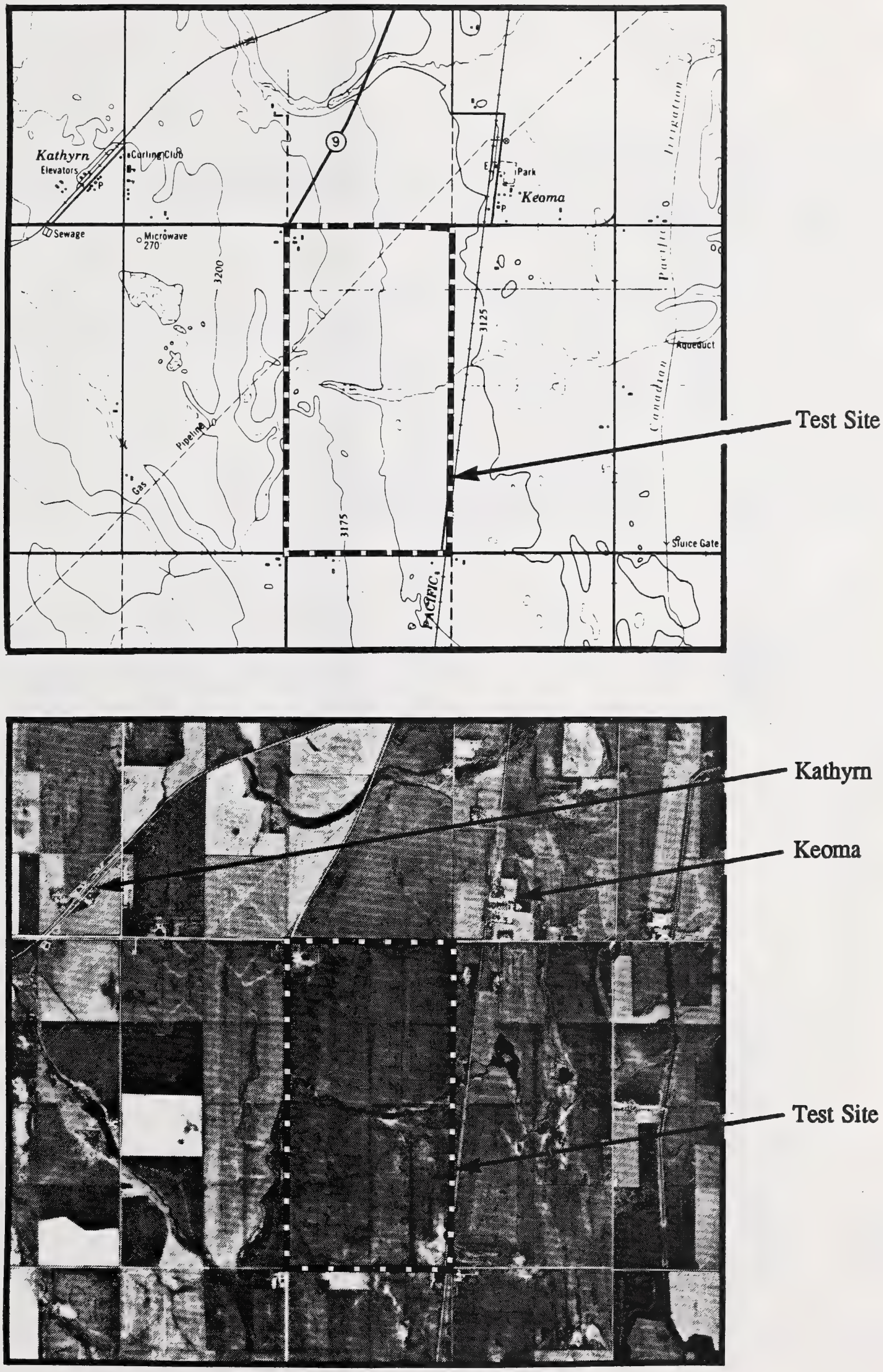

Figure 2.2

Reductions of Figures 2.4 and 2.5 Indicating the Location of the Test Site.

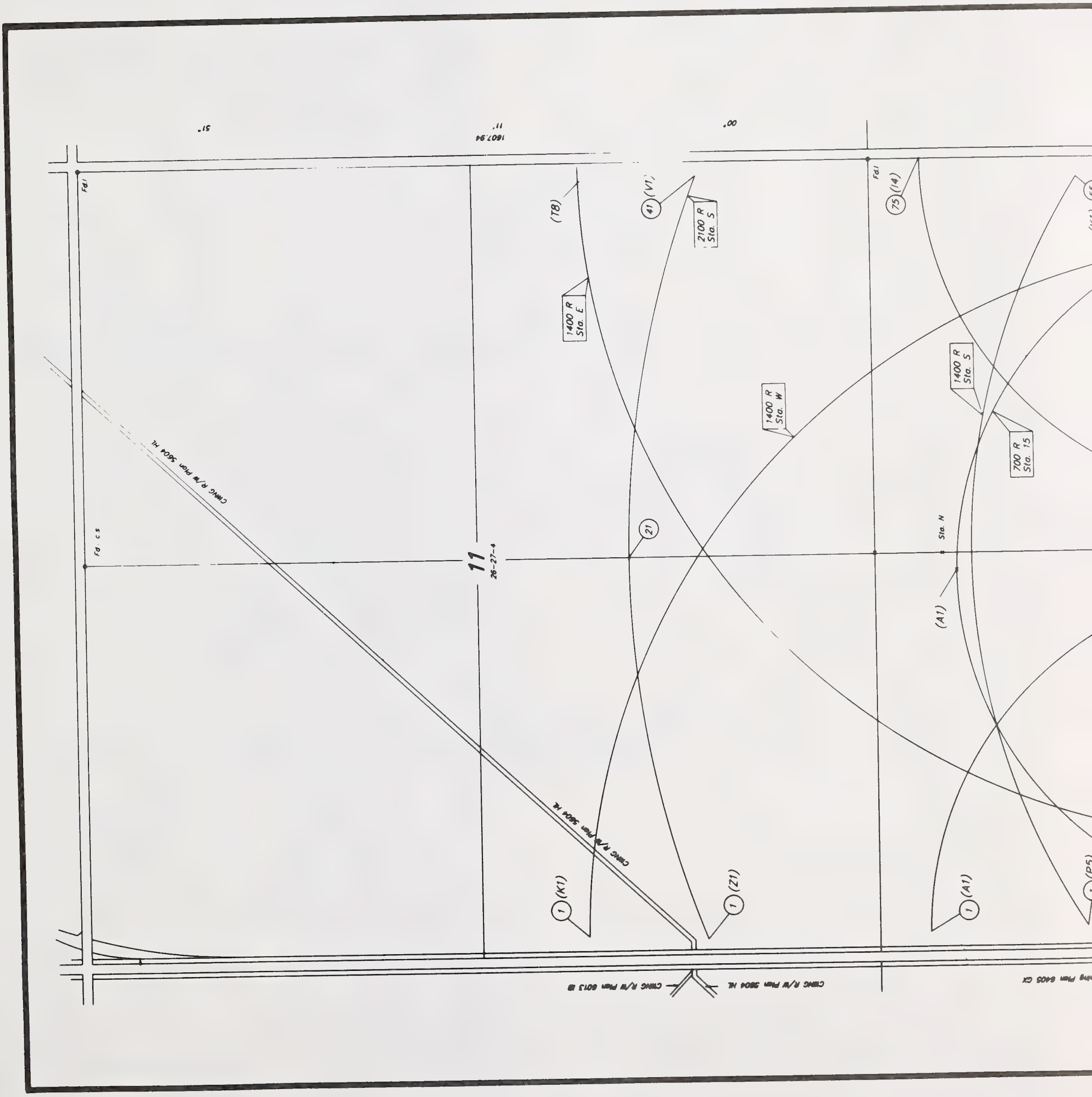
51°
1607.94
11'
00'
Fd.I
Fd. c s
(T8)
1400 R Sta. E
41 (V1)
2100 R Sta. S
75 (14)
1400 R Sta. W
1400 R Sta. S
700 R Sta. 15
11
26-27-4
21
Sta. N
(A1)
CWNG R/W Plan 5604 HL
1 (K1)
1 (Z1)
1 (A1)
(P5)
CWNG R/W Plan 6013 IB
CWNG R/W Plan 5604 HL
ing Plan 6405 CX

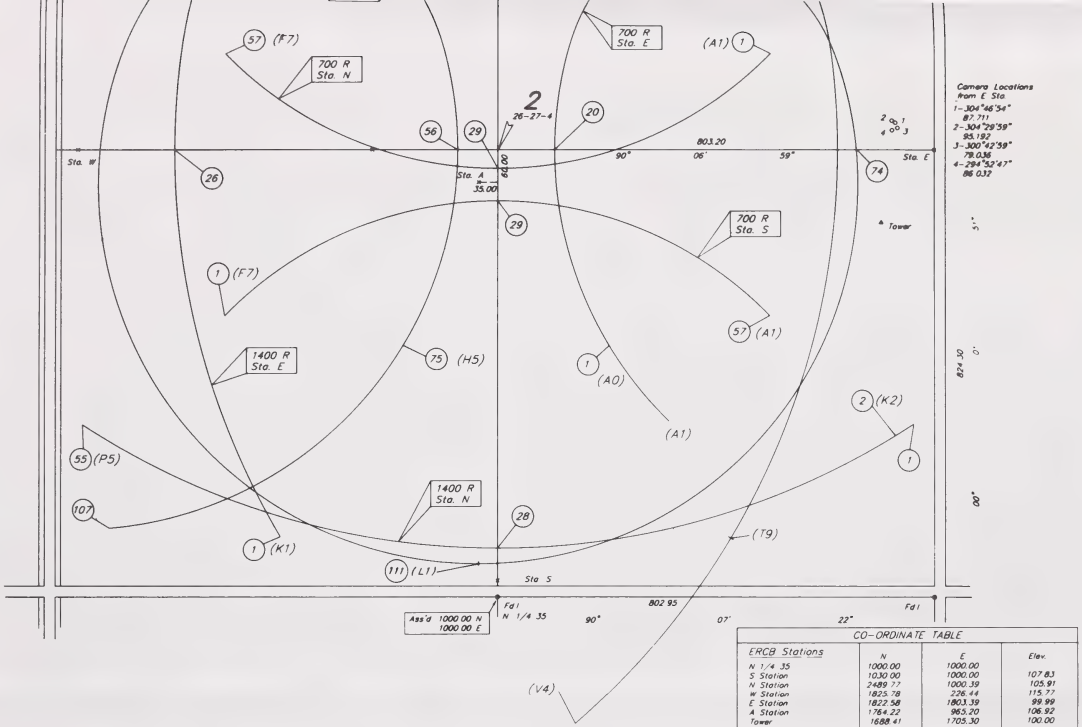

Camera Locations
from E Sta.
1-304°46'54"
87.711
2-304°29'59"
95.192
3-300°42'59"
79.036
4-294°52'47"
86.032

ENERGY RESOURCES CONSERVATION BOARD

Plan Showing

GAS RELEASE RADIUS POINTS

In

Sections 2 and 11 Tp. 26 Rge. 27 W.4 M.

SCALE 1:5000

JOB # E-1003-88

NOVEMBER 1988

ALL-WEST SURVEYS (1982) LTD.
249, 379 - 2nd Avenue S.W.
Calgary, Alberta T2P 0C5

Phone: (403) 234-7599

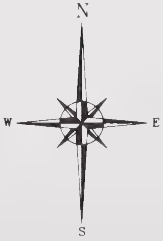

REVISIONS

January 3, 1989 (Table)
April 20, 1989 (Co-ord's added)
April 24, 1989
April 25, 1989
April 27, 1989

CO-ORDINATE TABLE

ERCB Stations	N	E	Elev.
N 1/4 35	1000.00	1000.00	
S Station	1030.00	1000.00	107.83
N Station	2489.77	1000.39	105.91
W Station	1825.78	226.44	115.77
E Station	1822.58	1803.39	99.99
A Station	1764.22	965.20	106.92
Tower	1688.41	1705.30	100.00
Camera #1	1872.61	1731.35	
Camera #2	1876.50	1724.94	
Camera #3 (Smoke Test)	1862.95	1735.44	
Camera #4 (Video)	1858.77	1725.34	
A Station 700R			
Sta 1 (A1)	2464.22	965.38	99.75
Sta 111 (L1)	1064.22	964.24	101.19
E Station 700R			
Sta 1 (A0)	1462.15	1203.32	104.05
(A1)	1321.40	1314.71	
Sta 75 (14)	2522.58	1805.39	99.82
E Station 1400R			
Sta 1 (K1)	1110.38	598.08	115.30
Sta 98 (T8)	3222.11	1767.14	98.36
Sta 99	3222.56	1797.14	98.83
S Station 700R			
Sta (F7)	1517.83	497.98	114.38
Sta 57 (A1)	1517.56	1502.28	101.15
S Station 1400R			
Sta 1 (P5)	2202.34	234.74	113.46
Sta 55 (K1)	2201.94	1765.87	99.48
S Station 2100R			
Sta 1 (Z1)	2979.65	219.69	111.98
Sta (V1)	2979.24	1781.33	97.70
N Station 700R			
C 9	1789.77	1000.21	106.76
C 0	1790.06	980.21	107.15
D 3	1794.36	920.37	108.00
D 4	1796.93	900.54	108.76
D 5	1800.06	880.78	109.52
D 6	1803.76	861.13	110.44
D 7	1808.02	841.58	110.86
Sta 1 (A1)	2001.94	1502.41	100.43
Sta 57 (F7)	2002.21	498.11	112.75
N Station 1400R			
M 7	1090.08	1030.02	106.86
Sta 1	1317.43	1765.65	97.96
Sta 2 (K2)	1301.30	1740.35	99.16
Sta 55 (P5)	1317.83	234.52	119.08
W Station 700R			
F 6	1824.36	926.44	108.56
F 7	1804.36	926.12	108.32
F 0	1744.53	921.71	107.91
Sta 1 (A1)	2525.78	227.29	110.41
Sta 75 (H5)	1462.92	825.05	108.8
Sta 107	1128.18	284.38	117.95
W Station 1400R			
Sta 1 (K1)	3225.73	238.38	108.64
Sta 99 (T9)	1108.69	1428.85	103.10
Sta 114 (V4)	765.55	1140.72	107.39

Figure 2.3

Gas Release Radius Points

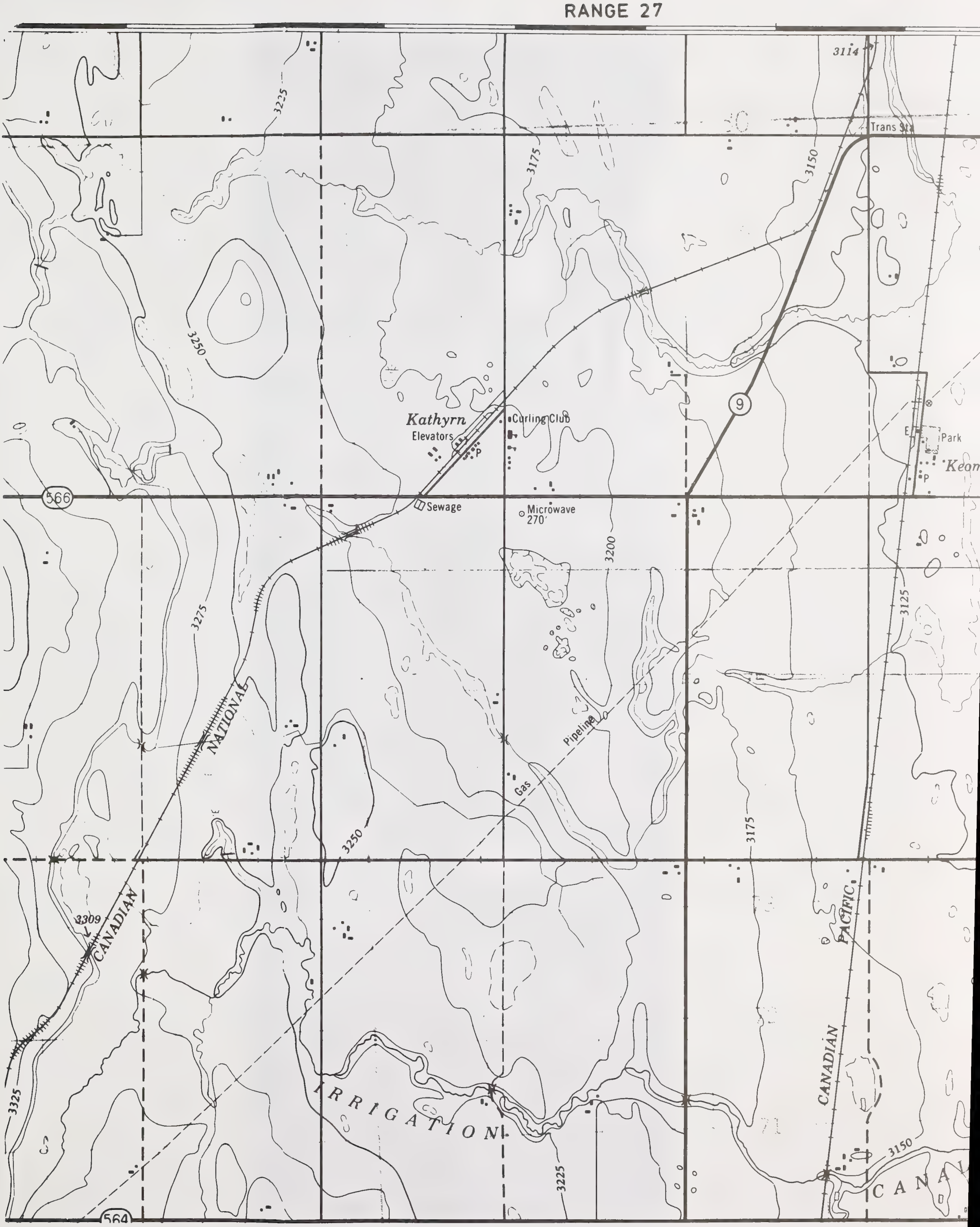
RANGE 27
3114
Trans Sta
3225
3175
3150
3250
Kathyrn
Elevators
Curling Club
P
9
E
Park
Keon
566
Sewage
Microwave
270'
3200
3125
3275
NATIONAL
Gas
Pipeline
3250
3175
3309
CANADIAN
CANADIAN
PACIFIC
IRRIGATION
3325
3225
3150
CANA
564

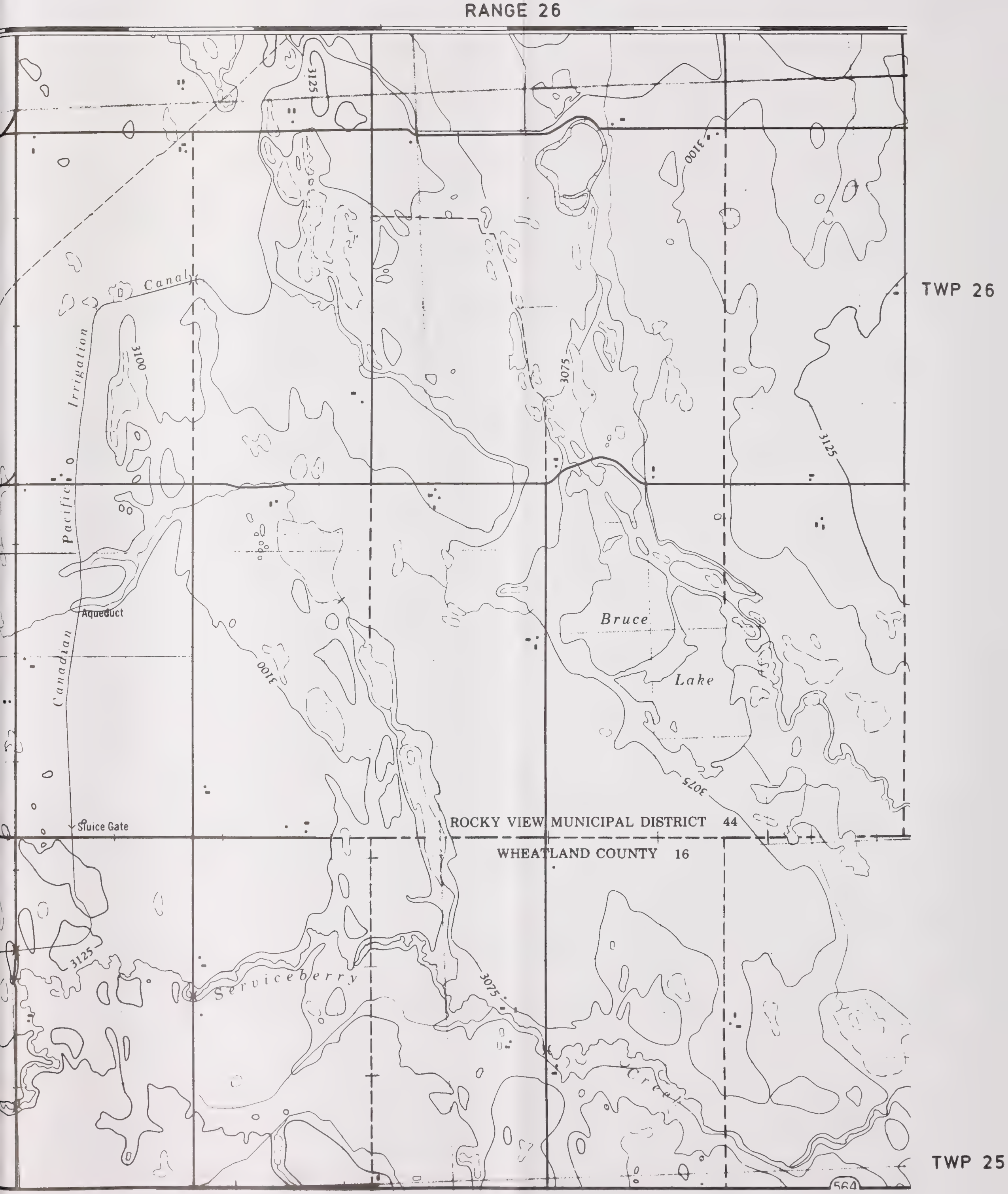

Figure 2.4 Topographical Map of Test Site and Surrounding Area

Aerial Photo of Test Site
and Surrounding Area

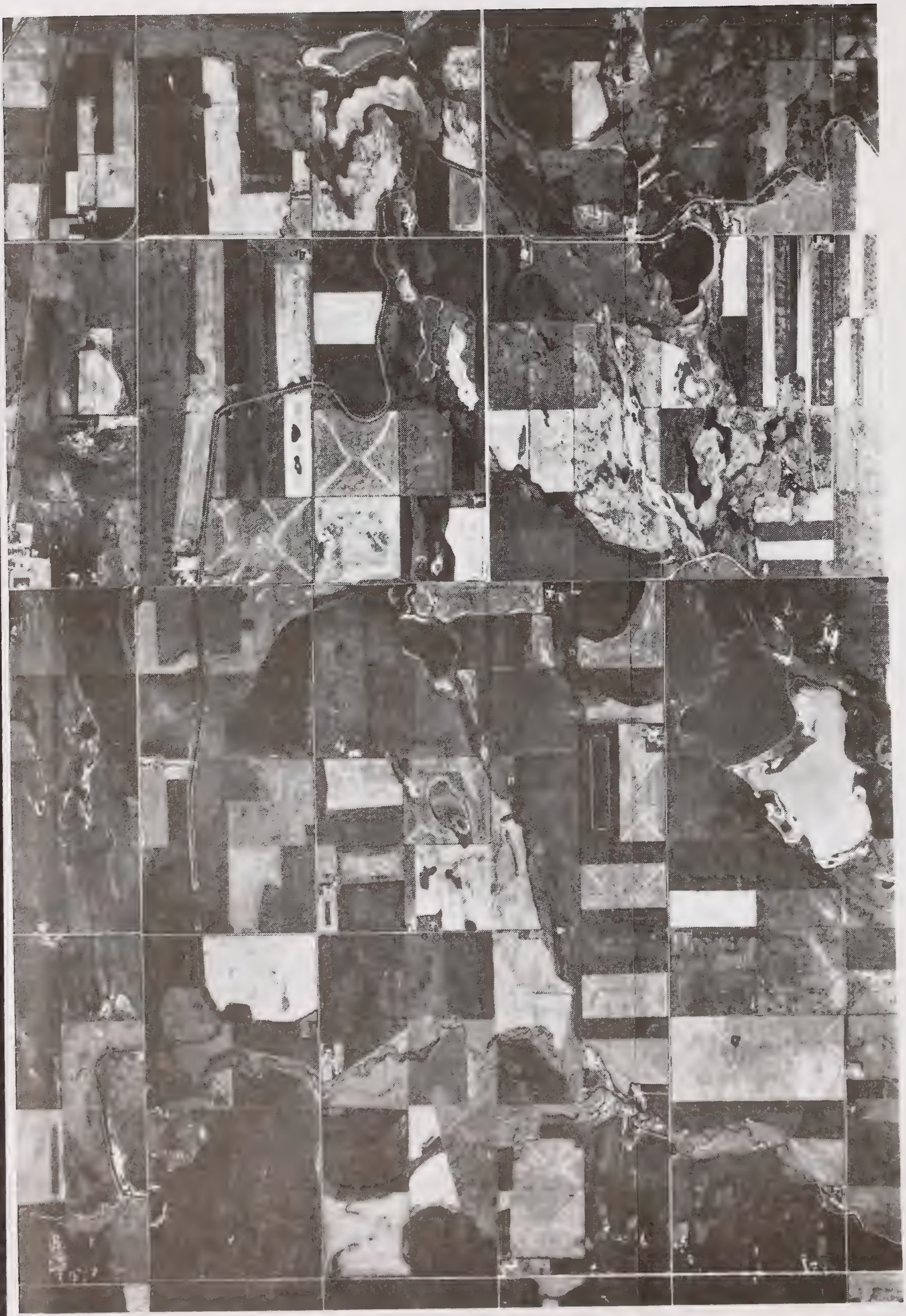

Figure 2.5 Aerial Photo of Test Site and Surrounding Area

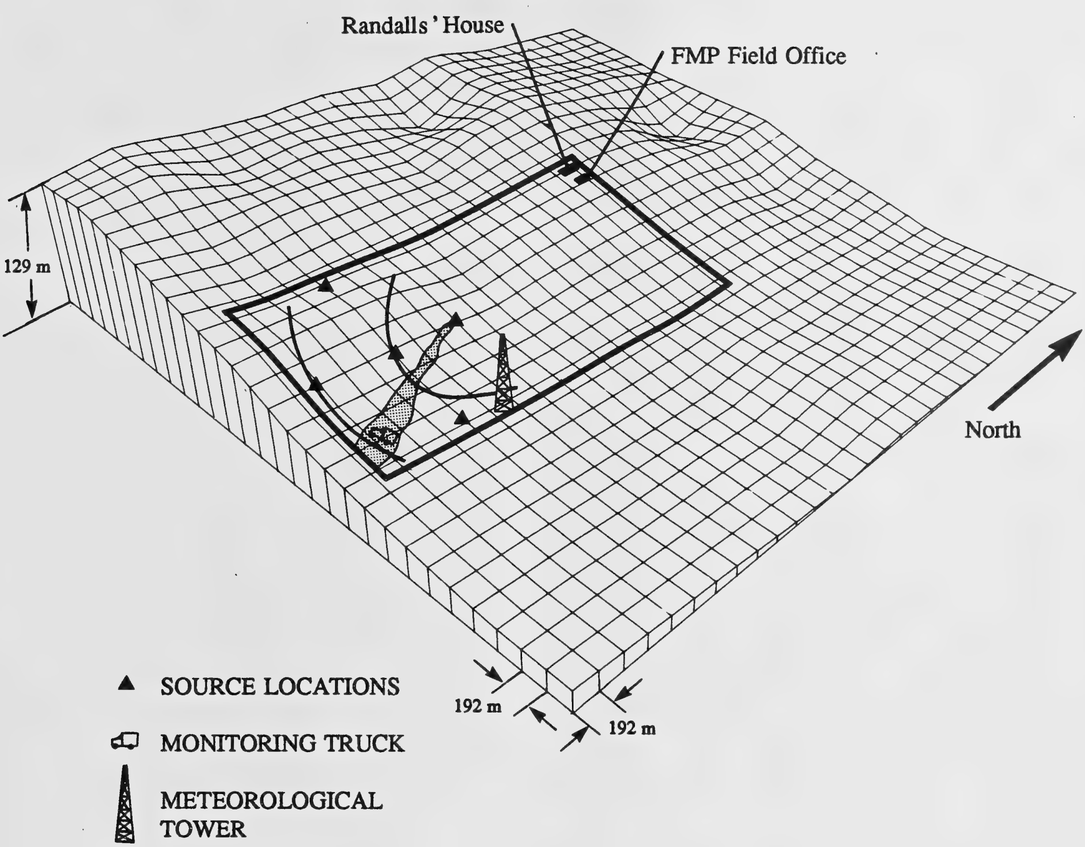

Figure 2.6

Perspective Terrain Diagram of Test Site and Surrounding Area.

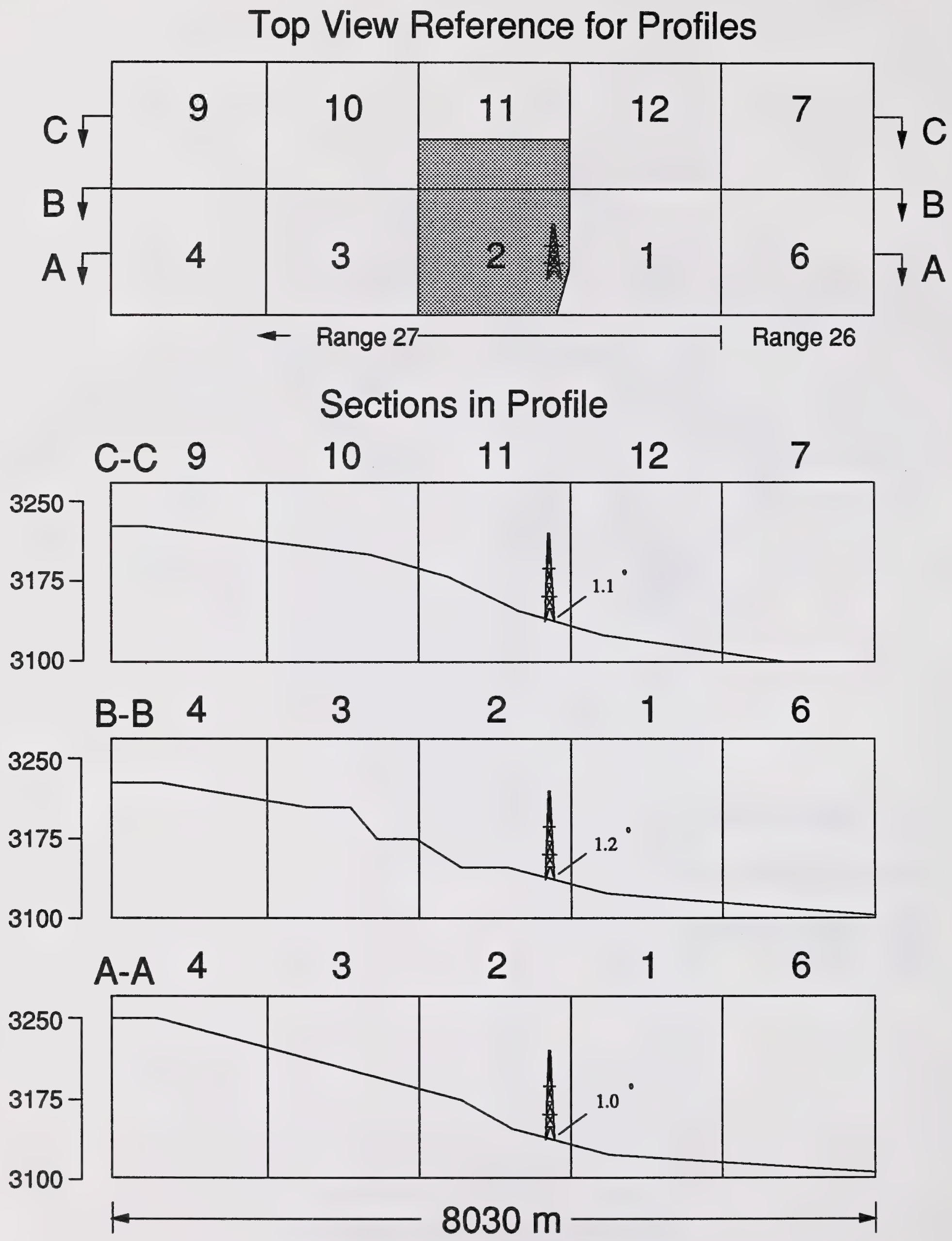

Top View Reference for Profiles

Sections in Profile

Figure 2.7

Section Profiles of Test Site and Surrounding Area. The Test Site is Shown as a Shaded Polygon and the Approximate Location of the Tower is Indicated. The Slope in Degrees at the Tower is Shown for Each Profile. The Elevation is in Feet Above Sea Level.

3 TRACER GAS RELEASE

3.1 Background

Atmospheric tracer technology has been developed to provide further understanding and quantification of atmospheric transport, transformation and dispersion processes. The technology has been applied to a variety of atmospheric situations which include

- Acid precipitation research
- Continental and global scale transport
- Dry deposition research
- Transport and dispersion
- Cloud dynamics.

The distance scales cover the full range of atmospheric motions ranging down to a few metres in the case of dry deposition research to the global scale in the case of climate change evaluations (Heiken 1986).

Tracer technology involves the release of a known compound (gaseous or particulate) into the atmosphere that can be unambiguously detected at low concentrations in the air. These tracers may be classified as either "tracers of opportunity" which are already in the atmosphere and may include atmospheric dust or anthropogenic emissions, or the release of "artificial tracers" which are compounds not normally present in the atmosphere.

An atmospheric tracer study involves both source release and sampling considerations. For the source release, known amounts of the tracer compound have to be measured precisely and emitted in such a manner as to simulate the desired source condition. The sampling methodology can range from the collection of integrated air samples (in plastic bags, syringes, evacuated bottles) which can be analysed promptly at a nearby or on-site laboratory, to the use of continuous analysers which can provide real-time measurements.

This section (Section 3) describes the tracer gas release system and hardware and the next section (Section 4) describes the tracer gas sampling methodology adopted for the Field Measurement Program.

3.2 Approach

3.2.1 Tracer Gas

To maximize the effectiveness of an atmospheric tracer, the selected tracer gas should

- Be non-reactive within the timeframe of interest
- Have a low background concentration in the study area
- Be harmless to users and the general public
- Be detectable at low concentrations
- Be available at a reasonable cost

These criteria incorporate both technical and practical considerations.

SF_6 has been used as a tracer gas for dispersion and transport studies. SF_6 is readily available in the liquefied form in compressed cylinders and its low boiling point allows for a controlled release as a gas from the cylinder to the atmosphere. SF_6 is primarily used as an electrical insulating gas for high voltage power switching equipment. The average background concentration is in the 1 to 2 parts per trillion (ppt) range (Dietz and Senum 1986). Properties of the SF_6 gas are as follows:

• Non-reactive:	Chemically and thermally stable.
• Non-toxic:	Odourless, colourless and tasteless, non-flammable and non-corrosive.
• Boiling point (-64 °C):	Gaseous at atmospheric conditions.
• Molecular mass (146.05 kilograms per kilomole (kg/kmol)):	Readily detectable by electron capture detector (ECD) at the ppt level.

The properties of SF_6 make it ideally suited as a tracer gas for both atmospheric and industrial hygiene studies. As a consequence, integrated and continuous ECD analyser hardware and technology are available commercially.

For the Field Measurement Program, clinical grade purity SF_6 (minimum 99.8% SF_6) was obtained from Medigas Alberta Ltd. The gas was provided in compressed cylinders as a liquid (cylinder size 1A contained 52.16 kg of SF_6).

3.2.2 Methodology

The objective of the source release is to simulate both elevated and ground release plumes that may result from a continuous unignited, H_2S well blowout. For the elevated release, a nominal plume height of 20-m was selected to coincide with typical plume heights expected in low wind speed, stable atmospheric conditions. Two alternative methods for releasing the plume at an elevated height were considered. The first was a fixed-location 20-m tower and the second was a ground-level fan that had sufficient power to provide for a 20 m plume rise. The latter was selected to provide flexibility for relocation during a test, should the winds change direction. For the ground release, a source with very little or no vertical momentum was simulated.

It is critical that any simulated source provides a means of adequately mixing the SF_6 stream into the atmosphere to produce a plume that has a neutral buoyancy and a plume that has a cross-sectional area that is the same order as the plumes expected from the well releases. If the former conditions are not met, gravitational settling will adversely affect the initial dilution of the plume. If the latter condition is not met, then the scales of turbulence that result in dispersion will not be readily accounted for.

3.3 Source Equipment

The hardware required for the source release can be classified as follows:

- Flow measurement hardware
- Ground release hardware
- Elevated release hardware
- Meteorological hardware.

The flow measurement instrumentation was required to provide an accurate measurement of the SF_6 release rate. During the tests, the release rate varied from 0.2 grams per minute (g/min) to 8 g/min and was predetermined primarily by the anticipated amount of dispersion and the limits of the sampling analyser range. A small fan and enclosure were used to simulate the ground source while a larger fan was used to simulate the elevated release. Supplementary meteorological measurements of wind speed and ambient temperature were made at the source with a 3-cup anemometer and a temperature probe. A portable 110/220 Volts AC (VAC) three-phase diesel-powered generator provided the electrical power needs for the source equipment.

3.3.1 Flow Measurement Hardware

Figure 3.1 shows the plumbing and electrical schematic of the SF_6 release and flow measurement system. The SF_6 gas was passed through a two-stage regulator and 6.4 millimetres outside diameter (mm O.D.) stainless steel tubing to a 6.4-mm needle valve which was used to control the flow. Stainless steel tubing of the same diameter was used to connect a mass flow transducer. Tygon tubing (9.5 mm O.D.) was used to carry the SF_6 gas to the release ports.

The mass flow was measured using a Matheson Model Series 8116 linear mass flow meter. The transducer (Model #H-5KM; Serial #6407) is constructed of Monel and is connected to the flow meter power supply indicator (Model #8116-0253; Serial #3975) with an electrical signal cable (transducer cable). Matheson indicated that its flow meter operates on a patented thermal principle that depends on the mass flow of the gas and its heat capacity.

The flow meter power supply/indicator is provided with an analog meter that responds to varying flow conditions and with a 0 to 5-Volts DC (VDC) output that is linear with flow rate. During the field tests, the output was directed to a Tylon Model FMT-3 totalizer which has a mechanical digital readout and a 0 to 5-VDC input. Output was also directed to a Campbell Scientific CR10 datalogger where the voltage was converted into engineering units at a 1-Hz sampling rate. For field tests 1 to 8, 3-minute average flow rates and standard deviations were calculated and for field tests 9 to 33, 1-minute averages and standard deviations were calculated and stored. The datalogger was programmed and data were monitored using a Tandy TRS-100 laptop computer. At the completion of each test, the data from the datalogger were downloaded to an IBM personal computer and stored on 5 1/4-inch floppy diskettes.

The flow meter and totalizer both require 110-VAC power which was supplied by a 110/220-VAC 3-phase diesel-powered electrical generator which supplied all the power needs for the source equipment. Power for the laptop computer and datalogger was supplied by DC batteries.

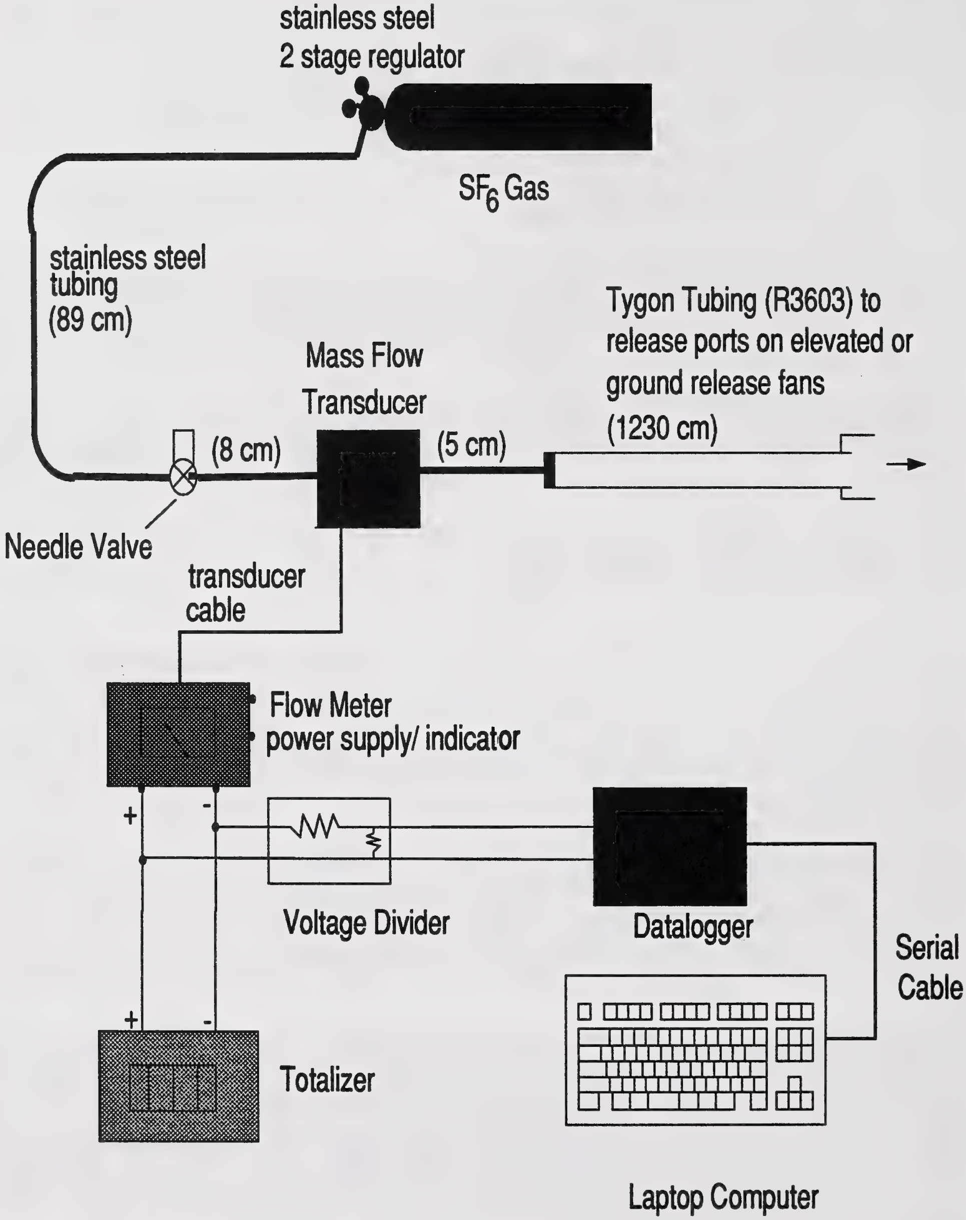

Figure 3.1

Schematic Showing the SF_6 Flow Measurement and Recording Hardware.

Calibration

Several calibrations of the flow measurement system were undertaken for each output: flow meter display, flow meter voltage output and totalizer output. In addition, calibration for two voltage ranges were determined (0 to 0.8 VDC and 0.8 to 5.5 VDC).

Actual flows were measured by passing SF_6 through a soap bubble meter. The bubble meter measurements were corrected from ambient conditions to a temperature and pressure of 0°C and 101.3 kilopascals(kPa) respectively. The measurements were not corrected for water vapour content in the SF_6. The amount is considered negligible (less than 2%).

For the low voltage range, the calibration curve is based on a linear fit to seven points within that range. The full-scale calibration is based on all points, including the low end (N = 50). Samples of the calibration points and curves for the mass flow rate are shown in Figure 3.2.

The linear regression coefficients for the volumetric and mass flow calibrations are presented in Table 3.1. The linear correlation coefficient between the observed values and predicted curves ranges from 0.995 to 0.999. For a voltage signal of 0.8 Volts, the difference between the high and low range calibration is approximately 5%. Typical differences between the data and curves are in the 4 to 8% range.

Table 3.1

Volumetric and Mass Flow Rate Calibration for the Source Flow Meter System.

Flow Meter Voltage Output (VDC)

Type	Applicable Range	Calibration
Volumetric Flow Rate (cm^3/min)	Voltage = 0.0 to 0.79 VDC Voltage = 0.8 to 5.5 VDC	$Q = (252.2*VDC) + 16.1$ $Q = (254.2*VDC) + 4.3$
Mass Flow Rate (g/min)	Voltage = 0.0 to 0.79 VDC Voltage = 0.8 to 5.5 VDC	$M = (1.644*VDC) + 0.1050$ $M = (1.657*VDC) + 0.0280$

Flow Meter Display (FMD)

Type	Applicable Range	Calibration
Volumetric Flow Rate (cm^3/min)	FMD = 0 to 799 cc/min FMD = 800 to 5000 cc/min	$Q = (0.268*FMD) - 8.5$ $Q = (0.257*FMD) - 13.0$
Mass Flow Rate (g/min)	FMD = 0 to 799 cc/min FMD = 800 to 5000 cc/min	$M = (0.00175*FMD) - 0.055$ $M = (0.00168*FMD) - 0.085$

Q = SF_6 volumetric flow rate (cm^3/min at 0° C and 101.3 kPa)

M = SF_6 mass flow rate (g/min)

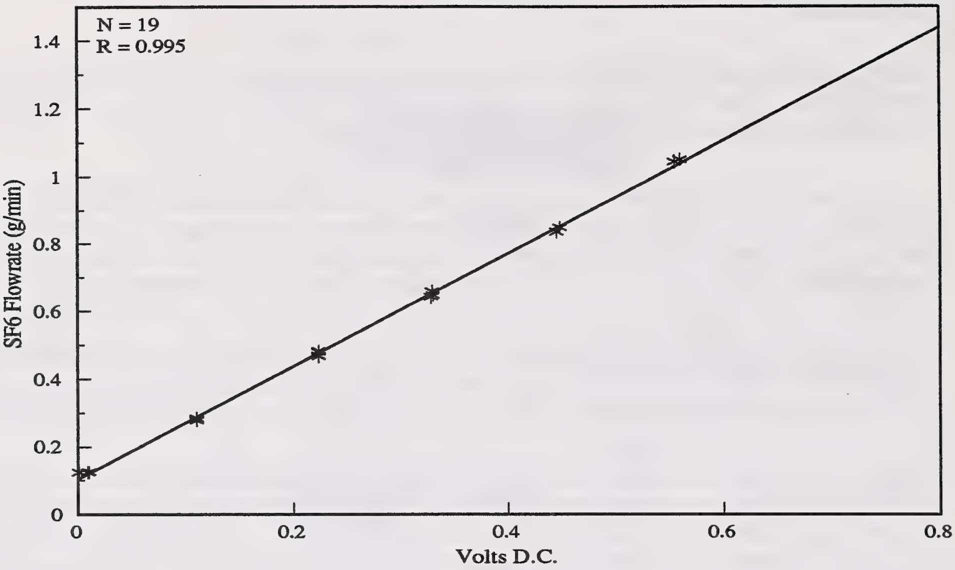

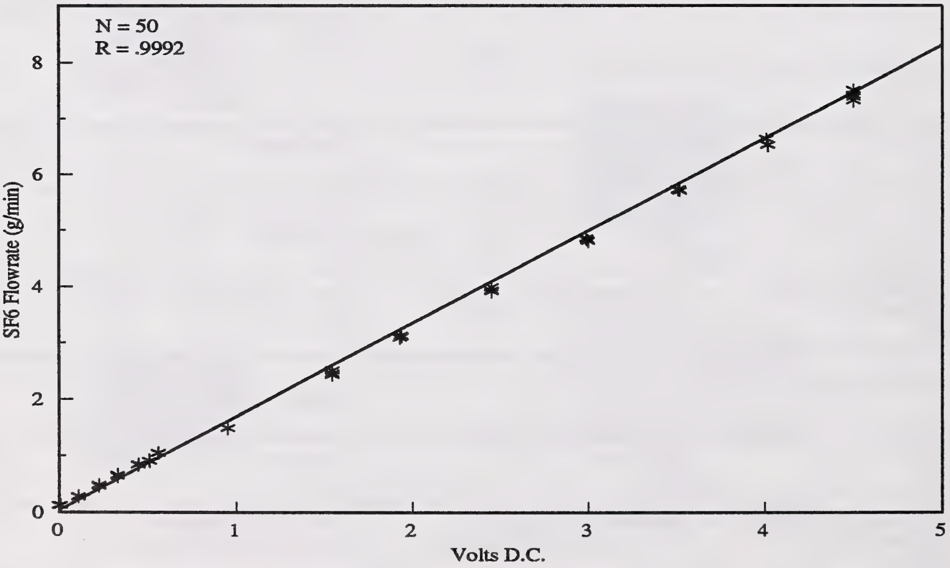

Figure 3.2

Mass Flow Rate Calibration (g/min) as a Function of Voltage.

3.3.2 Ground Source Hardware

The ground release consisted of a fan suspended in the centre of an octagonal-shaped enclosure. The enclosure was approximately 40 centimetres (cm) in height and 220 cm in diameter (Figure 3.3 and Photo 3.1). The lower face of the fan was at a height of 40 cm and the fan output was directed downward. The fan and enclosure were designed to induce mixing of SF_6 and air. A square shape was rejected at the design stage since it was thought that the sharp corners could result in some stagnation.

A Dayton (Model 4CS10-A) 61-cm domestic fan was used. The fan was driven by a 120-VAC (2.2 amp) motor and had three speed settings. The highest speed setting, which produced a nominal flow rate of 42.5 m^3/min, was used during the field tests.

A 9.5-mm O.D. copper tube was closed at one end and bent into a 45-cm diameter circle and attached to the bottom of the fan. A series of 0.158-cm diameter holes were drilled at 7.5-cm intervals. SF_6 was directed through 9.5-mm Tygon tubing which was connected to the open end of the copper tube.

Calibration

Because of the nature of the ground source, the fan flow rate was not measured. Calibration based on the nominal output of the fan indicates a downward velocity of 2.36 metres per second (m/s) based on a fan output area of 0.30 m^2. The total area of the octagon is 4.09 m^2. Simple conservation of mass would suggest a mean upward velocity of

$$\frac{0.30\,\mathrm{m}^2}{4.09\,\mathrm{m}^2} \cdot 2.36\mathrm{m/s} = 0.17\mathrm{m/s}$$

The above calculation assumes no flow recirculation or entrainment of outside air (other than that directed by the fan) into the enclosure.

3.3.3 Elevated Source Hardware

A Boyne Snowmaker fan was used to simulate an elevated source (Figure 3.4 and Photo 3.2). The fan was mounted such that the flow was vertical and had a nominal flow rate of 700 m^3/min. The 7-blade cast aluminum fan was rotated at 1 756 revolutions per minute (rpm) by a 15-BHP motor. For the field tests, the water supply hoses, water injection ports and pump used for snow making were disconnected from the fan.

A prefabricated metal shroud whose length was approximately equal to the fan diameter was added to the exhaust side of the fan (Figure 3.5). Six ports placed 60° apart were drilled 5 cm from the top of the shroud and two ports were drilled 180° apart 5 cm from the bottom of the shroud.

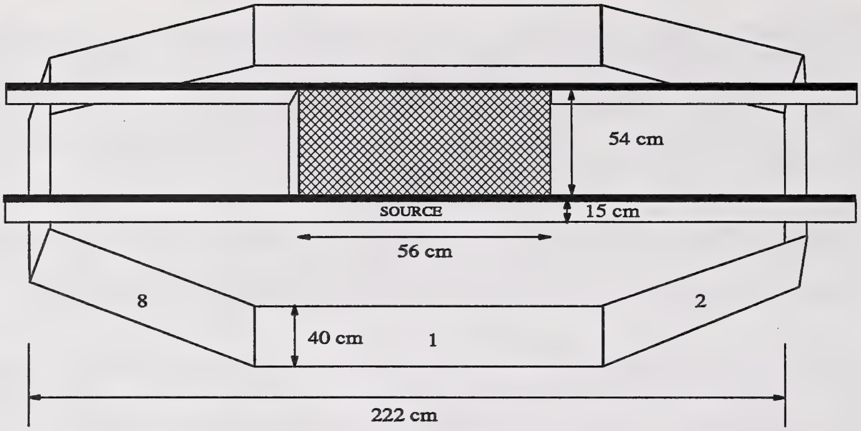

Figure 3.3

Ground Source for Tracer Gas Release.

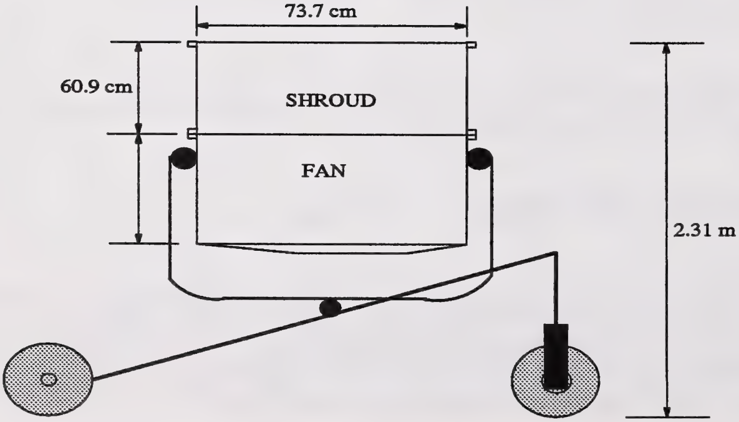

Figure 3.4

Elevated Source for Tracer Gas Release.

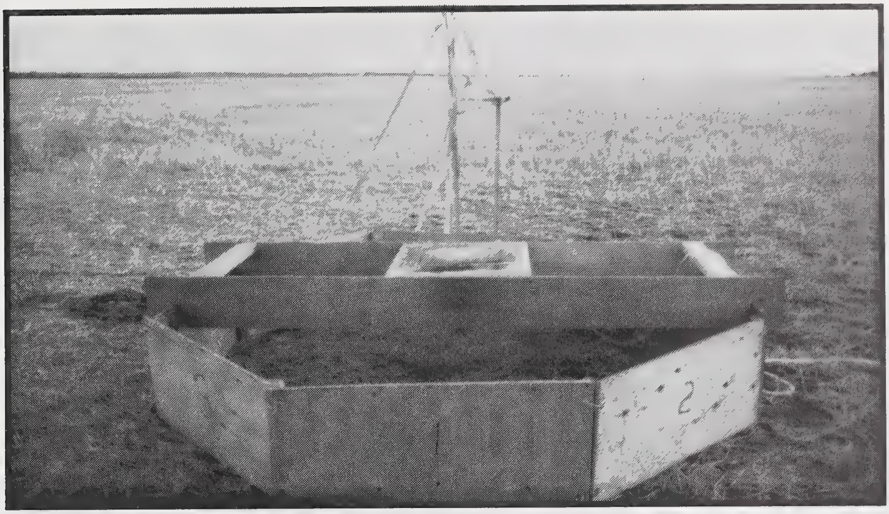

Photo 3.1

Ground Source for Tracer Gas Release.

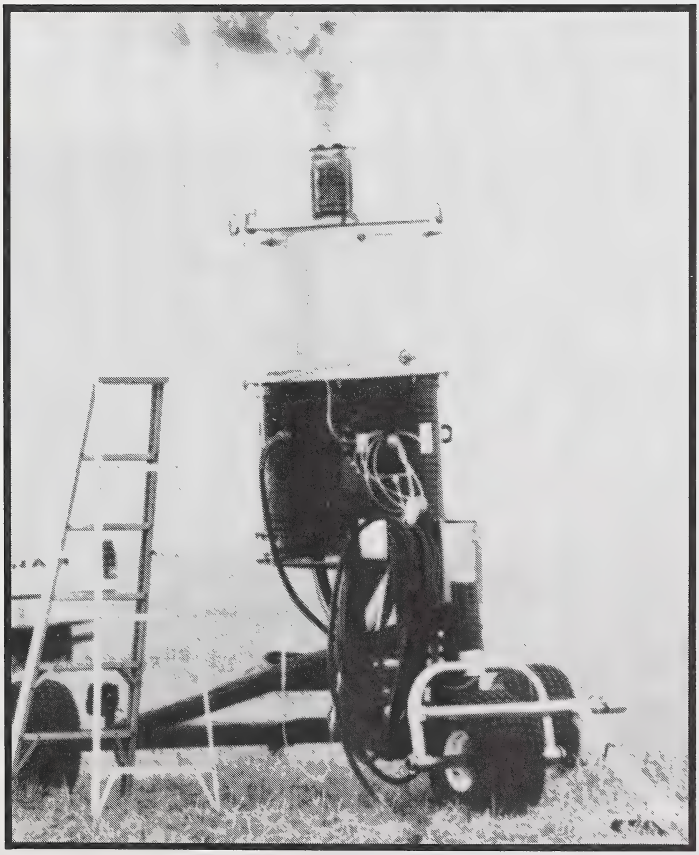

Photo 3.2

Elevated Source for Tracer Gas Release.

Photo 3.3

Fan Calibration Prior to Start of Field Tests.

Photo 3.4

Source Anemometer and Large Fan Used for Elevated Releases.

Photo 3.5

Flow Rate Instrumentation for the Source.

Photo 3.6

The SF_6 Cylinder and Tubing Connectors. The SF_6 had to be Stored Inside the Van, Particularly During Cold Temperatures.

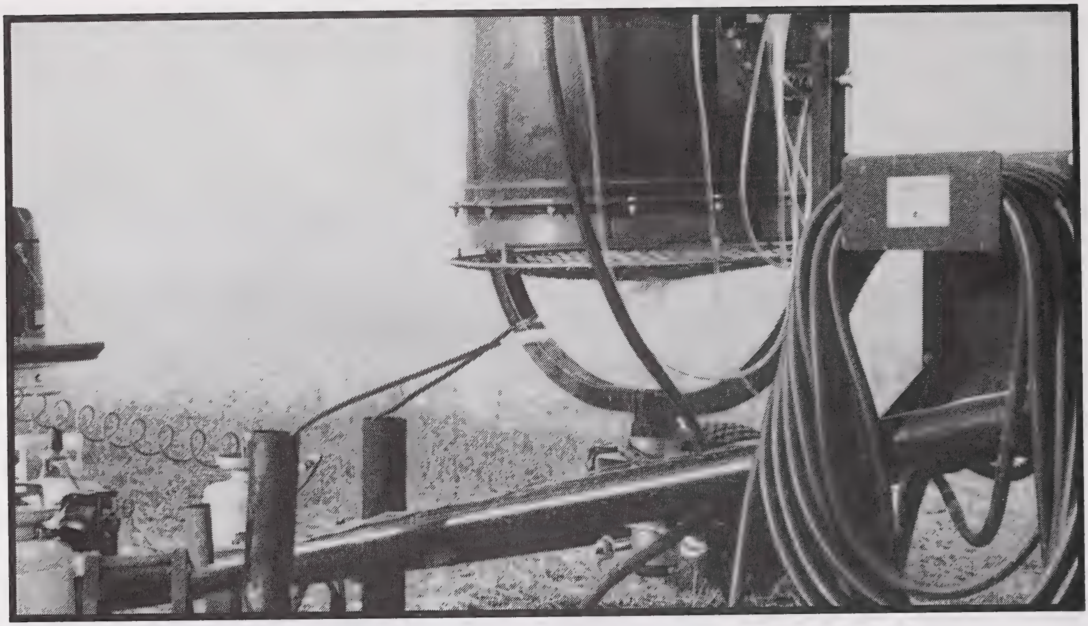

Photo 3.7

Example of Smoke Generation Equipment Tried for the Elevated Release Fan But Not Found Suitable.

Photo 3.8

Example of Smoke Generation Equipment Tried for the Ground Release Fan But Not Found Suitable.

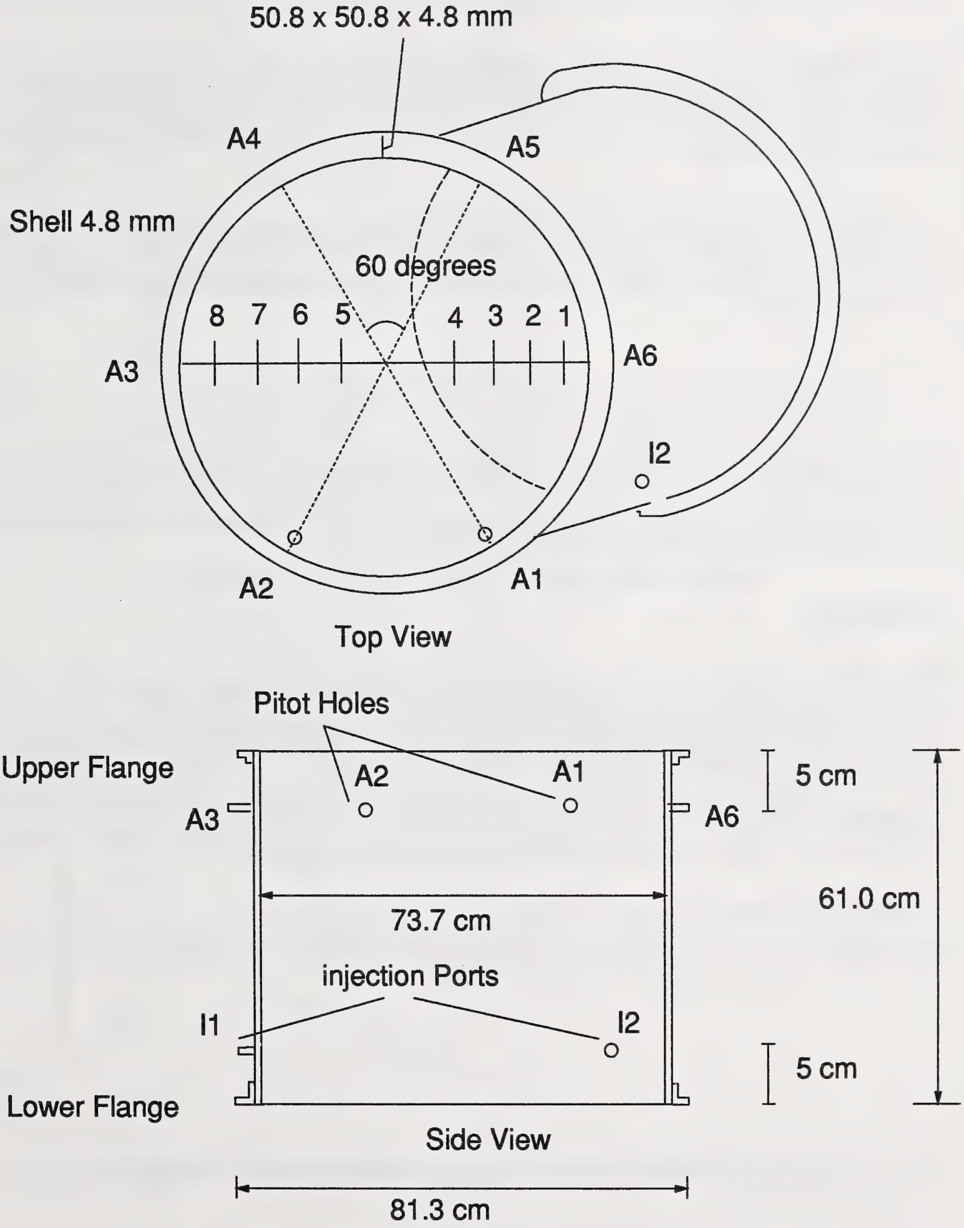

Figure 3.5

Elevated Source Port Layout for the Tracer Gas Release.

The two SF_6 injector ports (I1 and I2) were located near the bottom of the shroud. Copper tubing (9.5 mm O.D.) extended 12.5 cm into the shroud; outside the shroud, the two pieces of tubing connected to a tee fitting. The Tygon tubing from the SF_6 flow measurement system was connected to the tee fitting.

Six calibration ports (A1 to A6) were located near the top of the shroud. Two of these ports (A2 and A4) were used for flow measurements during each test. One copper tube (9.5 mm O.D.) was mounted flush with the inside of the shroud (A2), while another protruded 13.5 cm into the flow (A4).

A Dwyer Series 2 000 magnehelic differential pressure gauge was connected to the A2 and A4 calibrations points. The pressure differential (ΔP) across the high pressure port (A4) and the low pressure port (A2) was used to estimate the average momentum velocity (V_{mom}) from the equation:

$$V_{mom} = 1.06\sqrt{\Delta P} + 5.12 \tag{3.1}$$

where V_{mom} and ΔP have units of m/s and Pa respectively. The derivation of the above relationship will be further discussed in the following section. The magnehelic gauge accuracy is given as ± 2% full scale. Factory calibration of the gauge was checked against a Dwyer inclined manometer used for the pitot tube traverses.

Calibration

Pitot tube traverses using a 0.8-specific gravity inclined manometer across the flow were used to obtain impact and local stable pressure measurements, from which a velocity profile and the momentum velocity profile and the average momentum velocity could be calculated. Each profile consisted of eight sample points (1.5, 8.7, 13.7, 25.7, 48.7, 60.7, 65.7 and 72.9 cm). (The inside diameter of the shroud is 74.5 cm.) Concurrent measurements with the magnehelic differential pressure gauge, ambient pressure and ambient temperature were also recorded. Photo 3.3 shows part of the calibration procedure.

Figure 3.6 shows the average velocity profile measurement across the fan shroud. The decreased flow in the centre is due to the upstream obstruction caused by the fan motor. The velocity V_p at each point was calculated from

$$V_p = \sqrt{\frac{2\Delta P_p}{\rho}} \tag{3.2}$$

where ΔP_p is the difference between the impact and local static pressure (Pa) and ρ is the density of air (kg/m^3).

The average pressure difference:

$$\Delta P_{avg} = \frac{\sum_{p=1}^{8} \Delta P_p}{8} \tag{3.3}$$

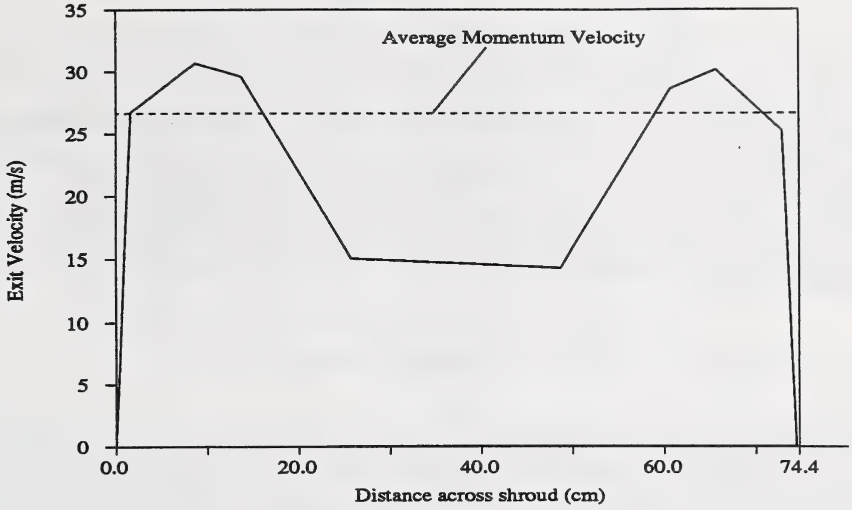

Figure 3.6

Observed Velocity Profile Across the Fan Shroud.

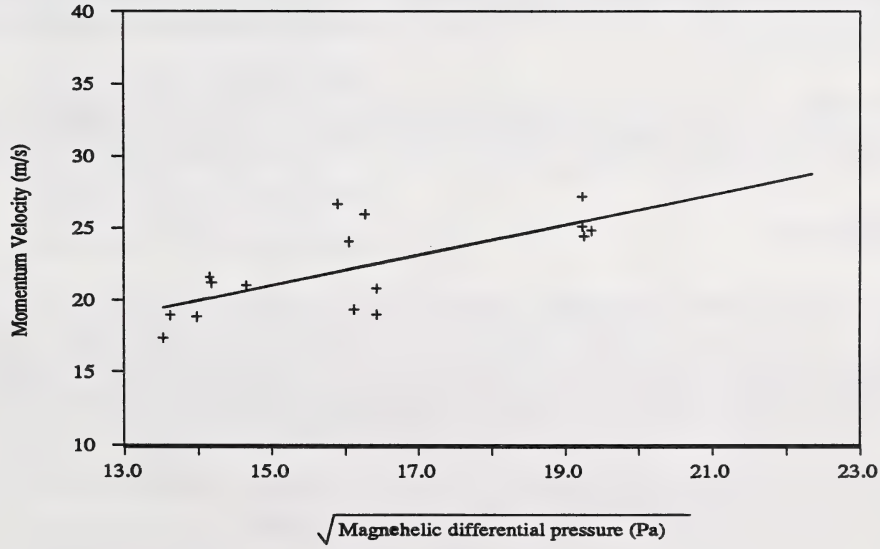

Figure 3.7

Exit Velocity Calibration Curve for the Elevated Release.

was calculated to determine the average momentum velocity for the relationship

$$V_{mom} = \sqrt{\frac{2\Delta P_{avg}}{\rho}} \tag{3.4}$$

The air flow volume and velocity were reduced by attaching screens to the fan intake. These allowed the average momentum velocity to be estimated as a function of varying concurrent magnehelic readings. Figure 3.7 shows the calibration curve derived for the fan. An inclined manometer filled with 0.8 specific gravity fluid was used for the calibration. The curve specifically gives the relationship between the calculated momentum velocity (m/s) and the square root of the differential pressure from the magnehelic gauge (Pa). The best fit line through the points is:

$$V_{mom} = 1.06\sqrt{\Delta P} + 5.12 \tag{3.5}$$

The linear correlation coefficient between predicted and observed values is 0.71. This equation was used in all the tests to estimate exit velocities from the elevated fan source. Further fan calibration information is contained in Appendix A1.

3.3.4 Meteorological Hardware

Meteorological measurements were obtained at the source during each test. A 10 cm O.D., 6.4 mm WT 6.1 m aluminum mast was installed in the bed of a half-ton pick-up truck as shown in Photo 3.4. A Qualimetrics Micro Response Model 2031 3-cup anemometer was mounted at the top of the mast (7.0 m above ground level) and a Campbell Scientific Model 107 temperature probe was mounted in a Gill naturally ventilated radiation shield 2.8 m above ground level.

The outputs from the Micro Response anemometer (VDC) and the 107 temperature probe were directed to the Campbell Scientific CR10 datalogger system. The data collection system was described in Section 3.3.1.

Calibration

The Micro Response anemometer, according to the manufacturer, has a threshold wind speed of 0.45 m/s, a distance constant of 1.5 m and an accuracy of ± 0.06 m/s. For tests 1 to 10, anemometer Serial #369 was used and had a measured output of 105 millivolts (mV) for 300 rpm (6.8 m/s). For tests 11 to 33, anemometer Serial #371 was used and had a measured output of 86 mV for 300 rpm (6.8 metres per second (m/s)).

The temperature sensor has an accuracy of ± 0.4 °C. Factory calibrations of the sensor and the CR10 datalogger algorithms for this sensor were accepted.

3.3.5 Field Set-Up Procedure

The SF_6 and the source flow measurement equipment were mounted on the back of a van which also pulled the trailer-mounted fan as shown in Photos 3.5 and 3.6. A half-ton pick-up truck was used to pull the generator trailer and served as a platform for the source meteorological instruments. The deployment procedures for each field test were as follows:

- Ensure generator fuel tank is filled
- Select a source location based on wind direction
- Transport fan and generator to source location
- Position source at source marker location and generator 30 m away from source
- Position van and truck 10 m away from source
- Power-up generator and connect voltage supply cables
- Connect flow meter, anemometer and temperature sensor cables to datalogger.

For the elevated release, the Tygon tubing carrying the SF_6 was connected to the fan inlet point. Two sections of Tygon tubing were used to connect the magnehelic differential pressure gauge to the high and low pressure points of the fan. For the ground release, the octagonal enclosure with the fan was set up. Tygon tubing carrying the SF_6 was connected to the injection manifold.

Following set-up, start-up and operating procedures for each test were as follows:

- Start generators and switch on fan
- Establish a specified SF_6 flow rate
- Adjust needle valve to obtain desired SF_6 flow rate
- Record start time and communicate to mobile analyser operators and tower personnel
- Every 15 minutes, manually record:

  Wind speed (datalogger display)
  Wind direction (tower)
  Flow meter reading
  Differential pressure
  Temperature (datalogger display)
  Totalizer reading
  Flow meter voltage (datalogger display).

Following each test, the shut-down procedures were as follows:

- Shut off SF_6 flow rate
- Record shut-off time and communicate to mobile analyser operators and tower personnel
- Decommission equipment and return to field offices
- Transfer datalogger data to IBM personal computer and store on 5 1/4-inch diskette
- File notes and diskette.

This procedure was employed for most of the field tests. For some of the tests which extended all night, manual readings were only taken at the beginning and the end of the test. Some of the tests also required the source location to be moved because of the changing wind direction.

3.4 Plume Rise for Elevated Source

The ground-level concentration of SF_6 from an elevated plume will be sensitive to the height of the plume above the ground. The Field Measurement Program, however, was not designed to produce detailed plume rise measurements for each field test. The approach selected to provide estimates of plume heights was based on standard plume rise model calculations based on source and meteorology data. The performance of this approach was to be confirmed using plume visualization techniques. The plume visualization tests were conducted separately from the tracer tests.

Plume visualization techniques involve the introduction of a particulate tracer into the plume to make it visible. The particulate tracer can consist of an oil fog resulting from the combustion of oil, soot particles resulting from the incomplete combustion of hydrocarbons or injection of small particles (e.g. Titanium dioxide) into the plume (Davies 1984).

3.4.1 Observed Plume Rise

For this study, a smoke pot designed for military use was used to produce a visible plume. The oxidation of hexachloroethane (C_2Cl_6) in the presence of zinc oxide (ZnO) and potassium nitrate (KNO_3) produces a visible zinc chloride ($ZnCl_2$) and calcium chloride ($CaCl_2$) smoke. Even though the smoke generators are not considered toxic in the general sense, prolonged exposure in a confined space is not recommended because of production of carbon monoxide and because $ZnCl_2$ can be irritating to the eyes, nose, throat and lungs. The smoke pots used for the study were manufactured by Hands Fireworks Inc. (Model SC39 Smoke Pot). An oil vaporizer was tested on both a ground and elevated release, as shown in Photos 3.7 and 3.8, but its output was erratic and this method was discarded.

The tracer tests were conducted during night-time hours to ensure stable atmospheric conditions. Plume visualization was not undertaken during the tests because of:

- Increased complexity to illuminate the plume at night
- Unknown impact of the smoke on the SF_6 analysers
- Increased exposure of field personnel to the smoke.

As a consequence, the plume rise tests were conducted just before sunset. The resulting smoke plumes were photographed and the slides were subsequently analysed to determine the trajectory of the plume. The analysis of the slides was in accordance with the Halitsky (1960) single camera method. Concurrent measurements of wind speed, wind direction and temperature profiles were obtained during each test. Details on the smoke pot reduction in jet momentum and plume trajectory determination are given in Appendices A2 and A3. Photos of the elevated release smoke plumes are shown in Photos 3.9 to 3.12 and photos of the ground release smoke plumes are shown in Photos 3.13 and 3.14.

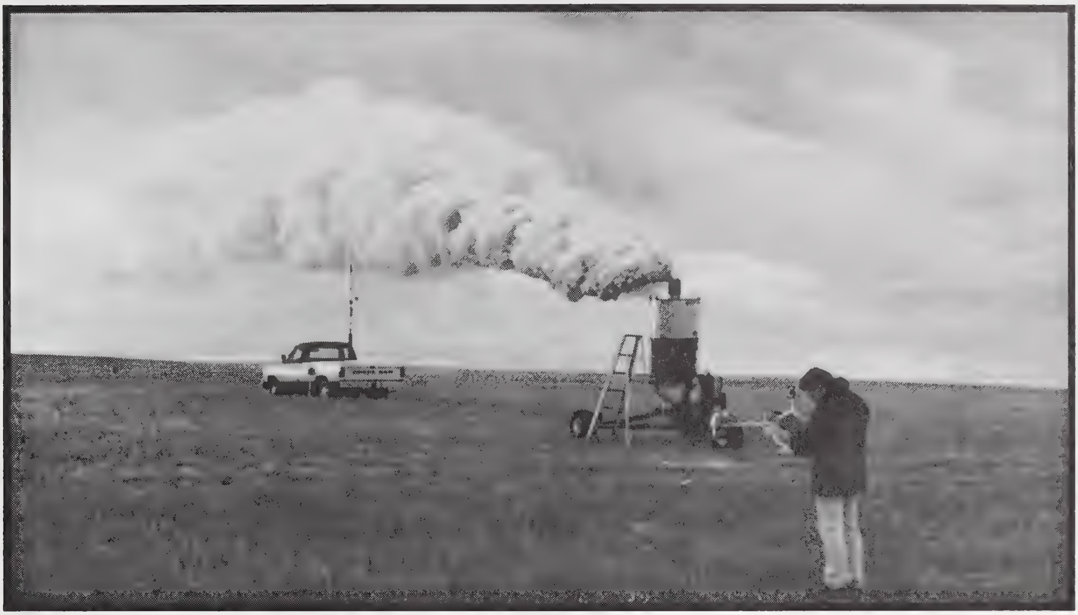

Photo 3.9

Smoke Plume Visualization With Elevated Release Fan Off.

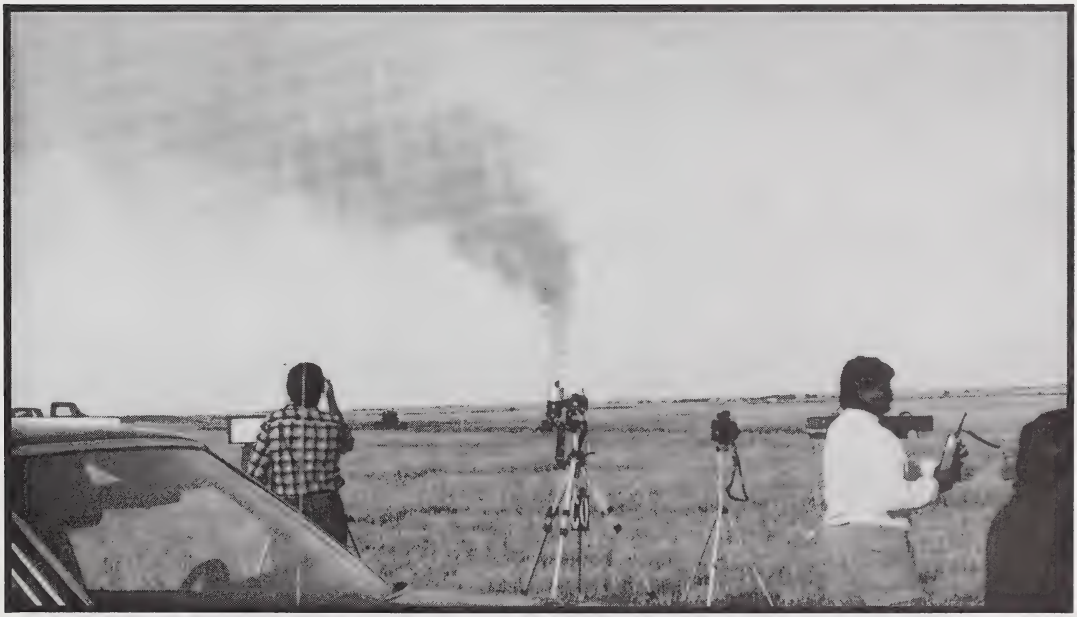

Photo 3.10

Smoke Plume Visualization With Elevated Release Fan On. Photographs and Video were Taken During the Smoke Tests.

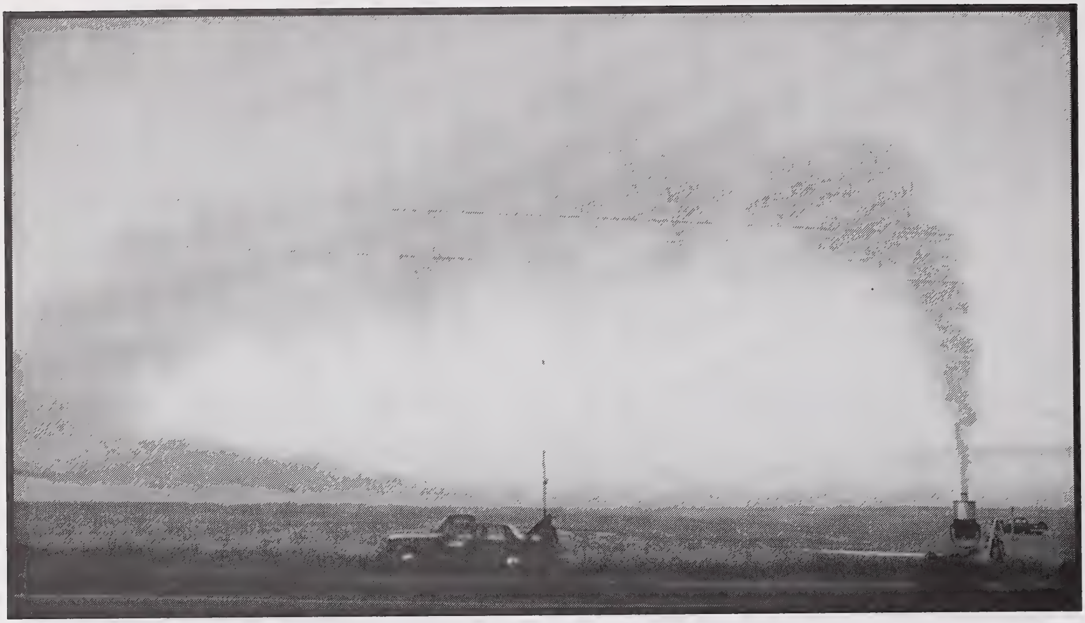

Photo 3.11

Smoke Plume Visualization With Elevated Release Fan On. Side View.

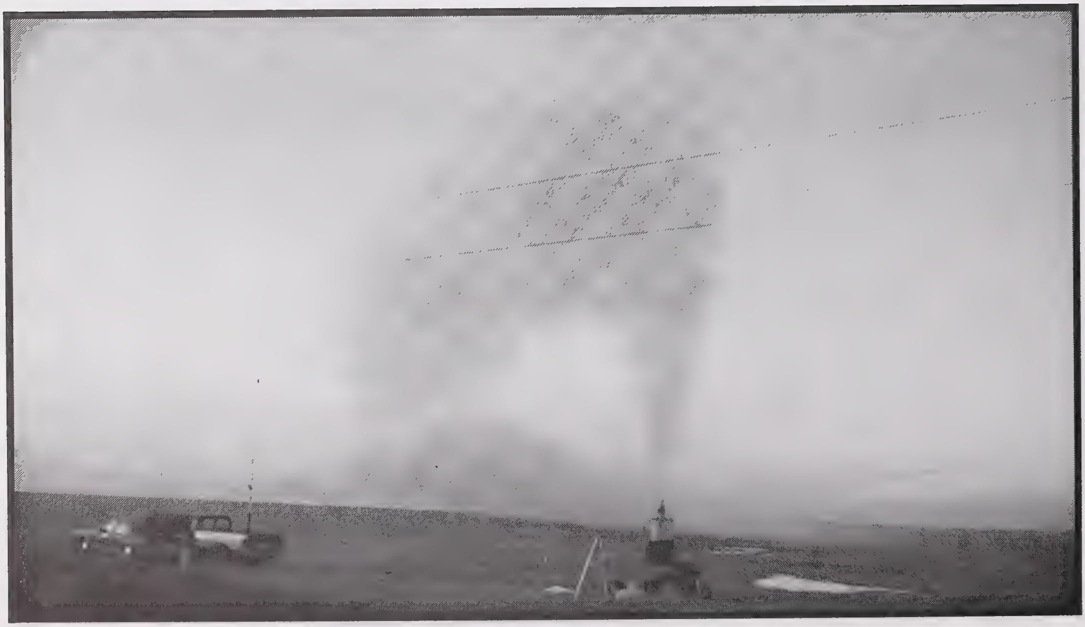

Photo 3.12

Smoke Plume Visualization With Elevated Release Fan On. Rear View.

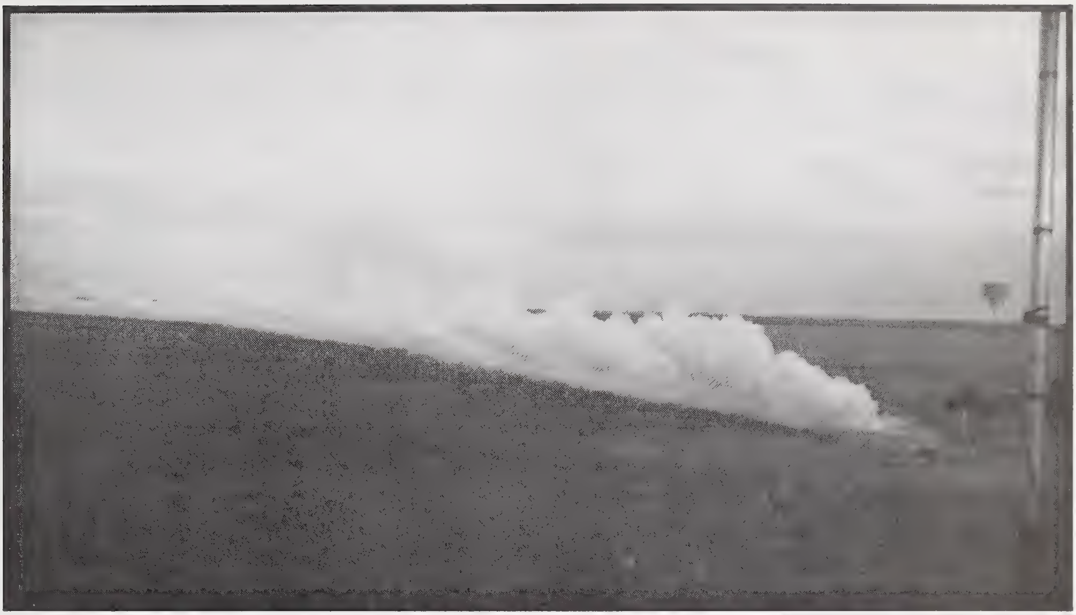

Photo 3.13

Smoke Plume Visualization With Ground Release Fan On. Side View. The Smaller House Fan was Used.

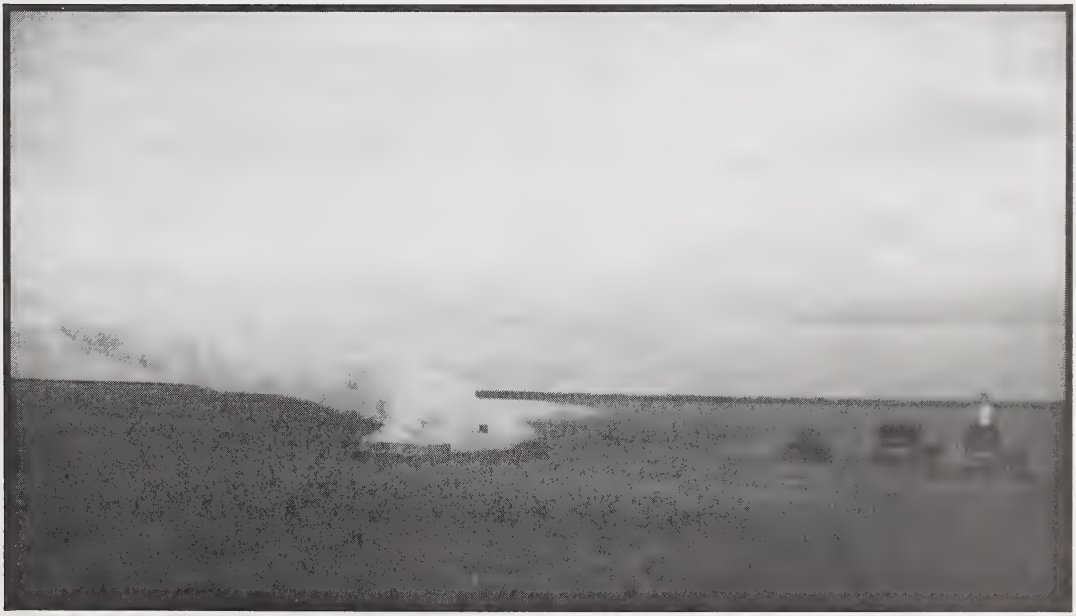

Photo 3.14

Smoke Plume Visualization With Ground Release Fan On. Rear View.

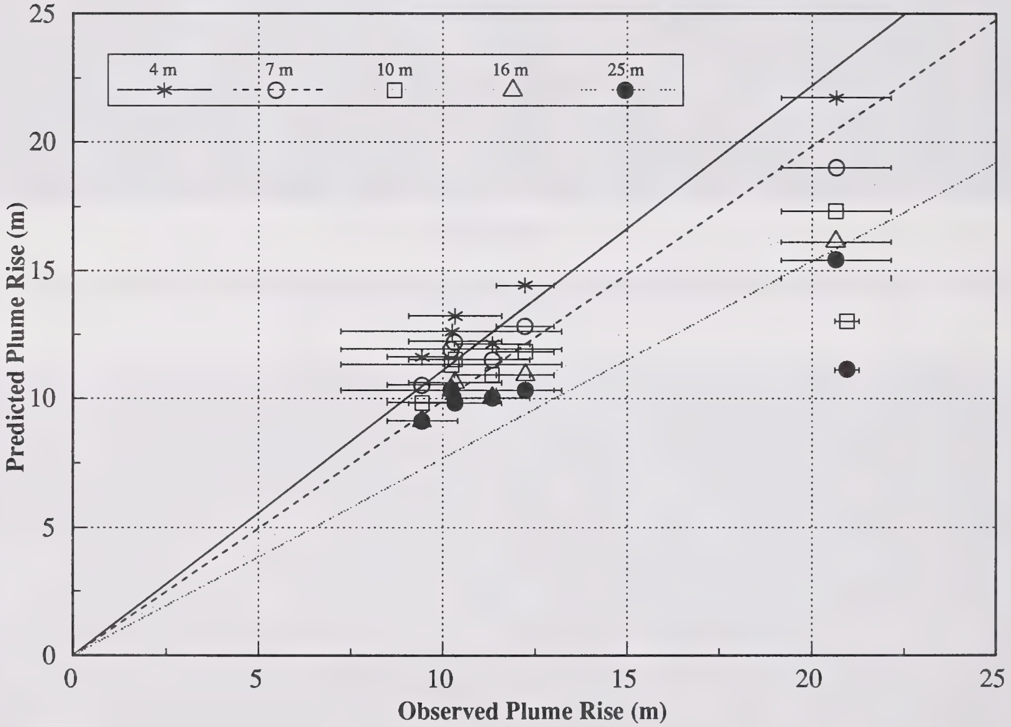

Figure 3.8

Comparison of Predicted and Observed Plume Rises for the Elevated Source Smoke Tests.

3.4.2 Predicted Plume Rise

The final plume rises were obtained from the analyses of the plume images on the slide. These values were then compared to selected plume rise formulas for momentum dominated plumes. For a vertical jet, the momentum flux (F_m) is given by:

$$F_m = \frac{\rho_s}{\rho_a}[V_s R_s]^2 \tag{3.6}$$

where:
ρ_s = density of the plume (kg/m^3)
ρ_a = density of the ambient air (kg/m^3)
V_s = exit velocity of the jet (m/s)
R_s = radius of the exit (m)

For this application $\rho_s = \rho_a$; $R_s = 0.3725$ m and V_s is available from the magnehelic differential pressure measurements and Equation 3.5.

For stable atmosphere, the plume height above ground level can be estimated from Briggs (1969, 1975):

$$H = h_s + 1.5\left(\frac{F_m}{US^{1/2}}\right)^{1/3} \tag{3.7}$$

where:
h_s = source height (2.3 m)
U = wind speed at source height (m/s)

The stability parameter S is given by:

$$S = \frac{g}{T}\left(\frac{\partial T}{\partial Z} + \Gamma\right) \tag{3.8}$$

where:
g = acceleration due to gravity (9.81 m/s^2)
T = ambient temperature (K)
$\frac{\partial T}{\partial Z}$ = temperature gradient (K/m)
Γ = adiabatic temperature gradient (0.0098 K/m)

The ambient temperature of the 2 m level and the temperature gradient over the 25 to 2 m layer from the tower were used to estimate the stability parameter S. Plume rises were estimated using wind speed data from the source anemometer (7 m) and from the four tower levels (4, 10, 16 and 25 m levels).

3.4.3 Comparison Between Observed and Predicted Plume Rise

Comparison between predicted and observed plume rise for each wind speed and test is shown in Figure 3.8. As expected, larger predicted plume rises result from the use of the smaller lower level wind speeds. The comparison shows the results for all smoke tests and wind speeds. The linear regression equation and correlation coefficient for each line fit are as follows:

Wind Speed Height (m)	N	Regression Equation	Correlation Coefficient
4	35	$P = 1.11 * O$	0.86
7	35	$P = 0.991 * O$	0.78
10	38	$P = 0.866 * O$	0.38
16	35	$P = 0.846 * O$	0.74
25	38	$P = 0.768 * O$	ND

ND = not defined ($R^2 < 0.0$)

Where P = the predicted plume rise (Equation 3.7) and O = observed plume rise extracted from the slides. The above correlations were forced to go through the origin ($P = 0$ and $O = 0$). The best correlation between predicted and observed plume rise was obtained using the wind speed observed at 4 m in Equation 3.7.

3.5 Data Reduction and Results

The 33 field tests were conducted over the period 18 October to 22 December 1988. The start and end times of each field test were defined by the SF_6 release times even though ambient concentration data could not be collected until the SF_6 plume reached the analyser and SF_6 concentration data were collected in some cases after the SF_6 release was shut down. The first test was conducted to determine field procedures and logistics rather than for the collection for data. As a consequence, tracer release and analyser data were only analysed for field tests 2 to 33.

As discussed in Section 2, fixed source locations (shown in Figure 3.9) were selected. For each test, the selected source was dependent on the wind direction with respect to the sampling arcs. On some nights, the source location was changed several times because of changes in wind direction.

Table 3.2 summarizes the dates, times, the source location and source type for each test. For field tests 2 to 20, the average duration for each field test was 4.9 hours (h). After test 20, an effort was made to focus on stationary monitoring with the source located at the centre and the average duration of field tests 21 to 33 was 15.0 hours. The tests were conducted during periods of darkness to increase the probability of stable atmospheric conditions.

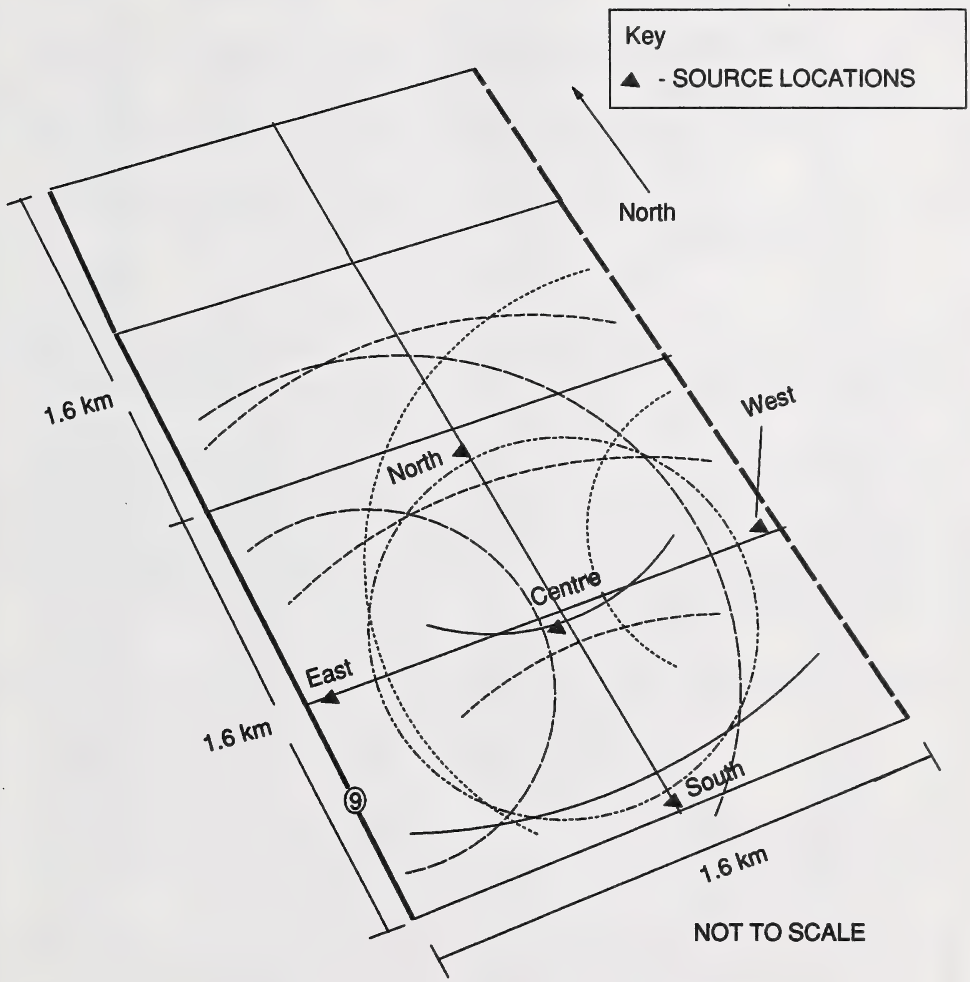

Figure 3.9

Location of the SF$_6$ Source Release Points.

Table 3.2

Summary of Field Measurement Program Source Data.

Field Test	Date	Time	Duration (h)	Source Location	Source Type
2	20 Oct 1988	20:11 to 22:12 22:50 to 00:41	1.0 1.9	South West	Elevated Elevated
3	24 Oct 1988	21:12 to 22.04 22:40 to 2:04 2:53 to 3:42 4:15 to 4:45	0.9 3.4 0.8 0.5	North West West East	Elevated Elevated Ground Ground
4	27 Oct 1988	18:51 to 21:10 21:28 to 23:18 23:18 to 1:12 2:02 to 3:17	2.3 1.8 1.9 1.3	West West West West	Elevated Ground Ground Elevated
5	28 Oct 1988	19:39 to 22:18	2.7	South	Elevated
6	31 Oct 1988	19:06 to 20:43 21:30 to 00:10	1.6 2.7	South West	Elevated Elevated
7	7 Nov 1988	18:54 to 20:52	2.0	West	Elevated
8	8 Nov 1988	18:28 to 20:52	2.4	West	Elevated
9	14 Nov 1988	17:22 to 21:25	4.0	South	Elevated
10	15 Nov 1988	17:04 to 18:10 18:10 to 21:45	1.1 3.4	South South	Elevated Elevated
11	16 Nov 1988	17:17 to 19:06 20:14 to 20:57 20:58 to 22:21 22:49 to 23:24 23:25 to 1:29	1.8 0.7 1.4 0.6 1.1	East West West West West	Ground Ground Ground Elevated Elevated
12	18 Nov 1988	17:45 to 1:57	8.2	South	Elevated
13	20 Nov 1988	17:33 to 00:43	7.2	Centre	Ground
14	24 Nov 1988	18:25 to 19:23	1.0	South	Elevated
15	26 Nov 1988	17:15 to 18:53 18:54 to 20:33 21:20 to 23:36	1.6 1.7 2.3	Centre Centre West	Ground Ground Elevated
16	2 Dec 1988	17:56 to 19:13 19:14 to 22:21 22:54 to 1:14	1.3 3.1 2.3	West West Centre	Elevated Elevated Elevated

Continued ...

Table 3.2 (Continued)

Summary of Field Measurement Program Source Data.

Field Test	Date	Time	Duration (h)	Source Location	Source Type
17	6 Dec 1988	17:36 to 20:34	3.0	North	Elevated
		20:57 to 23:33	2.6	West	Elevated
		00:06 to 1:33	1.5	North	Elevated
18	7 Dec 1988	17:26 to 18:36	1.2	East	Elevated
		19:01 to 20:56	1.9	Centre	Elevated
19	8 Dec 1988	17:50 to 18:25	1.6	South	Ground
		18:26 to 19:25	1.0	South	Ground
		20:11 to 21:13	1.0	West	Ground
		21:52 to 1:08	3.3	Centre	Ground
20	9 Dec 1988	17:10 to 23:23	6.2	Centre	Ground
21	10 Dec 1988	17:46 to 22:15	4.5	Centre	Ground
		23:31 to 8:30	9.0	Centre	Ground
22	11 Dec 1988	18:03 to 8:01	14.0	Centre	Ground
23	12 Dec 1988	16:49 to 8:22	15.6	Centre	Ground
24	13 Dec 1988	16:51 to 8:15	15.4	Centre	Ground
25	14 Dec 1988	17:17 to 17:39	0.4	Centre	Ground
		1:26 to 7:48	7.7	Centre	Ground
		17:40 to 1:25	6.4	Centre	Ground
26	15 Dec 1988	17:20 to 8:49	15.4	Centre	Ground
27	16 Dec 1988	17:32 to 8:04	14.6	Centre	Ground
28	17 Dec 1988	17:13 to 8:22	15.2	Centre	Ground
29	18 Dec 1988	16:53 to 8:40	15.8	Centre	Ground
30	19 Dec 1988	16:53 to 18:05	1.2	Centre	Ground
		18:06 to 18:51	0.8	Centre	Ground
		18:52 to 8:40	13.8	Centre	Ground
31	20 Dec 1988	17:50 to 8:40	14.9	Centre	Ground
32	21 Dec 1988	17:10 to 17:44	0.6	Centre	Ground
		17:45 to 1:47	8.0	Centre	Ground
		1:48 to 8:23	6.6	Centre	Ground
33	22 Dec 1988	16:39 to 18:00	1.3	Centre	Ground
		18:01 to 7:44	13.8	Centre	Ground

The total number of hours during which elevated and ground releases were conducted are as follows:

Test	Release Rate	Hours
2 to 20	Elevated Ground	60.8 32.5
21 to 33	Elevated Ground	0.0 195.0
Total 2 to 33	Elevated Ground	60.8 227.5

For tests 2 to 20, about 35% of the hours were associated with ground releases, while for tests 21 to 33, 100% of the hours were associated with ground releases.

3.5.1 SF_6 Release Rate

SF_6 release rates were available from the datalogger readings and from the manual observation of the flow meter. The datalogger data were not available for some tests and for some portions of other tests. For tests 3 to 9, the datalogger recorded 3-minute means and standard deviations; for tests 10 to 33, the datalogger recorded 1-minute means and standard deviations.

During the program, it was found that radio transmissions produced anomalous readings on the SF_6 flow meter. The radio transmissions did not affect the manual flow meter readings since the meter reading and a radio transmission did not occur simultaneously. Periods with radio transmissions were easily identified in the datalogger data by high standard deviations. These data were rejected and were not further analysed. The radio transmission interference, however, could not be factored out of the totalizer readings. As a consequence, the totalizer readings were not used in the data analysis.

Table 3.3 summarizes the flow meter and datalogger SF_6 release rates (the mean and standard deviations about the mean are shown in the table). The SF_6 release rates averaged 2.1 g/min with minimum and maximum values of 0.15 and 8.3 g/min, respectively. For tests 2 to 20, the manual flow meter readings were spread uniformly through the test period. For tests 21 to 33, the manual readings were limited to the beginning and the end of the field test. The standard deviations obtained from the flow meter readings are typically within 5% for the shorter tests (2 to 20) and within 10% for the longer tests (21 to 33). The agreement between the two sets of readings is generally within 10%.

Figures 3.10 and 3.11 show the SF_6 release rate for tests 10 and 26, respectively which provide a visual comparison of the two field program protocols. For the purposes of this field program, the SF_6 release rates were fairly uniform with time unless the flow rate was adjusted with the needle valve. Figures comparable to those shown are presented for each test in Appendix A4.

Table 3.3

Summary of SF_6 Release Rates for Each Test.

Field Test	Date	Time	Duration (h)	Datalogger Release Rate (g/min)	Flow meter Release Rate (g/min)
2	20 Oct 1988	20:11 to 22:12	1.0		2.94 ± 0.000
		22:50 to 00:41	1.9		2.94 ± 0.000
3	24 Oct 1988	21:12 to 22:04	0.9	4.23 ± 0.016	4.12 ± 0.002
		22:40 to 02:04	3.4		4.96 ± 0.000
		02:53 to 03:42	0.8	1.30 ± 0.032	1.26 ± 0.000
		04:15 to 04:45	0.5	2.60 ± 0.056	2.44 ± 0.000
4	27 Oct 1988	18:51 to 21:10	2.3	4.24 ± 0.012	4.15 ± 0.031
		21:28 to 23:18	1.8	1.64 ± 0.028	1.55 ± 0.050
		23:18 to 01:12	1.9	0.95 ± 0.035	0.84 ± 0.042
		02:02 to 03:17	1.3	N/A	4.96 ± 0.000
5	28 Oct 1988	19:39 to 22:18	2.7	2.52 ± 0.016	2.45 ± 0.011
6	31 Oct 1988	19:06 to 20:43	1.6	N/A	4.96 ± 0.000
		21:30 to 00:10	2.7	N/A	4.96 ± 0.000
7	7 Nov 1988	18:54 to 20:52	2.0	1.70 ± 0.015	1.61 ± 0.015
8	8 Nov 1988	18:28 to 20:52	2.4	4.26 ± 0.020	4.27 ± 0.218
9	14 Nov 1988	17:22 to 21:25	4.0	N/A	2.43 ± 0.004
10	15 Nov 1988	17:04 to 18:10	1.1	2.44 ± 0.046	2.47 ± 0.041
		18:10 to 21:45	3.4	4.08 ± 0.045	4.17 ± 0.050
11	16 Nov 1988	17:17 to 19:06	1.8	1.65 ± 0.062	1.61 ± 0.031
		20:14 to 20:57	0.7	2.35 ± 0.040	2.43 ± 0.008
		20:58 to 22:21	1.4	0.65 ± 0.015	0.65 ± 0.000
		22:49 to 23:24	0.6	2.32 ± 0.075	2.39 ± 0.042
		23:25 to 01:29	1.1	N/A	8.32 ± 0.001
12	18 Nov 1988	17:45 to 01:57	8.2	N/A	4.96 ± 0.027
13	20 Nov 1988	17:33 to 00:43	7.2	0.82 ± 0.015	0.82 ± 0.000
14	24 Nov 1988	18:25 to 19:23	1.0	4.63 ± 0.080	4.97 ± 0.018
15	26 Nov 1988	17:15 to 18:53	1.6	0.91 ± 0.024	0.82 ± 0.000
		18:54 to 20:33	1.7	0.55 ± 0.009	0.47 ± 0.000
		21:20 to 23:36	2.3	2.31 ± 0.098	2.44 ± 0.000

Continued ...

Table 3.3 (Continued)

Summary of SF_6 Release Rates for Each Test.

Field Test	Date	Time	Duration (h)	Datalogger Release Rate (g/min)	Flow meter Release Rate (g/min)
16	2 Dec 1988	17:56 to 19:13	1.3	3.08 ± 0.035	3.28 ± 0.000
		19:14 to 22:21	3.1	6.37 ± 0.067	6.62 ± 0.043
		22:54 to 01:14	2.3	6.43 ± 0.051	6.42 ± 0.000
17	6 Dec 1988	17:36 to 20:34	3.0	4.21 ± 0.023	4.12 ± 0.000
		20:57 to 23:33	2.6	5.02 ± 0.027	4.96 ± 0.000
		00:06 to 01:33	1.5	3.37 ± 0.028	3.28 ± 0.000
18	7 Dec 1988	17:26 to 18:36	1.2	5.01 ± 0.054	4.95 ± 0.016
		19:01 to 20:56	1.9	5.06 ± 0.020	4.96 ± 0.000
19	8 Dec 1988	17:50 to 18:25	1.6	N/A	0.82 ± 0.000
		18:26 to 19:25	1.0	3.38 ± 0.020	3.25 ± 0.043
		20:11 to 21:13	1.0	3.40 ± 0.060	3.28 ± 0.000
		21:52 to 01:08	3.3	0.74 ± 0.021	0.65 ± 0.000
20	9 Dec 1988	17:10 to 23:23	6.2	N/A	0.76 ± 0.000
21	10 Dec 1988	17:46 to 22:15	4.5	0.84 ± 0.037	0.82 ± 0.000
		23:31 to 08:30	9.0	0.92 ± 0.058	0.82 ± 0.000
22	11 Dec 1988	18:03 to 08:01	14.0	0.90 ± 0.038	0.82 ± 0.000
23	12 Dec 1988	16:49 to 08:22	15.6	0.87 ± 0.029	0.76 ± 0.000
24	13 Dec 1988	16:51 to 08:15	15.4	0.89 ± 0.061	0.95 ± 0.039
25	14 Dec 1988	17:17 to 17:39	0.4	0.84 ± 0.067	0.82 ± 0.000
		01:26 to 07:48	7.7	0.46 ± 0.026	0.38 ± 0.000
		17:40 to 01:25	6.4	N/A	N/A
26	15 Dec 1988	17:20 to 08:49	15.4	0.91 ± 0.023	0.85 ± 0.030
27	16 Dec 1988	17:32 to 08:04	14.6	0.92 ± 0.032	0.82 ± 0.000
28	17 Dec 1988	17:13 to 08:22	15.2	0.86 ± 0.013	0.82 ± 0.000
29	18 Dec 1988	16:53 to 08:40	15.8	0.96 ± 0.036	0.90 ± 0.087
30	19 Dec 1988	16:53 to 18:05	1.2	0.83 ± 0.035	0.82 ± 0.000
		18:06 to 18:51	0.8	0.43 ± 0.045	0.38 ± 0.000
		18:52 to 08:40	13.8	0.17 ± 0.013	0.12 ± 0.000
31	20 Dec 1988	17:50 to 08:40	14.9	0.48 ± 0.028	0.43 ± 0.044
32	21 Dec 1988	17:10 to 17:44	0.6	0.42 ± 0.021	0.38 ± 0.000
		17:45 to 01:47	8.0	0.92 ± 0.039	0.82 ± 0.000
		01:48 to 08:23	6.6	0.48 ± 0.014	0.47 ± 0.000
33	22 Dec 1988	16:39 to 18:00	1.3	0.84 ± 0.021	0.82 ± 0.000
		18:01 to 07:44	13.8	1.77 ± 0.070	1.65 ± 0.101

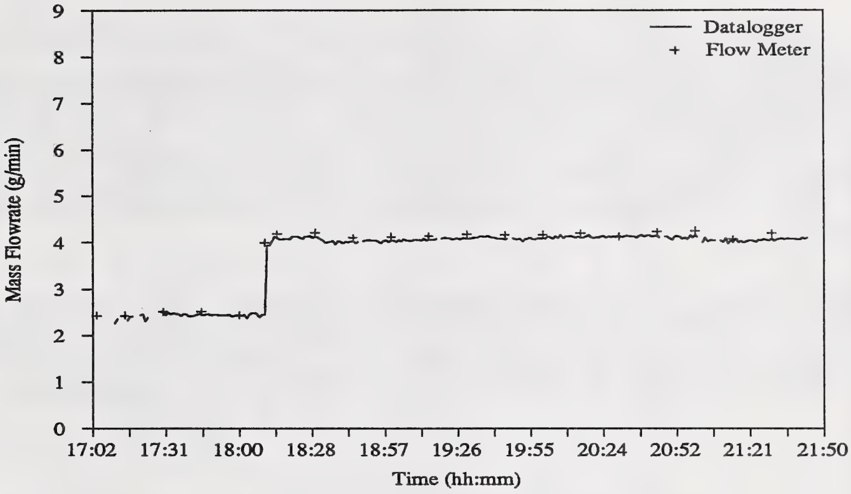

Figure 3.10

SF$_6$ Release Rate for Test 10.

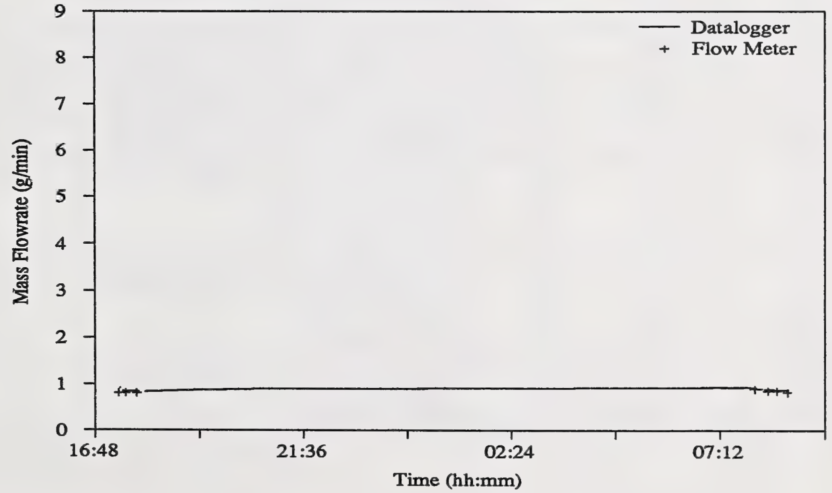

Figure 3.11

SF$_6$ Release Rate for Test 26.

3.5.2 Elevated Source Exit Velocity

The mean momentum exit velocity was calculated from the magnehelic differential pressure reading using the calibration Equation 3.5. The pressure reading was taken manually, typically once every 15 minutes. The resultant exit velocity therefore refers to a calibration temperature and pressure of 21.0 °C and 89.1 kPa, respectively. The ideal gas law can be used to compute the actual momentum velocity using actual temperature and pressure observations. The uncertainty in the magnehelic differential pressure gauge reading is ±20 Pa. This uncertainty results in an uncertainty of ±0.5 m/s in the mean momentum exit velocity.

Table 3.4 summarizes the mean momentum velocity during each test for the elevated releases. The mean velocity observed for the tests was 26.7 m/s, with minimum and maximum values of 26.2 at 28.3 m/s, respectively. The standard deviation values given in the table are typically in the same range as the uncertainty in the meter reading.

Table 3.4

Summary of Mean Momentum Velocity[(a)] From the Elevated Source.

Field Test	Date	Time	Duration (h)	Mean Momentum Velocity (m/s)
2	20 Oct 1988	20:11 to 22:12 22:50 to 00:41	1.0 1.9	26.3 ± 0.40 27.1 ± 0.29
3	24 Oct 1988	21:12 to 22:04 22:40 to 2:04	0.9 3.4	26.8 ± 0.32 26.2 ± 0.19
4	27 Oct 1988	18:51 to 21:10 2:02 to 3:17	2.3 1.3	26.4 ± 0.67 28.3 ± 0.00
5	28 Oct 1988	19:39 to 22:18	2.7	26.6 ± 0.22
6	31 Oct 1988	19:06 to 20:43 21:30 to 00:10	1.6 2.7	26.4 ± 0.11 26.6 ± 0.21
7	7 Nov 1988	18:54 to 20:52	2.0	26.5 ± 0.18
8	8 Nov 1988	18:28 to 20:52	2.4	26.5 ± 0.13
9	14 Nov 1988	17:22 to 21:25	4.0	26.3 ± 0.13
10	15 Nov 1988	17:04 to 18:10 18:10 to 21:45	1.1 3.4	26.5 ± 0.49 26.5 ± 0.49
11	16 Nov 1988	22:49 to 23:24 23:25 to 1:29	0.6 1.1	26.4 ± 0.33 26.4 ± 0.33
12	18 Nov 1988	17:45 to 1:57	8.2	26.8 ± 0.38
14	24 Nov 1988	18:25 to 19:23	1.0	26.3 ± 0.21
15	26 Nov 1988	21:20 to 23:36	2.3	27.5 ± 0.66
16	2 Dec 1988	17:56 to 19:13 19:14 to 22:21 22:54 to 1:14	1.3 3.1 2.3	26.6 ± 0.69 26.6 ± 0.69 27.0 ± 0.24
17	6 Dec 1988	17:36 to 20:34 20:57 to 23:33 00:06 to 1:33	3.0 2.6 1.5	26.8 ± 0.40 26.8 ± 0.65 26.6 ± 0.26
18	7 Dec 1988	17:26 to 18:36 19:01 to 20:56	1.2 1.9	27.1 ± 0.58 27.6 ± 0.08

[(a)] Normalized to 21.0 °C and 89.1 kPa

3.6

4 TRACER GAS SAMPLING

4.1 Introduction

Various sampling methods for measuring sulphur hexafluoride (SF_6) concentrations in the atmosphere have been developed for tracer studies. These include both instantaneous and time averaged sampling techniques. For atmospheric dispersion studies, these samplers are usually deployed uniformly along an arc located downwind of the tracer source. Samples can be collected from either mobile or stationary platforms.

Typically, the air samples are analysed in the field or a nearby laboratory using a small portable gas chromatograph. A molecular sieve column allows the SF_6 to pass through the column faster than oxygen (O_2). An electron capture detector (ECD) at the end of the column experiences a decrease in standing current that is proportional to the SF_6 concentration. Since ECD's also respond to oxygen, the SF_6 and the oxygen must be separated.

The discreet sample approach was not viewed as suitable for this study since the area of interest was short-term averaged concentration profiles for plumes which were expected to be 10 to 30 m in crosswind extent. The use of the individual sample technique would have required the deployment of "hundreds" of samplers at a typical spacing of 2 to 3 m to resolve the plume. Due to the expense and field logistics of maintaining such a network, a continuous SF_6 analyser was selected instead.

The continuous SF_6 analyser used in this work was developed at Washington State University (Brenner and Lamb 1985). This design has been successfully used in both mobile ground and airborne platforms. Three identical mobile SF_6 analyser systems were set up for the Field Measurement Program. The following sections describe the hardware setup and the data reduction procedures.

4.2 Hardware and System Design

4.2.1 Analyser System

A continuous SF_6 analyser (Scientech Inc., Pullman, Washington, USA) was mounted in the back seat of each of three, 3/4 ton crew-cab trucks for collection of concentration data (Figure 4.1 and Photos 4.1 to 4.5). These instruments were designed to provide continuous, real time data. The plumbing and electrical configurations for the analysers are shown in Figures 4.1 and 4.2, respectively.

To measure real time concentrations of SF_6, the ambient sample stream is drawn through the analyser's electron capture detector (ECD) continuously. To prevent the ECD from being saturated by ambient oxygen, the oxygen is removed from the sample stream by reaction with hydrogen over a palladium catalyst. The resulting exothermic reaction maintains the reactor temperature at approximately 200°C. At this temperature, other ambient fluorocarbons are destroyed before they reach the detector. The water vapor formed by the reaction is removed by a Nafion drier. The sample then flows through the electron capture detector, where the SF_6 causes a decrease in the detector standing current. This in turn is translated into an increase in the voltage output signal. Pressure pulsations, sample mixing, and dead volume have been minimized by locating the pump downstream of the reactor, drier and detector. The analyser typically has an SF_6 detection limit of less than 10 parts per trillion (ppt) (10 in 10^{12} parts) and a response time of 0.4 seconds.

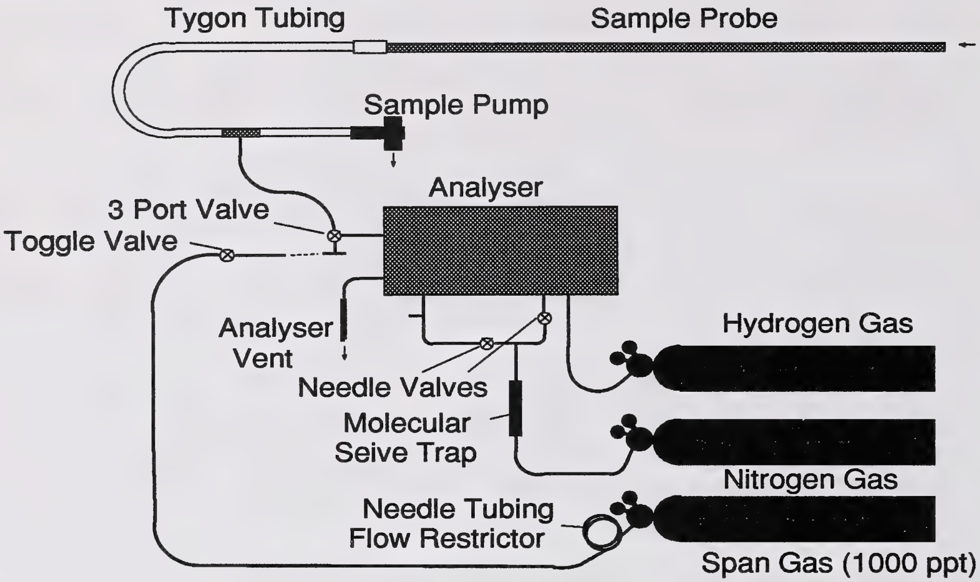

Figure 4.1

Analyser Plumbing Schematic.

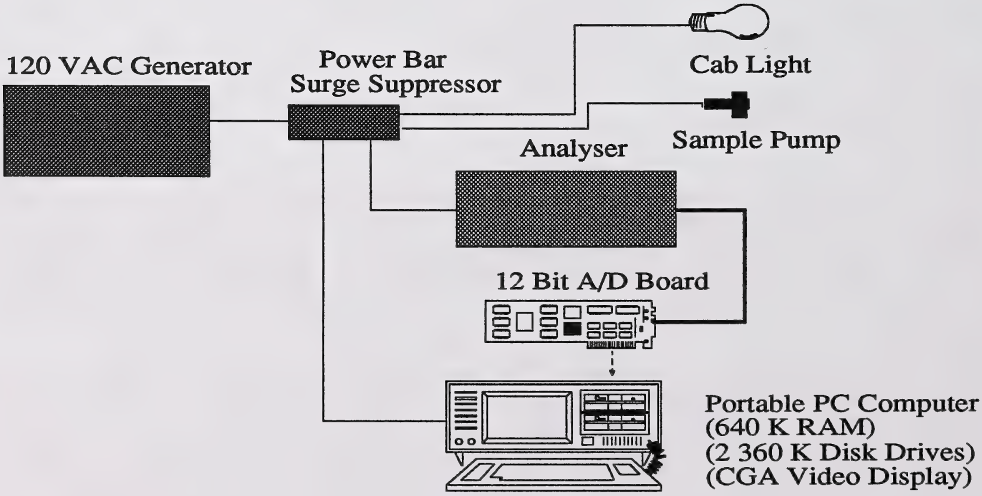

Figure 4.2

Analyser Electrical Schematic.

Photo 4.1

The Pick-up Box of One of the Tracer Trucks Containing Gas Cylinders and Generator.

Photo 4.2

The Three Identical Continuous Tracer Monitoring Trucks.

Photo 4.3

Full Range Calibrations Before and After the Tests Were Required.

Photo 4.4

Side View of Probe and Tubing Leading Into Analyser.

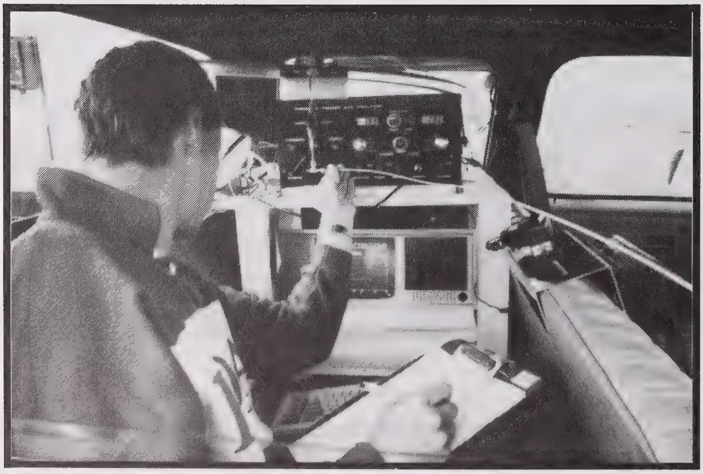

Photo 4.5

Inside View of Analyser and Portable Computer.

4.2.2 Inlet Manifold System

Outside air was drawn into the analyser through an inlet manifold system. The sample probe was 25.4 mm PVC pipe secured along the centreline of the truck. The inlet to the manifold was positioned 2 m ahead of the truck to minimize the effects of turbulence from the moving truck on the sampling. From above the cab, the air sample was drawn into the cab through 25.4 mm ID Tygon tubing which ran in through the back window. A small squirrel cage fan at the end of the manifold was used to draw air through the PVC sample probe.

The air sample was drawn into the analyser through 3.2 mm stainless steel tubing which ran from a tee in the Tygon tubing, located approximately 1 m ahead of the squirrel cage fan, to a three port valve at the inlet to the analyser.

To measure the total delay and response times of the combined analyser and manifold system, plug concentrations of tracer were introduced into the manifold inlet. A second channel of the data acquisition system was used to record a voltage signal at the same instant the tracer entered the probe. The data system was run at 10 Hz during these tests. Delay time (the time lag between the introduction of the tracer and the first response of the system) averaged approximately 6 seconds. Response time (the time required for the signal to reach 63% of the maximum response once the system has detected the tracer) averaged 1.1 seconds.

4.2.3 Supply Gas System

Nitrogen and hydrogen cylinders required by the analyser were mounted in the box of the truck. The gases were connected to the back panel of the analyser using 3.2 mm stainless steel tubing. Needle valves were installed in these lines to control flow rates. (Refer to Figure 4.1). The analyser required the following gas flow rates:

- Reactor Hydrogen: 20 to 30 cm^3/min
- Dryer Nitrogen: 200 to 250 cm^3/min
- Detector Nitrogen: 50 to 60 cm^3/min

A molecular sieve trap was installed in the line running from the nitrogen tank to the tee at the back panel of the analyser. A span gas cylinder with a nominal concentration of 1 000 ppt SF_6 was also mounted in the box of the truck to allow for span calibrations during the test. A 0.318 cm stainless steel line with a flow restrictor and toggle was used to deliver span gas to the analyser inlet.

4.2.4 Data Acquisition System

The output part of the analyser was connected to an MS-DOS personal computer with a 12 bit analog/digital board using a BNC cable. The computer was mounted in the back seat of the truck in a box lined with foam to reduce vibrations from the moving truck. All data were collected at 1 Hz using the computer program **D**ata **A**cquisition and **R**eduction Program for **T**racer (DART, Indaco Air Quality, Pullman, WA). Data were stored on 360 kB 5 1/4-inch floppy diskettes.

4.2.5 Power Generation System

A gasoline generator was mounted in the box of the truck to provide power for the analyser, computer, squirrel cage fan and additional cab lighting. A power bar surge suppressor was installed to reduce power surges that might damage equipment.

4.3 Analyser Performance and Operation

System response time was a critical parameter for this study. Tracer tests were conducted for relatively short downwind distances during a stable, calm atmospheric conditions. These conditions can result in rather narrow plumes with strong cross-wind concentration gradients. The real time, rapid response (approximately 1.1 seconds) of the system enables more precise determinations of the resultant plume boundaries and concentration gradients. The low detection limit of the analyser (less than 10 ppt) allows for easy detection downwind without having to release a large amount of the tracer gas.

For the most part, the SF_6 analysers performed well in the field. The most serious of the problems encountered during the study was a voltage response overshoot for the first few tests conducted. For the higher concentrations of SF_6 observed, overshoot on these tests ranged from 20% to 100%. This problem was remedied by thoroughly cleaning the electron capture detector (ECD) with methanol. For the following tests, overshoot generally did not exceed 10% of the steady state values and for the most part was not present at all.

Another problem encountered during data collection was associated with operators not recognizing oxygen breakthrough in the analyser. On several occasions this was a gradual process. Data collected when O_2 breakthrough was present to the time it was discovered had to be discarded.

Typically the analysers required one hour from start-up to stabilize or warm-up. During this one hour period, baseline drift was evident, especially towards the later tests at the end of the field study. A key to collecting accurate data was allowing the analysers sufficient time to warm up.

4.3.1 Calibration

The response of electron capture detectors in continuous analysers may change over time due to a variety of factors, including changes in temperature and pressure. To maintain measurement accuracy, the analysers were given a full-range calibration before and after each field test, with span gas checks performed at regular intervals during the tests. Seven SF_6 standards from Scott-Marrin, Inc. (+-5%, N.B.S. traceable), with nominal values ranging from 0 to 5 000 ppt, were injected via a tee at the analyser inlet from the manifold. This injection system provided both convenience and conservation of standard gases, since the flow at this point in the system is only a small fraction of the sampling manifold flow. Each standard was repeated three times for a minimum duration of 15 seconds.

The equivalence of injections at the calibration inlet versus tracer concentrations at the manifold inlet was verified by mounting a PVC tee on the manifold inlet and flowing sufficient standard past the inlet to prevent any dilution from ambient air. This response was found to be the same as the response of the same standard injected at the calibration inlet.

4.4 Monitoring Procedures

4.4.1 Sampling Arcs

The sampling arcs were surveyed on the 1 600 m x 2 400 m test site. These arcs were segregated into five groups corresponding to their appropriate source locations (i.e. south, north, east, west or centre). The sampling arc associated with the centre source location was a full 700 m radius circle. The sampling arcs associated with the other source locations were partial 700 m and 1 400 m radius arcs. A 2 100 m radius arc was associated with the south source (Figure 2.3). The angle covered by each arc can be found in Table 4.1.

Points along the arcs were marked with survey stakes. These stakes were 20 m apart for 700 m arcs and the circle, 30 m apart for 1 400 m arcs and 40 m apart for the 2 100 m arcs. A sign with a letter-number combination was placed on each stake (e.g. A1, A2, ... A0, B1, etc.). The 700 m arcs started with A1, the 1 400 m arcs with K1 or K2 and the 2 100 m arc with V1. The source locations were marked with three survey stakes in a triangle surrounding the surveyed source location.

Additional measurements were taken during the surveying to allow for the future calculation of single point elevations and arc elevation profiles but only certain single point elevations were actually calculated. The centre circle was added because large variations in wind directions at low wind speeds were encountered.

Table 4.1

Angle Coverage for Each Arc.

Source Location	Arc (m)	Angle (Degrees)
North	700 1 400	91.7 65.0
South	700 1 400 2 100	91.7 66.3 43.7
East	700 1 400	135.8 119.0
West	700 1 400	173.5 138.7
Centre	700	360.0

4.4.2 Mobile Analyser Operations

The purpose of the mobile sampling operations was to collect cross-wind profiles of SF_6 concentration at several distances downwind of the source. These profiles were collected repeatedly along each sampling arc during the test. It was expected that five to ten traverses would be collected each hour. Ideally, each sampling pass would begin outside the plume in clean air and end on the opposite side of the plume in clean air. The sampling passes were to be long enough to encompass the plume, but not extend to the entire distance of the arc.

During the traverse, the sampling locations were keyed into the personal computer system as the inlet of the sampling boom passed each location sign. The trucks were driven at a steady, slow rate during the traverse (approximately 5 km/hr). Observed plume centrelines were communicated between sampling trucks to facilitate plume tracking. After passing through the plume, the trucks would continue out of the plume for at least two to three sampling points. Any incorrect data system entries were noted on the sampling data sheets. Plume traverses were stored on floppy disk immediately after each pass.

Span checks were performed periodically throughout the test. While outside the plume, a nominal 1000 ppt standard was injected into the calibration inlet. As during the calibration, the injection was repeated three times to obtain a measure of the system precision.

4.4.3 Stationary Analyser Operations

The goal of the fixed analyser operations was to obtain continuous records of instantaneous concentration at a fixed point for uninterrupted periods of either 30 or 60 minutes.

During tests 1 to 20, one analyser would be moved to a location within the mean plume and operated for at least 33 minutes (to obtain a 30-minute block which overlaps ten 3-minute meteorological data blocks). The selection of a specific location was decided by the operator after consultation with the other mobile units, the source personnel and meteorological tower personnel as to the trend in plume and wind motions.

After the analyser was moved to a location, data were collected for 33 uninterrupted minutes on a single data file. If the plume impacted the fixed analyser for more than approximately 10% of the time during the 33 minutes and the trend in plume transport remained the same, the operation would be extended without stopping the data file for a second 30-minute period. After 63 minutes of operation, the file was normally stopped and a new file started or the analyser was moved to a new location depending upon the results of the last 30-minute period and current wind conditions.

For tests 21 to 33, the sampling trucks collected stationary data from approximately 16:00 to 08:00 the next morning. This approach was adopted during December to increase the amount of stationary tracer data collected. The data was collected whether or not the meteorological conditions met the low wind speed, stable conditions specified in the original scope of the work. Instead of 33 minute files, the files collected during this portion of the program were usually 3 to 4 hours in length. The three trucks would be set up approximately 60 to 100 m along the centre circle arc, with the plan being to bracket the meander of the plume between the outer trucks. As the wind shifted, one or more trucks would be moved to track the plume.

Span checks were performed periodically following the same procedures as outlined for the mobile systems. The span checks were stored on a separate file after a 33 or 63-minute data period was complete. However, if the analyser was located in the plume, data collection was resumed without performing a span. Span checks were performed only when the data record indicated no SF_6 was present.

4.5 Data Reduction

4.5.1 Data Handling and Back-Up

Two copies of each data disk were made immediately following each test. The original and one copy were returned to the ERCB. The original was stored as an archive copy, while the first copy was used for data reduction. The third copy was made later and stored at the field office for working purposes. Once the field portion of the program was over, the third set of data was stored at Concord Scientific's office in Calgary.

All of the data collected with the analyser data system were stored in a binary format as time in seconds, instrument response in computer A/D units, and location codes as entered. Each data file was accompanied by a separate comment file which contained file start time, any comments entered following data collection, and data on baseline segments.

4.5.2 Baseline Calculations

The first step in data reduction involved determining an instrument baseline. Baseline drift, which could be positive or negative, was accounted for by selecting segments of the continuous analyser record when the analyser was not in the plume. A linear best fit was calculated as the baseline for that segment. The baseline for regions between two baseline segments was a straight line between the endpoints (determined by the linear fit) of the two bordering segments. The first and last baseline segments were extrapolated through the regions before the first segment and after the last segment. Baseline noise was calculated as three times the standard deviation of the baseline voltage in a given segment. All voltages less than the sum of the baseline and the noise level were assigned a value of zero.

Baselines for traverses were calculated at the beginning and end of each traverse file. For stationary monitoring, baselines were calculated before and after any periods during which a major plume impact was observed and every 10 to 15 minutes during periods when the analyser was not in the plume.

4.5.3 Concentration Calculations

A power law relationship ($Concentration = C_a \cdot volt^{C_b}$) typical for electron capture detectors, was used to convert analyser voltage output to SF_6 concentrations. In most cases, this was accomplished for each test by determining coefficients C_a and C_b from a linear least-squares best fit of the logarithm of the voltage responses to the logarithm of the known concentrations of the standards. When the power law relationship for the upper concentration ranges (e.g. > 1 000 ppt) differed significantly from the relationship observed for the lower ranges, two sets of power law calibration coefficients were calculated and the voltage intercept determined. When the response of the analyser varied significantly with time, calibration coefficients were determined by interpolating between the pre-test and post-test calibration curves. If the power law relationship varied both with time and concentration, then a combined time-interpolation/two-range calibration curve was employed.

Although the analysers were only calibrated over the range of 0 to 5 000 ppt, concentrations as high as 10 000 ppt were occasionally observed during some field tests. Calibrations of one analyser over the range of 0 to 10 000 ppt subsequent to the field program indicated that the errors from extrapolating the lower range calibration are typically less than 15%.

4.5.4 Distance Calculation

The sampling grid consisted of a series of arcs and one circle, with surveyed markers at intervals of 20, 30 or 40 m. Each marker had a location code which was keyed in by the tracer analyser operator during data acquisition. After correcting for the sampling system delay time, the time, location code and arc distance were determined for each traverse file. The arc distance is the distance along the arc from point A1. For example, on an arc with a 20 m marker interval, C1 would be at an arc distance of 21•20 = 420 m from a specified origin. A linear interpolation was used to calculate arc distances in between markers. Given the location of each source, the distance of each arc from the source and the location of A1 on the arc, 2-dimensional coordinates (north and east from the section corner) were calculated for each sample in the traverse file. The transport direction was determined by the angle from due north of the source to the location of the centroid. This angle should correspond to mean wind direction.

4.6 DART Program

DART (**D**ata **A**cquisition **R**eduction Program for **T**racers, Indaco Air Quality Air Services, Inc., Pullman, WA) is a program developed to convert the voltage versus time data collected by the analyser systems into concentration versus distance using appropriate calibration data. Additionally, the program calculated a variety of plume concentration statistics for both traverse and stationary data.

For the traverse data, the peak SF_6 concentration, the shape of the cross-wind concentration distribution and a measure of the plume width were determined. In particular, the observed crosswind concentration distributions were compared to Gaussian distributions and the standard deviation of the cross-wind concentration was used as a measure of the plume width.

For the stationary data, factors such as maximum and mean concentrations, peak to mean ratios, plume intermittencies, concentration fluctuation intensities and concentration distributions were determined. These factors were calculated for each stationary one-half monitoring period.

4.6.1 Parameters Calculated from Traverse Data

Three methods were used to fit the cross-wind concentration data to a Gaussian distribution. There are the:

- "Moment" Method which is based on the second moment to determine plume statistics.

- "Hanna" Method which assumes the plume standard deviation can be determined from the 16 and 84 percentiles of the cross-wind integrated concentration.

- "Concentration Maximum" Method which forces a Gaussian distribution through the peak concentration observed during the traverse.

For some of the traverses, the beginning and the end points of the SF_6 cross-wind concentration profiles were clearly defined. In other cases, the beginning and end points were poorly defined due to what appeared to be concentration peaks occuring before and after the main portion of the plume. The concentration statistics for these profiles can be somewhat dependent on the width of the time window in terms of whether the window includes these peaks.

For the above reasons, two time windows were selected to calculate plume concentration statistics: one was selected for the Moment Method and another was selected for the Hanna and Concentration Maximum Methods. The Moment Method window was limited to exclude outlying points on the traverse. This is because the results calculated from this method can be strongly influenced by outliers. The identification of outlier points and the subsequent window required some subjective operator input. Generally, the following criteria were used as a guideline to exclude outlying points:

- If an abnormally long tail was associated with the main plume, then the edge of the window was taken as the point where the concentration descended to 10 to 15% of the peak concentration for that traverse.

- If a secondary peak was less than 20 to 25% of the peak concentration for that traverse, then the secondary peak was excluded from the window.

The window for the other methods included all the outlier parts and as a consequence was wider than that used for the Moment Method.

The DART program was used to generate one and two dimensional plots (see Figures 4.3 and 4.4) for traverse data. The one-dimensional plot shows concentration (ppt) versus distance (m) for both the actual data and a Gaussian approximation. The two-dimensional plot shows the plume (defined as any concentration greater than 10% of the maximum) in an easting and northing grid location.

Plume dimensions and transport direction were calculated from records of concentration and location. Location was determined by linear interpolation between known points which had been stored along with time-of-day and voltage output during data acquisition. The following statistics were computed for traverses using the Moment, Hanna and Concentration maximum methods:

- σ_{y_i} Instantaneous cross-wind spread (m)
- Maximum Concentration (ppt)
- Plume Centre on Arc (m)
- Mean Absolute Residual (% and ppt)

For the Second Moment Method:

$$\sigma_{y_i} = \left\{ \frac{\sum_{j=1}^{N} C_j (y_j - \bar{y})^2}{\sum_{j=1}^{N} C_j} \right\}^{1/2} \tag{4.4}$$

$$C_m = \frac{\int C\,dy}{\sqrt{2\pi}\,\sigma_y} \tag{4.5}$$

$$\bar{y} = \frac{\sum_{j=1}^{N} y_j C_j}{\sum_{j=1}^{N} C_j} \tag{4.6}$$

For the Hanna 2σ_y Method:

$$\sigma_{y_i} = \frac{1}{2}[y_{84} - y_{16}] \tag{4.7}$$

$$C_m = \frac{\int C\,dy}{\sqrt{2\pi}\,\sigma_y} \tag{4.8}$$

$$\bar{y} = y_{50} \tag{4.9}$$

where: y_{16} = 16th percentile of $\int C\,dy$
y_{50} = 50th percentile of $\int C\,dy$
y_{84} = 84th percentile of $\int C\,dy$

For the Concentration Maximum Method:

$$\sigma_{y_i} = \frac{\int C\,dy}{\sqrt{2\pi}\,C_m} \tag{4.10}$$

$$C_m = \max(C_j, C_{j+1}) \qquad j = 1 \quad \text{to} \quad N$$

$$\bar{y} = y_m = (y \quad \text{at} \quad C = C_m)$$

Mean residuals between predicted and observed concentrations were calculated as follows:

$$\text{Mean Residual (percent)} = \frac{\sum_{j=1}^{N} \left| \frac{C_{oj} - C_{pj}}{C_{oj}} \right|}{N} \cdot 100 \tag{4.11}$$

$$\text{Mean Residual (absolute)} = \sum_{j=1}^{N} \left| \frac{C_{oj} - C_{pj}}{C_{oj}} \right| \tag{4.12}$$

where: C_o = observed concentration
C_p = predicted concentration with the estimated σ_{y_i}, $\bar{y}$ and C_m

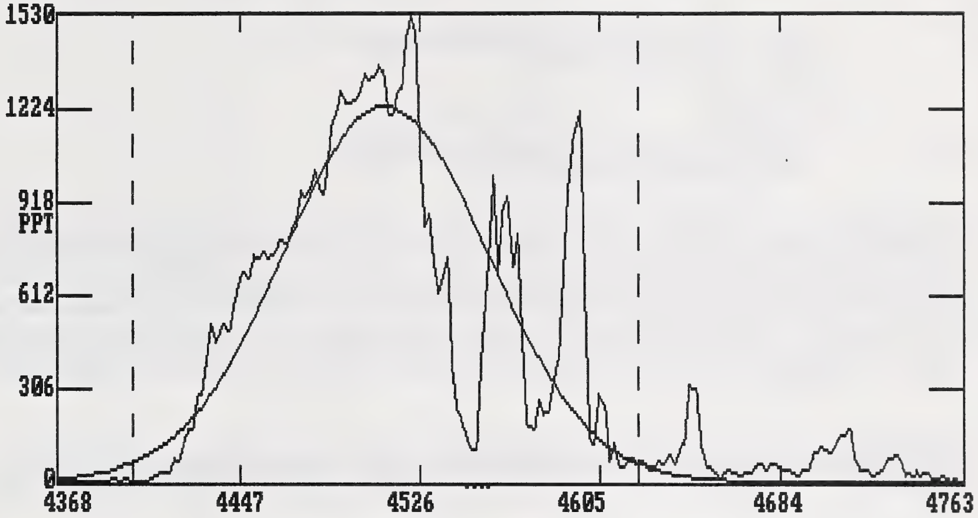

Figure 4.3

1-Dimensional Plot from DART - T13B25.

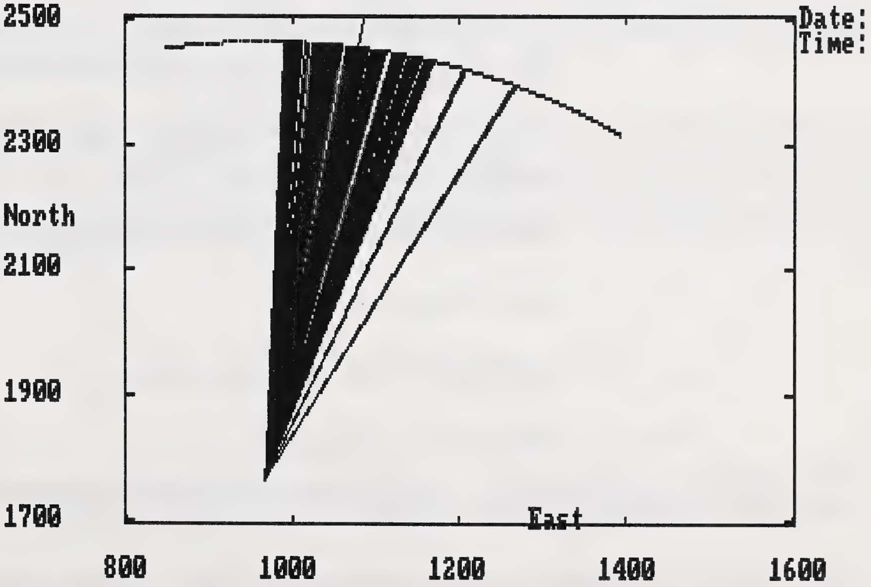

Figure 4.4

2-Dimensional Plot from DART - T13B25.

The following additional statistics were calculated using the Moment method:

- Cross-wind Integrated Concentration (ppt m)
- % in Moment Method (%)
- Skewness
- Kurtosis
- Centroid Location (northing and easting)
- Wind Transport Direction (deg)

Volume 2 presents a tabular and graphical summary for each traverse conducted during the study. The tabular portion presents the identification of the traverse and the traverse statistics discussed in this section. The graphical portion depicts the observed concentration file with a best-fit Gaussian distribution superimposed. The latter is based on the Moment Method and the time window for the portion of the profile that the Moment Method is based is also shown on the graph.

4.6.2 Parameters Calculated From Stationary Monitoring Data

For 30-minute stationary periods, the following statistics were computed:

C_m = Maximum Concentration (ppt)

$\overline{C}$ = Mean Concentration (ppt)

$\overline{C_m}$ = Conditional Mean Concentration (ppt)

I = Plume Intermittency - fraction of time the plume impacts the receptor during the sampling period

i = Concentration Fluctuation Intensity - ratio of the standard deviation to the mean which is $\frac{\sigma_c}{\overline{C}}$ (%)

i_p = Conditional Concentration Fluctuation Intensity

γ = Peak (99%) to Mean Ratio

σ_c = Standard deviation of concentration record

C_{50}, C_{99} = 50th and 99th Percentiles (ppt)

The conditional mean concentration and conditional concentration fluctuation intensity are computed by multiplying the plume intermittency by the appropriate value.

For data collected at a single location, the observed maximum (C_m) was reported and the absolute mean ($\overline{C}$) and concentration fluctuation intensity (i) were calculated as:

$$C_m = \mathrm{MAX}(C_j, C_{j+1})$$

$$\overline{C} = \frac{\sum_{j=1}^{N} C_j}{N} \tag{4.13}$$

$$i = \frac{\sigma_c}{\overline{C}} = \frac{\left[(1/N) \sum_{j=1}^{N} (C_j - \overline{C})^2 \right]^{1/2}}{\overline{C}} \tag{4.14}$$

The plume intermittency (I) calculation had to distinguish which portion of the 30-minute was impacted by the plume. The standard deviation of the instrument baseline noise was determined. All SF_6 concentrations less than three standard deviations from the baseline were regarded as zero. Concentrations greater than these standard deviations from the baseline were regarded as being impacted by the plume. A conditional mean $\overline{C_m}$ and concentration intensity i_p were calculated for non-zero concentration periods.

A probability distribution was determined by determining the fraction of time that the concentration was greater than nine selected concentration levels and above zero (which gives intermittency). The nine concentration levels are:

$$\exp[x \ln(C_m)] \tag{4.15}$$

where: $x = 0.1, 0.3, 0.5, 0.7, 0.8, 0.9, 0.95, 0.97$ and 0.99

From these results, the concentration of the 50th and 99th percentile were determined by linear interpolation. A peak-to-mean ratio (γ) was computed as the ratio of the 99th percentile to the mean concentration.

Volume 3 presents a tabular and graphical summary of each 30-minute stationary data block for those periods when the plume impacted on the monitor. There were a number of periods when the monitor was not in the plume and these periods were not analysed. The tabular portion presents the identification of the time period and the stationary statistics discussed in this section. The graphical depiction shows the concentration versus time profiles for the 30-minute period.

5 METEOROLOGICAL DATA

The monitoring program at the Kathyrn site was initiated to collect meteorological data on a continuous basis and to collect supplementary data during the tracer releases. In addition, meteorological data from off-site locations were retrieved to fulfill some of the program objectives.

5.1 On-site Data Collection

Much of our understanding of the physics of turbulence in the atmospheric boundary layer is a result of careful, tedious measurements made by the micrometeorological community. Unlike early measurements which relied on custom research-grade instrumentation, measurements today can be made with commercially available sensors and data processing systems. With the introduction of relatively low-cost microprocessor-based data acquisition hardware and software, the means, variances and fluxes of various meteorological parameters can now be measured in real time. This is in contrast to early measurements where data processing was typically undertaken after a field study using mainframe computing systems.

Measurements of mean and fluctuating components of wind and temperature at several levels are required to determine the boundary layer structure as the structure is strongly height dependent. Mean components are typically measured using sensors with 1 to 60 second response times. Fluctuating components require much faster response times (5 to 20 Hz).

A tower is commonly used as an instrument platform for micrometeorological sensors. The type, number and placement of the sensors on the tower is generally determined by available resources. As a general rule, however, a minimum of three observation levels are required and the spacing should be approximately logarithmic (Lenschow 1984).

5.1.1 Location

A 25 m tower was installed in the southeast quarter section of the study area (Figure 5.1). The selected location was based on a number of practical considerations which included:

- Maximizing the fetch over the study area for northerly, westerly and southerly winds. The least frequent winds were expected from the east. Nearby obstructions such as buildings, roadway ditches or clumps of trees were minimal in the selected area.

- Availability of a road access to facilitate installation, operation and maintenance. A road access runs north-south along the eastern edge of the study area. Since the road is used for local purposes only, it had the advantage of providing additional security.

- Minimizing the length of power line to provide electrical power to the station. Approximately 700 m of power line was required to connect to an existing power line running along the southern boundary of the study area.

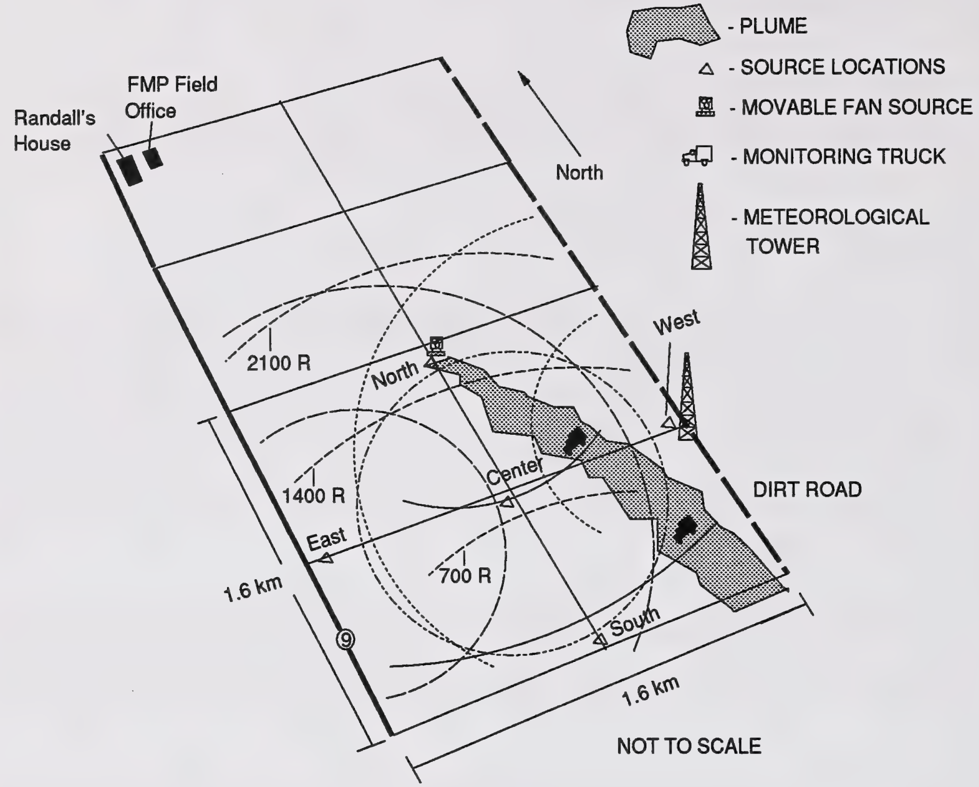

Figure 5.1

Schematic of Test Site.

- Minimizing crop damage. Since the station was installed during the summer prior to the crop removal, and would remain in place for a year, an effort was made to reduce damage to current and future crops.

In addition to the tower, the meteorological station consisted of shelters at the base of the tower for signal conditioning and data logging hardware, a 4.9 m x 2.7 m trailer to house additional data logging hardware and to provide a base for the release studies, an acoustic sounder and a temporary shelter for a tethersonde. The relative layout for the hardware associated with the meteorological station is shown in the overview given in Figure 5.2 and in Photos 5.1 and 5.2.

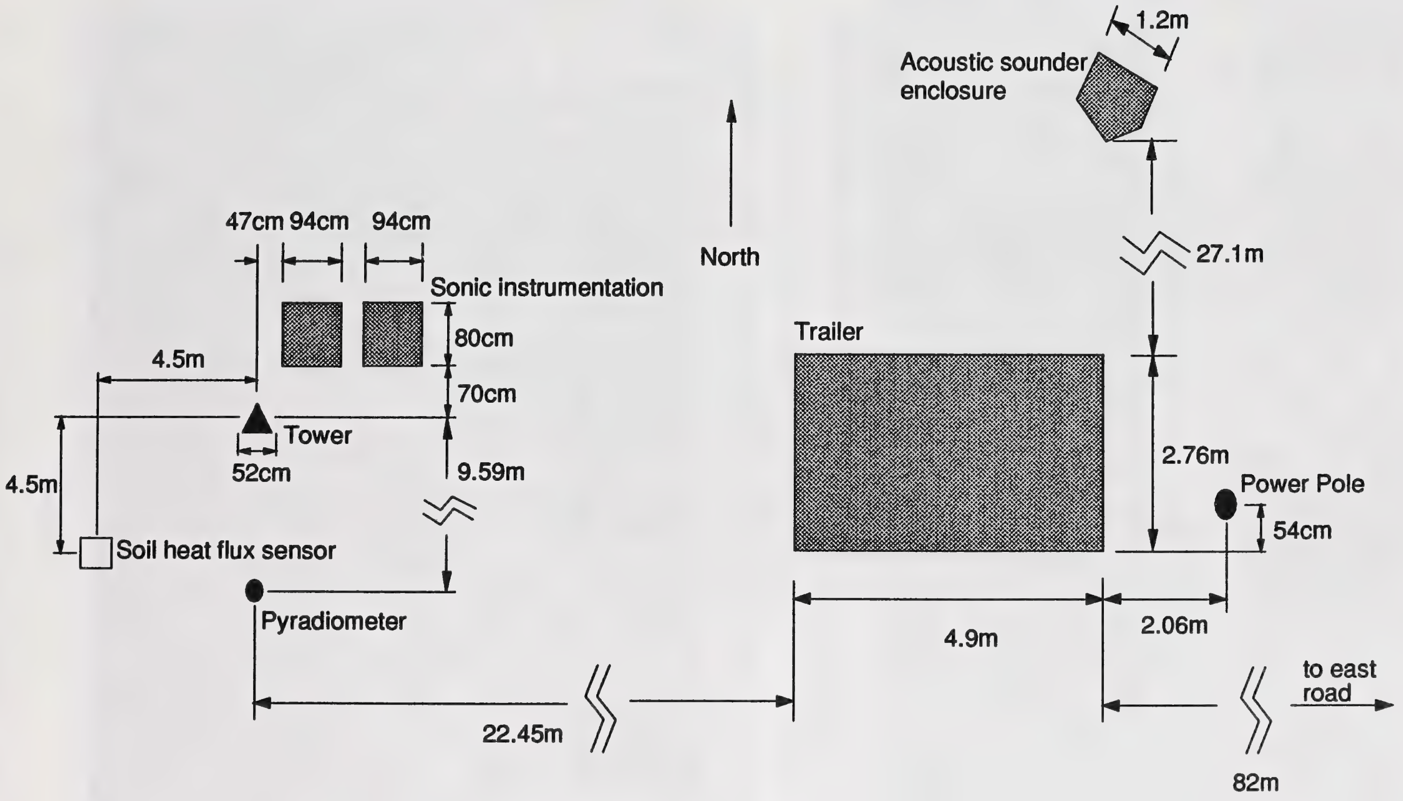

Figure 5.2

Overview of Meteorological Station (Not to Scale).

5.1.2 Station Overview

A 25 m guyed communications tower was used as a platform for the meteorological sensors employed in the study. The tower which had a triangular cross section, was installed such that one apex pointed north and one face pointed south. Photos 5.3 shows the instrumentation and Figure 5.3 shows the relative location of the sensors which were installed on the tower and the orientation of the sensor mounting booms. The primary instrumentation heights were at nominal 25, 16, 10 and 4 m levels. Detailed heights for each sensor are given in Table 5.1.

The presence of the tower, booms and the sensor itself can disturb the airflow in the immediate vicinity. For this reason, measurements obtained on the downwind side of the tower should be treated with caution due to induced turbulent wakes. Meteorological sensors, as a guideline, should not be installed closer than 1.5 times the tower width. As a further guideline, data analysis should be restricted to a sector which excludes wind directions through the tower and 30° on either side. For a sensor mounted at the minimum distance from the tower, the angle of acceptance is 270° (Kaimal 1984).

The face width of the communications tower was 0.52 m. Using the above guidelines, the sensor should be no closer than 0.78 m from the tower face. As can be seen from Table 5.1, the actual boom distances were greater than this value. During the design phase, consideration was given to the use of longer booms. This alternative was rejected to reduce levelling errors and to facilitate maintenance.

Other sensors which were installed at the station include a pressure sensor, a pyrradiometer to measure total incoming radiation, total outgoing radiation and net radiation, two heat flux plates to measure soil heat flux and an acoustic sounder to measure mixing height. The pressure sensor was located in one of the instrument shelters at the base of the tower. The pyrradiometer was mounted 1.2 m above the ground 9.6 m to the south of the tower. The heat flux plates were buried 10 cm in the ground 6.4 m to the southwest of the tower. The acoustic sounder was located 40 m to the northeast of the tower.

5.1.3 Sonic Anemometer System

Since one of the primary objectives of the program was to measure atmospheric turbulence under low wind speed, stable conditions, a low threshold, high frequency response anemometer is required. A sonic anemometer is ideally suited for this application. Unlike conventional anemometers consisting of rotating cups, propellers or vanes, a sonic anemometer does not have a mechanical linkage to the wind which can degrade frequency response, result in overspeeding or have a high starting threshold.

The sonic anemometer senses the wind by measuring the transit times of acoustic pulses travelling in opposite directions across a known path. The major limitation, in terms of frequency response, is the time averaging along the path length. For a path length of 15 cm, the lowest height for which vertical velocity variances can be obtained with reasonable accuracy is about 4 m. For heat flux measurements, this limitation can be relaxed (Kaimal 1984).

Photo 5.1

A View of the Meteorological Trailer, Tower, Acoustic Sounder Enclosure and Tethersonde Tent.

Photo 5.2

A View of the Inside of the Meteorological Trailer.

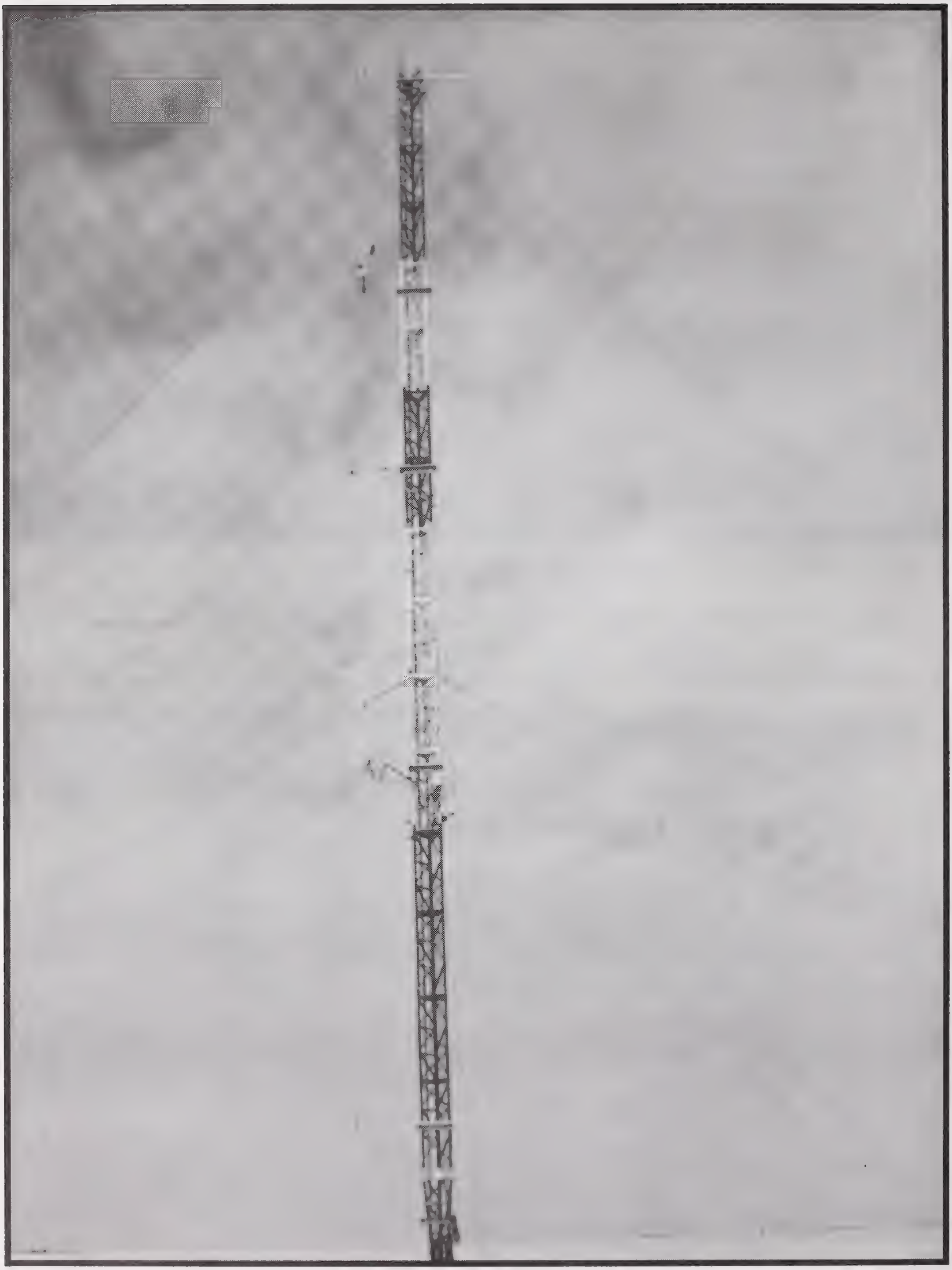

Photo 5.3

The Meteorological Tower Showing All the Instrumentation on it.

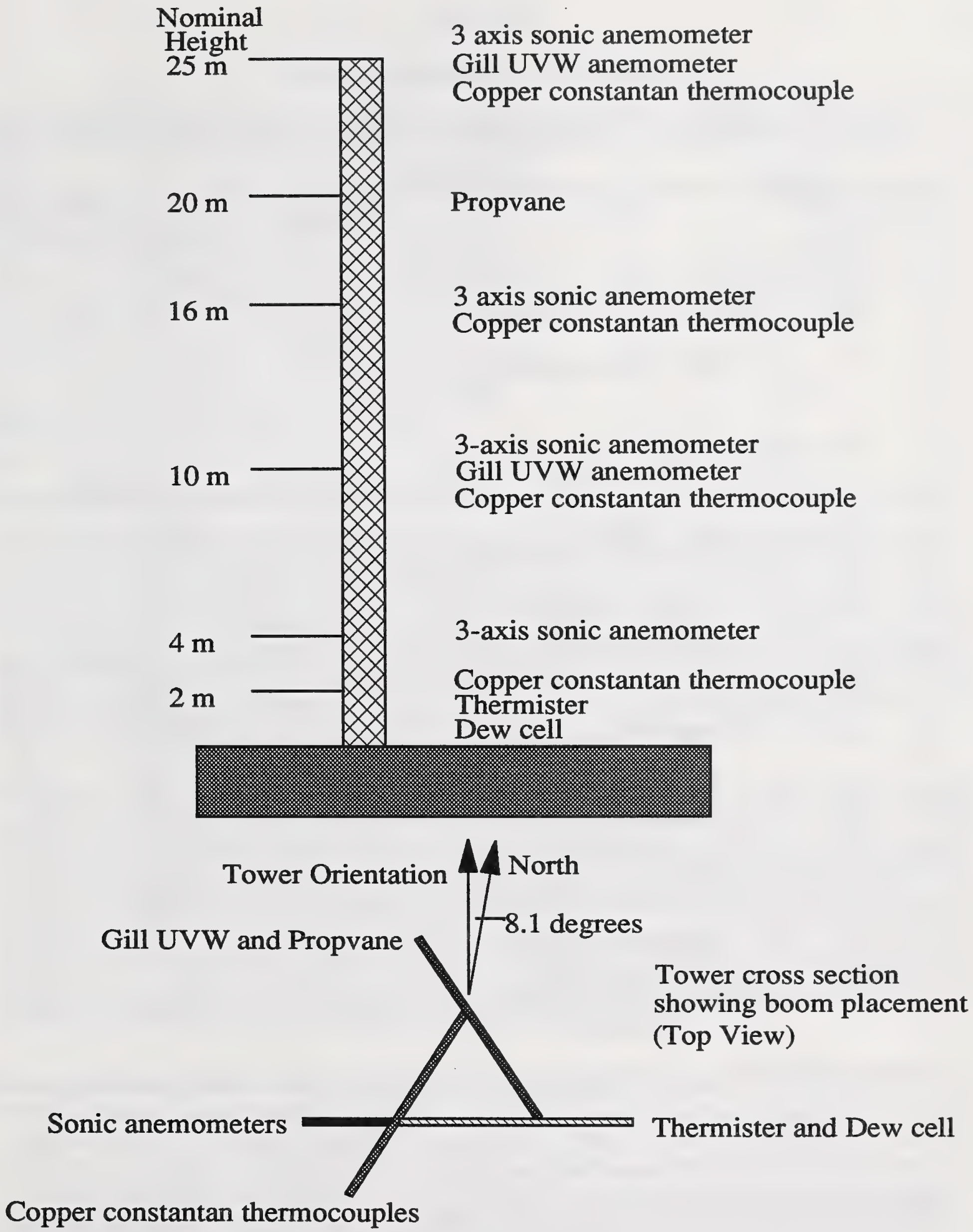

Figure 5.3

Schematic Showing the Relative Locations of Sensors on the Meteorological Tower.

Table 5.1

Details Concerning the Placement of Meteorological Sensors on the 25 m Tower.

Nominal Height (m)	Sensor	Parameter	Actual Height (m)	Boom Distance (m)
25	3-axis sonic anemometer	U,V	25.4	0.8
		W	25.2	1.2
25	Gill UVW anemometer	W	26.0	0.8
		U	25.7	0.8
		V	25.6	0.8
25	Copper constantan thermocouple	T	24.7	1.2
20	Propvane	S,θ	19.85	1.2
16	3-axis sonic anemometer	U,V	16.2	1.0
		W	15.9	1.2
16	Copper constantan thermocouple	T	15.5	1.2
10	3-axis sonic anemometer	U,V	10.0	1.0
		W	10.0	1.0
10	Gill UVW anemometer	W	10.0	0.9
		U	9.7	0.9
		V	9.6	0.9
10	Copper constantan thermocouple	T	9.6	1.0
4	3-axis sonic anemometer	U,V	3.9	1.1
		W	3.7	1.3
2	Copper constantan thermocouple	T	2.4	1.2
2	Thermister and relative humidity	T,RH	2.6	0.7

Four sonic anemometer units were used for this study. Three Applied Technologies Inc. SWS/3 Three-axis Wind Systems were used at the 4, 16 and 25 m levels of the tower (Photos 5.4 and 5.6). A single Kaijo Denki Co. Ltd. Model DAT 310 with the TR61A probe was mounted at the 10 m level of the tower (Photo 5.5). The sonic anemometers were three axis units capable of measuring two orthogonal horizontal components (U_m, V_m), the vertical wind (W_m) and temperature (T_m). Table 5.2 compares the characteristics of the two sonic anemometer systems used.

Table 5.2

Sonic Anemometer Specifications.

Manufacturer	Applied Technologies Inc.	Kaijo Denki Co. Ltd.
Model	SWS-201/3	DAT-310
Path length	15 cm	20 cm
Measurement range		
Horizontal wind	0 to 20 m/s	0 to 25 m/s
Vertical wind	-5 to 5 m/s	-5 to 5 m/s
Temperature	-20 to 50°C	-10 to 40°C
Accuracy		
Wind	±0.1% or 0.05 m/s	±1%
Temperature	±1%	±1%
Resolution		
Wind	0.01 m/s	0.005 m/s
Temperature	0.01°C	0.025°C

The Applied Technologies anemometers use a microcomputer based electronic system to control the sample rate and calculate wind speeds. The sample output is a nominal 10 Hz, with each sample being comprised of 20 individual measurements. The actual sample output of the units provided for the study were typically about 9.3 Hz. Due to the alignment of the U_m and V_m axes of the anemometer, partial shadowing of the acoustic path can cause velocity readings to be underestimated. The electronics in the system incorporates a correction factor to compensate for the shadowing effect. The output of the Applied Technology system is directed as an ASCII data string to an RS232 interface operating at 9600 baud.

In contrast to the Applied Technologies system with orthogonally positioned horizontal sensors, the Kaijo Denki system with the TR-61A probe has horizontal axes which are separated by 120 degrees. The Kaijo Denki probe orientation has the advantage of sampling the same volume in space which should allow for a better estimation of the momentum flux term. The Kaijo Denki system uses an analogue signal processing unit which incorporates a transformation of co-ordinates to provide the horizontal wind vector in orthogonal co-ordinates. The output of the Kaijo Denki system is an analogue voltage which is proportional to wind speed and temperature. The Kaijo Denki system output is based on 10 measurements per second providing a sample rate of 10 Hz.

The Kaijo Denki system has a limited angle of acceptance due to the non-orthogonal nature of the horizontal wind transducers. Ideally the probe is most accurate when facing into the wind, providing a 120 degrees angle of acceptance. The probe was mounted on a platform which could be rotated manually. When the station was unmanned the probe was positioned in a fixed orientation facing west (261.9°). During a tracer release, the probe was manually oriented into one of four positions to ensure the probe faced into the wind (141.9°, 171.9°, 261.9° and 351.9°).

Figure 5.4 shows the schematic of the signal processing for the sonic anemometer systems. While the sonic anemometer probes were all mounted on the tower, the corresponding electronic data processing units were housed in the instrument enclosures located at the base of the tower. A Campbell Scientific 21X datalogger was used as an analog to digital converter to transform the Kaijo Denki values (U_m, V_m, W_m and T_m) into a serial output (10 Hz). The four serial outputs were transmitted to an NEC 386 microcomputer located in the trailer. A Digiboard four channel serial port card was used to overcome the MS-DOS limitation of two serial ports.

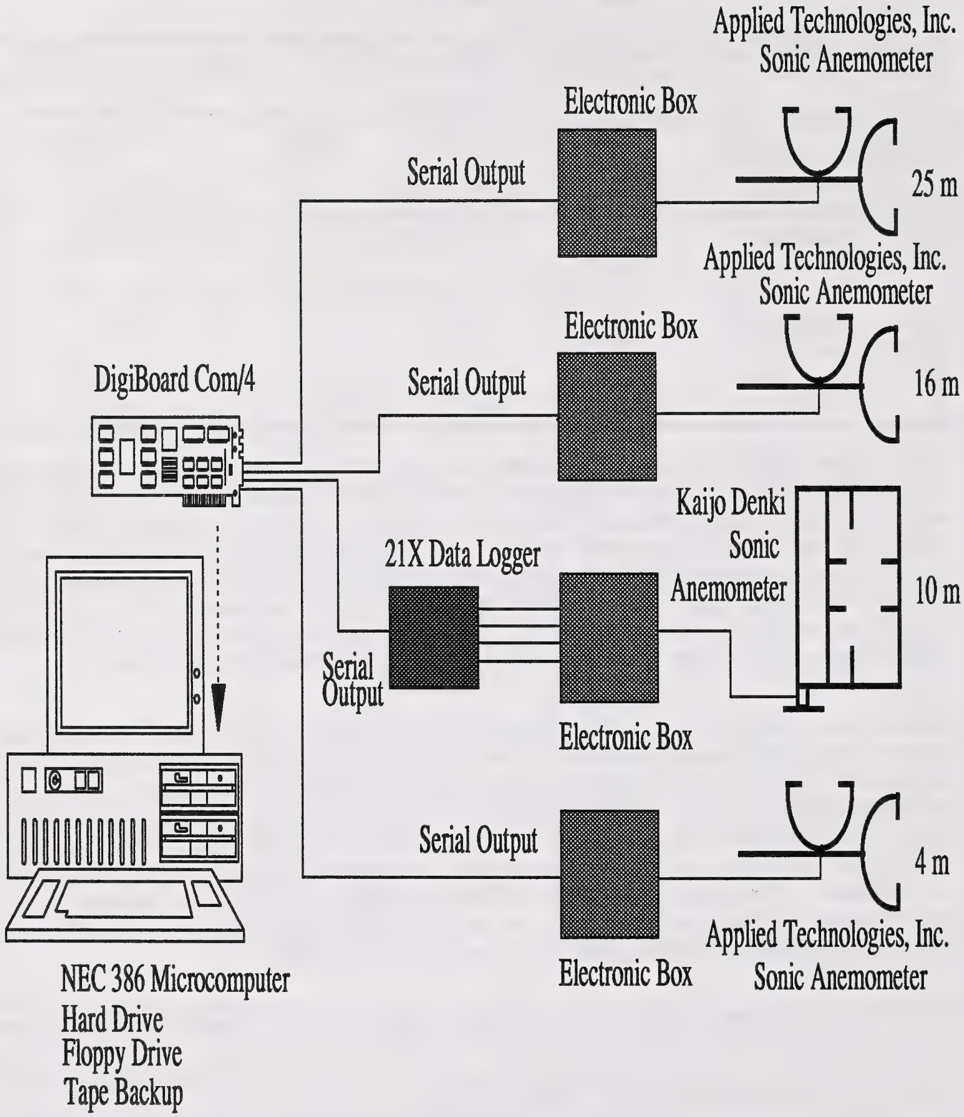

Figure 5.4

Schematic of Signal Processing for Sonic Anemometers.

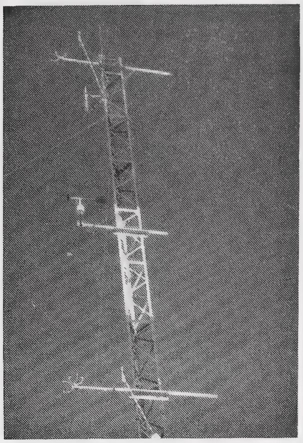

Photo 5.4

16 and 25 m Level Anemometer Sensors. Note the Back-up Equipment.

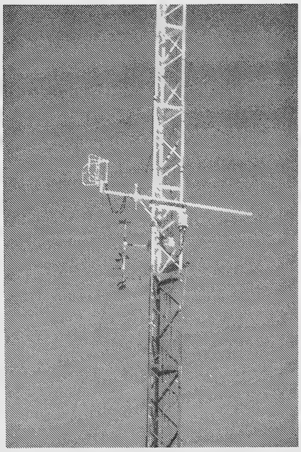

Photo 5.5

10 m Level Kaijo-Denke Anemometer.

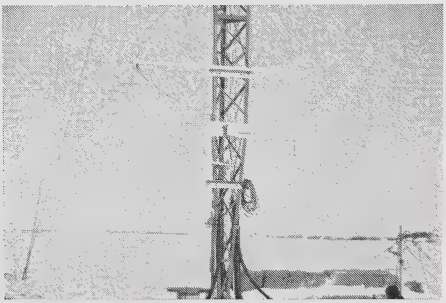

Photo 5.6

4 m Level Applied Technologies Anemometer.

Photo 5.7

As Mentioned in Section 3.3.4, A Mast-Mounted Anemometer was Located at the Source

A program was written in Microsoft C using the Greenleaf communications package to calculate 3-minute mean, variance and co-variance terms from the nominal 10 Hz data. Mean wind speed and direction ($\overline{S}$, $\overline{\theta}$), heat flux (H_o), friction velocity (U^*) and Monin-Obukhov lengths (L) were also calculated. Data were written to the floppy diskette and the hard drive. Selected parameters were written to screen to provide a measure of system performance. During the tracer release tests, high frequency 10 and 25 m data were written to hard disk. At the end of each test, the high frequency data files were transferred to a 40 Mb streaming tape drive back-up unit.

5.1.4 Conventional Sensor System

Wind Sensors

Two conventional Gill UVW propellor anemometers were mounted at the 10 and 25 m levels. The purpose of these sensors were two-fold; first to serve as back-up instrumentation for the sonic anemometers, and second to allow for a comparison of a high frequency response instrument with a conventional one. The latter comparison will evaluate the utility of using the lower cost propeller anemometer in an operational setting.

The Gill UVW propeller anemometer system consists of three DC generators which produce voltages that are proportional to the wind speed. The anemometers were initially equipped with 23 cm low threshold, high sensitivity propellers with propeller extensions to improve the response of the instrument at low speeds. The characteristics of the 23 cm propellers are as follows:

Range	0 to 30 m/s
Threshold	0.1 to 0.2 m/s
Distance Constant	1.0 m

The nominal calibration of 500 mV at 1800 rpm was within 0.1% of the actual output during calibration. This rotation rate corresponds to a horizontal wind speed of 9.18 m/s.

Starting on May 5, 1989, adverse weather conditions (higher winds, rain, hail) resulted in significant damage to the propellors. As the propellors were damaged, they were replaced. On June 26, 1989, the propellors were finally replaced with a more robust 19 cm propellor whose characteristics are:

Range	0 to 40 m/s
Threshold	0.2 to 0.3 m/s
Distance Constant	0.8 m

For these propellors, a rotation rate of 1800 rpm corresponds to a horizontal wind speed of 9.00 m/s. No changes were made to the datalogger algorithms for these new propellors.

The Gill UVW propeller anemometers have frequently been used for turbulence assessments. One of their limiting factors, especially for vertical wind near the ground, is the limited frequency response. In addition, due to departures from the ideal cosine response, correction factors should be applied to wind values measured with these wind sensors. Below 1 m/s, the propeller response is non-linear. Since the primary interest of this study is low wind speeds, a correction factor was implemented to account for this non-linear response.

A Gill Propvane was used primarily to provide a visual indication of wind direction and wind speed and to serve as a confirmation during the system installation and data logging program development portion of the project. The 18 cm diameter propeller drives a DC voltage generator whose voltage is proportional to the wind speed. The generator output is a nominal 2400 mV at 1800 rpm (8.8 m/s). The wind direction is determined from a 1 kΩ potentiometer which can provide a wind direction that is proportional to the voltage produced.

During the tracer releases a wind anemometer was located at the release point at a height of 7 m. The instrumentation was discussed in Section 3.3.4 and is shown in Photo 5.7.

Temperature and Relative Humidity Sensors

The vertical temperature gradient is used as a measure of thermal stability of the atmosphere. The gradient is determined by placing temperature sensors at various heights on the tower. For this project, the selected heights were at the nominal 2, 10, 16 and 25 m levels.

Limitations on the accuracy of atmospheric temperature measurements result primarily from shielding (radiation and ventilation hardware) concerns rather than the inherent uncertainty of the sensor itself. For the temperature sensors selected for this project, the RM Young Gill motor aspirated ventilation shields were used. For the combined temperature-relative humidity sensor, the Qualimetrics Inc. motor-aspirated radiation shield was used.

For the temperature profile measurements, copper-constantan thermocouple junctions were used to ensure reliable measurements. The thermocouple leads were all kept a constant length and confirmed to be within 0.01°C of each other by immersing in an ice-water bath.

The combined temperature-relative humidity sensor was a Campbell Scientific 201 thermistor and RH probe which contains a Fenwal UUT-SIJI thermister and a Phys-Chemical Research Model PC RC-11 relative humidity sensor. Factory calibration for the sensors was accepted.

Radiation Sensor

A Qualimetrics pyrradiometer (Model 3040-A) was used to measure total downward radiation, total upward radiation and net radiation. The spectral sensitivity of the sensor is from 0.3 to 60 µm. Lupolene domes protect the measuring surfaces from wind and moisture. To prevent internal condensation on these domes, they were pressurized continuously by a stream of nitrogen gas. The sensor was mounted 1.5 m above the ground. Every attempt was made to minimize and limit foot traffic in the vicinity of the pyrradiometer. Factory calibrations for the pyrradiometer were initially accepted and later were revised based upon re-calibrations conducted at the conclusion of the study. The revised calibration factors were applied to all of the data.

Pressure Sensor

A Qualimetrics analog output barometer (Model 1705) was used to measure atmospheric pressure. The sensing device consists of a piezo-resistance transducer whose resistance changes with pressure. Built-in signal conditioning produces a voltage which is proportional to pressure. The sensor was mounted in one of the electronic enclosures at the base of the tower. The pressure sensor was calibrated by using the pressure measurements from Calgary International Airport.

Data Logging

Two dataloggers (Campbell Scientific 21X and CR-21) were used for the conventional meteorological sensors to convert electrical voltage signals to engineering units and to calculate appropriate averages and standard deviations. The output of the dataloggers were directed to cassette tape units as the primary storage medium and to printer units as the back-up storage medium. The dataloggers were located in the electronic enclosures at the base of the tower while the cassette tape and printer units were located in the trailer.

Figure 5.5 shows the electronic schematic associated with the conventional meteorological sensors. Also indicated in the figure are the electronic enclosure heaters which were turned on and off by the CR-21 when the shelter temperatures dropped below 0°C.

Table 5.3 lists the input channels for each datalogger. The output channels represent three-minute average values. The sampling rate for the 21X was user programmed for 1 Hz; the sampling rate for the CR-21 was fixed at once every 10 seconds.

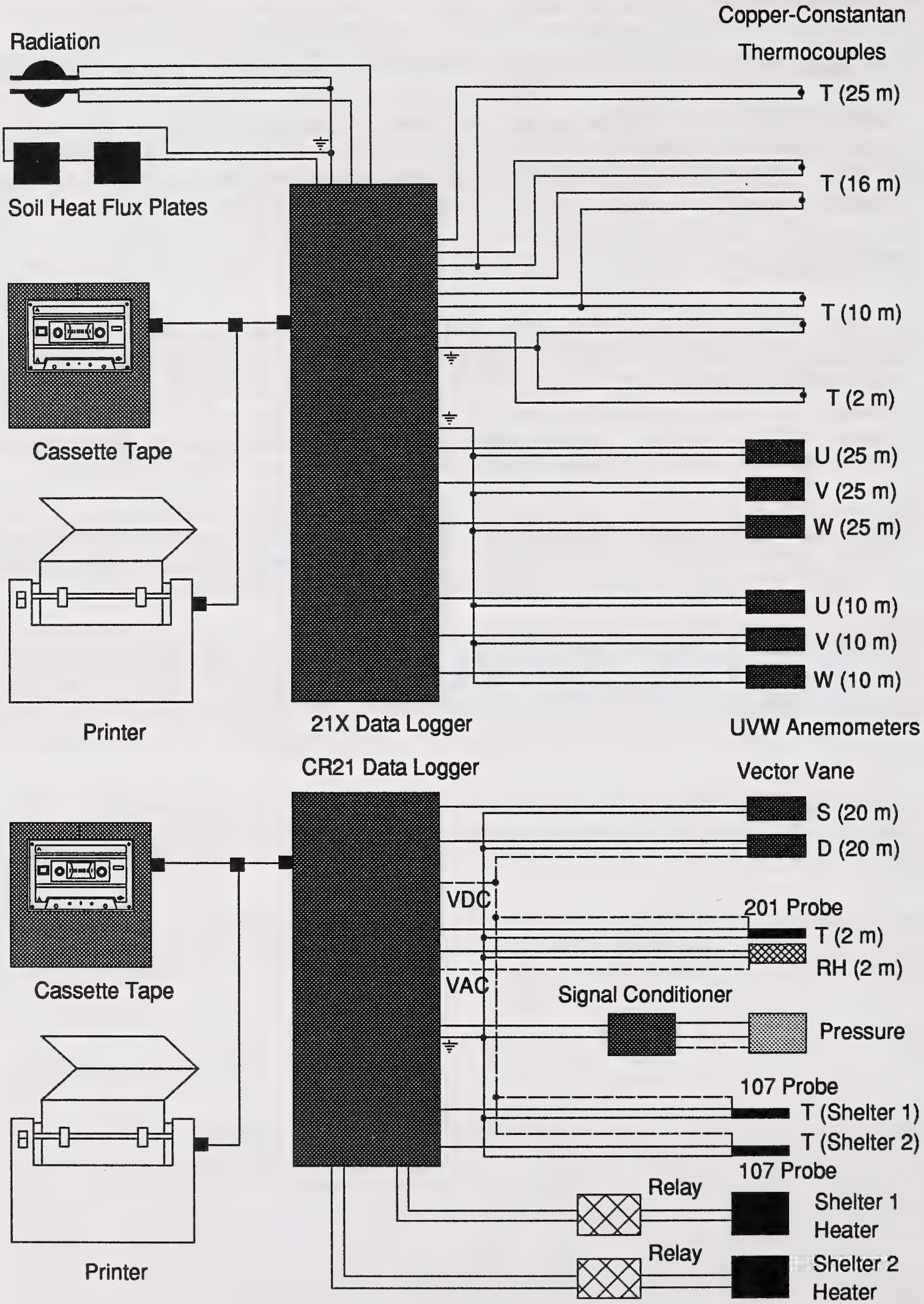

Figure 5.5

Schematic of Signal Processing for Conventional Meteorological Instruments.

Table 5.3

Input Channels of the 21X and CR-21 Dataloggers.

Datalogger	Input Channel	Symbol	Parameter
21X	1	T_{25}	25 m thermocouple temperature
21X	2	$\Delta T(25-16)$	Temperature difference (25 m - 16 m)
21X	3	T_{16}	16 m thermocouple temperature
21X	4	$\Delta T(16-10)$	Temperature difference (16 m - 10 m)
21X	5	T_{10}	10 m thermocouple temperature
21X	6	$\Delta T(10-2)$	Temperature difference (10 m - 2 m)
21X	7	T_2	2 m thermocouple temperature
21X	8	U_m	25 m Gill UVW horizontal wind
21X	9	V_m	25 m Gill UVW horizontal wind
21X	10	W_m	25 m Gill UVW vertical wind
21X	11	U_m	10 m Gill UVW horizontal wind
21X	12	V_m	10 m Gill UVW horizontal wind
21X	13	W_m	10 m Gill UVW vertical wind
21X	14	I_{RAD}	Incoming radiation flux
21X	15	O_{RAD}	Outgoing radiation flux
21X	16	S_{FLUX}	Soil heat flux
CR-21	1	T_{S1}	Shelter 1 temperature
CR-21	2	T_{S2}	Shelter 2 temperature
CR-21	3	S	20 m Propvane wind speed
CR-21	4	T_{2R}	2 m thermister temperature
CR-21	5	RH	2 m relative humidity
CR-21	6	P	Ground ambient pressure
CR-21	7	θ	20 m Propvane wind direction

5.1.5 Acoustic Sounder System

An Aerovironment Inc. Model 300 acoustic sounder was used to obtain a continuous record of acoustic back scatter from atmospheric discontinuities. The returned back scatter or echo is produced by turbulence in the atmosphere. The back scatter is displayed on a chart recorder from which the depth of the mixing layer or inversion heights can be abstracted.

The acoustic system consists of a transducer mounted at the focal point of a parabolic dish which is directed vertically. A plywood/foam enclosure is used to minimize outside noise interference and to reduce the noise impact produced by the sounder on nearby residents. The acoustic sounder control and recorder unit was placed inside the trailer.

Two systems were employed during the study. The first one, obtained from Alberta Environment in Edmonton, was used from 8 September 1988 to 4 November 1988. The range of this instrument was 0 to 500 m with a resolution of 25 m. The second unit, obtained from Mount Royal College in Calgary was installed when the Alberta Environment unit failed. The replacement unit had a range of 0 to 750 m with a resolution of 25 m. Once Alberta Environment's unit was repaired, it was returned to the site on 2 June 1989. The Alberta Environment unit operated intermittently after it was reinstalled. Due to the discontinuous nature of the acoustic sounder data collection, no analysis of the data was undertaken for the summer period (April to October).

The acoustic sounder charts were date stamped whenever an operator visited the meteorological station. At the end of the chart, the chart was labelled for subsequent analysis. The acoustic sounder trace is produced on a facsimile recorder which deteriorates rapidly with handling. To provide a permanent record and to facilitate data extraction, the charts were cut up into 12 or 24 hour segments (depending on chart speed) and photographed on to 35 mm slides. The 35 mm slides were then projected on to a screen to allow mixing layer depths to be determined. Figure 5.6 shows a sample of the mixing height variation with time of day. See Appendix D2 for final plots and examples of slides.

5.1.6 Tethersonde

During the tracer release periods, depending on weather and manpower availability, periodic ascents and descents with an instrumented tethersonde were made. The tethersonde was released northeast of the tower. The tethersonde system consisted of the following components:

- Balloon, cable and winch assembly. A 3.25 m^3 helium filled balloon was used to carry the instrument package. A winch assembly controls the rate of ascent and descent.

- The instrument package consisting of wind direction, wind speed, temperature and relative humidity sensors and an FM crystal controlled transmitter.

- The ground station consists of a receiver and a microprocessor to produce digital and analog outputs. A modified HP-97 programmable printer calculator was used to print out data from the ground station. In addition, the digital output was also directed to a cassette tape. During data reduction, it was discovered no usable data were on the cassette tape, so all data were entered from the hard copy printout into files manually.

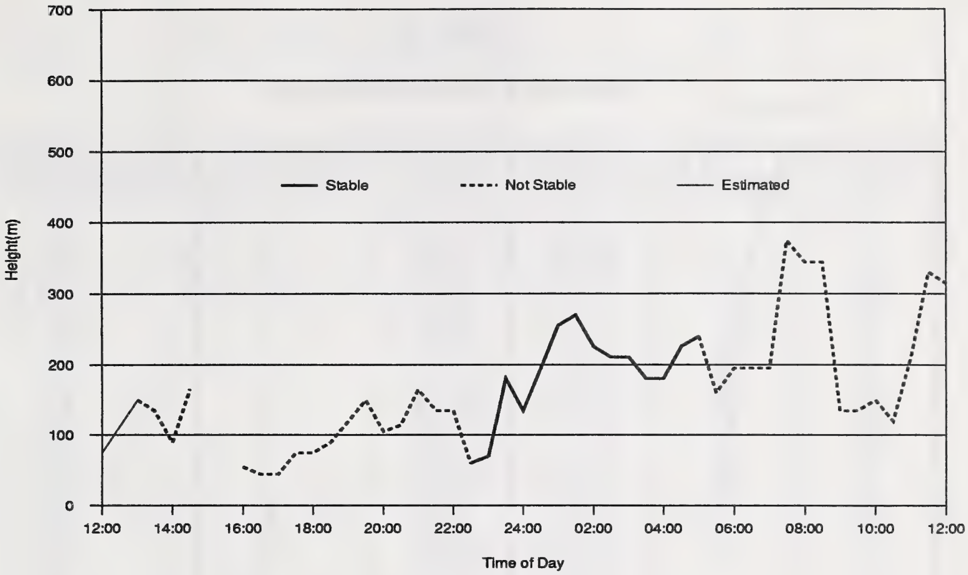

Figure 5.6

Example Plot of Acoustic Sounder Data.

The paper tape from the ground station of the tethersonde recorded the following information:

- Elapsed time from turning on ground station (minutes)
- Change in pressure from reference pressure (millibars)
- Ambient temperature (°C)
- Dew point temperature (°C)
- Wind speed (m/s)
- Wind direction (degrees)
- Battery voltage (% power remaining)

The paper tapes were marked for the ascent time, the time the balloon reached the top, the time the descent started, the time the balloon reached ground-level again and the time when the power was turned off on the ground. The data were plotted to determine the temperature, temperature difference, wind direction and wind speed as a function of height.

Table 5.4 summarizes the tethersonde ascents and descents which were made during the tracer releases. Figure 5.7 shows sample wind speed, wind direction, temperature and dewpoint temperature profiles. See Appendix D1 for final plots. The maximum height above the ground level is also indicated in the table. The height was generally less than 90 m and was restricted due to Ministry of Transport regulations.

Table 5.4

Record of Tethersonde Releases.

Release #	Launch #	Date	Time[a]	Tracer Test	Max Height (m)
01	2	24 Oct	20:47	3	69
02	3	24 Oct	21:32	3	46
03	4	24 Oct	22:32	3	75
04	6	24 Oct	23:37	3	132
05	7	25 Oct	00:22	3	76
06	8	25 Oct	01:12	3	70
07	9	25 Oct	02:08	3	57
08	10	25 Oct	03:07	3	66
09	11	25 Oct	03:47	3	65
10	12	25 Oct	04:37	3	69
11	3	27 Oct	22:32	4	84
12	4	28 Oct	00:02	4	72
13	1	28 Oct	19:32	5	56
14	1	31 Oct	20:47	6	69
15	2	31 Oct	21:47	6	69
16	1	8 Nov	18:47	8	75
17	2	8 Nov	19:32	8	84
18	3	8 Nov	20:32	8	89
19	1	14 Nov	17:42	9	50
20	2	14 Nov	18:34	9	48
21	3	14 Nov	19:22	9	61
22	4	14 Nov	20:12	9	63
23	2	16 Nov	18:52	11	64
24	3	16 Nov	21:04	11	76
25	4	16 Nov	23:32	11	76
26	2	18 Nov	20:57	12	78
27	3	18 Nov	22:02	12	78
28	4	18 Nov	23:02	12	70
29	1	20 Nov	18:27	13	76
30	2	20 Nov	19:10	13	61
31	3	20 Nov	20:42	13	61
32	5	20 Nov	23:02	13	61
33	6	20 Nov	23:54	13	69
34	1	26 Nov	17:47	15	85
35	2	26 Nov	18:47	15	73
36	1	2 Dec	18:22	16	52
37	3	2 Dec	20:22	16	90
38	2	6 Dec	18:42	17	80
39	3	6 Dec	19:42	17	74
40	1	8 Dec	18:27	19	69
41	2	8 Dec	21:07	19	75
42	1	9 Dec	18:07	20	48
43	2	9 Dec	19:19	20	60
44	3	9 Dec	20:27	20	60

(a) Beginning of the ascent

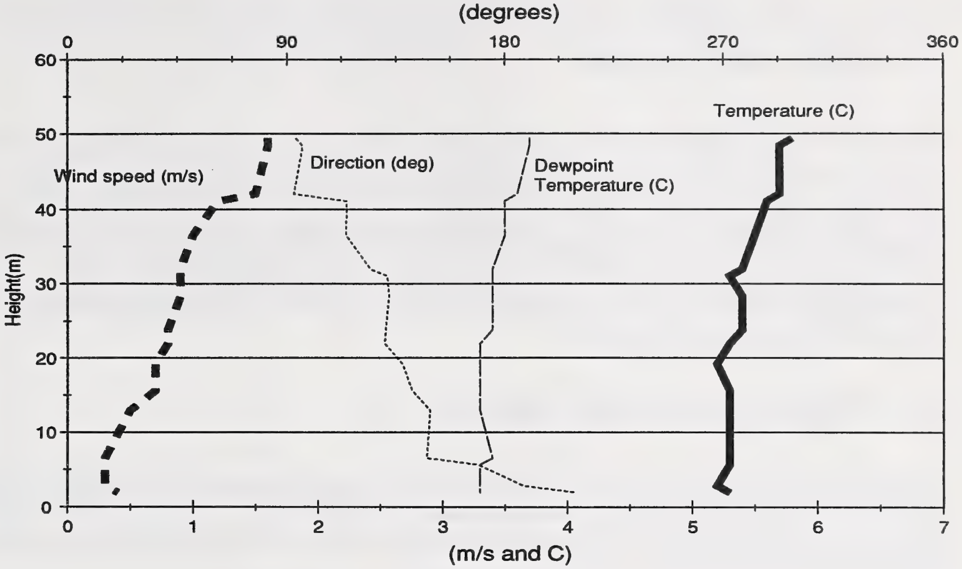

Figure 5.7

Example Plot of Tethersonde Data.

5.2 Off-Site Data Collection

To determine the representativeness of the data collected on-site and to evaluate the utility of nearby airport data for dispersion evaluations, off-site data from three sources were obtained. The first source of data is from Calgary International Airport which is located 24 km to the southwest of the site. The second source of data is from the Acid Deposition Research Program (ADRP) Crossfield East air quality monitoring station (Legge, 1988). The Crossfield East site is 32 km to the northwest of the study site. The third source is compliance ambient air quality monitoring stations located 16 km west and 32 km to the north of the study site (Figure 5.8).

5.2.1 Calgary International Airport

Weather data has been officially collected in the Calgary area since July 1884. Between 1884 and 1939, the monitoring site was moved several times within a 3 km radius of downtown. In 1939, the site was moved out to the airport and the anemometer is currently located at a height of 10 m.

The airport is situated on flat land at an elevation of 1 067 m above sea level. The land falls away to the valley of Nose Creek, 1.6 km to the west, and then rises to Nose Hill located 6.4 km to the west. To the east, the generally rolling ground levels off to flat prairie land.

The following types of observations are collected at Calgary International Airport:

- Synoptic observations provided in a numerical code based on World Meteorological Organization regulations. Observations are taken at 6 hour intervals (00:00, 06:00, 12:00 and 18:00 GMT) and include: sky condition, wind speed, wind direction, visibility, weather, obstructions to vision, pressure, temperature, dew point, precipitation, cloud amount and special phenomena.

- Hourly observations are taken once each hour and include observations of sky conditions, visibility, weather, obstruction to vision, pressure, temperature, humidity, wind speed, wind direction, cloud amount and obscuring phenomena.

Both the synoptic and hourly observations made at Calgary Airport (and other airports) have been designed to satisfy the weather forecast requirements of the aviation industry and of the general public. As a consequence, the data collected may be of limited use for the dispersion boundary layer assessments. For example, the wind data collected at the airport represent one-minute averages taken every hour up until the end of 1984. In 1985, two-minute average wind data are used. Neither may be representative of hourly average values frequently required for environmental purposes.

Atmospheric turbulence levels are frequently inferred from airport measurements. For example, Turner's scheme categorizes turbulence based on wind speed (to recognize wind speed generated turbulence) and solar radiation index (to recognize surface heating and cooling effects on turbulence) (Turner 1964). The solar radiation index is based on time of day, time of year, latitude and cloud cover.

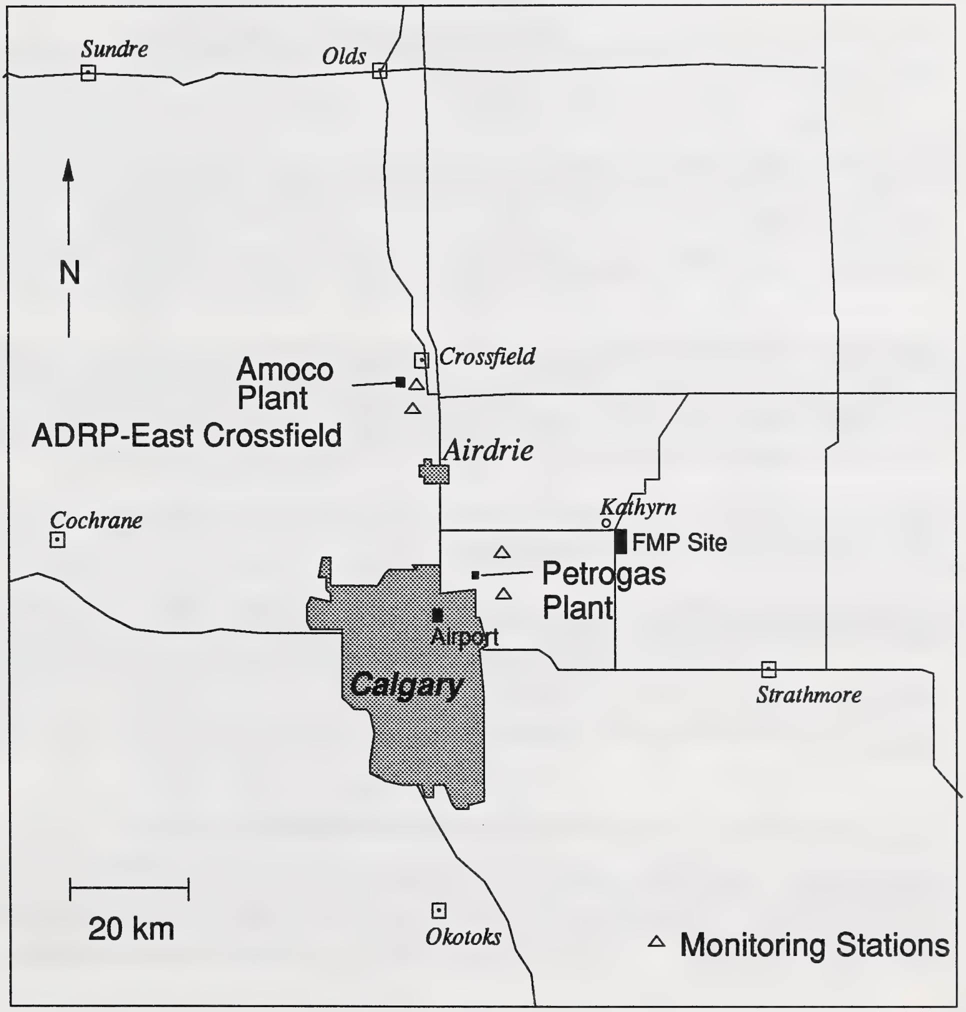

Figure 5.8

Location of Off-site Meteorological Stations.

For the purpose of this study, the following observations were obtained: pressure, temperature, cloud cover, wind speed, wind direction, snow depth and snowing indicator. All of these, except snow depth, are available on an hourly basis from Atmospheric Environment Service (AES) in HLY01 record format (AES 1983). Snow depth information is available on a daily basis in DLY04 record format (AES 1983).

5.2.2 ADRP East Crossfield

The East Crossfield site was established to collect background air quality and meteorological data as part of the ADRP. The air quality station operated from 1 November 1985 to 31 October 1987. The site is located at an elevation of 1158 m MSL amid flat cultivated terrain.

The site was instrumented to measure wind speed at the 5.8 and 10 m levels of a 10 m tower. The data are of particular interest to this study since 2 minute average, 10 minute average and 1 hour average data are available. Qualimetrics models 2020 and 2031 Micro Response Wind Vane Anemometers were used to measure horizontal wind data and a Gill Propeller Anemometer model 2072B was used to measure vertical wind at the 10 m level.

Means and standard deviations of the collected wind data were retrieved from the ADRP data base for this project. This data base provides a longer time period than is available at the Kathyrn site which can assist in determining the temporal representativeness of the data collected in the study area. The shorter averaging times expressed in multiples of 2 minutes offer an advantage over other stations which simply collect hourly average data.

5.2.3 Compliance Monitoring Data

Large industrial facilities in Alberta are required to establish monitoring stations in the vicinity of their operations to record changes in the ambient air quality. These stations are equipped with sensors to record hourly-average wind speeds and directions. The closest stations to the study site are located 16 km and 32 km to the west of the study area. They are the Petrogas Balzac gas plant stations (2) and the Amoco Crossfield gas plant station, respectively.

The Petrogas station is equipped with a Weather Measure model W102-P anemometer mounted at the 10 m level. The Amoco station is equipped with Climatronics Mark 4 anemometers mounted at the 17 and 30 m levels. All observations are recorded on an hourly basis and monthly reports are provided to Alberta Environment as part of the operating requirements for the plant. For this assessment, hourly average wind data were obtained from the plant operators.

5.3 Meteorological Data Organization and Reduction

To facilitate data analysis, several different file formats were used to archive the meteorological data collected. Specifically these file formats include:

Quality-controlled sonic anemometer data.
Quality-controlled conventional meteorology data.
Working-level 3-minute average data.
Working-level 30-minute average data.
Quality-controlled high-frequency sonic anemometer data.

The quality-controlled data files archived meteorological information collected at the station. The working-level data files involve integration and preprocessing of files. The following discussion documents the format of these files and discusses the procedures which were taken to generate the files.

5.3.1 Quality-Controlled Sonic Anemometer Data

The format for the 3-minute average sonic anemometer data is presented in Table 5.5. Each file consists of 1440 records (3-day period) with 63 fields. Each field is represented by at least one blank character and all fields are represented by numeric characters only. Missing data are represented by a "-99".

The correction angles are dependent on the sonic anemometer and correct the wind direction reading from the anemometer co-ordinate system to true north. For the three Applied Technologies Inc. systems, the correction angle (θ_{CAT}) is 171.9°. That is 171.9° has to be added to the sonic anemometer wind direction value to provide a wind direction in conventional co-ordinates (e.g. N=0°, E=90°,S=180° and W=270°). The correction angle (θ_{CKD}) for the Kaijo Denki system is dependent on its orientation.

Position 1 (Anemometer facing North)	351.9°
Position 2 (Anemometer facing South)	171.9°
Position 3 (Anemometer facing West)	261.9°
Position 4 (Anemometer facing Southeast)	141.9°

It is also important to note the measured parameters in Table 5.5 refer to the anemometer co-ordinate system and are denoted by the subscript "m" to differentiate from the conventional coordinate system. The speed $\overline{S}$ is given by:

$$\overline{S} = \sqrt{(\overline{U_m})^2 + (\overline{V_m})^2} \tag{5.1}$$

and the direction by:

$$\overline{\theta} = \theta_c + \tan^{-1}(\overline{U}_m / \overline{V}_m) \tag{5.2}$$

where θ_c = correction angle (θ_{CAT} or θ_{CKD}).

Table 5.5

Quality-Controlled Sonic Anemometer Data File Format (three-minute average).

Field	Symbol	Description	Units	Format
1	No	Case (1 to 1440)		dddd
2	MON	Month (01 to 12)		dd
3	DAY	Day (01 to 31)		dd
4	YR	Year (88 to 89)		dd
5	HH	Hour (00 to 23)		dd
6	MM	Minute (00 to 59)		dd
7	θ_{CAT}	Correction angle (AT)	(°)	ddd.d
8	θ_{CKD}	Correction angle (KD)	(°)	ddd.d
9	$COUNT$	Number of data points		dddd
10	$\overline{U_m}$	4 m horizontal wind	(m/s)	ddd.dd
11	$\overline{V_m}$	4 m horizontal wind	(m/s)	ddd.dd
12	$\overline{W_m}$	4 m vertical wind	(m/s)	ddd.dd
13	$\overline{T_m}$	4 m sonic temperature	(°C)	ddd.d
14	$\overline{U_m^2}$	4 m (horizontal wind)^2	$(m/s)^2$	ddddd.ddd
15	$\overline{V_m^2}$	4 m (horizontal wind)^2	$(m/s)^2$	ddddd.ddd
16	$\overline{W_m^2}$	4 m (vertical wind)^2	$(m/s)^2$	ddddd.ddd
17	$\overline{U_m V_m}$	4 m momentum cross product	$(m/s)^2$	ddddd.ddd
18	$\overline{W_m T_m}$	4 m temperature cross product	(°C·m/s)	ddddd.ddd
19	$\overline{V_m W_m}$	4 m momentum cross product	$(m/s)^2$	ddddd.ddd
20	$\overline{U_m W_m}$	4 m momentum cross product	$(m/s)^2$	ddddd.ddd
21	$\overline{S}$	4 m wind speed	(m/s)	ddd.dd
22	$\overline{\theta}$	4 m wind direction	(°)	ddd.d
23 to 36		Same as 9 to 22 for 10 m level		
37 to 50		Same as 9 to 22 for 16 m level		
51 to 64		Same as 9 to 22 for 25 m level		

The measured values are denoted by a subscript 'm' which corresponds to the anemometer system. The overbar denotes a 3-minute average.

Figure 5.9 illustrates the correction angle and co-ordinate system parameters for the two anemometer systems. Only the Kaiji Denki Position 3 orientation is shown.

During the collection of the sonic anemometer data, spurious results were observed under certain conditions. These failures were more frequent with the Applied Technologies systems and were associated with an ice or frost build-up on the transducers or when a transducer failed. The observed values were identified as spurious by looking at sudden changes in the time series or by comparing with other sensors.

5.3.2 Quality-Controlled Conventional Meteorological Data

The format for the 3-minute average conventional meteorological data is presented in Table 5.6. Again, each file consists of 1440 records (3-day period, with 41 fields). Each field is separated by at least one blank character and all fields are represented by numeric characters only. Missing data is represented by "-99".

The $\overline{U}_m$, $\overline{V}_m$ and $\overline{W}_m$ wind components are corrected for departures from the ideal cosine propeller response. These correction factors are supplied with the system documentation and are also presented in Gill (1975). The true wind speed is given by:

$$U_m = C_1 U_{mu} \tag{5.3}$$

$$V_m = C_2 V_{mu} \tag{5.4}$$

$$W_m = C_3 W_{mu} \tag{5.5}$$

where the "m" denotes the corrected values and the subscript "mu" denotes the uncorrected values. The value of C_3 is equal to 1.25 since the cosine curve in the region of 90 ± 30° is nearly a straight line. The correction factors C_1 and C_2 depend on the ratio:

$$R = \frac{\mathrm{MIN}(U_{mu}, V_{mu})}{\mathrm{MAX}(U_{mu}, V_{mu})} \tag{5.6}$$

If $U_{mu} > V_{mu}$, then:

$$C_1 = 0.998 + 0.019R + 0.111R^2 \tag{5.7}$$

$$C_2 = 1.249 + 0.024R - 0.028R^2 - 0.300R^3 + 0.187R^4 \tag{5.8}$$

and if $V_{mu} > U_{mu}$, then:

$$C_1 = 1.249 + 0.024R - 0.028R^2 - 0.300R^3 + 0.187R^4 \tag{5.9}$$

$$C_2 = 0.998 + 0.019R + 0.111R^2 \tag{5.10}$$

The above polynomials are regression curve-fits to the correction factor values presented in Gill (1975).

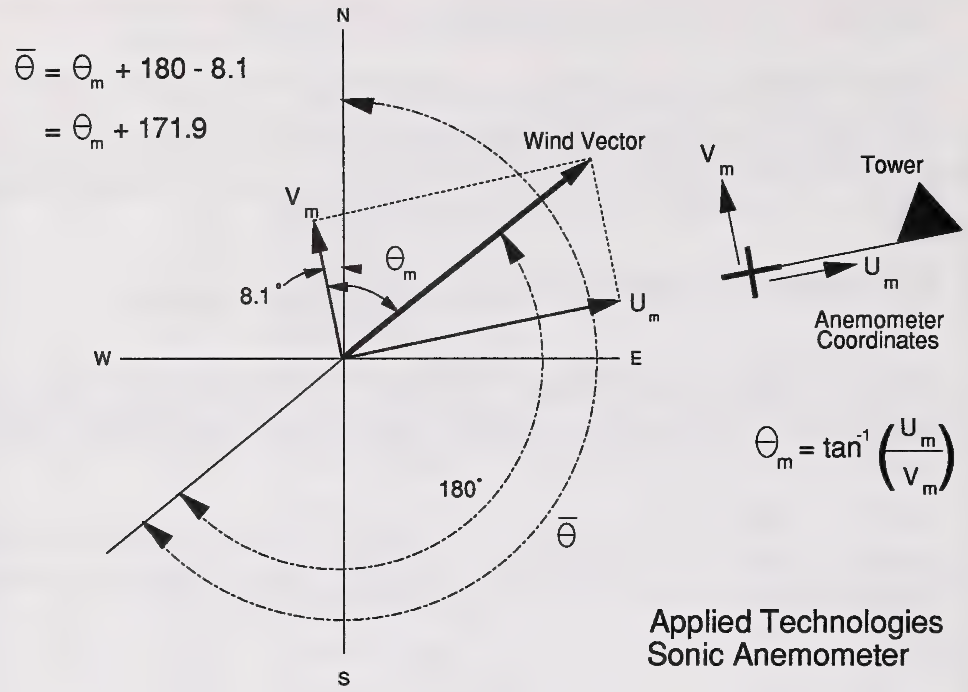

Applied Technologies
Sonic Anemometer

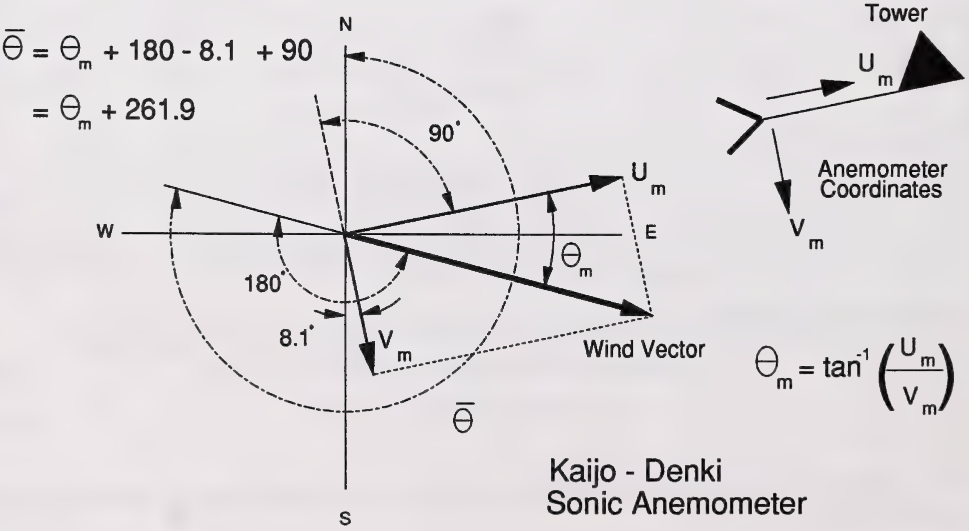

Kaijo - Denki
Sonic Anemometer

Figure 5.9
Correction Angles for the Sonic Anemometers.

Table 5.6

Quality-Controlled Conventional Meteorological Data File Format (three-minute average).

Field	Symbol	Description	Units	Format
1	No	Case (1 to 1440)		dddd
2	MON	Month (01 to 12)		dd
3	DAY	Day (01 to 31)		dd
4	YR	Year (88 to 89)		dd
5	HH	Hour (00 to 23)		dd
6	MM	Minute (00 to 59)		dd
7	$\overline{U_m}$	25 m Gill UVW horizontal wind	(m/s)	ddd.dd
8	$\overline{V_m}$	25 m Gill UVW horizontal wind	(m/s)	ddd.dd
9	$\overline{W_m}$	25 m Gill UVW vertical wind	(m/s)	ddd.dd
10	$\overline{S}$	25 m Gill UVW wind speed	(m/s)	ddd.dd
11	$\overline{\lvert S \rvert}$	25 m Gill UVW vector magnitude	$(m/s)^2$	ddd.dd
12	$\overline{\theta}$	25 m Gill UVW wind direction	$(m/s)^2$	ddd.d
13	σ_θ	25 m Gill UVW standard deviation of $\overline{\theta}$	(°)	ddd.d
14	σ_W	25 m Gill UVW standard deviation of $\overline{W}$	$(m/s)^2$	dd.ddd
15 to 22		Same as 7 to 14 for 10 m Gill UVW		
23 to 26		Same as 10 to 13 for 20 m Propvane		
27	$\overline{T_{25}}$	25 m thermocouple temperature	(°C)	ddd.d
28	$\overline{T_{16}}$	16 m thermocouple temperature	(°C)	ddd.d
29	$\overline{T_{10}}$	10 m thermocouple temperature	(°C)	ddd.d
30	$\overline{T_2}$	2 m thermocouple temperature	(°C)	ddd.d
31	$\overline{T_{2R}}$	2 m thermister temperature	(°C)	ddd.d
32	$\overline{\Delta T(25-16)}$	Temperature difference (25 m - 16 m)	(°C)	dd.ddd
33	$\overline{\Delta T(16-10)}$	Temperature difference (16 m - 10 m)	(°C)	dd.ddd
34	$\overline{\Delta T(10-2)}$	Temperature difference (10 m - 2 m)	(°C)	dd.ddd
35	$\overline{T_{S1}}$	Shelter 1 temperature	(°C)	ddd.d
36	$\overline{T_{S2}}$	Shelter 2 temperature	(°C)	ddd.d
37	$\overline{I_{RAD}}$	Incoming radiation flux	(W/m^2)	dddd.d
38	$\overline{O_{RAD}}$	Outgoing radiation flux	(W/m^2)	dddd.d
39	$\overline{N_{RAD}}$	Net radiation flux	(W/m^2)	dddd.d
40	$\overline{S_{FLUX}}$	Soil heat flux	(W/m^2)	dddd.d
41	$\overline{P}$	Ground ambient pressure	(kPa)	ddd
42	$\overline{RH}$	2 m relative humidity	(%)	ddd

The measured values are denoted by a subscript "*m*" which corresponds to the anemometer system.
The overbar denotes a 3-minute average.

In addition to the cosine correction, the $\overline{U_m}$, $\overline{V_m}$ and $\overline{W_m}$ values were corrected for non-linear response at low wind speeds. The correction factor is based on the use of different relationships between wind speed and voltage when the wind is less than 0.9 m/s than when it is greater, and is based on a polynomial curve fit to the calibration curve. The relationships used are as follows:

$$S = 0.09 + 0.0185(\text{voltage}) \qquad S > 0.9\text{m/s} \qquad (5.11)$$

$$S = 0.188 + 0.0131(\text{voltage}) + 0.0000667(\text{voltage})^2 \qquad S < 0.9\text{m/s} \qquad (5.12)$$

This correction factor was applied prior to the cosine correction procedures and tries to account for non-linear propeller response. It has the disadvantage, however, of producing a minimum wind speed of 0.188 m/s during periods when the propeller is not turning.

The cosine response correction factor and the low wind speed correction factor were programmed into the 21X datalogger. The 3 minute averages of wind speed, wind direction, standard deviations of wind components and the means of all the other parameters were obtained from the 21X programming efforts.

5.3.3 Sonic Temperature Correction

The estimates of the heat flux term $\overline{W'T'}$ were based on sonic anemometer temperature measurements. While the sonic anemometer (T_s) has the advantages of representing the same volume of air as the vertical velocity (W) measurement at the same sampling frequency, it can be contaminated by the wind component normal to the acoustic path (Kaimal 1969). The true temperature fluctuates T' can be written as a function of the sonic temperature fluctuation T_s'

$$T' = T_s' + \frac{2\overline{TU}}{\overline{C}^2} U' \qquad (5.13)$$

where $\overline{U}$ = average horizontal wind speed

$\overline{C}$ = speed of sound

U' = horizontal wind speed fluctuation

When temperature fluctuations are large (as in unstable conditions), then $\overline{T'} \approx \overline{T_s'}$ (and $\overline{W'T'} \approx \overline{W'T_s'}$). When the temperature fluctuations are small (as in very stable conditions), then $\overline{T'} < \overline{T_s'}$ (and $\overline{W'T'} < \overline{W'T_s'}$).

To evaluate the effects of using the sonic temperature rather than the true temperature fluctuation, both $\overline{W'T_s'}$ and $\overline{W'T'}$ were calculated using Equation 5.13 from the high frequency 10 and 25 m sonic anemometer wind and temperature data. Figure 5.10 shows the median difference $\overline{W'T_s'} - \overline{W'T'}$ as a function of wind speed and two observation heights. For high wind speeds, the departure from zero increases with further increases in wind speed.

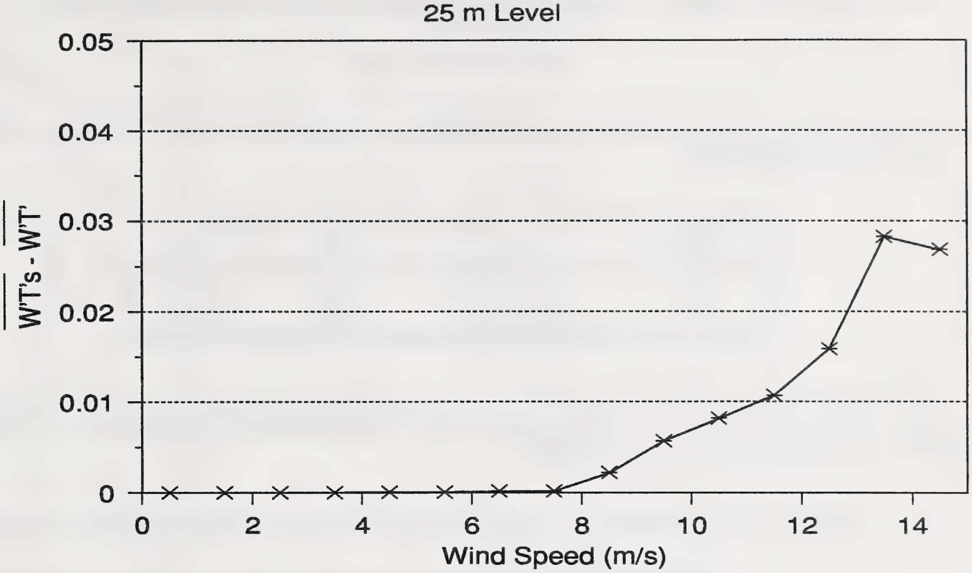

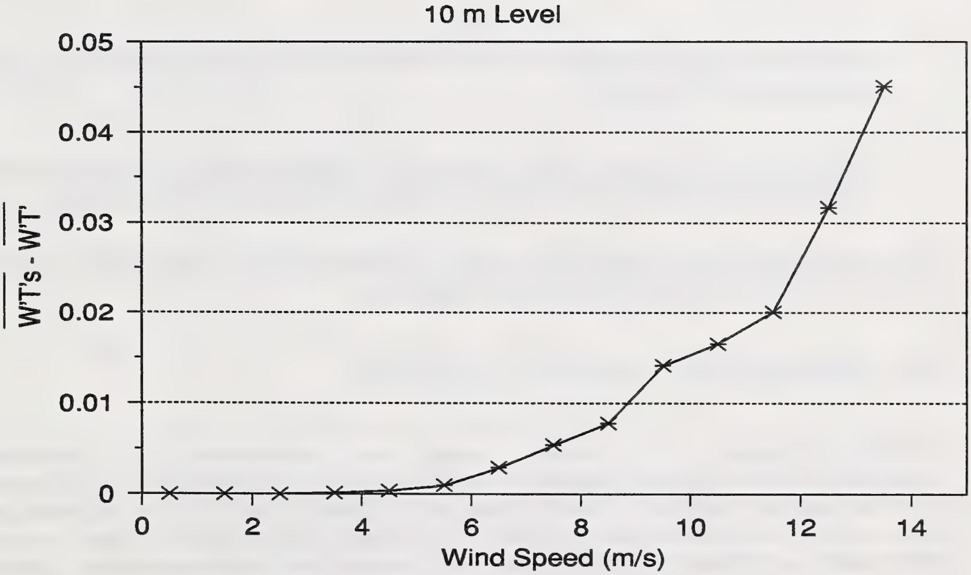

Figure 5.10

The Median Difference Between the Uncorrected ($\overline{W'T'_s}$) and the True ($\overline{W'T'}$) Heat Flux Term as a Function of Wind Speed.

The median curves shown in Figure 5.10 were fitted to the power law relationship:

$$\overline{W'T_s'} - \overline{W'T'} = aU^b \tag{5.14}$$

and a correlation coefficient providing a measure of goodness of fit was calculated. The results were found to be:

Level	a	b	R^2
10	$8.22 \bullet 10^{-7}$	4.208	0.9876
25	$9.04 \bullet 10^{-9}$	5.634	0.9604

As shown in Figure 5.11, the power law correction greatly reduced the median difference for the large wind speeds. Based on these results, the following corrections to the Field Measurement Program data were made:

- The 10 m level correction was applied only to the Kaijo Denki anemometer (10 m).
- The 25 m level correction was applied to the Applied Technologies anemometer (4, 16 and 25 m).
- Equation 5.14 was applied to all the 3-minute working level meteorology sonic anemometer $\overline{W'T'}$ values.
- For the meteorology data which were used to analyse the SF_6 tracer observations, concurrent high frequency data were available and Equation 5.13 was used.

While the corrections thus applied are not exact, they do nonetheless attempt to account for the cross-wind contamination of the sonic temperature.

5.3.4 Working-level 3-minute Average Data

Selected components of the 3-minute average sonic anemometer and conventional meteorological data files were merged to provide working level files which could be used for subsequent data analysis. Certain parameters in Tables 5.5 and 5.6 were redundant and were removed to facilitate data analysis. Co-ordinate transformations from the sonic anemometer co-ordinate systems to natural wind co-ordinates were undertaken. (Natural wind co-ordinates: U is along the direction of the wind; V is the cross-wind component ($\overline{V} \equiv 0$); and W is the vertical wind direction). In addition, selected atmospheric boundary layer parameters were calculated.

The format for the working-level 3-minute average meteorological data file is presented in Table 5.7. As with the quality-controlled data files, each file consists of 1440 records (3 day period) with 88 fields. Each field is separated by at least one blank character and all fields are represented by numeric characters only. Again, missing data are represented by "-99".

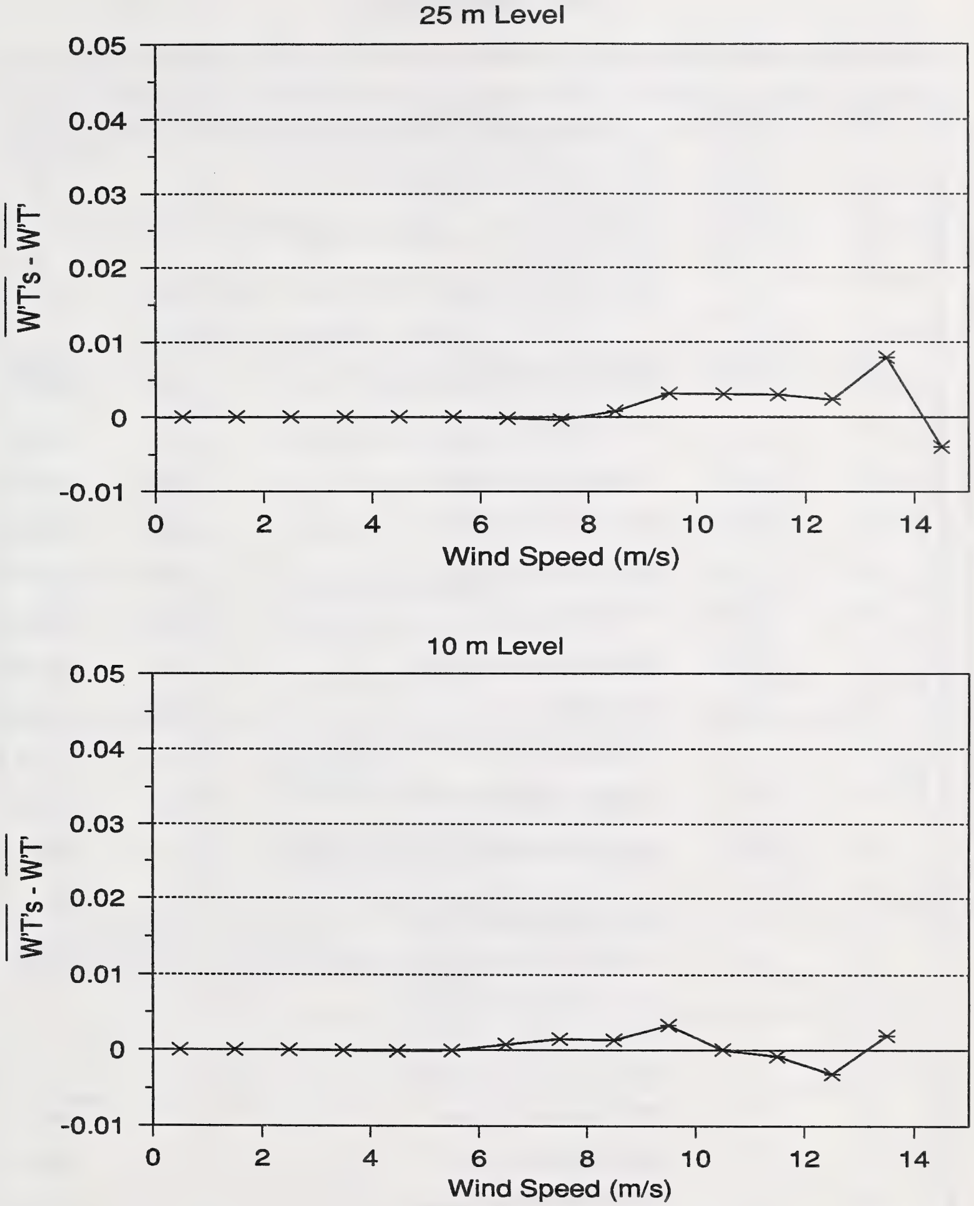

Figure 5.11

The Median Difference Between the Corrected ($\overline{W'T'_s}$) and the True ($\overline{W'T'}$) Heat Flux Term as a Function of Wind Speed.

Table 5.7

Working Level Meteorological Data File Format (3-minute and 30-minute average).

Field	Symbol	Description	Units	Format
1	*No*	Case		dddd
2	*MON*	Month (01 to 12)		dd
3	*DAY*	Day (01 to 31)		dd
4	*YR*	Year (88 to 89)		dd
5	*HH*	Hour (00 to 23)		dd
6	*MM*	Minute (00 to 59)		dd
7	θ_{CKD}	Correction angle (KD)	(°)	ddd.d
8	*COUNT*	Number of data points		ddddd
9	$\overline{S}$	4 m along-wind speed	(m/s)	ddd.dd
10	$\overline{\theta}$	4 m wind direction	(°)	ddd.d
11	$\overline{(U')^2}$	4 m along-wind variance	$(m/s)^2$	ddd.ddd
12	$\overline{(V')^2}$	4 m cross-wind variance	$(m/s)^2$	ddd.ddd
13	$\overline{(W')^2}$	4 m vertical wind variance	$(m/s)^2$	ddd.ddd
14	$\overline{W'T'}$	4 m heat flux product	(°C·m/s)	ddd.ddd
15	$\overline{U'W'}$	4 m momentum flux product	$(m/s)^2$	ddd.ddd
16	$\overline{H_o}$	4 m heat flux	(W/m^2)	ddddd.d
17	$\overline{U*}$	4 m friction velocity	(m/s)	dd.dd
18	$\overline{L}$	4 m Monin-Obukhov length	(m)	ddddd.d
19	$\overline{Z/L}$	4 m stability parameter		dd.dddd
20	σ_θ	4 m standard deviation of $\overline{\theta}$	(°)	ddd.d
21	σ_W	4 m standard deviation of $\overline{W}$	(m/s)	dd.ddd
22	σ_ϕ	4 m standard deviation of $\overline{\phi}$ or $\tan^{-1}(\sigma_W/\overline{S})$	(°)	dd.ddd
23 to 36		Same as 8 to 22 for 10 m level		
37 to 50		Same as 8 to 22 for 16 m level		
51 to 64		Same as 8 to 22 for 25 m level		
65	$\overline{R_f}$	Flux Richardson Number		ddd.dd
66	$\overline{R_b}$	Bulk Richardson Number		ddd.dd
67	$\overline{R_g}$	Gradient Richardson Number		ddd.dd
68	$\overline{S}$	25 m Gill UVW wind speed	(m/s)	ddd.dd
69	$\overline{\theta}$	25 m Gill UVW wind direction	$(m/s)^2$	ddd.d
70	σ_θ	25 m standard deviation of $\overline{\theta}$	$(m/s)^2$	ddd.d
71	σ_W	25 m standard deviation of $\overline{W}$	$(m/s)^2$	dd.ddd
72	σ_ϕ	25 m standard deviation of $\overline{\phi}$ or $\tan^{-1}(\sigma_W/\overline{S})$	(°)	dd.ddd

Continued ...

Table 5.7 (Continued)

Working Level Meteorological Data File Format (3-minute and 30-minute average).

73 to 77		Same as 68 to 72 for 10 m Gill UVW		
78	$\overline{T_{2R}}$	2 m thermister temperature	(°C)	ddd.d
79	$\overline{\Delta T(25-16)}$	Temperature difference (25 m - 16 m)	(°C)	dd.ddd
80	$\overline{\Delta T(16-10)}$	Temperature difference (16 m - 10 m)	(°C)	dd.ddd
81	$\overline{\Delta T(10-2)}$	Temperature difference (10 m - 2 m)	(°C)	dd.ddd
82	$\overline{I_{RAD}}$	Incoming radiation flux	(W/m^2)	dddd.d
83	$\overline{O_{RAD}}$	Outgoing radiation flux	(W/m^2)	dddd.d
84	$\overline{N_{RAD}}$	Net radiation flux	(W/m^2)	dddd.d
85	$\overline{S_{FLUX}}$	Soil heat flux	(W/m^2)	dddd.d
86	$\overline{P}$	Ground ambient pressure	(kPa)	ddd
87	$\overline{RH}$	2 m relative humidity	(%)	ddd
88	$\overline{\rho}$	2 m ambient air density	(kg/m^3)	dd.dd
89*	SC	Snow Cover Indicator (See note below) (Yes = 1; No = 0)		d
90*	$\overline{Z_I}$	Mixing Height (See note below)	(m)	dddd
91*	PG_S	Calgary Airport PG class	(1 to 6)	d
92*	PG_W	Site PG class (Williamson and Krenmayer)	(1 to 6)	d
93*	PG_B	Site PG class (Bowen *et al*)	(1 to 6)	d

The overbar denotes a time average.
* These values are in the 30-minute average files only.

Co-ordinate transformation for the sonic anemometer data were taken using the following relationships. The variances specifically were estimated using:

$$\sigma_U^2 = \overline{(U')^2} = \left[\left(\overline{U_m^2} - (\overline{U_m})^2\right)\right]\sin^2\overline{\theta} + \left[\left(\overline{V_m^2} - (\overline{V_m})^2\right)\right]\cos^2\overline{\theta} + 2[\overline{U_m V_m} - \overline{U_m}\,\overline{V_m}]\sin\overline{\theta}\cos\overline{\theta} \tag{5.15}$$

$$\sigma_V^2 = \overline{(V')^2} = \overline{V_m^2}\cos^2\overline{\theta} + \overline{U_m^2}\sin^2\overline{\theta} - 2\overline{U_m}\,\overline{V_m}\cos\overline{\theta}\sin\overline{\theta} \tag{5.16}$$

$$\sigma_W^2 = \overline{(W')^2} = \overline{W_m^2} - (\overline{W_m})^2 \tag{5.17}$$

The heat and momentum flux terms were estimated using:

$$\overline{W'T'} = \overline{W_m T} - \overline{W_m}\,\overline{T} \tag{5.18}$$

$$\overline{U'W'} = (\overline{U_m W_m} - \overline{U_m}\,\overline{W_m})\sin\overline{\theta} + (\overline{V_m W_m} - \overline{V_m}\,\overline{W_m})\cos\overline{\theta} \tag{5.19}$$

Boundary layer values were calculated from the following relationships. For example, the heat flux, H, is given by:

$$H = \rho C_p \overline{W'T'} \tag{5.20}$$

where: $C_p = 1003$ J/(kg K)
ρ = density of air (kg/m^3)

similarly the friction velocity, $\overline{U*}$, is given by:

$$\overline{U*} = [-\overline{U'W'}]^{1/2} \tag{5.21}$$

The Monin-Obukhov length, $\overline{L}$, is given by:

$$\overline{L} = -\frac{\overline{U*}^3\,\overline{T}}{\mathrm{kg}\,\overline{W'T'}} \tag{5.22}$$

The stability parameter, $\overline{Z/L}$, is given by:

$$\overline{Z/L} = Z/\overline{L} \tag{5.23}$$

where: Z = height of the measurement.

The standard deviation of the wind direction σ_θ is given by:

$$\sigma_\theta \approx \tan^{-1}\left(\frac{\sigma_V}{\overline{S}}\right) = \tan^{-1}\left[\frac{\sqrt{\overline{(V')^2}}}{\overline{S}}\right] \tag{5.24}$$

Similarly, the standard deviation of the vertical wind direction elevation angle is given by:

$$\sigma_\phi \approx \tan^{-1}\left(\frac{\sigma_W}{\overline{S}}\right) = \tan^{-1}\left[\frac{\sqrt{\overline{(W')^2}}}{\overline{S}}\right] \tag{5.25}$$

The Richardson Flux Number, R_f, is estimated from:

$$R_f = \left[\frac{g/\overline{T}}{(\partial U/\partial Z)}\right]\frac{\overline{W'T'}}{\overline{U'W'}} \tag{5.26}$$

where:

$$\frac{\partial U}{\partial Z} = \frac{\overline{U_{10}} - \overline{U_4}}{10-4}$$

The Bulk Richardson Flux Number (R_b) is estimated from:

$$R_b = \frac{g Z_1 Z_2}{\overline{T}\,\overline{U}^2}\frac{\partial\theta}{\partial Z} \tag{5.27}$$

where:

$$\frac{\partial\theta}{\partial Z} = \frac{\theta_{10} - \theta_2}{10-2}$$

The Richardson Gradient Number R_g is estimated from:

$$R_g = \frac{g}{T}\frac{(\partial\theta/\partial Z)}{(\partial U/\partial Z)^2} \tag{5.28}$$

where:

$$\frac{\partial\theta}{\partial Z} = \frac{1}{2}\left[\left(\frac{T_{10} - T_2}{10-2}\right) + \left(\frac{T_{16} - T_{10}}{16-10}\right)\right] - \Gamma$$

$$\frac{\partial U}{\partial Z} = \frac{1}{2}\left[\left(\frac{U_{10} - U_4}{10-4}\right) + \left(\frac{U_{16} - U_{10}}{16-10}\right)\right]$$

and Γ = dry adiabatic lapse rate = 0.0098 K/m.

The density of the air ρ (kg/m³) is given by:

and

$$\rho = \frac{\overline{P}10^{-3}MW}{TR_u} \tag{5.29}$$

where:
$\overline{P}$ = pressure (kPa)
MW = molecular mass (kg/kmol)
R_u = 8314 (J/(kmole K))
T = temperature (K)

For dry air $MW = 28.964$ kg/kmol

5.3.5 Working-level 30-minute Average Data

In addition, 30-minute average data files were constructed from the working-level 3-minute average data file. The format of the 30-minute average data files is nearly identical to the 3-minute average files (Table 5.7). Each 30-minute average data file consists of up to 1488 records (1 month) with 93 fields.

The sonic data were combined to produce 30-minute averages from the quality controlled sonic anemometer data (Table 5.5) using the following relationship:

$$\overline{U_m(30)} = \frac{\sum_{i=1}^{N} \text{Count}_i \cdot \overline{U_m(3)_i}}{\sum_{i=1}^{N} \text{Count}_i} \tag{5.30}$$

where N is the number of 3-minute averages available to form the 30-minute average ($N \leq 10$). Similar relationships to the above were used to form 30-minute averages of the means, variances, flux terms, cross products and derived boundary layer parameters (Fields 8 to 64 in Table 5.7).

For the conventional meteorological data, 30-minute averages of mean parameters were estimated using:

$$\overline{x(30)} = \frac{\sum_{i=1}^{N} x(3)_i}{N} \tag{5.31}$$

where x is one of the fields 65 to 88 (Table 5.7). The above averaging method, however, is not suitable for standard deviation values (Fields 70, 71, 72, 75, 76 and 77), in which case the following should be used:

$$\overline{\sigma_x(30)} = \left\{ \frac{\sum_{i=1}^{N} \overline{\sigma_x(3)}^2}{N} + \frac{\sum_{i=1}^{N} \{x_i(3) - \overline{x(30)}\}^2}{N} \right\}^{1/2} \tag{5.32}$$

The first term provides the contributions of high frequency fluctuations ($t < 3$ minutes) while the second term provides the contribution of low frequency fluctuations ($3 < t < 30$ minutes).

5.3.6 High-Frequency Sonic Anemometer Data

The three orthogonal wind speed components and the sonic temperature were written directly to the hard disk on the NEC 386 computer. Data storage requirements on the hard disk ranged from 1.03 Mb per hour of data collected for the 25 m sensor to 1.11 Mb per hour for the 10 m sensor. At the conclusion of the field test, the high frequency data files were backed up on a streaming tape drive. The tape was used again to transfer the data to the ERCB mainframe computer system via an IBM-PC with an identical tape backup unit.

5.4 Data Recovery

Table 5.8 presents the data recovery efficiency as a percentage for each of the meteorological sensors. During the winter period, the overall data recovery varied from 75 to 84%. The highest data recovery was associated with the Kaijo-Denki system. For the Applied Technologies systems, the highest data recoveries were associated with the lower sensors. This is probably due to a shorter cable length and easier access. Data recoveries for the three other sensors during the winter period were typically 85 to 90%.

For the summer period, the data recovery of the Applied Technologies 16 and 25 m systems decreased due to major periods of downtime in June and July. The instruments had to be removed and repaired because of a power supply problem. The 25 m UVW anemometer data recovery efficiency decreased with time. During the quality control of the data, it became apparent that the 25 m UVW sensor was underestimating the winds. This was probably due to problems with the transducers or bearings. For the other sensors, the data recoveries were similar to those observed during the winter season.

5.5 Surface Roughness Z_o

The logarithmic wind profile has generally been established as describing the vertical variation of wind speed with height. The vertical wind speed variation is dependent upon the surface roughness of the ground. A measure of the roughness of the ground is the aerodynamic surface roughness factor, Z_o, which is defined as the height where $\overline{U}$ goes to zero. It is usually determined from measured wind profiles and can be thought of representing the eddy size at the surface (Panofsky and Dutton 1984). Values of Z_o can vary from 0.01 cm over a smooth ice surface to several hundreds of cm over urban areas. The larger the value of Z_o, the more efficiently horizontal momentum is being transferred to the ground.

Table 5.8 Winter

Data Recovery Efficiency.

				Month			
	OCT	NOV	DEC	JAN	FEB	MAR	OVERALL WINTER
4 meter sonic anemometer							
mean terms	63.6	91.0	91.2	84.0	91.5	97.1	82.2
variance terms	62.1	89.4	89.3	82.3	88.4	94.2	80.2
flux terms	63.4	90.7	90.7	83.7	91.2	96.8	81.8
10 meter sonic anemometer							
mean terms	71.0	91.6	91.6	84.7	94.8	98.8	84.0
variance terms	70.6	91.3	91.1	84.3	94.1	98.4	83.6
flux terms	70.8	91.1	91.3	84.4	94.6	98.5	83.7
16 meter sonic anemometer							
mean terms	76.7	89.8	82.9	80.0	90.2	94.4	80.5
variance terms	76.1	89.3	82.9	80.3	89.2	94.0	80.2
flux terms	72.7	87.4	79.3	76.9	89.4	94.1	78.5
25 meter sonic anemometer							
mean terms	76.7	89.8	82.9	80.0	90.2	94.4	80.5
variance terms	72.7	89.6	87.6	78.9	87.9	56.4	74.0
flux terms	73.1	89.8	88.0	79.4	88.7	45.6	72.6
10 meter UVW anemometer							
mean terms	33.2	99.7	92.5	99.3	100.0	100.0	85.2
variance terms	33.2	99.7	92.6	99.3	100.0	100.0	85.2
25 meter UVW anemometer							
mean terms	33.2	99.7	92.6	99.2	100.0	100.0	85.2
variance terms	33.2	99.7	92.5	99.2	100.0	100.0	85.2
Temperature Profiles							
mean terms	70.7	99.7	92.0	99.2	100.0	100.0	88.9
Other meteorological variables							
Radiation	90.1	97.5	92.5	98.4	99.7	98.8	90.1
Soil heat flux	70.7	99.7	91.9	99.3	100.0	100.0	88.9
Pressure	47.6	99.0	100.0	91.9	91.4	99.4	85.0
Relative humidity	47.4	98.2	99.6	91.1	91.2	99.0	84.6
Density	46.8	98.9	99.9	91.7	91.3	99.4	84.9

Table 5.8 Summer

Data Recovery Efficiency.

	Month							
	APR	MAY	JUN	JUL	AUG	SEP	OCT	OVERALL SUMMER
4 meter sonic anemometer								
mean terms	88.7	66.2	62.4	78.7	73.8	93.3	96.6	79.5
variance terms	87.8	66.0	62.3	78.4	73.6	93.2	96.3	79.1
flux terms	88.0	66.0	62.3	78.4	73.6	93.2	96.6	79.2
10 meter sonic anemometer								
mean terms	93.7	86.0	94.5	88.9	77.2	99.2	99.3	91.0
variance terms	93.2	87.6	94.1	88.4	77.0	98.0	96.5	90.5
flux terms	94.0	87.8	94.4	88.8	77.3	98.9	98.4	91.1
16 meter sonic anemometer								
mean terms	92.9	46.9	6.3	0.0	70.1	91.7	95.7	57.7
variance terms	91.7	46.3	6.2	0.0	69.5	90.9	94.9	55.1
flux terms	92.8	46.9	6.2	0.0	69.3	91.4	95.6	55.5
25 meter sonic anemometer								
mean terms	56.5	22.8	15.9	1.6	49.6	96.2	97.6	46.5
variance terms	55.5	22.5	15.6	1.6	48.9	94.9	96.4	45.8
flux terms	56.1	21.8	15.6	1.5	49.4	94.9	97.1	46.0
10 meter UVW anemometer								
mean terms	92.9	68.9	72.5	87.6	98.4	95.5	94.3	87.0
variance terms	88.1	61.3	70.8	83.9	92.5	94.7	93.5	83.3
25 meter UVW anemometer								
mean terms	93.0	39.9	58.1	39.3	35.5	18.1	2.9	42.1
variance terms	91.5	39.3	60.1	39.7	35.6	18.5	2.9	42.2
Temperature Profiles								
mean terms	96.9	93.3	99.8	90.4	99.8	99.1	99.8	96.8
Other meteorological variables								
Radiation	95.8	90.3	96.0	88.3	97.5	98.0	99.3	94.8
Soil heat flux	97.1	93.3	99.8	90.5	93.6	99.3	100.0	96.0
Pressure	100.0	100.0	100.0	99.0	98.4	99.9	100.0	99.6
Relative humidity	99.3	99.3	98.7	20.9	84.3	91.6	99.6	83.5
Density	100.0	100.0	100.0	78.1	98.4	99.8	100.0	96.2

The roughness length is dependent upon the nature of the surface and on the height above the ground. Typically at low levels ($Z < 10$ m), the surface roughness is dependent upon the height of local (~ 100 m) ground cover. Above 10 m, nearby terrain irregularities can increase the roughness length. The nature of the ground cover can have a seasonal dependence. For example, during the winter, a smooth snow surface will have a smaller surface roughness ($Z_o \sim 0.2$ cm) than a mature crop during the summer ($Z_o \sim 5$ cm). Similarly it can depend on wind speed since the wind can change the nature of the surface (for example waves over water).

The surface roughness factor was calculated from the logarithmic wind profile relationship which was solved for Z_o:

$$\overline{U} = \frac{\overline{U^*}}{k} \ln\left(\frac{Z}{Z_o}\right) \tag{5.33}$$

where the friction velocity U^* was estimated from:

$$\overline{U^*} = (-\overline{U'W'})^{1/2} \tag{5.34}$$

where $k = 0.4$ (von Karman constant) and $\overline{U}$ is the mean wind speed at height Z. The above logarithmic profile is applicable to neutral atmospheric conditions. Three-minute average values for $\overline{U}$ and $\overline{U'W'}$ for periods when the wind speed $\overline{U}$ was greater than 5 m/s were used to estimate Z_o. In addition, wind data were excluded if the tower was upwind of the anemometer.

Table 5.9 shows the mean values for Z_o as a function of month, season and observation height. The results in the table indicate the following:

- The 4 m and 10 m Z_o values are similar (~ 0.5 cm for winter, ~ 2.8 cm for summer).
- The 16 m and 25 m Z_o values tend to be larger than those observed at the lower levels (16 m: 1.3 cm for winter; 4.3 cm for summer) (25 m: 1.7 cm for winter; 7.2 cm for summer).

There appears to be a tendency for Z_o to increase with increasing height above the ground.

The mean Z_o values given in Table 5.9 were plotted as a function of month for each observation height (Figure 5.12). The results indicate the following:

- The Z_o values are typically 1 to 2 cm when the surface is covered with crop stubble (Oct, Nov, Dec).
- During periods with snow cover, the Z_o values are in the 0.5 cm range (Jan, Feb, Mar).
- During the period following the snow cover, the Z_o values associated with the remaining stubble and newly growing crop is again in the 1 to 2 cm range (Apr, May, Jun).
- As the crop matured and increased in height (~ 1 m), the Z_o values are in the 6 to 10 cm range (Jul, Aug, Sep).

- The decrease in the Z_o value from August to September is associated with the swathing of the crop which took place on 23 August 1989.

The above measured surface roughness values are consistent with those reported in the literature (Panofsky and Dutton 1984):

• Cut grass (3 cm)	0.7 cm
• Fairly level grass plains	0.7 to 2 cm
• Uncut grass	2.5 cm
• Long grass (60 cm)	5 cm

According to the Alberta Environment (1988) surface roughness classification system, the site would range from roughness class 1 (Z_o = 1.0 cm) for "cultivated fields, young agricultural crops" to roughness class 2 (Z_o = 10 cm) for "mature agricultural crops".

Table 5.9

Surface Roughness Z_o (cm) as a Function of Month and Height.

	Anemometer Height (m)				
Month	4	10	16	25	Mean
Oct	1.2	0.9	1.7	6.0	3.0
Nov	1.3	0.9	2.4	2.4	1.9
Dec	0.9	0.7	1.6	1.2	1.1
Jan	0.1	0.1	0.5	0.1	0.3
Feb	0.3	0.2	1.2	1.5	0.9
Mar	0.2	0.2	0.4	0.7	0.4
Winter Mean	0.6	0.5	1.3	1.7	1.1
Apr	1.1	1.2	1.9	4.1	2.1
May	0.4	0.8	2.0	4.8	1.2
Jun	1.4	0.7	n/a	n/a	0.6
Jul	8.1	6.3	n/a	n/a	6.9
Aug	6.7	6.5	9.5	12.3	9.6
Sep	2.7	3.0	5.9	11.3	6.7
Summer Mean	2.9	2.8	4.3	7.2	4.2

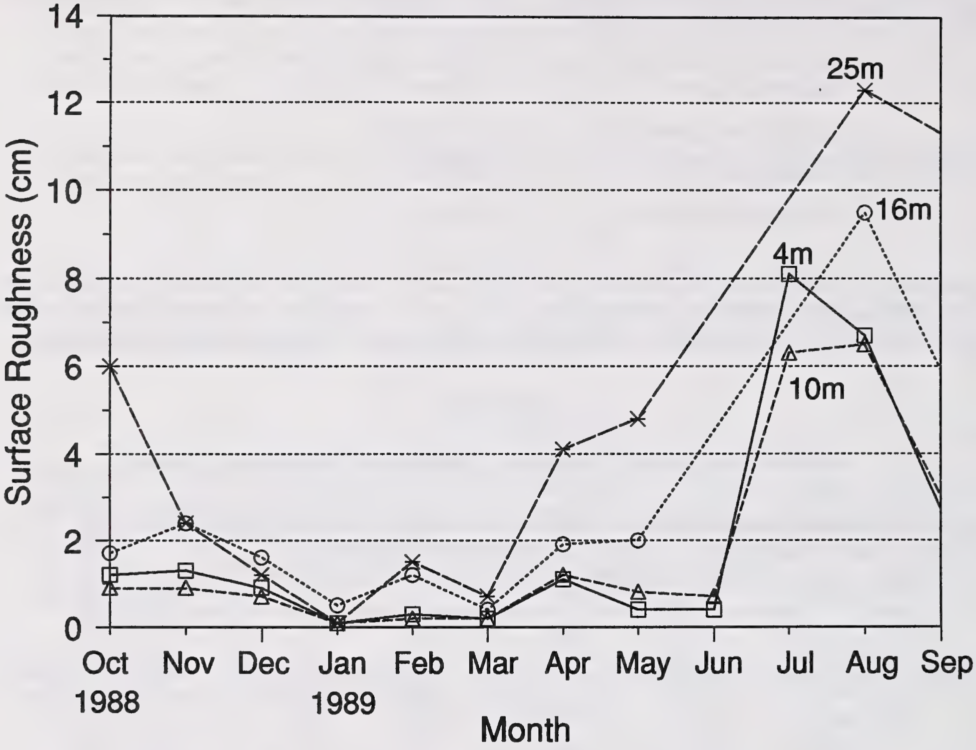

Figure 5.12

Mean Estimated Values for the Aerodynamic Surface Roughness as a Function of Time of Year.

6 DATA INTEGRATION

The hardware, data collection methodology and data reduction procedures for the three types of data collected during the Field Measurement Program have been discussed. Specifically, the three data types are comprised of:

- Tracer gas source data (Section 3)
- Tracer gas sampling data (Section 4)
- Concurrent meteorology data (Section 5).

To facilitate the interpretation and evaluation of these data, relevant portions of the data sets were integrated prior to the detailed assessment. This section of the report discusses the integration of these data sets, which can be viewed as a final step in the data reduction process.

6.1 Traverse Data

Traverse data were collected at pre-determined downwind distances of 700, 1400, and 2100 m. During the collection of these data, wind speeds averaged 3 m/s, with most of the values occurring between 1 and 5 m/s. The following table indicates the time for a plume from the source to be transported to the analyser:

Wind Speed (m/s)	Transport Time (minutes)		
	700 m	1400 m	2100 m
1	12	23	35
3	4	8	12
5	2	5	7

Compared to the 3-minute averaging period associated with the meteorological data, plume transport times for low wind speed cases (~ 1 m/s) can become significant. For the source data, which are relatively invariant with time, the transport time is less significant.

Each traverse has associated beginning (t_s) and end (t_f) times, from which an average time (t_a) for the traverse can be computed from:

$$t_a = t_s + \frac{t_f - t_s}{2} = \frac{t_f + t_s}{2} \tag{6.1}$$

For a symmetric distribution, this average time will correspond to the time of the peak concentration. The time to transport the SF_6 plume from the source to the sampling arc was estimated by integrating backwards in time using the 3-minute average wind speeds at 4 and 10 m. The integration was performed as a summation over 3-minute time blocks ($\Delta t = 180s$):

$$d = \sum_{i=1}^{n} \Delta t V_i \tag{6.2}$$

The summation starts with time block i in which t_a falls and ends with the time block in which distance d first exceeds the downwind distance (700, 1400 or 2100 m). The transport time is defined as $n\Delta t$ and all meteorological data were averaged over this period. The procedures for averaging meteorological means and variances were discussed in Section 5.3.5.

The number of time blocks over which the meteorological data were averaged is summarized in Table 6.1. The most frequent number of occurrences for the 700, 1400, and 2100 m distances are 2, 3, and 7 time periods respectively. These correspond to nominal transport times of 3 to 6, 6 to 9 and 18 to 21 minutes, respectively.

The SF_6 tracer gas release rates were relatively invariant with time. Abrupt release rate changes were primarily associated with source start-up and source shut-down. If source monitoring was re-initiated after a source shut-down, no observations were usually taken until the study area had been "flushed" by the wind. On a few occasions however, abrupt changes were made during a field test if the tracer gas analyser observations were not within the SF_6 analyser range. Sampling done during these transitional periods was not included in the data set.

Each traverse is represented by a single record consisting of 79 fields. The data can be broadly grouped into the following categories:

- Fields 1 to 12: Sampling identification, date and time.
- Fields 13 to 19: Sampling location and source conditions.
- Fields 20 to 34: Traverse statistics using the Moment, Hanna and Concentrations Maximum methods.
- Fields 35 to 40: Additional traverse statistics.
- Fields 41 to 55: Sonic anemometer data (4 m level).
- Fields 56 to 70: Sonic anemometer data (10 m level).
- Fields 71 to 79: Additional meteorological data.

This data file provided the basis for the traverse data assessment. The format of this file is given in Table 6.2.

6.2 Stationary Data

Stationary data were collected at the 700 and 1400 m downwind distances. As discussed in Section 5, 3-minute average SF_6 concentrations were obtained from these data. The meteorological and source data were corrected for each 3-minute period by using the corresponding transport time method which was described for the traverse data.

Each 3-minute period is represented by a single record consisting of 63 fields.

- Fields 1 to 12: Sampling identification, date and times.
- Fields 13 to 19 and 22 to 24: Sampling location and source conditions.
- Fields 20 and 21: Mean concentration, peak concentration.
- Fields 25 to 39: Sonic anemometer data (4 m level).
- Fields 40 to 54: Sonic anemometer data (10 m level).
- Fields 55 to 63: Additional meteorological data.

This data file provided the basis for the stationary data assessment. The format of this file is given in Table 6.3.

Table 6.1

Number of Time Blocks Which Meteorological Data Were Averaged Over to Reflect the Transport Time.

Number of 3-Minute Time Periods	Number of Occurrences 700 m	1400 m	2100 m
1 (3 minutes)	96	2	0
2	277	35	3
3	135	95	1
4	45	59	4
5 (15 minutes)	11	32	5
6	5	13	3
7	3	4	2
8	1	2	0
9	1	1	0
10 (30 minutes)	0	0	0
11	1	4	0
12	0	0	0
13	0	4	0
14	0	0	0
15 (45 minutes)	0	0	0
16	0	1	0
17	0	1	0
18	0	0	0
19	0	0	0
20 (60 minutes)	0	0	0
Total	552	279	18

Table 6.2

Integrated Traverse Data File Format.

Field	Variable	Unit
1	Field Test	1 to 33
2	Analyser[(a)]	1, 2 or 3
3	Traverse Number	
4	Month	10, 11 or 12
5	Day	1 to 31
6	Year	1988
7	Start Hour	0 to 23
8	Start Minute	0 to 59
9	Start Second	0 to 59
10	Finish Hour	0 to 23
11	Finish Minute	0 to 59
12	Finish Second	0 to 59
13	Arc Code[(b)]	1 to 5
14	Source Code[(c)]	1 to 5
15	Distance (m)	700, 1400 or 2100
16	Number of Time Intervals	
17	Release Height Code[(d)]	6 or 7
18	SF_6 Release Rate	(g/min)
19	Fan Velocity	(m/s)
	Moment Method	
20	Sigma y	(m)
21	Mean Absolute Percentage	
22	Mean Absolute Residual Concentration	(ppt)
23	Maximum Concentration	(ppt)
24	Centroid Position	(m)
25 to 29	Same as 20 to 24 for Hanna Method	
30 to 34	Same as 20 to 24 for Concentration Maximum Method	
35	Cross-wind Integrated Concentration	(ppt m)
36	Skewness	
37	Kurtosis	
38	Transport Angle	(degrees)
39	Easting Co-ordinate	(m)
40	Northing Co-ordinate	(m)
	4 m Sonic Data	
41	Counts	
42	Wind Speed	(m/s)
43	Wind Direction	(degrees)
44	$\overline{U'^2}$	$(m/s)^2$

Continued ...

Table 6.2 (Continued)

Integrated Traverse Data File Format

Field	Variable	Unit
	4 m Sonic Data	
45	$\overline{V'^2}$	$(m/s)^2$
46	$\overline{W'^2}$	$(m/s)^2$
47	$\overline{W'T'}$	(m K/s)
48	$\overline{U'W'}$	$(m/s)^2$
49	H_o	(W/m^2)
50	$U*$	(m/s)
51	L	(m)
52	Z/L	
53	σ_θ	(degrees)
54	σ_W	(m/s)
55	σ_ϕ	(degrees)
56 to 70	Same as 41 to 55 for 10 m Sonic Data	
71	Ambient Temperature	(°C)
72	$T_{25} - T_{16}$	(°C)
73	$T_{16} - T_{10}$	(°C)
74	$T_{10} - T_2$	(°C)
75	Incoming Radiation	(W/m^2)
76	Outgoing Radiation	(W/m^2)
77	Net Radiation	(W/m^2)
78	Soil Heat Flux	(W/m^2)
79	Mixing Height	(m)

(a) Analyser Code
1 = Analyser A
2 = Analyser B
3 = Analyser C

(b) Arc Code
1 = Centre Sampling Circle
2 = North Sampling Arcs
3 = East Sampling Arcs
4 = South Sampling Arcs
5 = West Sampling Arcs

(c) Source Code
1 = Centre Source Location
2 = North Source Location
3 = East Source Location
4 = South Source Location
5 = West Source Location

(d) Release Height Code
6 = Surface Release
7 = Elevated Release

Table 6.3

Integrated Stationary Data File Format.

Field	Variable	Unit
1	Field Test	1 to 33
2	Analyser[(a)]	1, 2 or 3
3	Traverse Number	
4	Month	10, 11 or 12
5	Day	1 to 31
6	Year	1988
7	Start Hour	0 to 23
8	Start Minute	0 to 59
9	Start Second	0 to 59
10	Finish Hour	0 to 23
11	Finish Minute	0 to 59
12	Finish Second	0 to 59
13	Arc Code[(b)]	1 to 5
14	Source Code[(c)]	1 to 5
15	Distance (m)	700, 1400 or 2100
16	Number of Time Intervals	
17	Release Height Code[(d)]	0 or 1
18	SF_6 Release Rate	(g/min)
19	Fan Velocity	(m/s)
20	Mean SF_6 Concentration	(ppt)
21	Peak SF_6 Concentration	(ppt)
22	Northing Co-ordinate	(m)
23	Easting Co-ordinate	(m)
24	Transport Angle	(degrees)
	4 m Sonic Data	
25	Counts	
26	Wind Speed	(m/s)
27	Wind Direction	(degrees)
28	$\overline{U'^2}$	$(m/s)^2$
29	$\overline{V'^2}$	$(m/s)^2$
30	$\overline{W'^2}$	$(m/s)^2$
31	$\overline{W'T'}$	(m K/s)
32	$\overline{U'W'}$	$(m/s)^2$
33	H_o	(W/m^2)
34	$U*$	(m/s)
35	L	(m)
36	Z/L	
37	σ_θ	(degrees)
38	σ_W	(m/s)
39	σ_ϕ	(degrees)

Continued ...

Table 6.3 (Continued)

Integrated Stationary Data File Format.

Field	Variable	Unit
40 to 54	Same as 25 to 39 for 10 m Sonic Data	
55	Ambient Temperature at 2 m	(°C)
56	T_{25} - T_{16}	(°C)
57	T_{16} - T_{10}	(°C)
58	T_{10} - T_2	(°C)
59	Incoming Radiation	(W/m^2)
60	Outgoing Radiation	(W/m^2)
61	Net Radiation	(W/m^2)
62	Soil Heat Flux	(W/m^2)
63	Mixing Height	(m)

(a) Analyser Code
1 = Analyser A
2 = Analyser B
3 = Analyser C

(b) Arc Code
1 = Centre Sampling Circle
2 = North Sampling Arcs
3 = East Sampling Arcs
4 = South Sampling Arcs
5 = West Sampling Arcs

(c) Source Code
1 = Centre Source Location
2 = North Source Location
3 = East Source Location
4 = South Source Location
5 = West Source Location

(d) Release Height Code
0 = Surface Release
1 = Elevated Release

6.3 Traverse Data Summary

As indicated in Sections 3.3 and 3.5, field tests were conducted over the period 18 October to 22 December 1988. The observed traverse and stationary data from field tests 2 to 33 were analyzed since the first test was conducted to determine field procedures.

In total, 846 traverses through the plume were obtained at sampling distances of 700, 1 400 and 2 100 m. These were associated with both elevated and surface SF_6 releases.

The ratio of the observed SF_6 concentration (χ) divided by the SF_6 emission rate (Q) is referred to as the normalized SF_6 concentration. For the purposes of the Field Measurement Program, the dimensions of the χ/Q ratio are ppt/(g/min). The normalized concentration is a measure of the relative dilution in the atmosphere and allows individual plume traverses from one test to be compared to another test when the SF_6 emission rates may vary. Large χ/Q values are associated with small dilution and small χ/Q values are associated with large dilution.

The following table indicates the extreme values and the central tendencies for the χ/Q values observed during the Field Measurement Program. The values were based on 846 individual traverses and the χ values were taken as the peak concentration observed during the individual traverses.

χ/Q (ppt/(g/min))

Elevated Releases	700 m	1 400 m	2 100 m
Minimum	8	2	8
Mean	233	206	78
Maximum	1 447	1 673	361
5 Percentile	11	7	8
Median	171	128	44
95 Percentile	1 079	690	361
Number	262	220	18

χ/Q (ppt/(g/min))

Surface Releases	700 m	1 400 m	2 100 m
Minimum	45	7	-
Mean	2 825	1 210	-
Maximum	11 398	4 363	-
5 Percentile	103	7	-
Median	2 472	378	-
95 Percentile	8 981	4 363	-
Number	313	33	0

The largest χ/Q values were associated with surface releases and observations at 700 m. These values were about 10 times larger than those associated with elevated measures.

6.3.1 Worst Case Meteorological Conditions

As the majority of the traverses were associated with 700 m distances (elevated and surface releases) and 1 400 m distances (elevated releases only), these three cases were examined in more detail to identify the meteorological conditions which were associated with the 20 largest χ/Q values in each class. The results are presented in Tables 6.4, 6.5 and 6.6. Specifically, the meteorological conditions in the table include the 10 m level wind speed (U_{10}), heat flux at 10 m (H_o), the temperature gradient from the 10 and 2 m levels ($\partial T/\partial Z$), the Monin-Obukhov stability parameter (Z/L), lateral absolute (σ_v) and relative (σ_θ) turbulence intensity measurements, and the vertical absolute (σ_w) and relative (σ_ϕ) turbulence intensity measurements. The derived cross-wind spread of the plume (σ_{yi}) as determined from the second Moment Method is also shown.

For the 700 m traverses associated with elevated releases (Table 6.4), the following points are noted for the 20 largest χ/Q values:

- Sixteen of the 20 largest χ/Q values occurred during Test 15 which was conducted on 26 November 1988.
- The average plume width (σ_{yi}) was 14.6 m with an observed range from 10.3 to 22.7 m.
- The average 10 m level wind speed (U_{10}) was 3.8 m/s with an observed range from 1.7 to 5.1 m/s.
- The average 10 to 2 m temperature gradient ($\partial T/\partial Z$) was 0.19 K/m.
- The average lateral temperature intensity (σ_θ) was 3.4 degrees with an observed range for 1.4 to 14.9 degrees. The second largest(σ_θ) value was 3.9 degrees.
- The average vertical turbulence intensity (σ_ϕ) was 2.2 degrees with an observed range from 0.7 to 10.3 degrees. The second largest(σ_ϕ) value was 2.5 degrees.

For the 1 400 m traverses associated with elevated releases (Table 6.5, the following points are noted for the 20 largest χ/Q values:

- Nine of the 20 largest χ/Q values occurred during Test 15 which was conducted on 26 November 1988.
- The average plume width (σ_{yi}) was 28.1 m with an observed range from 15.1 to 45.1 m.
- The average 10 m level wind speed (U_{10}) was 3.9 m/s with an observed range from 3.0 to 5.6 m.

Table 6.4

Summary of the 20 largest χ/Q Values Observed at 700 m and Associated with Elevated Releases.

Rank	Test	Date	Start Time	End Time	χ/Q ppt/(g/min)	σ_{yi} (m)	U_{10} (m/s)	Heat$_{10}$ (W/m^2)	$\frac{\partial T}{\partial Z}$ (K/m)	Z/L	σ_V (m/s)	σ_θ (degrees)	σ_W (m/s)	σ_ϕ (degrees)
1	15	26-Nov-88	21:41:54	21:43:24	1447	12.7	3.9	-16.4	0.207	1.47	0.18	2.68	0.112	1.66
2	15	26-Nov-88	22:57:39	22:59:09	1150	14.6	3.9	-13.4	0.106	6.06	0.20	2.93	0.152	2.23
3	15	26-Nov-88	22:04:28	22:05:48	1140	12.4	4.0	-7.3	0.182	4.63	0.23	3.39	0.178	2.58
4	15	26-Nov-88	21:23:08	21:25:53	1096	18.9	3.1	2.8	0.253	---	0.17	3.21	0.669	1.23
5	15	26-Nov-88	21:53:16	21:54:41	1093	10.9	3.8	-9.0	0.177	100.00	0.21	3.10	0.150	2.25
6	6	31-Oct-88	22:49:37	22:52:17	1092	22.7	1.7	-15.9	0.258	---	0.44	14.90	0.302	10.33
7	15	26-Nov-88	23:08:26	23:09:51	1079	13.0	3.9	-5.8	0.144	1.72	0.10	1.39	0.108	1.57
8	15	26-Nov-88	21:58:40	22:00-00	1061	10.3	3.6	-12.9	0.180	0.43	0.14	2.25	0.100	1.58
9	15	26-Nov-88	22:51:48	22:53:13	1044	14.9	4.2	-9.5	0.117	---	0.21	2.96	0.171	2.36
10	15	26-Nov-88	22:43:12	22:44:42	879	15.3	4.0	-11.1	0.127	5.28	0.20	2.84	0.145	2.05
11	15	26-Nov-88	23:26:49	23:28:19	788	15.1	4.0	-10.4	0.205	3.72	0.12	1.70	0.089	1.27
12	15	26-Nov-88	23:20:47	23:22:07	778	13.0	4.2	-1.8	0.211	0.12	0.14	1.84	0.539	0.73
13	15	26-Nov-88	23:02:02	23:03:27	720	13.3	3.7	-9.3	0.110	4.11	0.23	3.50	0.142	2.18
14	15	26-Nov-88	22:14:28	22:15:53	715	14.2	3.7	-9.3	0.143	3.78	0.25	3.91	0.114	1.77
15	15	26-Nov-88	22:25:52	22:27:31	705	12.5	3.5	-10.0	0.159	17.91	0.19	3.16	0.155	2.54
16	6	31-Oct-88	23:15:26	23:16:56	695	18.2	4.3	-14.5	0.241	---	0.28	3.74	0.109	1.46
17	7	07-Nov-88	20:45:02	20:46:52	668	15.9	5.1	-17.5	0.260	0.63	0.28	3.16	0.155	1.74
18	15	26-Nov-88	23:32:25	23:34:05	624	17.6	3.8	-4.5	0.242	---	0.13	1.87	0.581	0.87
19	5	28-Nov-88	21:45:21	21:45:21	621	10.8	3.7	---	0.093	0.65	0.18	2.82	0.141	2.17
20	15	26-Nov-88	21:34:18	21:34:18	606	16.6	3.6	-3.0	0.303	2.82	0.13	2.06	0.084	1.33

Table 6.5

Summary of the 20 largest χ/Q Values Observed at 1 400 m and Associated with Elevated Releases.

Rank	Test	Date	Start	End	χ/Q	σ_{yi}	U_{10}	Heat_{10}	$\frac{\partial T}{\partial Z}$	Z/L	σ_v	σ_θ	σ_w	σ_ϕ
			Time	Time	ppt/(g/min)	(m)	(m/s)	(W/m^2)	(K/m)		(m/s)	(degrees)	(m/s)	(degrees)
1	15	26-Nov-88	21:28:33	21:31:33	1673	34.1	3.3	-0.9	0.289	---	0.19	3.26	0.616	1.05
2	15	26-Nov-88	21:27:56	21:30:01	1471	34.1	3.2	1.2	0.269	---	0.24	4.33	0.059	1.05
3	3	25-Oct-88	01:56:29	01:59:17	843	15.1	3.9	-7.8	0.198	2.76	0.13	1.93	0.087	1.28
4	3	25-Oct-88	02:06:38	02:09:04	737	21.6	3.9	-6.1	0.194	4.23	0.21	3.07	0.097	1.44
5	15	26-Nov-88	23:17:43	23:20:23	699	23.5	4.2	-5.8	0.186	---	0.12	1.64	0.095	1.28
6	9	14-Nov-88	19:01:28	19:04:28	690	29.7	3.2	-9.8	0.062	0.72	0.22	3.93	0.189	3.38
7	7	07-Nov-88	20:52:23	20:57:23	677	23.3	5.1	-37.3	0.215	20.21	0.53	5.94	0.156	1.75
8	15	26-Nov-88	23:08:47	23:11:17	662	21.1	3.9	-7.4	0.140	1.30	0.14	1.98	0.104	1.53
9	7	07-Nov-88	20:28:56	20:30:11	640	18.1	5.6	-4.2	0.353	---	0.25	2.57	0.089	0.92
10	3	25-Oct-88	00:31:19	00:34:45	634	37.0	3.6	0.5	0.421	---	0.13	2.05	0.034	0.54
11	15	26-Nov-88	21:40:18	21:43:18	625	35.6	4.1	-6.6	0.256	2.14	0.17	2.43	0.119	1.68
12	9	14-Nov-88	18:51:00	18:54:20	611	37.4	3.0	-7.7	0.075	0.28	0.23	4.34	0.194	3.67
13	15	26-Nov-88	22:00:57	22:03:47	597	25.8	3.9	-6.6	0.192	0.45	0.23	3.41	0.128	1.88
14	15	26-Nov-88	23:02:26	23:04:06	588	23.3	3.8	-10.0	0.115	5.92	0.23	3.45	0.141	2.15
15	9	14-Nov-88	18:56:40	18:59:20	580	25.9	3.1	-11.1	0.069	0.48	0.25	4.48	0.205	3.74
16	9	14-Nov-88	18:42:58	18:48:18	554	45.1	3.1	-7.9	0.085	0.49	0.27	4.91	0.178	3.28
17	7	07-Nov-88	20:46:20	20:48:40	551	24.2	5.2	-13.8	0.274	2.45	0.25	2.82	0.147	1.63
18	15	26-Nov-88	21:54:34	21:57:44	526	28.7	3.7	-12.2	0.174	3.55	0.27	4.22	0.137	2.11
19	3	25-Oct-88	02:09:42	02:12:51	518	31.3	3.8	-8.8	0.202	---	0.25	3.82	0.105	1.60
20	15	26-Nov-88	22:06:52	22:09:17	512	27.8	3.7	-10.1	0.169	2.01	0.29	4.48	0.183	2.81

Table 6.6

Summary of the 20 largest χ/Q Values Observed at 700 m and Associated with Surface Releases.

Rank	Test	Date	Start Time	End Time	χ/Q ppt/(g/min)	σ_{yi} (m)	U_{10} (m/s)	Heat$_{10}$ (W/m^2)	$\frac{\partial T}{\partial Z}$ (K/m)	Z/L	σ_V (m/s)	σ_θ (degrees)	σ_W (m/s)	σ_ϕ (degrees)
1	11	16-Nov-88	21:20:40	21:22:00	11 398	14.2	2.6	-1.3	0.642	2.14	0.14	2.97	0.446	0.97
2	31	20-Dec-88	18:49:32	18:52:47	11 232	25.8	2.9	127.9	0.527	---	0.25	4.90	0.169	3.36
3	31	20-Dec-88	00:37:26	00:45:06	11 116	15.7	3.5	-11.7	0.312	0.42	0.32	5.29	0.181	2.99
4	25	14-Dec-88	18:05:15	18:06:15	10 833	8.5	2.6	-0.1	0.857	---	0.11	2.36	0.058	1.31
5	15	26-Nov-88	18:19:07	18:21:07	10 415	11.4	1.3	-0.3	1.026	0.34	0.12	5.46	0.029	1.27
6	30	19-Dec-88	18:21:32	18:23:08	10 205	14.1	4.7	-19.0	0.188	10.23	0.19	2.32	0.146	1.79
7	30	19-Dec-88	18:17:15	18:18:45	9 324	10.3	4.6	-16.9	0.192	10.08	0.18	2.20	0.137	1.69
8	15	26-Nov-88	18:24:35	18:26:20	8 981	16.3	1.3	-0.2	1.028	0.25	0.11	4.69	0.029	1.28
9	15	26-Nov-88	18:06:50	18:09:05	8 944	14.1	1.0	-0.6	1.025	---	0.12	6.67	0.039	2.14
10	11	16-Nov-88	22:26:23	22:29:33	8 782	21.2	3.0	-1.9	0.564	---	0.18	3.39	0.069	1.32
11	15	26-Nov-88	18:41:08	18:42:28	8 445	10.3	2.2	-2.3	0.953	4.40	0.19	4.86	0.044	1.15
12	15	26-Nov-88	18:13:14	18:15:14	8 387	14.9	1.1	-0.8	1.051	---	0.22	11.80	0.022	1.21
13	15	26-Nov-88	19:02:04	19:03:44	7 842	9.7	2.6	0.1	0.841	-0.04	0.17	3.70	0.056	1.25
14	11	16-Nov-88	21:55:40	22:01:20	7 614	26.9	2.4	-0.8	0.684	---	0.14	3.40	0.038	0.93
15	15	26-Nov-88	19:48:21	19:50:31	7 458	20.1	3.0	-1.0	0.672	---	0.19	3.67	0.073	1.42
16	27	16-Dec-88	19:16:52	19:18:17	7 179	13.6	2.9	-8.6	0.742	3.62	0.29	5.65	0.086	1.68
17	30	19-Dec-88	17:55:01	17:56:31	7 133	12.9	4.2	-8.5	0.371	5.62	0.21	2.86	0.089	1.22
18	11	16-Nov-88	21:14:36	21:16:16	7 114	26.9	2.5	-1.4	0.662	56.89	0.14	3.22	0.048	1.09
19	30	19-Dec-88	17:44:36	17:45:56	6 781	13.2	4.8	-10.3	0.270	13.57	0.21	2.49	0.065	0.78
20	13	20-Nov-88	18:31:08	18:39:28	6 779	58.9	0.3	-0.2	0.517	0.12	0.22	32.82	0.051	8.74

- The average 10 to 2 m temperature gradient ($\partial T/\partial Z$) was 0.20 K/m.

- The average lateral turbulence intensity (σ_θ) was 3.5 degrees with an observed range from 1.6 to 5.9 degrees.

- The average vertical turbulence intensity (σ_ϕ) was 1.9 degrees with an observed range from 0.5 to 3.7 degrees.

The meteorological conditions associated with these 1 400 m traverses (Table 6.5) are similar to those associated with the 200 m elevated traverses (Table 6.4). The average plume width between 700 and 1 400 m increased from 14.6 to 28.1. The χ/Q values at 700 and 1 400 m were similar (from about 560 to 1 560 ppt/(g/min)).

For the 700 m traverses associated with surface releases (Table 6.6), the following points are noted for the 20 largest χ/Q values:

- Seven of the 20 largest χ/Q values occurred during Test 15 which was conducted on 26 November 1988.

- The average plume width (σ_{yi}) was 17.9 m with an observed range from 8.5 to 58.9 m.

- The average 10 m level wind speed (U_{10}) was 3.9 m/s with an observed range from 0.3 to 4.8 m/s.

- The average 10 to 2 m temperature gradient ($\partial T/\partial Z$) was 0.66 K/m.

- The average lateral turbulence intensity (σ_θ) was 5.7 degrees with an observed range from 2.2 to 32.8 degrees.

- The average vertical turbulence intensity (σ_ϕ) was 1.9 degrees with an observed range from 0.8 to 8.7 degrees.

Again, the meteorological conditions associated with the χ/Q values listed in Table 6.6 are similar to those associated with the elevated releases (Tables 6.4 and 6.5). The average 700 m surface release plume width of 18.0 metres is about 20% greater than that associated with elevated releases at 700 m (14.6 m). The χ/Q values associated with the surface releases were almost 10 times those associated with the elevated releases.

In summary, the largest normalized plume centreline concentrations were associated with:

- Surface releases.

- Mean 10 m level wind speeds of 3.8 to 3.9 m/s for elevated releases and 10 m level wind speed of 2.7 m/s for surface releases.

- Mean 10 to 2 m level temperature gradients of 0.2 K/m for elevated releases and 0.7 K/m for surface releases.

- Mean (σ_θ) values of 3.3 to 3.4 degrees for elevated releases and 5.7 degrees for surface releases.

- Mean (σ_ϕ) values of 1.9 to 2.2 degrees of elevated releases and surface releases.

The meteorological conditions can be referred to as the "worst case" meteorological conditions in the sense they were associated with the largest χ/Q values.

6.3.2 Individual Field Test Summary

Tables 6.7 and 6.8 present an overall summary on a field test basis of the range of wind speed values observed during each traverse and the range of χ/Q values observed during each test. The summary results have been classified according to source type (elevated or surface) and according to downwind distance (700, 1 400 or 2 100 m). The time of the field tests and corresponding source conditions are documented in Tables 6.4 and 6.5.

Table 6.7 presents the results for the elevated releases. It is clear that Test 15 leads to the largest χ/Q values and was associated with mean wind speeds of 3.8 to 3.9 m/s. Test 14 was associated with a mean wind speed of less than 2 m/s. The χ/Q values for Test 14 (based on only 3 traverses) are about 20 times less than that for Test 15.

Table 6.8 presents the results for the surface releases. The tests with the largest χ/Q values are Tests 30 (7984), 25 (5874) and 15 (4786). The corresponding average 10 m level wind speeds for these tests are 4.7, 3.3 and 2.6 m/s, respectively. Tests 32 and 33 were associated with mean 10 m level wind speeds less than 2 m/s. The χ/Q values for these tests (279 and 142) are about 30 times less than those associated with Tests 30, 25 and 15.

Table 6.7

Summary of the Range of Values of χ/Q and Wind Speed During the Individual Field Tests for Elevated Releases.

Field Test	No. of Traverses	Distance (m)	χ/Q (ppt/(g/min)) Mimimum	Mean	Maximum	U_{10} (m/s) Minimum	Mean	Maximum
2	21	700	11	45	179	2.1	2.9	4.2
2	13	1 400	2	37	94	2.1	2.9	4.0
3	0	700	---	---	---	---	---	-
3	21	1 400	3	240	843	0.9	3.3	3.9
4	14	700	26	121	298	2.3	2.8	3.4
4	18	1 400	21	162	438	2.3	2.9	3.5
5	13	700	127	283	621	3.6	3.9	4.4
5	3	1 400	363	401	442	3.6	3.8	4.0
6	6	700	59	572	1 092	1.7	2.5	4.3
6	9	1 400	15	171	496	1.3	2.6	4.0
7	11	700	135	333	668	4.6	5.0	5.4
7	12	1 400	51	342	677	4.6	5.1	5.6
8	3	700	51	207	315	2.6	2.9	3.1
8	7	1 400	7	102	458	2.5	3.0	3.4
9	22	700	42	204	343	3.1	4.4	7.1
9	21	1 400	53	284	690	3.0	4.4	8.2
9	4	2 100	9	35	60	5.7	6.4	7.1
10	16	700	10	80	366	1.7	2.6	3.9
10	17	1 400	10	91	291	1.8	2.7	3.9
11	11	700	14	151	582	1.3	2.1	2.8
11	9	1 400	13	109	372	1.3	2.1	2.8
12	13	700	12	105	290	1.4	2.1	2.9
12	31	1 400	4	88	394	1.6	2.4	3.6
12	14	2 100	8	90	361	1.9	2.6	3.4
14	1	700	62	62	62	1.7	1.7	1.7
14	2	1 400	7	23	38	1.1	1.4	1.7
15	20	700	412	849	1 447	3.1	3.8	4.2
15	16	1 400	383	656	1 673	3.2	3.9	4.3
16	39	700	9	182	545	0.1	3.0	4.6
16	9	1 400	24	133	487	0.3	2.0	3.2
17	46	700	57	204	416	1.6	2.4	4.9
17	30	1 400	40	189	426	1.7	2.2	3.5
18	25	700	8	170	603	0.8	3.3	5.2
18	2	1 400	22	40	57	1.2	1.5	1.9

Table 6.8

Summary of the Range of Values of χ/Q and Wind Speed During the Individual Field Tests for Surface Releases.

Field Test	No. of Traverses	Distance (m)	χ/Q (ppt/(g/min)) Mimimum	Mean	Maximum	U_{10} (m/s) Minimum	Mean	Maximum
3	2	1 400	7	9	10	3.1	3.4	3.8
4	18	700	224	2 617	5 061	1.6	2.3	3.1
4	8	1 400	122	1 240	2 847	1.8	2.2	3.0
11	9	700	107	4 396	11 398	0.9	2.3	3.0
11	18	1 400	18	1 593	4 363	0.6	1.9	3.0
13	45	700	53	2 633	6 779	0.3	2.3	3.8
15	41	700	62	4 786	10 415	0.6	2.6	3.5
19	24	700	49	2 927	6 356	1.7	3.4	4.6
19	5	1 400	56	345	720	1.9	2.8	3.3
20	45	700	103	2 316	4 8097	0.9	3.1	4.7
21	27	700	1 162	2 613	4 580	4.0	4.5	5.1
22	11	700	258	437	820	4.7	6.5	7.9
23	14	700	133	855	1 579	4.9	6.8	9.7
24	14	700	194	839	2 489	1.7	5.4	8.3
25	8	700	3 593	5 874	10 833	2.3	3.3	4.0
26	10	700	1 152	1 841	2 612	4.4	5.3	5.6
27	16	700	1 598	3 261	7 179	2.7	4.6	5.5
29	6	700	427	1 575	2 557	1.7	2.3	3.1
30	6	700	6 479	7 985	10 205	4.2	4.7	5.2
31	8	700	531	4 316	11 232	2.3	2.7	3.5
32	4	700	176	279	380	0.4	1.0	1.4
33	7	700	45	142	317	0.7	1.2	1.7

7 TRACER GAS ASSESSMENT

This preliminary analysis of the tracer gas assessment is based on the 846 SF_6 plume traverse profiles and on the 439 one-half hour stationary SF_6 concentrations.

7.1 Traverse Data

For the purposes of assessment, the traverse data were grouped according to source type (elevated or ground) and downwind distance (700, 1400 or 2100 m). The number of individual traverses that fall into each group are summarized below:

Frequency of Occurrence

Source Type	Distance (m)			Total
	700	1400	2100	
Elevated Surface	262 (31%) 313 (37%)	220 (26%) 33 (4%)	18 (2%) 0 (0%)	500 (59%) 346 (41%)
Total	575 (68%)	253 (30%)	18 (2%)	846 (100%)

Most of the traverses are associated with the 700 m distance (68%) and elevated (59%) sources.

Volume 2 presents basic statistics associated with each of the 846 traverses. Plots of the actual concentration profiles and corresponding fitted Gaussian profiles (based on the Moment method) for each of the traverses are also presented in Volume 2.

The traverse data were analysed with respect to the following:

- Assessment of Gaussian plume approximation,
- Comparison of alternate methods for calculating crosswind plume spreads (σ_{y_i}),
- Identification of concurrent meteorological conditions,
- Evaluation of instantaneous plume spreads (σ_{y_i}),
- Evaluation of time-averaged plume spreads (σ_{y_c}), and
- Comparison of predicted and observed centreline concentrations.

The results of these analyses are presented in the following sections.

7.1.1 Gaussian Plume Approximation

The Gaussian plume dispersion model approximation assumes that the crosswind and vertical plume concentration profiles have a normal or a Gaussian probability distribution. The peak concentration is defined by the plume centreline, with the concentrations decreasing to zero with increasing distance from either side from the centreline. The standard deviation of the crosswind component (σ_y) can be calculated from the tracer traverse profiles.

As described in Section 4, the Moment method was one of three techniques used to fit Gaussian distributions to the observed concentration profiles. Sample observed crosswind profiles are shown in Figures 7.1 and 7.2 along with the corresponding predicted Gaussian profiles. In some cases, observed and predicted profiles are virtually indistinguishable, while for others, the observed profiles are skewed or even bimodal. The profiles shown in the figures represent instantaneous plume profiles and not time-averaged profiles in spite of the finite travel time required through the plume (see Section 7.1.4 for further clarification of the difference between instantaneous and time-averaged profiles).

As described in Section 4, one of the properties of the Gaussian distribution is symmetry about the centreline (Skewness coefficient = 0). If the bulk of the data are biased to the left of the mean, the distribution is positively skewed with a positive Skewness coefficient. If the bulk of the data are biased to the right of the mean, the distribution is negatively skewed with a negative Skewness coefficient. Samples of positively and negatively skewed distributions are shown in Figure 7.2. The following table summarizes the mean Skewness coefficients for each traverse grouping:

Mean Skewness

Source Type	Distance (m)			Combined
	700	1400	2100	
Elevated	0.00	0.00	-0.20	0.00
Ground	0.16	0.05	N/A	0.15
Combined	0.09	0.01	-0.20	0.06

From the above table, the overall mean skewness is 0.06. Figure 7.3 shows the frequency distribution of the skewness coefficients for all 846 crosswind profiles. The symmetry of the skewness coefficient distribution about zero suggests on the average, the SF_6 concentration profiles can be reasonably approximated by a Gaussian distribution. It is interesting to note that the departure from a Gaussian distribution (skewness coefficient = 0) appears to be randomly or normally distributed.

Another property of the Gaussian distribution is the measure of the "peakedness" or kurtosis. A Gaussian distribution has a kurtosis coefficient of 3.0. Distributions that are more peaked than the Gaussian distribution have kurtosis coefficients that are greater than 3.0. Similarly, distributions that are flatter than the Gaussian distribution have kurtosis coefficients that are less than 3.0. Samples of profiles with kurtosis coefficients less than and greater than 3.0 are also shown in Figure 7.2. The following table summarizes the mean kurtosis coefficient for each traverse grouping:

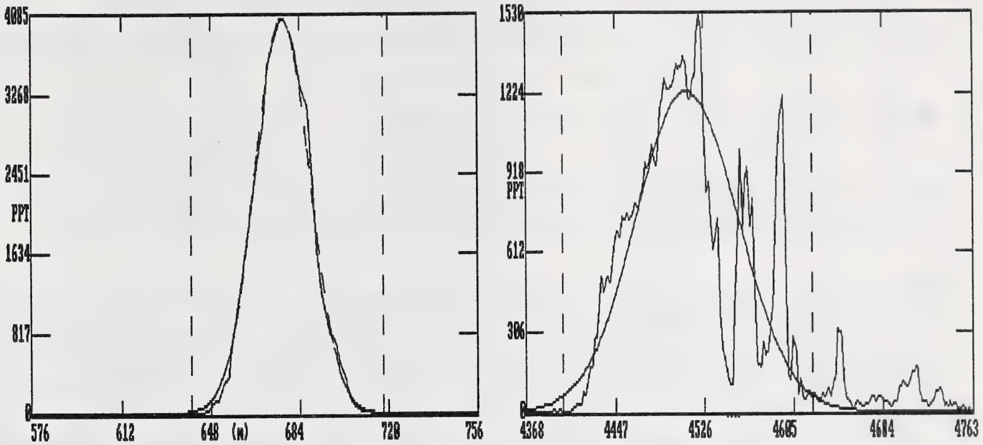

σ_{yi} = 10.9 m
Skewness = 0.016
Kurtosis = 2.8

σ_{yi} = 45.4 m
Skewness = 0.25
Kurtosis = 2.4

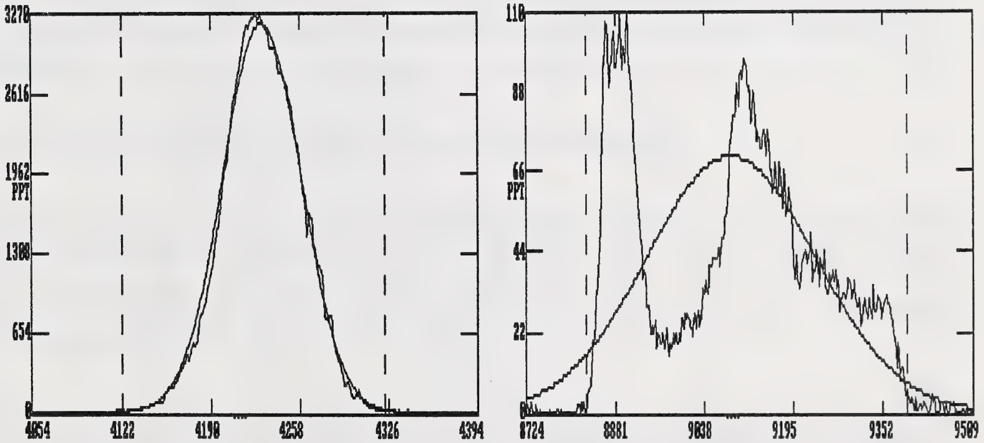

σ_{yi} = 29.5 m
Skewness = -0.077
Kurtosis = 2.92

σ_{yi} = 148.9 m
Skewness = -0.045
Kurtosis = 1.95

Figure 7.1

Selected Examples of the Crosswind SF_6 Concentration Profiles. The Corresponding Gaussian Profiles Determined From the Moment Method are Shown for the Purposes of Comparison.

Positive Skewness **Negative Skewness**

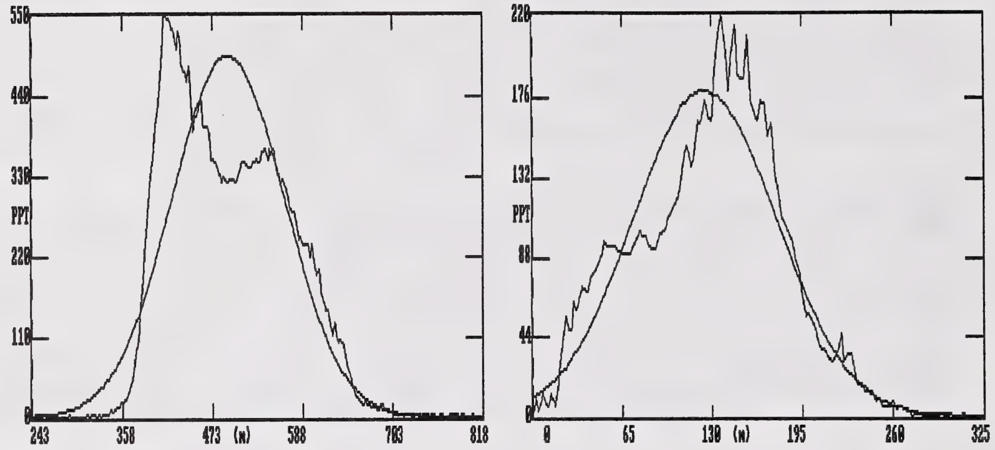

$\sigma_{yi} = 72.0$ m
Skewness = 0.372
Kurtosis = 2.39

$\sigma_{yi} = 52.5$ m
Skewness = -0.109
Kurtosis = 2.54

Kurtosis > 3.0 **Kurtosis < 3.0**

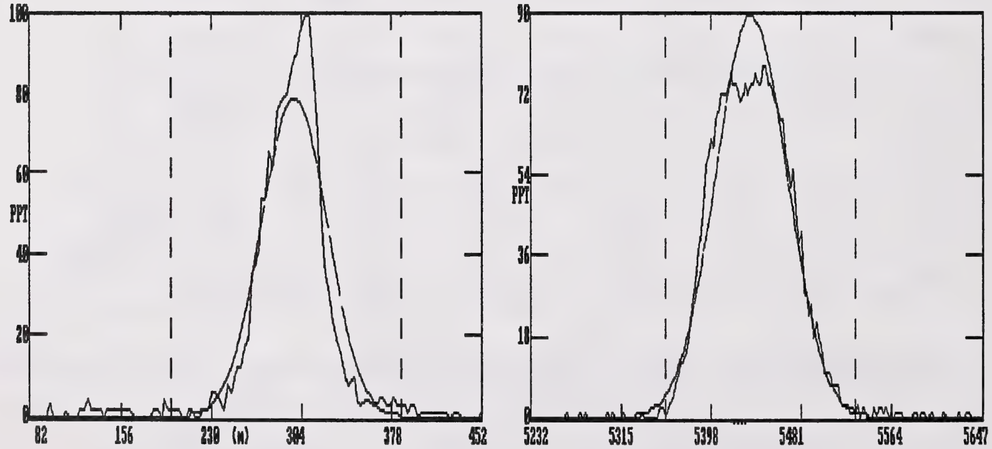

$\sigma_{yi} = 26.8$ m
Skewness = -0.083
Kurtosis = 4.15

$\sigma_{yi} = 32.6$ m
Skewness = 0.175
Kurtosis = 2.4

Figure 7.2

Selected Examples of Crosswind SF_6 Concentration Profiles Illustrating Positive Skewness, Negative Skewness, Kurtosis > 3.0 and Kurtosis < 3.0.

Mean Kurtosis

Source Type	Distance (m)			Combined
	700	1400	2100	
Elevated	2.79	3.04	2.92	2.91
Ground	3.00	2.82	N/A	2.98
Combined	2.91	3.01	2.92	2.94

From the above table, the overall mean kurtosis is 2.94. Figure 7.4 shows the frequency distribution of the kurtosis coefficients for all 846 crosswind profiles. Most of the traverses have kurtosis coefficients between 2.25 and 2.75 indicating that the observed SF_6 concentration profiles are slightly less peaked than a Gaussian distribution. The next most frequent kurtosis coefficient range is 2.75 to 3.25 which is the expected range for a Gaussian distribution.

In summary, an analysis of 846 individual plume crosswind profiles indicated that many of the observed profiles closely approximate the Gaussian distribution, while others showed significant variance from the Gaussian distribution. For the 846 profiles, the mean skewness and kurtosis coefficients of 0.06 and 2.94, respectively, indicate on the average that the plume crosswind profile can be adequately represented by a Gaussian distribution. This conclusion is based on a semi-quantitative statistical review of the data. More formalized quantitative statistics evaluating the goodness of fit were not viewed as necessary to confirm this point.

7.1.2 Alternate Plume Spread Calculation Methods

As discussed in Section 4, two alternate methods for determining the crosswind spread were used in addition to the "Moment" method. These methods are referred to as the "Hanna" and "Concentration Maximum" methods. The plume spread (σ_y or sigma y) and the maximum concentration obtained from the fitted Gaussian distribution are dependent on the method used.

The Moment and Hanna methods both attempt to produce Gaussian concentration profiles based on the observed SF_6 concentration profiles. The Moment method can be biased by smaller concentration subpeaks which may occur in the "tail" regions of the observed profiles. The Hanna method attempts to overcome this bias by using only data between the 16 and 84 percentile concentration values. The Concentration Maximum method, on the other hand, forces a Gaussian distribution to pass through the peak instantaneous concentration for each profile.

In turbulence studies, the Gaussian concentration profile is defined to represent the ensemble average concentration profile. Due to the stochastic nature of turbulence, the fine details of turbulence for a given traverse are not known. The ensemble average concentration profile is therefore better represented by either the Moment or Hanna plume spread values. The Concentration Maximum method which is based on an individual instantaneous peak, does not represent an ensemble average. The method does however better represent the observed peak concentration (by definition).

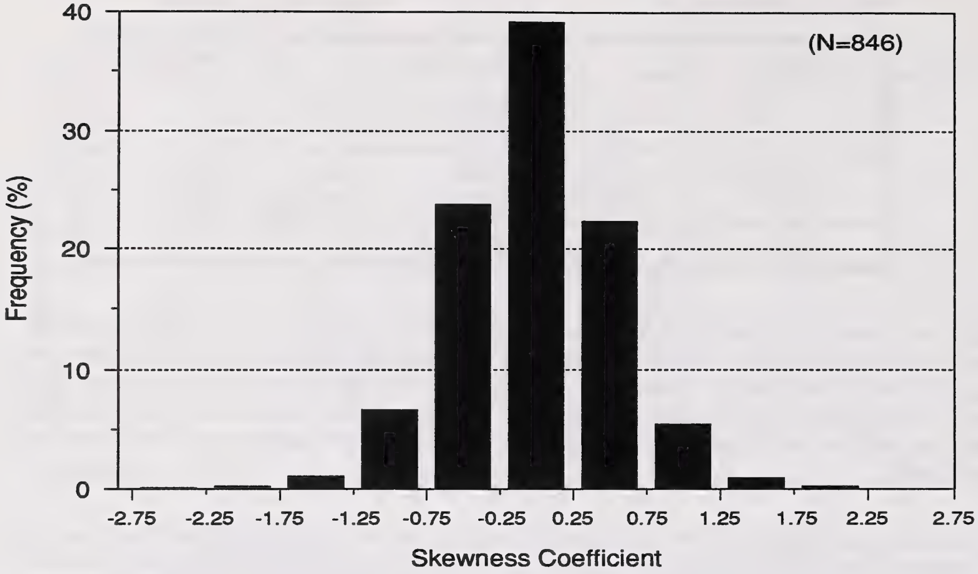

Figure 7.3

Histogram of Skewness Coefficients for the 846 Crosswind Traverses. (For a Normal Distribution, the Skewness Coefficient = 0.0).

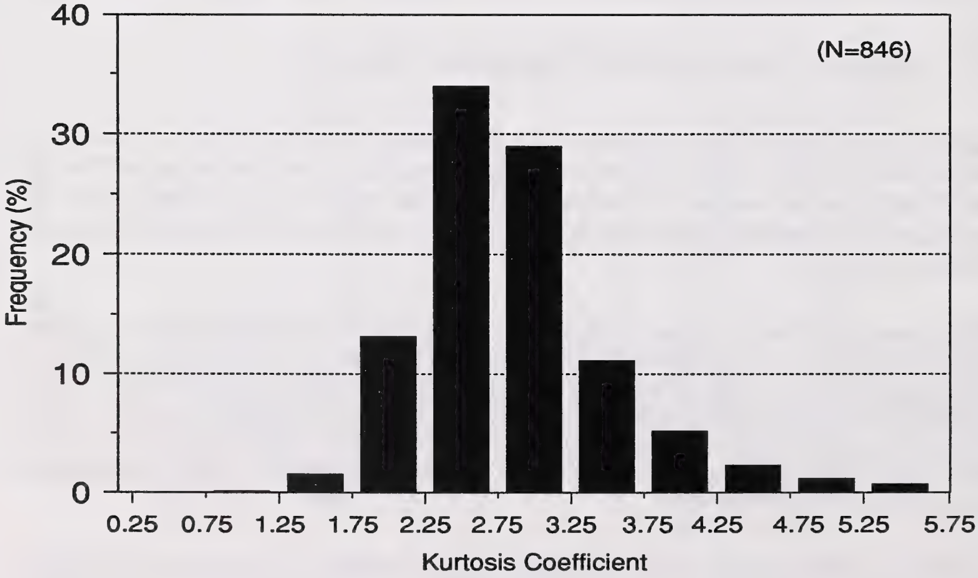

Figure 7.4

Histogram of Kurtosis Coefficient for the 846 Crosswind Traverses. (For a Normal Distribution, the Kurtosis Coefficient = 3.0).

Table 7.1 summarizes the mean plume spreads calculated from each of the three methods. Generally, the plume spreads predicted using the Hanna method are about 10% larger than those predicted using the Moment method. Similarly, the plume spreads predicted using the Concentration Maximum method are about 20% less than those predicted using the Moment method.

Table 7.1

Comparison of the Three Methods for Calculating Plume Spreads (σ_{y_i}).

Source Type and Distance (m)	Mean Plume Sigma (m)		
	Moment	Hanna	Concentration Maximum
Elevated			
700	35	39	29
1400	56	61	43
2100	92	99	71
Ground			
700	36	42	27
1400	73	81	57

Table 7.2 summarizes the normalized peak concentrations calculated from each of the three methods. The concentrations that were observed in the field have been normalized by the SF_6 release rates to allow the comparison of concentrations from one field test to another. Generally, the peak concentrations predicted using the Hanna method are similar to those predicted using the Moment method. The peak concentrations predicted using the Moment method are about 85% of the actual concentrations which define the Concentration Maximum method.

Table 7.2

Comparison of the Three Methods for Calculating the Normalized Peak Concentration.

Source Type and Distance (m)	Normalized Concentration [(ppt)/(g/min)]		
	Moment	Hanna	Concentration Maximum
Elevated			
700	230	229	260
1400	203	203	250
2100	78	76	98
Ground			
700	2811	2900	3404
1400	1182	1157	1282

The Hanna and Moment methods generally predict similar plume spreads (within 10%) and similar peak concentrations (within 1%). The peak concentrations predicted with either of these two methods, however, underpredicts the peak observed concentration, which defines the Concentration Maximum method, by 18%. As a consequence, the Concentration Maximum method underpredicts the plume spreads to conserve mass.

The Moment method plume spreads and concentration maximum data were selected for subsequent data analysis because of the close agreement with the Hanna method. This does not mean, however, that the Concentration Maximum method will be ignored since it, by definition, provides a better indicator of peak concentrations that were observed in the field.

7.1.3 Concurrent Meteorology

The traverse data were obtained during night time hours, during which the stability of the atmosphere was primarily stable and neutral. This section provides an overview summary of the meteorological conditions that were observed when traverses were obtained. The meteorological data have been averaged over the transport time for the plume to reach the analyzer for each traverse. For the presentation of the meteorological data, all the statistics have been delineated according to the distance at which the data were collected.

7.1.3.1 Wind Speed

Figures 7.5 and 7.6 show histograms of the 4 and 10 m level wind speeds observed during the plume traverses. The histograms are subgrouped according to downwind distance and represent averages over the transport time. The following table summarizes the wind speed statistics presented in the histogram:

Distance	Height	Wind Speed (m/s)		
(m)	(m)	Minimum	Maximum	Mean
700	4	0.2	9.1	2.3
700	10	0.1	9.6	3.3
1400	4	0.2	7.2	2.0
1400	10	0.3	8.2	2.9
2100	4	1.2	6.2	2.6
2100	10	1.8	7.1	3.4

Mean wind speeds are generally in the 2 to 3 m/s range with maximum values in the 6 to 9 m/s range. The 10 m level wind speeds are typically 1.4 times larger than those observed at the 4 m level. The number of occurrences of wind speeds less than 2 m/s are summarized below:

Distance (m)	10 m Level (Number)	4 m Level (Number)
700	84 (15.1%)	274 (49.6%)
1400	38 (17.3%)	148 (53.2%)
2100	3 (16.7%)	9 (50.0%)

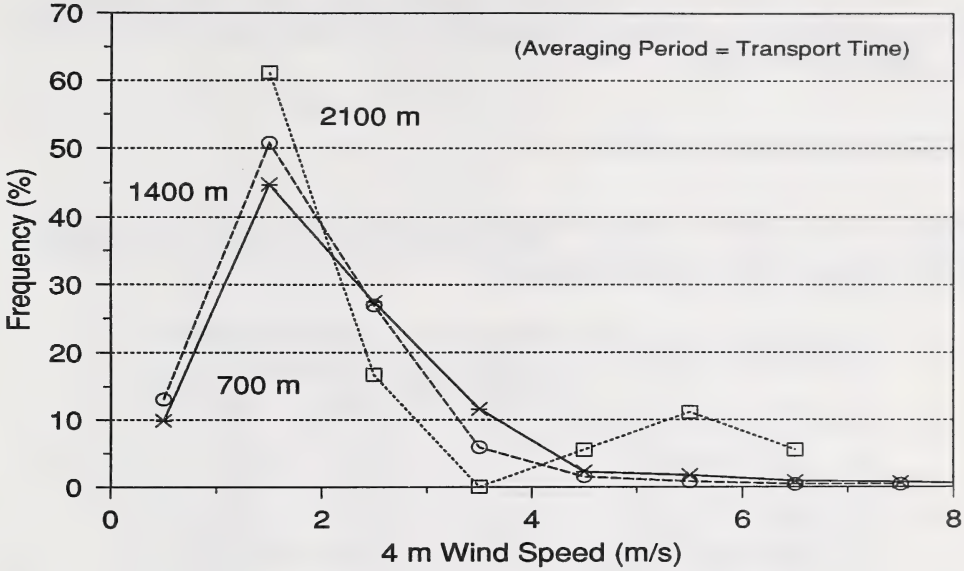

Figure 7.5

4 m Level Wind Speed Observed During the Plume Traverses.

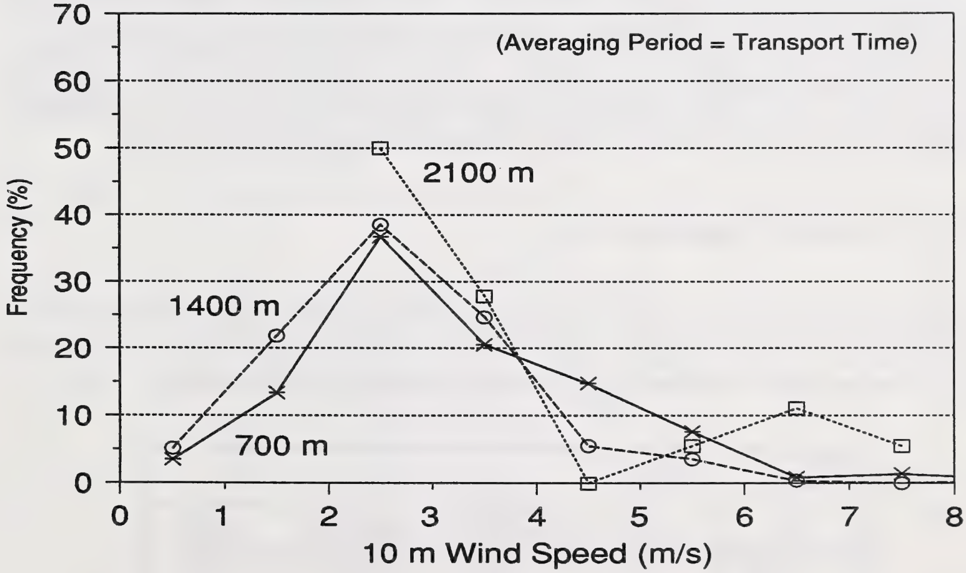

Figure 7.6

10 m Level Wind Speed Observed During the Plume Traverses.

About 15 to 17 per cent of all the traverse data were associated with 10 m wind speeds less than 2 m/s. Similarly, about 50 per cent of all traverse data were associated with 4 m level wind speeds less than 2 m/s.

7.1.3.2 Temperature Gradient

Figures 7.7 and 7.8 show the vertical temperature gradient between the 10 and 2 m level and the 25 and 2 m level, respectively. The following table summarizes the temperature gradient statistics for each downwind distance:

Distance	Elevation	Temperature Gradient (K/m)		
(m)	(m)	Minimum	Maximum	Mean
700	10-2	-0.02	1.05	0.25
700	25-2	-0.01	0.45	0.15
1400	10-2	-0.02	0.79	0.20
1400	25-2	-0.01	0.51	0.13
2100	10-2	-0.01	0.07	0.03
2100	25-2	-0.01	0.12	0.07

Temperature gradients that are more negative than -0.01 K/m (for example: -0.05 K/m) are associated with thermally unstable atmospheres, while those that are larger than -0.01 K/m (for example: 0.0 K/m) are associated with thermally stable atmospheres. The majority of the traverses clearly occur during periods when the temperature gradients indicate a thermally stable atmosphere. As expected, the magnitude of the temperature gradients for the lower layer (10 to 2 m) is larger than those for the upper layer (25 to 2 m). The limited amount of data associated with the 2100 m distance indicates the inverse is true.

7.1.3.3 Vertical Turbulence (σ_ϕ)

Figures 7.9 and 7.10 show histograms of the 4 and 10 m level vertical wind fluctuation (σ_ϕ or sigma phi) observed during the plume traverses and averaged over the transport time. The following table summarizes the σ_ϕ statistics presented in the histograms:

Distance	Height	σ_ϕ (degrees)		
(m)	(m)	Minimum	Maximum	Mean
700	4	0.5	23.4	3.7
700	10	0.2	28.8	2.8
1400	4	0.8	23.4	4.0
1400	10	0.3	11.7	2.6
2100	4	1.9	4.5	3.3
2100	10	0.8	4.6	2.4

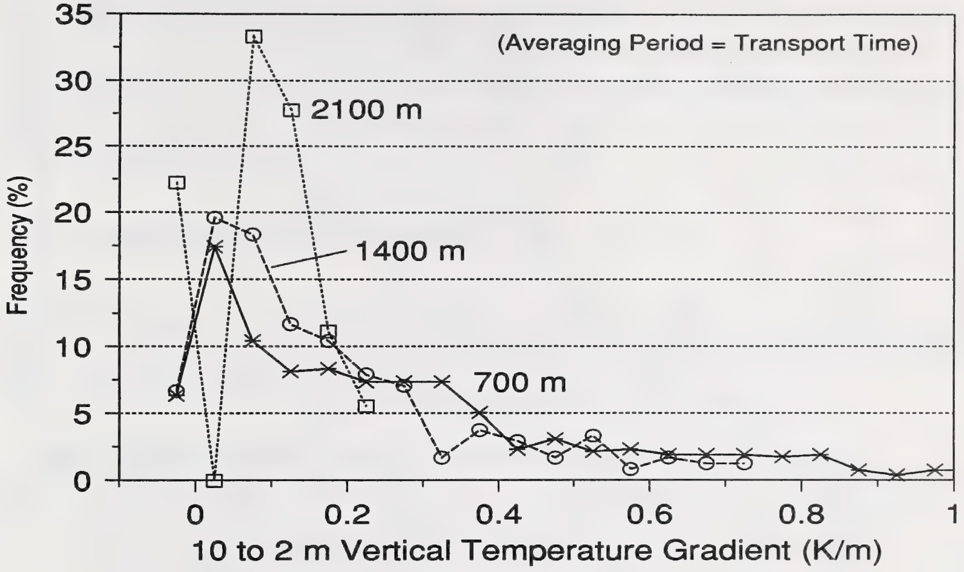

Figure 7.7

10 to 2 m Vertical Temperature Gradient Observed During the Plume Traverses.

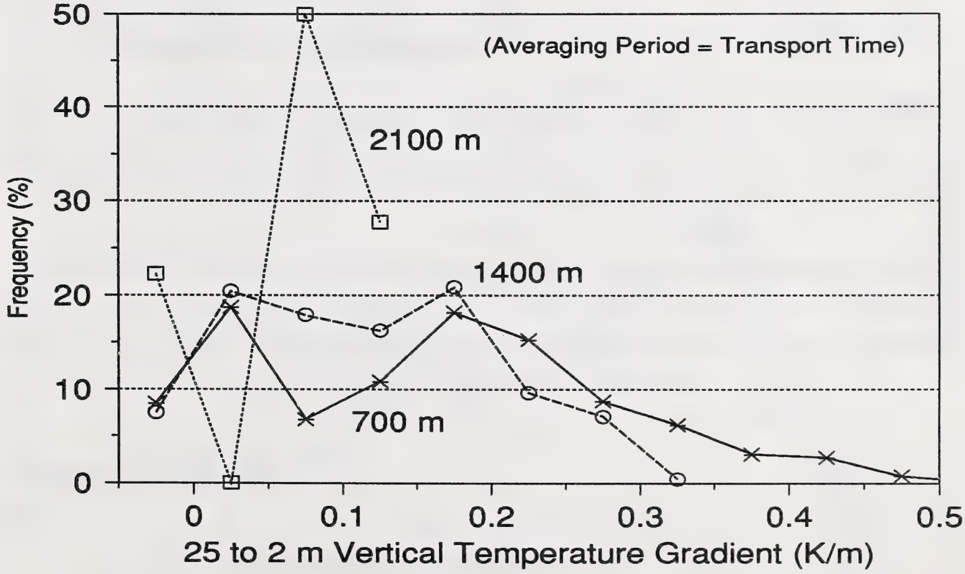

Figure 7.8

25 to 2 m Vertical Temperature Gradient Observed During the Plume Traverses.

About 15 to 17 per cent of all the traverse data were associated with 10 m wind speeds less than 2 m/s. Similarly, about 50 per cent of all traverse data were associated with 4 m level wind speeds less than 2 m/s.

7.1.3.2 Temperature Gradient

Figures 7.7 and 7.8 show the vertical temperature gradient between the 10 and 2 m level and the 25 and 2 m level, respectively. The following table summarizes the temperature gradient statistics for each downwind distance:

Distance (m)	Elevation (m)	Temperature Gradient (K/m)		
		Minimum	Maximum	Mean
700	10-2	-0.02	1.05	0.25
700	25-2	-0.01	0.45	0.15
1400	10-2	-0.02	0.79	0.20
1400	25-2	-0.01	0.51	0.13
2100	10-2	-0.01	0.07	0.03
2100	25-2	-0.01	0.12	0.07

Temperature gradients that are more negative than -0.01 K/m (for example: -0.05 K/m) are associated with thermally unstable atmospheres, while those that are larger than -0.01 K/m (for example: 0.0 K/m) are associated with thermally stable atmospheres. The majority of the traverses clearly occur during periods when the temperature gradients indicate a thermally stable atmosphere. As expected, the magnitude of the temperature gradients for the lower layer (10 to 2 m) is larger than those for the upper layer (25 to 2 m). The limited amount of data associated with the 2100 m distance indicates the inverse is true.

7.1.3.3 Vertical Turbulence (σ_ϕ)

Figures 7.9 and 7.10 show histograms of the 4 and 10 m level vertical wind fluctuation (σ_ϕ or sigma phi) observed during the plume traverses and averaged over the transport time. The following table summarizes the σ_ϕ statistics presented in the histograms:

Distance (m)	Height (m)	σ_ϕ (degrees)		
		Minimum	Maximum	Mean
700	4	0.5	23.4	3.7
700	10	0.2	28.8	2.8
1400	4	0.8	23.4	4.0
1400	10	0.3	11.7	2.6
2100	4	1.9	4.5	3.3
2100	10	0.8	4.6	2.4

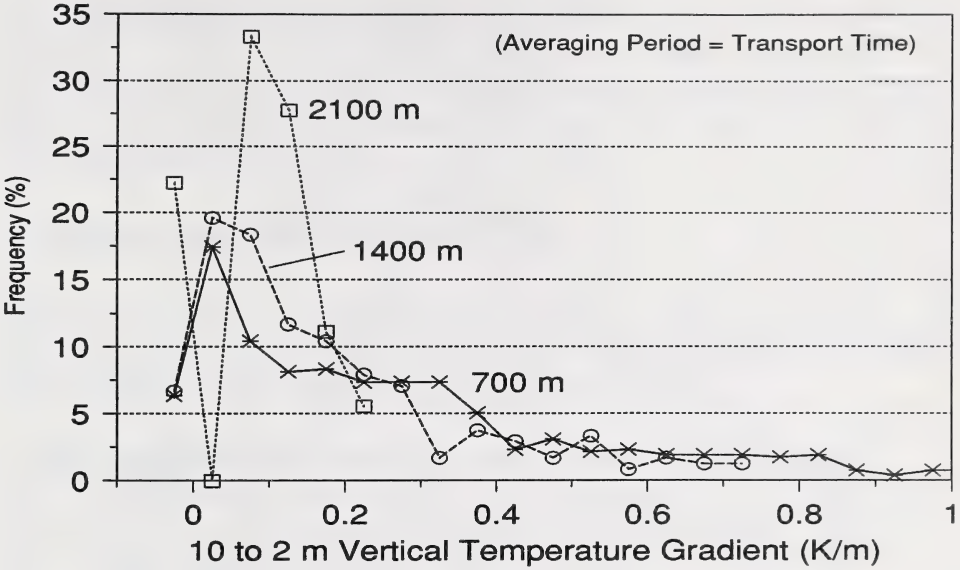

Figure 7.7

10 to 2 m Vertical Temperature Gradient Observed During the Plume Traverses.

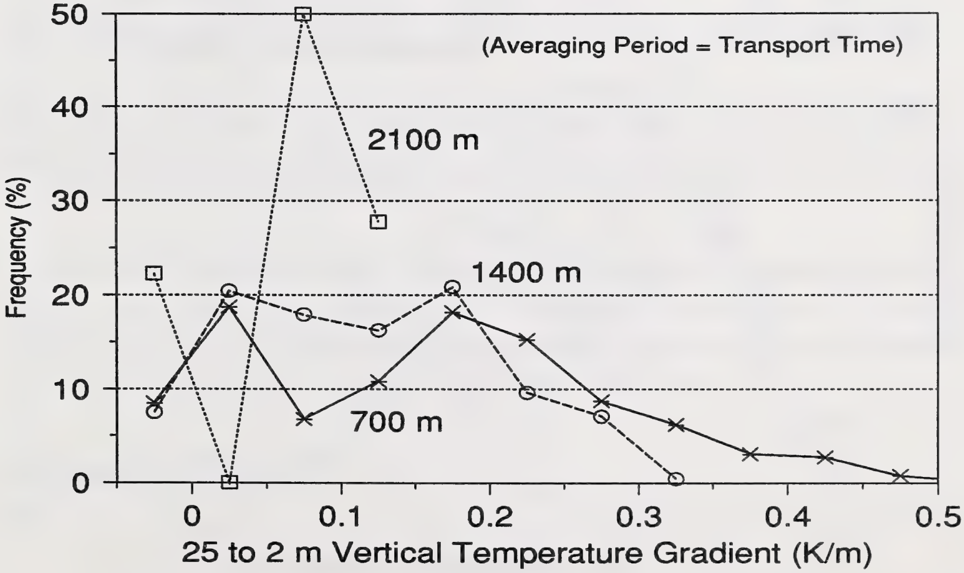

Figure 7.8

25 to 2 m Vertical Temperature Gradient Observed During the Plume Traverses.

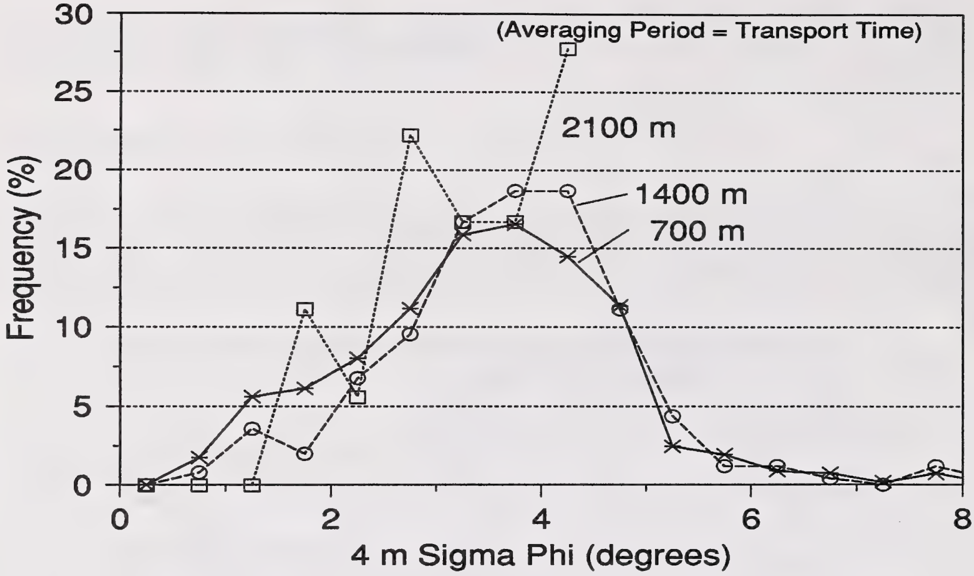

Figure 7.9

4 m Level σ_ϕ Observed During the Plume Traverses.

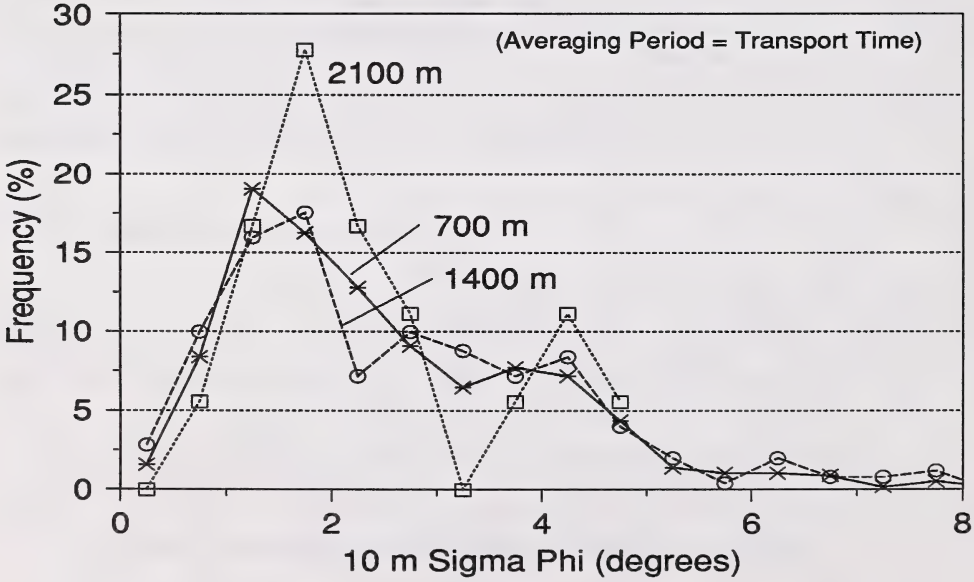

Figure 7.10

10 m Level σ_ϕ Observed During the Plume Traverses.

The mean values of σ_ϕ tend to decrease with increasing height. This is expected since $\sigma_\phi \approx \sigma_W/U$. If σ_W is essentially constant with increasing height and U increases with increasing height, then σ_ϕ will show a $1/U$ dependence on wind speed (see Sections 8.2.4 and 8.3.8). For the 700 and 1400 m traverses, the 4 and 10 m level σ_ϕ value were about 3.9 and 2.7 degrees, respectively.

7.1.3.4 Horizontal Turbulence (σ_θ)

Figures 7.11 and 7.12 show histograms of the 4 and 10 m level horizontal wind fluctuation (σ_θ or sigma theta) observed during the plume traverses and averaged over the transport time. The following table summarizes the σ_θ statistics:

Distance (m)	Height (m)	σ_θ (degrees)		
		Minimum	Maximum	Mean
700	4	1.8	73.1	8.6
700	10	0.6	82.9	5.9
1400	4	2.0	69.6	10.4
1400	10	0.7	60.6	6.7
2100	4	6.0	17.6	10.0
2100	10	4.0	11.5	7.3

The mean values of σ_θ tend to decrease with increasing height for the same reason that σ_ϕ decreases with increasing height ($\sigma_\theta \approx \sigma_V/U$ see Sections 8.2.3 and 8.3.8). For the traverses, the mean 4 and 10 m level σ_θ values are 9.7 and 6.6 degrees respectively.

The σ_θ frequency distributions tend to show a log-normal type of distribution with a long tail to the right of the mode. For the 4 m σ_θ values, the 90 percentiles are 14, 22 and 16 degrees for the 700, 1400 and 2100 m distance traverses, respectively. Corresponding σ_θ values for the 10 m level are 10, 12 and 11 degrees, respectively.

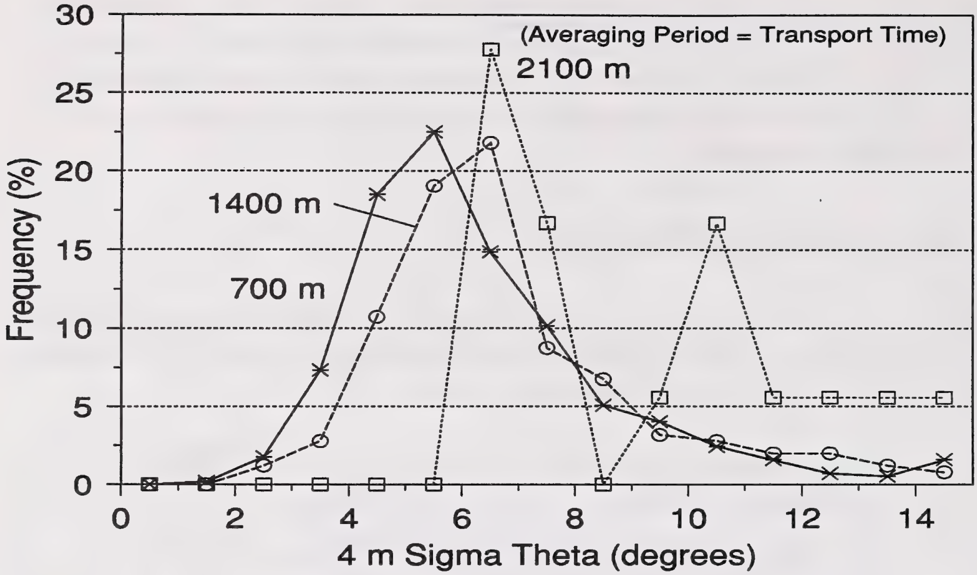

Figure 7.11

4 m Level σ_θ Observed During the Plume Traverses.

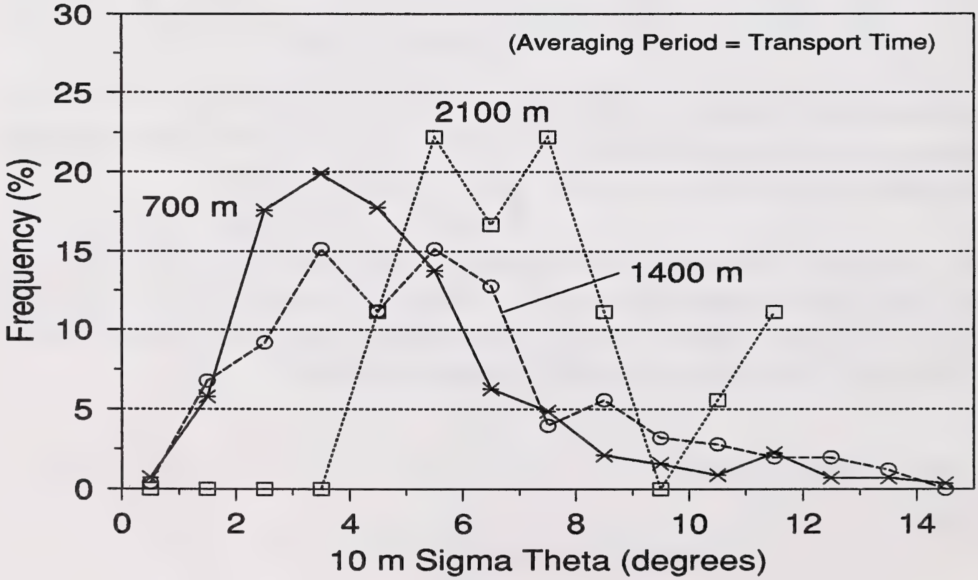

Figure 7.12

10 m Level σ_θ Observed During the Plume Traverses.

7.1.3.5 Heat Flux (H_o)

Figure 7.13 shows the heat flux derived from the 10 m level sonic anemometer during the plume traverses and averaged over the transport time. The majority of the heat flux values tend to be clustered around $H_o = 0$ W/m^2 with some extreme outliers. The following table summarizes the heat flux statistics:

Distance (m)	Mean H_o (W/m^2)
700	-7.7
1400	-4.7
2100	0.0

Heat flux values less than zero tend to be associated with stable atmospheres (see Section 8.3.2). For the 700, 1400 and 2100 m traverses, 84, 83 and 78 per cent of traverses, respectively, were less than 0.0 W/m^2. For the 700, 1400 and 2100 m traverses, 71, 87 and 89 per cent of the cases, respectively, were within the range -10 to 10 W/m^2.

7.1.3.6 Friction Velocity *(U*)*

Figure 7.14 shows the friction velocity derived from the 10 m level sonic anemometer during the plume traverses and averaged over the transport time. The following table summarizes the friction velocity statistics:

Distance	*U** (m/s)		
(m)	Minimum	Maximum	Mean
700	0.00	0.65	0.12
1400	0.00	0.41	0.10
2100	0.01	0.41	0.14

The most frequently occurring values of *U** are in the 0.05 to 0.10 m/s range. The mean values are relatively constant for all traverse distances.

7.1.3.7 Monin-Obukhov Stability Parameter (*Z/L*)

Figure 7.15 shows the Monin-Obukhov stability parameter (*Z/L*) derived from the 10 m level sonic anemometer data and averaged over the transport time. Positive values of *Z/L* are associated with stable atmospheres. For the 700, 1400 and 2100 m traverses, 84, 89 and 73 percent of the *Z/L* values are positive.

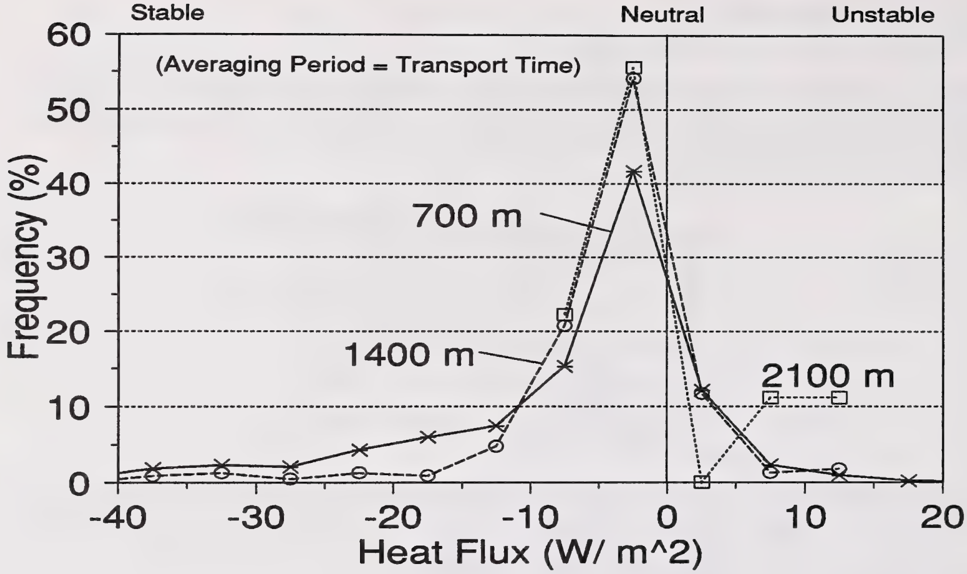

Figure 7.13

Heat Flux (W/m^2) Observed During the Plume Traverses.

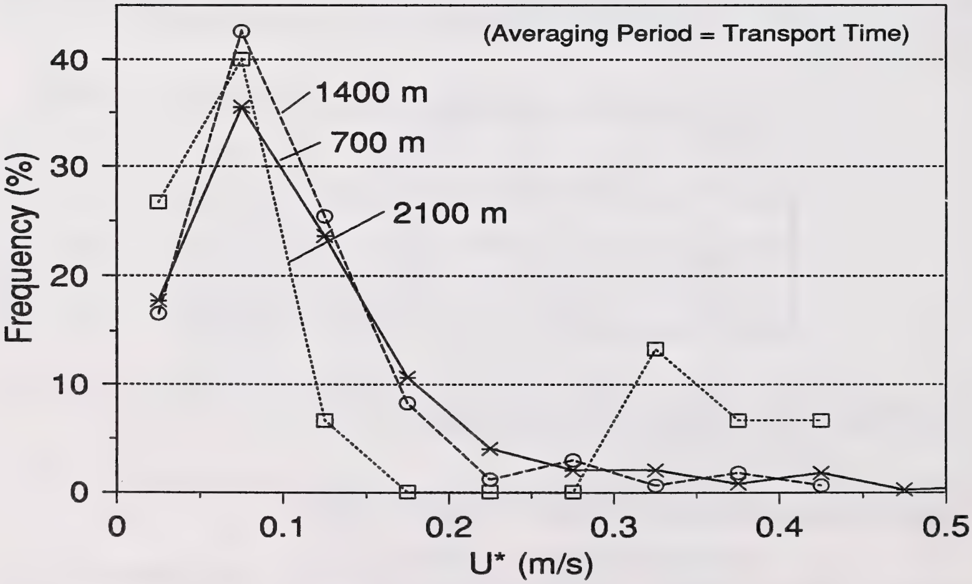

Figure 7.14

U* (m/s) Observed During the Plume Traverses.

7.1.3.8 Meteorology Summary

The meteorological conditions during which the plume traverse data were collected have been summarized. The meteorological conditions represent a wide range of stable and neutral atmospheric conditions. The meteorological conditions can be summarized below:

- About 50 per cent of the traverses were associated with 4 m level wind speeds less than 2 m/s.
- About 16 per cent of the traverses were associated with 10 m level wind speeds less than 2 m/s.
- Mean vertical temperature gradients in the 10 to 2 m layer were about 0.2 K/m with extreme maximum values up to 1 K/m.
- Mean σ_ϕ values were typically 3 to 4 degrees, with minimum values less than 1 degree.
- Mean σ_θ values were typically 6 to 10 degrees, with minimum values of 1 to 2 degrees.
- About 80 per cent of the traverses were associated with negative heat flux values (and positive values of the Monin-Obukhov stability parameter).

These conditions, during which the traverse data were collected, appear to have met one of the objectives of the Field Measurement Program, namely the collection of traverse data during low wind speed, stable atmospheric conditions.

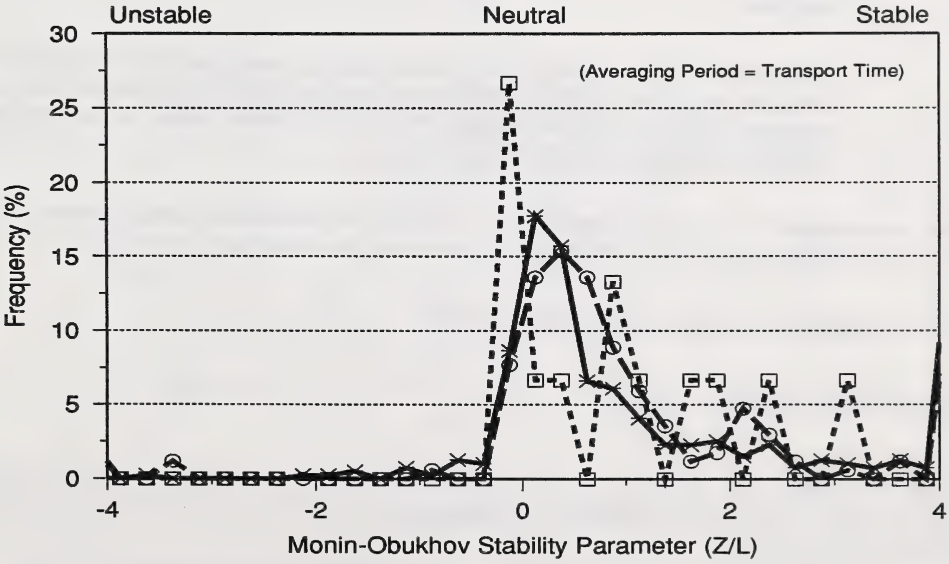

Figure 7.15

Monin-Obukhov Stability Parameter (*Z*/*L*) Observed During the Plume Traverses.

7.1.4 Instantaneous Plume Spreads

The cross wind plume spreads (σ_y) used in dispersion models represent time-averaged plume spreads at fixed locations downwind of a source. The horizontal plume spread generally increases with increasing averaging time. For a given set of plume spreads used in these models, the averaging period is either stated explicitly or implied. The Field Measurement Program plume spreads derived from each traverse represent the "instantaneous" or "relative dispersion" plume spread. It is tempting to assign an averaging period to each measured plume spread based on the speed of the traverse through the plume. As pointed out by Davison and Leavitt (1979), this practice is incorrect. A rapid traverse determines the instantaneous spread accurately, whereas a slow traverse results in a scatter about the true instantaneous value. The relative dispersion or instantaneous plume spread is **not** the same as the time-averaged plume spread normally used in dispersion models.

There are a number of processes that control the lateral dispersion and position of a plume as it moves downwind from a source:

- **Turbulent motions** result in the entrainment of ambient air into the plume and the extrainment of plume material into the surrounding air. This process is dominated by turbulent motions in the atmosphere that are of the same scale as the plume cross-section.

- **Meandering motions** result in the lateral displacement of the plume by turbulent motions in the atmosphere that are much larger in scale than the plume cross-section. For sufficiently large averaging periods, the separation of the turbulent and meander component may be difficult without a detailed spectra analysis.

- **Wind shear enhancement** due to wind direction variations with height will result in an enhancement of dispersion over an equivalent situation with a vertically uniform wind direction profile. This enhancement is not usually addressed by dispersion models.

The interpretation of the plume spreads derived from the individual plume traverses will have to recognize that all three of the above processes can occur simultaneously.

7.1.4.1 Observed Instantaneous Values

Cross-wind Spread σ_{y_i}

Figure 7.16 shows the frequency distribution of the observed instantaneous plume spreads as a function of downwind distance and source type. The following observations can be drawn from the figure:

- For a downwind distance of 700 m, the most frequent spreads for an elevated release are in the 10 to 30 m range. For a ground release, the corresponding spreads are in the 10 to 20 m range.

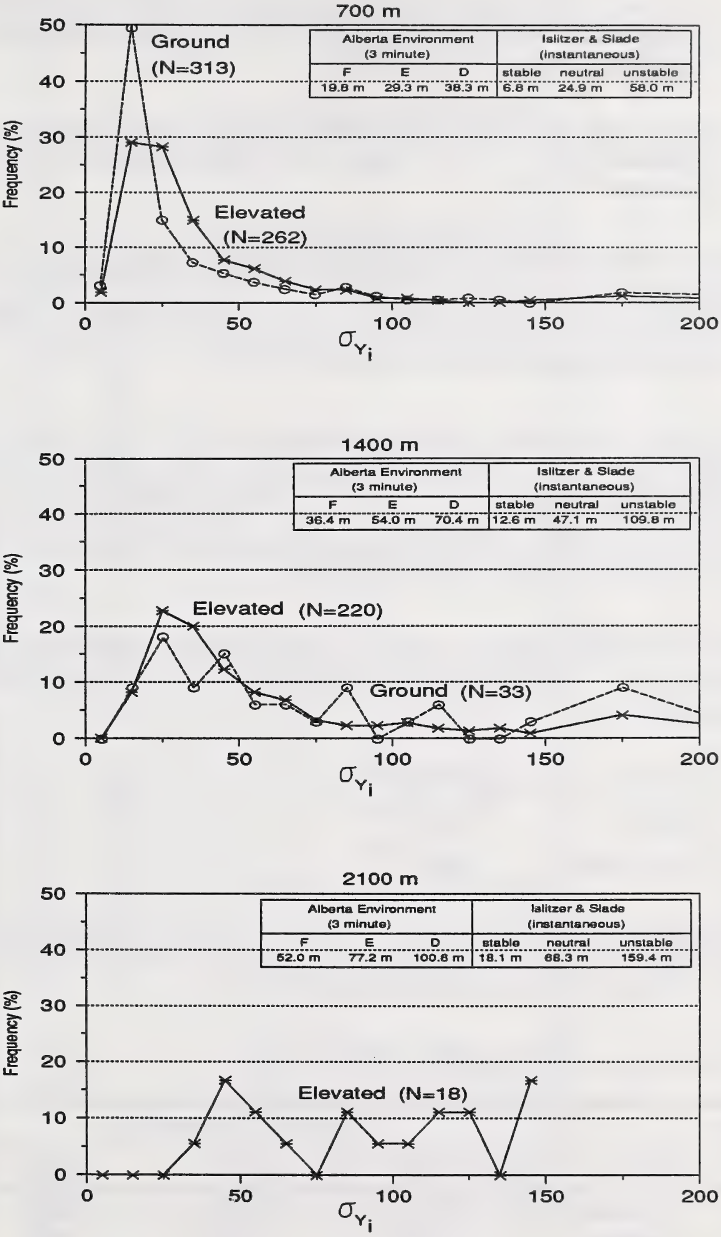

Figure 7.16

Plume Spread Frequency Distribution for Elevated and Ground Releases and Downwind Distances of 700, 1400 and 2100 m. The Predicted Values from Alberta Environment and Islitzer & Slade are Presented at the Top of the Figure.

- For a downwind distance of 1 400 m, the most frequent spreads for an elevated release are in the 20 to 40 m range. For a ground release, the corresponding spreads are in the 30 to 50 m range.

- For a downwind distance of 2 100 m, the most frequent spreads are in the 40 to 50 and the 140 to 150 m ranges. Data from this distance are only available for elevated releases.

The frequency distributions tend to be highly skewed, indicating that significantly larger plume spreads were observed at all downwind distances than could be indicated by the mode. These large values may be a result of either the measurement technique accompanied by a systematic wind direction shift during a plume traverse or due to enhanced dispersion due to large wind direction shear during the traverses.

For the purposes of comparison, the time-averaged or relative dispersion plume spreads predicted using the Alberta Environment (1988) guideline model approach are shown in the figure. These predicted spreads refer to a three-minute averaging period and a surface roughness Z_o of 1 cm. The plume spreads appropriate to the downwind distance for neutral (Stability Class D) and stable conditions (Stability Classes E and F) are shown. The predicted values are in the same range as the observed values.

Islitzer and Slade (1968) reviewed a number of field experiments concerning instantaneous plume spread values. Their suggested relationships for σ_{y_i} (m) based on an empirical fit to the data are as follows:

• Unstable	$0.14\,x^{0.92}$
• Neutral	$0.06\,x^{0.92}$
• Very Stable	$0.02\,x^{0.89}$

where x is the downwind distance in (m). The very stable values represent the limit of the most stable data that were available for the review. Applications of the above relationships to the 700, 1 400 and 2 100 m sampling are as follows:

Instantaneous Plume Spread σ_{y_i} (m)

	Downwind Distance (m)		
Stability	700	1 400	2 100
Unstable	58.0	109.8	159.4
Neutral	24.9	47.1	68.3
Very Stable	6.8	12.6	18.1

These values are also shown on Figure 7.16. The stable instantaneous values are about one third the Alberta Environment time averaged values. Figure 7.16 indicates about 4% of the 700 m plume spreads (σ_{y_i}) are less than 10 m and about 9% of the 1 400 m plume spreads are less than 20 m. Tables 7.3 and 7.4 summarize the times and meteorological conditions when the 700 m and 1 400 m plume spreads were less than 10 and 20 m, respectively. The meteorological conditions shown in the tables include 10 m level wind speed (U_{10}), heat flux at 10 m (H_o), the temperature gradient from the 10 to 2 m levels ($\partial T/\partial Z$), the

Table 7.3

Summary of 700 m Traverses Where the σ_{y_i} Values are Less Than 10 m.

TEST	DATE	START TIME	END TIME	SOURCE TYPE	σ_{y_i} (m)	U_{10} (m/s)	H_o (W/m^2)	$\frac{\partial T}{\partial Z}$ (K/m)	Z/L	σ_V (m/s)	σ_θ (degrees)	σ_W (m/s)	σ_ϕ (degrees)	$\frac{\chi}{Q}$ $\left(\frac{ppt}{(g/min)}\right)$
T05A02	28-Oct-88	19:40:26	19:41:56	Elevated	9.0	3.9	---	0.19	0.16	0.05	0.80	0.037	0.55	21
T05A05	28-Oct-88	20:09:56	20:13:06	Elevated	9.3	3.9	---	0.20	---	0.08	1.15	0.051	0.74	248
T05A08	28-Oct-88	20:38:35	20:40:15	Elevated	8.0	4.4	---	0.18	---	0.10	1.30	0.078	1.01	202
T11C24	16-Nov-88	23:10:33	23:13:53	Elevated	9.4	2.5	2.1	0.21	---	0.21	4.72	0.071	1.60	767
T15C14	26-Nov-88	19:02:04	19:03:44	Ground	9.7	2.6	0.1	0.28	-0.04	0.17	3.70	0.056	1.25	7842
T16C26	02-Dec-88	23:51:00	23:52:20	Elevated	8.3	4.1	-2.0	0.15	---	0.09	1.27	0.066	0.94	39
T19C19	08-Dec-88	22:41:33	22:43:13	Ground	10.0	3.6	-11.3	0.19	0.83	0.22	3.48	0.152	2.43	4190
T20B19	09-Dec-88	19:01:01	19:03:11	Ground	9.9	3.3	-7.4	0.19	2.46	0.20	3.37	0.094	1.62	3148
T20B51	09-Dec-88	23:19:23	23:21:23	Ground	8.4	4.4	-20.9	0.21	---	0.20	2.56	0.182	2.34	2531
T25C09	14-Dec-88	18:05:15	18:06:15	Ground	8.5	2.6	-0.1	0.30	---	0.11	2.36	0.058	1.31	10858
T25C13	14-Dec-88	18:29:45	18:30:35	Ground	9.4	3.3	-0.9	0.29	---	0.06	1.11	0.037	0.64	5193
T27C02	16-Dec-88	17:36:27	17:37:37	Ground	8.8	5.5	-21.6	0.39	---	0.26	2.72	0.134	1.40	1960
T27C03	16-Dec-88	17:41:23	17:42:23	Ground	8.5	5.2	-16.6	0.38	---	0.24	2.63	0.150	1.64	3327
T27C04	16-Dec-88	17:47:10	17:48:00	Ground	6.3	5.1	-32.4	0.39	25.88	0.20	2.29	0.118	1.34	2905
T31C02	20-Dec-88	17:56:52	18:02:12	Ground	6.1	2.4	77.7	0.32	-7.05	0.75	17.14	0.230	5.44	533

Table 7.4

Summary of 1400 m Traverses Where the σ_{y_i} Values are Less Than 20 m.

TEST	DATE	START TIME	END TIME	SOURCE TYPE	σ_{y_i} (m)	U_{10} (m/s)	H_o (W/m^2)	$\frac{\partial T}{\partial Z}$ (K/m)	Z/L	σ_V (m/s)	σ_θ (degrees)	σ_W (m/s)	σ_ϕ (degrees)	χ/Q $\left(\frac{ppt}{(g/min)}\right)$
T03C19	25-Oct-88	01:35:09	01:37:29	Elevated	18.8	3.33	-0.07	0.186		0.116	2.00	0.061	1.06	392
T03C20	25-Oct-88	01:56:29	01:59:17	Elevated	15.1	3.90	-7.82	0.174	2.746	0.131	1.93	0.087	1.28	844
T03C21	25-Oct-88	02:13:31	02:15:59	Elevated	17.3	3.72	-7.82	0.180		0.251	3.87	0.099	1.53	738
T05B12	28-Oct-88	21:41:22	21:15:29	Elevated	15.0	3.60		0.142	0.905	0.220	3.49	0.166	2.63	443
T07B02	07-Nov-88	19:02:21	19:04:31	Elevated	11.5	4.92	-4.58	0.198	0.768	0.456	5.30	0.063	0.73	37
T07C08	07-Nov-88	20:33:06	20:34:26	Elevated	16.9	5.10	-9.79	0.266	0.424	0.148	1.66	0.097	1.09	391
T07C08	07-Nov-88	20:28:56	20:30:11	Elevated	18.1	5.56	-4.23	0.272		0.250	2.57	0.089	0.92	639
T09B10	14-Nov-88	18:37:01	18:38:50	Elevated	16.3	3.23	-7.47	0.041	0.366	0.345	6.09	0.147	2.61	208
T09B23	14-Nov-88	20:11:56	20:14:11	Elevated	16.8	3.71	1.13	-0.009	-0.034	0.384	5.92	0.279	4.30	338
T09B25	14-Nov-88	20:26:12	20:28:57	Elevated	12.1	5.16	6.76	-0.011	-0.045	0.572	6.32	0.466	5.15	156
T09B26	14-Nov-88	20:34:02	20:36:42	Elevated	11.9	8.16	13.26	-0.014	-0.029	0.637	4.46	0.515	3.61	52
T11A06	16-Nov-88	20:36:16	20:37:36	Ground	10.3	0.88	0.18	0.156		0.355	21.91	0.052	3.40	401
T11B11	16-Nov-88	20:30:44	20:32:06	Ground	10.6	0.90	0.29	0.159	-12.451	0.362	21.94	0.057	3.60	222
T11B12	16-Nov-88	20:37:02	20:39:22	Ground	19.1	0.88	0.18	0.156		0.355	21.91	0.052	3.40	135
T11B25	16-Nov-88	23:03:10	23:08:00	Elevated	19.6	2.72	1.81	0.219	-0.166	0.342	7.17	0.122	2.58	19
T12B20	18-Nov-88	21:15:53	21:17:43	Elevated	15.4	1.81	-2.40	0.038	0.511	0.163	5.13	0.072	2.26	18
T12B45	19-Nov-88	01:24:15	01:25:35	Elevated	19.8	2.28	-6.01	0.091	1.007	0.346	8.63	0.112	2.81	92
T15B34	26-Nov-88	22:31:50	22:34:50	Elevated	20.0	4.33	-4.23	0.182	0.608	0.179	2.36	0.109	1.45	473
T15B40	26-Nov-88	23:24:17	23:26:04	Elevated	17.8	4.19	-1.03	0.154	0.053	0.226	3.09	0.096	1.32	469
T16C09	02-Dec-88	19:55:19	20:01:09	Elevated	17.7	3.24	3.20	0.167		0.351	6.19	0.102	1.81	94
T16C11	02-Dec-88	20:28:41	20:32:11	Elevated	14.6	2.66	0.20	0.111	-0.058	0.255	5.48	0.108	2.32	200

Monin-Obukhov stability parameter (Z/L), lateral absolute (σ_V) and relative (σ_θ) turbulence intensity measurements, and the vertical absolute (σ_W) and relative (σ_ϕ) turbulence intensity measurements. The last column shows the χ/Q values for each traverse.

The minimum σ_{y_i} values obtained from the Field Measurement Program traverses are as follows:

- 700 m σ_{y_i} (minimum) = 6.1 m
- 1 400 m σ_{y_i} (minimum) = 10.3 m
- 2 100 m σ_{y_i} (minimum) = 39.0 m

For the 700 and 1 400 m sampling arcs, the minimum observed Field Measurement Program values are slightly smaller than the empirical relationships given by Islitzer and Slade. There is therefore some comfort that the minimum observed Field Measurement Program values are indeed representative of minimum values that could be observed under very stable conditions. For the 2 100 m sampling arc, the minimum observed Field Measurement Program value is about twice that derived from the Islitzer and Slade suggested relationships. As the 2 100 m sampling arc data were based on 18 traverses, we can conclude that the traverses were not made during very stable conditions.

For the 700 m traverses, the smallest σ_{y_i} values are associated with an average 10 m level wind speed of 3.79 m/s. The minimum wind speed is 2.42 m/s. The mean values for σ_ϕ and σ_θ are 1.62 and 2.23 degrees, respectively. The average temperature gradient was 0.257 K/m (or 25.7 K/100 m) indicating very stable atmospheric conditions. It is interesting to compare the results from Figure 7.3 with the results in Tables 6.4 and 6.6. The latter tables identified the largest normalized SF_6 concentrations observed at 700 m. Of the 40 values identified in these latter tables, only two are associated with σ_{y_i} values less than 10 m. Tables 6.4, 6.6 and 7.3 indicate average "worst case" wind speeds of 2.7 and 3.9 m/s.

For the 1 400 m traverses, the smallest σ_{y_i} values are associated with an average 10 m level wind speed of 3.54 m/s; the minimum value is 0.88 m/s. The mean values for σ_ϕ and σ_θ are 2.37 and 7.0 degrees, respectively. The average temperature gradient was 0.136 K/m (or 13.6 K/100 m), again indicating a relatively stable atmosphere. It is also interesting to compare the results from Table 7.4 with the results in Table 6.5. The latter table identified the 20 largest normalized SF_6 concentrations observed at 1400 m. Of the 20 values identified, only 2 are associated with σ_{y_i} values less than 20 m. Tables 6.5 and 7.4 indicate average "worst case" wind speeds of 3.5 to 3.9 m/s.

In Tables 7.3 and 7.4 there are what appear to be some anomalies based on the presumption that small plume sigma values are associated with stable conditions which are characterized by reduced turbulence. These anomalies include:

- The relatively large σ_ϕ and σ_θ (5.44 and 17.14 degrees, respectively) associated with the smallest 700 m σ_{y_i} value of 6.1 m (Traverse T31C02).

- The large positive heat flux (77.74 W/m^2) and negative Z/L value (-7.0) associated with the same traverse as above (Traverse T31C02).
- The large σ_θ values (> 20 degrees) associated with some of the 1 400 m σ_{y_i} values (Traverses T11A06, T11B11 and T11B12). These were also associated with the smallest wind speeds (< 1 m/s).
- The positive heat flux values and negative Z/L values associated with the traverses indicate slightly unstable conditions.

The anomaly concerning the sign of the heat flux and Z/L values is discussed in Section 8.3.2. Due to time constraints on the project the other anomalies were not explored further. One of the key findings from the results presented in these tables is that the smallest plume spreads appear to be associated with wind speeds of 3 to 4 m/s rather than the wind speeds less than 1 m/s. In addition the smallest σ_{y_i} values are not necessarily associated with the largest normalized concentration (χ/Q) values.

In Figure 7.17 the median values of σ_{y_i} are plotted versus Pasquill-Gifford Stability Class (PG). The PG class was based on a STAR analysis Calgary airport data. The cross-wind spread appears to increase from PG Class E to PG Class F. This would suggest that the PG class F condition may be accompanied by plume meander.

Vertical Spread σ_{z_i}

Vertical plume spreads (σ_{z_i}) were not measured during the Field Measurement Program due to the difficulty and expense associated with collecting vertical SF$_6$ concentration profiles. It is for this reason that vertical sampling of plumes has been extremely limited. The vertical plume spread can be estimated from the measured surface concentrations **if** the vertical profile shape is known (Briggs 1988).

There are two ways to estimate the vertical plume spread. The first is to base the estimate on the Gaussian plume spread approximation and to estimate σ_{z_i} from:

$$\sigma_{z_i} = \frac{Q \cdot 10^{12}}{\pi \sigma_{y_i} U \chi_i} \exp\left(\frac{-H^2}{2\sigma_z^2}\right)$$

which is the generic Gaussian dispersion model equation (Section 7.3.1) solved for σ_{z_i}. For ground-based releases, the exponential term becomes unity and σ_{z_i} can be directly estimated. The terms in the above equation are:

Q = SF$_6$ release rate (m^3/s)
U = wind speed at 4 m (m/s)
χ_i = SF$_6$ peak concentration (ppt)
σ_{z_i} = instantaneous crosswind spread (m).

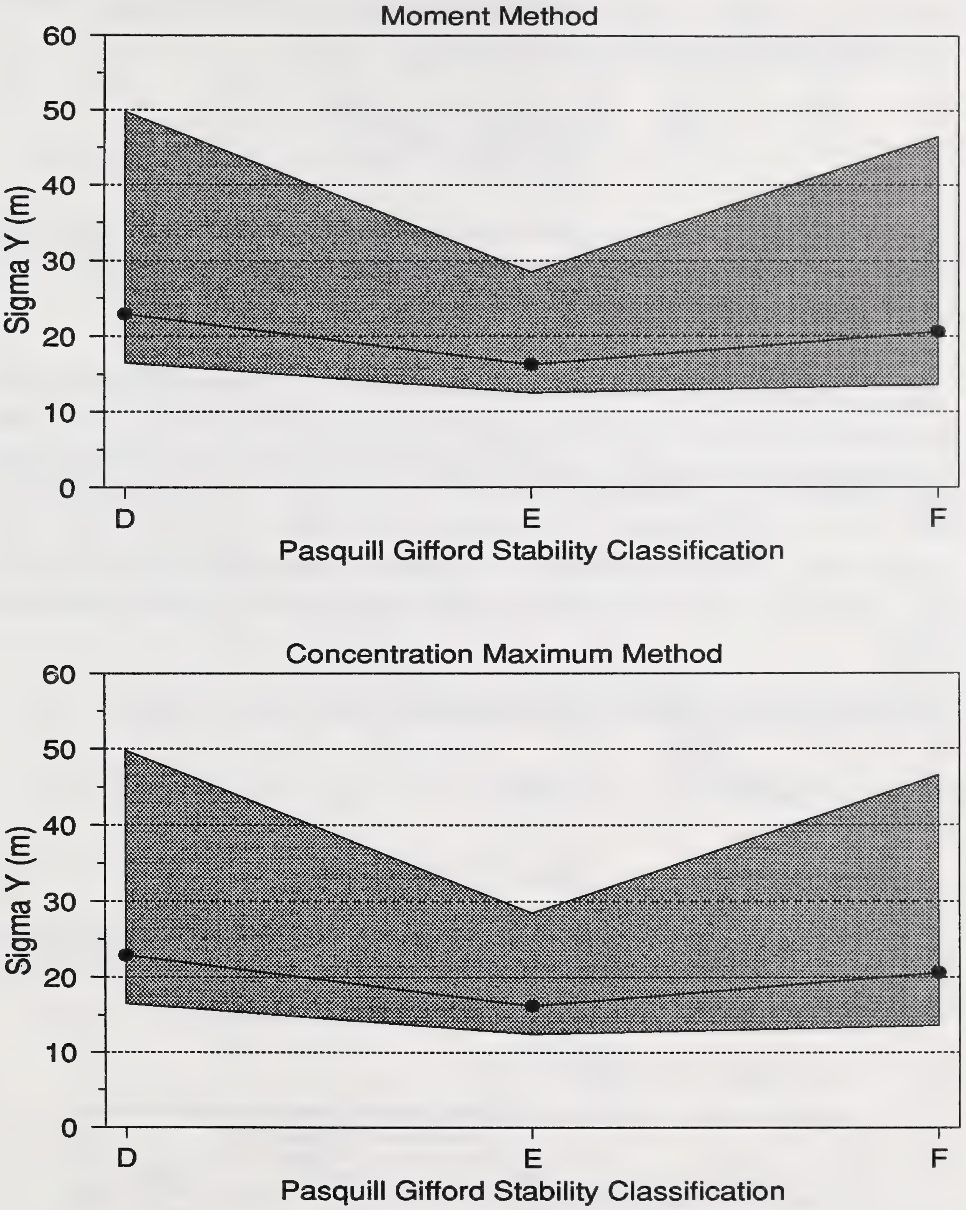

Figure 7.17

Median Values of σ_y

as a Function of Pasquill-Gifford Stability Class. Elevated and Ground Release Data for Moment Method and Concentration Maximum Method. The Shaded Envelope Indicates the 25 and 75 Percentile Limits.

Alternately, σ_{z_i} may be estimated from crosswind integrated concentration χ_{CWI} which is also based on the Gaussian plume approximation. In this case:

$$\sigma_{z_i} = \frac{2Q \cdot 10^{12}}{\sqrt{2\pi}\, U \chi_{CWI}} \exp\left(\frac{-H^2}{2\sigma_z^2}\right)$$

Similarly, for ground-based sources the exponential term becomes unity. The method based on the χ_{CWI} rather than χ_i is more attractive in that it is less dependent on the computational procedures used to estimate χ_i and σ_{y_i}.

While it is recognized that the second method has advantages in the estimation of σ_{z_i}, the first method was selected out of computational convenience. The estimation of σ_{z_i} from the Field Measurement Program focussed the analysis on the traverse concentration profiles associated with surface releases and assuming H = 0 m. Only downwind distances of 700 and 1 400 m were considered. The estimated values for σ_{z_i} were compared to the instantaneous σ_{z_i} relationships proposed by Islitzer and Slade (1968) and to Islitzer and Slade (1968) and to the time-averaged σ_z relationships proposed by Alberta Environment (1988).

The Islitzer and Slade (1968) suggested relationships for σ_{z_i} (m) are as follows:

• Unstable	$0.53\,x^{0.73}$
• Neutral	$0.15\,x^{0.70}$
• Very Stable	$0.05\,x^{0.61}$

where x is the downwind distance in (m). Again, the very stable values represent the limit of the most stable data that were available for the review. Application of the above relationships to the 700, 1 400 and 2 100 m sampling are as follows:

Instantaneous Plume Spread σ_{z_i} (m)

	Downwind Distance (m)		
Stability	700	1 400	2 100
Unstable	63.3	104.9	141.0
Neutral	14.7	23.9	31.7
Very Stable	2.7	4.2	5.3

Figure 7.18 shows the σ_{z_i} frequency distributions for neutral and stable conditions. The stability was based on the Pasquill-Gifford class derived from concurrent Calgary airport observations using the STAR preprocessor (Section 8.5.1) Under stable conditions (at a distance of 700 m), about and 31 and 64% of the σ_{z_i} values are less than 5 and 10 m

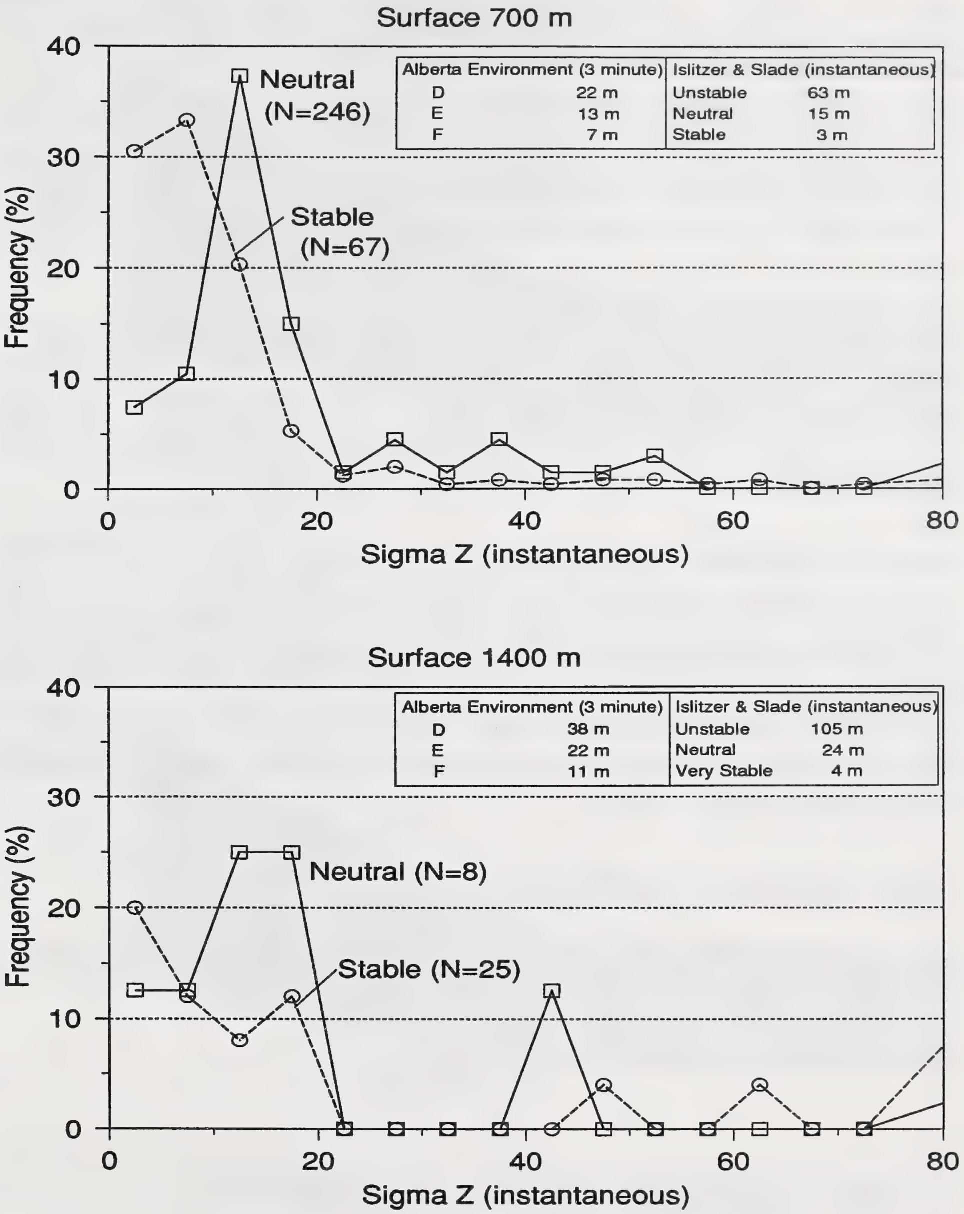

Figure 7.18

Frequency Distribution of σ_{z_i} for Neutral (PG Class D) and Stable (PG Classes E and F) Conditions for 700 and 1400 m. The Islitzer & Slade Instantaneous Values and Alberta Environment Values for σ_z are Presented at the Top of the Figure.

respectively. These are consistent with the predicted values proposed by Alberta Environment and Islitzer and Slade for stable conditions. Under neutral conditions (at a distance of 700 m) about 38% of the σ_{z_i} values are in the 10 to 15 m range. These are consistent with the predicted values proposed by Islitzer and Slade and are less than the Alberta Environment neutral values. At 1 400 m (stable conditions), about 20% of the σ_{z_i} values are less than 5 m; these are consistent with the Islitzer and Slade values and less than Alberta Environment values. Similarly, at 1 400 m (neutral conditions) about 50% of the σ_{z_i} values are in the 10 to 20 m range; these are less than the Islitzer and Alberta Environment values.

It is interesting to note that some of the estimated σ_{z_i} values are relatively large (greater than 20 m). Their relatively large values can be attributed to a failure in the Gaussian model to correctly account for the actual crosswind or vertical concentration profiles. For example, Horst (1979) suggests the vertical plume spread for a surface release follows an exponential rather than a Gaussian form. It is for this reason that different dispersion formulations have been used for surface and elevated releases (eg. van Ulden 1978).

Figure 7.19 compares the calculated σ_{z_i} values obtained using the moment and concentration maximum methods, categorized by Pasquill-Gifford stability classes (PG). The PG class was based on a STAR analysis of Calgary airport data. Very little difference between the field data fitting methods is evident. The vertical spread appears to increase from PG class E to PG class F. A similar trend was observed for the crosswind spread σ_{y_i} (Figure 7.17). For σ_{y_i}, the increase was attributed to meander. However, since the same trend was observed for both σ_{y_i} and σ_{z_i}, it may be due to the inability of the STAR method to differentiate between E and F stability classes.

7.1.4.2 Theoretical Considerations

In finite difference form, the instantaneous or relative dispersion can be estimated from Pasquill and Smith (1983, page 156):

$$\Delta\sigma_{y_i} = \frac{2}{3}\beta\frac{\sigma_V^2}{U^2}\Delta x \qquad (7.1)$$

Assuming that the ratio of the Lagrangian to Eulerian time scales (β) can be given by Panofsky and Dutton (1984, page 252):

$$\beta = \frac{\sqrt{\pi}U}{4\sigma_V} \qquad (7.2)$$

and that:

$$\sigma_{y_i}(x=0) \ll \sigma_{y_i}(x=x_1) \qquad (7.3)$$

where x_l = 700, 1 400 or 2 100 m sampling distances, then:

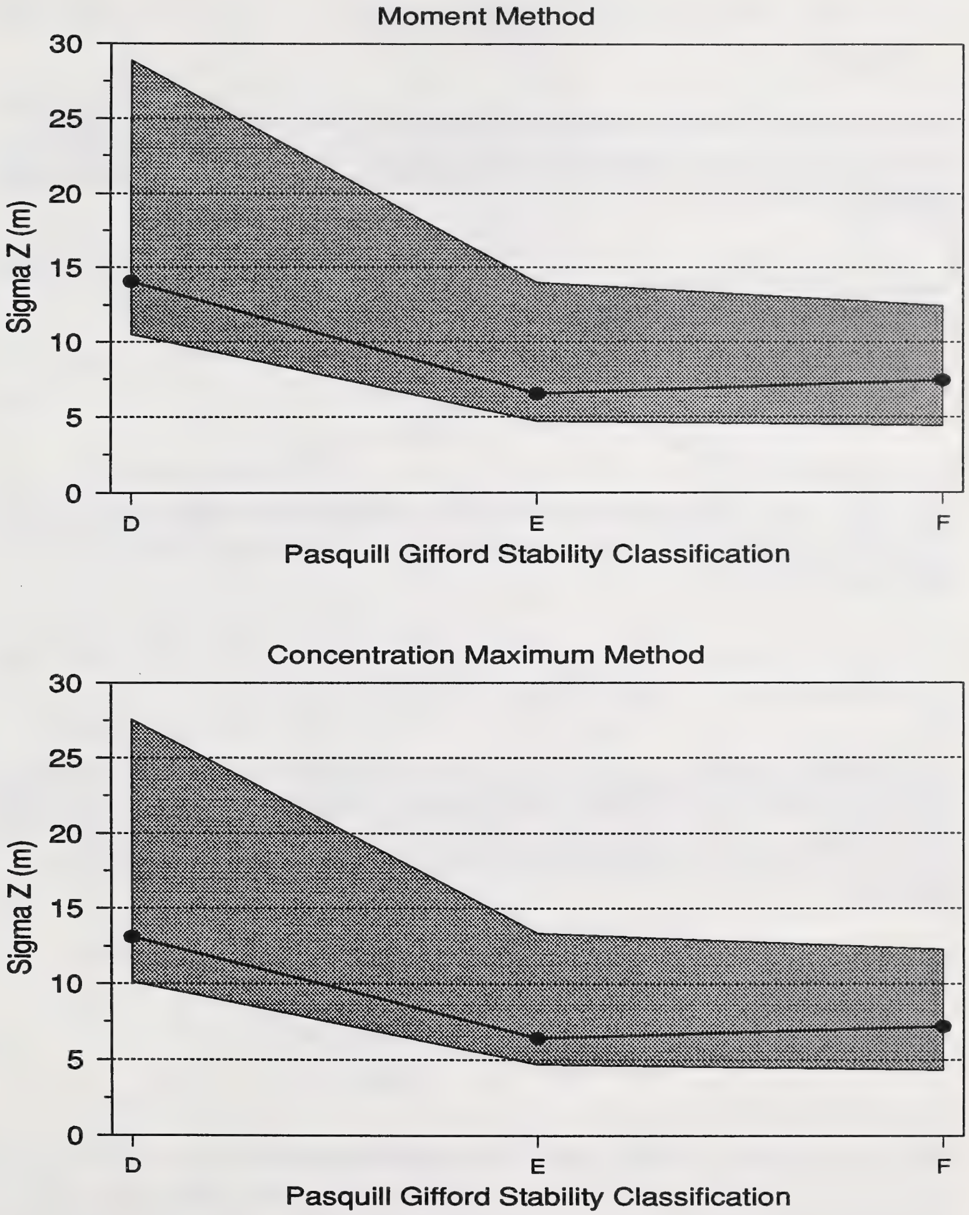

Figure 7.19

Median Value of σ_{z_i} as a Function of Pasquill-Gifford Stability Class. Ground Releases Data for Moment Method and Concentration Maximum Method. The Shaded Envelope Indicates the 25 and 75 Percentile Limits.

$$\sigma_{y_i} = 0.3\frac{\sigma_V}{U}x \quad \approx 0.3\sigma_\theta x \tag{7.4}$$

The estimate of σ_y is based on turbulence in a uniformly homogeneous atmosphere. In the real world, the variation of wind direction with height will enhance the horizontal spread (Pasquill and Smith, 1983). This effect is most obvious under stable conditions and/or long travel times.

Pasquill and Smith's discussion on the wind direction shear enhancement is based on Smith (1965). The enhancement of crosswind spread by wind shear can be given by:

$$WDE = \frac{\sqrt{\sigma_{y_i}^2(t) + \sigma_{y_i}^2(s)}}{\sigma_{y_i}(t)} \tag{7.5}$$

where $\sigma_y(s)$ is the wind shear term and $\sigma_y(t)$ is the turbulence term. The ratio of the wind shear term to the turbulence term can be estimated from (Pasquill and Smith 1983, Davison and Leavitt 1979):

$$\frac{\sigma_{y_i}(s)}{\sigma_{y_i}(t)} = \left(\frac{1}{12}\right)^{1/2} \frac{\tan|\alpha|}{\Delta Z}\left(\frac{\sigma_W}{\sigma_V}\right)\left(\frac{t_{wl}}{t_{vl}}\right) \quad x \tag{7.6}$$

where α is the wind direction difference over the vertical layer ΔZ. The terms t_{wl} and t_{vl} are the integral time scales for the vertical and cross-wind components of turbulence. As a first approximation, t_{wl}/t_{vl} can be assumed to be equal to unity. While this approximation is valid for neutral conditions, departures of the ratio t_{wl}/t_{vl} from unity may be expected for stable conditions.

The enhanced plume spread can be estimated by combining Equations 7.4 to 7.6:

$$\sigma_{y_i} = \frac{0.3\sigma_V x}{U}\sqrt{1 + \frac{1}{12}\frac{\tan^2|\alpha|}{(\Delta Z)^2}\left(\frac{\sigma_W}{\sigma_V}\right)^2 x^2} \tag{7.7}$$

This expression for σ_y refers explicitly to instantaneous dispersion and accounts for the wind direction shear enhancement. The above expression still assumes that both σ_V and U are essentially constant with height. Specifically, it assumes these values are constant over the layer bounded by the height of the plume (upper surface) and the height of the receptor (lower surface). It is therefore important that representative values for σ_V and U be selected when comparing predicted and observed values.

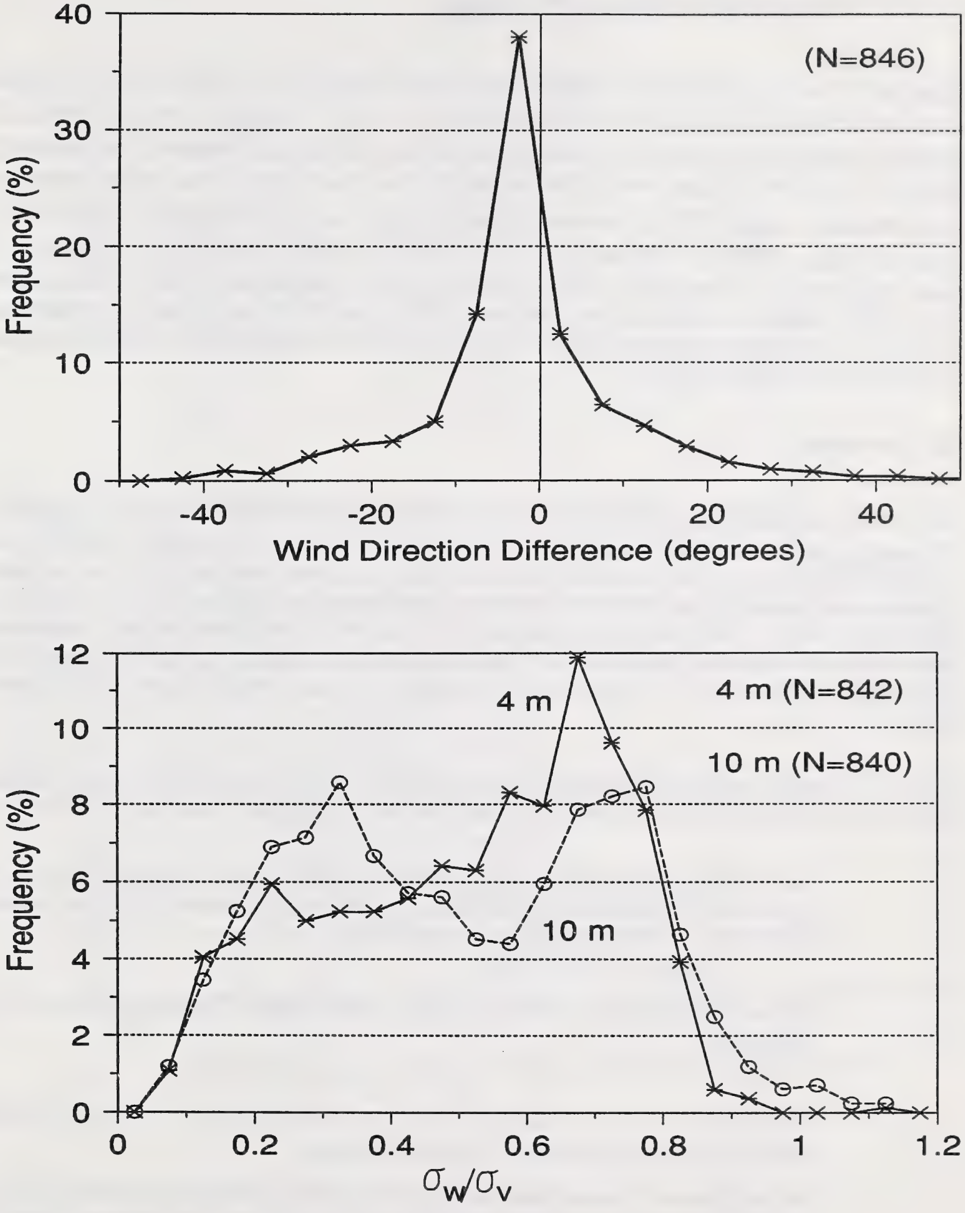

Figure 7.20

Frequency Distribution of Wind Direction Difference (α) Over the 4 and 10 m Level, and σ_W/σ_V during the Times of the Traverses.

7.1.4.3 Comparison to Observed Values

Equation 7.7 was applied to the Field Measurement Program data where α is the wind direction difference over the 4 to 10 m layer ($\Delta Z = 6$ m). The ratio σ_W/σ_V was obtained from the 4 and 10 m levels and applied to the surface and elevated releases, respectively. Figure 7.20 shows the frequency distribution of α and σ_W/σ_V for periods when traverses were obtained. About 30% of the wind shear $|\alpha|$ values exceed 10 degrees. The median observed σ_W/σ_V ratios are 0.55 and 0.50 at the 4 and 10 m levels, respectively. Figure 7.21 shows the frequency distribution of the wind direction enhancement (*WDE*). About 30% of the *WDE* values are less than two and about 10% of the *WDE* values are more than six. The *WDE* values greater than six indicate that the *WDE* term can have a significant effect on the crosswind plume spread.

All Traverses

The median predicted σ_{y_i} values are plotted as functions of the observed values. The degree of scatter about the median is indicated by the shaded band that is bounded by the 25 and 75 percentile values. A minimum of 5 values in each class was required for a comparison. The observed values include those obtained from the Moment method and the Concentration Maximum method. All the plots shows the 1:1 line which indicates perfect agreement between observations and predictions. In addition, the plots also show the median predicted value based on Equation 7.4 which does not include the wind direction shear enhancement term.

Figure 7.22 shows the results for all downwind distances and source release types. For the observed values based on the Moment method, the following comments can be made:

- The 1:1 line falls between the wind direction shear enhanced predicted values (Equation 7.7 is depicted by a solid line) and the non-enhanced predicted values (Equation 7.4 is depicted by a dashed line).
- For small observed σ_{y_i} values (< 10 m), both models (Equations 7.7 and 7.4) overpredict.
- For large observed σ_{y_i} values (> 70 m), better agreement is obtained between the observed and Equation 7.7 predicted values.
- For the observed values based on the Concentration Maximum method, the 1:1 line falls between the wind direction shear enhanced predicted values (Equation 7.7) and the non-enhanced values (Equation 7.4) for observed σ_{y_i} values larger than 70 m.

The results presented in Figure 7.22 indicate that the wind direction shear term can be important in its contribution to enhancing the plume spreads. The largest number of observed plume spreads were associated with elevated and surface 700 m traverses (68%), and elevated 1 400 m traverses (26%). Therefore, only these observed plume spreads were compared to model (Equation 7.7) predictions. The results of these comparisons are shown in Figures 7.23 to 7.25.

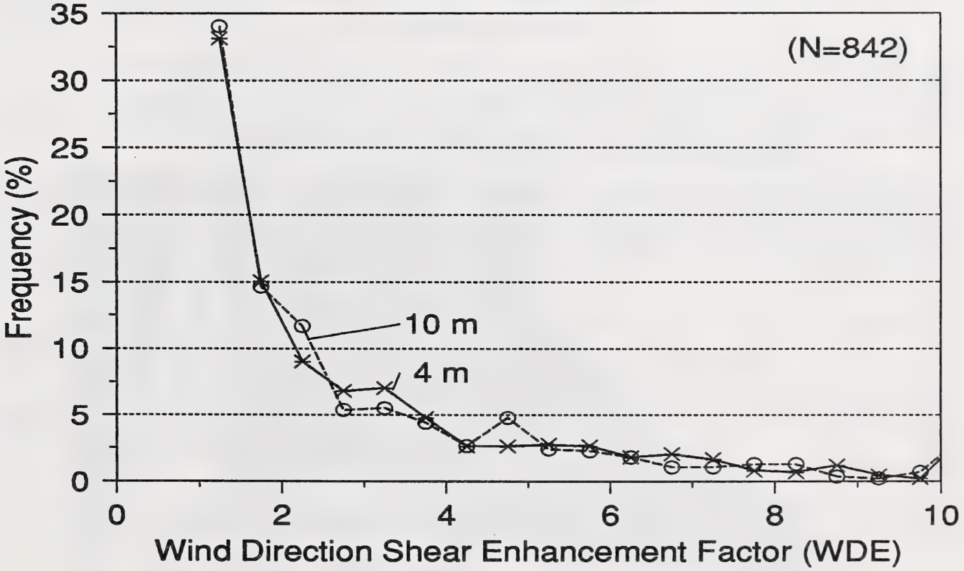

Figure 7.21

Frequency Distribution of Wind Shear Enhancement Factor (*WDE*) to the Crosswind Plume Spread.

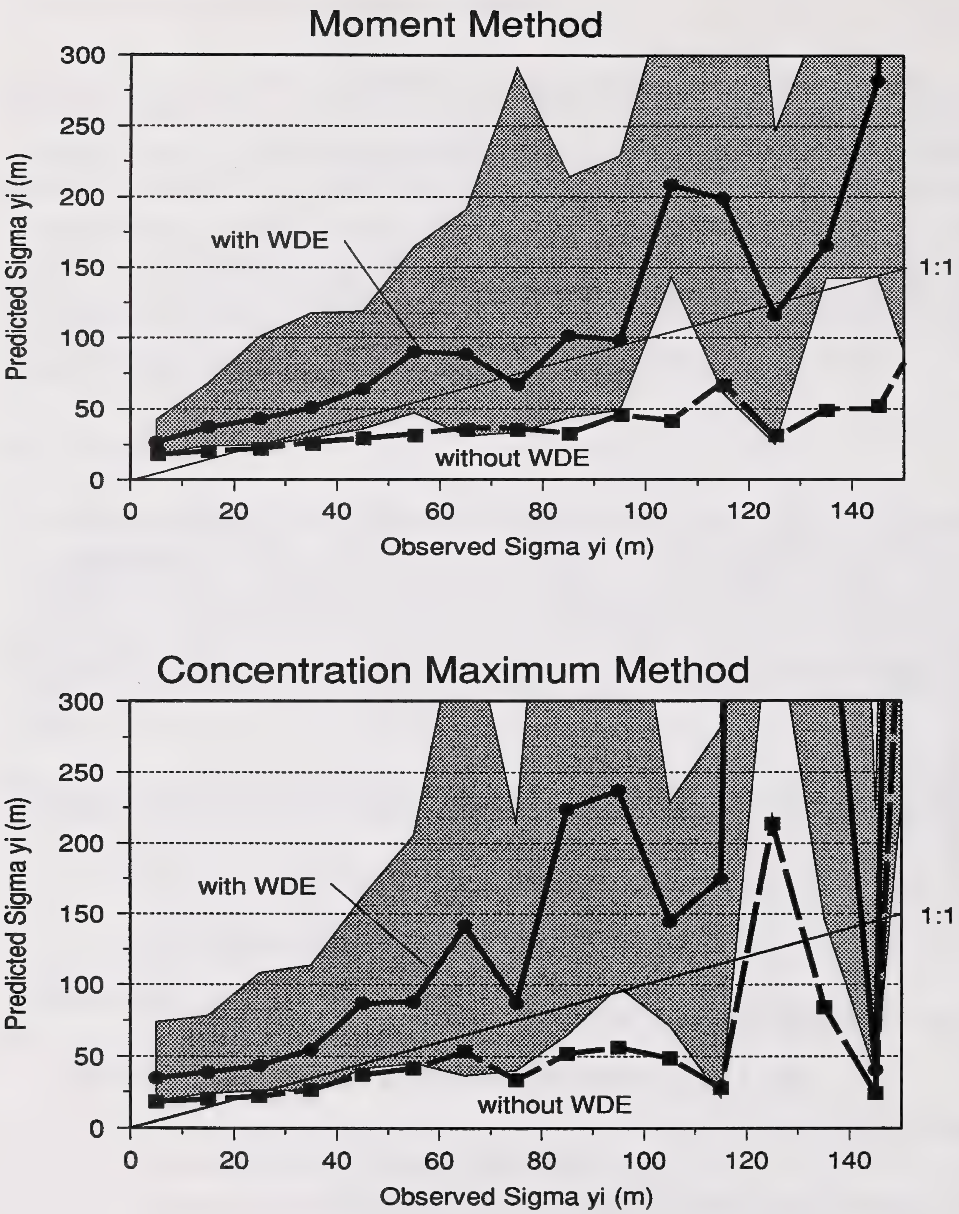

Figure 7.22

Comparison of Instantaneous Predicted and Observed Plume Spreads (σ_{y_i}) for All Source Types (Elevated and Ground) and all Sampling Arcs (700, 1400 and 2100 m). The Dashed Line Represents the Median Values Without *WDE* Factor. The Shaded Envelope Indicates the 25 and 75 Percentile Limits.

Ground Release (700 m) Traverses

Figure 7.23 shows the results for surface releases and a downwind distance of 700 m. For the observed values based on the Moment method, the following comments can be made:

- For observed plume spreads (σ_{y_i}) less than 20 m, the Equation 7.4 model overpredicts.
- For observed plume spreads (σ_{y_i}) less than 60 m, the Equation 7.7 overpredicts the plume spreads.
- For plume spreads (σ_{y_i}) greater than 60 m, the agreement between the observations and the predicted values are better.

For the observed values based on the Concentration Maximum method, the following comments can be made:

- For observed values less than 60 m, the predicted values based on wind direction shear enhanced term tend to overpredict. In the same range, the agreement between predicted values based on no wind shear tend to be in better agreement.

Both graphs in Figure 7.23 indicate that for observed values less than 10 m, overpredictions result. The shaded band indicates considerable scatter between predictions and observations. The incorporation of wind shear enhancement in the predictions can sometimes increase the agreement between observations and predictions.

Elevated Release (700 m) Traverses

Figure 7.24 shows the results for elevated releases and a downwind distance of 700 m. The results presented in the figure indicate that:

- For small observed plume spreads ($\sigma_{y_i} < 60$ m), the agreement between the model and observations are qualitatively good.
- For large plume spreads ($\sigma_{y_i} > 60$ m), the Moment method observations are less than the predicted values, and the Concentration Maximum observations are larger than the predicted values.

The shaded band indicates less uncertainty with the elevated releases than with the surface releases. The predicted values based on Equation 7.4 are significantly smaller than those observed, which indicates that wind direction shear term cannot always be neglected.

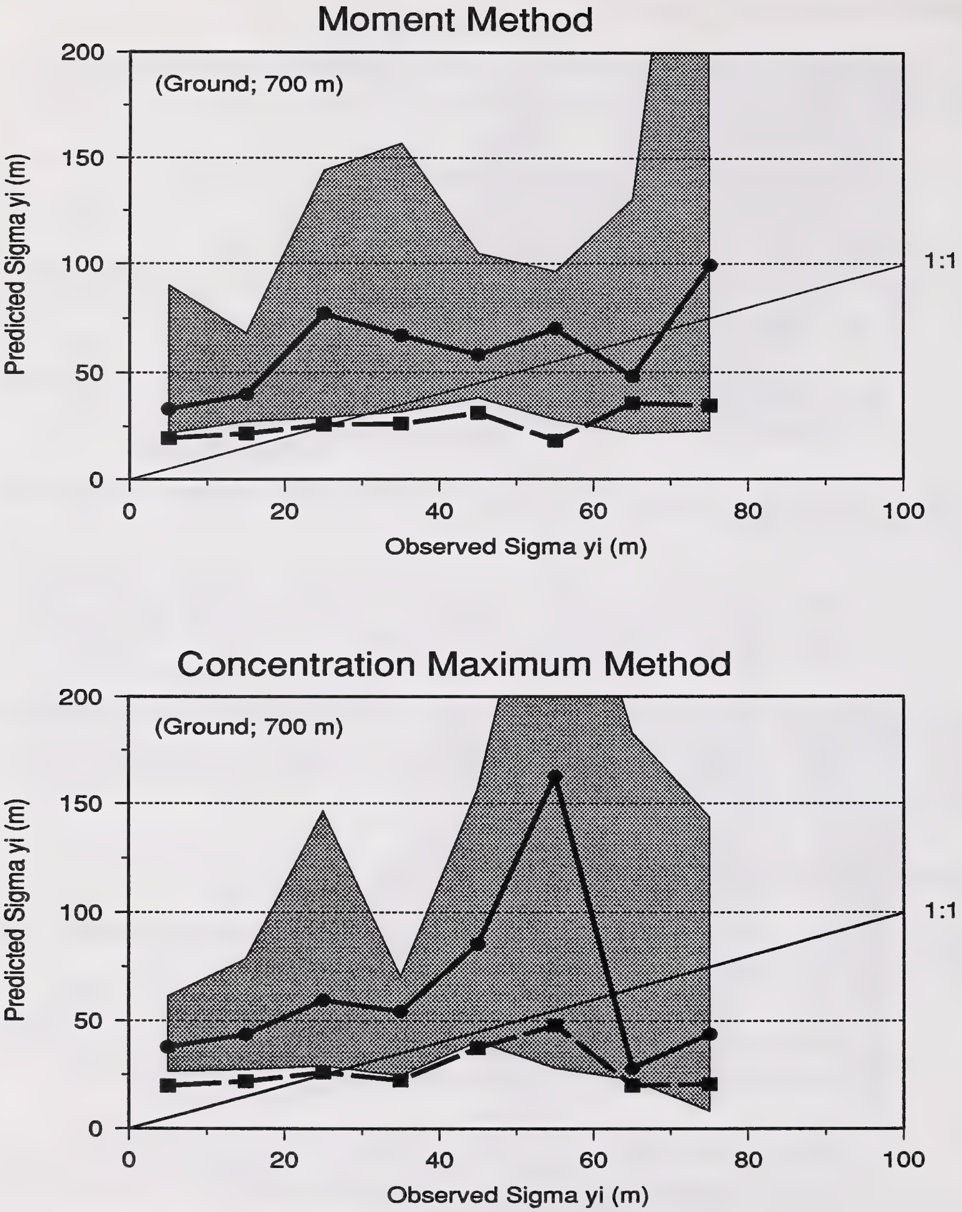
Moment Method

Concentration Maximum Method

Figure 7.23

Comparison of Instantaneous Predicted and Observed Plume Spreads (σ_{y_i}) for Ground Source, 700 m Data. The Dashed Line Represents the Median Values Without *WDE* Factor. The Shaded Envelope Indicates the 25 and 75 Percentile Limits.

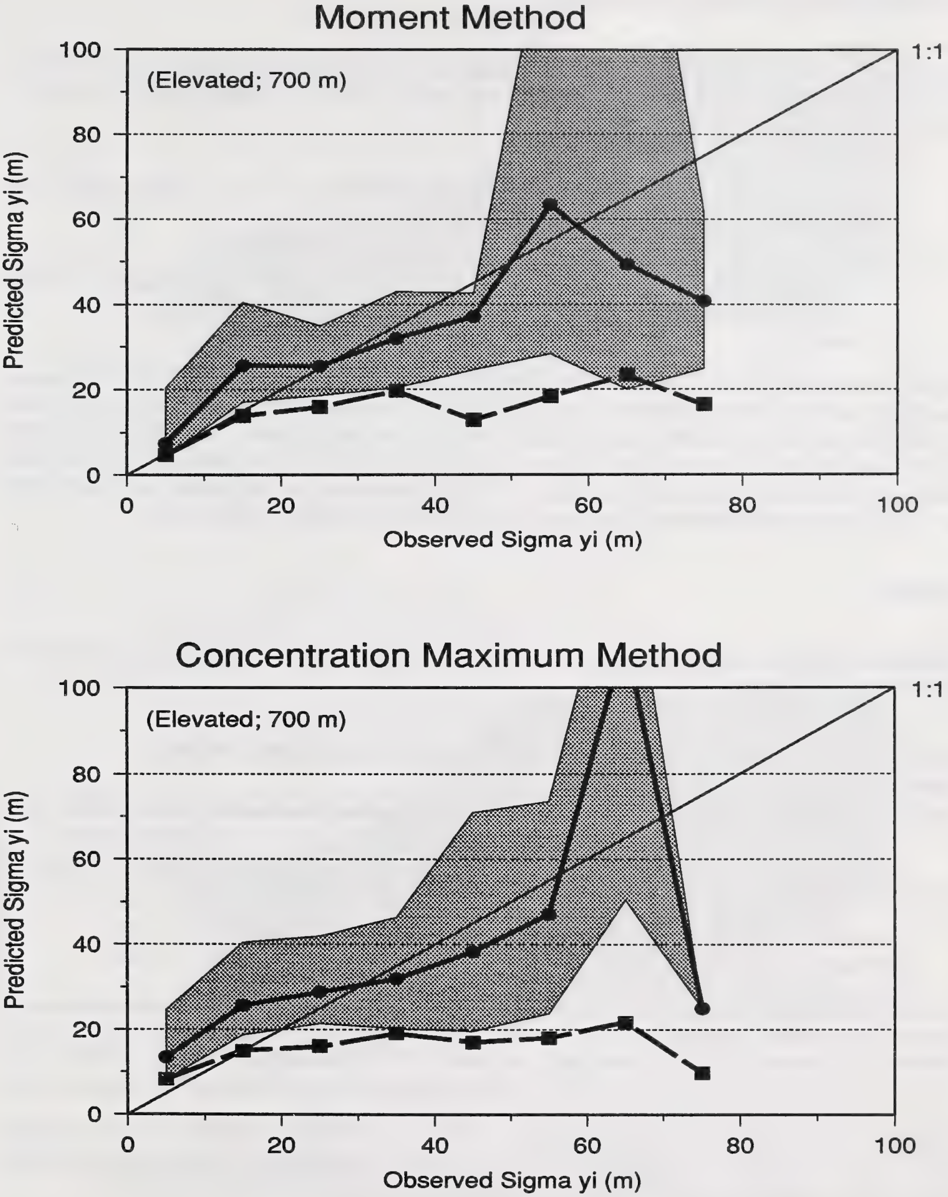

Figure 7.24

Comparison of Instantaneous Predicted and Observed Plume Spreads (σ_{y_i}) for Elevated Source, 700 m Data. The Dashed Line Represents the Median Values Without *WDE* Factor. The Shaded Envelope Indicates the 25 and 75 Percentile Limits.

Elevated Release (1 400 m) Traverses

Figure 7.25 shows the results for elevated releases and a downwind distance of 1 400 m. For the observed values based on the Moment method, the following comments can be made:

- The predicted values are systematically shifted by 50 m to values which are larger than those observed.

- There appears to be a better agreement between predicted and observed values when the wind shear term is not included in the predicted values.

Similar conclusions can be made from the observed values based on the Concentration Maximum method. As can be seen from both comparison plots, there is considerable scatter between the median predicted plume spreads and the observed values. The predicted values based on Equation 7.4 are similar to those observed, indicating that wind direction shear does not appear to be as important at 1 400 m. This is somewhat in contrast to the expectation that wind direction shear should be more important for the larger travel time.

Summary

The following tables indicates the percent of the predictions that were within a factor of two of the observed values:

Percent Within a Factor of Two (with Wind Direction Shear Enhancement);
(Equation 7.7).

Traverses	Moment Method	Concentration Maximum Method
All (Figure 7.19)	44	39
Ground, 700 m (Figure 7.20)	36	32
Elevated, 700 m (Figure 7.21)	63	60
Elevated, 1 400 m (Figure 7.22)	37	32

The best agreement appears to be with the elevated release plume spreads observed at a downwind distance of 700 m when approximately 60% are within a factor of two. The observed plume spreads (σ_{y_i}) were not well correlated with the standard deviation of the horizontal wind direction fluctuation (σ_θ). As the correlation is based on atmospheric turbulence in a uniform atmospheric layer, the lack of correlation should not be surprising in the stable boundary layer where large wind direction shears can be observed.

The addition of a shear correction term was found to increase the qualitative agreement between the median predicted and observed values for all distances. In summary, a preliminary analysis of the plume spread data indicates that the model represented in Equation 7.7 appears to be best able to predict the elevated release plume spreads at a downwind distance of 700 m.

From the following table with no wind shear enhancement it is interesting to note that 1 400 m level agreement has increased substantially:

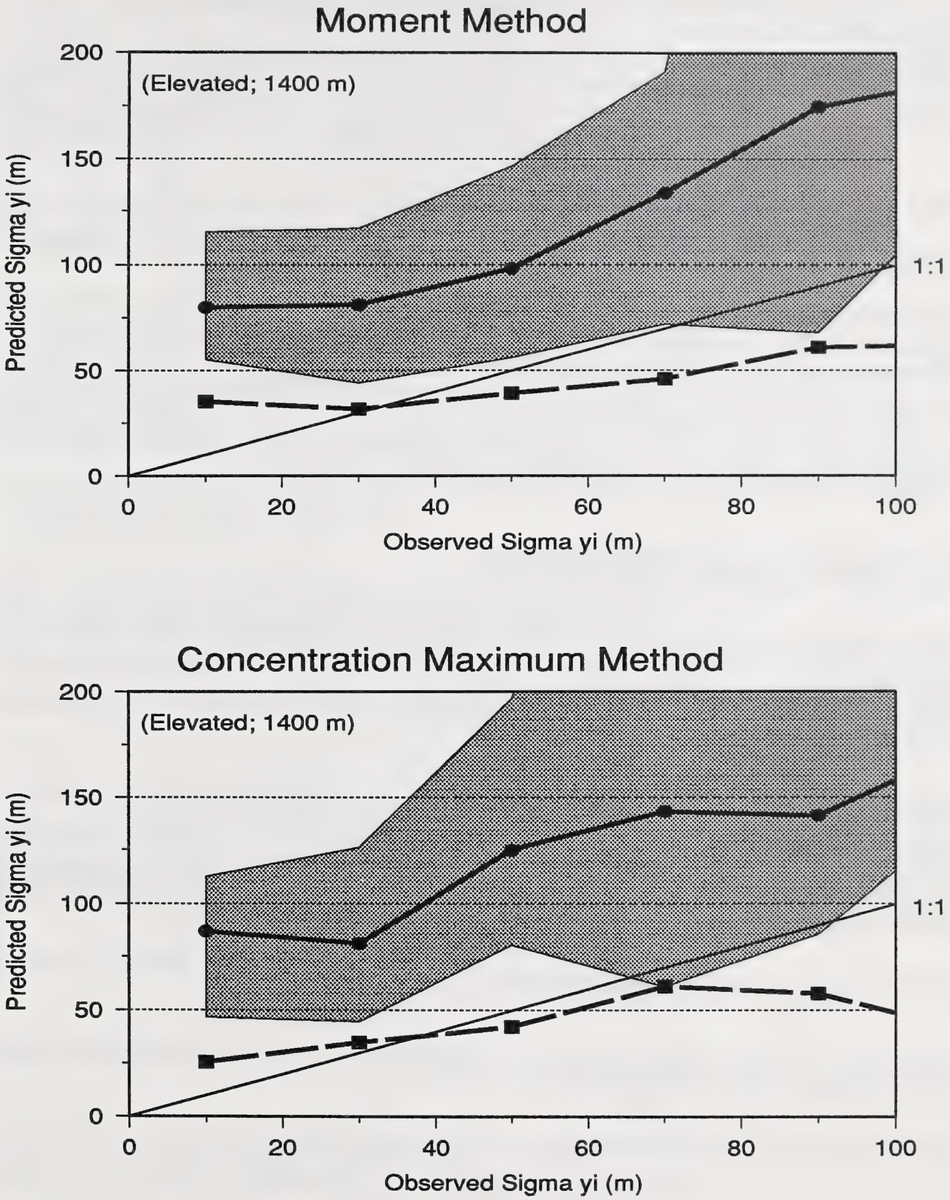

Figure 7.25

Comparison of Instantaneous Predicted and Observed Plume Spreads (σ_{y_i}) for Elevated Source, 1400 m Data. The Dashed Line Represents the Median Values Without *WDE* Factor. The Shaded Envelope Indicates the 25 and 75 Percentile Limits.

Percent Within a Factor of Two (No Wind Direction Shear Enhancement); (Equation 7.4).

Traverses	Moment Method	Concentration Maximum Method
All (Figure 7.19)	64	66
Ground, 700 m (Figure 7.20)	64	64
Elevated, 700 m (Figure 7.21)	58	64
Elevated, 1 400 m (Figure 7.22)	71	72

The thrust of this preliminary analysis of the data has been to focus on all the traverses and not on case studies. To further define the ability to predict instantaneous plume spreads, it is recommended that a case study approach be adopted. The case study approach should focus on selecting periods that are characterized by relatively stationary and horizontally homogeneous wind and turbulence conditions. This can be specifically accomplished by selecting periods where a sequence of individual traverse profiles are relatively uniform with time and accompanied by a relatively uniform wind direction.

7.1.5 Time-Averaged Plume Spreads

The discussion in the previous section focussed on the instantaneous or relative dispersion plume spreads (σ_{y_i}). The (σ_{y_i}) values were based on individual crosswind SF_6 concentration profiles. The plume spread values used in dispersion models are based on time-averaged values at fixed locations downwind of a source.

Time-averaged or composite plume spreads (σ_{y_c}) can be estimated from a series of instantaneous plume spreads (σ_{y_i}). Longer term plume spreads (typically representing one-half or one hour) will be more influenced by meandering motions. The following sections discuss the estimation of composite plume spreads from the traverse data.

7.1.5.1 Theoretical Considerations

The longer-term plume spreads can be estimated from the instantaneous plume spreads using the relationship (Hanna 1983):

$$\sigma_{y_c}^2(t) = \left(\frac{1}{N}\sum_{n=1}^{N}\sigma_{y_i}(n)\right)^2 + \frac{1}{N}\sum_{n=1}^{N}(Y_n - \overline{Y})^2 \qquad (7.8)$$

where:

$\sigma_{y_c}(t) =$ composite plume spread from N plume traverses
$t =$ specified averaging period
$\sigma_{y_i}(n) =$ individual plume spread from a single plume traverse
$Y_n =$ plume centroid position from a single plume traverse
$\overline{Y} =$ average centroid position of N plume traverses

The first term on the right is the measure of the relative diffusion while the second term is the measure of the plume meander. The meander term can contribute significantly to the overall plume spread for averaging times of about one hour (Hanna 1983), particularly under low wind speed, stable conditions. To evaluate the importance of the relative diffusion and meander terms, the instantaneous plume spreads (Moment method) were used to estimate one-half and one-hour average plume sigmas using Equation 7.8.

The ratio of the composite plume spread for one-half and one-hour averaging periods to the relative plume spread can be derived from Equation 7.1:

$$M\left(\frac{\text{Composite}}{\text{Relative}}\right)=\frac{\left(\frac{1}{N}\sum_{n=1}^{N}\sigma_{y_i}(i)\right)^2+\frac{1}{N}\sum_{n=1}^{N}(Y_n-\overline{Y})^2}{\left(\frac{1}{N}\sum_{n=1}^{N}\sigma_{y_i}(i)\right)^2} \tag{7.9}$$

If the meander term is very small, then this ratio will approach unity. As the meander term increases, the ratio will also increase.

Time-averaged or composite plume spreads can be calculated as a function of downwind distance and meteorology from the following relationship (Irwin 1983):

$$\sigma_{y_c}=\frac{\sigma_v}{U}xf_y \tag{7.10}$$

where σ_V and U are the standard deviation of the crosswind wind speed and the horizontal wind speed respectively. The function f_y is a non-dimensional function of travel time which is equal to unity at travel time $(x/U)=0$ and decreases with increasing travel time. For near neutral and stable conditions, Draxler's (1976) proposed values for f_y can be used:

Elevated Releases:

$$f_y=\frac{1}{1+0.9\sqrt{x/(1000\,U)}} \tag{7.11}$$

Ground Releases:

$$f_y=\frac{1}{1+0.9\sqrt{x/(300\,U)}} \tag{7.12}$$

Equation 7.10 can be rewritten in terms of the standard deviation of the horizontal wind direction standard deviation (σ_θ):

$$\sigma_{y_c}=\sigma_\theta xf_y \tag{7.13}$$

Equation 7.13, in conjunction with Equations 7.11 and 7.12, can be used to predict the plume spread knowing the downwind distance x, the mean transport wind speed U and the wind direction standard deviation σ_θ. For the purposes of model assessment, two estimations of σ_θ were used. The first is based on the average σ_θ calculated from:

$$\sigma_{\theta_1} = \sqrt{\left(\frac{1}{N}\sum_{n=1}^{N}\sigma_{\theta_n}\right)^2 + \frac{1}{N}\sum_{n=1}^{N}(\bar{\theta}-\theta_n)^2} \qquad (7.14)$$

where the first term is a measure of the turbulence component and the second term is a measure of the meander component. This expression for σ_θ, however, does not include the enhancement due to wind direction shear. For this reason, a second σ_θ was calculated from:

$$\sigma_{\theta_2} = \sqrt{\left(\frac{1}{N}\sum_{n=1}^{N}\sigma_{\theta_n}\right)^2 \left(1+\frac{1}{12}\frac{\tan^2\alpha}{\Delta Z^2}\left(\frac{\sigma_W}{\sigma_V}\right)^2 x^2\right)^{1/2} + \frac{1}{N}\sum_{n=1}^{N}(\bar{\theta}-\theta_n)^2} \qquad (7.15)$$

This enhanced σ_θ accounts for turbulence, plume meander, wind direction shear and can be used in Equation 7.13. The correction factor for wind shear used in the above equation is the same that was applied to the instantaneous releases.

7.1.5.2 Observed Values

The 846 individual SF_6 concentration profiles were scanned and blocked into nominal one-half and one-hour groupings. A total of 173 one-half hour and 83 one-hour groupings were created from the data. These blocks formed the basis of the time-averaged plume spread assessment.

For the purposes of assessment, the time-averaged data were also grouped according to source type, (elevated or ground) and downwind distance (700, 1 400 or 2 100 m). The number of one-half data periods that fall into each group are summarized below:

Frequency of Occurrence (1/2 hour).

Source Type	Distance (m)			Total
	700	1 400	2 100	
Elevated	60 (35%)	45 (26%)	4 (2%)	109 (63%)
Ground	58 (34%)	6 (4%)	0 (0%)	64 (37%)
Total	118 (69%)	51 (29%)	4 (2%)	173 (100%)

Most of the one-half hour data periods are associated with the 700 m distance (69%) and elevated sources (63%).

For the purposes of comparison, the equivalent table for the one-hour data periods were also grouped according to source type and downwind distance:

Frequency of Occurrence (1 hour).

Source Type	Distance (m)			Total
	700	1 400	2 100	
Elevated	26 (31%)	21 (25%)	2 (3%)	49 (59%)
Ground	30 (36%)	4 (5%)	0 (0%)	34 (41%)
Total	56 (67%)	25 (30%)	2 (3%)	83 (100%)

There are about one-half the number of one-hour data periods as there are one-half hour data periods. Most of the one-hour data periods are associated with the 700 m distance (67%) and elevated sources (59%)

The average number of traverses which comprise the calculated one-half and one-hour average values are given in the following table:

Mean Number of Traverses per Averaging Period (N).

Source Type	Distance (m)	Averaging Period	
		0.5 hour	1.0 hour
Elevated	700	3.8	6.8
	1 400	3.7	6.4
	2 100	3.3	5.5
Ground	700	4.3	7.4
	1 400	3.2	5.3

As the mean number of averaging periods per traverse are relatively small, some uncertainty will be associated with each nominal one-half and one-hour data period.

Figure 7.26 shows the frequency distribution of the ratio of the composite plume spread to the relative plume spread (m) for one-half and one-hour averaging periods. The results of the histogram can be summarized as follows:

Averaging Period	$M\left(\frac{\text{Composite}}{\text{Relative}}\right)$		
(h)	Minimum	Maximum	Mean
0.5	1.0	24.0	3.9
1.0	1.1	13.7	4.6

The maximum value of the ratio indicates considerable meander can occur which will have the effect of significantly increasing the time-averaged dispersion σ_{y_c}. These maximum values are not significantly different from those reported in the literature by others (e.g. Hanna, 1983, reported ratios in the 5 to 10 range).

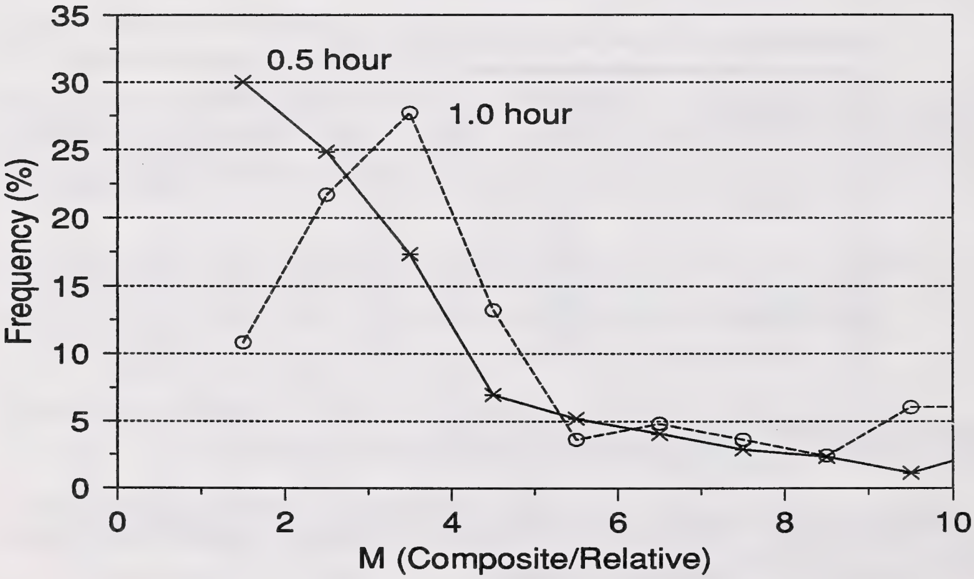

Figure 7.26

Histogram of Composite Plume Spread (σ_{y_c}) to Relative Dispersion (σ_{y_i}) Ratio for One-half Hour and One-hour Averaging Periods (All Stability Classes).

While significant increases are noted, about 30 and 11 percent of the ratios for the one-half and one-hour averaging periods, respectively, fall into the 1 to 2 range. For the one-half hour spreads, the most frequent ratios of composite to relative dispersion plume spreads are in the 1 to 2 range. For the one-hour plume spreads, the most frequent ratios are in the 3 to 4 range. This difference indicates the increased wind variability (meander) with the larger averaging period. The minimum values of the ratio for the one-half and one-hour averaging period, however, indicate that wind direction can remain fairly constant over a one-hour period.

The previous results of the ratio M were based upon all stability classes (neutral and stable) and wind speeds. It is useful to review how the ratio varies with wind speed and atmospheric stability. It is expected that plume meander would be present and produce larger values of the ratio when low wind speeds and low levels of turbulence (stable conditions) are present.

Figure 7.27 shows the median values of the ratio M as a function of 10 m level wind speed for one-half and one-hour averaging periods. The wind speed was obtained from the nearest one-half hour average observation period. For the one-half hour ratios, the median values tend to be about 2.8 for wind speeds less than 4 m/s, increasing to a maximum of 5.3 at a wind speed of 5 m/s. The one-hour ratio follows a similar trend with a fairly uniform value of about 3.8 for wind speeds less than 4 m/s, increasing to 6.8 for a wind speed of 5 m/s. This finding indicates that, contrary to our initial expectation, plume meander can be even more important in terms of increasing the overall time-averaged plume spreads for moderate wind speeds (4 to 5 m/s range) than for low wind speeds (0 to 3 m/s range).

Figure 7.28 shows the median value of the ratio M as a function of the Monin-Obukhov stability parameter (Z/L). For stable conditions, (Z/L > 0), the ratio M tends to initially increase with increasing stability (increasing Z/L) up to Z/L value of 0.8 and then decreases with further increases in stability. This latter change is in contrast with our initial expectation but is nonetheless consistent with the wind speed dependency.

Figures 7.27 and 7.28 indicate the median ratios tend to be in the 2 to 10 range for a wide range of wind speeds and Z/L values. These median values represent enhanced dispersion with the longer averaging periods. However, it should be noted that about 25% of the one-half hour average ratios are between 1 and 2 resulting in minimal enhanced dispersion. For the one-hour average case, there is a tendency for meander to enhance dispersion by a minimum of 2 to 3 for the low wind and low turbulence cases.

7.1.5.3 Comparison to Observed Values

Equation 7.13 was applied to the Field Measurement Program data to predict one-half average plume spreads. Both the non-enhanced and wind shear enhanced σ_θ values were used. The α value was obtained over the 4 to 10 m layer ($\Delta Z = 6$ m). The ratio of σ_W/σ_V, wind direction θ and the standard deviation σ_θ were obtained from the 4 to 10 m levels for the surface and elevated releases, respectively. Draxler's surface and elevated f_y functions (Equations 7.11 and 7.12) were applied to the surface and elevated releases, respectively.

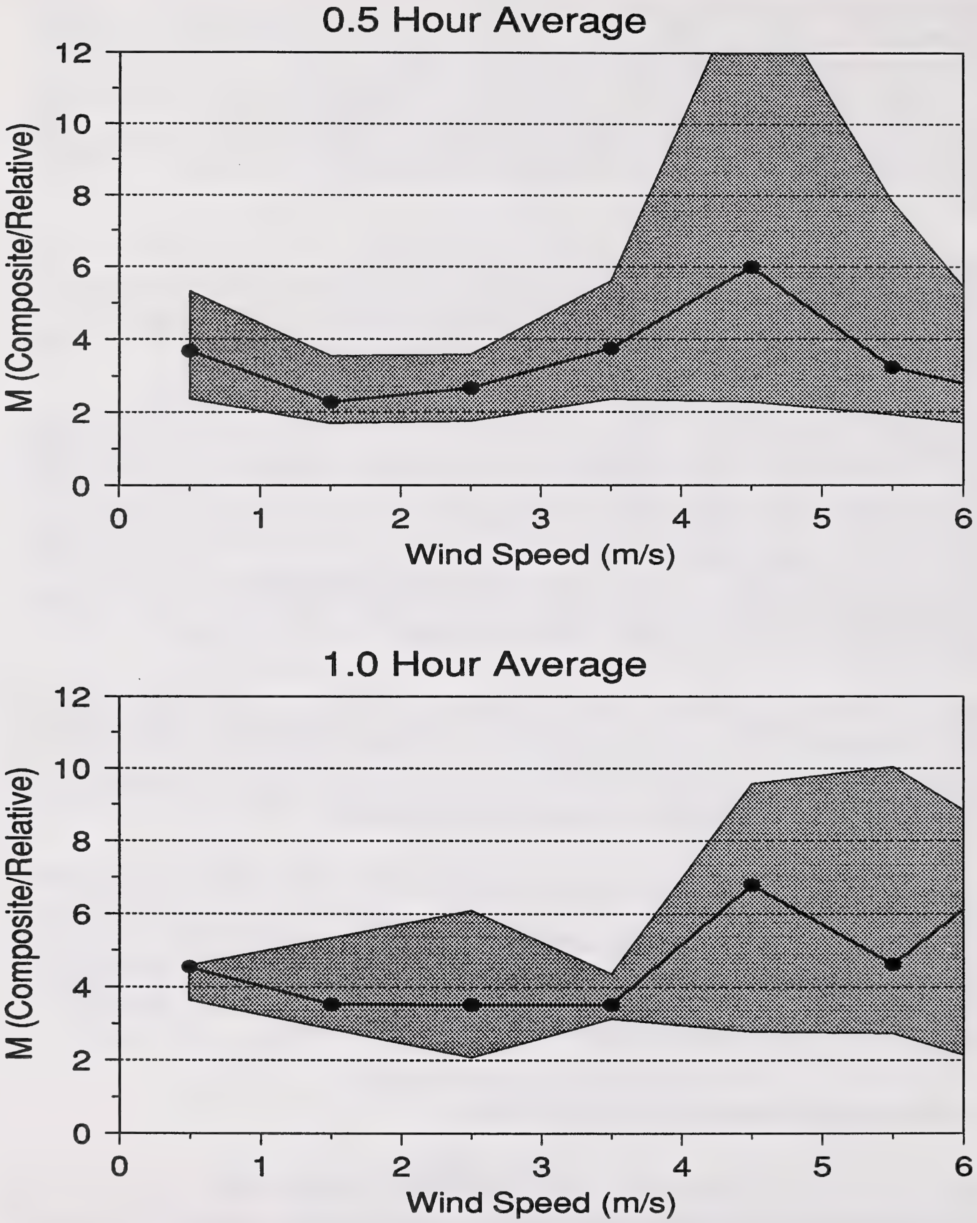

Figure 7.27

Median Value of Ratio *M* as a Function of Wind Speed for One-half Hour and One-hour Averaging Periods. The Shaded Envelope Indicates the 25 and 75 Percentile Limits.

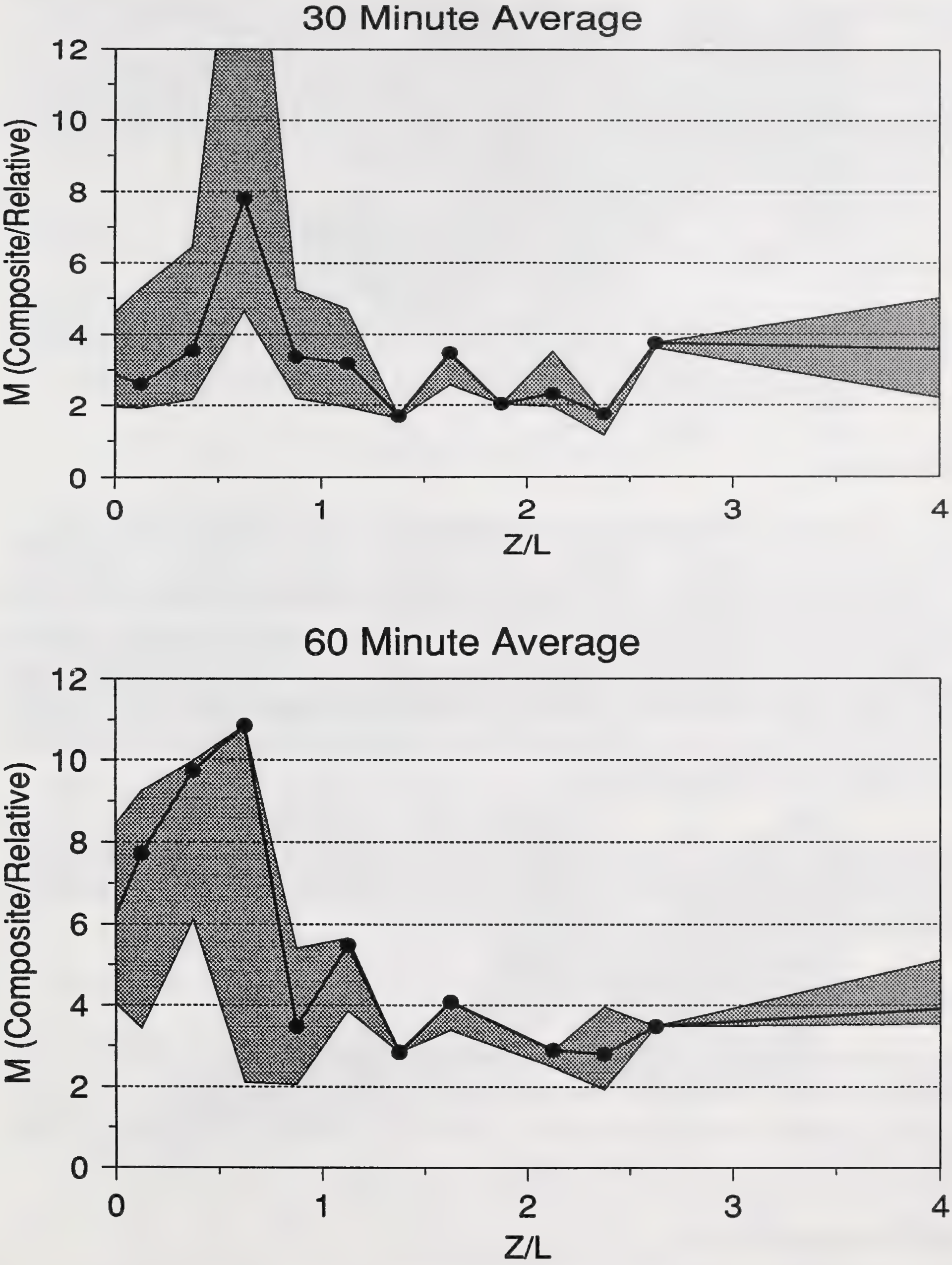

Figure 7.28

Median Value of Ratio *M* as a Function of *Z/L* for One-half Hour and One-hour Average Periods. The Shaded Envelope Indicates the 25 and 75 Percentile Limits.

Like the instantaneous traverses, the median predicted values are plotted in Figures 7.29 to 7.32 as functions of the observed value. The scatter about the median is indicated by a shaded band that is bounded by the 25 and 75 percentile values. The figures also show the one-half hour average plume spreads which are predicted using the Alberta Environment dispersion model algorithm (Alberta Environment 1988). The values shown are based on a surface roughness factor of 1.0 cm and an averaging period of 30 minutes. The Alberta Environment general expression for the crosswind spread is:

$$\sigma_{y_c} = ax^{0.88} \tag{7.16}$$

where x is the distance (m) and a is a stability dependent constant. For Pasquill stability classes D, E and F, values for this constant are 0.190, 0.145 and 0.098, respectively. Similarly the Islitzer and Slade instantaneous plume sigmas (σ_{y_i}) are also shown in the figure.

All Traverses

The overall results for all source types and sampling arcs are presented in Figure 7.29. In general, there is reasonable agreement between the median predicted values which incorporate wind direction shear effects and the observed values. When the wind direction shear effects are not accounted for, the median predictions are less than the observed values. For small observed values of $\sigma_{y_c} < 75$ m, the median predicted values without the wind shear adjustment factor tend to agree better with the observed values than the predicted values which accounts for wind shear. For the larger observed values of $\sigma_{y_c} > 100$ m, better agreement between the median predicted and observed values are obtained by incorporating wind shear effects in the predictions.

The predicted and observed comparison data were further subdivided into 700 m (surface source), 700 m (elevated source), 1 400 m (elevated source) and plotted in Figures 7.31, 7.32 and 7.33. Because of the relatively small number of data points and the inherent scatter in the data, consistent trends are difficult to identify.

Ground Release (700 m) Traverses

Figure 7.30 shows the results for surface releases and a downwind distance of 700 m. The results presented in the figure indicate that for small observed values of $\sigma_{y_c} < 50$ m, both models overpredict. For larger values of σ_y ($50 \text{ m} < \sigma_{y_c} < 150$ m), there is some qualitative agreement between observed and predicted values which include wind shear effects.

Elevated Releases (700 m)

Figure 7.31 shows the results for elevated releases and a downwind distance of 700 m. The results presented in the figure indicate that the predicted σ_{y_c} values are independent of the observed values indicating poor predictive capabilities.

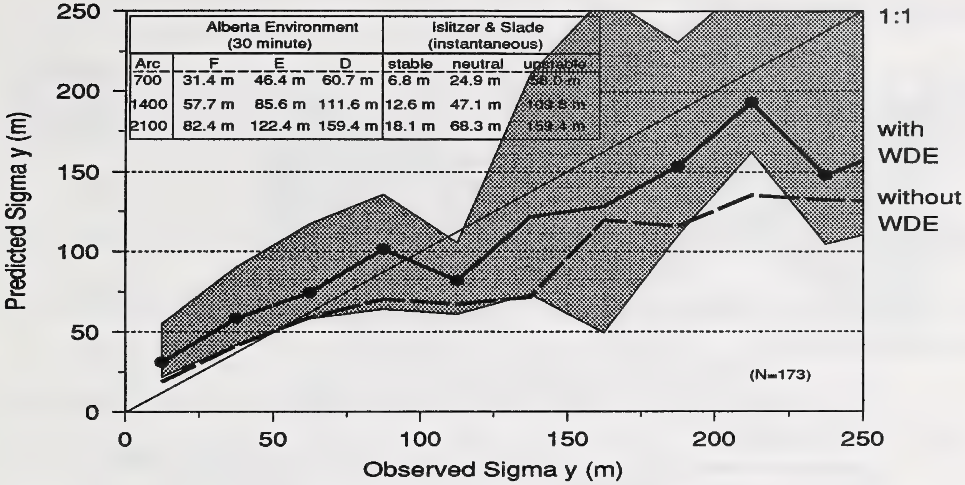

Figure 7.29

Comparison of Predicted and Observed 1/2 Hour Average Plume Spreads (σ_{y_c}) for All Source Types (Elevated and Ground) and all Sampling Arcs (700, 1400 and 2100 m). The Predicted Alberta Environment and Islitzer & Slade Values are Presented at the Top of the Figure. The Dashed Line Represents the Median Values Without *WDE* Factor. The Shaded Envelope Indicates the 25 and 75 Percentile Limits.

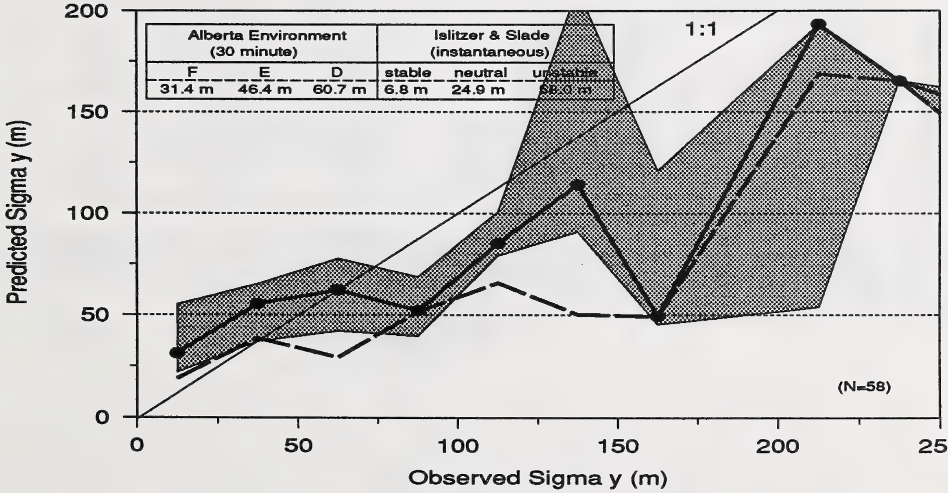

Figure 7.30

Comparison of Predicted and Observed 1/2 Hour Average Plume Spreads (σ_{y_c}) for Ground Source, 700 m Data. The Predicted Alberta Environment and Islitzer & Slade Values are Presented at the Top of the Figure. The Dashed Line Represents the Median Values Without *WDE* Factor. The Shaded Envelope Indicates the 25 and 75 Percentile Limits.

Elevated Releases (1 400 m)

Figure 7.32 shows the results for elevated releases and a downwind distance of 1 400 m. The results presented in the figure indicate some qualitative agreement between observed and predicted values which do not include the wind shear enhancement term. For observed σ_{y_c} values less than 50 m, both models overpredict.

Summary

The following table indicates the percent of the predictions that were within a factor of two of the observed values:

Percent Within a Factor of Two. (Wind Direction Shear Enhancement; Equations 7.13 and 7.15).

Traverse	One-half hour Predictions
All (Figure 7.26)	64
Ground, 700 m (Figure 7.27)	62
Elevated, 700 m (Figure 7.28)	71
Elevated, 1 400 m (Figure 7.29)	62

Percent Within a Factor of Two. (No Wind Direction Shear Enhancement; Equations 7.13 and 7.14).

Traverse	One-half hour Predictions
All (Figure 7.26)	69
Ground, 700 m (Figure 7.27)	57
Elevated, 700 m (Figure 7.28)	74
Elevated, 1 400 m (Figure 7.29)	76

In summary, the time-averaged observed plume spreads tend to agree best without wind direction shear enhancement except for the ground release at 700 m. This is different than the previous observations for the instantaneous spreads in Section 7.1.4.3.

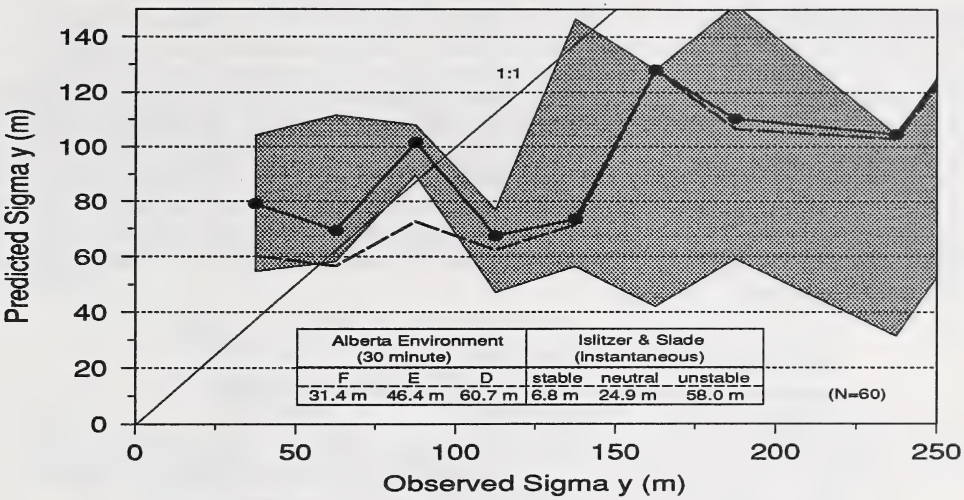

Figure 7.31

Comparison of Predicted and Observed 1/2 Hour Average Plume Spreads (σ_{y_c}) for Elevated Source, 700 m Data. The Predicted Alberta Environment and Islitzer & Slade Values are Presented at the Bottom of the Figure. The Dashed Line Represents the Median Values Without *WDE* Factor. The Shaded Envelope Indicates the 25 and 75 Percentile Limits.

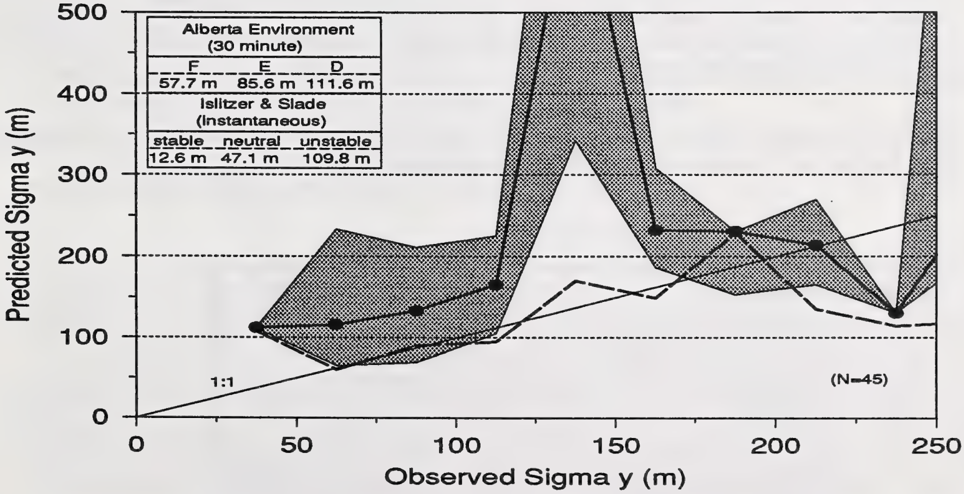

Figure 7.32

Comparison of Predicted and Observed 1/2 Hour Average Plume Spreads (σ_{y_c}) for Elevated Source, 1400 m Data. The Predicted Alberta Environment and Islitzer & Slade Values are Presented at the Top of the Figure. The Dashed Line Represents the Median Values Without *WDE* Factor. The Shaded Envelope Indicates the 25 and 75 Percentile Limits.

7.2 Stationary Data

The stationary data were collected to provide a measure of the time varying concentrations at a fixed point. Unlike the traverse data, the stationary data were not grouped according to distance. The stationary data were saved for one-half hour average periods only when the analyser recorded non-zero SF_6 concentrations during that one-half hour period. Due to plume meander and shifts in wind direction, the stationary monitors frequently recorded zero SF_6 concentrations. These latter periods were neither saved nor analysed. The following table indicates the delineation of one-half hour periods according to source type and downwind distance:

Number of one-half hour periods.

Source Type	Distance (m)		Total
	700 m	1400 m	
Elevated	1 (0.2%)	35 (8.0%)	36 (8%)
Surface	397 (90.4%)	6 (1.4%)	403 (92%)
Total	398 (91%)	41 (9%)	439 (100%)

Most of the stationary data were collected at the 700 m distance (91%) and most are associated with surface (ground-level) releases (92%).

Appendix B presents basic statistics associated with each of the one-half hour periods. In addition to the basic statistics, plots of the time series concentration for each one-half hour period are also presented in the appendix.

The one-half hour data file was further subdivided into three-minute average time periods. The number of three-minute periods are summarized below.

Number of three-minute periods.

Source Type	Distance (m)		Total
	700 m	1400 m	
Elevated	6 (0.1%)	328 (6.2%)	334 (6%)
Surface	4874 (92.5%)	63 (1.2%)	4937 (94%)
Total	4880 (92%)	391 (7.4%)	5271 (100%)

Similar to the one-half hour periods, only three-minute periods with non-zero SF_6 concentration data were saved for analysis.

Dispersion models are frequently used to predict a mean concentration value over a specified averaging period. Certain air quality work, such as toxicity and odour concerns, is concerned with peak (near instantaneous) concentration values. For this reason, the peak-to-mean ratios of the observed concentrations are of interest. Additional analyses of the Field Measurement Program data in terms of intermittency, conditional statistics and turbulence spectra are the subject of a separate study and are not discussed in this report and only a limited analysis of the stationary data will be undertaken in this report.

Several peak-to-mean ratios are available from this work collected in the field. These include:

- Instantaneous peak to 30-minute mean,
- Peak 99% to 30-minute mean, and
- Instantaneous peak to 3-minute mean.

All were addressed in this study. Tests were also undertaken to evaluate the sens'itivity of the ratios to selected meteorology valuables.

Figures 7.33, 7.34 and 7.35 show the frequency distributions of the instantaneous peak to 30-minute means, 99% peak to 30-minute means and the instantaneous peak to the 3-minute means, respectively. The results can be summarized as follows:

- The most frequent instantaneous peak to 30-minute mean ratios are in the 3 to 7 range.
- The most frequent 99% peak to 30-minute mean ratios are in the 3 to 5 range.
- The most frequent instantaneous peak to 3-minute mean ratios are in the 1 to 3 range.

These results are typical of those found in other studies. For example, peak to mean ratios of 2 to 5 in stable conditions were reported in Peterson (1989).

7.3 Predicted SF_6 Centreline Concentrations

A simple Gaussian dispersion plume model was used to predict plume centreline SF_6 concentrations. The predicted values were then compared to the observed values that were obtained from each traverse. The traverse data were evaluated rather than the stationary data as the stationary data were typically off the centreline. To arrive at observed concentration values two methods were used, one based on the Gaussian distribution from the Moment method and the other one based on the Concentration Maximum method. Each method provided one maximum concentration value for each traverse. To arrive at the predicted concentration values five different options were used. These options ranged from incorporating σ_{y_i} values obtained in the field to σ_{y_c} obtained in the literature. These are discussed in section 7.3.2.

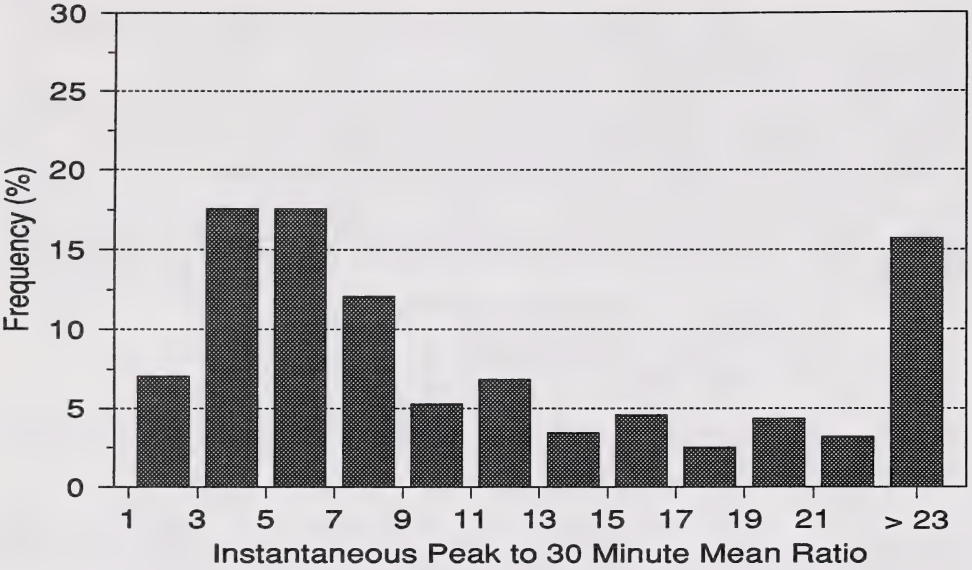

Figure 7.33

Frequency Distribution of the Instantaneous Peak SF_6 Concentration to the 30 Minute Mean SF_6 Concentration.

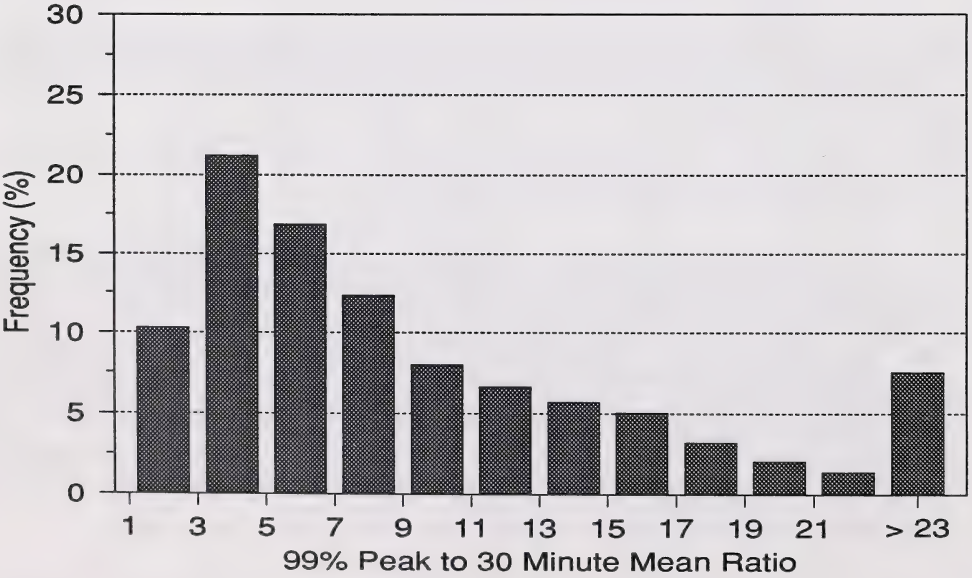

Figure 7.34

Frequency Distribution of the 99% Peak SF_6 Concentration to the 30 Minute Mean SF_6 Concentration.

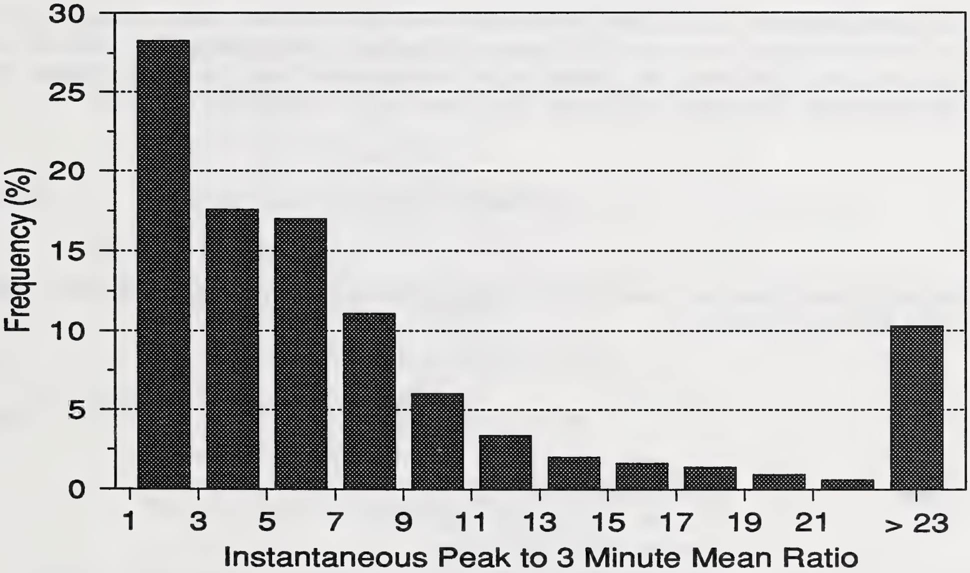

Figure 7.35

Frequency Distribution of the Instantaneous Peak SF_6 Concentration to the 3 Minute Mean SF_6 Concentration.

7.3.1 Gaussian Model Formulations

SF_6 concentrations, χ (ppt), are predicted from the simple Gaussian relationship:

$$\chi = \frac{Q \cdot 10^{12}}{\pi \sigma_y \sigma_z U} \exp\left(-\frac{H^2}{2\sigma_z^2}\right) \qquad (7.17)$$

where:

Q = SF_6 release rate (m^3/s)
σ_y = lateral plume standard deviation (m)
σ_z = vertical plume standard deviation (m)
U = wind speed at plume height (m/s)
H = plume height (m)

For ground releases, the 4 m level wind speeds were used and for elevated releases, the 10 m level wind speeds were used. For ground releases, the plume height was taken as 1 m and for elevated releases, the plume height was estimated from momentum plume rise considerations. For neutral conditions, the plume height is given by:

$$H = h_s + \frac{6 V_s R_s}{U} \qquad (7.18)$$

For stable conditions, the plume height is taken as the minimum of the neutral value or the stable value predicted by:

$$H = h_s + 1.5 \left[\frac{V_s^2 R_s^2}{U S^{1/2}}\right]^{1/3} \qquad (7.19)$$

where:

h_s = fan height (2.3 m)
V_s = fan exit velocity (m/s)
R_s = fan radius (0.3725 m)
U = 10 m wind speed (m/s)
S = stability parameter given by

$$S = \frac{g}{T}\left(\frac{\partial T}{\partial Z} + \Gamma\right)$$

where:

g = acceleration due to gravity (9.81 m/s^2)
T = ambient temperature at 2 m (K)
$\partial T / \partial Z$ = vertical temperature gradient 2 to 25 m (K/m)
Γ = adiabatic temperature gradient 0.0098 (K/m)

These formulations amount to what was called the simple Gaussian model.

7.3.2 Model Comparison Input Options

Five sets of plume spread data were used in the simple concentration model (Equation 7.17). These include:

- **Option 1** (Field σ_{y_i})

  σ_{y_i} = observed value based on Moment method

  $\sigma_{z_i} = 0.3\ \sigma_W x/U$ (similar to Equation 7.4)

- **Option 2** (Field σ_{y_i})

  σ_{y_i} = observed value based on Concentration Maximum method

  $\sigma_{z_i} = 0.3\ \sigma_W x/U$ (similar to Equation 7.4)

- **Option 3** (Field σ_V)

  $\sigma_{y_i} = 0.3\ \sigma_V x/U$ (Equation 7.4)

  $\sigma_{z_i} = 0.3\ \sigma_W x/U$ (similar to Equation 7.4)

- **Option 4** (Field σ_V)

  $\sigma_{y_i} = 0.3\ \sigma_V x\ WDE/U$ (Equation 7.7)

  $\sigma_{z_i} = 0.3\ \sigma_W x/U$ (similar to Equation 7.4)

- **Option 5** (Alberta Environment σ)

  $\sigma_{y_c} = ax^{0.88}$ (Equation 7.16)

  $\sigma_{z_c} = bx^c$ (similar to Equation 7.16)

The first two methods are based on using the observed value of σ_{y_i} as collected in the field by both the Moment and Concentration Maximum methods. The third and fourth methods are based on using field meteorology without accounting for, and then with accounting for wind direction shear. The fifth method is based on using the composite time-averaged (3-minute) Alberta Environment plume spread formulations σ_{y_c} for a surface roughness of $Z_o = 1.0$ cm. For the fifth case, the stability class was determined from a STAR analysis of Calgary International Airport data, where the constants, (a, b and c), are a function of stability class:

Stability Class	D	E	F
a	0.125	0.0916	0.0623
b	0.1077	0.077	0.0623
c	0.81	0.78	0.72

Options one to five range from maximum to minimum use of on-site data and provide a measure of the simple Gaussian formulation to predict the observed SF_6 concentrations.

7.3.3 Performance Measures

The performance of the simple Gaussian model was evaluated using standard statistical and graphical procedures. Considerable effort has been made to determine the appropriate performance measures for dispersion models (Hanna 1975, Cox 1988). A wide variety of performance indices have been suggested since it is difficult to arrive at a single quantitative index of accuracy. Unfortunately there is a temptation to get carried away and compute a multitude of statistical measures and comparisons which can make it even more difficult to arrive at the bottom line answer on "How well does the model work?".

Performance measures can be obtained from observed and predicted data sets that are either paired or unpaired in time and/or space. If a large data base exists and the goal is to obtain an understanding of model physics, then paired data sets are preferable. If the model performance is to be compared to the ability of the model to predict maximum values for regulatory purposes, then unpaired data sets can be used. The US EPA (Cox 1988) protocol for screening and testing a model for regulatory use is based on unpaired data.

For the evaluation of the simple Gaussian model, the following parameters were calculated for each set of observed and predicted data sets:

- Mean observed ($\overline{O}$) and predicted ($\overline{P}$) concentrations. The ratio of mean predicted to observed ($\overline{P/O}$ and $\overline{P}/\overline{O}$). For perfect agreement $\overline{O} = \overline{P}$ and $\overline{P/O} = \overline{P}/\overline{O} = 1.0$.

- Median observed ($\tilde{O}$) and predicted ($\tilde{P}$) concentrations. The ratio of mean predicted to observed ($\widetilde{P/O}$ and $\tilde{P}/\tilde{O}$). For perfect agreement $\tilde{O} = \tilde{P}$ and $\tilde{P}/\tilde{O} = \widetilde{P/O} = 1.0$.

- The average bias which is defined from:

  $$\overline{d} = \Sigma\frac{(O_i - P_i)}{N}$$

  which like $\overline{P/O}$ $\overline{P}/\overline{O}$, $\widetilde{P/O}$ and $\tilde{P}/\tilde{O}$ will indicate whether the model generally over or underpredicts. For perfect agreement $\overline{d} = 0.0$.

- The Pearson product-moment correlation coefficient:

  $$r = \frac{\Sigma(O_i - \overline{O})(P_i - \overline{P})}{\sqrt{\Sigma(O_i - \overline{O})^2 \Sigma(P - \overline{P})^2}}$$

  which presumes a linear relationship between O_i and P_i. This correlation coefficient should be used as a measure or relative rather than absolute measure of model performance. For example, in a recent EPRI model development project, an improved model resulted in an r value of 0.58, a significant improvement over the CRSTER model value of 0.14 (Ventekram 1988). For perfect agreement r = 1.0.

- The slope (S) and intercept (B) obtained from a least squares fit of P_i as function of O_i. This method presumes a linear relationship between P_i and O_i. For perfect agreement $\overline{B} = 0$ and $\overline{M} = 1.0$.

- The relative mean absolute error (RMAE) was computed from:

$$RMAE = \frac{\Sigma | O - P |}{N\overline{O}}$$

  For perfect agreement RMAE = 0.0

- The mean relative error (MRE) was computed from:

$$MRE = \left\{ \frac{2}{N} \Sigma \left(\frac{[P_i - O_i]}{[P_i + O_i]} \right)^2 \right\}^{1/2}$$

  For perfect agreement MRE = 0.0

- Percent of predictions within a specified factor of the observation. For this evaluation, the specified factors are 2 and 3. Ideally, perfect agreement would give 100% within these factors.

- Hanna's (1975) dimensionless mean square error (*M*) from:

$$M = \frac{\overline{(P - O)^2}}{(\overline{P}\overline{O})}$$

  A lower value of *M* indicates a better model. The method gives larger concentrations more weight because the difference $\overline{P} - \overline{O}$ will be influenced by the larger concentrations. A perfect model would have an *M* value of zero; the best available models have *M* values of order 1. Models with poor performance have high *M* values.

The above statistical performance measures were applied to paired data sets. For unpaired data sets, the cumulative frequency distributions of the normalized predicted and observed concentrations are presented graphically. The US EPA suggests that the fractional bias (FB) be calculated from unpaired data.

$$FB = 2\frac{(\overline{O} - \overline{P})}{(\overline{O} + \overline{P})}$$

where $\overline{O}$ and $\overline{P}$ refer to the 25 highest observed and predicted values.

The previously discussed performance measures were applied to the traverse data obtained from the Field Measurement Program. While these measures are by no means complete, they will provide a preliminary evaluation on the ability of simple Gaussian model to predict plume centreline concentrations.

7.3.4 Model Performance - Paired Data

Table 7.5 presents the performance statistics for different combinations of the observed and predicted data sets. The results from the table indicates the following:

- The poorest performance of all the options was with Option 4. The model generally underpredicts. This option incorporated a wind direction shear enhancement term in the estimation of σ_{y_i}. This increased σ_{y_i} and decreased the predicted concentrations.

- For the other options, there is no one option which stands out as being the best. Generally speaking, the best performances were obtained when the predictions were compared to the observations based on the Moment method.

  For example: the minimum bias is associated with Option 5; the maximum correlation coefficient (r) with the Option 1 predictions; the maximum percentage within a factor of 2 with the Option 2 predictions and the maximum percentage within a factor of 3 with the Option 1 prediction. The minimum Hanna *M* values are associated with Option 2 and 5 predictions.

Table 7.6 presents the performance statistics for a subset of the available data set. Specifically, the subset includes:

- Ground Releases when the 4 m level tower wind speed was less than 3 m/s and when Calgary airport observations indicated a Pasquill-Gifford stability class E or F. The number of traverses that meet these criteria is 191 compared to the 704 in the full data set.

- Elevated releases when the 10 m level tower wind speed was less than 3 m/s and when Calgary airport observations indicated a Pasquill-Gifford stability class E or F. The number of traverses that meet this criteria is 119 compared to the 704 in the full data set.

From the table, the following comments can be derived:

- For ground releases, the simple Gaussian model on the average underpredicts for all options. Options 1, 2 and 3 show a general improvement of predictions within a factor of 2 and 3. For Options 3 and 4, the percentage decreases.

  One of the difficulties with a ground release is that the Gaussian approximation in the vertical may not be valid. This is why alternate dispersion models have been developed for surface releases. For example, Horst (1979) assumed the vertical spread is exponential rather than Gaussian.

Table 7.5

Comparison of Model Performance Statistics.

	MEAN O	MEAN P	MEAN $\frac{P}{O}$	$\frac{MEAN\ P}{MEAN\ O}$	MEDIAN O	MEDIAN P	MEDIAN $\frac{P}{O}$	$\frac{MEDIAN\ P}{MEDIAN\ O}$	AVG. BIAS	r (P vs. O)	SLOPE	INTERCEPT	RMAE	MRE	% WITHIN FACTOR OF 2	% WITHIN FACTOR OF 3	HANNA'S M
OPTION 1																	
Moment	1304	1040	0.82	0.80	902	769	0.77	0.85	262	0.43	0.36	580	0.65	0.68	50	68	35.6
Maximum	1561	1040	0.66	0.67	1069	769	0.66	0.72	518	0.40	0.27	624	0.65	0.69	47	64	116.7
OPTION 2																	
Moment	1304	1234	0.97	0.95	902	878	0.90	0.97	67	0.39	0.38	747	0.70	0.69	51	67	2.0
Maximum	1561	1234	0.79	0.79	1069	878	0.74	0.82	324	0.44	0.35	698	0.66	0.67	51	67	38.5
OPTION 3																	
Moment	1304	1167	0.94	0.90	902	810	0.85	0.90	135	0.27	0.26	838	0.79	0.71	43	63	8.4
Maximum	1561	1167	0.76	0.75	1069	810	0.72	0.76	391	0.29	0.23	823	0.73	0.70	45	63	59.3
OPTION 4																	
Moment	1304	573	0.39	0.44	902	337	0.42	0.37	729	0.19	0.12	426	0.79	0.82	29	50	501.5
Maximum	1561	573	0.32	0.37	1069	337	0.35	0.32	985	0.21	0.11	410	0.78	0.85	27	46	766.0
OPTION 5																	
Moment	1304	1304	1.17	1.0	902	859	1.05	0.95	-2	0.23	0.26	1055	0.71	0.80	42	58	3.5
Maximum	1561	1304	0.95	0.84	1069	859	0.89	0.80	254	0.24	0.22	1054	0.70	0.75	41	60	3.0

O = Observed centreline SF_6 concentration (ppt) for the moment or concentration maximum method.

P = Predicted centreline SF_6 concentration (ppt) from one of Option 1 to 5 (Options 1 to 4 assume instantaneous plume spreads, while Option 5 assumes a 3 minute average plume spread).

Table 7.6

Comparison of Model Performance Statistics for Low Wind Speed Stable Conditions.

	All Cases			Stable Ground $U_4 < 3$ m/s			Stable Elevated $U_{10} < 3$ m/s		
	$\frac{MedianP}{MedianO}$	% Within Factor of 2	% Within Factor of 3	$\frac{MedianP}{MedianO}$	% Within Factor of 2	% Within Factor of 3	$\frac{MedianP}{MedianO}$	% Within Factor of 2	% Within Factor of 3
OPTION 1									
Moment	0.85	50	68	0.38	51	79	3.01	29	47
Maximum	0.72	47	64	0.34	42	69	2.49	32	48
OPTION 2									
Moment	0.97	51	67	0.43	55	80	3.45	29	43
Maximum	0.82	51	67	0.39	52	79	2.84	29	47
OPTION 3									
Moment	0.90	43	63	0.40	25	59	3.17	27	39
Maximum	0.76	45	63	0.35	28	52	2.62	32	47
OPTION 4									
Moment	0.37	29	50	0.17	17	38	1.32	33	59
Maximum	0.31	27	46	0.15	15	35	1.09	35	60
OPTION 5									
Moment	1.19	42	58	0.53	51	70	4.22	22	34
Maximum	1.01	41	60	0.47	55	70	3.49	24	44

O = Observed centreline SF_6 concentration (ppt) for the moment or concentration maximum method.

P = Predicted centreline SF_6 concentration (ppt) from one of Option 1 to 5 (Options 1 to 4 assume instantaneous plume spreads, while Option 5 assumes a 3 minute average plume spread).

- For elevated releases, the simple Gaussian model overpredicts by a factor of about 3 for all options except for Option 4. For Option 4, the median P over median O ratio indicates relatively good agreement.

  Option 4 includes wind direction shear enhancement in the estimation of the crosswind spread. The improvement in model performance for this meteorological subset may indicate that wind shear enhanced dispersion is important for low wind, stable conditions.

7.3.5 Model Performance - Unpaired Data

Unpaired data performance was undertaken for Option 5 model predictions only. Cumulative frequency distributions of normalized concentrations were subdivided into the following groups:

- Elevated and ground releases, 700 and 1 400 m receptor distance (all cases),
- Ground release, 700 m receptor distance,
- Ground release, 1 400 m receptor distance,
- Elevated release, 700 m receptor distance, and
- Elevated release, 1 400 m receptor distance.

The normalized concentration (χ/Q) were defined as the observed plume centreline concentration defined by the Moment Method (ppt) divided by the SF_6 source release rate (g/min). The normalization allows comparison of all traverse data even though the release rates were varied between the tests. The largest χ/Q ratios represent the lowest dilution factors and are indicative of potential "worst case" meteorological scenarios.

The fractional bias (FB) was only computed for the "all cases" data set and was based on the 25 highest normalized concentration pairs. The computed value for Option 5 is 0.101. Values of the fractional bias that are equal to -0.67 (+0.67) are equivalent to overpredictions (underpredictions) by a factor of two. Models associated with computed FB values that are between -0.67 and +0.67 are deemed to have passed an initial test for consideration as a regulatory model (Cox 1988).

Figure 7.36 shows the cumulative frequency distributions for surface releases (700 and 1 400 m) for Option 5 based predictions. For the 700 m concentrations, the cumulative frequency distributions for the observed and predicted values are similar for normalized concentration values up to 4 000 ppt/(g/min). These values include 73% of the data. For normalized concentrations between 4 000 and 12 000 ppt/(g/min), the model under predicts. For normalized concentrations greater than 12 000 ppt/(g/min), the model over predicts by a factor of up to 2.5. For the 1 400 m concentrations, the cumulative frequency distributions are similar for normalized concentration values of up to 3 000 ppt/(g/min). These values include 80% of the data. For normalized concentrations greater than this value, the simple Gaussian model overpredicts by a factor of up to 2.5.

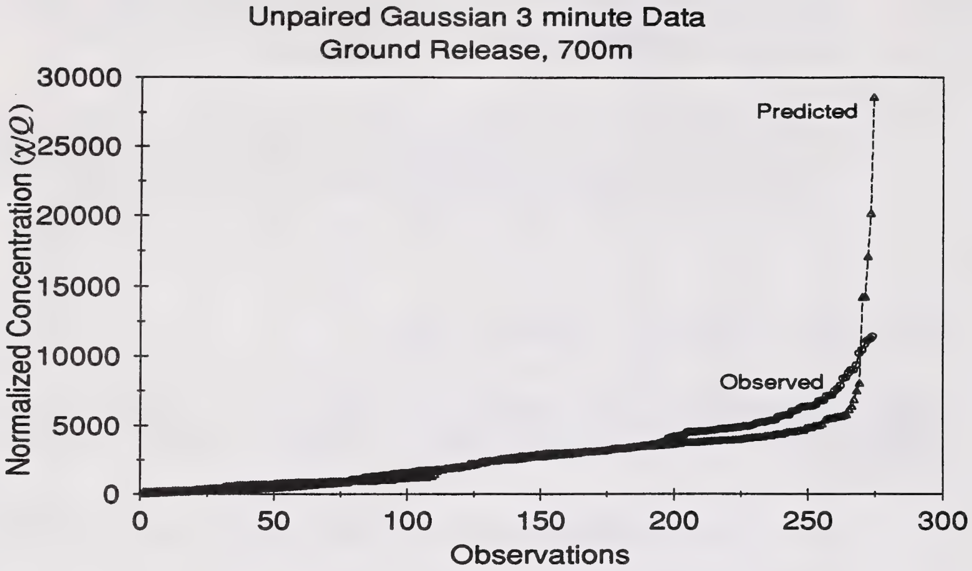

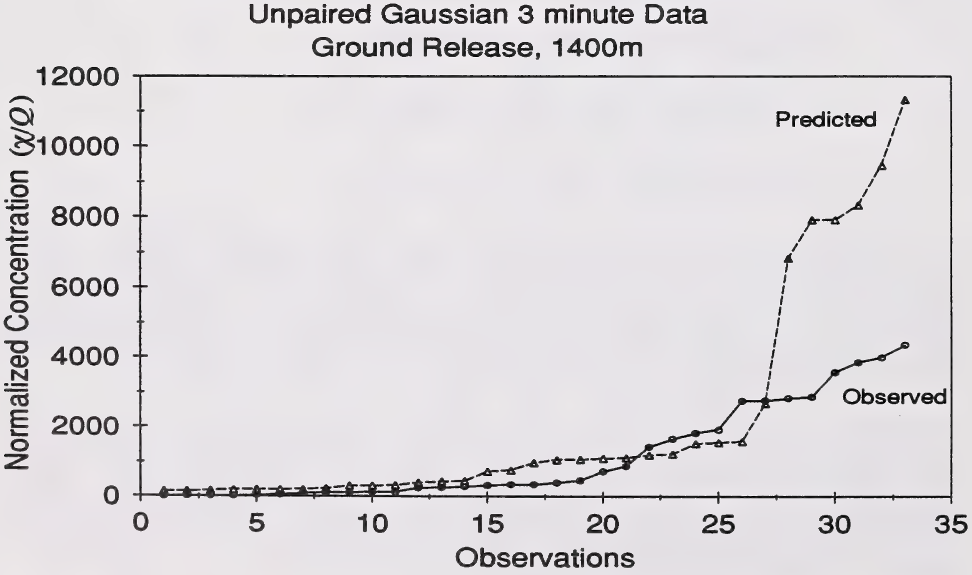

Figure 7.36

Cumulative Frequency Distributions of Observed and Predicted Normalized SF_6 Concentration [ppt/(g/min)] for Surface Releases.

Figures 7.37 shows the cumulative frequency distributions for elevated releases (700 and 1400 m) for Option 5 predictions. For the 700 m concentrations, the simple Gaussian model overpredicts for normalized concentrations less than 150 ppt/(g/min). These values include 36% of the data. For normalized concentrations between 150 and 350 ppt/(g/min), the predicted and observed values are in agreement. For normalized concentrations greater than 350 ppt/(g/min), the simple Gaussian model tends to underpredict by a factor of up to 1.7. For the 1400 m concentrations, the model predictions and observations appear to be in agreement for normalized concentrations less than 300 ppt/(g/min). For normalized concentrations greater than this value, the model tends to underpredict by a factor of up to 2.8.

7.3.6 Comments

For the paired data analysis, the lowest overall simple Gaussian model performance was associated with the option which included wind direction shear. The wind shear enhancement produced larger σ_{y_i} values which resulted in a consistent underprediction. For all the other options, mean and median predictions are comparable to the corresponding observations, and about 40 to 50% of the predictions are within a factor of two.

A subset of the data set based on low wind speed ($U < 3$ m/s), stable conditions were evaluated. For **ground** releases, the model tends to **underpredict** by a factor of about 2.5 for options 1, 2, 3 and 5. In contrast, for **elevated** releases, the model tends to **overpredict** by a factor of about 3 for all options except Option 4. For Option 4, there is better agreement between predicted and observed.

The unpaired data analysis focussed on Option 5 only. For **ground** releases, the model tended to **overpredict** by a factor of up to 2.5 for the largest normalized concentrations. For the **elevated** releases, the model tends to **underpredict** by a similar factor for the largest normalized concentrations. The direction of prediction tendencies are opposite to what was found for the paired analysis. Considering the difficulties in trying to pair data in time and space there is a higher degree of confidence in the unpaired data analysis. It must also be noted that for this unpaired analysis 3-minute sigma values were used. If a smaller averaging time were used to try to approximate instantaneous sigmas then the concentrations would have been higher.

These findings indicate the potential problems which may arise when using an entire data set to compare model predictions with observations. In particular, competing effects may indicate a certain level of performance that may not necessarily be indicated by a data subset. For this reason it is important to use subsets based on source type and meteorology to fully evaluate a model's performance. Further analysis of this type is contained in Volume 4, the model evaluation document.

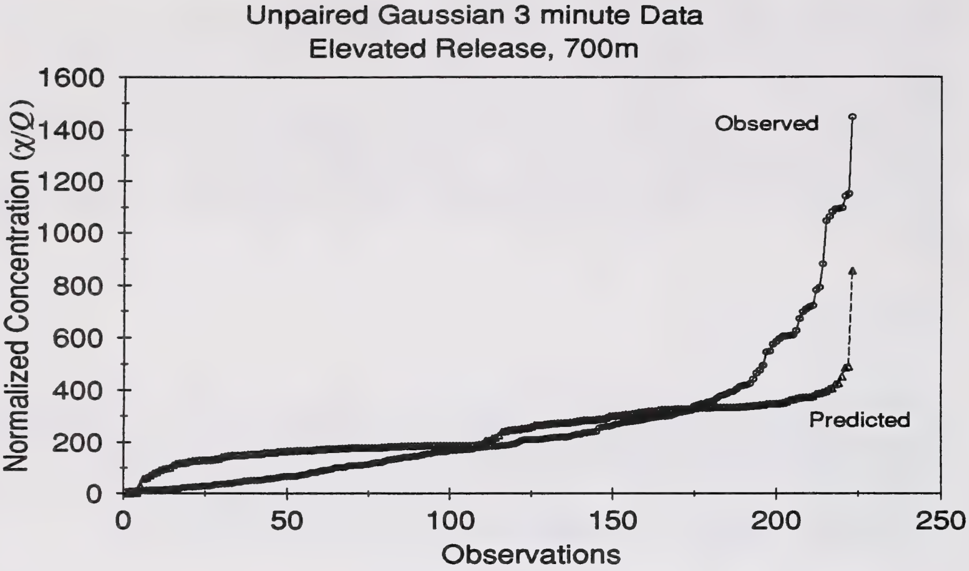

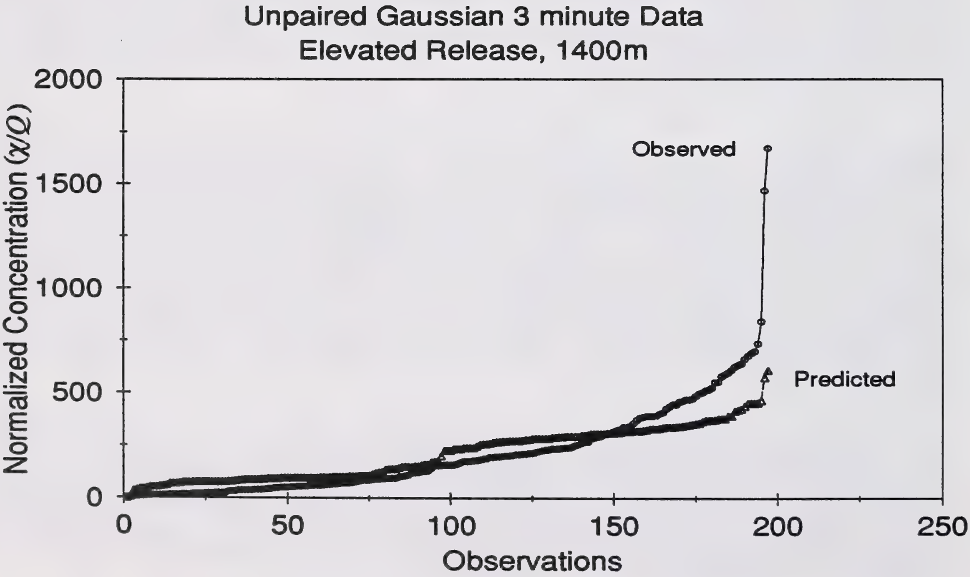

Figure 7.37

Cumulative Frequency Distributions of Observed and Predicted Normalized SF_6 Concentration [ppt/(g/min)] for Elevated Releases.

8 METEOROLOGICAL DATA ASSESSMENT

In addition to supporting the tracer gas observations, the meteorological data were used to provide information to help understand processes that affect the dispersion of plumes from both uncontrolled sour gas and controlled stack releases. To meet this end, a number of quasi-independent meteorological objectives for the Field Measurement Program were identified. The first six months of data (October 1988 to March 1989) were analyzed to meet the identified objectives. The second six months of data (April to October 1989) were analyzed for selected objectives. The data analysis and results are presented in this section for both periods.

8.1 Meteorology Objectives

A brief description of eight identified objectives and the rationale for each objective follow:

- **Field Measurement Site (Kathyrn) Climatology**

  A climatological summary of important measured and derived meteorological variables provided an overview of the range and distribution of observed conditions at the Field Measurement Program site.

- **Boundary Layer Parameterization**

  The vertical variation of mean and turbulence related meteorological variables is essential in understanding the effect of turbulence on dispersion in the boundary layer. The observed vertical variations of mean values (θ, U), turbulence values (σ_ϕ, σ_θ) and flux based values (H_o, U^*) were compared to other boundary layer studies and the theoretical understanding of boundary layer behavior.

  A number of different methods have been used to categorize atmospheric stability and turbulence in plume dispersion models. These methods are based on observations of atmospheric wind and/or temperature profiles. Direct measurements of turbulence include observations of σ_θ or σ_ϕ. Indirect methods include observations of temperature gradient, heat flux and wind speed, or the estimation of stability indicators such as the Richardson Number, Monin-Obukhov Length and Kazanski-Monin Length. These stability indicators recognize both thermal and mechanical contributions to atmospheric turbulence.

- **Low Wind, Low Turbulence Statistics**

  The largest hazard zones associated with low-level releases of toxic gases are associated with low wind speed, stable atmospheric conditions. The persistence of these conditions can assist in determining the duration and downwind extent of hazard zones. Wind data from the Kathyrn site and from the Acid Deposition Research Program (East and West Crossfield) sites (Legge 1988) were reviewed for persistence. The Kathyrn wind data were further reviewed to determine minimum wind and turbulence levels.

- **Meteorological Preprocessor**

  Various meteorological preprocessor schemes have been used to classify atmospheric turbulence classes from meteorological observations. The Turner (1969) scheme is the most commonly used for application oriented dispersion modelling and is based on routine observations of wind speed and cloud cover at airports. The scheme is used to derive the discrete Pasquill-Gifford stability classes (A through F). More recently, efforts have been made to classify turbulence as a continuous variable rather than a discrete variable and to use stability parameters as the measure of turbulence.

  This objective compares various direct and indirect measures of turbulence with the Pasquill-Gifford stability classes. This comparison provides an indication of how well the Pasquill-Gifford classes can be related to field measurements.

  In addition, the performance of meteorological preprocessor schemes based on sensible heat flux was evaluated. The sensible heat flux was used with boundary-layer formulations to estimate the friction velocity (U^*) and the Monin-Obukhov length (L) which were then compared to the corresponding values derived from field measurements.

- **Spatial Representativeness**

  On-site meteorological data are frequently required to undertake air quality impact assessments (Standards and Approvals 1989). Meteorological data are often available from nearby airports (Atmospheric Environment Service) and/or air monitoring trailers (industry). The difference between on-site and off-site data depends on the distance between the two sites and the nature of the intervening terrain.

  Detailed comparisons of meteorological parameters from the Kathyrn site were compared to corresponding values observed at the Calgary International Airport. Mean parameters that were compared include pressure, temperature, relative humidity, wind speed and wind direction. Similarly, wind speed and direction observed at the Kathyrn site were compared to those observed at the Petrogas Balzac and Amoco Crossfield East plants.

- **Averaging Time**

  Empirical power law relationships are frequently used in dispersion models to convert meteorological turbulence measurements (Eg. σ_θ) from one averaging period to another for time periods ranging from 3 minutes to 3 hours. The power law exponent is sometimes allowed to be dependent on atmospheric stability. The vertical turbulence component (σ_ϕ) is usually assumed to be independent of averaging period.

  The 10 and 25 m sonic data collected at high frequency during the Field Measurement Program were used to determine temporal variations of σ_θ and σ_ϕ for time periods between 1 and 3 minutes and for time periods between 3 minutes and 1 hour.

- **Anemometer Comparison**

  UVW propeller anemometers have been frequently used to obtain measurements of atmospheric turbulence. These UVW anemometers have response times that can limit high frequency turbulence measurements. Sonic anemometers, on the other hand, have the sensitivity and high frequency response times suitable for turbulence measurements. Sonic anemometers, however, are considerably more expensive than UVW anemometers ($10 000 to $20 000 versus $2 000) and also can require more support hardware in the field.

  The Kathyrn meteorological tower is instrumented with both types of instruments at the 10 and 25 m levels. Comparisons of wind speed, wind direction and wind standard deviations were made.

- **Mixing Height**

  The depth of the mechanical mixing layer can have a significant effect on the dispersion of plumes emitted into the mixing layer. Plumes that are trapped in the mechanical mixing layer can produce larger ground-level concentrations than those that disperse above the mixing layer. The mixing height data available from the Field Measurement Program were reviewed and compared to selected analytical relationships for predicting mixing depth.

8.2 Field Measurement Site (Kathyrn) Climatology

As was seen in Chapter 5, a relatively large number of meteorological parameters were measured and derived from the field observations at the Kathyrn site. To facilitate the interpretation of these parameters for both the tracer gas evaluation and for the individual meteorological objectives, an overview of selected parameters is presented. The selected parameters include measured temperature (T), wind speed (U), lateral turbulence intensity (σ_θ) and vertical turbulence intensity (σ_ϕ). Derived parameters include heat flux (H_o), friction velocity (U^*), gradient Richardson number (R_g), and Monin-Obukhov stability parameter (Z/L).

The data are presented in two formats: frequency distributions and diurnal variations of medians. Both formats are presented on a monthly basis (October 1988 through to September 1989 inclusive). The October 1989 data were not evaluated for this objective. The plots are based on one-half hour average data. The data analyses were performed separately for the first and second six months. All of the figures in this section are on two pages. The first six months (October 1988 to March 1989) are referred to as "winter," while the second six months (April to September 1989) are referred to as "summer."

8.2.1 Temperature

Figure 8.1 shows the frequency distribution of the 2 m level temperature for each month. The overall statistics with respect to temperature (°C) are given in the following table:

Month	Minimum (°C)	Mean (°C)	Maximum (°C)
October 1988	-12.9	2.2	21.5
November	-24.5	-1.8	15.2
December	-27.6	-6.4	16.8
January 1989	-35.8	-8.8	7.2
February	-33.9	-10.4	9.2
March	-33.4	-7.2	11.4
April	-9.6	5.7	24.1
May	-3.2	11.0	27.6
June	3.9	15.8	31.3
July	1.3	16.6	30.9
August	5.1	15.0	30.8
September	-5.5	10.5	26.7

As can be seen from the above summary table and Figure 8.1, the meteorological data were obtained over a wide range of temperatures with an overall minimum of -35.8°C in January and maximum of 31.9°C in August. The monthly mean temperatures were compared with Calgary International Airport 30 year mean monthly temperatures (AES 1982). Four of the months were outside one standard deviation of the corresponding 30 year mean. November was about 5°C warmer, December was about 9°C warmer and May and June were about 2°C warmer than average.

Figure 8.2 shows the monthly 2 m level median temperature as a function of time of day. The diurnal variation with afternoon maximum and early morning minimum temperatures are clearly shown. For December and January, the months with minimum solar input, smaller diurnal variations were observed in comparison to the other months. The largest diurnal variation of 12°C was observed in July.

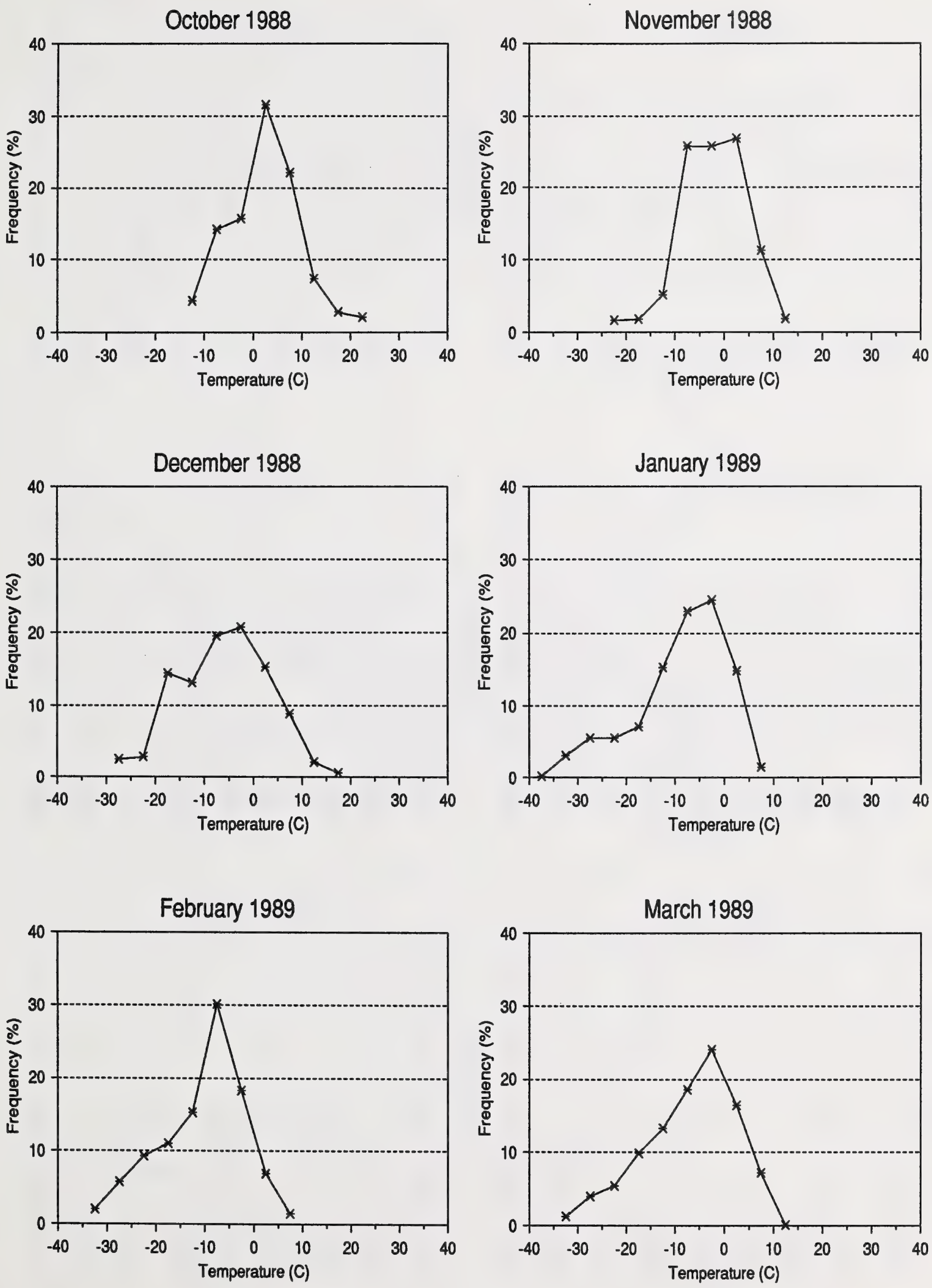

Figure 8.1 Winter

Monthly Frequency Distributions of 2 m Level Temperature.

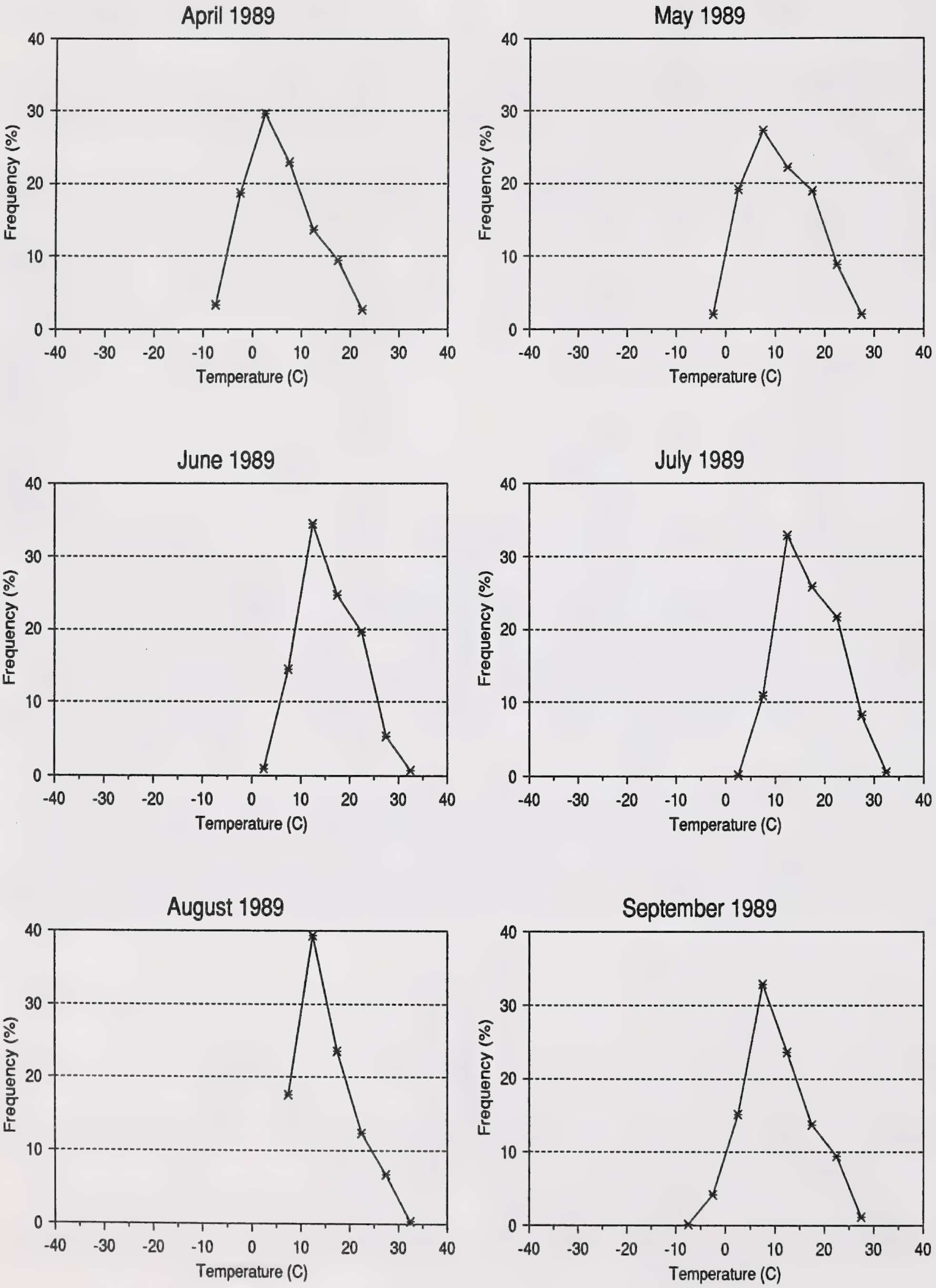

Figure 8.1 Summer

Monthly Frequency Distributions of 2 m Level Temperature.

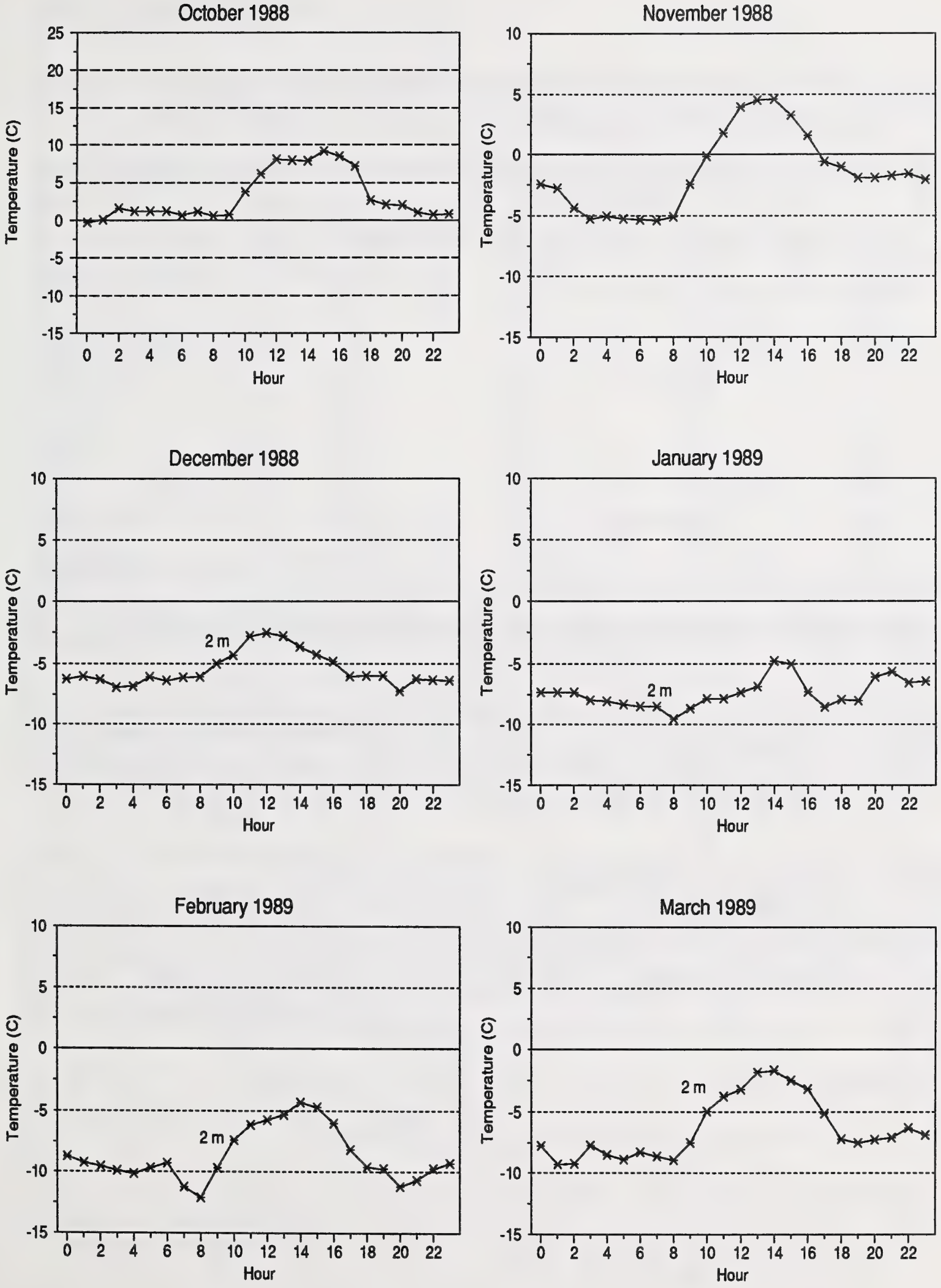
October 1988

November 1988

December 1988

January 1989

February 1989

March 1989

Figure 8.2 Winter

Median 2 m Level Temperature as a Function of Time of Day and Month.

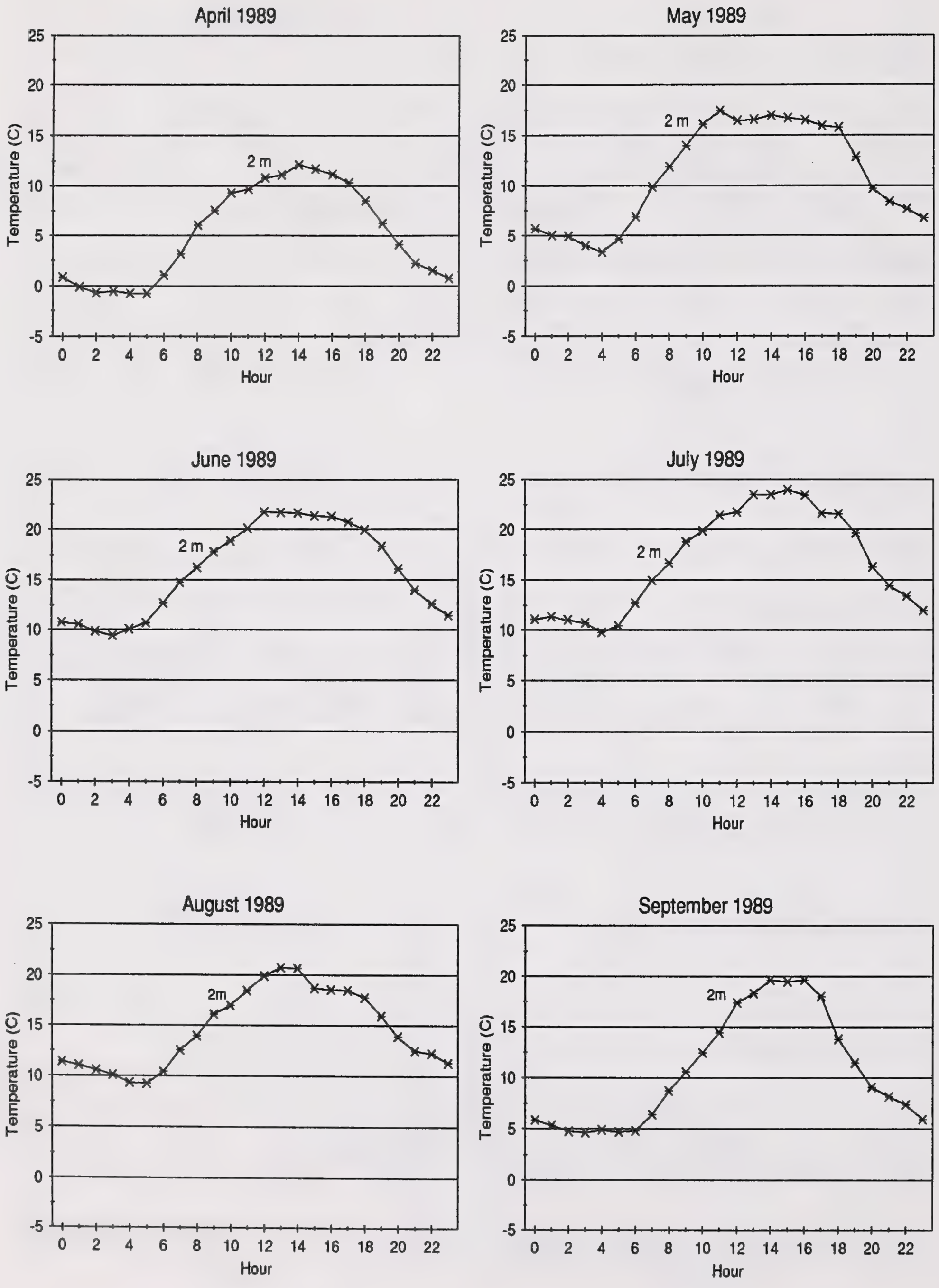

Figure 8.2 Summer

Median 2 m Level Temperature as a Function of Time of Day and Month.

8.2.2 Wind Speed

Figure 8.3 shows the frequency distributions for the 4, 10, 16 and 25 m level wind speeds for each month. The median wind speeds (m/s) observed during each month are as follows:

Month	Median (m/s)			
	4 m	10 m	16 m	25 m
October 1988	2.6	3.5	4.4	5.1
November	3.0	3.8	4.6	5.1
December	2.9	3.7	4.8	5.4
January 1989	4.3	5.2	6.6	6.7
February	3.6	4.2	5.3	5.8
March	3.0	3.3	4.1	4.7
April	2.6	3.1	3.8	4.4
May	3.8	4.6	5.2	n/a
June	3.7	4.1	n/a	4.7
July	2.1	3.1	n/a	n/a
August	2.3	2.9	3.7	4.9
September	2.6	3.3	4.3	4.7

Due to problems with the sonic anemometer, 16 m wind data are not available for June and July and 25 m wind data are not available for May and July.

The median wind speeds increase with increasing height for all months. The largest median wind speeds were observed during the month of May. One objective of the Field Measurement Program was to focus on low wind speeds. During the months of October, November and December, 16.1% of the 10 m level winds were less than 2 m/s.

Figure 8.4 shows the monthly 4, 10, 16 and 25 m level median wind speeds as a function of time of day. Again, the trend for wind speeds to increase with increasing height is evident. No consistent diurnal trend was noted for the winter months. While October wind speeds had a tendency to be larger in the afternoon, February and March wind speeds had a tendency to be smaller during the afternoon. A more consistent diurnal trend was noticed for the summer months. During the summer months, the wind speed tended to increase during the day and decrease during the night.

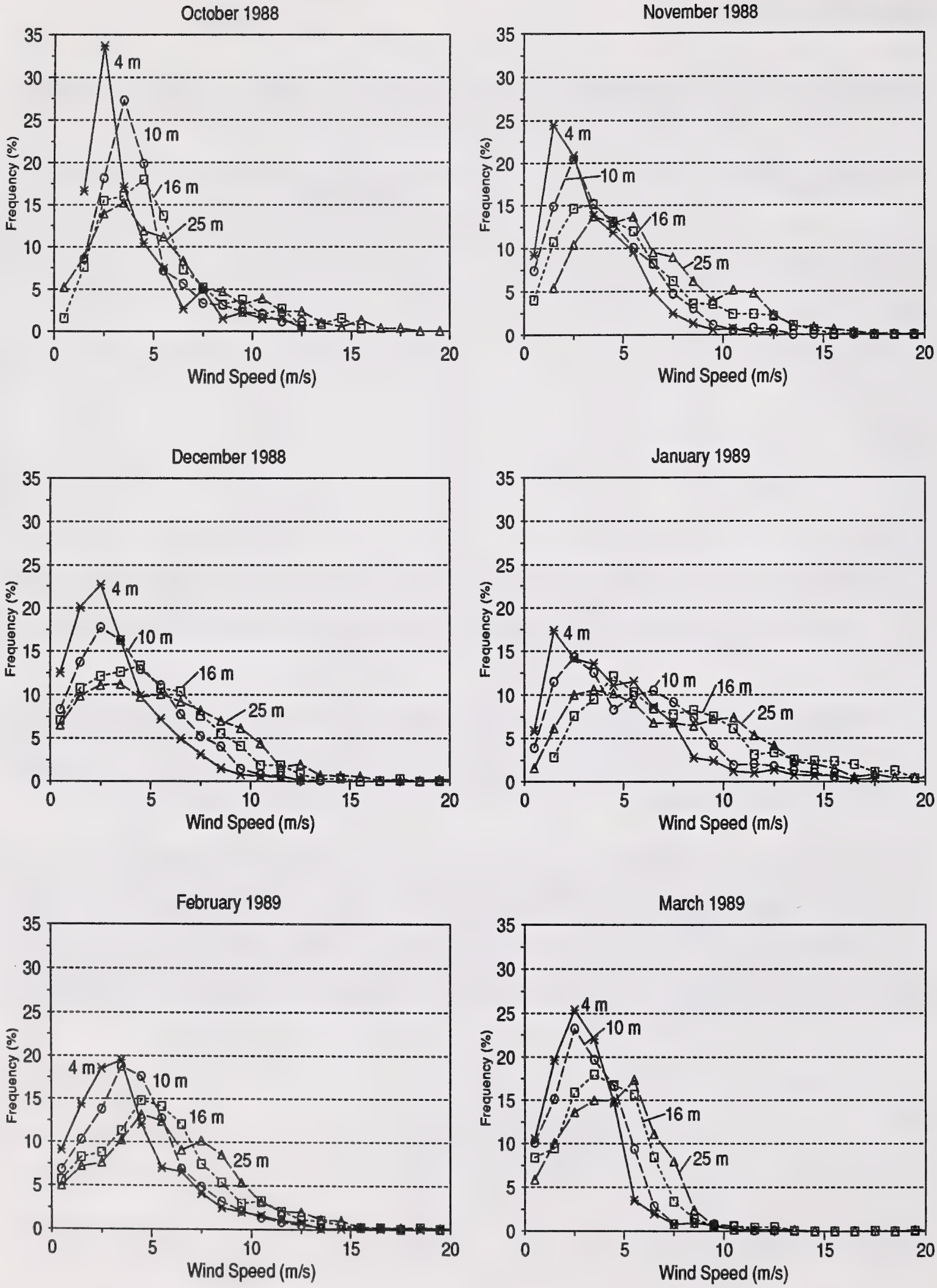

Figure 8.3 Winter

Monthly Frequency Distributions of 4, 10, 16 and 25 m Level Windspeeds.

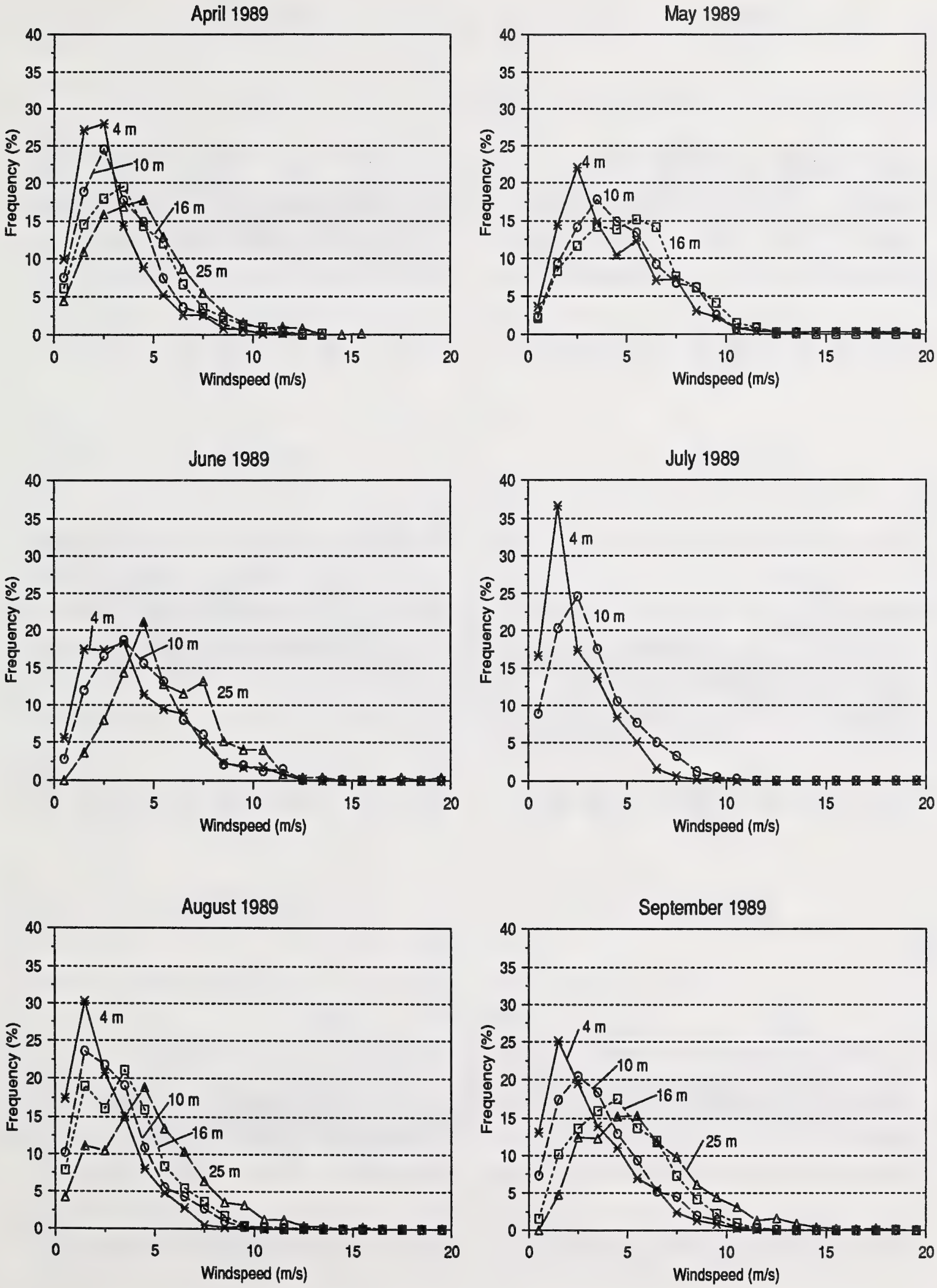

Figure 8.3 Summer

Monthly Frequency Distributions of 4, 10, 16 and 25 m Level Windspeeds.

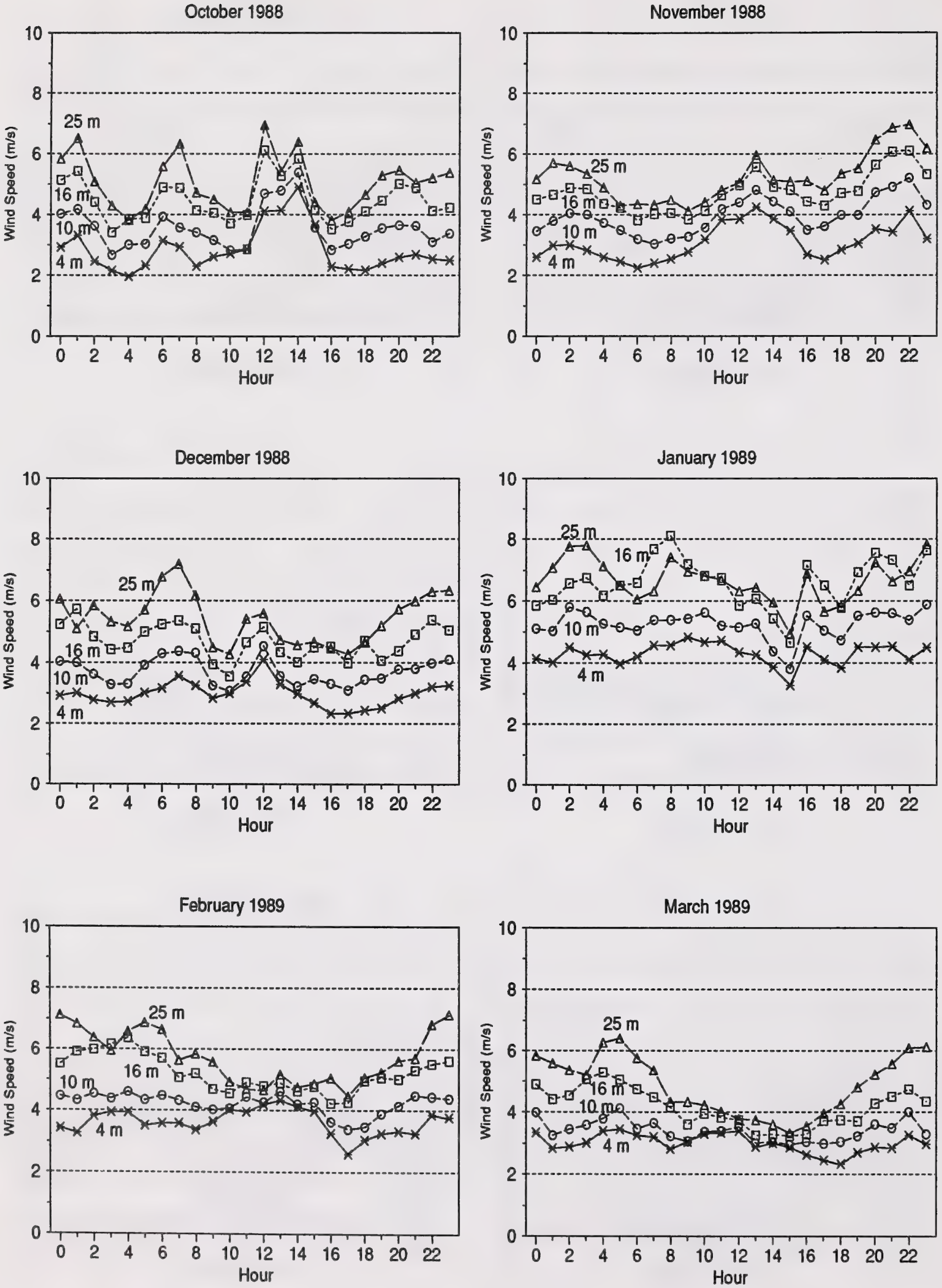

Figure 8.4 Winter

Median 4, 10, 16 and 25 m Level Windspeeds as a Function of Time of Day and Month.

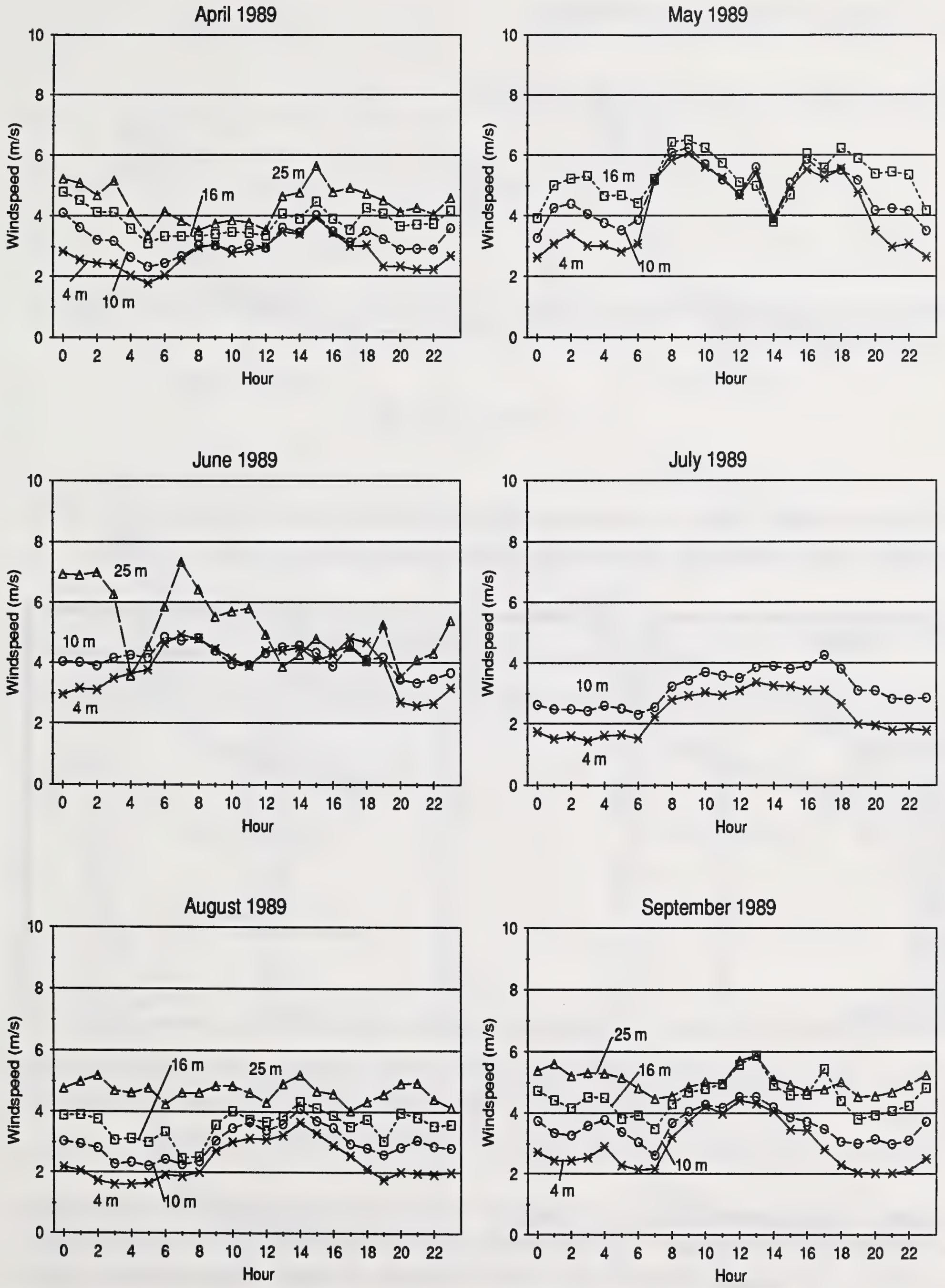

Figure 8.4 Summer

Median 4, 10, 16 and 25 m Level Windspeeds as a Function of Time of Day and Month.

8.2.3 Lateral Turbulence Intensity

The lateral turbulence intensity (i_y) is defined as:

$$i_y = \frac{\sigma_V}{\overline{U}} \qquad (8.1)$$

which can be expressed as either a fraction or a percentage. For air pollution studies, the lateral turbulence intensity can be approximated by

$$i_y \approx \sigma_\theta = \tan^{-1}\left(\frac{\sigma_V}{\overline{U}}\right) \approx \frac{\sigma_V}{\overline{U}}$$

for small σ_θ angles. Figure 8.5 shows the monthly frequency distributions for the 4, 10, 16 and 25 m level values of σ_θ. The median values of σ_θ for each month are as follows:

Month	Median (degrees)			
	4 m	10 m	16 m	25 m
October 1988	9.4	8.2	7.5	7.2
November	9.4	7.9	7.0	6.4
December	8.4	7.2	6.5	5.9
January 1989	7.4	6.3	5.9	5.6
February	6.7	5.4	5.5	5.0
March	8.2	7.0	6.7	6.2
April	10.8	9.3	9.0	8.8
May	9.9	9.0	8.4	n/a
June	10.0	9.9	n/a	13.1
July	13.4	10.8	n/a	n/a
August	13.6	10.9	10.5	7.2
September	11.1	9.3	10.4	7.6

The median σ_θ values have a tendency to decrease with increasing height with an overall average 10 m value of 8.4 degrees or 15%. The smallest median σ_θ values were observed in February. The largest median σ_θ values were observed in July and August.

Figure 8.6 shows the monthly 4, 10, 16 and 25 m level median lateral turbulence intensities as a function of time of day. At night, the σ_θ values can decrease with increasing height. In contrast, the daytime σ_θ values can remain constant or increase with increasing height. The median σ_θ values tend to be fairly uniform with time of day for the winter months, but show a definite diurnal trend of increased daytime values for the summer months. During the summer, the median values during the night tend to be in the 5 to 10 degree range, and during the day they tend to be in the 15 to 20 degree range.

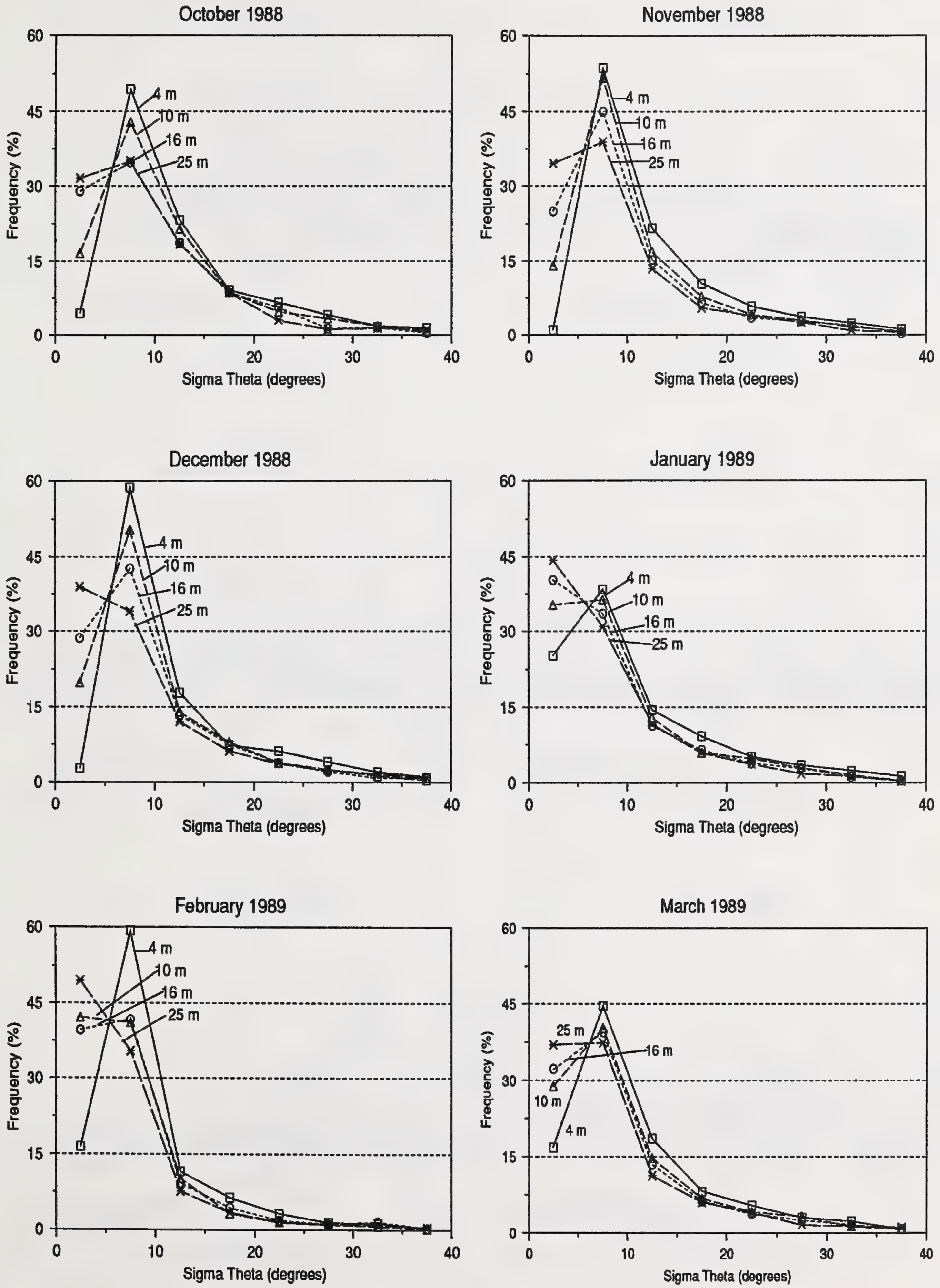

Figure 8.5 Winter

Monthly Frequency Distributions of 4, 10, 16 and 25 m Level Lateral Turbulence Intensities (σ_θ).

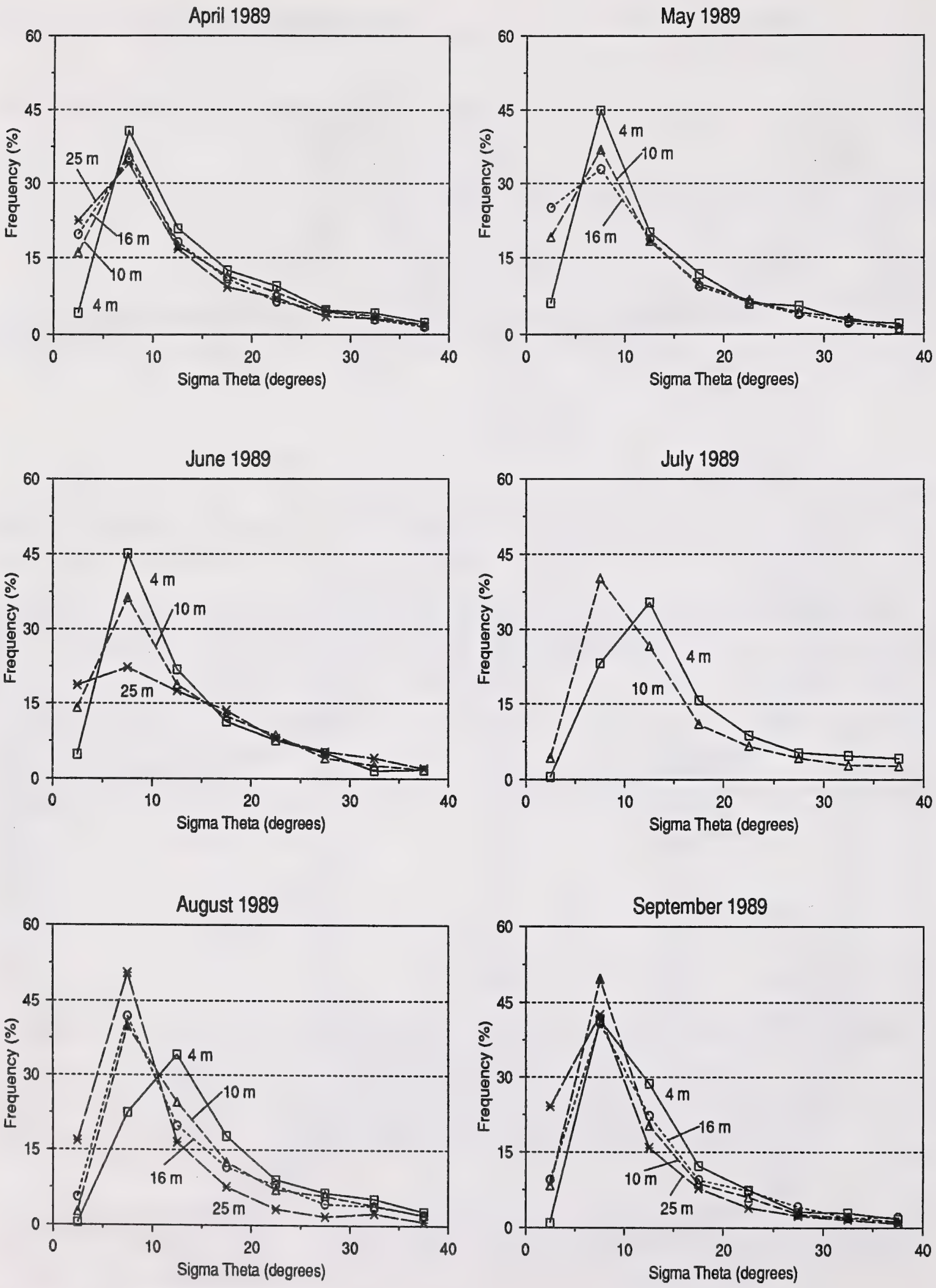

Figure 8.5 Summer

Monthly Frequency Distributions of 4, 10, 16 and 25 m Level Lateral Turbulence Intensities (σ_θ).

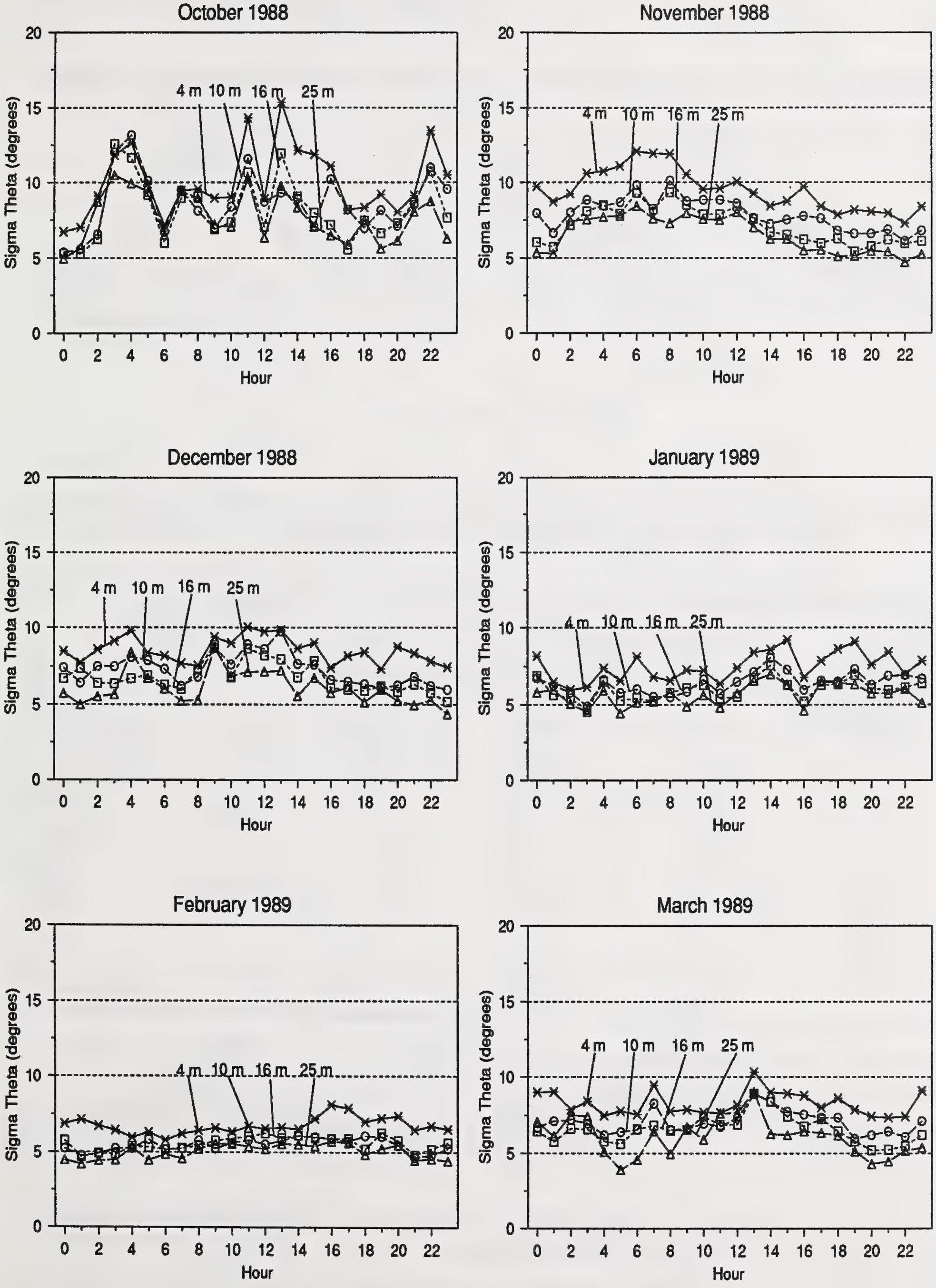

Figure 8.6 Winter

Median 4, 10, 16 and 25 m Level Lateral Turbulence Intensities (σ_θ) as a Function of Time of Day and Month.

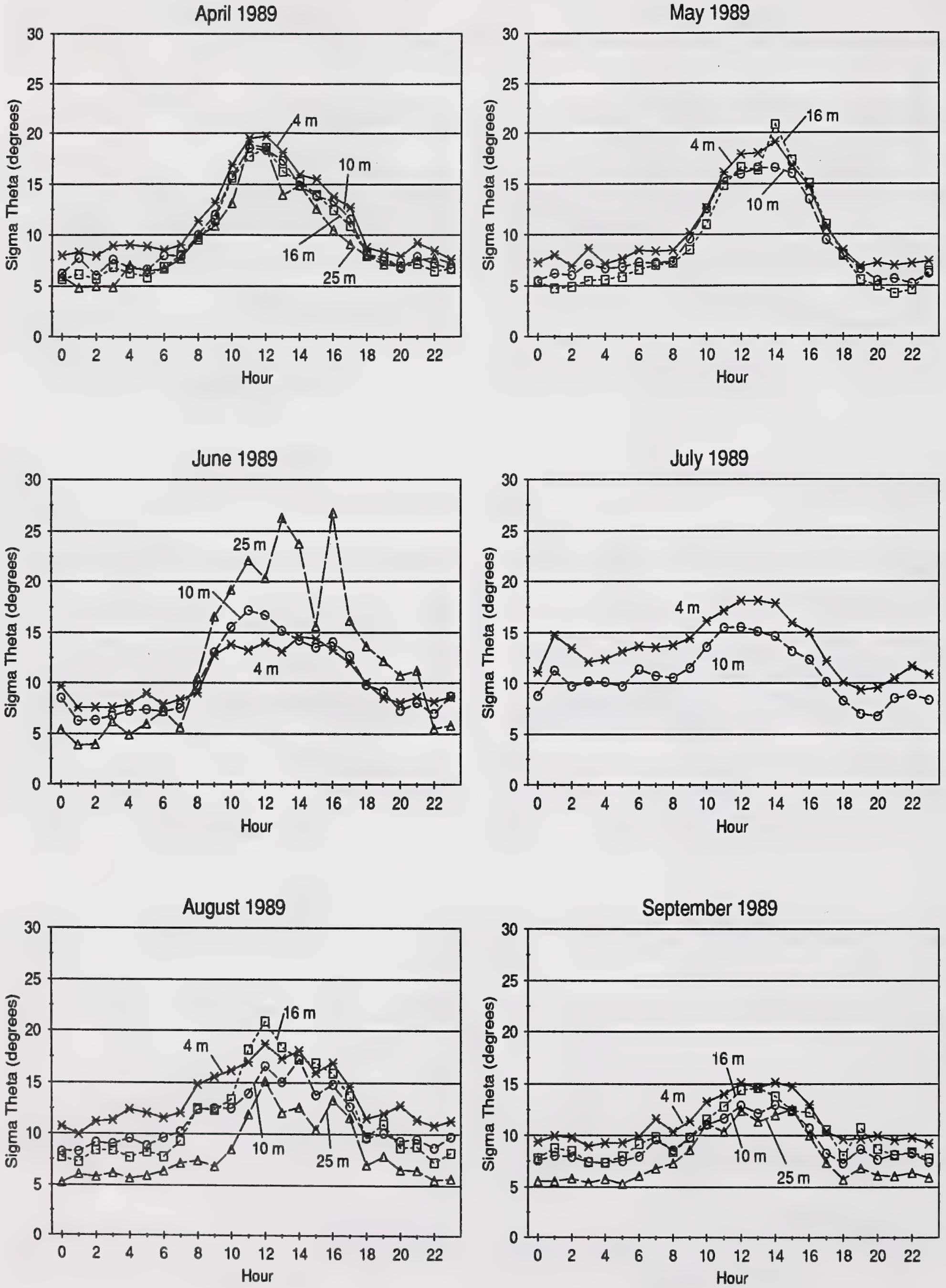

Figure 8.6 Summer

Median 4, 10, 16 and 25 m Level Lateral Turbulence Intensities (σ_θ) as a Function of Time of Day and Month.

8.2.4 Vertical Turbulence Intensity

Similar to the lateral turbulence intensity, the vertical turbulence intensity i_z is defined as:

$$i_z = \frac{\sigma_W}{\overline{U}} \tag{8.2}$$

which can be expressed as a fraction or a percentage. The vertical turbulence intensity can be approximated by:

$$i_z \approx \sigma_\phi = \tan^{-1}\left(\frac{\sigma_W}{\overline{U}}\right) \approx \frac{\sigma_W}{\overline{U}}$$

for small angles. Figure 8.7 shows the monthly frequency distributions for the 4, 10, 16, 25 m level values of σ_ϕ. The median values of σ_ϕ for each month are as follows:

Month	Median (degrees)			
	4 m	10 m	16 m	25 m
October 1988	4.2	3.5	3.1	2.9
November	4.2	3.9	3.1	2.8
December	4.1	3.8	3.0	2.6
January 1989	2.7	2.6	2.1	1.9
February	3.1	3.1	2.5	2.5
March	2.8	3.0	2.4	2.2
April	4.3	4.2	3.5	3.7
May	3.7	4.0	3.5	4.6
June	3.9	4.1	n/a	5.5
July	6.4	5.6	n/a	n/a
August	6.3	5.9	4.9	4.1
September	5.1	5.0	4.3	3.9

The median σ_ϕ values also have a tendency to decrease with increasing height. The overall average 10 m value of 4.1 degrees or 7% is about one-half that observed for σ_θ. The smallest median σ_ϕ values were observed in January. The largest median σ_ϕ values were observed in July and August.

Figure 8.8 shows the monthly 4, 10, 16 and 25 m level median vertical turbulence intensities as a function of time of day. There is a definite tendency for σ_ϕ to increase during the day and decrease during the night for the winter and summer months. At night, the σ_ϕ values tend to decrease with increasing height. In contrast, the daytime σ_ϕ values can remain constant or increase with increasing height. The summer months show a more pronounced daytime increase than the winter months. The diurnal variation is least noticeable at the 4 m level and during December and January, the months with the lowest solar radiation. The diurnal variation is the greatest during April when night-time values are typically 2 to 4 degrees and daytime values peak in the 8 to 10 degree range.

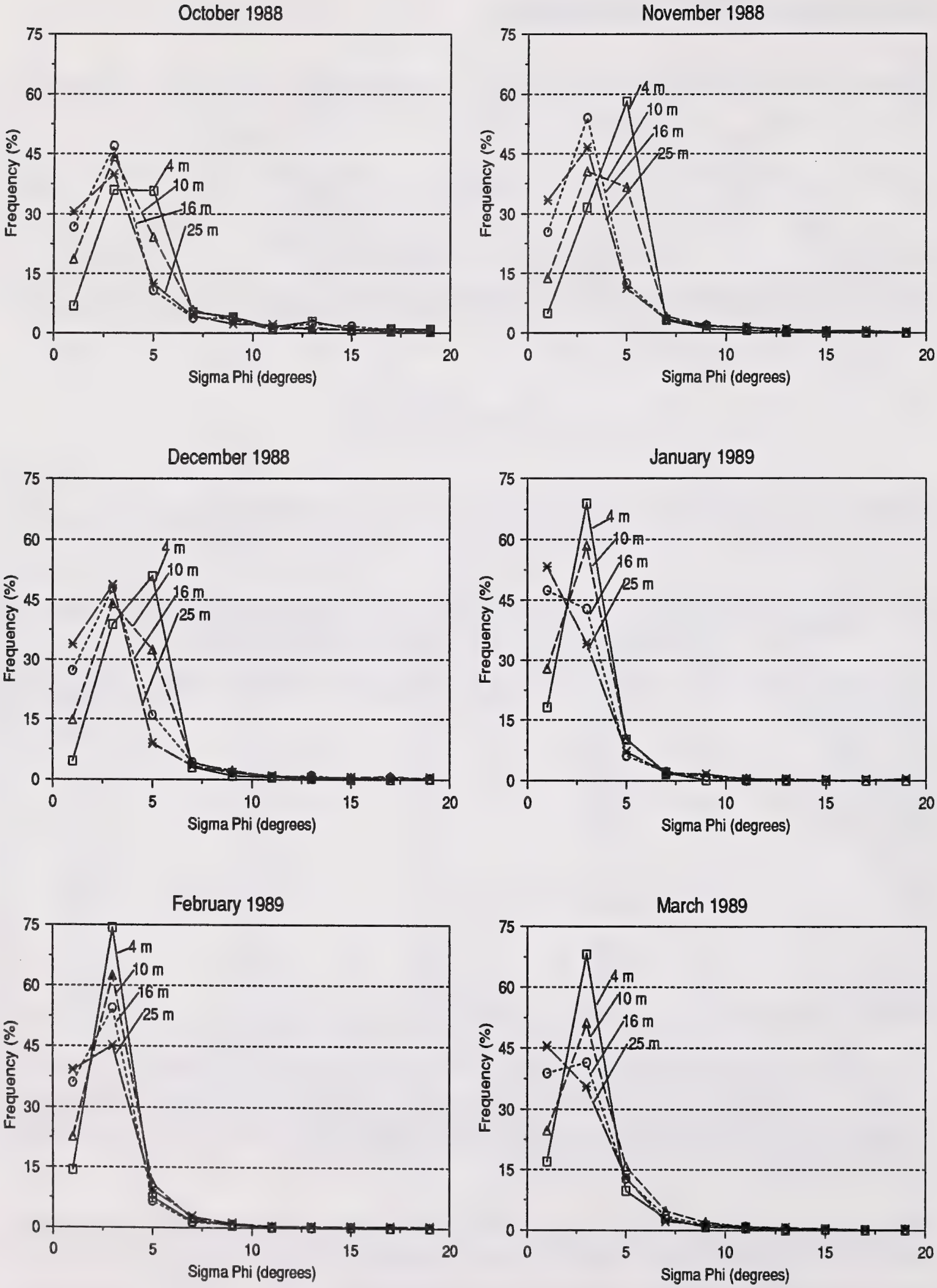

Figure 8.7 Winter

Monthly Frequency Distributions of 4, 10, 16 and 25 m Level Vertical Turbulence Intensities (σ_ϕ).

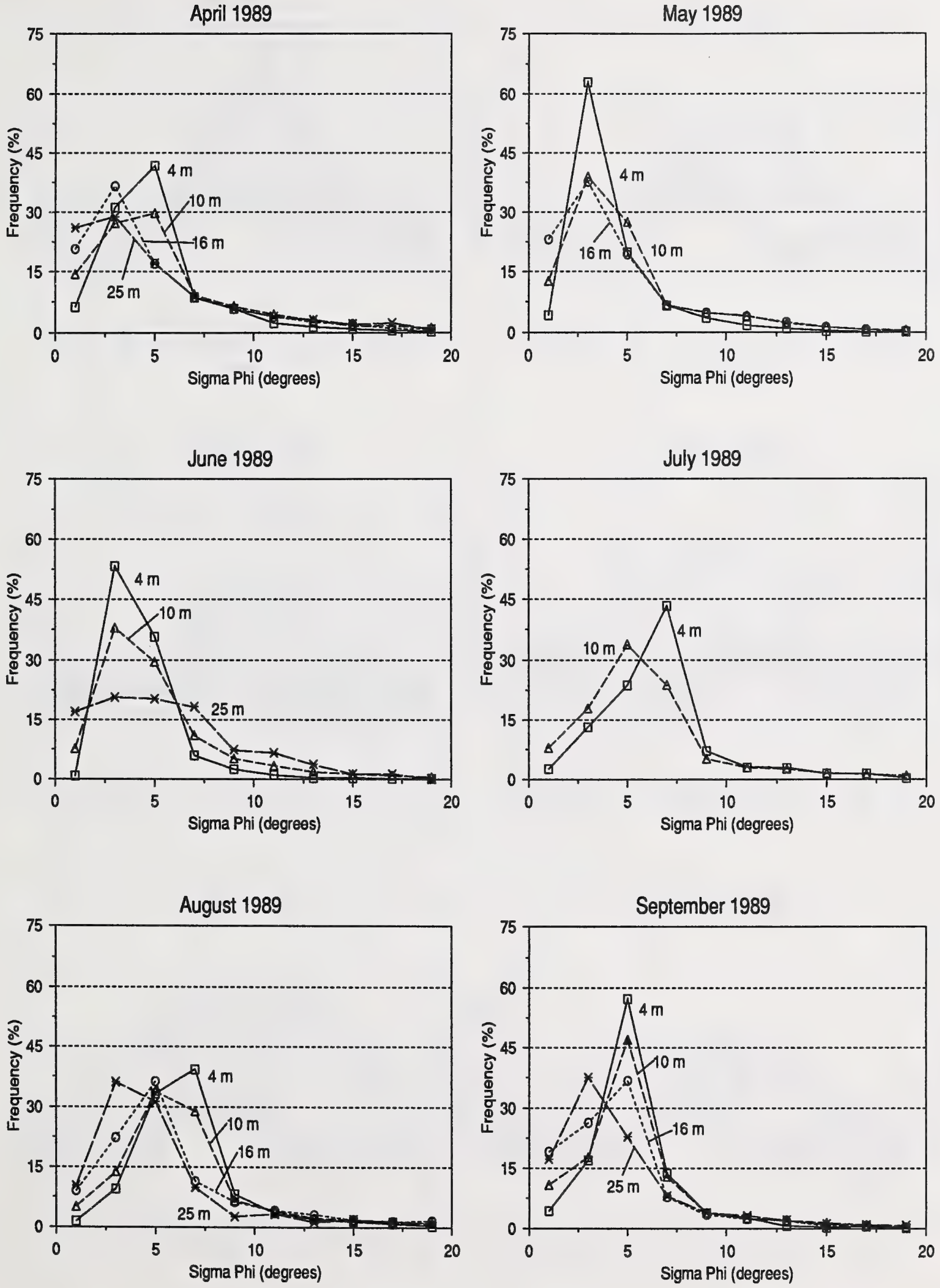

Figure 8.7 Summer

Monthly Frequency Distributions of 4, 10, 16 and 25 m Level Vertical Turbulence Intensities (σ_ϕ).

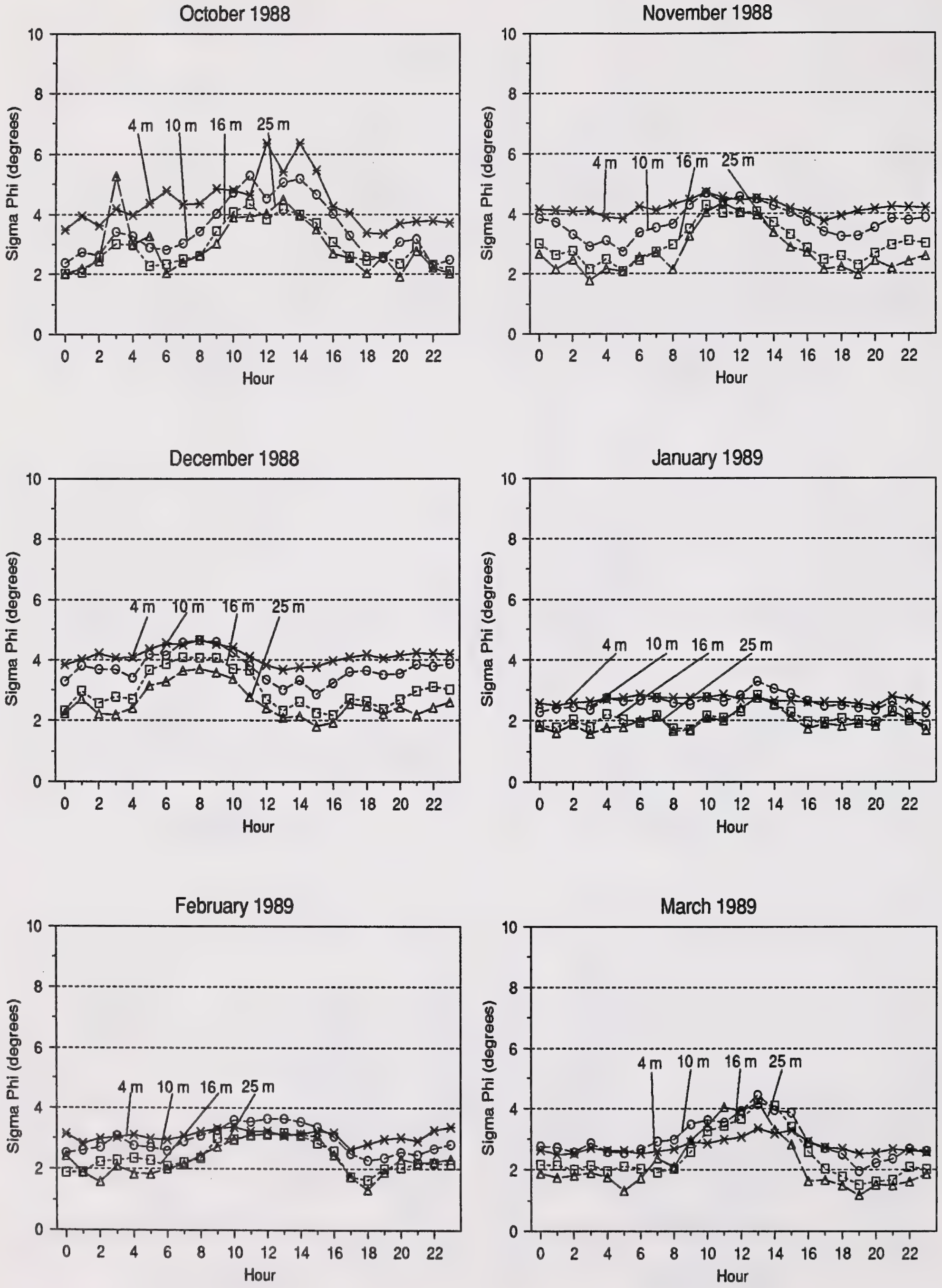

Figure 8.8 Winter

Median 4, 10, 16 and 25 m Level Vertical Turbulence Intensities (σ_ϕ) as a Function of Time of Day and Month.

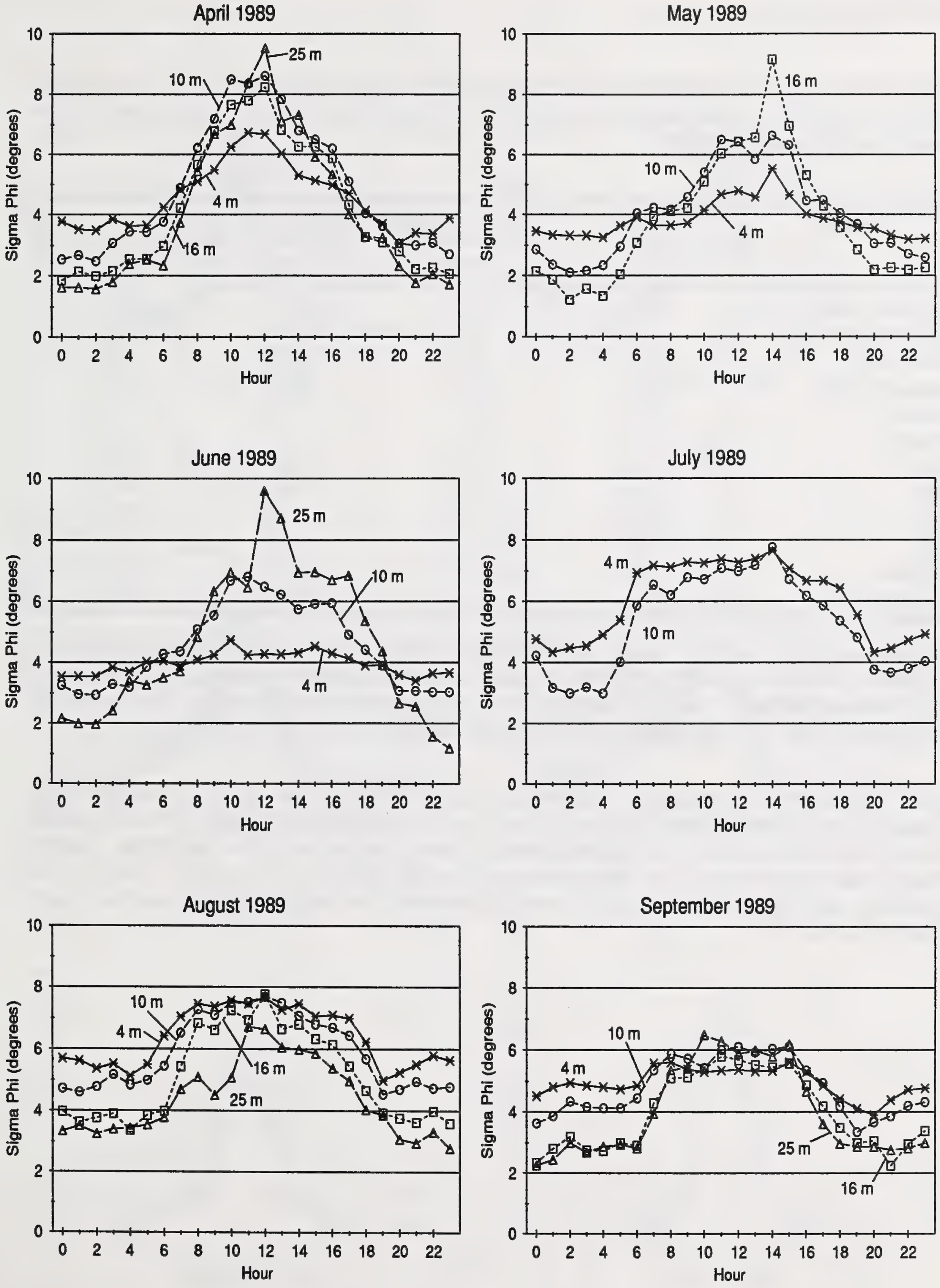

Figure 8.8 Summer

Median 4, 10, 16 and 25 m Level Vertical Turbulence Intensities (σ_ϕ) as a Function of Time of Day and Month.

8.2.5 Heat Flux

The heat flux (H_o) was calculated from the sonic anemometer values of $\overline{W'T'}$. Figure 8.9 shows the frequency distribution for the 4, 10, 16 and 25 m levels for each month. The median values are as follows:

Month	Median (W/m^2)			
	4 m	10 m	16 m	25 m
October 1988	-9.0	-5.6	-8.0	-6.6
November	-7.2	-6.5	-6.8	-5.9
December	-10.8	-8.7	-13.6	-6.8
January 1989	-18.6	-15.3	-15.2	-13.8
February	-10.1	-8.1	-8.8	-3.8
March	-2.4	-1.1	-1.1	0.0
April	2.8	4.2	2.7	8.0
May	4.7	13.7	10.1	n/a
June	13.2	12.2	n/a	37.1
July	3.7	6.1	n/a	n/a
August	3.9	4.4	6.0	-1.6
September	-0.1	2.3	4.4	18.5

The median 10 m heat flux values are the smallest during January and largest during May and June. There is a tendency for the median heat flux values to increase with increasing height, although there is some scatter in the results presented in the table. The frequency distributions shown in the figure indicate small variations between the four levels.

Figure 8.10 shows the monthly 4, 10, 16 and 25 m level median heat flux values as a function of time of day. They tend to be larger during the day than during the night. For November through to March, there is a relatively small diurnal variation in the heat flux. During January, the median heat flux values are negative for all hours of the day. For April to September, significant diurnal variations were observed. The largest median heat flux values occurred in May.

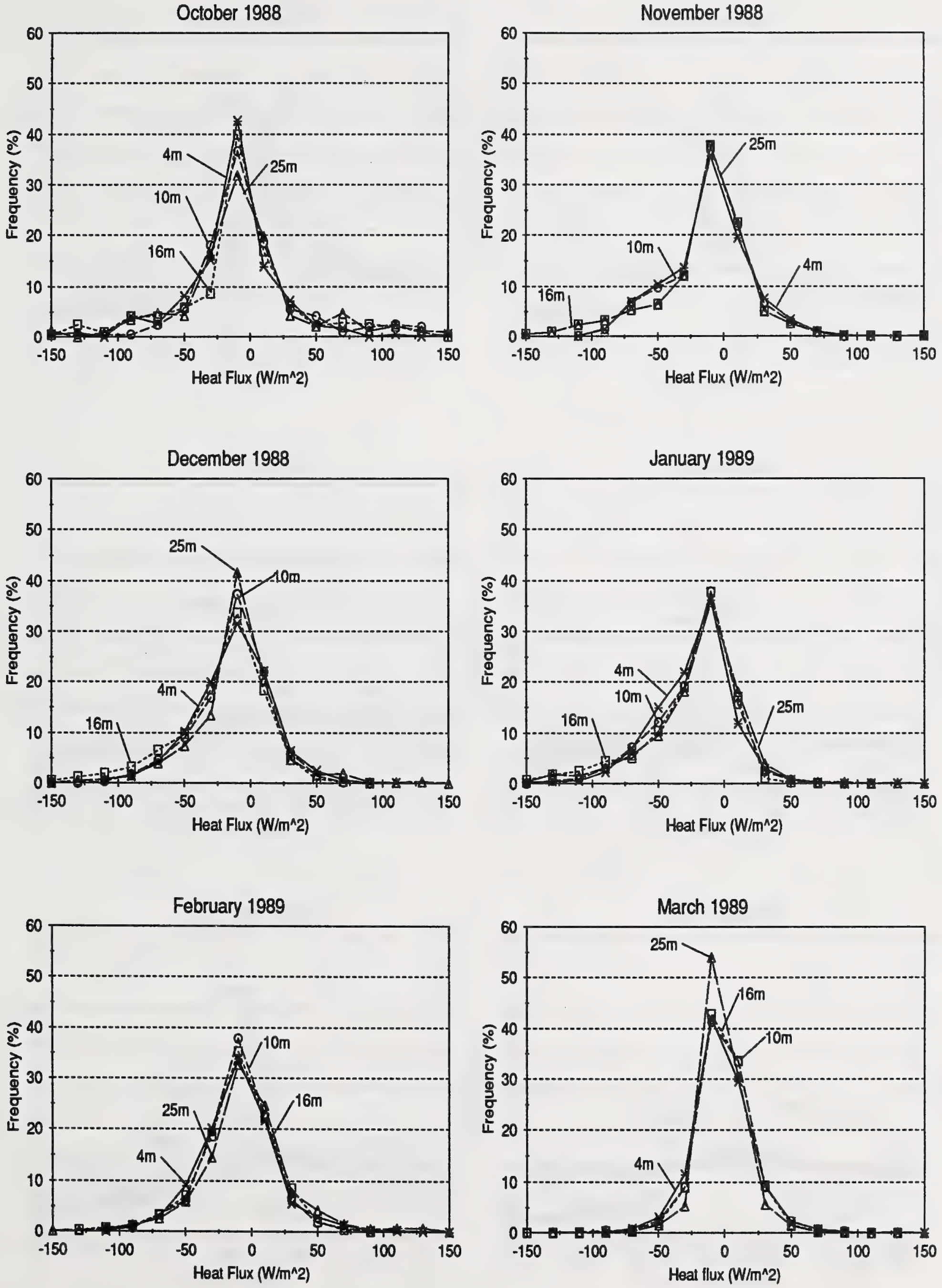

Figure 8.9 Winter

Monthly Frequency Distributions of 4, 10, 16 and 25 m Heat Fluxes.

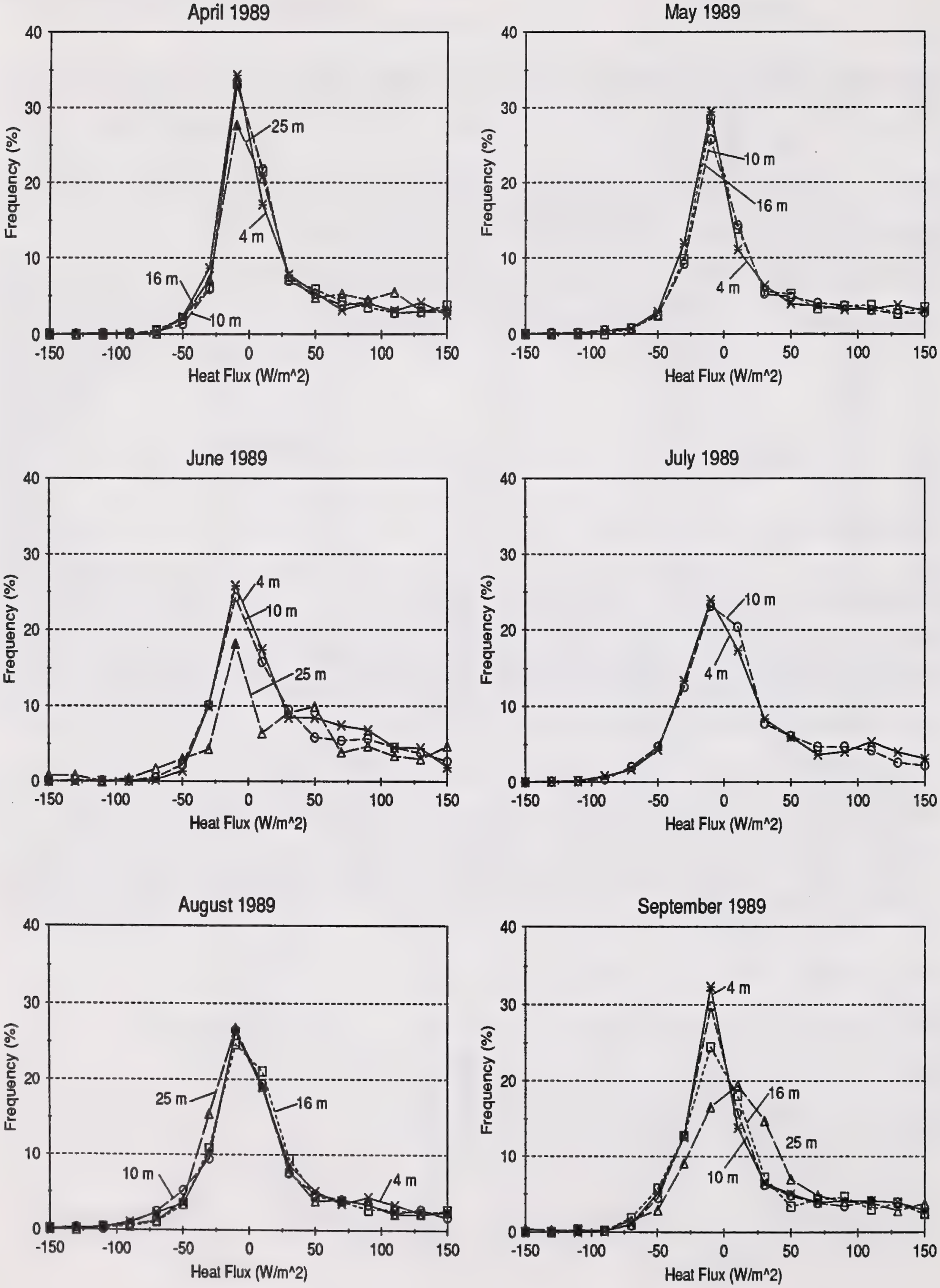

Figure 8.9 Summer

Monthly Frequency Distributions of 4, 10, 16 and 25 m Heat Fluxes.

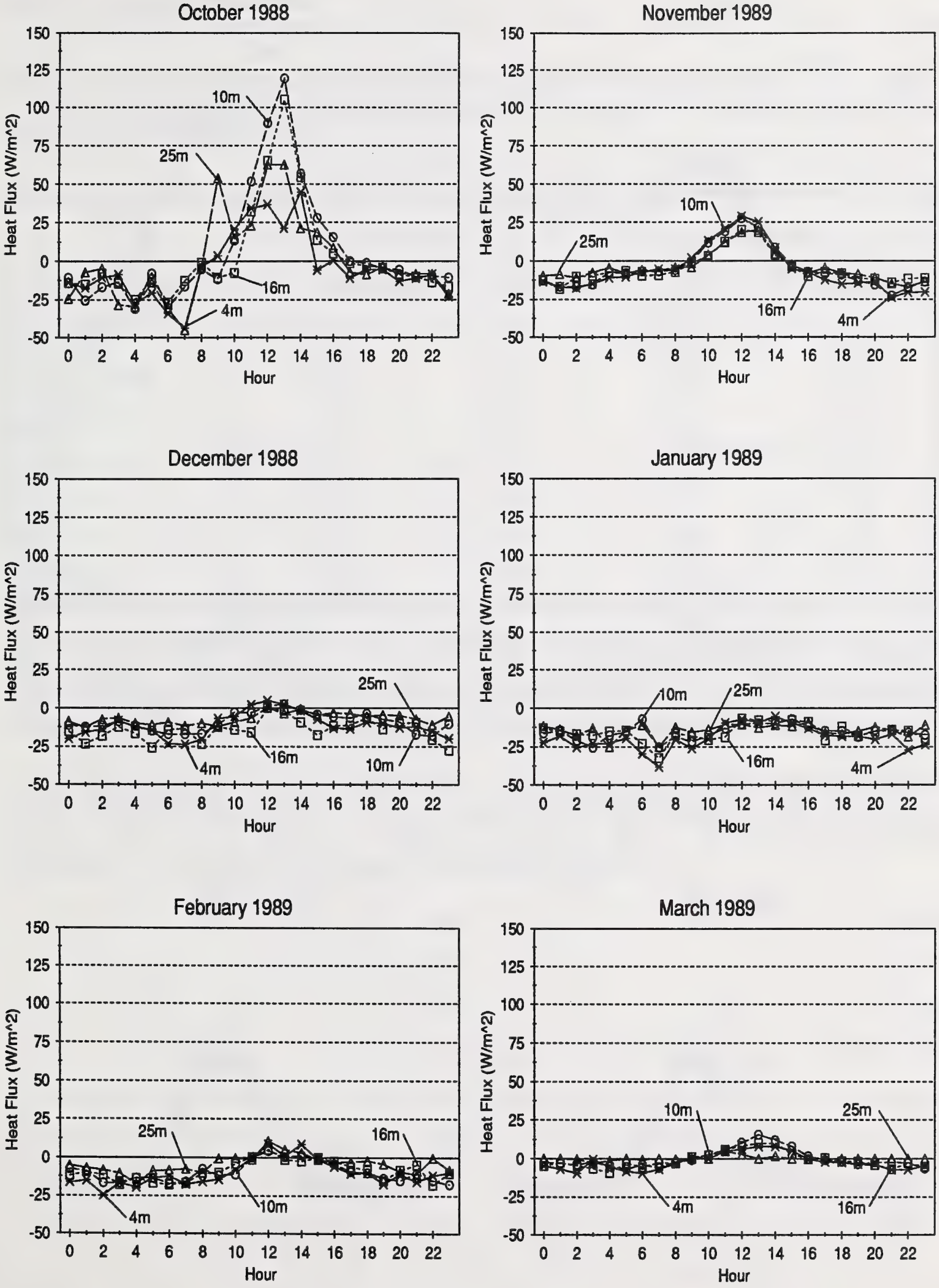

Figure 8.10 Winter

Median 4, 10, 16 and 25 m Level Heat Fluxes as a Function of Time of Day and Month.

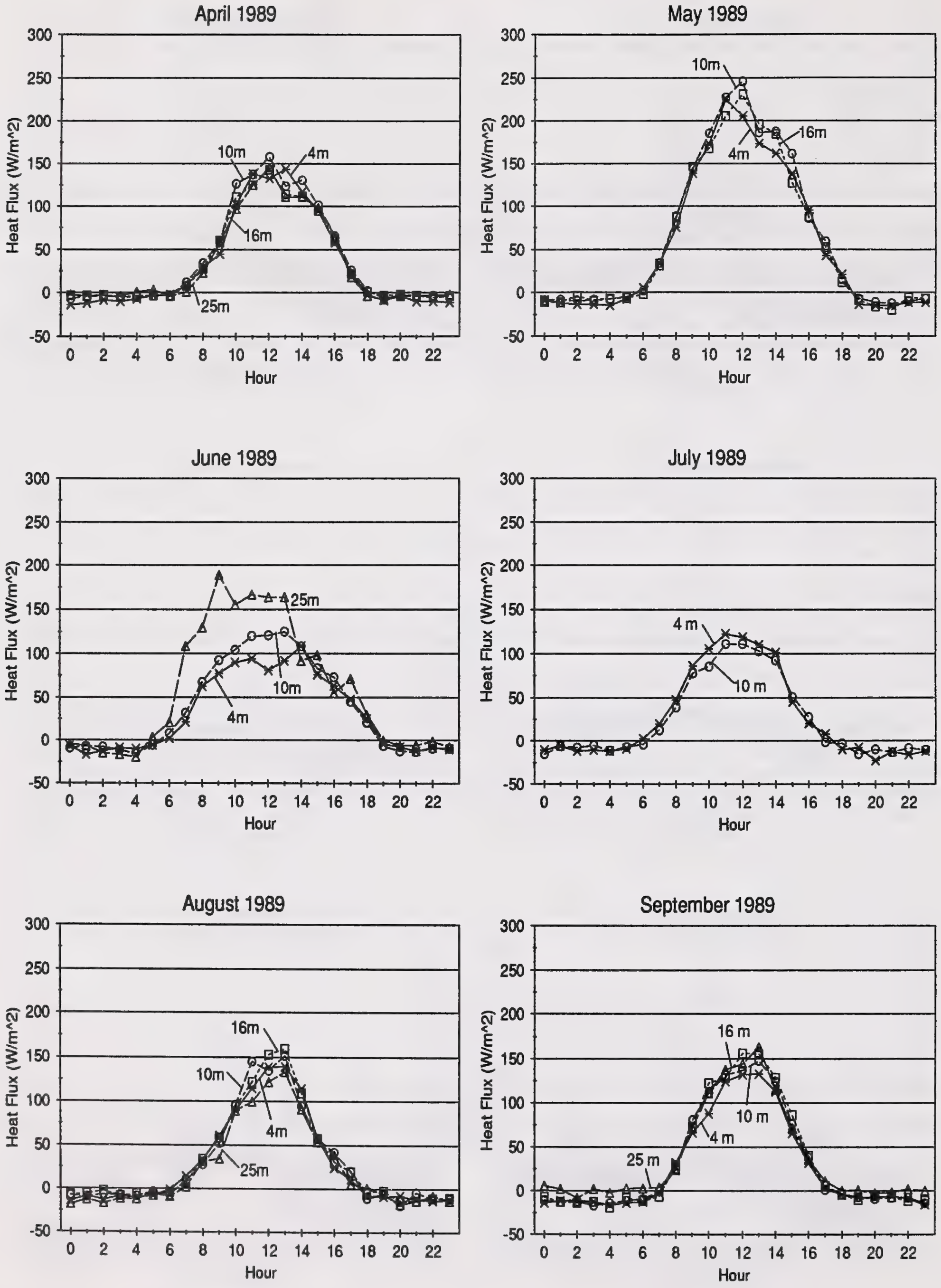

Figure 8.10 Summer

Median 4, 10, 16 and 25 m Level Heat Fluxes as a Function of Time of Day and Month.

8.2.6 Friction Velocity

The friction velocity (*U**) was calculated from the sonic anemometer values of $\overline{U'W'}$. Figure 8.11 shows the monthly frequency distribution for *U** at the 4, 10, 16 and 25 m levels. The median values are as follows:

Month	Median (m/s)			
	4 m	10 m	16 m	25 m
October 1988	0.17	0.16	0.20	0.24
November	0.19	0.19	0.21	0.21
December	0.18	0.18	0.21	0.19
January 1989	0.16	0.17	0.21	0.19
February	0.17	0.16	0.18	0.19
March	0.12	0.11	0.13	0.13
April	0.18	0.18	0.20	0.21
May	0.24	0.20	0.24	0.27
June	0.24	0.21	n/a	n/a
July	0.22	0.23	n/a	n/a
August	0.24	0.23	0.24	0.33
September	0.23	0.23	0.25	0.26

The monthly 4 and 10 m level median *U** values are similar. The monthly 16 and 25 m level median *U** values are also similar, but larger than the 4 and 10 m values. Apart from this variation, the overall tendency is for *U** to be uniform with height. The frequency distributions shown in Figure 8.11 indicate small variations among the four levels.

Figure 8.12 shows the monthly 4, 10, 16 and 25 m level median values as a function of time of day. The diurnal variations of friction velocity are similar to the diurnal variations of wind speed shown in Figure 8.4. Unlike wind speed, friction velocity does not vary consistently with height when plotted as a function of time of day.

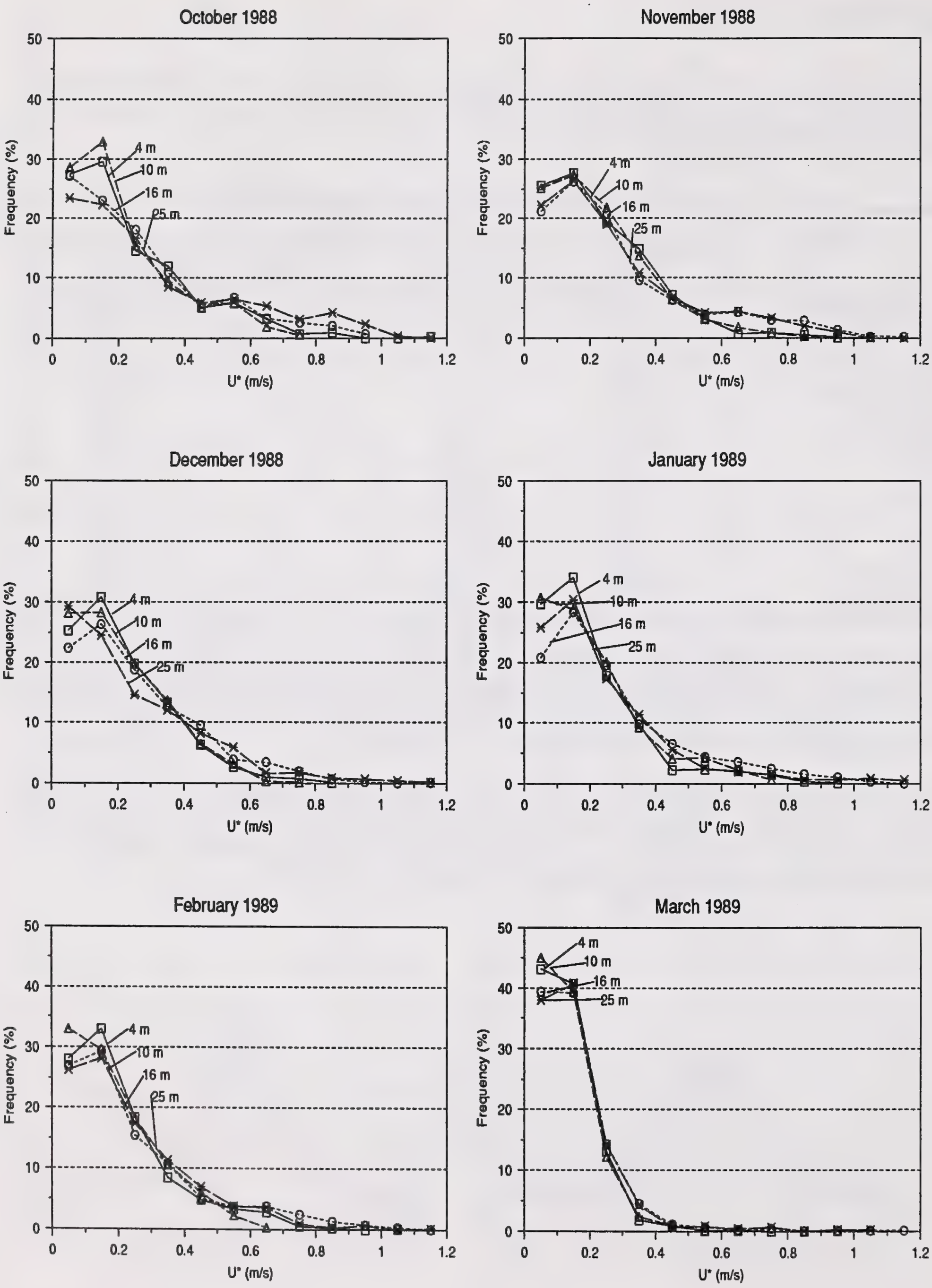

Figure 8.11 Winter

Monthly Frequency Distributions of 4, 10, 16 and 25 m Level Friction Velocities (*U).**

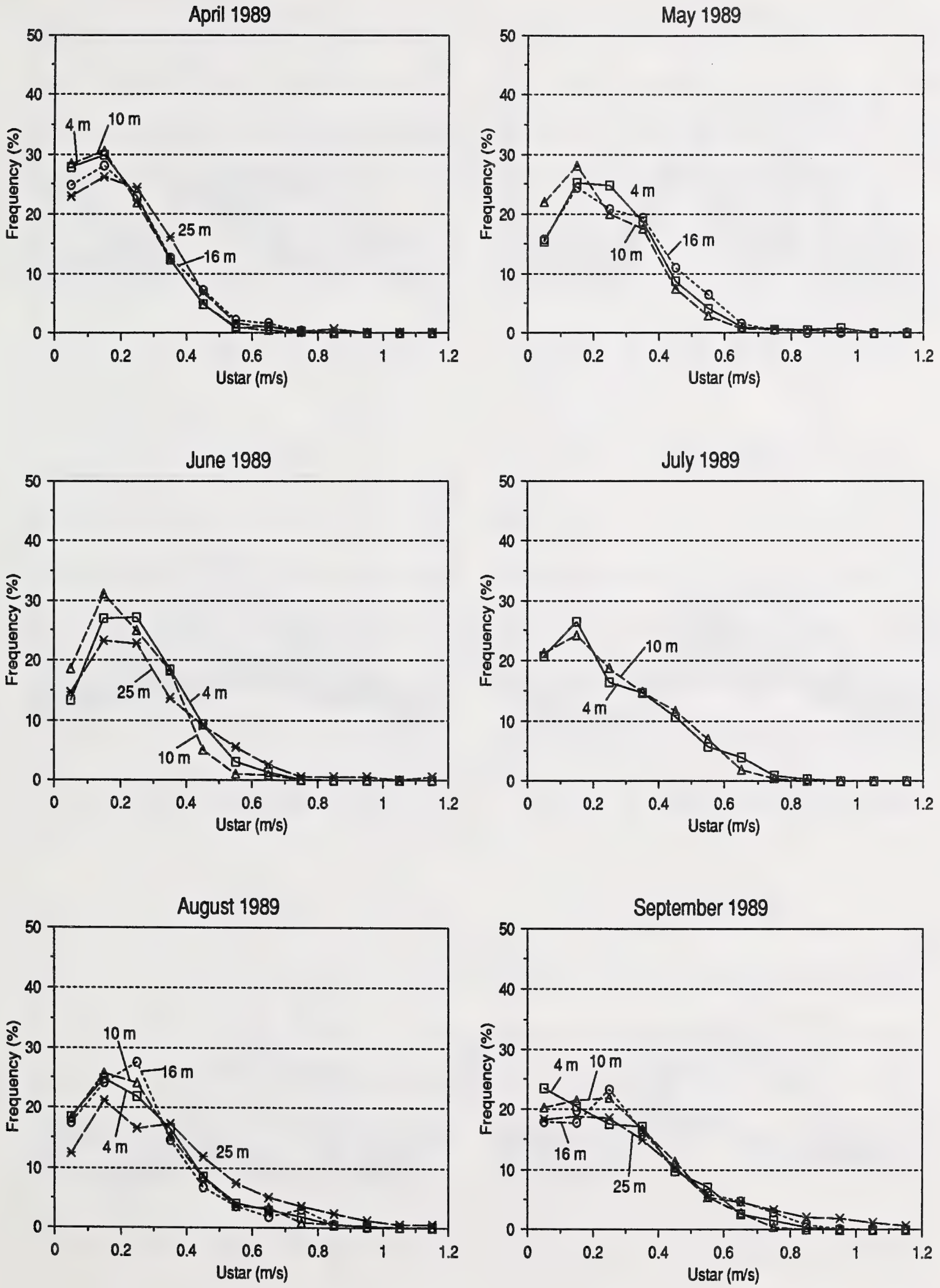

Figure 8.11 Summer

Monthly Frequency Distributions of 4, 10, 16 and 25 m Level Friction Velocities (*U).**

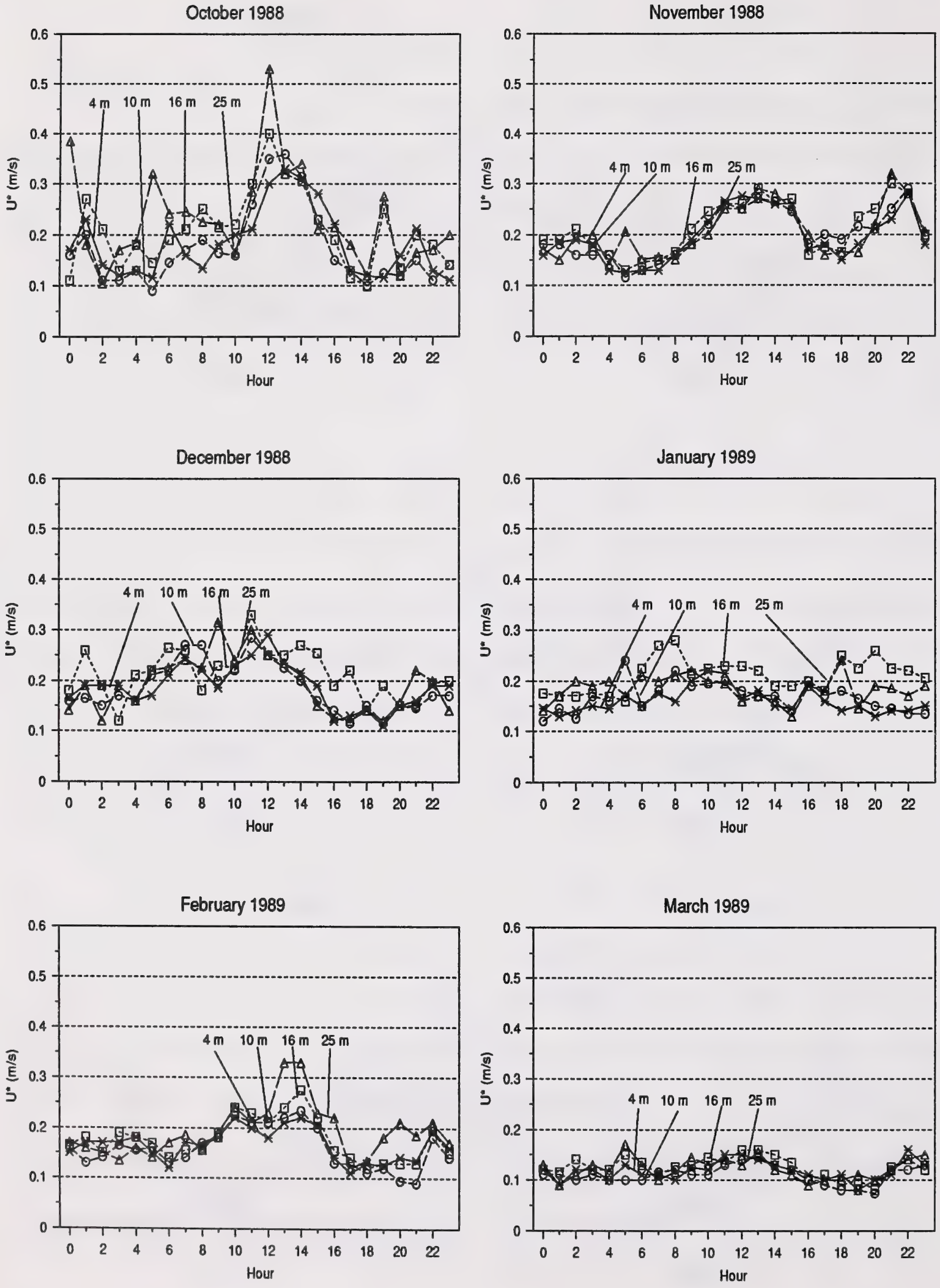
October 1988

November 1988

December 1988

January 1989

February 1989

March 1989

Figure 8.12 Winter

Median 4, 10, 16 and 25 m Level Friction Velocity (*U) as a Function of Time of Day and Month.**

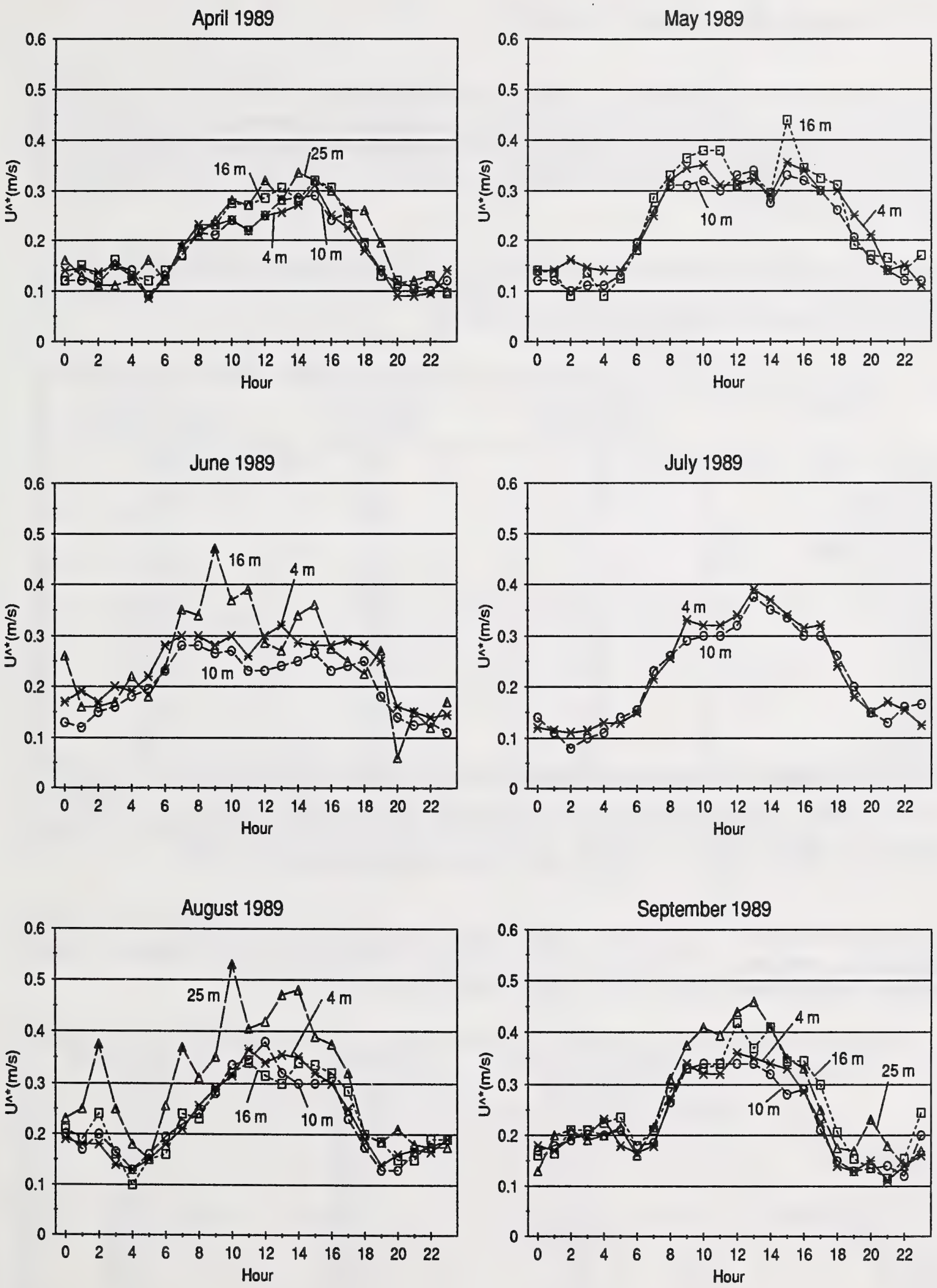

Figure 8.12 Summer

Median 4, 10, 16 and 25 m Level Friction Velocity (*U) as a Function of Time of Day and Month.**

8.2.7 Gradient Richardson Number

The gradient Richardson number is based on the ratio ($[(\partial\theta/\partial Z)/(\partial U/\partial Z)^2]$). The gradient Richardson number (R_g) represents the relative importance of convective to mechanical turbulence. R_g is positive during stable conditions and negative during unstable conditions. An R_g value greater than the critical Richardson number of 0.25 indicates a tendency for laminar flow conditions.

Figure 8.13 shows the frequency distribution of the 10 m level gradient Richardson number for each month. The following table summarizes the frequency (%) of unstable, stable and super critical conditions that occur for each month:

Month	Negative R_g (Unstable)	Positive R_g (Stable)	$R_g > 0.25$ (Super Critical)
October 1988	21	79	34
November	21	79	28
December	17	83	27
January 1989	9	91	33
February	34	66	25
March	47	53	27
April	49	51	21
May	51	49	15
June	n/a	n/a	n/a
July	n/a	n/a	n/a
August	45	55	15
September	38	62	21

On the average, stable conditions occur 67% of the time. Stable conditions were the most frequent during the month of January. Unstable conditions were most frequent during May. On average, the tendency for laminar stable flow was calculated to be 25%.

Figure 8.14 shows the 25 percentile, median and 75 percentile monthly values of the gradient Richardson number as a function of time of day. The highest hourly minimum, overall monthly median and lowest hourly median values are as follows:

Month	Highest Hourly Median	Monthly Median	Lowest Hourly Median
October 1988	0.41	0.12	-0.35
November	0.26	0.08	-0.15
December	0.18	0.09	0.01
January 1989	0.21	0.14	0.08
February	0.20	0.08	-0.10
March	0.25	0.03	-1.38
April	0.24	0.01	-1.45
May	0.26	-0.01	-2.12
June	n/a	n/a	n/a
July	n/a	n/a	n/a
August	0.14	0.02	-0.42
September	0.25	0.05	-0.58

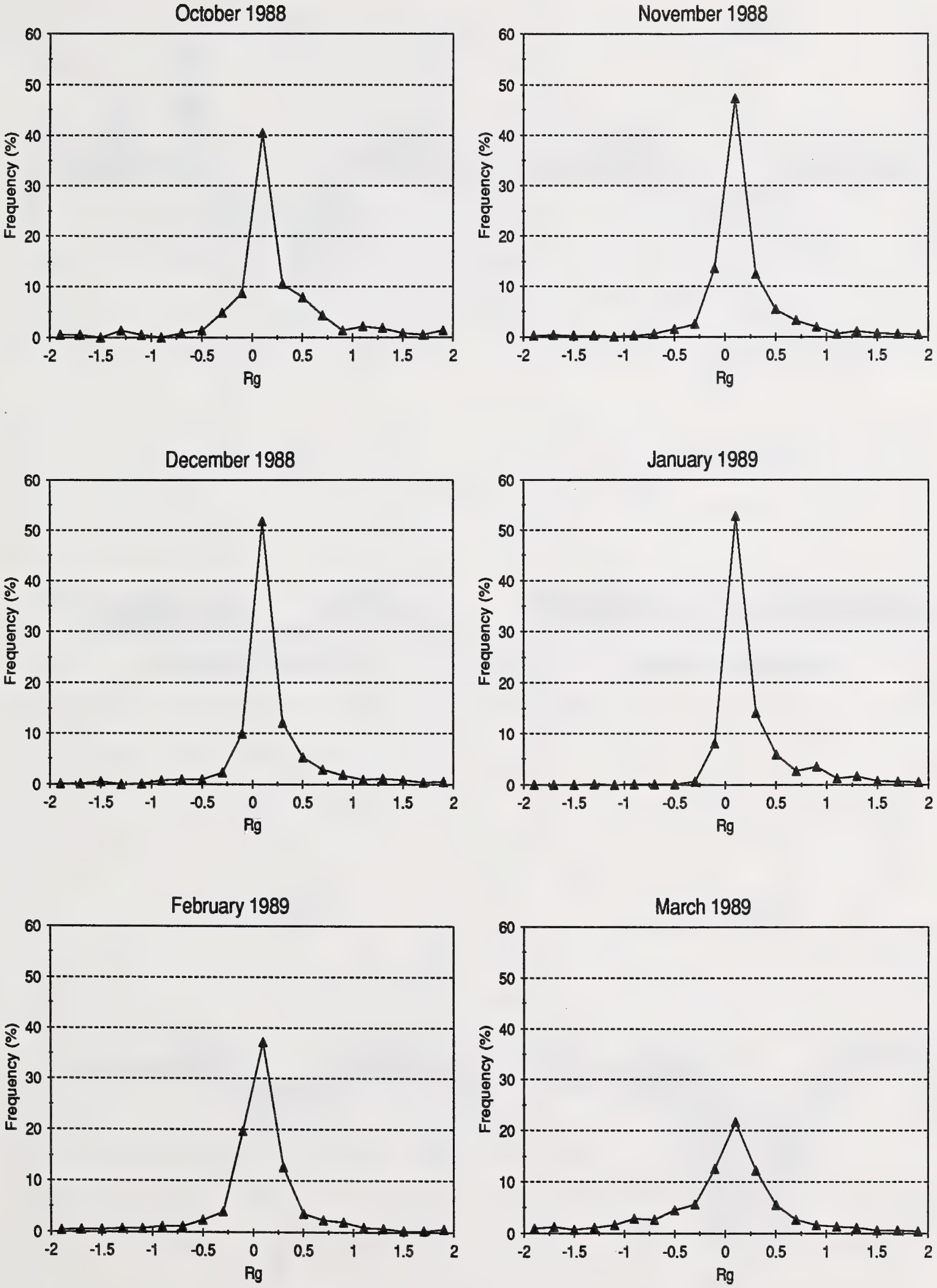

Figure 8.13 Winter

Monthly Frequency Distributions of 4, 10, 16 and 25 m Level Richardson Gradient Number.

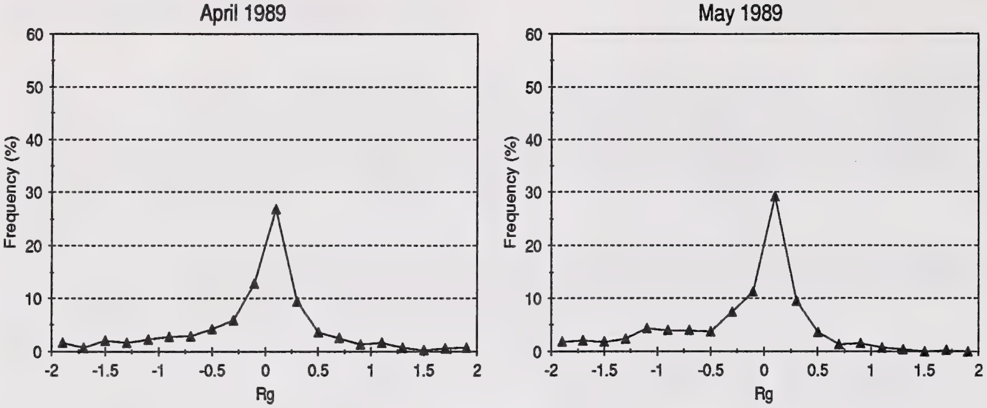

June 1989

July 1989

No Data Available

No Data Available

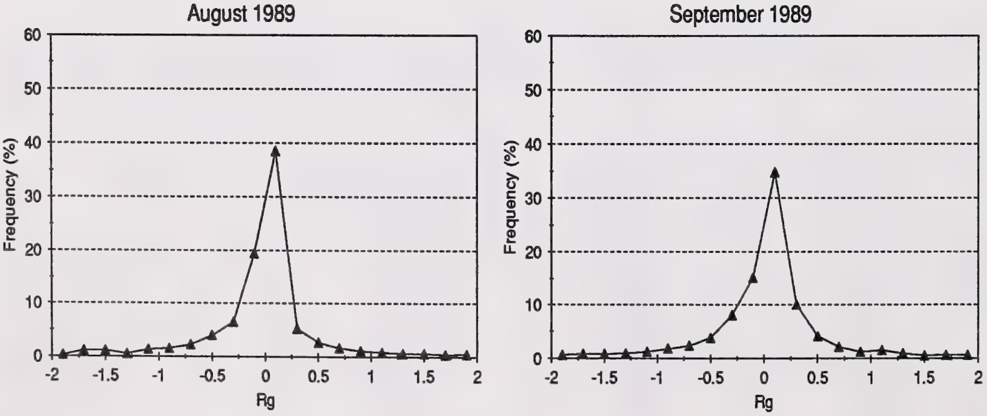

Figure 8.13 Summer

Monthly Frequency Distributions of 4, 10, 16 and 25 m Level Richardson Gradient Number.

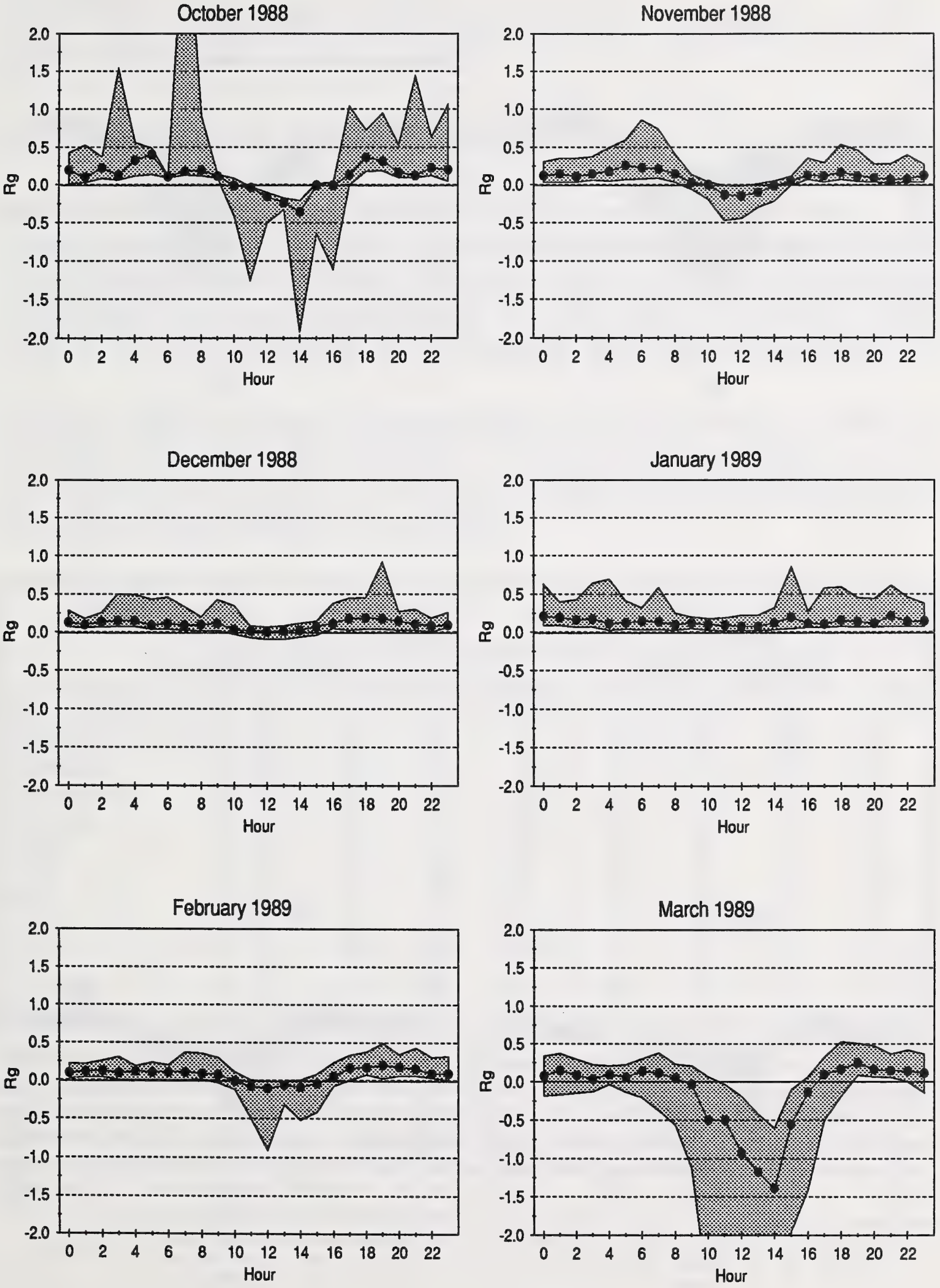

Figure 8.14 Winter

Median 4, 10, 16 and 25 m Level Richardson Gradient Number as a Function of Time of Day and Month.

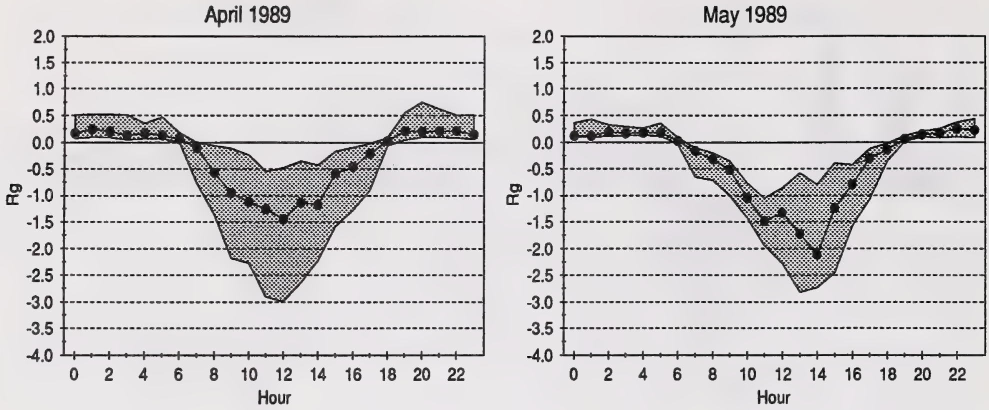

June 1989

July 1989

No Data Available

No Data Available

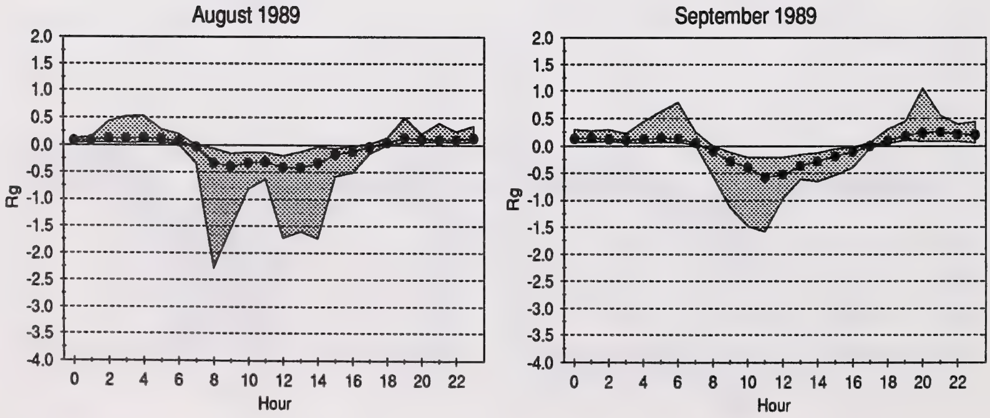

Figure 8.14 Summer

Median 4, 10, 16 and 25 m Level Richardson Gradient Number as a Function of Time of Day and Month.

Maximum hourly median values at night support the assumption that more stable conditions occur at night. Minimum hourly median values during the day support the assumption that more unstable conditions occur during the day.

8.2.8 Monin-Obukhov Stability Parameter

The Monin-Obukhov Stability Parameter (*Z/L*) is based on measurements of the Monin-Obukhov length (*L*) at each level. Values of *L* are dependent on the ratio $U^{*3}/\overline{W'T'}$. The *Z/L* stability parameter is the ratio of buoyant production of turbulence to wind shear production of turbulence. *Z/L*, like the gradient Richardson number, is positive for stable conditions and negative for unstable conditions. The *Z/L* stability parameter is more useful than R_g since it is a known function of height within the surface layer (Kaimal 1988).

Figure 8.15 shows the frequency distribution of the 4, 10, 16 and 25 m level *Z/L* values for each month. The frequency distributions shown for *Z/L* should only be used for comparative purposes because of the variable *Z/L* bin sizes. Variable bin sizes were selected to increase the resolution as *Z/L* approached zero. The following table summarizes the frequency (%) of unstable and stable conditions for each month:

Month	Negative *Z/L* (Unstable)				Positive *Z/L* (Stable)			
	4 m	10 m	16 m	25 m	4 m	10 m	16 m	25 m
October 1988	29	35	31	36	71	65	69	64
November	32	32	31	30	68	68	69	70
December	33	28	23	30	67	72	77	70
January 1989	19	21	17	22	81	79	83	78
February	36	35	34	42	64	65	66	58
March	45	50	48	53	55	50	52	47
April	52	54	56	63	45	45	43	36
May	51	57	56	n/a	43	42	43	n/a
June	59	59	n/a	n/a	37	41	n/a	n/a
July	54	55	n/a	n/a	44	44	n/a	n/a
August	52	52	57	45	42	46	42	53
September	47	49	51	64	48	50	48	35

The *Z/L* prediction of stable and unstable conditions is relatively invariant with height. On the average, stable conditions occur 56% of the time. The *Z/L* method predicts fewer stable conditions the R_g method (67%). Stable conditions were most frequent during January, the month when the smallest hourly median heat fluxes were observed. Unstable conditions were most frequent in June, one of the months when the largest median heat fluxes were observed.

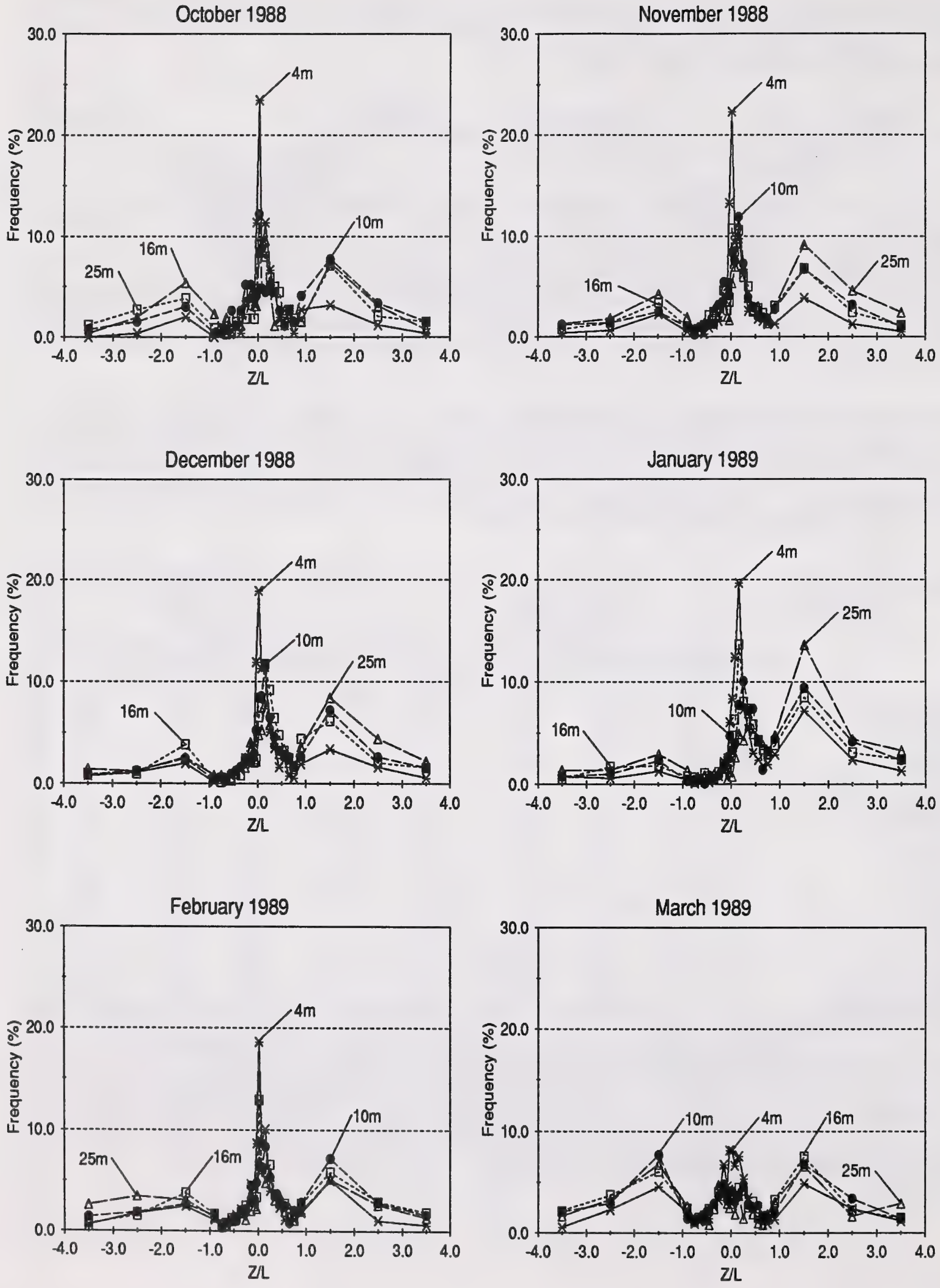
October 1988

November 1988

December 1988

January 1989

February 1989

March 1989

Figure 8.15 Winter

Monthly Frequency Distributions of 4, 10, 16 and 25 m Level Monin-Obukhov Stability Parameter (*Z/L*).

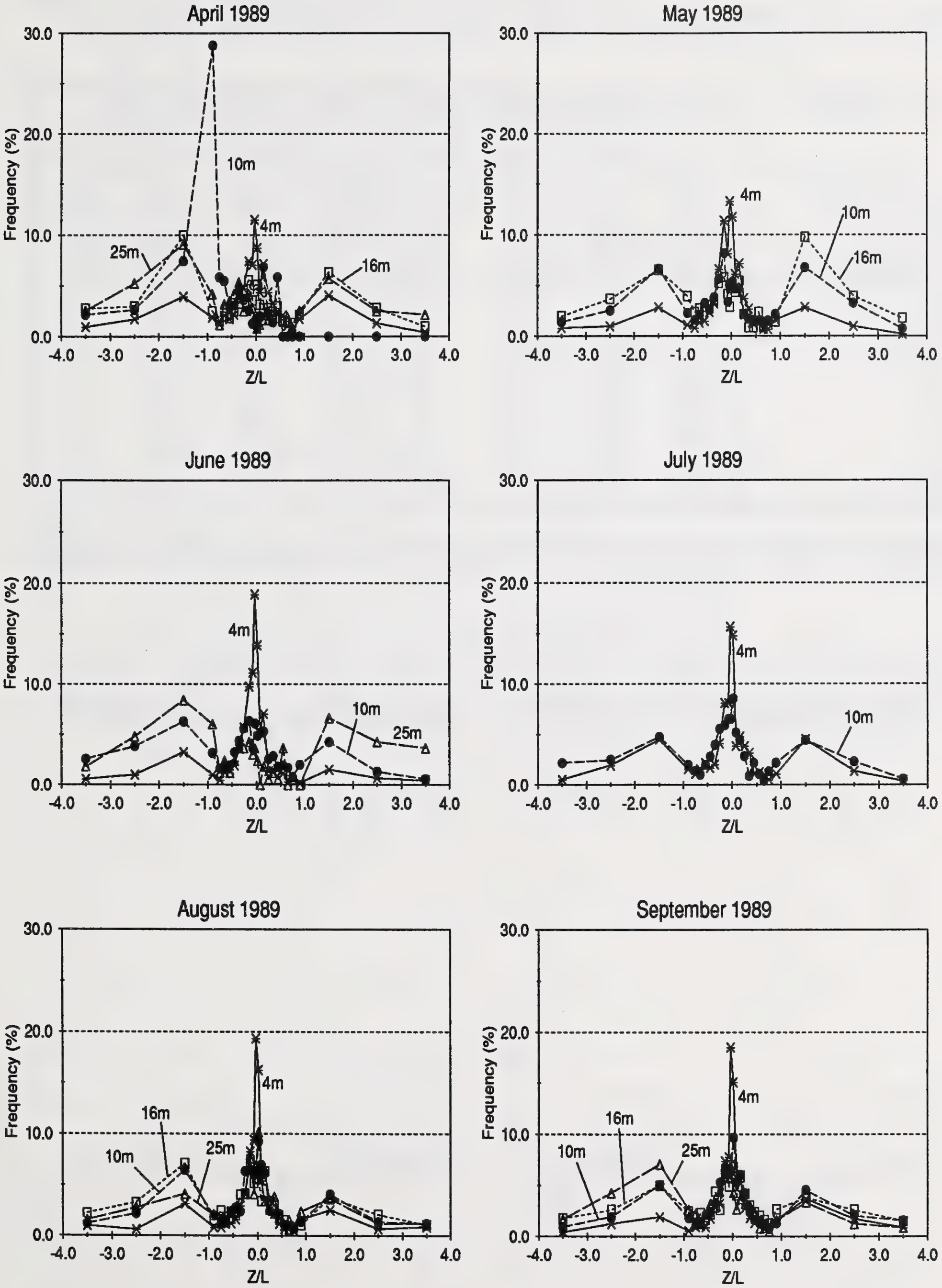

Figure 8.15 Summer

Monthly Frequency Distributions of 4, 10, 16 and 25 m Level Monin-Obukhov Stability Parameter (*Z*/*L*).

Figure 8.16 shows the monthly 4, 10, 16 and 25 m level median values as a function of time of day. The median night-time maximum and day-time minimum values are as follows:

Month	Night-time Maximum Z/L				Day-time Minimum Z/L			
	4 m	10 m	16 m	25 m	4 m	10 m	16 m	25 m
October 1988	0.40	2.53	0.64	3.48	-0.05	-0.26	-0.19	-0.32
November	0.18	0.46	0.53	0.61	-0.05	-0.15	-0.17	-0.31
December	0.11	0.40	0.46	1.14	-0.02	-0.00	-0.00	-0.00
January 1989	0.29	0.87	0.57	1.11	0.04	0.15	0.09	0.27
February	0.17	0.92	0.36	0.42	-0.03	-0.15	-0.05	-0.12
March	0.23	0.51	0.81	0.87	-0.15	-0.51	-0.46	-0.87
April	0.51	0.59	0.87	1.47	-0.46	-0.83	-1.13	-1.49
May	0.20	0.97	2.14	n/a	-0.33	-1.07	-1.54	n/a
June	0.18	0.53	n/a	n/a	-0.18	-1.03	n/a	n/a
July	0.34	0.97	n/a	n/a	-0.14	-0.49	n/a	n/a
August	0.08	0.23	0.15	0.49	-0.13	-0.43	-0.14	-0.37
September	0.15	0.49	0.97	0.27	-0.14	-0.37	-0.64	-0.69

During the day, there is a tendency for negative values of Z/L to occur indicating the presence of unstable conditions. During the night, Z/L tends to be positive indicating stable conditions.

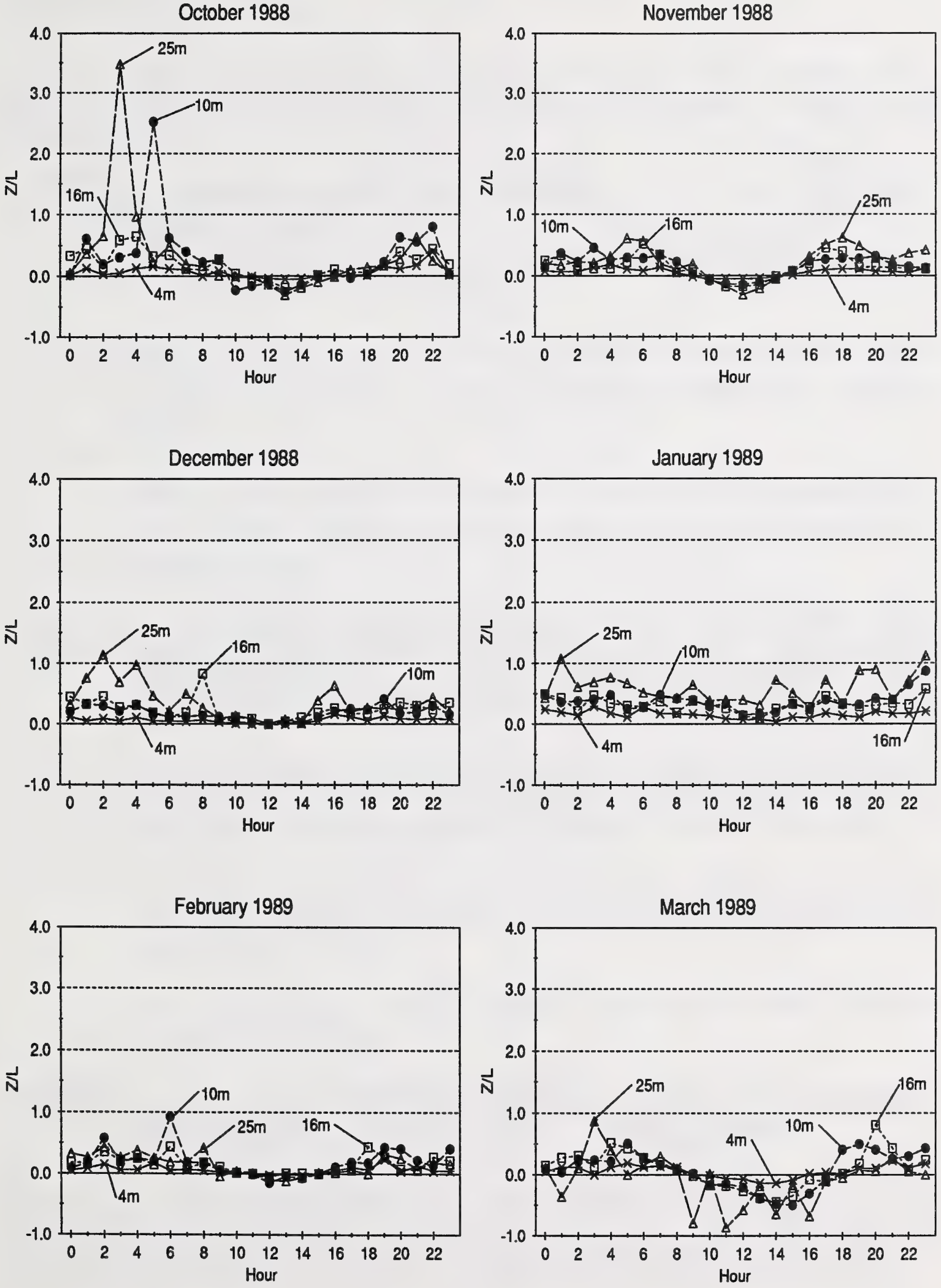

Figure 8.16 Winter

Median 4, 10, 16 and 25 m Level Monin-Obukhov Stability Parameter (*Z*/*L*) as a Function of Month.

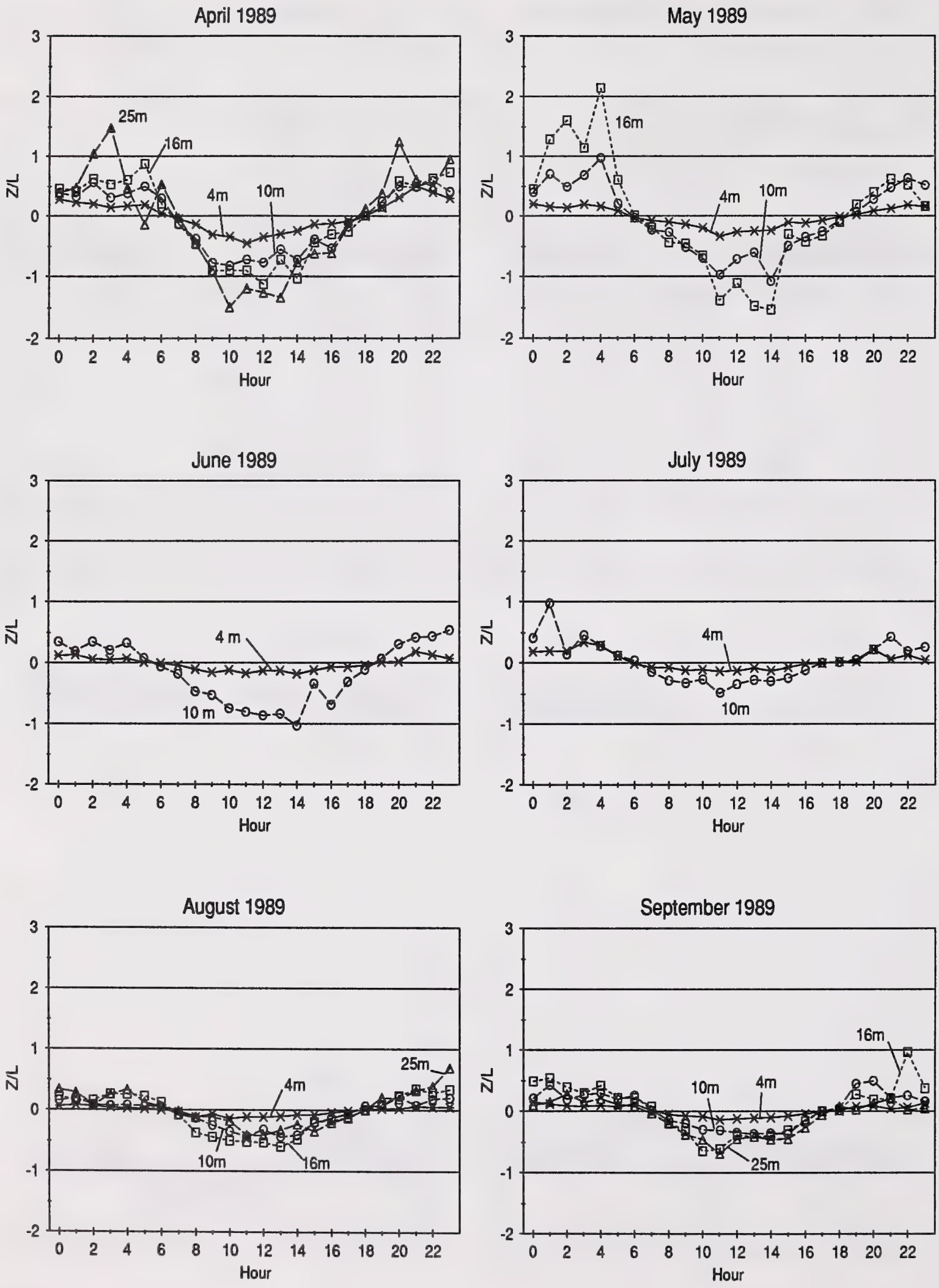

Figure 8.16 Summer

Median 4, 10, 16 and 25 m Level Monin-Obukhov Stability Parameter (*Z/L*) as a Function of Month.

8.2.9 Comments

The data collection period was performed over one year (October 1988 to September 1989) during which a wide range of meteorological conditions were observed. An overview of the data indicates:

- Temperatures ranged from -35.8 to 31.9°C.
- Median wind speeds increase with increasing height. The mean 4 m value of 3.0 m/s increases to 5.3 m/s at 25 m.
- Median lateral turbulence intensities (σ_θ) decrease with increasing height during the night. During the day, σ_θ can remain constant or increase with increasing height.
- Median vertical turbulence intensities (σ_ϕ) decrease with increasing height during the night. During the day, σ_ϕ can also remain constant or increase with increasing height.
- During the night median heat fluxes were negative. Positive median values were observed during the day for all months except January. While there was some scatter with the median values, similar frequency distributions were observed at all four observation levels.
- The diurnal variation of median friction velocities coincided with the variations of the median wind velocities. The median friction velocity frequency distributions and diurnal variations were relatively invariant with height.
- The gradient Richardson number indicated that stable conditions occurred 67% of the time. Gradient Richardson numbers greater than the critical value of 0.25 occurred 25% of the time.
- The Monin-Obukhov stability parameter indicated that stable conditions occurred 56% of the time.
- January, the month with the smallest hourly median heat fluxes had the most frequent occurrence of stable conditions.

The objective of the tracer component of the Field Measurement Program was to collect tracer data during low wind speed, stable atmospheric conditions. Wind speeds at the 10 m level were less than 2 m/s about 16% of the time during October, November and December. During these months, stable conditions were estimated to occur 70 to 80% of the time.

8.3 Boundary Layer Parameterization

The lowest layer of the atmospheric boundary layer can be mathematically described (or parameterized) in terms of wind and temperature profiles. The boundary layer is also characterized by vertical and horizontal turbulent fluctuations which determine the dispersion of pollutants. The relationship between these vertical profiles and turbulence levels have been summarized in micrometeorology textbooks (e.g. Lumley and Panofsky 1964, Haugen 1973, Panofsky and Dutton 1984, Kaimal 1988). The data and conclusions contained within these textbooks represent a synthesis of scientific publications and their associated field and/or laboratory studies.

Many fundamental relationships describing the atmosphere have been derived from carefully screened data to isolate selected behavior characteristics. The screening process usually ensures that stationary, horizontally homogeneous turbulent processes dominate. As the data collected during the Field Measurement Program include non-stationary, horizontally non-homogeneous and non-turbulent processes, more scatter in the Field Measurement Program results can be expected when they are compared to comparable values from the scientific literature.

Several boundary layer relationships were evaluated using the Field Measurement Program data. The analysis focussed on 8 064 one-half hourly averages from the winter period (16 October 1988 to 3 April 1989) and on 9 792 one-half hourly averages from the summer period (3 April to 23 October 1989). The first six months (October 1988 to March 1989) of data is referred to as "winter" data. The next seven months (April to October 1989) of data is referred to as "summer" data.

To minimize the effects of "outlier data", median values were used to delineate trends. To provide an indication of the scatter about the mean, the 25 and 75 percentiles are shown where deemed appropriate. A comparison of wind speeds using the different anemometers indicates some uncertainty with the Applied Technology Sonic Anemometers data when recorded wind speeds exceed 10 m/s (Section 8.8). For this reason, sonic anemometer data from the 4, 16 and 25 m levels were removed from the data set when they recorded wind speeds exceeding 10 m/s.

8.3.1 Drainage and Non-drainage Winds

As indicated in Section 2, the average west/east slope of the study area is one degree. As a consequence of this slope, drainage winds were frequently observed during the data collection program. Figure 8.17 shows selected wind speed and direction profiles indicating the presence of low level wind maxima associated with drainage air flow. The non-drainage flows shown in the figure indicate a uniform wind speed increase with height and a fairly constant wind direction with height. For the 24 October and 8 November profiles, the depth of the drainage layer is 20 to 30 m and the drainage layer wind directions are westerly (270°). Above the drainage layer, the wind directions are northeasterly and easterly (45° and 90°, respectively). For the 25 October profile, even though low level maximum wind speeds were observed, the wind directions are southeasterly to southerly (135 to 180°) indicating low level wind speed maximums may not always be associated with drainage flow from the west.

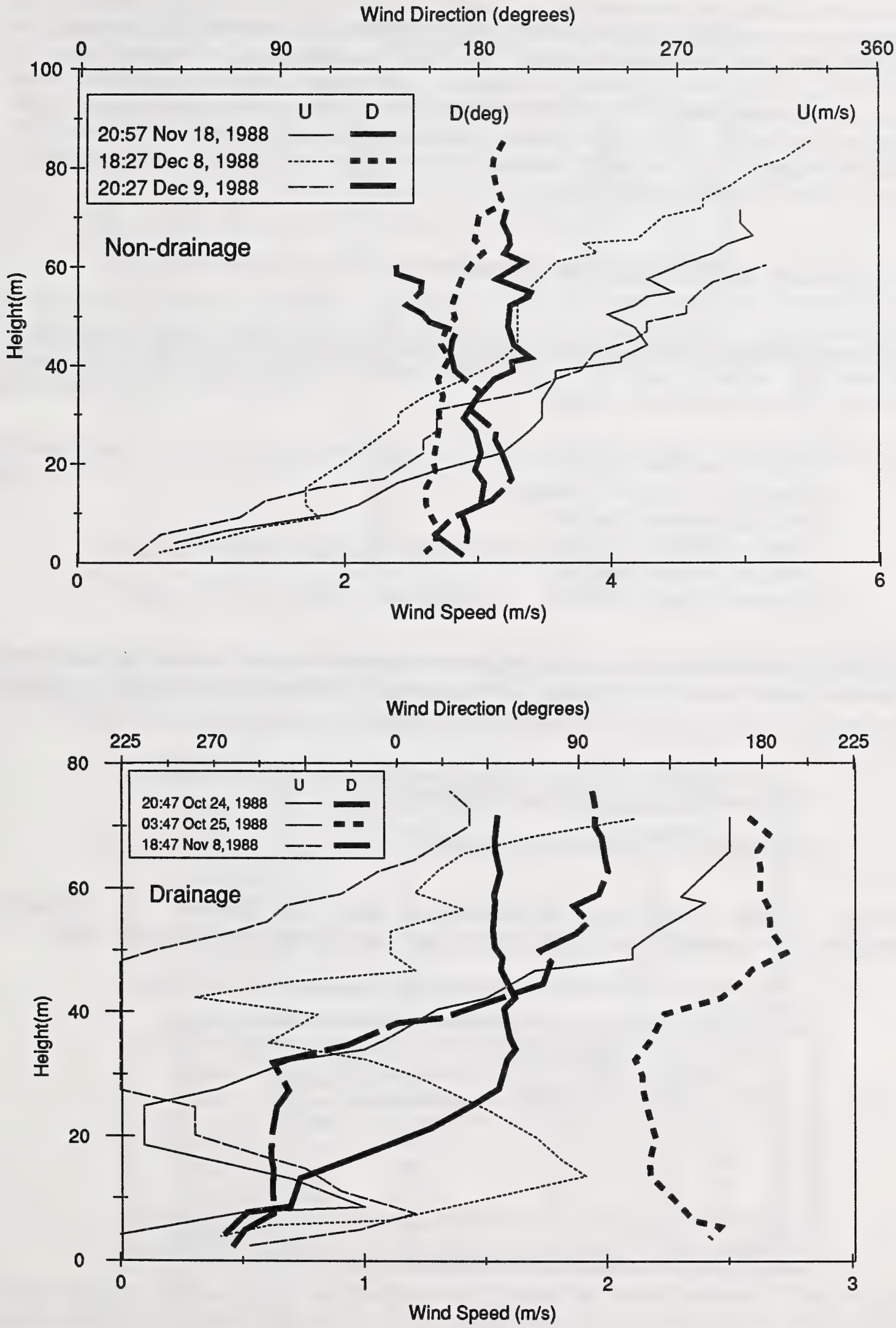

Figure 8.17

Selected Non-drainage and Drainage Flow Wind Speed and Direction Profiles.

As many boundary layer relationships are based on turbulent, non-drainage conditions, it is important to separate drainage and non-drainage conditions prior to effecting a comparison of observations with these relationships. The flow was classified as drainage when U_4 exceeded U_{16}, U_4 exceeded U_{25} or U_{10} exceeded U_{25}. The method uses non-adjacent (in the vertical sense) anemometers to ensure a positive wind shear defines non-drainage flow conditions. During the winter, non-drainage and drainage conditions occur 93.4 and 6.6% of the time, respectively. During the summer, non-drainage and drainage conditions occur 97.6 and 2.4% of the time, respectively.

8.3.2 Primary Stable/Unstable Criteria

A number of different stability parameters have been used to broadly classify atmospheric turbulence into unstable and stable conditions and to quantify the magnitude of the turbulence. These parameters include:

• Flux Richardson Number	R_f
• Gradient Richardson Number	R_g
• Bulk Richardson Number	R_b
• Monin-Obukhov Length	L
• Monin-Obukhov Stability	Z/L
• Kazanski-Monin Stability	K

The above terms are defined such that negative values correspond to unstable conditions and positive values to stable conditions. Given a normal wind speed increase with increasing height, the sign of R_f, L, Z/L and K depend only on the sign of the heat flux term $\overline{W'T'}$.

- Positive $\overline{W'T'}$ = unstable atmospheres, and
- Negative $\overline{W'T'}$ = stable atmospheres.

A review of the non-drainage meteorological data files indicate the following frequencies (%) of unstable and stable conditions at the four sonic anemometer levels:

Winter

Level (m)	Positive $\overline{W'T'}$ (Unstable)	Negative $\overline{W'T'}$ (Stable)
4	33	67
10	35	65
16	34	66
25	37	63
Mean	35	65

Summer

Level (m)	Positive $\overline{W'T'}$ (Unstable)	Negative $\overline{W'T'}$ (Stable)
4	47	53
10	43	57
16	45	55
25	36	64
Mean	43	57

On the average, all four levels are in agreement with each other predicting the occurrence of unstable and stable conditions 35 and 65% of the time, respectively for the winter, and 43 and 57% of the time, respectively for the summer. These numbers are consistent with those presented in Section 8.2.8.

Similarly, the sign of R_g and R_b depends only on the sign of the potential temperature gradient $\partial\theta/\partial Z$:

- Negative $\partial\theta/\partial Z$ = unstable atmospheres, and
- Positive $\partial\theta/\partial Z$ = stable atmospheres.

The following tables compare the predicted frequencies (%) of unstable and stable atmospheres using the sign of $\partial\theta/\partial T$ criteria:

Winter

Level (m)	Negative $\partial\theta/\partial T$ (Unstable)	Positive $\partial\theta/\partial T$ (Stable)
2 and 25	21	79
2 and 16	21	79
2 and 10	17	83
Mean	20	80

Summer

Level (m)	Negative $\partial\theta/\partial T$ (Unstable)	Positive $\partial\theta/\partial T$ (Stable)
2 and 25	42	58
2 and 16	44	56
2 and 10	44	56
Mean	44	56

On the average, all three levels are in agreement, predicting the occurrence of unstable and stable conditions 20 and 80% of the time, respectively for the winter, and 44 and 56%, respectively for the summer. These numbers differ slightly from those presented in Section 8.2.7 because of the exclusion of drainage flows.

The two methods ($\overline{W'T'}$ and $\partial\theta/\partial Z$), however, are not in close agreement with each other. The following table compares the joint frequency of stable and unstable atmosphere using the sign of $\overline{W'T'}$ and $\partial\theta/\partial Z$ criteria:

Winter

	Stable (Positive $\partial\theta/\partial Z$)	Unstable (Negative $\partial\theta/\partial Z$)	Total
Stable (Negative $\overline{W'T'}$)	3774 (60%)	334 (5%)	4108 (65%)
Unstable (Positive $\overline{W'T'}$)	1217 (19%)	960 (16%)	2177 (35%)
Total	4991 (79%)	1294 (21%)	6285 (100%)

Summer

	Stable (Positive $\partial\theta/\partial Z$)	Unstable (Negative $\partial\theta/\partial Z$)	Total
Stable (Negative $\overline{W'T'}$)	3275 (41%)	197 (2%)	3472 (43%)
Unstable (Positive $\overline{W'T'}$)	1331 (17%)	3176 (40%)	4507 (57%)
Total	4606 (58%)	3373 (42%)	7979 (100%)

The table is based on $\overline{W'T'}$ measured at the 10 m level and $\partial\theta/\partial Z$ over the 2 to 25 m layer. The results indicate:

- $\overline{W'T'}$ and $\partial\theta/\partial Z$ are in agreement 76% of the time in the winter and 81% of the time in the summer.
- When $\overline{W'T'}$ indicates a stable atmosphere, $\partial\theta/\partial Z$ indicates a stable atmosphere 92% of the time for the winter, and 95% of the time for the summer.
- When $\partial\theta/\partial Z$ indicates a stable atmosphere, $\overline{W'T'}$ indicates a stable atmosphere 76% of the time for the winter, and 71% of the time for the summer.
- When $\overline{W'T'}$ indicates an unstable atmosphere, $\partial\theta/\partial Z$ indicates an unstable atmosphere 46% of the time for the winter, and 70% of the time for the summer.
- When $\partial\theta/\partial Z$ indicates an unstable atmosphere, $\overline{W'T'}$ indicates an unstable atmosphere 76% of the time for the winter and 95% of the time for the summer.

Without a prior knowledge or preference for one method over the other, this analysis indicates less uncertainty with either method for predicting the occurrence of stable conditions. At this stage, it is not clear whether the difference between these two methods relates to some fundamental unknown in terms of atmospheric behavior or to uncertainties with instrument behavior. It may be due to the difficulty in measuring $\overline{W'T'}$ based on sonic anemometer values of T' under low turbulence conditions (see Section 5). To assess boundary layer relationships, it was decided to use the data set where both $\overline{W'T'}$ and $\partial\theta/\partial Z$ agree in terms of predicting stable or unstable conditions. This data set represents 4734 one-half hour periods from the non-drainage file (76% of the non-drainage file) for the winter period. For the summer period, the data set represents 6451 one-half hour periods from the non-drainage file (81% of the non-drainage file).

8.3.3 Surface Layer Stability Relationships

In the surface layer, the Gradient Richardson Number (R_g), Flux Richardson Number (R_f) and Monin-Obukhov Stability Parameter (Z/L) are interrelated according to the following relationships (Kaimal 1988):

- Stable Conditions ($0 \leq Z/L \leq 2$)

$$R_G = (Z/L)/(1 + 4Z/L) \tag{8.3}$$

$$R_F = R_G \tag{8.4}$$

- Unstable Conditions ($-2 \leq Z/L \leq 0$)

$$R_G = Z/L \tag{8.5}$$

$$R_F = (1 + 16|Z/L|)^{1/4} R_G \tag{8.6}$$

Figure 8.18 compares the predicted relationships between R_g, R_f and Z/L with median values obtained from the Field Measurement Program. The shaded areas represent the spread between the 25 and 75 percentile values. The figures indicate the following:

- There appears to be much less scatter for stable conditions than for unstable conditions during the winter. For the summer months the scatter appears to be similar for stable and unstable conditions.

- Under stable conditions, median values of the gradient Richardson number appear to be underestimated while the median values of the flux Richardson number show better agreement with the theoretical relationship.

- Under unstable conditions, the correct decreasing trend for R_g and R_f with decreasing Z/L is predicted. With the scatter, it is difficult to make further quantitative statements regarding the predictability of R_g. For unstable conditions, R_f is under predicted.

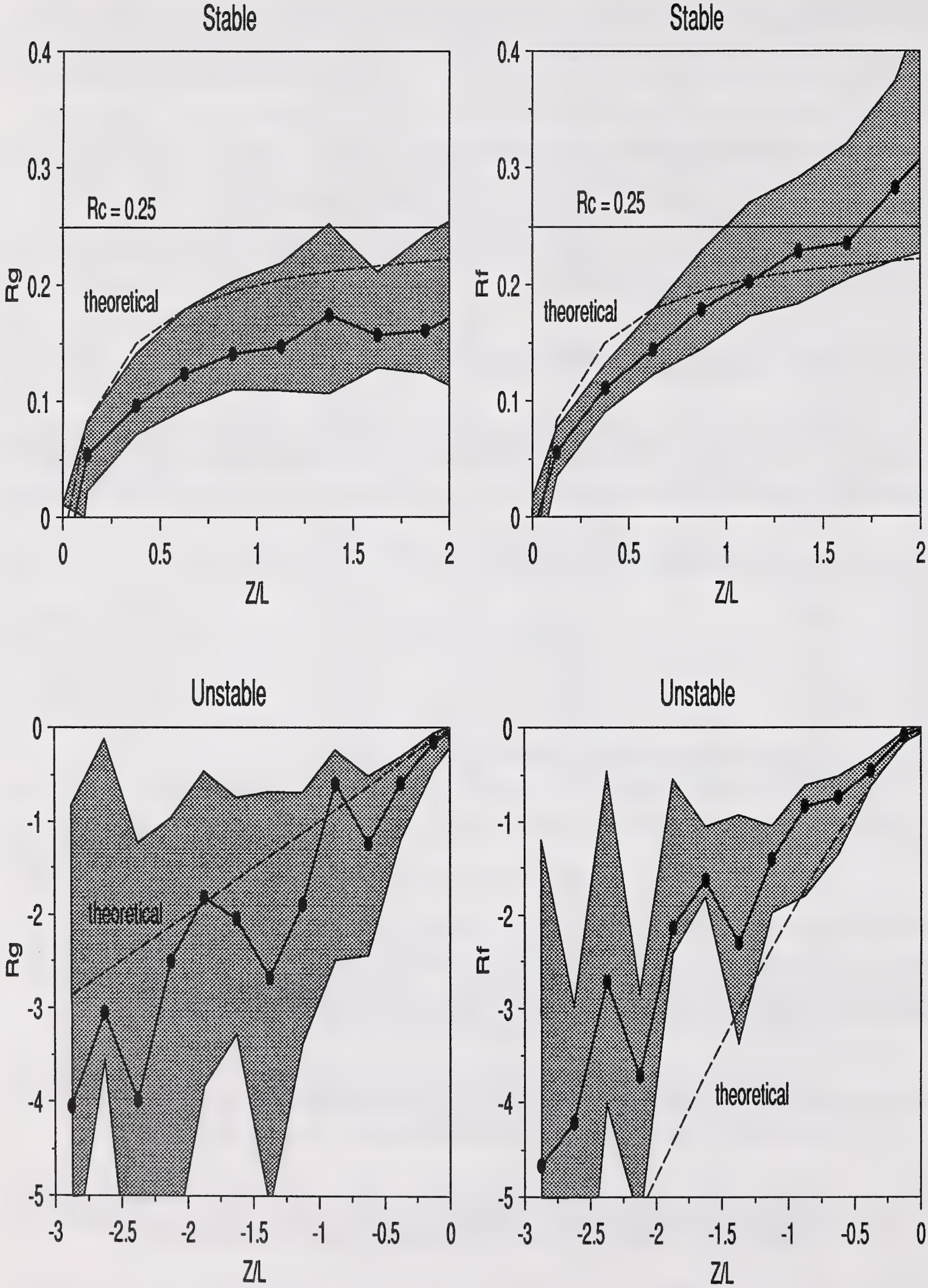

Figure 8.18 Winter

Comparison of Predicted and Observed Interrelationships among R_g, R_f and Z/L. The Shaded Envelope Indicates the 25 and 75 Percentile Limits. Theoretical Relationships are Shown as a Dashed Line.

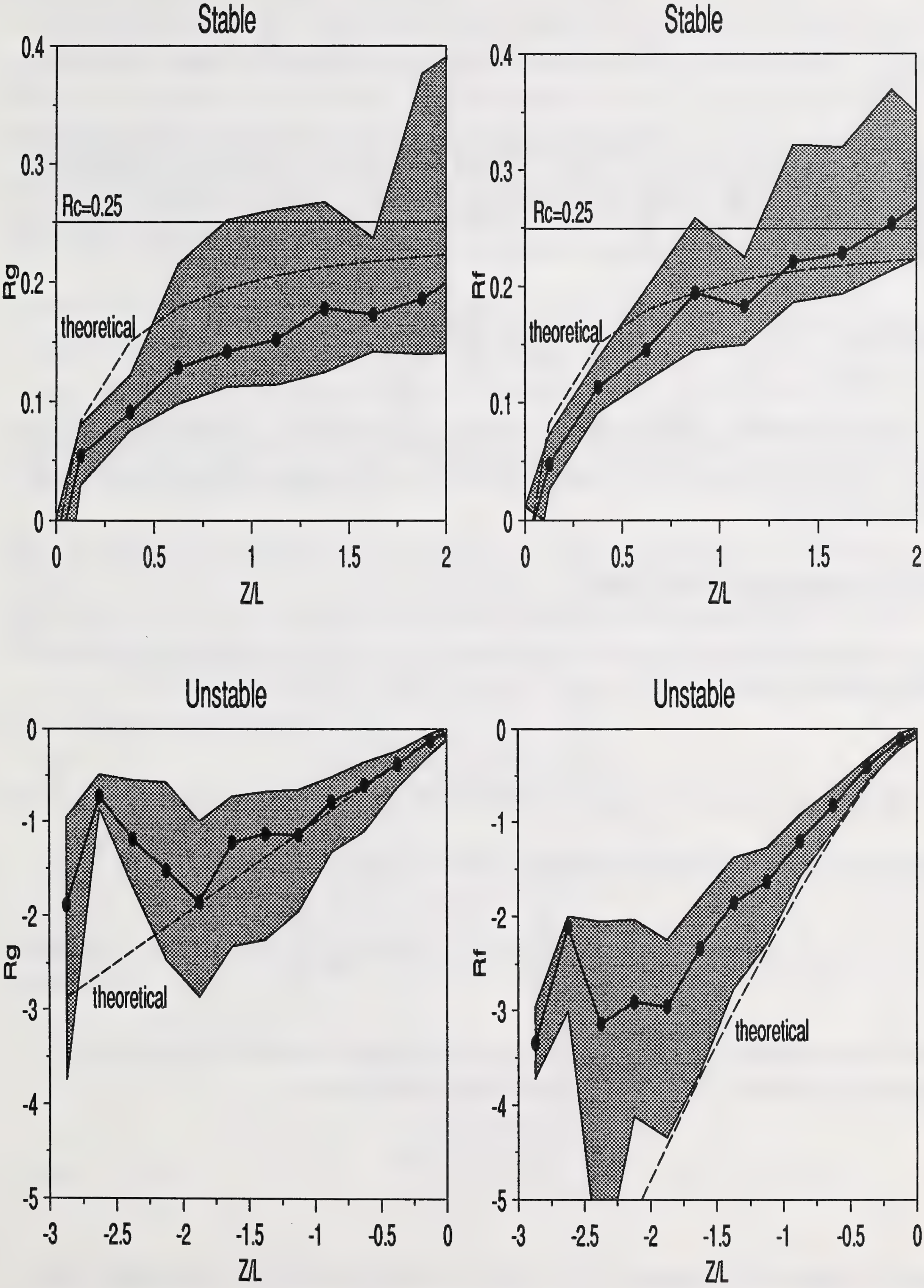

Figure 8.18 Summer

Comparison of Predicted and Observed Interrelationships among R_g, R_f and Z/L. The Shaded Envelope Indicates the 25 and 75 Percentile Limits. Theoretical Relationships are Shown as a Dashed Line.

Both R_g and R_f depend on the wind shear gradient $\partial U/\partial Z$. This gradient is small for unstable conditions and any small absolute calibration errors will result in large uncertainties in both R_g and R_f. The uncertainty will be compounded for R_g since the wind shear gradient term is squared.

For stable conditions ($R_f = R_g$), theory and observations indicate the presence of a limiting critical Richardson number R_c of 0.25. When R_g is less than R_c, mechanical turbulence persists but is damped by thermal stratification. When R_g is larger than R_c, turbulence disappears and non-turbulent laminar flow appears (Panofsky and Dutton 1984). The median values shown in Figure 8.18 indicate that both R_g and R_f tend to be less than R_c.

Gradient Richardson numbers significantly larger than R_c were calculated from the Field Measurement Program data. Even though this may be partly due to instrumentation uncertainties, R_g values in excess of R_c have been observed by others (Kondo *et al* 1978, Zamora 1983). For example, when a low level wind speed maximum or minimum occurs, the wind shear gradient ($\partial U/\partial Z$) can become very small resulting in large positive values of R_g (Strimaitis *et al* 1981). This complex behavior of R_g with height is one of the reasons why the Monin-Obukhov stability parameter is often preferred as a stability indicator for the surface layer.

8.3.4 Normalized Wind Shear

Surface similarity theory is based on the hypothesis that the normalized wind shear in the surface layer is a function of Z/L only. The normalized wind shear is defined by:

$$\phi_m = \left(\frac{kZ}{U*}\right)\left(\frac{\partial U}{\partial Z}\right) \qquad (8.7)$$

For the Field Measurement Program data, $\partial U/\partial Z$ at 10 m calculated from:

$$\frac{\partial U}{\partial Z} = \frac{1}{2}\left[\frac{U_{16}-U_{10}}{16-10}+\frac{U_{10}-U_4}{10-4}\right] = \frac{U_{16}-U_4}{16-4} \qquad (8.8)$$

and $U*$ computed from $[\sqrt{-\overline{U'W'}}]_{10m}$ were used to calculate normalized wind shear ϕ_m. For unstable atmospheres, a proposed empirical relationship for ϕ_m is:

$$\phi_m = \left(1+16\left|\frac{Z}{L}\right|\right)^{1/4} \qquad (8.9)$$

which is valid over the range $-2 \le Z/L \le 0$. For stable conditions, the Businger stable relationship:

$$\phi_m = 1 + 5Z/L \qquad (8.10)$$

has been frequently used and is valid over the range $0 \leq Z/L \leq 1$ (Kaimal 1988).

Figure 8.19 compares the predicted normalized wind shear with median values from the field data. The shaded areas show the 25 and 75 percentile limits. The predicted ϕ_m values agree fairly well with the median values observed over the range $-3 \leq Z/L < 1$. For Z/L larger than one, the ϕ_m prediction fails and median values tend to level off to a constant value of 6 in the winter and 8 in the summer. This departure is consistent with what has been reported by others (Hicks 1976, Carson and Richards 1978). Hicks suggested an alternate form for ϕ_m:

$$\phi_m = 8 - \frac{4.25}{Z/L} + \frac{1}{(Z/L)^2} \tag{8.11}$$

for Z/L greater than 0.5. This relationship is shown in Figure 8.19 as a dashed line. The agreement with the median values shown in the figure is much better than the stable Businger relationship for large Z/L values.

Figure 8.19 also shows the normalized wind shear as a function of the Gradient Richardson Number (R_g). For $R_g < 0.25$, the same qualitative behavior is observed as for the Z/L dependence. At $R_g > 0.25$, the non dimensional wind shear behavior changes significantly. This value corresponds to the critical Richardson number and the transition from turbulent to laminar flow.

8.3.5 Wind Speed Ratios

The wind speed increase with increasing height is usually expressed by the log-linear profile:

$$U = \frac{U*}{k}\left[\ln\left(\frac{Z}{Z_o}\right) - \psi\left(\frac{Z}{L}\right)\right] \tag{8.12}$$

where $\psi(Z/L)$ is the stability parameter. The ratio of wind speeds at two heights can therefore be given by:

$$\frac{U_1}{U_2} = \frac{\left[\ln\left(\frac{Z_1}{Z_o}\right) - \psi_1\left(\frac{Z_1}{L}\right)\right]}{\left[\ln\left(\frac{Z_2}{Z_o}\right) - \psi_2\left(\frac{Z_2}{L}\right)\right]} \tag{8.13}$$

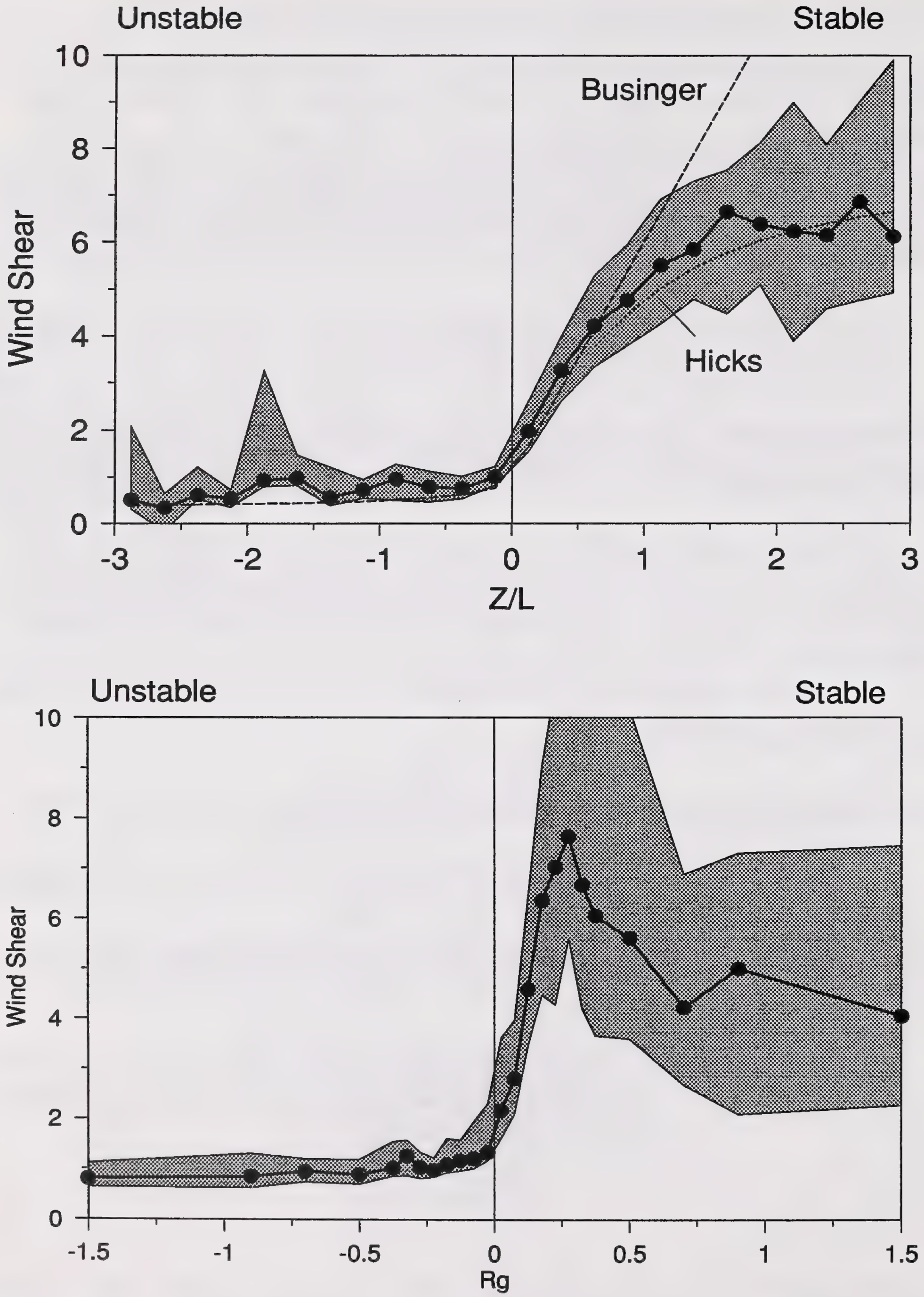

Figure 8.19 Winter

Comparison of Predicted and Observed Normalized Wind Shear ϕ_m as a Function of Z/L and R_g. The Shaded Envelope Indicates the 25 and 75 Percentile Limits.

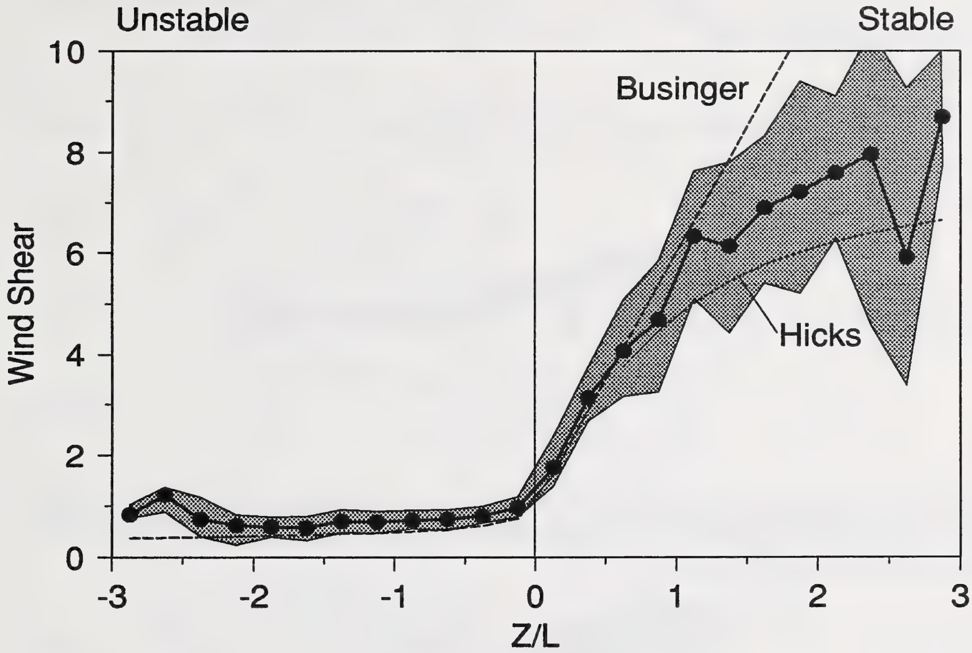

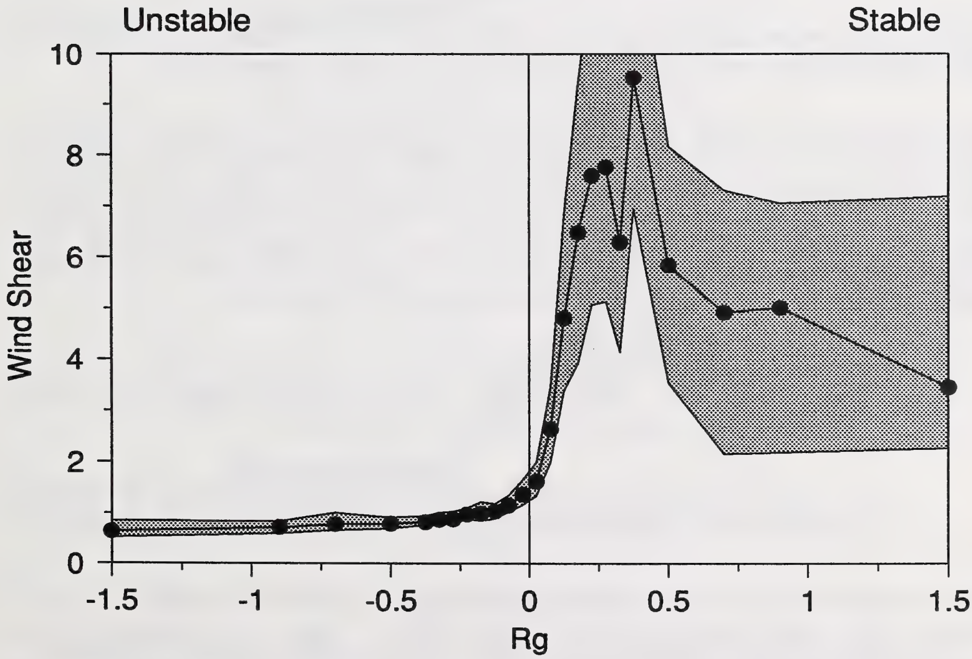

Figure 8.19 Summer

Comparison of Predicted and Observed Normalized Wind Shear ϕ_m as a Function of Z/L and R_g. The Shaded Envelope Indicates the 25 and 75 Percentile Limits.

For unstable conditions, $\psi(Z/L)$ can be estimated from the Businger-Dyer expression (Panofsky and Dutton 1984):

$$\psi(Z/L) = \ln\left[\left(\frac{1+x^2}{2}\right)\left(\frac{1+x}{2}\right)^2\right] - 2\tan^{-1}x + \frac{\pi}{2} \qquad (8.14)$$

where:

$$x = \left(1 - \frac{16Z}{L}\right)^{1/4} \qquad (8.15)$$

For stable conditions, the most commonly used relationship is:

$$\psi(Z/L) = -5\left(\frac{Z}{L}\right) \qquad (8.16)$$

This stable relationship is equivalent to the normalized wind shear given by the Businger stable relationship (Equation 8.10). This stable relationship, however, fails for $Z > L$. Van Ulden and Holtslag (1985) indicate that:

$$\psi(Z/L) = -17\left[1 - \exp\left\{-0.29\left(\frac{Z}{L}\right)\right\}\right] \qquad (8.17)$$

provides better performance over a larger height range. This relationship is arithmetically equivalent to the Hicks relationship for normalized wind shear (Equation 8.11).

The theoretical and observed wind speed ratios U_{10}/U_4, U_{16}/U_4 and U_{25}/U_4 were compared by plotting the ratio as a function of $1/L$ (Figure 8.20). The theoretical relationships are shown for the wind speed ratios using surface roughness values (Z_o) of 0.1 and 1 cm for the winter period. For the summer period, the theoretical wind speed ratios are given using Z_o values of 1 and 10 cm. The observed median values of L are based on 10 m data. The shaded areas represent the 25 and 75 percentile limits. The results given in the figure indicate good agreement between predicted and observed results. In particular:

- Surface roughness values in the vicinity of the tower appear to be in the 0.1 to 1 cm range for the winter months. For the summer months, the surface roughness values appear to be in the 1 to 10 cm range.

- For stable conditions, the van Ulden and Holtslag relationship for $\psi(Z/L)$ provides better agreement than the normally used value given in Equation 8.16.

The Field Measurement Program data supports the use of the Hicks relationship for ϕ_m and the van Ulden and Holtslag relationship for $\psi(Z/L)$. These two relationships are arithmetically consistent and equivalent.

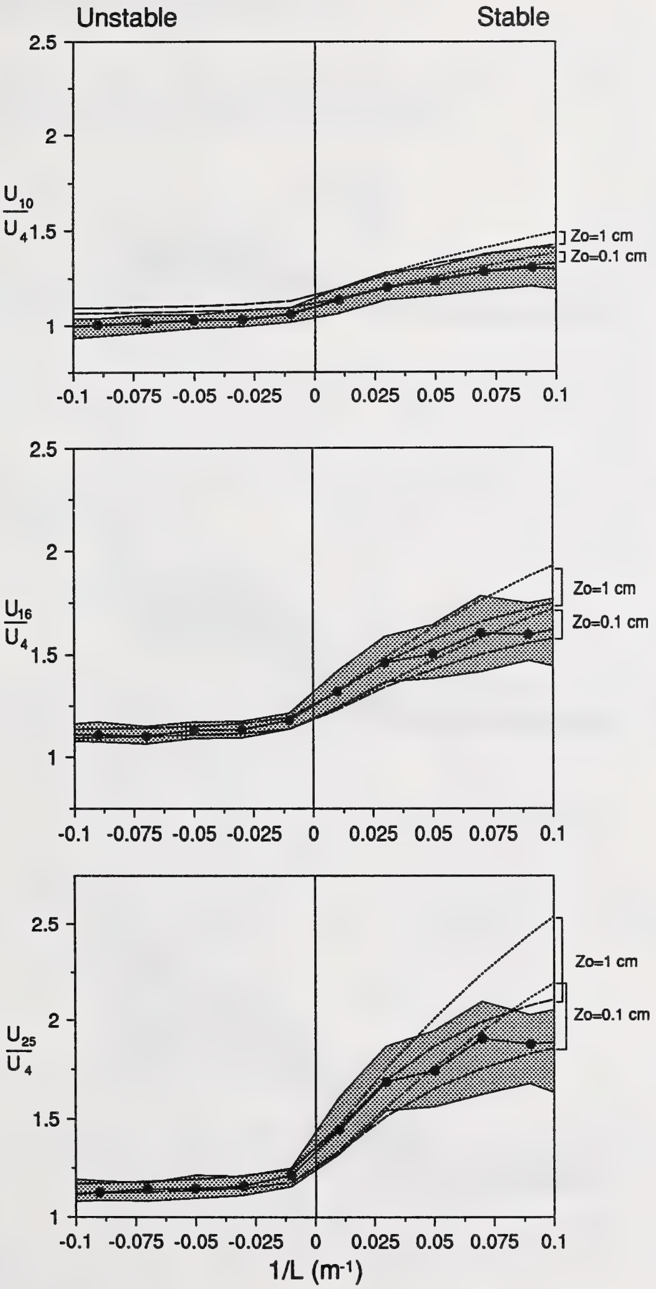

Figure 8.20 Winter

Predicted and Observed Wind Speed Ratios as a Function of *1/L*. The Shaded Envelope Indicates the 25 and 75 Percentile Limits. The Dotted Lines Represent the Predicted Relationships Using the Normal $\psi(Z/L)$ Expression While the Dashed Line Represents the van Ulden and Holtslag $\psi(Z/L)$ for Stable Conditions.

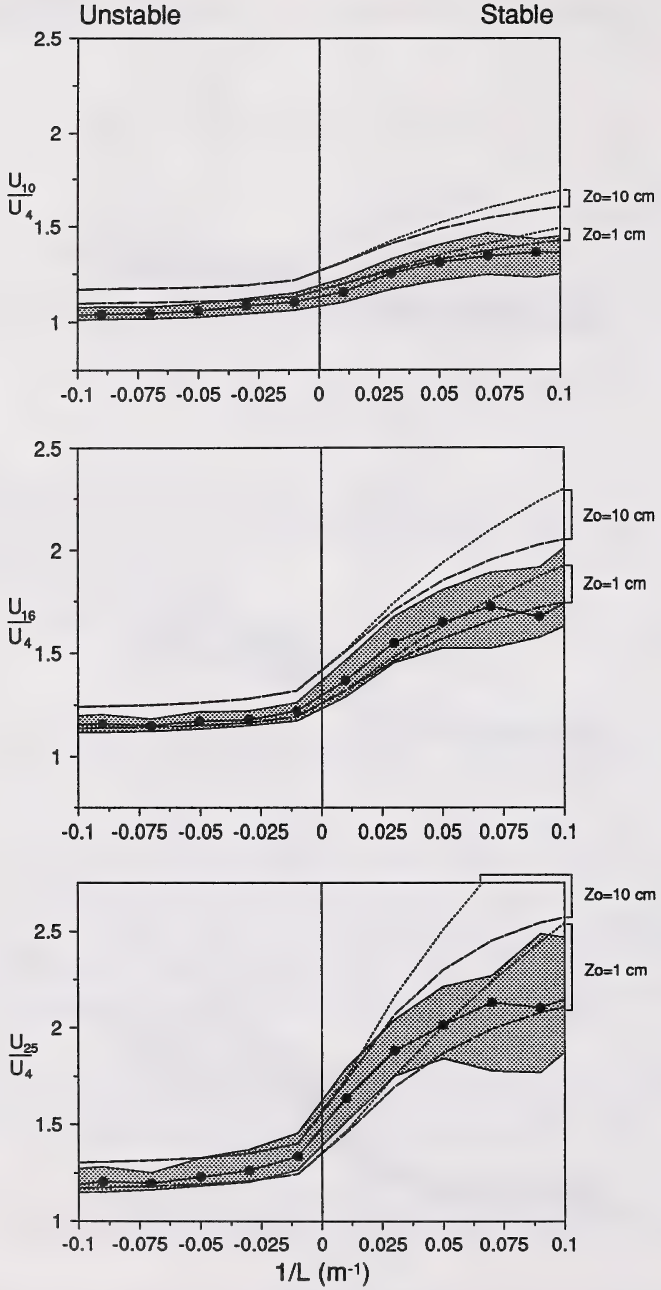

Figure 8.20 Summer

Predicted and Observed Wind Speed Ratios as a Function of *1/L*. The Shaded Envelope Indicates the 25 and 75 Percentile Limits. The Dotted Lines Represent the Predicted Relationships Using the Normal $\psi(Z/L)$ Expression While the Dashed Line Represents the van Ulden and Holtslag $\psi(Z/L)$ for Stable Conditions.

8.3.6 Normalized Thermal Stratification

Surface similarity theory also requires that the normalized thermal stratification is a function of Z/L. The normalized thermal stratification is defined by:

$$\phi_H = \left(\frac{kZ}{T^*}\right)\frac{\partial\theta}{\partial Z} \tag{8.18}$$

where the scaling temperature T^* is given by:

$$T^* = \frac{-\overline{W'T'}}{U^*} \tag{8.19}$$

For the Field Measurement Program, ϕ_H was calculated using the following expression for the potential temperature gradient:

$$\frac{\partial\theta}{\partial Z} = \frac{1}{2}\left[\frac{T_{16}-T_{10}}{16-10} + \frac{T_{10}-T_2}{10-2}\right] + \Gamma \tag{8.20}$$

and using $\overline{W'T'}$ and U^* from the 10 m sonic anemometer observations. Γ is the adiabatic lapse rate (0.0098 K/m). For unstable atmospheres, a proposed empirical relationship for ϕ_H is:

$$\phi_h = (1 + 16|Z/L|)^{-1/2} \tag{8.21}$$

which is valid over the range $-2 \leq Z/L \leq 0$. For stable atmospheres, the relationship:

$$\phi_h = 1 + 5Z/L \tag{8.22}$$

for the range $0 \leq Z/L \leq 1$ has been used (Webb 1970).

Figure 8.21 compares the predicted normalized thermal stratification with median values from the field data. The shaded areas represent the 25 and 75 percentile limits. The predicted ϕ_H values agree fairly well with the median values over the range $-3 \leq Z/L \leq 0.5$. For Z/L larger than 0.5, the ϕ_H predictions fail and median values tend to level off to a constant value of four. An extension of Hicks form for ϕ_M to ϕ_H suggests that the normalized thermal stratification is better given by:

$$\phi_H = 5.1 - \frac{1.3}{Z/L} + \frac{0.11}{(Z/L)^2} \tag{8.23}$$

for $Z/L > 0.5$. This relationship is shown in the Figure as a dashed line. The agreement with the median values is much better than that for the Webb relationship (Equation 8.22).

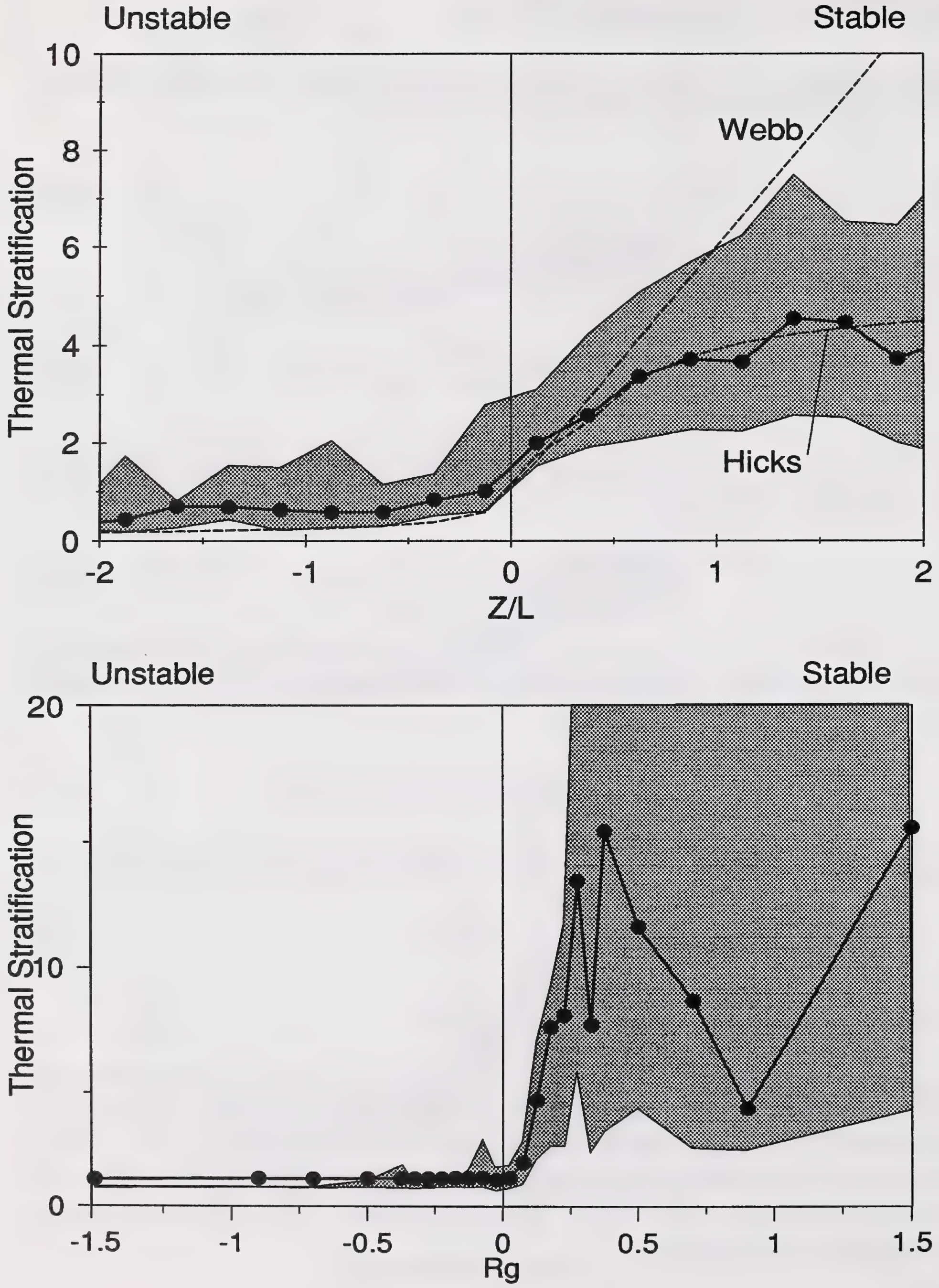

Figure 8.21 Winter

Comparison of Predicted and Observed Normalized Thermal Stratification ϕ_h as a Function of Z/L and R_g. The Shaded Envelope Indicates the 25 and 75 Percentile Limits.

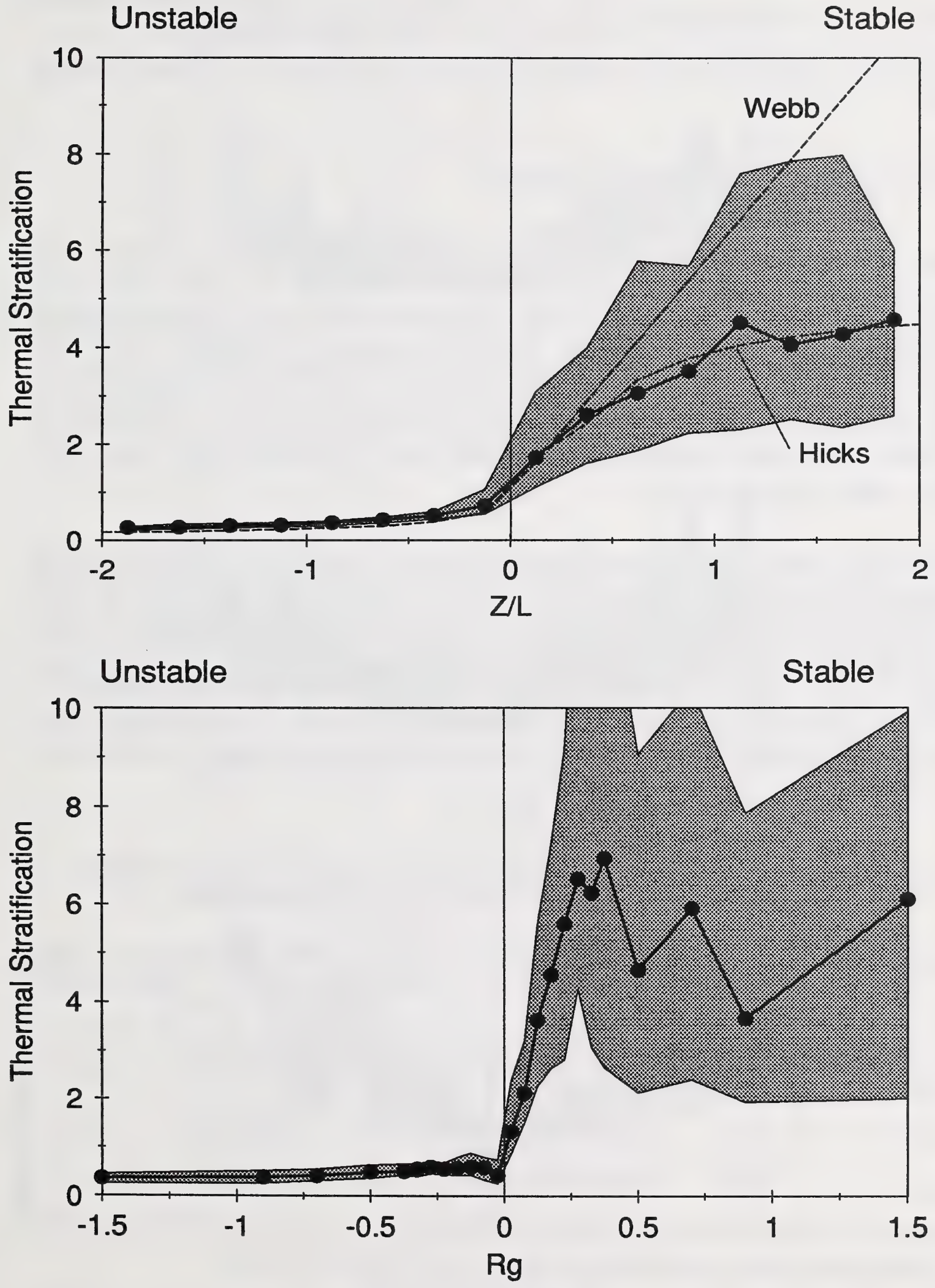

Figure 8.21 Summer

Comparison of Predicted and Observed Normalized Thermal Stratification ϕ_h as a Function of *Z/L* and R_g. The Shaded Envelope Indicates the 25 and 75 Percentile Limits.

Figure 8.21 also shows the normalized thermal stratification (ϕ_H) as a function of the Gradient Richardson Number (R_g). For $R_g > 0.25$, there is no clear relationship between ϕ_H and R_g. This value corresponds to the critical Richardson number transition from turbulent to laminar flow.

8.3.7 Variance of Wind Components

Monin-Obukhov similarity requires that the standard deviations of the wind components (σ_U, σ_V, and σ_W) normalized by the friction (U^*) are functions of Z/L in the surface layer. For purely mechanical conditions when $Z/L = 0$, the normalized standard deviations should be constant and independent of height. For these mechanically turbulent situations, the ratios of the standard deviation to the friction velocity for flat terrain are given in Table 8.1. These values are given by Panofsky and Dutton (1984) and represent an average from nine sites. The bracketed values indicate the range observed at the nine sites. The normalized σ_W values were found to be independent of terrain type. For rolling terrain, larger values for σ_U and σ_V can be expected.

Figure 8.22 shows the normalized standard deviations as a function of Z/L for unstable (negative Z/L) and stable (positive Z/L) conditions. The observations shown in the figure are based on one-half hourly average values when the 10 m level wind direction was within the Kaijo-Denki angle of acceptance. The normalized standard deviations tend to show minimum values for purely mechanically turbulent situations (Z/L=0). These minimum values are also given in Table 8.1. The minimum normalized standard deviations for σ_V and σ_W fall within the ranges reported by Panofsky and Dutton. The σ_U minimum value is larger than expected for flat terrain and falls within the expected range for rolling terrain.

Table 8.1

Comparison of Normalized Variance From the Field Measurement Program With Those Reported by Others for Neutral Conditions.

	Panofsky and Dutton (1984)		Field Measurement Program(a)		Hicks (1978)
	Mean	Range	$Z/L = 0$	$R_g = 0$	$R_g = 0$
σ_u/U^*	2.39	(2.30 to 2.45)	2.72, 2.66	2.85, 2.75	2.6
σ_v/U^*	1.92	(1.73 to 2.20)	2.05, 2.13	2.03, 2.02	2.0
σ_W/U^*	1.25	(1.10 to 1.40)	1.3, 1.35	1.39, 1.36	1.4

(a) - The first value is for the winter period, the second value is for the summer period.

The normalized standard deviations can also be plotted as a function of the Gradient Richardson Number (Figure 8.23). The normalized standard deviations corresponding to neutral conditions (R_g=0) are also given in Table 8.1. Hicks (1978) replotted the Kansas experiment data as a function of Gradient Richardson Number and his results for neutral conditions (R_g=0) are also found in Table 8.1. These values are consistent with those obtained from the Field Measurement Program.

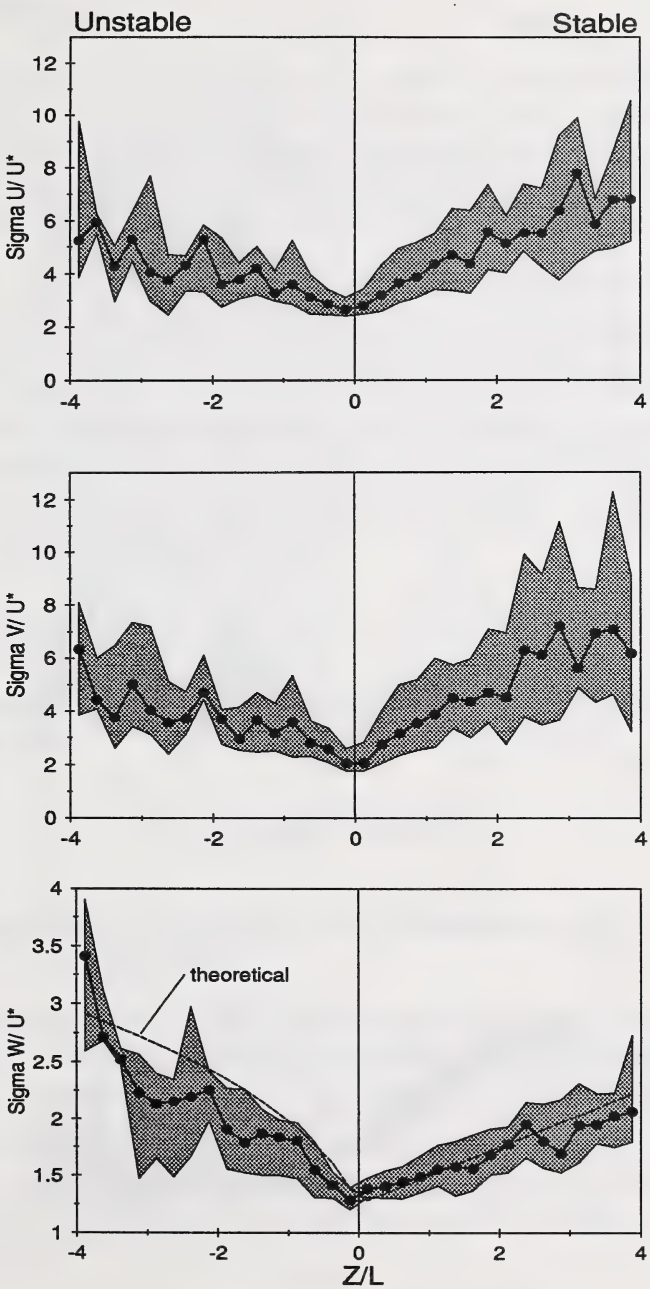

Figure 8.22 Winter

Normalized Standard Deviations (σ_U/U^*, σ_V/U^*, σ_W/U^*) as a Function of Z/L. The Shaded Envelope Indicates the 25 and 75 Percentile Limits.

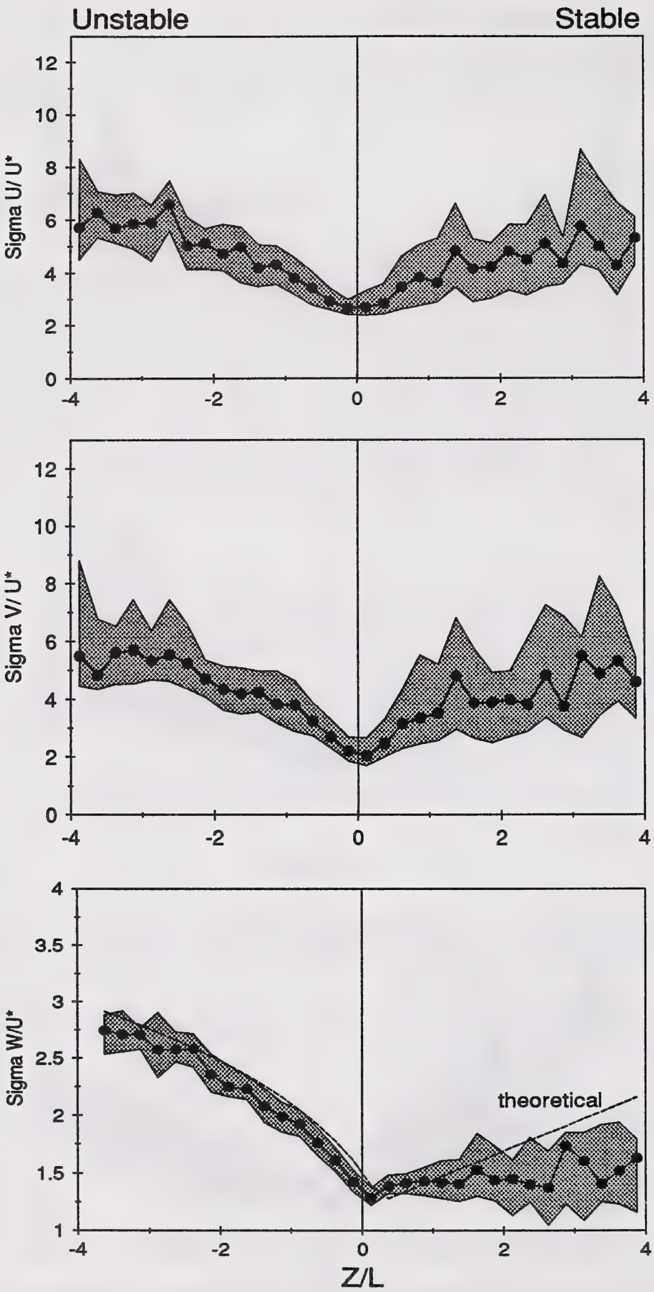

Figure 8.22 Summer

Normalized Standard Deviations (σ_U/U^*, σ_V/U^*, σ_W/U^*) as a Function of *Z/L*. The Shaded Envelope Indicates the 25 and 75 Percentile Limits.

Horizontal Velocity

For stable conditions, the normalized σ_U and σ_W values are expected to be constant as long as Z/L is not large. As Z/L becomes large, the normalized σ_U and σ_W can also become large and unpredictable. This is due to low frequency fluctuations not associated with turbulence (Panofsky and Dutton 1984). The results from the Field Measurement Program indicate that both the normalized σ_U and σ_W values tend to increase with increasing $|Z/L|$ values.

Hicks (1981), however, indicates some of the observed increases may be due to nondimensional inter-relationships between variables. To overcome this problem, Hicks recommends plotting the normalized values as a function of the Gradient Richardson Number (R_g) instead of Z/L. Figure 8.23 shows the median normalized standard deviations as a function of the Gradient Richardson Number. The results plotted as a function of R_g differ from those plotted as a function of Z/L (Figure 8.22). In particular, the normalized σ_U and σ_V values tend to be relatively constant for unstable conditions when plotted as a function of R_g. In contrast, the normalized σ_U and σ_V values tend to increase with increasing instability when plotted as a function of Z/L. Both the R_g and Z/L plots indicate that σ_U and σ_V increase with increasing stability for stable conditions.

Vertical Velocity

For unstable conditions (Z/L negative) the normalized σ_W is given by (Panofsky and Dutton 1984, Kaimal 1988):

$$\frac{\sigma_W}{U*} = 1.25[1-3(Z/L)]^{1/3} \tag{8.28}$$

This relationship is shown in Figure 8.22. The Field Measurement Program results tend to support the use of this relationship.

For stable conditions, there is little agreement between the expected relationship for the behavior of $\sigma_W/U*$. Merry and Panofsky (1976) and Mortensen *et al* (1987) show an increase of the ratio with increasing Z/L. Hicks (1981) states that this apparent increase may not be real and may be due to nondimensional inter-relationships between variables. For this reason, Panofsky and Dutton (1984) recommend that the normalized σ_W for stable conditions be set equal to its neutral value (1.32). The winter data from the Field Measurement Program, however, support the increase of the normalized σ_W with increasing Z/L. For stable conditions, Kaimal (1988) indicates that:

$$\frac{\sigma_W}{U*} = 1.25[1+0.2(Z/L)] \tag{8.29}$$

is valid for Z/L less than 1. The above relationship supports the increase with increasing Z/L and is shown in Figure 8.22. The winter data from the Field Measurement Program

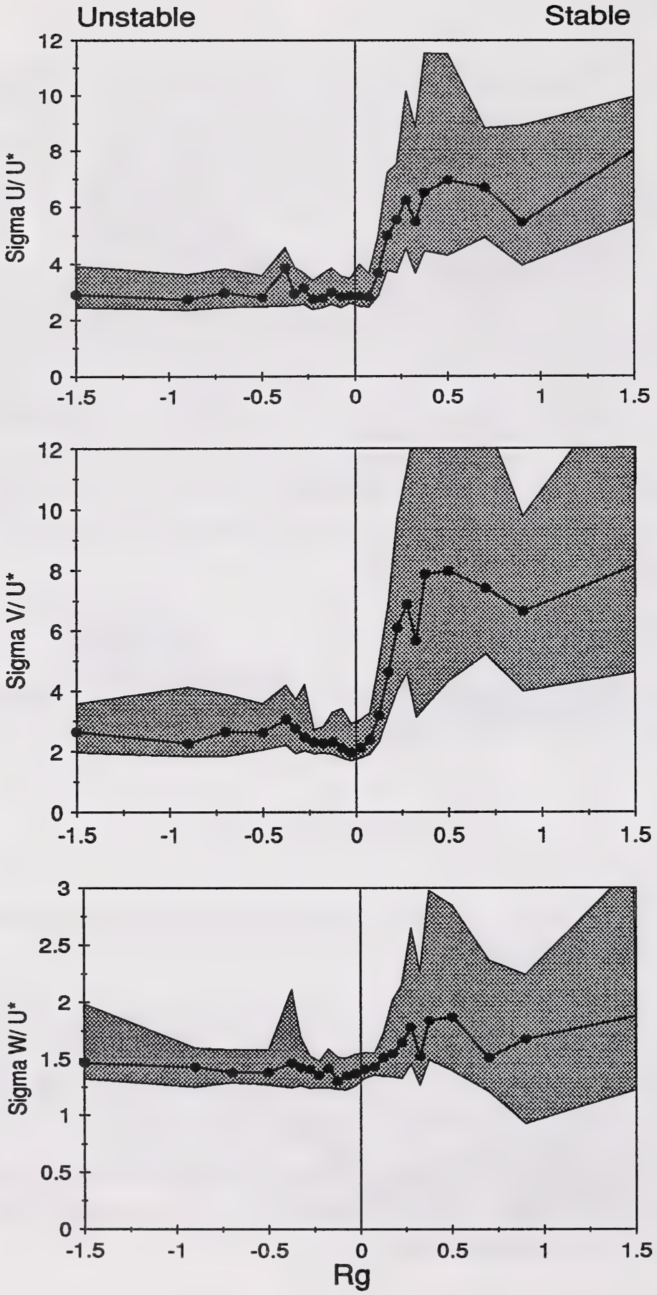

Figure 8.23 Winter

Normalized Standard Deviations (σ_U/U^*, σ_V/U^*, σ_W/U^*) as a Function of R_g. The Shaded Envelope Indicates the 25 and 75 Percentile Limits.

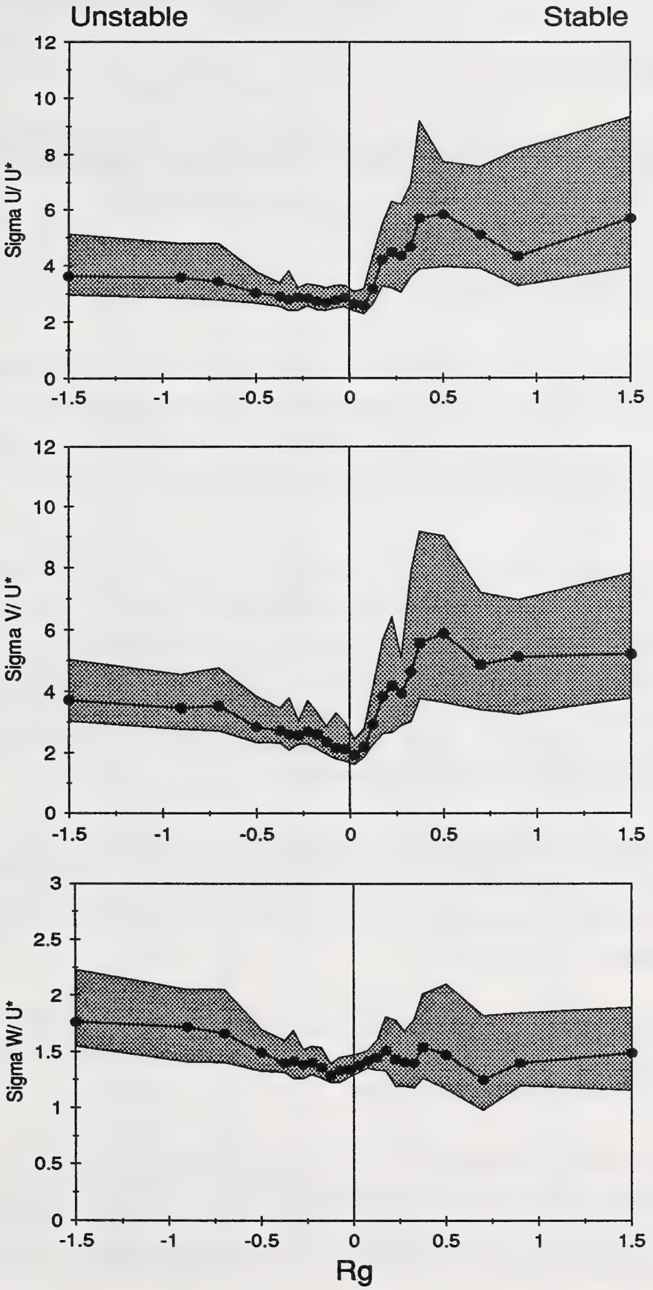

Figure 8.23 Summer

Normalized Standard Deviations (σ_U/U^*, σ_V/U^*, σ_W/U^*) as a Function of R_g. The Shaded Envelope Indicates the 25 and 75 Percentile Limits.

tend to support this relationship over a much wider Z/L range. The summer data, however show that σ_W/U^* tends to remain constant with increasing stability which tends to support Panofsky and Dutton (1984).

The normalized vertical standard deviation as a function of the Gradient Richardson Number (R_g) is shown in Figure 8.23. The normalized σ_W values tend to be relatively constant for both unstable and stable conditions when plotted as a function of R_g.

8.3.8 Vertical Profiles of Variance

The turbulence intensities σ_θ and σ_ϕ were shown to decrease with increasing height (Sections 8.2.3 and 8.2.4 respectively). The vertical variations of the wind standard deviations (σ_U, σ_V, σ_W, σ_θ and σ_ϕ) as a function of atmospheric stability were evaluated. The 10 m level Z/L value was used as the stability indicator. The results are presented in Table 8.2 and may be summarized as:

- For unstable and near neutral conditions ($-3 < Z/L < 1$), the median values of σ_U and σ_V results are relatively constant with height. For extremely stable conditions ($Z/L > 2$), there is an indication for the median σ_U values to increase with increasing height. This increase, however, is relatively small and is within the scatter of the data. The largest σ_U and σ_V values are associated with near neutral conditions ($-1 < Z/L < 1$) during the winter and unstable and neutral conditions ($Z/L < 1$) during the summer.

- For unstable conditions ($Z/L < -1$), there is a tendency for σ_W to increase with height. For near neutral and stable conditions ($Z/L > -1$), σ_W is relatively constant with height. The largest 10 m σ_W values are associated with near neutral conditions ($-1 < Z/L < 1$).

- For all stability classes, median values of σ_θ decrease with increasing height. The relative decrease with height is the largest for stable conditions and the smallest for unstable conditions.

- For unstable conditions ($-3 < Z/L < -1$), the median values of σ_ϕ increase with increasing height. For near neutral conditions ($-1 < Z/L < 0$), the median values of σ_ϕ tend to remain constant with height while for stable conditions ($Z/L > 0$), the median values of σ_ϕ decrease with increasing height.

The above observations have certain practical considerations in as much as observations of σ_θ and σ_ϕ are frequently used in air quality impact assessments to characterize plume dispersion. It is clear that the vertical variation of these parameters has to be taken into account.

Table 8.2 Winter

Median Wind Standard Deviations σ_U, σ_V and σ_W (m/s) and σ_θ and σ_ϕ (degrees) as a Function of Height and Stability.

Wind Component	Z/L_{10} Class	Height (m)			
		4	10	16	25
σ_U	-3 to -2	0.49	0.47	0.53	0.51
	-2 to -1	0.46	0.43	0.41	0.41
	-1 to 0	0.70	0.64	0.66	0.67
	0 to 1	0.70	0.68	0.77	0.77
	1 to 2	0.50	0.50	0.54	0.54
	2 to 3	0.47	0.48	0.56	0.58
σ_V	-3 to -2	0.48	0.49	0.49	0.48
	-2 to -1	0.42	0.41	0.40	0.42
	-1 to 0	0.59	0.54	0.59	0.56
	0 to 1	0.56	0.55	0.61	0.59
	1 to 2	0.45	0.47	0.52	0.56
	2 to 3	0.46	0.49	0.53	0.52
σ_W	-3 to -2	0.18	0.25	0.27	0.32
	-2 to -1	0.17	0.22	0.22	0.23
	-1 to 0	0.27	0.31	0.32	0.33
	0 to 1	0.27	0.29	0.27	0.26
	1 to 2	0.18	0.18	0.16	0.14
	2 to 3	0.16	0.16	0.14	0.14
σ_θ	-3 to -2	14.0	13.2	13.2	13.0
	-2 to -1	10.1	9.3	8.3	8.0
	-1 to 0	8.0	7.0	6.7	6.3
	0 to 1	7.3	6.2	5.6	4.9
	1 to 2	8.3	6.7	6.0	5.3
	2 to 3	9.3	7.7	7.1	5.8
σ_ϕ	-3 to -2	5.1	6.2	5.9	6.4
	-2 to -1	3.6	4.5	3.4	4.5
	-1 to 0	4.0	4.1	3.8	3.9
	0 to 1	4.0	3.6	2.8	2.3
	1 to 2	3.4	2.5	1.7	1.4
	2 to 3	3.2	2.5	1.9	1.7

Table 8.2 Summer

Median Wind Standard Deviations σ_U, σ_V and σ_W (m/s) and σ_θ and σ_ϕ (degrees) as a Function of Height and Stability.

Wind Component	Z/L_{10} Class	Height (m)			
		4	10	16	25
σ_U	-3 to -2	0.87	0.94	0.97	0.98
	-2 to -1	0.94	0.95	0.98	0.99
	-1 to 0	1.04	0.99	1.02	1.12
	0 to 1	0.69	0.67	0.71	0.75
	1 to 2	0.39	0.40	0.46	0.44
	2 to 3	0.34	0.39	0.44	0.52
σ_V	-3 to -2	0.93	0.88	0.95	1.02
	-2 to -1	0.93	0.89	0.94	0.95
	-1 to 0	0.93	0.86	0.98	0.93
	0 to 1	0.55	0.55	0.62	0.58
	1 to 2	0.37	0.39	0.43	0.43
	2 to 3	0.33	0.33	0.38	0.39
σ_W	-3 to -2	0.29	0.42	0.46	0.54
	-2 to -1	0.31	0.44	0.46	0.54
	-1 to 0	0.39	0.47	0.48	0.53
	0 to 1	0.30	0.32	0.29	0.28
	1 to 2	0.16	0.16	0.13	0.12
	2 to 3	0.13	0.13	0.11	0.13
σ_θ	-3 to -2	21.6	19.5	18.9	17.7
	-2 to -1	17.6	16.1	15.6	14.6
	-1 to 0	11.7	9.9	10.1	9.2
	0 to 1	9.0	7.3	7.1	5.7
	1 to 2	9.4	7.2	6.6	4.9
	2 to 3	9.5	7.2	5.9	5.6
σ_ϕ	-3 to -2	7.7	9.2	9.0	8.9
	-2 to -1	6.0	7.7	7.3	7.8
	-1 to 0	5.0	5.3	4.8	5.0
	0 to 1	4.7	4.2	3.3	2.8
	1 to 2	3.7	2.6	1.6	1.5
	2 to 3	3.5	2.3	1.5	1.8

8.3.9 Vertical Profiles of Fluxes

The lowest portion of the boundary layer, called the surface layer, is qualitatively defined as that part of the boundary layer immediately above the surface. The height of the surface layer is usually defined as 10% of the mixing height. Heat and momentum fluxes are usually treated as constants in the surface layer even though they normally decrease slowly with height. For practical purposes, the fluxes are defined as constant if they vary by 10% or less. The treatment of the surface layer often assumes that the heat flux (H_o) friction velocity (U^*) and Monin-Obukhov length (L) do not change with height (Panofsky and Dutton 1984).

The heat flux and friction velocity were shown to be relatively invariant with height (Sections 8.2.5 and 8.2.6, respectively). The vertical variations of H_o, U^*, and L as a function of atmospheric stability were evaluated and are shown in Table 8.3. The 10 m level Z/L value was used as the stability indicator. The results are presented in Table 8.3 and may be summarized as:

- As was seen in Section 8.2.5, there is a trend for median heat flux values to decrease with increasing height. The trend, however, is not clearly delineated for all stability categories. As was seen in the frequency distributions given in Section 8.2.5, the variation among the four levels is smaller than that suggested from the median values.

- As was seen in Section 8.2.6, there is a tendency for U^* to remain constant with height. The larger U^* values are observed during near neutral conditions.

- The vertical variation of L values does not indicate a clear trend for decreasing or increasing with increasing height. Values of L may therefore be fairly uniform with height.

The median values of H_o, U^* and L indicate that these parameters are fairly uniform over the height range 4 to 25 m.

8.3.10 Comments

In summary, the results of the Boundary Layer Parameterization evaluation indicated the following:

- Non-drainage flow conditions occurred 93 and 98 % of the time in the winter and summer, respectively. Low level wind speed maximums were not always associated with drainage flow conditions.

- The primary indicators of stable versus unstable conditions are $\overline{W'T'}$ and $\partial\theta/\partial Z$. These indicators were in agreement 76 and 81 % of the time in the winter and summer, respectively.

- The interrelationships between R_g, R_f and Z/L stability indicators were compared to the findings of others. The Field Measurement Program results showed some qualitative agreement with the findings of others.

Table 8.3

Median H_O, U^* and L as a Function of Height and Atmospheric Stability.

Parameter	Z/L_{10} Class	Height (m)			
		4	10	16	25
		Winter			
H_O	-3 to -2	19	29	15	22
	-2 to -1	11	17	11	7
	-1 to 0	13	16	12	13
	0 to 1	-20	-19	-20	-14
	1 to 2	-17	-15	-12	-7
	2 to 3	-13	-14	-8	-7
U^*	-3 to -2	0.12	0.11	0.12	0.12
	-2 to -1	0.13	0.11	0.12	0.12
	-1 to 0	0.23	0.23	0.24	0.23
	0 to 1	0.22	0.20	0.24	0.21
	1 to 2	0.14	0.11	0.14	0.11
	2 to 3	0.12	0.09	0.12	0.11
L	-3 to -2	-5	-4	-7	-6
	-2 to -1	-11	-8	-11	-6
	-1 to 0	-63	-65	-47	-43
	0 to 1	32	36	44	33
	1 to 2	12	7	14	9
	2 to 3	6	4	13	8
		Summer			
H_O	-3 to -2	88	100	95	95
	-2 to -1	99	114	109	108
	-1 to 0	66	68	68	73
	0 to 1	-18	-18	-17	-13
	1 to 2	-11	-15	-8	0
	2 to 3	-10	-14	-5	2
U^*	-3 to -2	0.19	0.17	0.21	0.23
	-2 to -1	0.23	0.21	0.23	0.24
	-1 to 0	0.35	0.33	0.36	0.38
	0 to 1	0.25	0.22	0.22	0.23
	1 to 2	0.12	0.11	0.11	0.09
	2 to 3	0.10	0.09	0.10	0.11
L	-3 to -2	-6	-4	-7	-11
	-2 to -1	-11	-7	-11	-11
	-1 to 0	-45	-37	-45	-58
	0 to 1	48	50	37	34
	1 to 2	11	7	7	0
	2 to 3	7	4	5	3

- For stable conditions, the median values of R_g support the presence of a critical Richardson Number at 0.25.

- The dependence of normalized wind shear (ϕ_M) on Z/L is in agreement with the findings of others over the range $-3 < Z/L < 1$. For stable conditions ($Z/L > 1$), Hick's alternate form for the normalized wind shear gives much better agreement with the observations.

- The field observation data support the use of the log-linear wind speed profile for all stability conditions. The Businger-Dyer expression for $\psi(Z/L)$ under unstable conditions agreed with the observations. For stable conditions, the van Ulden and Holtslag relationship for $\psi(Z/L)$ gave much better agreement for $Z > L$ than the normally used $\psi(Z/L) = -5(Z/L)$.

- The normalized thermal stratification (ϕ_H) dependence on Z/L is in agreement with others for the range $-3 < Z/L < 0.5$. An alternate form for ϕ_H is proposed for $Z/L > 0.5$ which is an extension of the Hick's form for ϕ_M.

- The normalized wind standard deviation values (σ_U/U^*, σ_V/U^* and σ_W/U^*) under mechanically dominated turbulence conditions are consistent with the findings of others. The normalized σ_U and σ_V and values increase with increasing stability for stable conditions.

- The normalized σ_W values for stable conditions increase with increasing stability when plotted as a function of Z/L and remain relatively constant with increasing stability when plotted as a function of R_g. This contradiction is perhaps a result of non-dimensional interrelationships between variables.

- The following height dependence for the wind standard deviations were found:
  - Median σ_U and σ_V values are relatively constant with height for neutral and unstable conditions. For stabile conditions, there is a tendency for median values to increase with increasing height.
  - Median σ_W values tend to increase with increasing height for unstable conditions. For neutral and stable conditions, the median σ_W values are relatively constant with height.
  - Median σ_θ values decrease with increasing height for all stability conditions.
  - Median σ_ϕ values increase with height for unstable conditions.
  - Median σ_ϕ values decrease with increasing height for stable conditions.

- Over the first 25 m, median values of H_o, U^* and L appear to be relatively constant with height.

The analysis of meteorology data collected from the Field Measurement Program tends to be in agreement with the findings of others and as such supports the matematical relationships used for the behavior of the surface layer.

8.4 Low Wind, Low Turbulence Statistics

The largest predicted hazard zones associated with a low-level release of toxic gases have been associated with low wind speed, stable atmospheric conditions (Alp *et al* 1987). The persistence of these winds can assist in the determination of the duration and downwind extent of hazard zones. Wind data from the Field Measurement Program site, the Acid Deposition Research Program Crossfield West site and Calgary International airport were reviewed to determine the frequency of low wind speed occurrences.

Similarly, largest hazard zones are associated with low turbulence levels. The Field Measurement Program turbulence data were reviewed to determine whether minimum turbulence levels in the atmosphere could be defined.

8.4.1 Low Wind Speed Analysis

Wind speed persistance is intuitively defined as the length of time that a given wind speed will last before shifting to a new value. In practice, wind speed persistance is difficult to define since the wind speed constantly varies with time and is dependent on the averaging period adopted. For the purposes of this assessment, persistance was defined by the following terms:

- **Frequency**: The frequencies of low wind speeds conditions were determined for selected averaging periods ranging from 1/2 to 8 h. The averaging was based on fixed non-moving time blocks.

- **Duration**: The duration that a wind speed persisted within a given wind speed range was determined in multiples of the one-half hour blocks. The wind speed classes were 1 m/s in width. The sequential wind speed time series were scanned to determine the duration that a given wind speed class persisted. When the wind speed shifted to another class, then a new persistance class was determined.

In some cases, the above definitions relating to persistance were applied to all the data, in other cases only stable conditions were considered.

Frequency Analysis (FMP)

The 10 m level sonic anemometer based wind speeds collected during the Field Measurement Program (FMP) were analysed to determine the frequency wind speeds less than 3 m/s occurred. The Field Measurement Program data set represents a nominal 12 month period from October 1988 to October 1989. The effects of averaging the wind over periods ranging from one-half to eight hours were also assessed.

For the study period, 16 189 one-half hourly average 10 m level wind speeds were available, representing an overall data recovery efficiency of 91.3%. The minimum and maximum wind speeds were 0.1 and 21.1 m/s respectively. The overall mean wind speed was 4.1 m/s.

The following table indicates the frequency of occurrence for wind speeds in wind selected wind speed classes:

All Stability (FMP)

Wind Speed Class (m/s)	Percentage Occurrence (%)
0 to 1	4.0
0 to 2	17.5
0 to 3	36.5

Overall, 10 m level wind speeds less than 2 m/s were observed 17.5% of the time.

The frequency of low wind speeds and stable atmospheric conditions was also determined. For the purposes of this assessment, stable conditions were defined by three criteria:

- Negative net radiation ($Q_{net} < 0$)
- Positive potential temperature gradient ($\partial\theta/\partial Z > 0$)
- Negative 10 m level heat flux term ($\overline{W'T'} < 0$).

The following table shows the frequency of occurence for low wind speeds under stable atmosphere conditions:

Stable Conditions Only (FMP)

Wind Speed Class (m/s)	Percentage Occurence (%)		
	$Q_{net} < 0$	$\frac{\partial\theta}{\partial Z} > 0$	$\overline{W'T'} < 0$
0 to 1	2.3	2.7	1.8
0 to 2	9.9	11.0	7.4
0 to 3	21.8	23.6	16.4

The $\overline{W'T'}$ criteria indicate fewer stable cases than the other two. The reason for this was discussed in Section 8.3.2. On the average, wind speeds less than 2 m/s and stable conditions were observed 10.5% of the time.

Longer-term Averages (FMP)

Wind speed frequency distributions for averaging periods ranging from 1/2 to 8 hours were prepared from the 10 m sonic anemometer observations. Average wind speeds for time periods from 1 to 8 hours were observed using fixed non-moving block averages for the winter and summer periods. All atmospheric stability classes were used.

The frequency distributions are summarized in Table 8.4 and Figures 8.24 and 8.25. Figure 8.24 shows the frequency distribution for wind speeds less than 3 m/s whereas Figure 8.25 shows the frequency distributions for wind speeds up to 10 m/s. The shapes of the frequency

Table 8.4

Wind Speed Frequencies for Averaging Times From 1/2 Hour to 8 Hours.

Avg Time	0.5h	1h	2h	3h	4h	5h	6h	7h	8h
Wind Speed (m/s)	Frequency								
Winter									
0.0 to 0.5	43	12	1	2	0	0	0	0	0
0.5 to 1.0	274	119	45	18	8	7	5	3	1
1.0 to 1.5	370	187	90	57	44	29	19	16	16
1.5 to 2.0	488	225	116	69	52	42	36	31	24
2.0 to 2.5	592	320	151	109	73	57	49	34	33
2.5 to 3.0	724	369	187	125	86	76	63	56	39
3.0 to 3.5	707	350	193	127	110	86	65	55	57
3.5 to 4.0	627	322	176	110	88	58	52	49	49
4.0 to 4.5	601	289	133	86	73	60	48	39	33
4.5 to 5.0	514	265	121	103	64	57	44	49	31
5.0 to 5.5	448	230	122	71	52	41	45	31	34
5.5 to 6.0	384	178	83	49	39	34	29	20	12
6.0 to 6.5	280	147	64	46	46	26	22	19	19
6.5 to 7.0	254	129	61	56	28	30	20	19	15
7.0 to 7.5	214	106	59	36	20	17	21	12	13
7.5 to 8.0	157	81	42	20	19	16	14	8	11
8.0 to 8.5	154	61	40	21	25	11	7	10	7
8.5 to 9.0	127	59	26	24	10	12	6	11	6
9.0 to 9.5	85	52	22	11	10	9	3	2	4
9.5 to 10.0	66	39	17	15	6	6	5	2	3
> 10.0	236	106	47	25	21	14	13	9	7
Total	7345	3646	1796	1180	874	688	566	475	414
Summer									
0.0 to 0.5	48	12	2	1	1	0	0	0	0
0.5 to 1.0	277	111	35	14	7	4	1	1	1
1.0 to 1.5	587	293	133	93	63	41	29	21	15
1.5 to 2.0	750	386	202	123	80	78	59	53	43
2.0 to 2.5	840	440	240	166	131	95	94	80	64
2.5 to 3.0	921	485	247	164	139	115	89	64	66
3.0 to 3.5	949	471	235	172	123	101	92	78	73
3.5 to 4.0	799	397	212	151	132	88	75	89	59
4.0 to 4.5	693	338	192	113	75	81	70	45	63
4.5 to 5.0	566	308	151	110	79	63	52	52	46
5.0 to 5.5	512	254	127	92	75	68	52	44	42
5.5 to 6.0	431	223	104	74	59	45	45	38	23
6.0 to 6.5	296	163	92	55	35	19	23	24	23
6.5 to 7.0	288	135	71	40	31	38	28	20	12
7.0 to 7.5	231	117	45	44	35	18	11	13	12
7.5 to 8.0	179	89	46	26	17	19	9	11	10
8.0 to 8.5	127	59	31	17	16	15	10	6	8
8.5 to 9.0	89	49	22	12	16	5	7	5	3
9.0 to 9.5	63	33	18	13	1	4	4	3	3
9.5 to 10.0	53	28	13	6	4	3	4	2	1
> 10.0	145	63	26	18	13	8	5	4	4
Total	8844	4454	2244	1504	1132	908	759	653	571

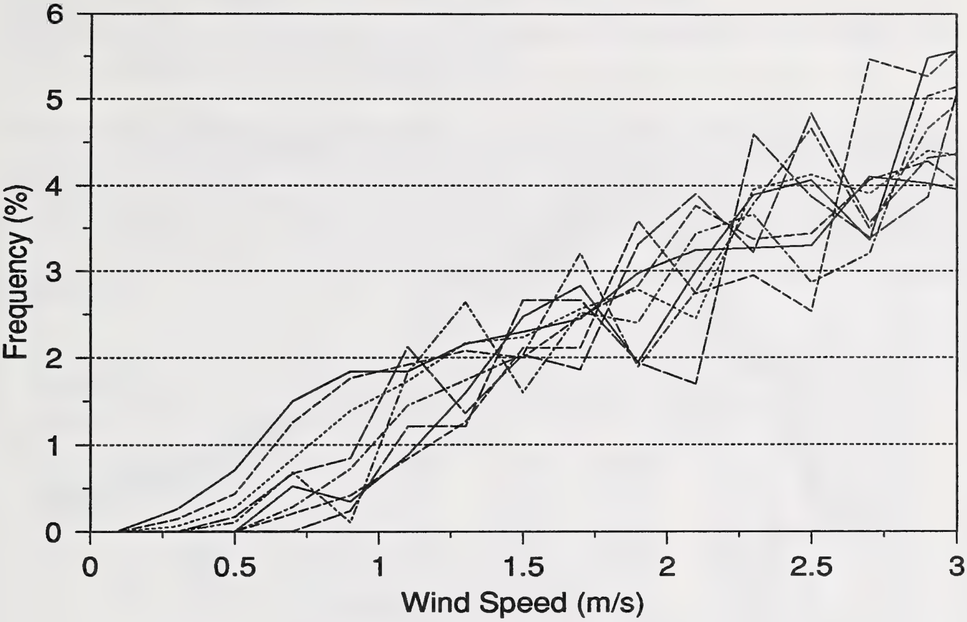

(Winter)

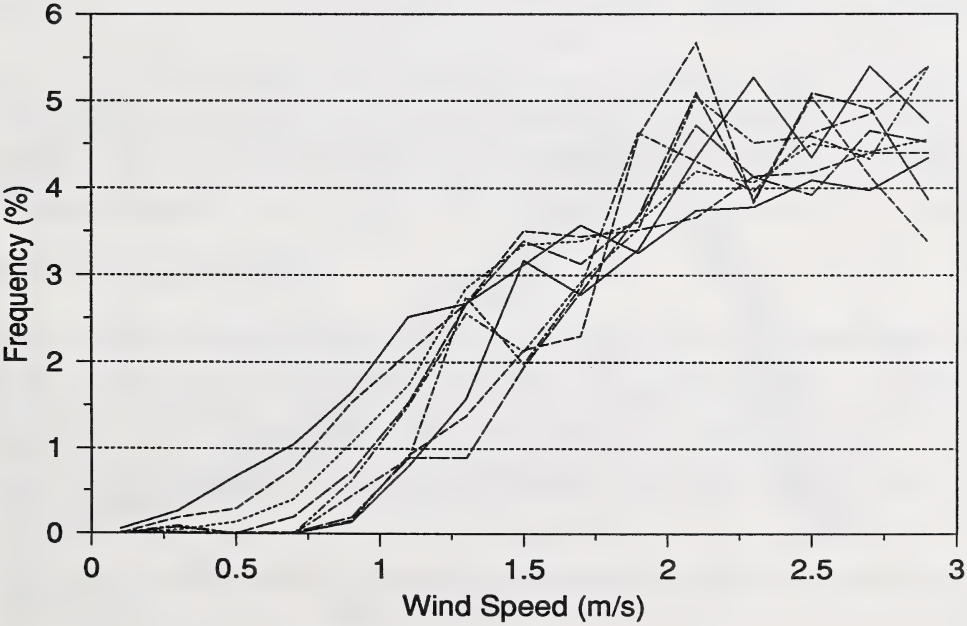

(Summer)

Figure 8.24

Longer Averaging Times Analysis - Kathyrn.
Wind Speed Frequencies for Averaging Times from 1/2 to 8 hours. 0 to 3 m/s Scale.

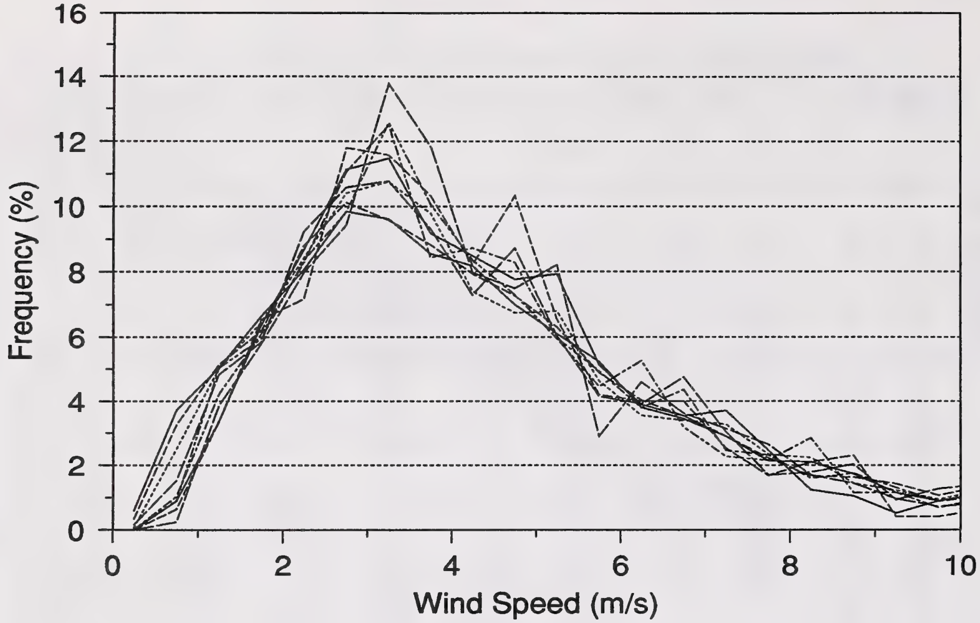

(Winter)

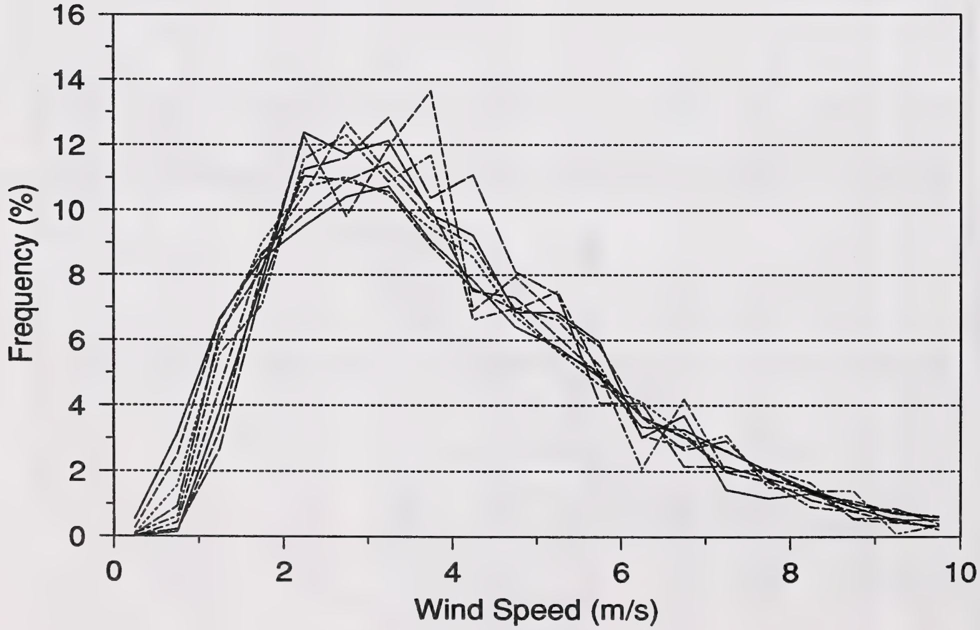

(Summer)

Figure 8.25

Longer Averaging Time Analysis - Kathyrn.
Wind Speed Frequencies for Averaging Times from 1/2 to 8 Hours. Full Scale.

distributions shown in Figure 8.25 are somewhat independent of the averaging period. The shapes of the low wind speed portion of the frequency distributions shown in Figure 8.24, however, are dependent on the averaging period.

In terms of the application of these results, it is useful to ask a question like, "How many times a year could wind speeds less than 1 m/s occur?" This type of question can be addressed using the data in Table 8.4. The following table indicates the number of occurrences per year of wind speeds less than 1 m/s, 2 m/s and 3 m/s for averaging periods ranging from 1/2 hour to 8 hours. The results in the table have been normalized for an 8 760 hour year and are presented in terms of absolute frequency as well as on a percentage basis (values in parenthesis).

Averaging	Wind Speed						Periods in
Period (h)	< 1 m/s (%)		< 2 m/s (%)		< 3 m/s (%)		a Year
0.5	694	(4.0)	3069	(17.5)	6398	(36.5)	17 250
1	274	(3.1)	1454	(16.5)	3199	(36.5)	8 760
2	90	(2.0)	972	(22.3)	1866	(42.6)	4 380
3	38	(1.3)	410	(14.0)	1023	(35.0)	2 920
4	17	(0.8)	277	(12.6)	745	(34.0)	2 190
5	12	(0.7)	220	(12.6)	596	(34.0)	1 752
6	6	(0.4)	163	(11.2)	488	(33.4)	1 460
7	4	(0.3)	138	(11.0)	397	(31.7)	1 251
8	2	(0.2)	110	(10.0)	334	(30.5)	1 095

The smallest wind speed class appears to be the most sensitive to the averaging period (as was indicated in Figure 8.24). One-half hour average wind speeds less than 2 m/s can be expected 17.5% of the time; in contrast an 8 average wind speed less than 2 m/s can be expected 10% of the time. An 8 hour average wind speed less than 2 m/s can be expected 110 times per year.

Frequency Analysis (ADRP)

The 10 m level Crossfield West data from the ADRP program were based on two years of hourly average data from November 1985 to October 1987. For this period, 16 152 hourly average wind speeds were available, representing an overall recovery efficiency of 92.2%. The minimum and maximum wind speeds were 0.3 and 20 m/s, respectively. The overall mean wind speed was 4.1 m/s (the same mean as the Field Measurement Program). Wind speed frequency distributions for the ADRP Crossfield West site are given in Appendix D5.

The following table indicates the frequency of occurrence for wind speeds in selected wind speed classes:

All Stability Conditions (ADRP)

Wind Speed Class (m/s)	Percentage Occurrence (%)
0 to 1	5.5
0 to 2	20.3
0 to 3	35.0

Overall, 10 m level wind speeds less than 2 m/s were observed 20.3% of the time. This compares to the corresponding Field Measurement Program value of 17.5%.

The frequency of low wind speeds and stable atmospheric conditions was also determined. For the purposes of this assessment, stable conditions were defined by two criteria:

- Negative net radiation ($Q_{net} < 0$)
- Positive potential temperature gradient ($\partial\theta/\partial Z > 0$).

The following table shows the frequency of occurrence for low wind speeds under stable atmospheric conditions:

Stable Conditions Only (ADRP)

Wind Speed Class (m/s)	Percentage Occurrence (%)	
	Q_{net}	$\frac{\partial\theta}{\partial Z} > 0$
0 to 1	2.7	2.1
0 to 2	10.2	9.0
0 to 3	17.9	16.1

On the average, wind speeds less than 2 m/s and stable conditions were observed 9.6% of the time. This compares to the corresponding Field Measurement Program value of 10.5%.

Frequency Analysis (Calgary Airport)

Prior to the Field Measurement Program, the wind speed data reported on the hour at Calgary International airport were reviewed. This review was conducted to determine the best time of the year to undertake the Field Measurement Program. The airport data analysis were based on five years of data from 1980 to 1984 and the resultant frequency distributions are presented in Appendix D4. Over this period, wind speeds less than 1.5 m/s (3 knots) were observed 19% of the time. Wind speeds less than 1.5 m/s occurred more than 20% of the time during the months of August, October, November and December.

Duration Analysis (FMP)

Wind speed durations were determined from the one-half hour 10 m level wind speed files for the winter period only. This period represents 7 344 one-half hour averages from October 1988 to March 1989. The wind speed durations were determined for wind speed classes 1 m/s in width for wind speeds less than 5 m/s and for wind speed classes 2.5 m/s in width for wind speeds greater than 5 m/s. The durations were expressed in multiples of the one-half hour base period.

The results of the analysis are presented in Table 8.5. The data from the table were used to determine the duration and frequency of one-half hourly average wind speeds less than selected values (1, 2 and 3 m/s). The results were then normalized for an 8 760 hour year and presented in Table 8.6. For this period, wind speeds less than 2 m/s occurred 16% of the time. Of this 16%, 3.81% of the wind speeds less than 2 m/s lasted for 1/2 hour only; 3.21% lasted for 1 hour only; 0.65% lasted for 3 hours; and 0.14% lasted for 5 hours.

Duration Analysis (FMP and ADRP)

Wind speed durations were also determined from the FMP three-minute average 10 m level wind data for the full nominal one-year period (October 1988 to March 1989). Similar durations were also determined from the ADRP Crossfield East and Crossfield West two-minute average wind data from the 10 m levels. The ADRP data were grouped into Year 1 (1984/85) and Year 2 (1985/86).

The results are plotted in Figure 8.26 as contours of time (minutes) which are functions of frequency (%) and wind speed (m/s). The following provides an example of data extraction and interpretation for the plots. Consider a Field Measurement Program wind speed of 6.5 m/s.

- 84% of the 6.5 m/s wind speeds persist for up to 6 minutes
- 52% of the 6.5 m/s wind speeds persist for up to 9 minutes
- 20% of the 6.5 m/s wind speeds persist for up to 20 minutes
- 10% of the 6.5 m/s wind speeds persist for up to 30 minutes.

All plots indicate that wind speeds in the 5 to 8 m/s range tend to be more persistent than other wind speed ranges.

The contour patterns for the two years of ADRP data are similar, but both are different from the Kathyrn Field Measurement Program. Broadly speaking, a given wind speed tends to persist twice as long at the Kathyrn site than at the ADRP site.

Table 8.5

FMP Duration Analysis for the Period October 1988 to March 1989.

Time	Wind Speed Class (m/s)												
(h)	0-1	1-2	2-3	3-4	5-7.5	7.5-10	10-12.5	12.5-15	15-17.5	17.5-20	20-22.5	22.5-25	
0.5	65	215	324	343	333	172	91	39	13	2	1	1	1599
1.0	27	91	145	154	129	101	50	17	2	1	0	0	1434
1.5	24	53	67	68	60	57	27	4	2	1	0	0	1089
2.0	10	29	37	35	24	34	18	5	0	0	0	0	768
2.5	4	12	23	19	20	27	9	2	1	0	0	0	585
3.0	2	6	14	11	5	18	6	4	1	0	0	0	402
3.5	3	6	9	7	2	15	12	2	0	0	0	0	392
4.0	1	2	1	7	4	8	0	1	0	0	0	0	192
4.5	0	2	0	7	2	12	1	0	1	0	0	0	225
5.0	1	0	6	1	2	2	0	0	0	0	0	0	120
5.5	0	0	1	0	2	7	1	0	1	0	0	0	132
6.0	0	0	1	0	1	2	1	1	0	0	0	0	72
6.5	0	0	0	0	0	2	0	0	0	0	0	0	26
7.0	0	1	0	0	0	4	1	0	0	0	0	0	84
7.5	1	0	0	0	0	0	1	0	0	0	0	0	30
8.0	0	0	0	0	0	3	0	0	0	0	0	0	48
8.5	0	0	0	0	0	1	0	0	0	0	0	0	17
9.0	0	0	0	0	0	1	0	0	0	0	0	0	18
9.5	0	0	0	0	0	1	1	0	0	0	0	0	38
10.0	0	0	0	0	0	0	0	0	0	0	0	0	0
10.5	0	0	0	0	0	1	0	0	0	0	0	0	21
11.0	0	0	0	0	0	0	0	0	0	0	0	0	0
11.5	0	0	0	0	0	1	0	0	0	0	0	0	23
12.0	0	0	0	0	0	0	0	0	0	0	0	0	0
12.5	0	0	0	0	0	0	0	0	0	0	0	0	0
13.0	0	0	0	0	0	0	0	0	0	0	0	0	0
13.5	0	0	0	0	0	0	0	0	0	0	0	0	0
14.0	0	0	0	0	0	0	0	0	0	0	0	0	0
14.5	0	0	0	0	0	1	0	0	0	0	0	0	29
												Total	7344

Table 8.6

Occurrence of Wind Speed Duration for Selected Wind Speed Classes (Normalized for an 8 760 hour year).

Duration (h)	< 1 m/s		< 2 m/s		< 3 m/s		Number of Periods in a Year
	N	%	N	%	N	%	
0.5	155	0.89	668	3.81	1441	8.22	17520
1.0	64	0.74	282	3.21	627	7.16	8760
1.5	57	0.98	184	3.15	344	5.88	5840
2.0	24	0.54	93	2.12	181	4.14	4380
2.5	10	0.27	38	1.09	93	2.66	3504
3.0	5	0.16	19	0.65	52	1.80	2920
3.5	7	0.29	21	0.86	43	1.72	2503
4.0	2	0.11	7	0.33	10	0.44	2190
4.5	0	0.00	5	0.25	5	0.25	1947
5.0	2	0.14	2	0.14	17	0.95	1752
5.5	0	0.00	0	0.00	2	0.15	1593
6.0	0	0.00	0	0.00	2	0.16	1460
6.5	0	0.00	0	0.00	0	0.00	1348
7.0	0	0.00	2	0.19	2	0.19	1251
7.5	2	0.20	2	0.20	2	0.20	1168
8.0	0	0.00	0	0.00	0	0.00	1095
Total		4.32		15.99		33.91	

N = number of occurrences that consecutive 1/2 hour wind speed values were of the given duration and less than the specified speed.

% = $(N/N_{tot}) \times 100$ where N_{tot} = number of periods in a year = 8 760/period (h).

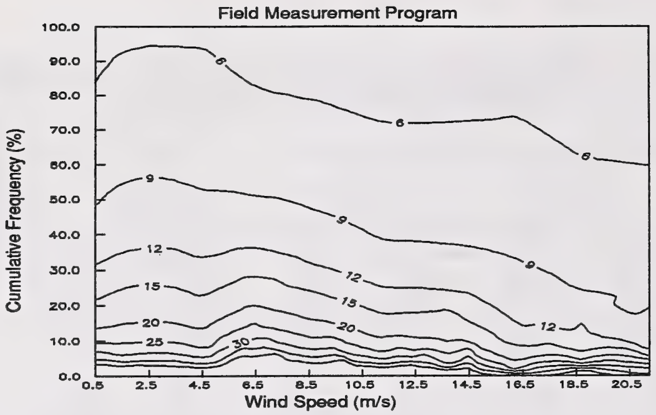

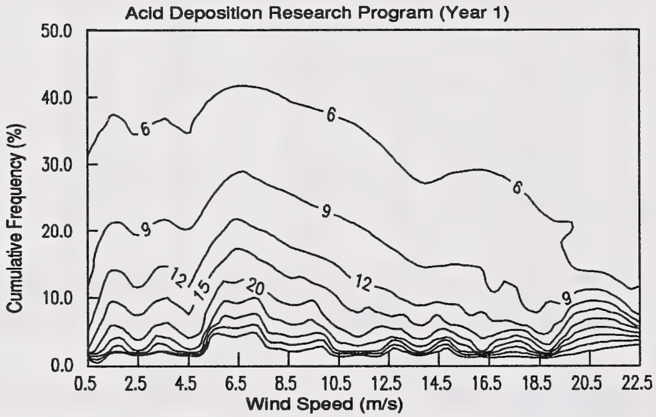

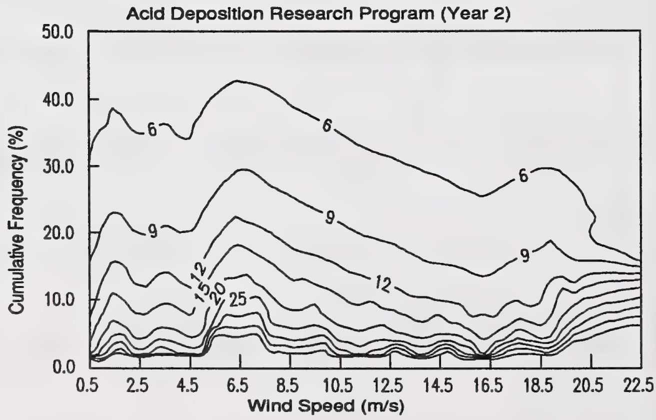

Figure 8.26

Short Averaging Time Analysis.
Wind Persistence Contours as a Function of Wind Speed. Contour Interval of 5 Minutes for Values Longer Than 15 Minutes.

The table below summarizes the persistence of wind speeds less than 2 m/s from Figure 8.26.

Short Averaging Time Analysis
Persistence and Duration of Wind Speeds Less than 2 m/s.

Persistence (%)	Duration (minutes) Kathyrn	 ADRP (Year 1)	 ADRP (Year 2)
100	3	2	2
50	10	4	4
25	15	7	7
20	18	9	9
10	25	14	15
5	35	20	20
1	55	3	25

Again, the results support the findings that winds were more persistent at the Kathyrn site. One percent of the wind speeds less than 2 m/s persisted for about one hour at the Kathyrn site. In contrast, one percent of the wind speeds less than 2 m/s persisted for 1/2 hour at the ADRP sites.

Comments

The issue of persistence relates to the duration of a given meteorological condition to occur. The duration is important when dispersion models are used to predict air quality changes. As the models usually incorporate steady-state assumptions, it is important that the model is not applied to a condition which has a duration that is less than the travel time from the source to a specified receptor.

Persistence in this application addresses more than just the wind speed: wind direction and atmospheric persistence also important factors. This preliminary assessment focussed mainly on wind speed. A more rigorous assessment would include the other parameters as well. Qualitatively, persistence should be limited by the normal diurnal variation of these parameters.

8.4.2 Minimum Turbulence Levels

One of the program objectives was to determine whether the atmosphere is characterized by a minimum turbulence level. To address this objective, the frequency distributions of the wind fluctuations σ_U, σ_V and σ_W were determined. These frequency distributions were then compared to the instrument baseline by recording wind data under zero wind speed conditions. In addition, the frequency distributions of σ_θ and σ_ϕ were also determined.

To determine the impact of sonic anemometer instrument noise on the frequency distributions, "zero air" tests were conducted. This consisted of placing the sonic anemometer in an enclosed chamber out of the wind. The results for each anemometer based on a one-hour period are given in Table 8.7. The table provides both the mean and turbulence components. The following conclusions can be made:

- The average zero air values for the mean wind components is about 0.04 m/s. At one level, a value of 0.11 m/s was observed.
- The average zero air values for the turbulence components σ_U and σ_V was 0.05 m/s. For σ_W, the average value was 0.01 m/s. Even though the transducers are symmetric for all axis, the gain is different for the vertical component. This lower gain appears to result in systematic σ_W values that are smaller than the horizontal values.

Table 8.7

Sonic Anemometer Zero Air Test Results.

Component (m/s)	4 m	10 m	16 m	25 m
U	-0.01	-0.04	0.05	0.08
V	0.01	0.01	0.05	0.02
W	0.03	0.01	-0.01	0.11
σ_U	0.01	0.02	0.11	0.08
σ_V	0.01	0.03	0.02	0.10
σ_W	0.01	0.01	0.01	0.01

Note: Applied Technologies sonic systems were located at 4, 16 and 25 m.
Kaijo-Denki Sonic system was located at 10 m.

The above findings are based on one "zero-air" test conducted at the end of the study.

Figure 8.27 shows the frequency distributions for the 10 m level σ_U, σ_V and σ_W values. The figure indicates that the σ_U and σ_V are about the same magnitude while the σ_W values are about one-third the σ_U and σ_V values. The frequency distributions indicate that σ_U and σ_V are dependent on averaging period while σ_W is somewhat independent of averaging period. (See Section 8.7). The summer frequency distributions indicate the more frequent occurrence of larger σ_U, σ_V and σ_W values than those for the winter. The summer σ_W frequency distribution is particularly interesting in that a bimodal distribution was observed. The first peak is likely due to stable night-time conditions while the second peak is likely due to unstable (convective) daytime conditions.

Figure 8.28 shows the frequency distribution values for small σ_U, σ_V and σ_W values. The zero-air test results are superimposed on both the winter and summer values. For the 3-minute average σ_U and σ_V values, the observed distribution and the zero-air test distributions overlap indicating any minimum turbulence levels taper off and disappear into

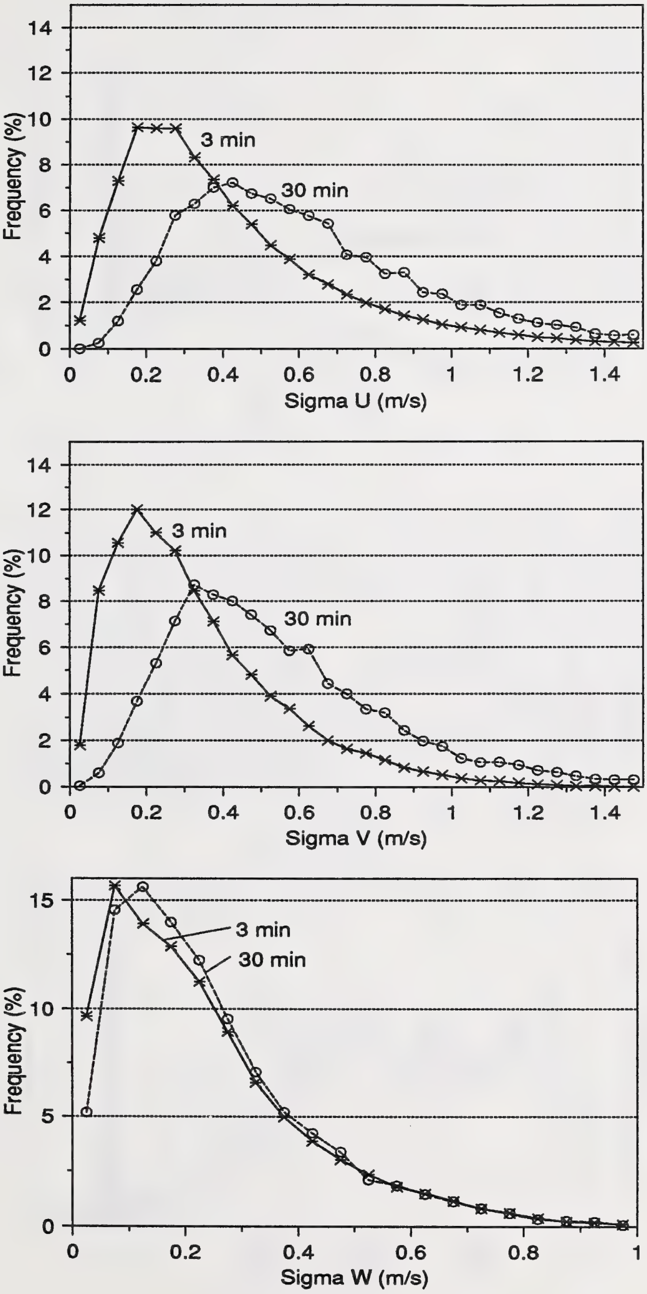

Figure 8.27 Winter

Observed 10 m Level Frequency Distribution for σ_U, σ_V and σ_W.

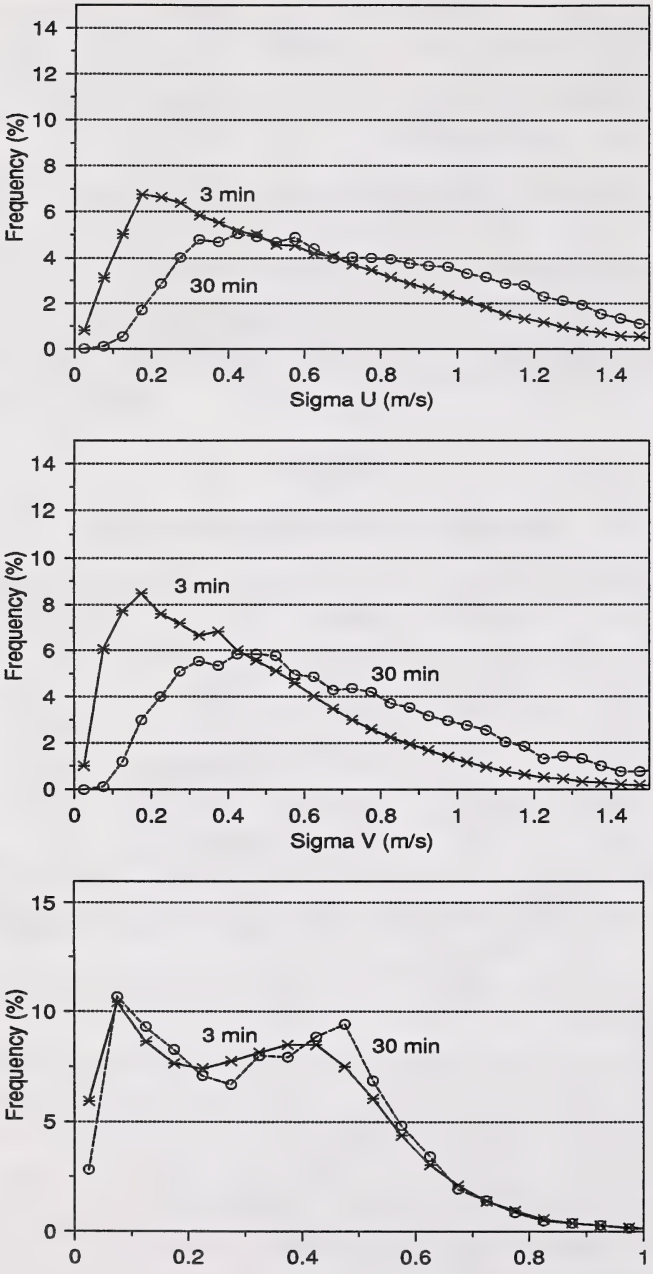

Figure 8.27 Summer

Observed 10 m Level Frequency Distribution for σ_U, σ_V and σ_W.

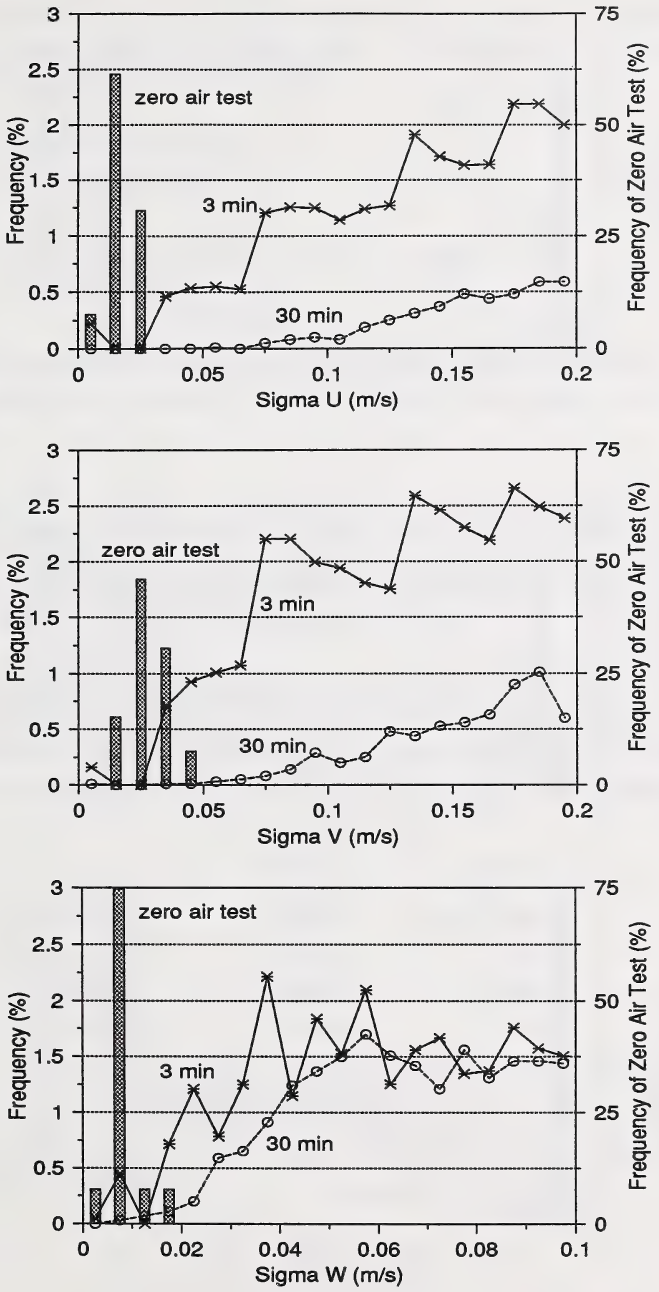

Figure 8.28 Winter

Observed 10 m Level Frequency Distribution for Small σ_U, σ_V and σ_W. The Results of the Zero Air test are Shown as Bars.

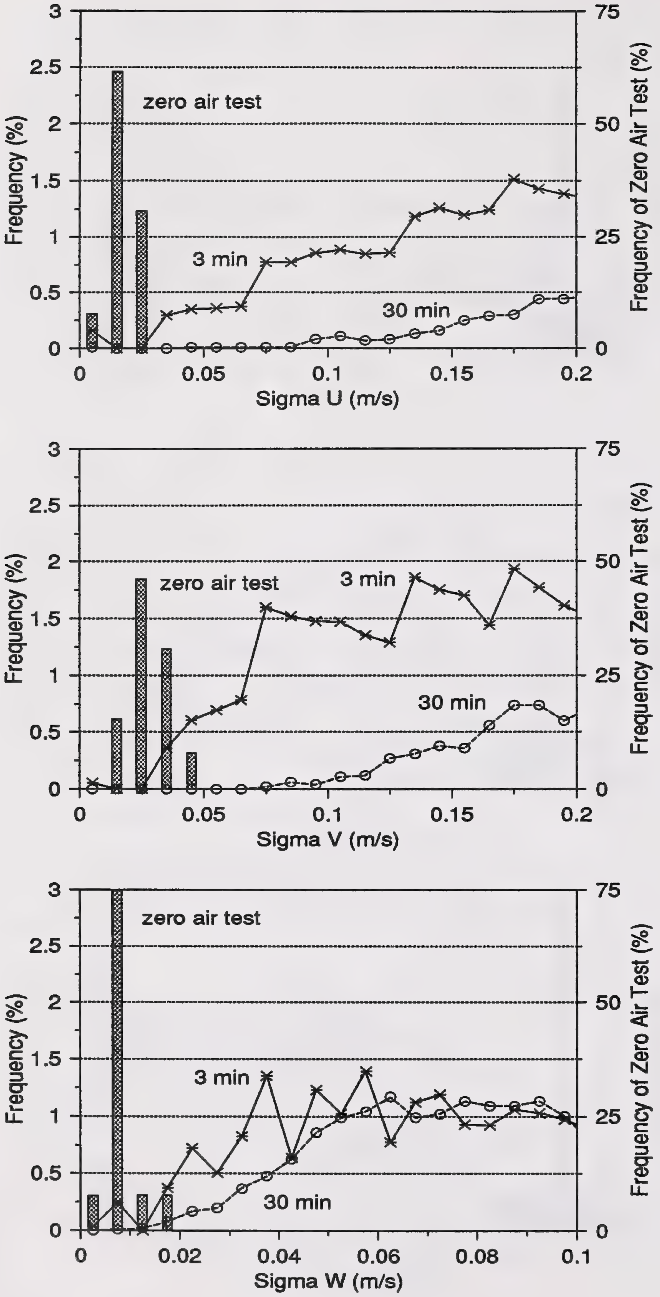

Figure 8.28 Summer

Observed 10 m Level Frequency Distribution for Small σ_U, σ_V and σ_W. The Results of the Zero Air test are Shown as Bars.

the instrument noise. For the 30-minute average σ_U and σ_V values, there appears to be much less of an overlap with the instrument noise. These implies that 30-minute minimum turbulence levels may be defined as follows:

σ_U (winter) = 0.065 m/s
σ_U (summer) = 0.085 m/s

σ_V (winter) = 0.045 m/s
σ_V (summer) = 0.075 m/s

For the vertical component, both the 3 and 30-minute average values for σ_W slowly decrease and disappear into the instrument noise. As such, it is not possible to define a minimum value for σ_W.

Selected cumulative frequency distribution values were extracted from the frequency distributions shown in Figure 8.27. These values are presented in Table 8.8. The one-percentile turbulence levels for the 3-minute average values are comparable to the noise level of the sonic anemometers. The one-percentile levels for the 30-minute average values are much larger than the noise levels.

Figure 8.29 shows the frequency distribution of the 10 m level σ_θ and σ_ϕ values for the 3 and 30-minute averaging periods. Figure 8.30 shows the frequency distribution for small values of σ_θ and σ_ϕ. The frequency distribution for σ_θ is dependent on averaging time while that for σ_ϕ is independent of averaging time. The most frequent occurrence of σ_θ and σ_ϕ are:

	Winter	Summer
• σ_θ(3-minute)	4 degrees	5 degrees
• σ_θ(30-minute)	5 degrees	7 degrees
• σ_ϕ(3-minute)	3 degrees	5 degrees
• σ_ϕ(30-minute)	3 degrees	5 degrees

For σ_θ, there appears to be a minimum value of 1.5 to 2.0 degrees for the 30-minute averaging period. For the 3-minute σ_θ, the minimum value is almost 0.5 degrees. For the 30-minute σ_ϕ, the minimum value is about 0.25 degrees. For the 3-minute σ_ϕ, there does not appear to be a cut-off or a minimum.

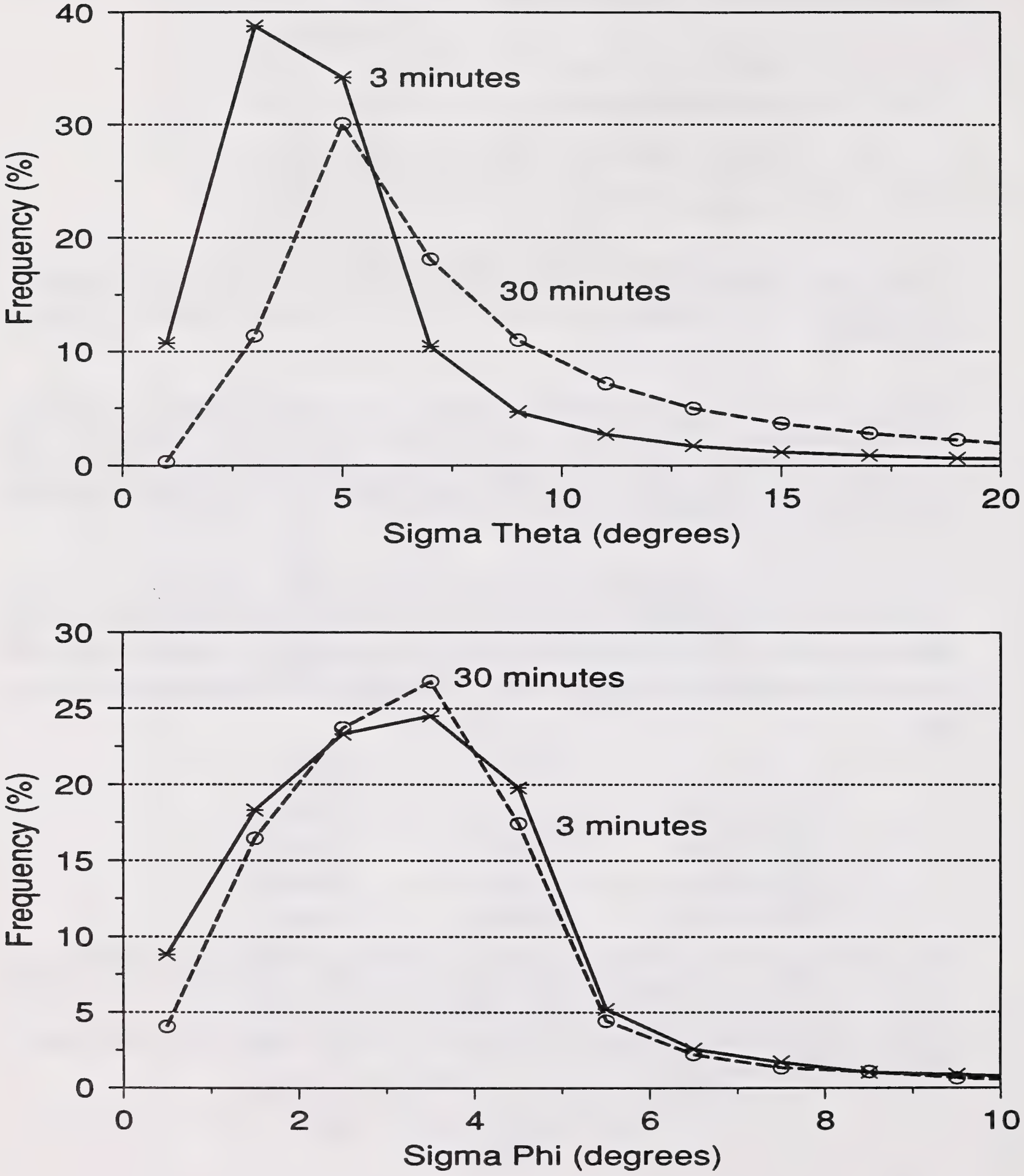

Figure 8.29 Winter

Frequency Distributions of 3 and 30 Minute Sigma Theta (σ_θ) and Sigma Phi (σ_ϕ).

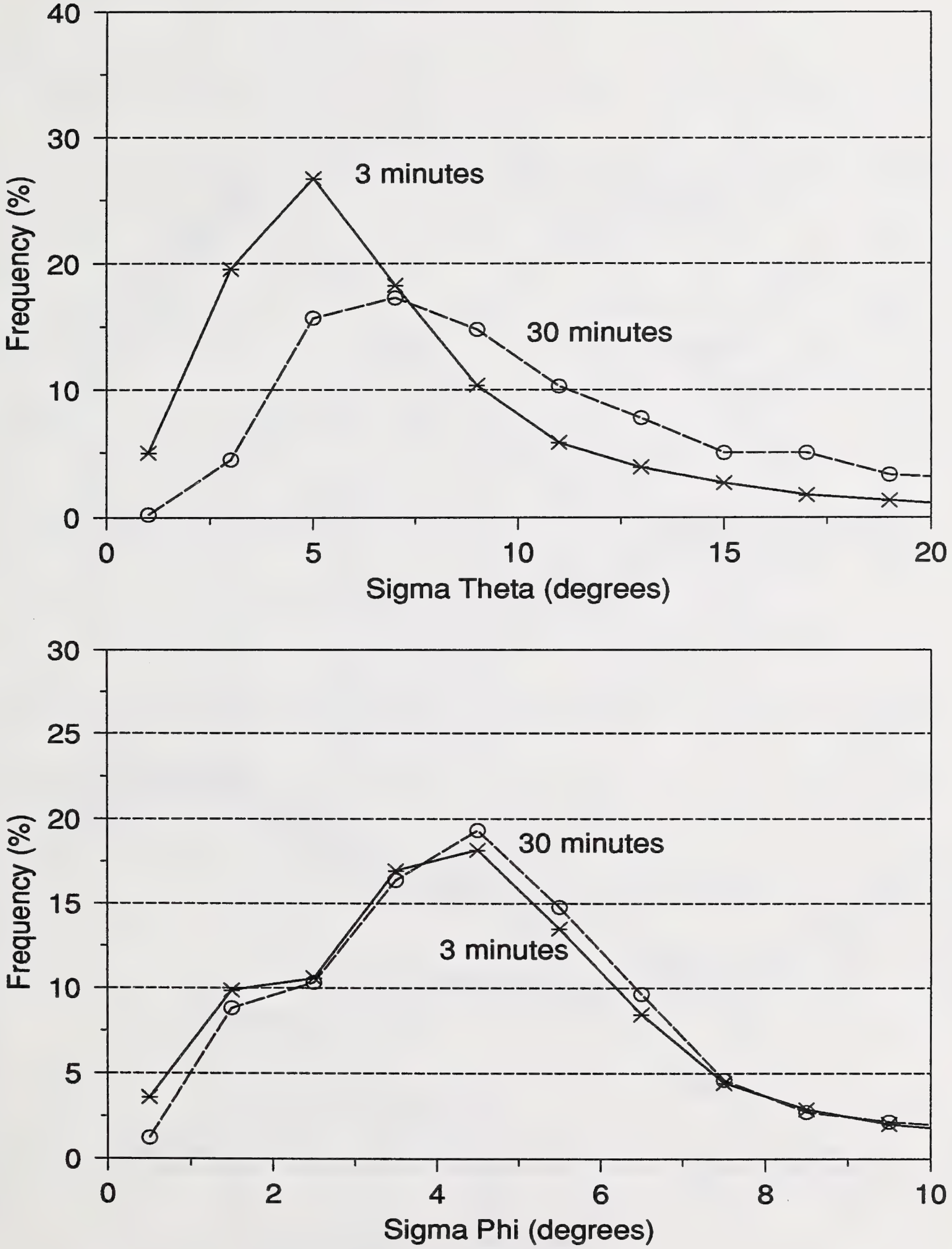

Figure 8.29 Summer

Frequency Distributions of 3 and 30 Minute Sigma Theta (σ_θ) and Sigma Phi (σ_ϕ).

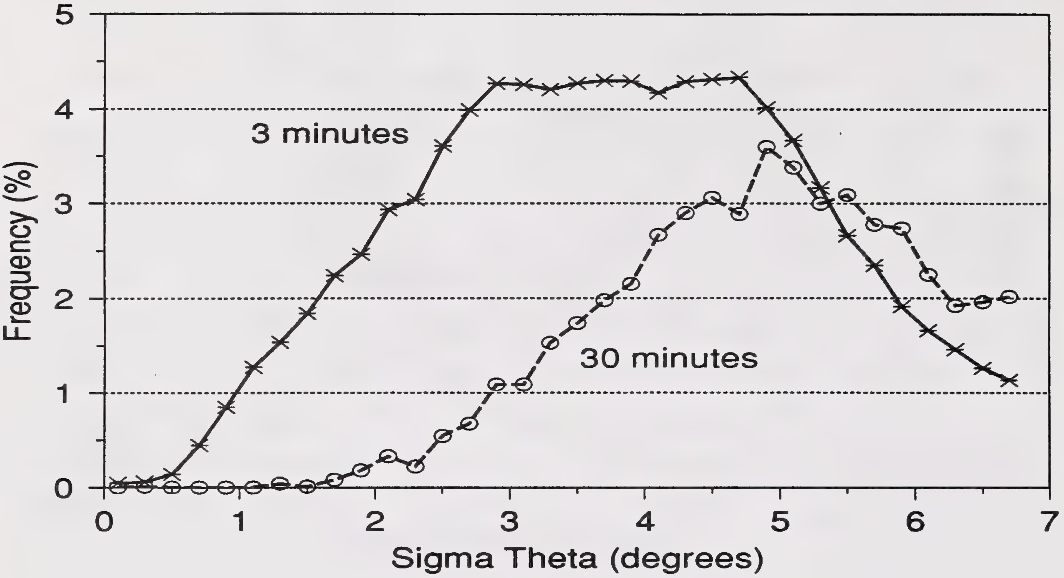

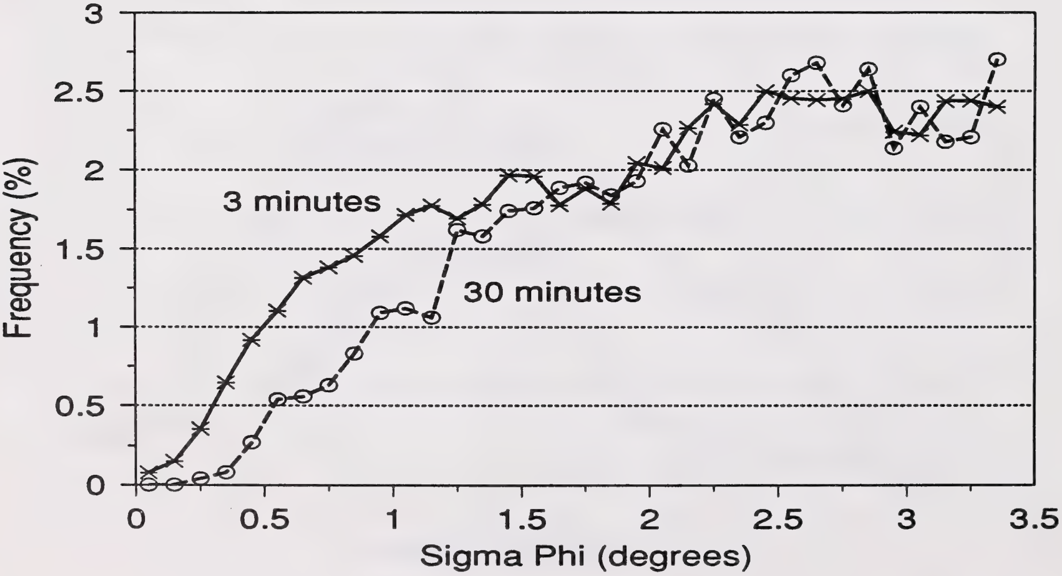

Figure 8.30 Winter

Frequency Distributions of 3 and 30 Minute Sigma Theta (σ_θ) and Sigma Phi (σ_ϕ).

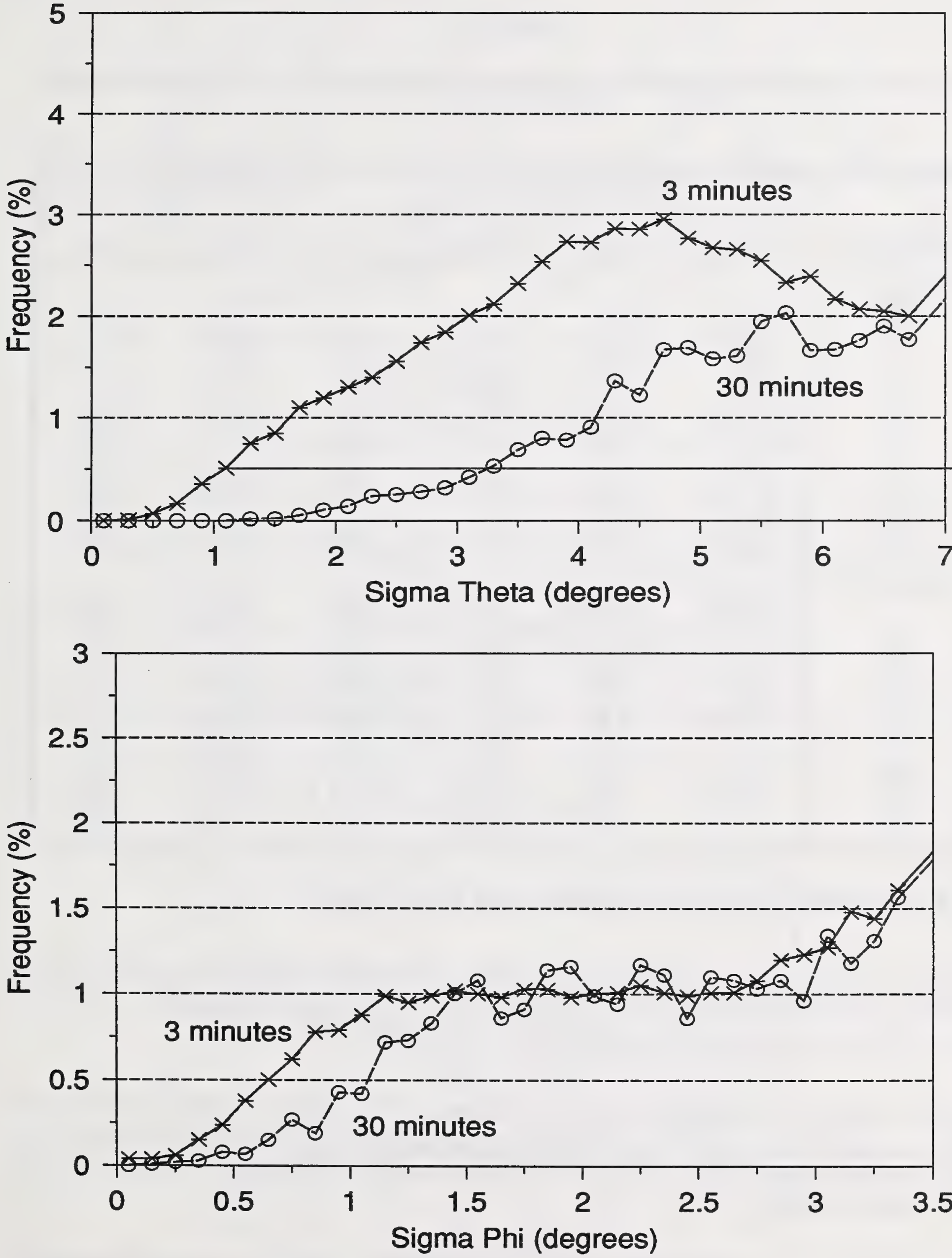

Figure 8.30 Summer

Frequency Distributions of 3 and 30 Minute Sigma Theta (σ_θ) and Sigma Phi (σ_ϕ).

Table 8.8

Cumulative Frequency Distribution Values of Observed 10 m Level Wind Standard Deviations (m/s).

Percentile	3 Minutes			30 Minutes		
	σ_U	σ_V	σ_W	σ_U	σ_V	σ_W
Winter						
1	0.045	0.045	0.016	0.14	0.12	0.03
5	0.10	0.08	0.04	0.22	0.19	0.05
10	0.13	0.10	0.05	0.27	0.24	0.07
25	0.21	0.17	0.10	0.39	0.34	0.13
50	0.35	0.28	0.19	0.57	0.49	0.20
75	0.56	0.45	0.32	0.84	0.71	0.32
90	0.86	0.65	0.49	1.17	0.98	0.49
95	1.09	0.80	0.61	1.46	1.20	0.60
99	1.58	1.12	0.81	n/a	n/a	0.81
Summer						
1	0.056	0.053	0.027	0.16	0.14	0.04
5	0.12	0.10	0.05	0.25	0.21	0.06
10	0.17	0.14	0.08	0.31	0.27	0.08
25	0.29	0.23	0.16	0.46	0.41	0.16
50	0.54	0.41	0.33	0.74	0.63	0.33
75	0.83	0.65	0.37	1.08	0.95	0.48
90	1.14	0.91	0.69	1.41	1.30	0.59
95	1.34	1.09	0.69	1.66	1.59	0.67
99	1.77	1.49	0.85	2.50	1.99	0.89

8.4.3 Turbulence Level Dependence on Wind Speed

As the wind speed decreases, the mechanically generated turbulence levels will also decrease. To determine turbulence behavior under low wind speeds, the wind fluctuations (σ_U, σ_V and σ_W; also σ_θ and σ_ϕ) were plotted as a function of wind speed.

Figure 8.31 shows the median σ_U, σ_V and σ_W values as a function of averaging period (3 and 30-minute) and wind speed. For the 30-minute values, the wind speed bins are 0.67 m/s in width, for the 3-minute values, the wind speed bins are 0.5 m/s in width. The results shown in the figure indicate:

- The winter 3 and 30-minute and summer 3-minute average σ_U values converge to 0.25 m/s as the wind speed approaches zero. The summer 30-minute average σ_U values converge to 0.35 m/s as the wind speed approaches zero.

- The winter 3 and 30-minute average σ_V values converge to 0.25 m/s as the wind speed approaches zero. The summer 3 and 30-minute average σ_V values converge to 0.2 and 0.35 m/s, respectively, as the wind speed approaches zero.

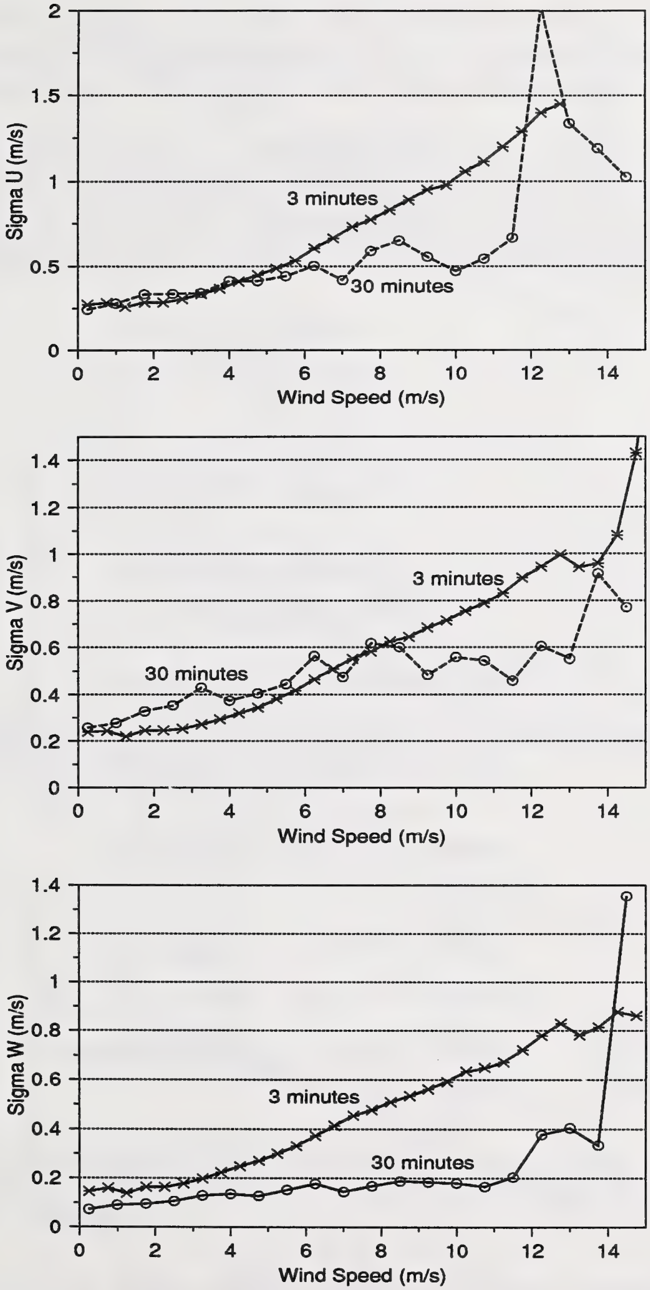

Figure 8.31 Winter

6 Month Averaged 3 and 30 Minute σ_U, σ_V and σ_W as a Function of Wind Speed.

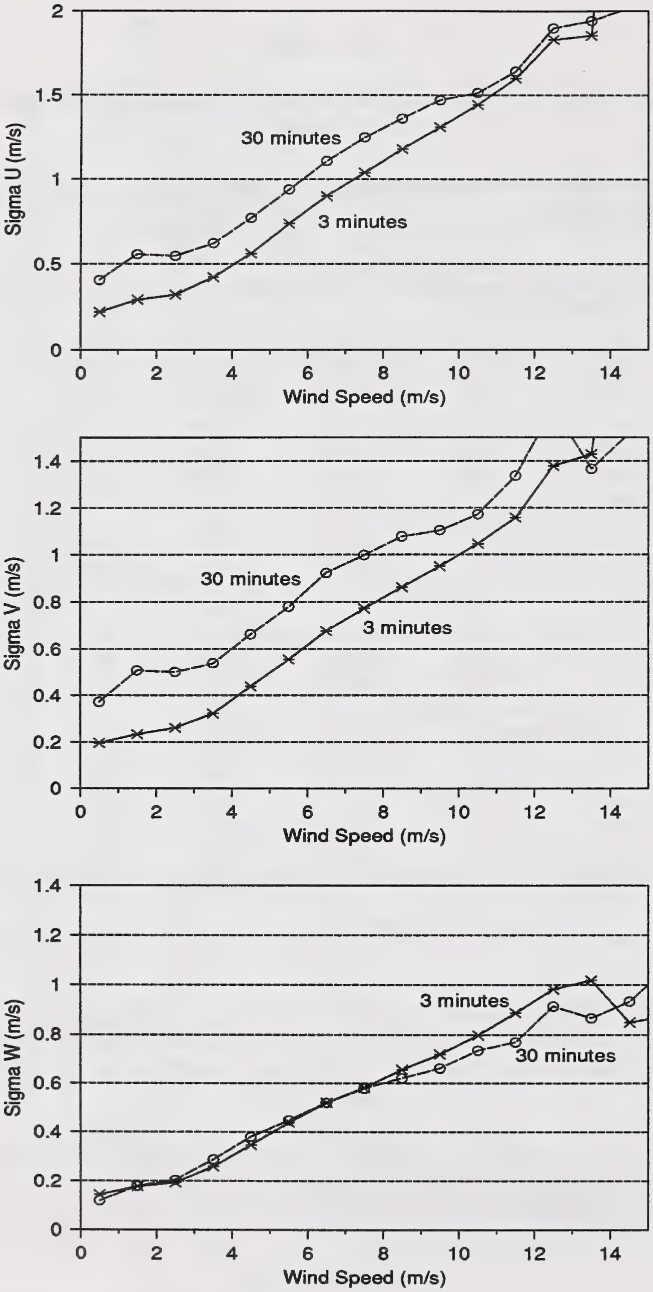

Figure 8.31 Summer

6 Month Averaged 3 and 30 Minute σ_U, σ_V and σ_W as a Function of Wind Speed.

- The winter 3-minute and summer 3 and 30-minute average σ_W values converge to 0.175 m/s as the wind speed approaches zero. The summer 30-minute average σ_W values converge to 0.09 m/s as the wind speed approaches zero.

A linear relationship expressing σ_U, σ_V and σ_W as a function of wind speed can be obtained. The 3-minute σ_U, σ_V and σ_W relationships can be fitted to a curve which passes through the origin. The σ_U, σ_V and σ_W values tend to depart from the linear relationships through the origin for wind speeds less than 3 m/s. The linear relationships are given as:

$$\sigma_U = 0.11\,U \text{ (winter)}$$
$$\sigma_U = 0.14\,U \text{ (summer)}$$

$$\sigma_V = 0.075\,U \text{ (winter)}$$
$$\sigma_V = 0.100\,U \text{ (summer)}$$

$$\sigma_W = 0.060\,U \text{ (winter)}$$
$$\sigma_W = 0.076\,U \text{ (summer)}$$

where σ_X and the wind speed are in m/s.

Combining Equation 8.12 (using $\psi(Z/L) = 0$) (Section 8.3.5) with the normalized variances given by Panofsky and Dutton (1984), it can be shown that:

$$\begin{aligned} \sigma_U = \frac{2.39k}{\ln(Z/Z_o)}U \quad &= 0.103\,U \text{ (winter)} \\ &= 0.138\,U \text{ (summer)} \\ \sigma_V = \frac{1.92k}{\ln(Z/Z_o)}U \quad &= 0.083\,U \text{ (winter)} \\ &= 0.111\,U \text{ (summer)} \\ \sigma_W = \frac{1.25k}{\ln(Z/Z_o)}U \quad &= 0.054\,U \text{ (winter)} \\ &= 0.072\,U \text{ (summer)} \end{aligned}$$

The above equation assumes $k = 0.4$, $Z = 10$ m and $Z_o = 0.1$ cm for winter and $Z_o = 1$ cm for summer. The slopes derived from Figure 8.31 are somewhat in agreement with the log-linear wind profile relationship.

Figure 8.32 shows the median σ_θ and σ_ϕ values as a function of averaging period (3 and 30-minute) and wind speed. The results shown in the figure indicate:

- The 3-minute σ_θ tends to remain constant at 5 degrees for wind speeds greater than 5 m/s for the winter and 6 degrees for wind speeds greater than 3 m/s during the summer.

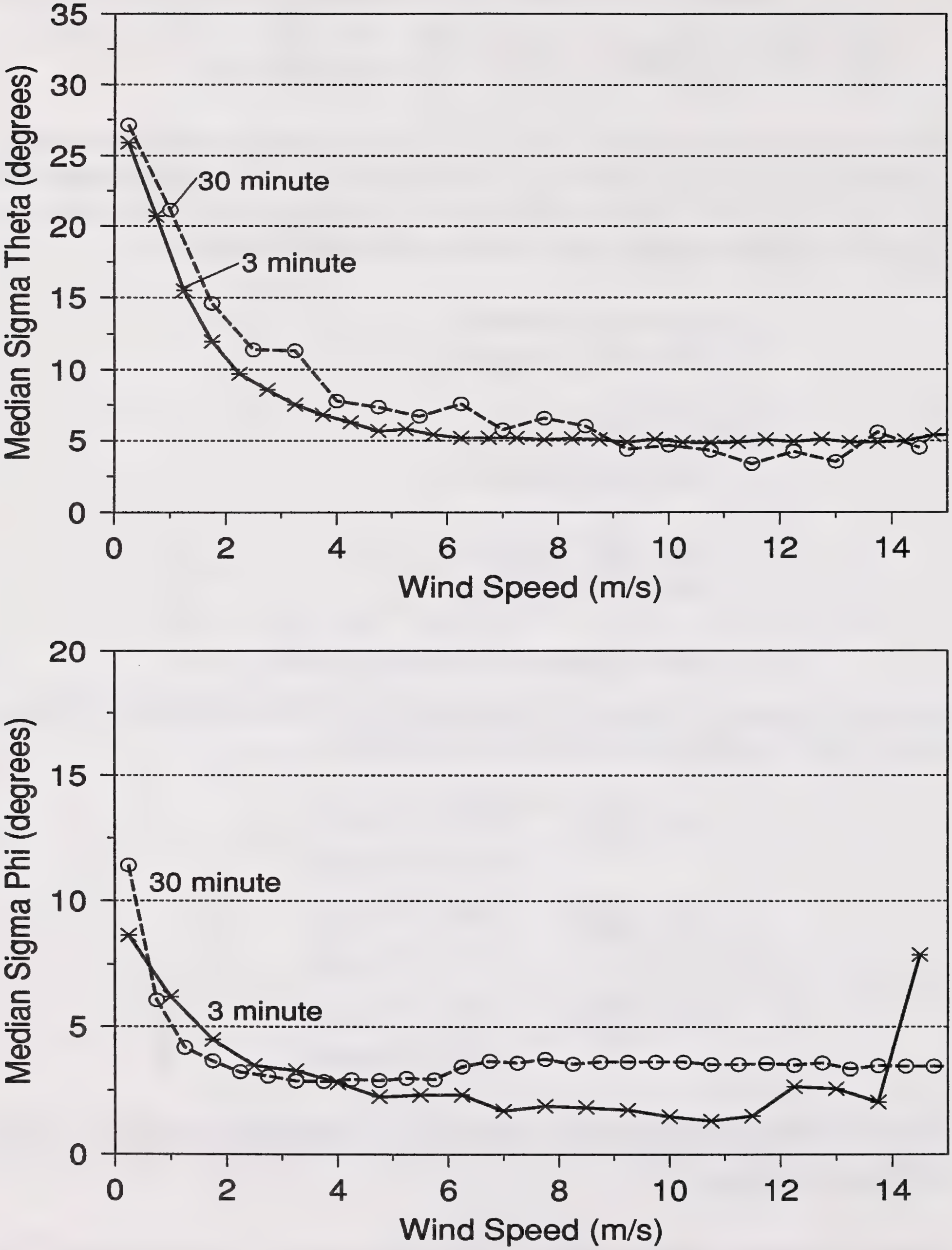

Figure 8.32 Winter

6 Month Averaged 3 and 30 Minute σ_θ and σ_ϕ as a Function of Wind Speed.

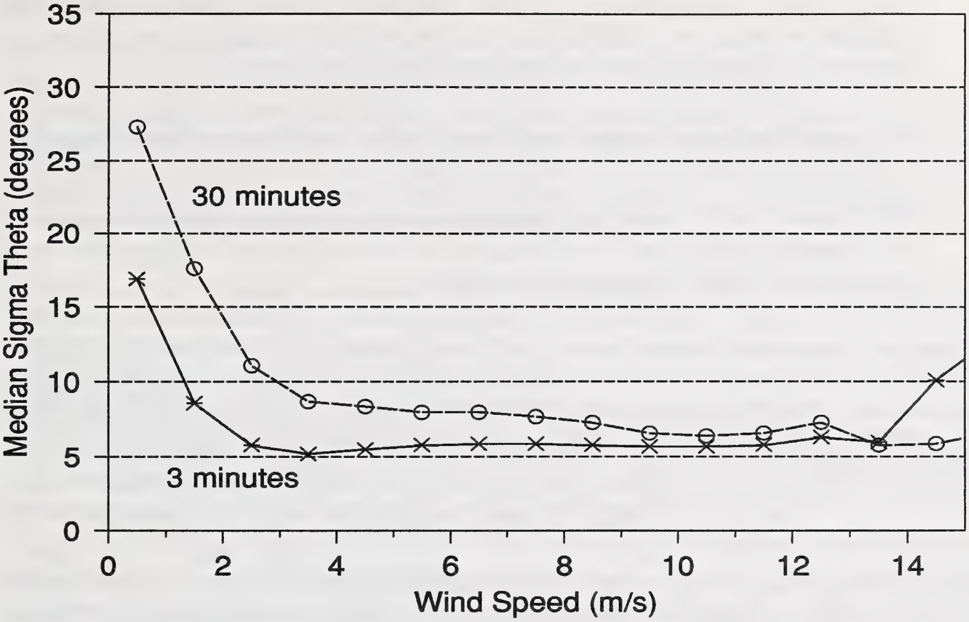

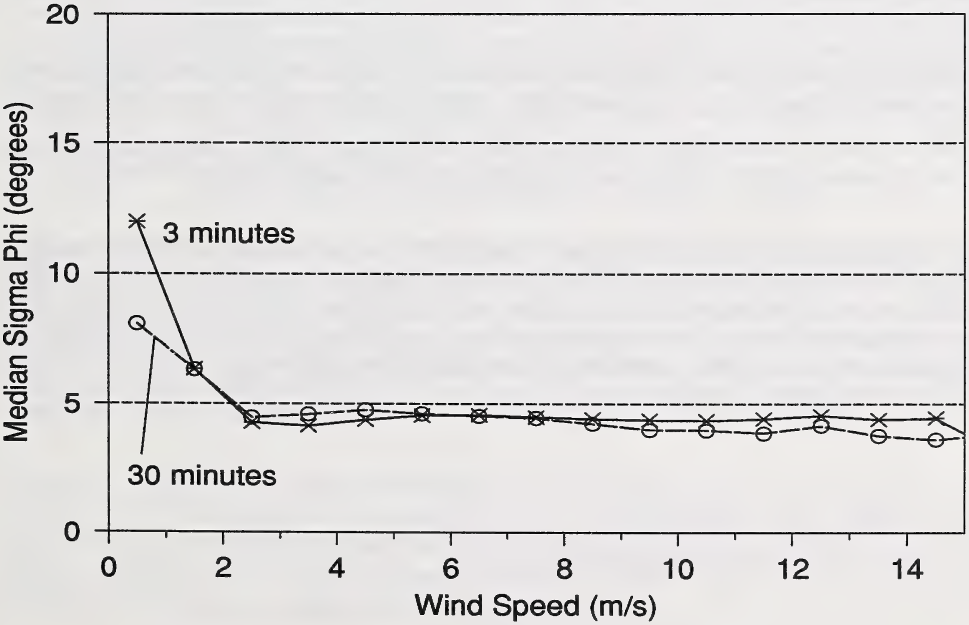

Figure 8.32 Summer

6 Month Averaged 3 and 30 Minute σ_θ and σ_ϕ as a Function of Wind Speed.

- The 30-minute σ_θ decreases slowly from 7 degrees at a wind speed of 7 m/s to about 4 degrees at a wind speed of 12 m/s during the winter, and during the summer decreases between the same wind speed values from about 8 to 6 degrees.

- The larger 30-minute σ_θ values for wind speeds less than 9 m/s may be due to meander.

- The 3-minute and 30-minute σ_ϕ values tend to remain constant at about 3 degrees for wind speeds greater than 3 m/s during the winter and at about 4 degrees for wind speeds greater than 3 m/s during the summer.

These findings are consistent with other field investigations which have been conducted in the Calgary area. For example, Leahey *et al* (1988) found that $\sigma_W = 0.06$ U for wind speeds greater than 3.5 m/s. This compares to the Field Measurement Program results which found $\sigma_W = 0.06$ U (winter) and $\sigma_W = 0.076$ U (summer) for wind speeds greater than 3.0 m/s. Both the Leahey *et al* and Field Measurement Program results indicated that the median values for σ_ϕ are about 3 to 4 degrees for wind speeds greater than 3 m/s. Leahey *et al* also found that hourly values for σ_θ were generally in the 7 to 10 degree range for wind speeds greater than 3 m/s. This compares to the Field Measurement Program results when the one-half hourly σ_θ values were in the 4 to 10 degree range for winter and 6 to 10 degree range for summer.

For the σ_U, σ_V and σ_W plots (Figure 8.31) departures from linearity occurred when the wind speed was less than 3 m/s. Similary for the σ_θ and σ_ϕ plots (Figure 8.32), the three minute values are not constant when the wind speeds are less than 3 m/s. The σ_θ and σ_ϕ values seem to increase significantly as the wind speed decreases below 3 m/s.

The preceding implies that minimum turbulence levels are associated with wind speeds of about 3 m/s. As the wind speed decreases below 3 m/s, the lateral (σ_θ) and vertical (σ_ϕ) turbulence intensities increase significantly. For wind speeds greater than 3 m/s, the along wind dilution increases. This conclusion supports the findings of the tracer program in which the smallest plume spreads were associated with mean wind speeds of 3.74 m/s (700 m) and 3.54 m/s (1400 m).

8.5 Meteorological Preprocessor

Pasquill (1960) defined six turbulence classes on the basis of net radiation and wind speed. These turbulence classes became the basis of the Pasquill-Gifford (PG) stability classes frequently used by regulatory models. These classes range from unstable (Classes A, B and C) to neutral (Class D) to stable (Classes E and F). Various algorithms have been used to correlate a given set of meteorological conditions to a PG class. These algorithms have become known as meteorological preprocessors.

One of the most frequently used meteorological preprocessors is the STAR (Stability Array) program which is based on a method proposed by Turner (1964). This method uses routine airport observations of wind speed, cloud cover, time of day and time of year to determine a PG stability class. Since then, other investigators have attempted various methods to estimate the PG class based on more direct, on-site measurements of radiation or turbulence. Two of these methods were applied to the Field Measurement Program observations. The first, proposed by Williamson and Krenmayer (1980), is based on wind speed, net radiation and whether it is day or night. The second, proposed by Bowen *et al* (1983), is based on wind speed, solar radiation and whether it is day or night.

More recent models use meteorological preprocessors which classify turbulence as a continuous variable and are based on heat flux estimates. These preprocessors have been described in van Ulden and Holtslag (1985), the MESOPUF II model (Scire *et al* 1984), the Ontario Ministry of Environment models (OME 1987) and the CTDM model (Paine 1988). These second generation meteorological preprocessors are based on obtaining estimates of heat flux (H_o) and then determining the friction velocity (U^*), the Monin-Obukhov length (L) and, in the case of convective conditions, the convective velocity scale (W^*).

8.5.1 Pasquill - Gifford Stability Class

Figure 8.33 shows the PG frequency distribution predicted using the three methods. The STAR method was based on the Calgary International Airport data. The two other methods were based on site specific data (10 m wind speed, net radiation, solar radiation and 2 to 10 m temperature gradient). Compared to the on-site methods, the STAR method over predicted Class D and under predicted Class E conditions. The Bowen *et al* method, compared to the other methods, over predicted Classes B and C conditions and under predicted Class D conditions.

Table 8.9 compares the on-site stability class determination methods with those from the airport. The Williamson and Krenmayer and STAR methods agree on the stability class 49.1% of the time. The two methods are within ± one stability class 87.7% of the time. The Bowen *et al* and STAR methods agree on the stability class 51.3% of the time. The two methods are within ±one stability class 90.4% of the time.

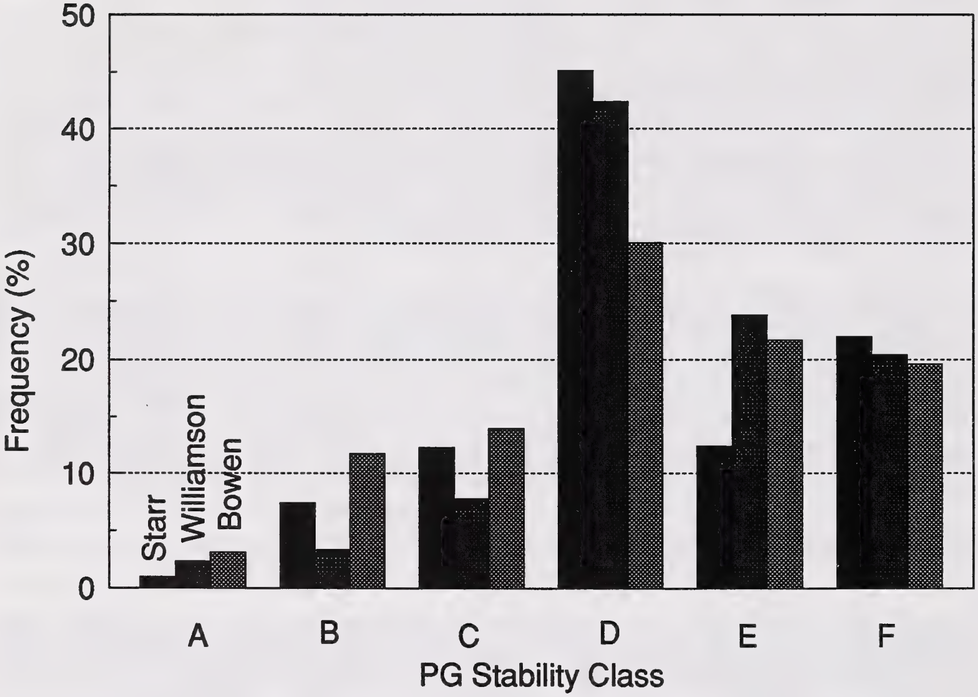

Figure 8.33

Frequency Distribution of Predicted PG Classes Using Calgary Airport and Field Measurement Program Data.

Table 8.9

Comparison of Stability Classes determined by Various Methods (Frequency in %).

(N = 15 657)

Williamson and Krenmayer PG Class	Airport STAR PG Class					
	A	B	C	D	E	F
A	0.5	1.3	0.4	0.1	0.0	0.0
B	0.2	1.7	1.0	0.4	0.0	0.0
C	0.2	1.8	2.9	2.9	0.1	0.0
D	0.1	2.3	6.5	27.9	2.7	2.7
E	0.0	0.1	0.6	9.0	5.4	8.8
F	0.0	0.3	0.6	4.4	4.4	10.7

(N = 15 673)

Bowen *et al* PG Class	Airport STAR PG Class					
	A	B	C	D	E	F
A	0.6	1.6	0.7	0.3	0.0	0.0
B	0.4	3.5	4.3	2.9	0.3	0.3
C	0.0	1.5	4.2	7.3	0.5	0.5
D	0.0	0.4	1.7	22.2	2.7	3.0
E	0.0	0.1	0.6	7.6	5.1	8.2
F	0.0	0.3	0.7	4.4	3.8	10.3

8.5.2 Pasquill - Gifford Stability Class Versus Meteorology Parameters

Selected meteorological observations, direct turbulence measurements and stability indicators were compared for the ability to delineate the PG classes as defined by the airport observations:

Meteorological Observations

- Wind Speed (U),
- Potential temperature gradient ($\partial\theta/\partial Z$),
- Net radiation (Q_{net}), and
- Heat Flux (H_o).

Direct Turbulence Measurements

- Standard deviation of lateral wind speed (σ_V),
- Standard deviation of vertical wind speed (σ_W),
- Standard deviation of wind direction (σ_θ), and
- Standard deviation of vertical wind angle (σ_ϕ).

Stability Indicators

- Gradient Richardson Number (R_g),
- Bulk Richardson Number (R_b),
- Monin-Obukhov Stability Parameter (Z/L), and
- Kazanski-Monin Length (KM).

The basis for all the above parameters is the 10 m level wind data. For $\partial\theta/\partial Z$, the gradient is taken over the 2 to 10 m level. The cumulative frequency distributions for the above parameters were plotted for each PG stability derived from the airport observations using the Turner STAR, Williamson and Krenmayer and Bowen *et al* methods. The delineation ability will depend on the orderly separation of the cumulative frequency distributions with either increasing or decreasing stability, the separation of the frequency distributions and the steepness of the slope of the frequency distribution.

Figure 8.34 shows the cumulative frequency distributions for the meteorological observations (U, $\partial\theta/\partial Z$, Q_{net} and H_o). The results are:

- The wind speed (U) method is unable to differentiate between stable and unstable conditions. The frequency distributions indicate that high wind speeds tend to be associated with stability class D.

- The potential temperature gradient ($\partial\theta/\partial Z$) method provides a good separation between unstable and stable conditions but is unable to clearly distinguish the difference between the individual unstable classes. The stable cases appear to be well delineated for the STAR classifiction.

- The net radiation (Q_{net}) method provides a good separation between unstable and stable conditions but is unable to distinguish between the individual stable classes.
- The heat flux (H_o) method provides a clear separation between unstable and other conditions but is unable to distinguish between the classes for neutral and stable conditions.

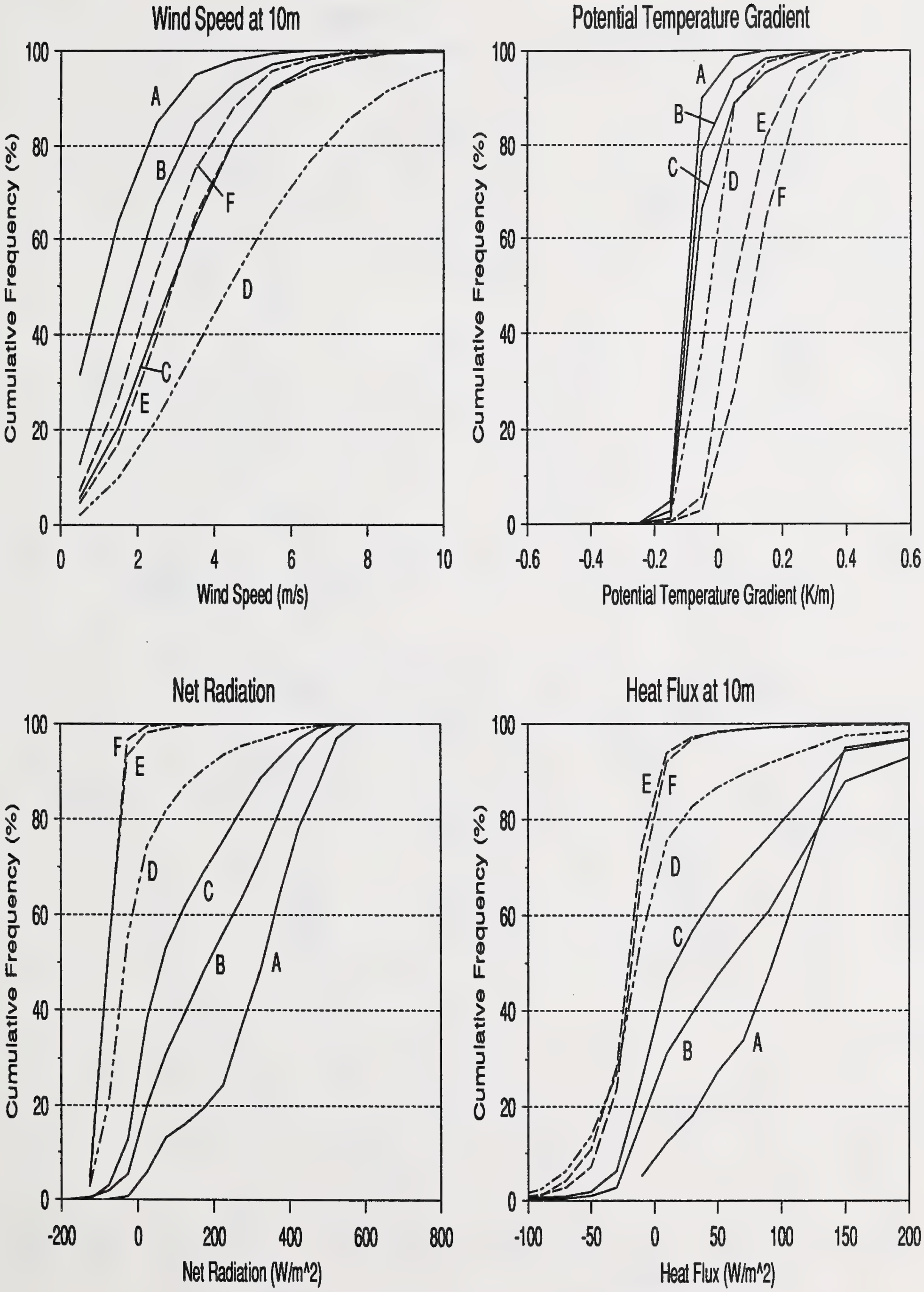

Figure 8.34 STAR

Cumulative Frequency Distribution of U, $\partial T/\partial Z$, Q_{net} and H_o as a Function of the STAR PG Stability Class.

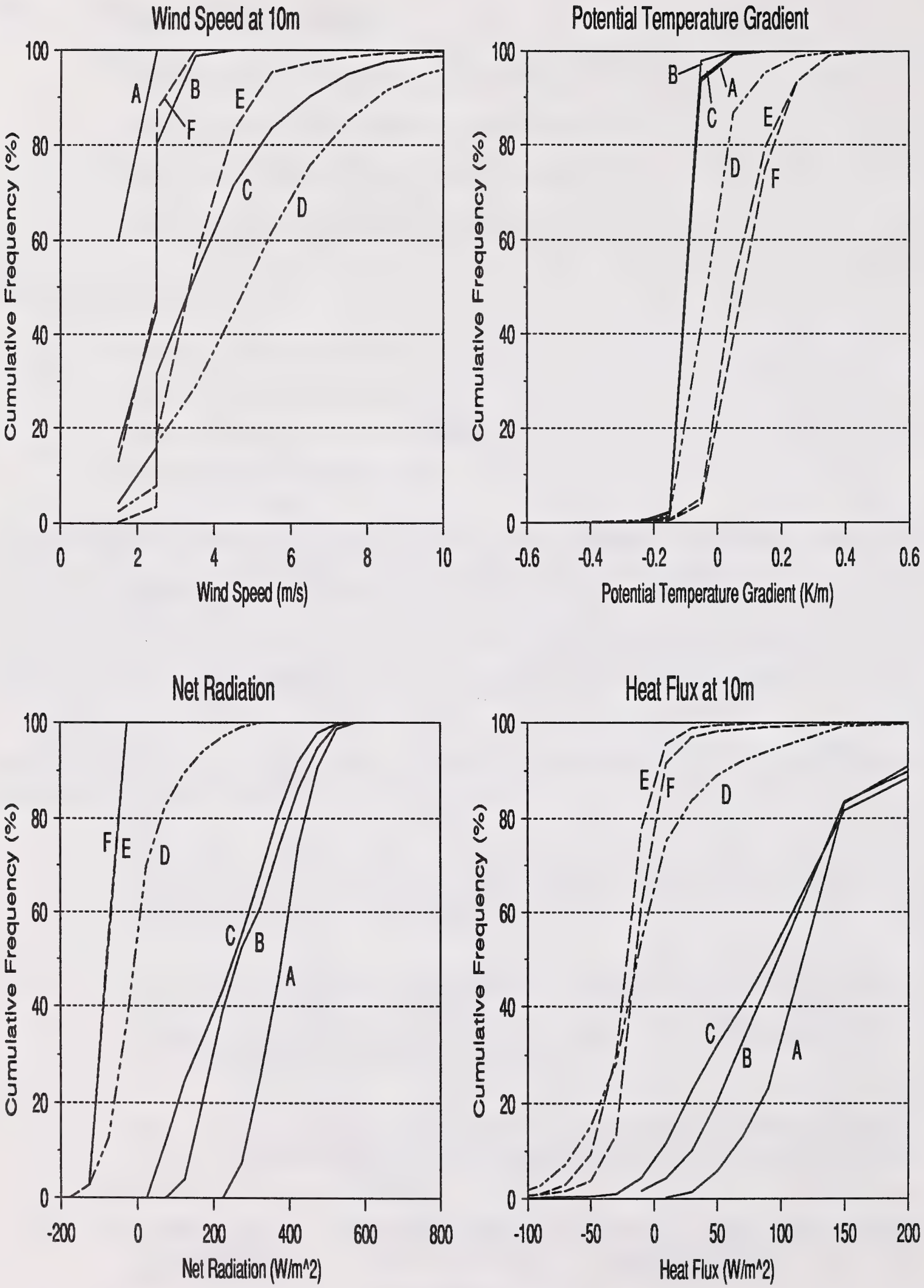
Wind Speed at 10m

Potential Temperature Gradient

Net Radiation

Heat Flux at 10m

Figure 8.34 Williamson and Krenmayer

Cumulative Frequency Distribution of U, $\partial T/\partial Z$, Q_{net} and H_o as a Function of the Williamson and Krenmayer PG Stability Class.

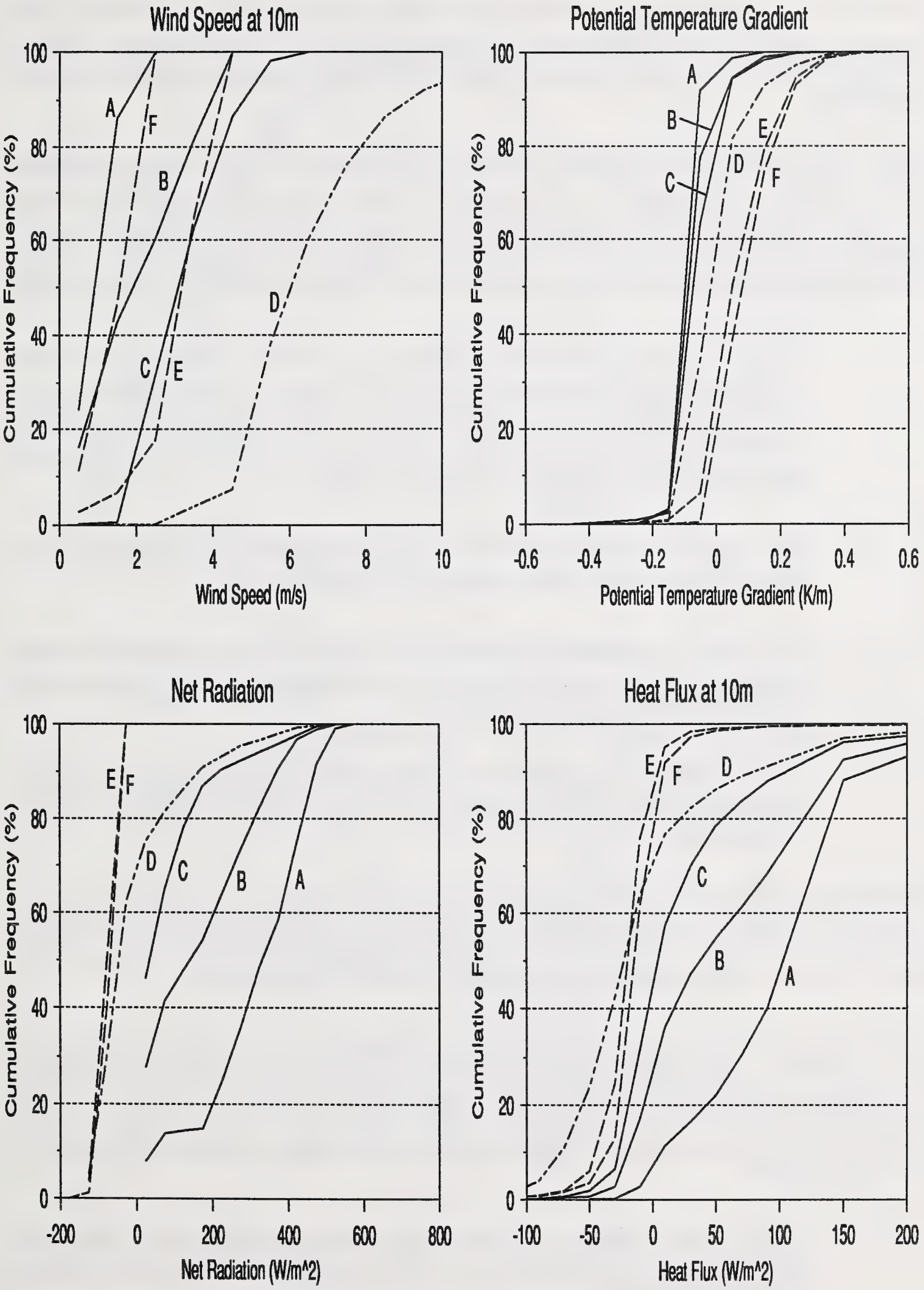
Wind Speed at 10m

Potential Temperature Gradient

Net Radiation

Heat Flux at 10m

Figure 8.34 Bowen *et al*

Cumulative Frequency Distribution of U, $\partial T/\partial Z$, Q_{net} and H_o as a Function of the Bowen PG Stability Class.

Collectively U, $\partial\theta/\partial Z$ and Q_{net} were used to define the PG class. Individually, these parameters fail to delineate the classes. The $\partial\theta/\partial Z$ method is a commonly used indicator (U.S. N.R.C. 1974). The method appears to determine only the presence of stable or unstable conditions.

Figure 8.35 shows the cumulative frequency distributions for the direct turbulence measurements (σ_V, σ_W, σ_θ and σ_ϕ). The standard deviations σ_V and σ_W are direct measures of turbulence and the standard deviations σ_θ and σ_ϕ are measures of turbulence intensity. Intuitively, one would expect that the standard deviations would be small for stable atmospheres and increase with increasing instability. The results from the figure indicate:

- The lateral wind standard deviation (σ_V) method indicates an orderly progression in delineating the STAR PG classes. For the Williamson and Krenmayer classes, the σ_V method fails to distinguish between individual unstable classes. For the Bowen *et al* classes, the σ_V method fails to distinguish between individual unstable and neutral classes.

- The vertical wind standard deviation (σ_W) method fails to distinguish between the individual unstable and neutral classes for all methods.

- The lateral and standard deviation (σ_θ) method fails to distinguish between stable and neutral classes. For the two on-site methods there is considerable overlap between Classes C and F.

- The vertical wind standard deviation (σ_ϕ) method indicates a somewhat orderly delineation except for some difficulty in distinguishing between individual stable classes.

The purpose of the PG class is to delineate atmospheric turbulence in terms of the impact on plume behavior. As the standard deviations of the winds can be related directly to atmospheric turbulence, the inability of the standard deviations to clearly correspond to a given PG class is not a reassuring confirmation of the PG class definition.

Figure 8.36 shows the cumulative frequency distributions for the stability indicators (R_g, R_b, Z/L and KM). The selected stability indicators have been used as alternate measures of delineating atmospheric turbulence. They recognize the contribution of both thermal and mechanical processes to atmospheric turbulence. Unlike the PG classes, these stability indicators classify turbulence as a continuous rather than a discrete variable. The results in the figure indicate:

- The Gradient Richardson Number (R_g) method appears to show a reasonably good delineation among stability classes B through to F. The stability class A is almost off the scale.

- The Bulk Richardson Number (R_b) method shows good delineation for all stability classes for the STAR PG classes and the Williamson and Krenmayer PG classes. For the Bowen PG classes, there is poor differentiation between Class C and D.

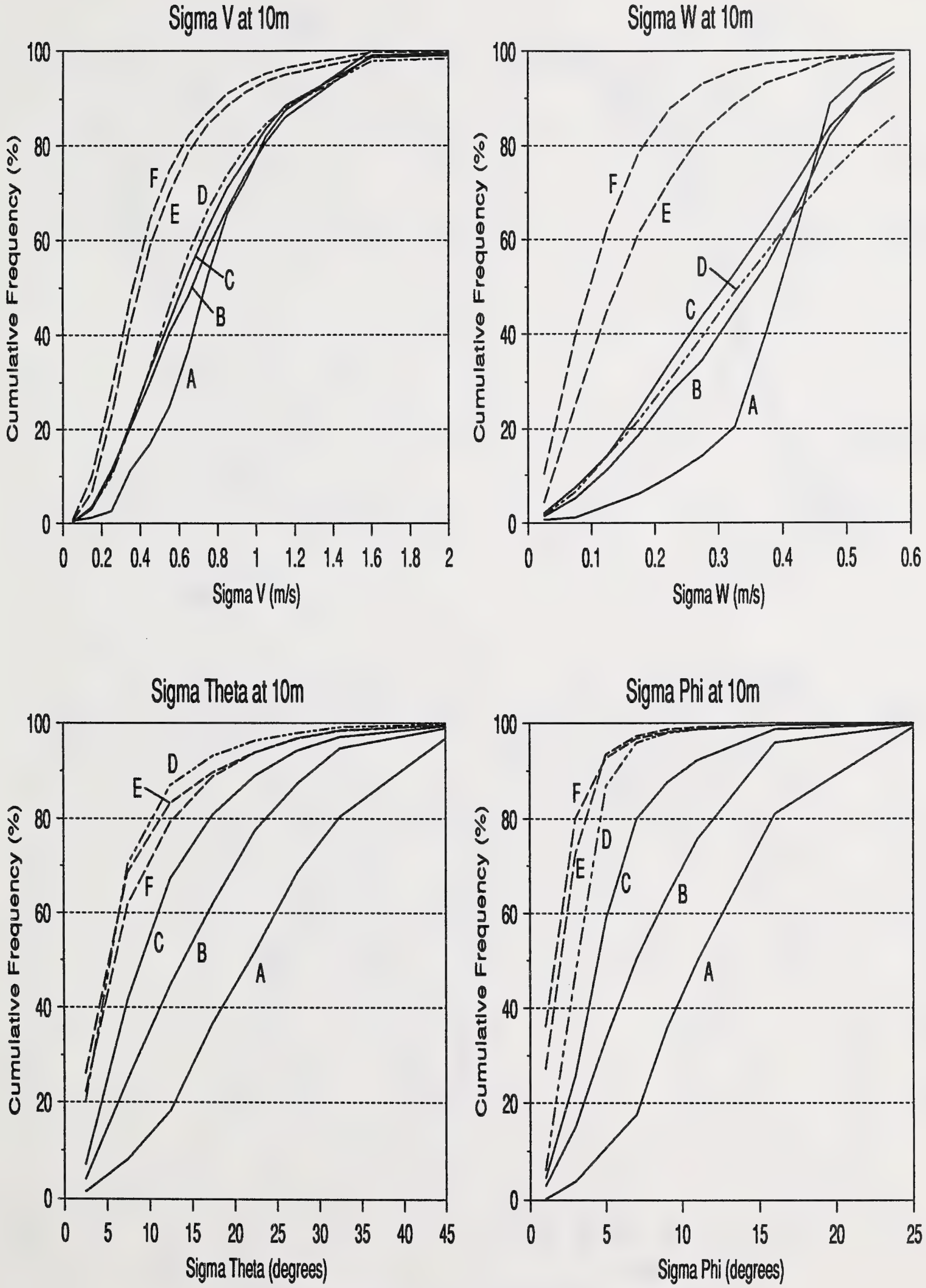

Figure 8.35 STAR

Cumulative Frequency Distribution of σ_V, σ_W, σ_θ, σ_ϕ as a Function of the STAR PG Stability Class.

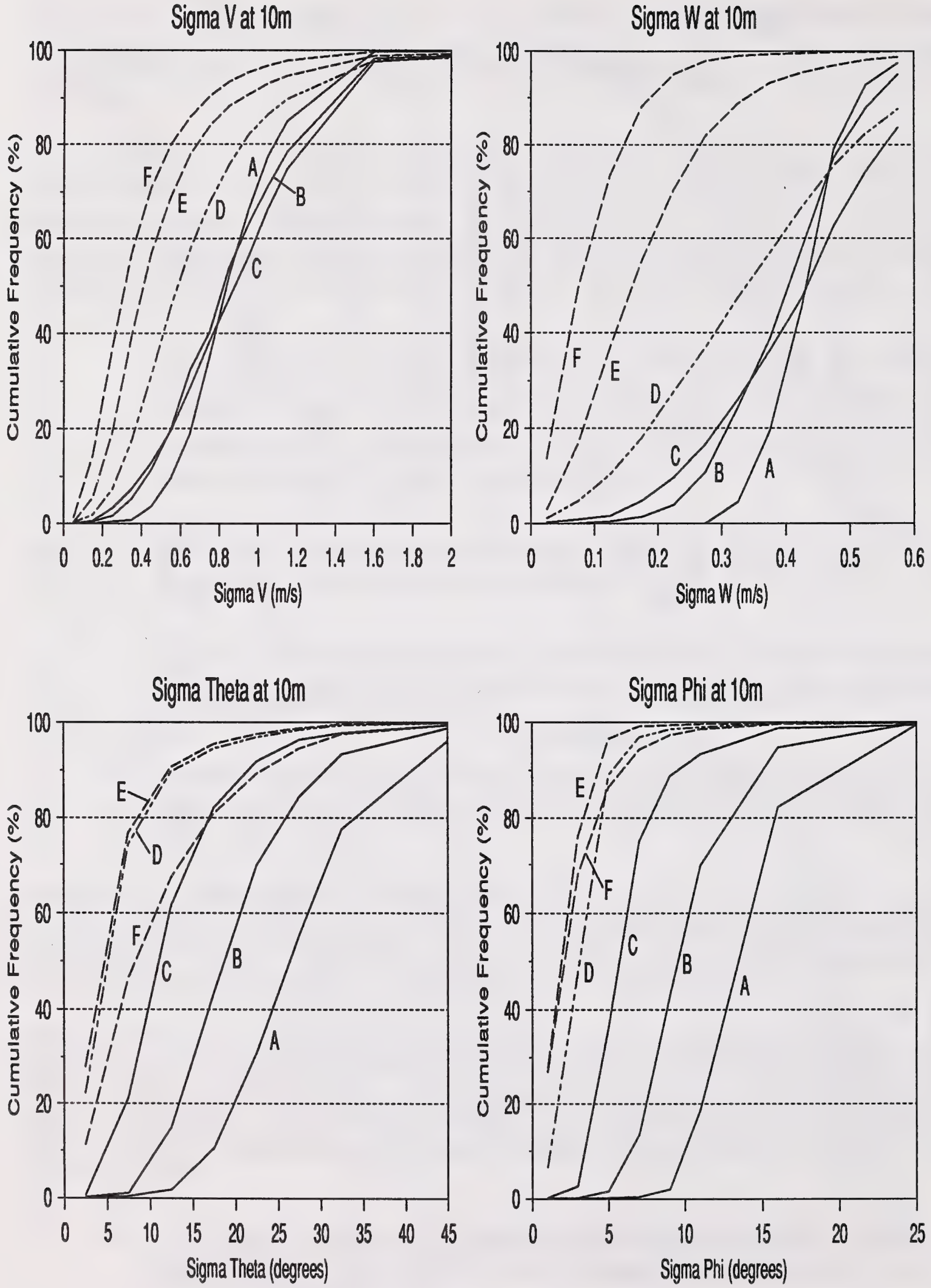

Figure 8.35 Williamson and Krenmayer

Cumulative Frequency Distribution of σ_V, σ_W, σ_θ, σ_ϕ as a Function of the Williamson and Krenmayer PG Stability Class.

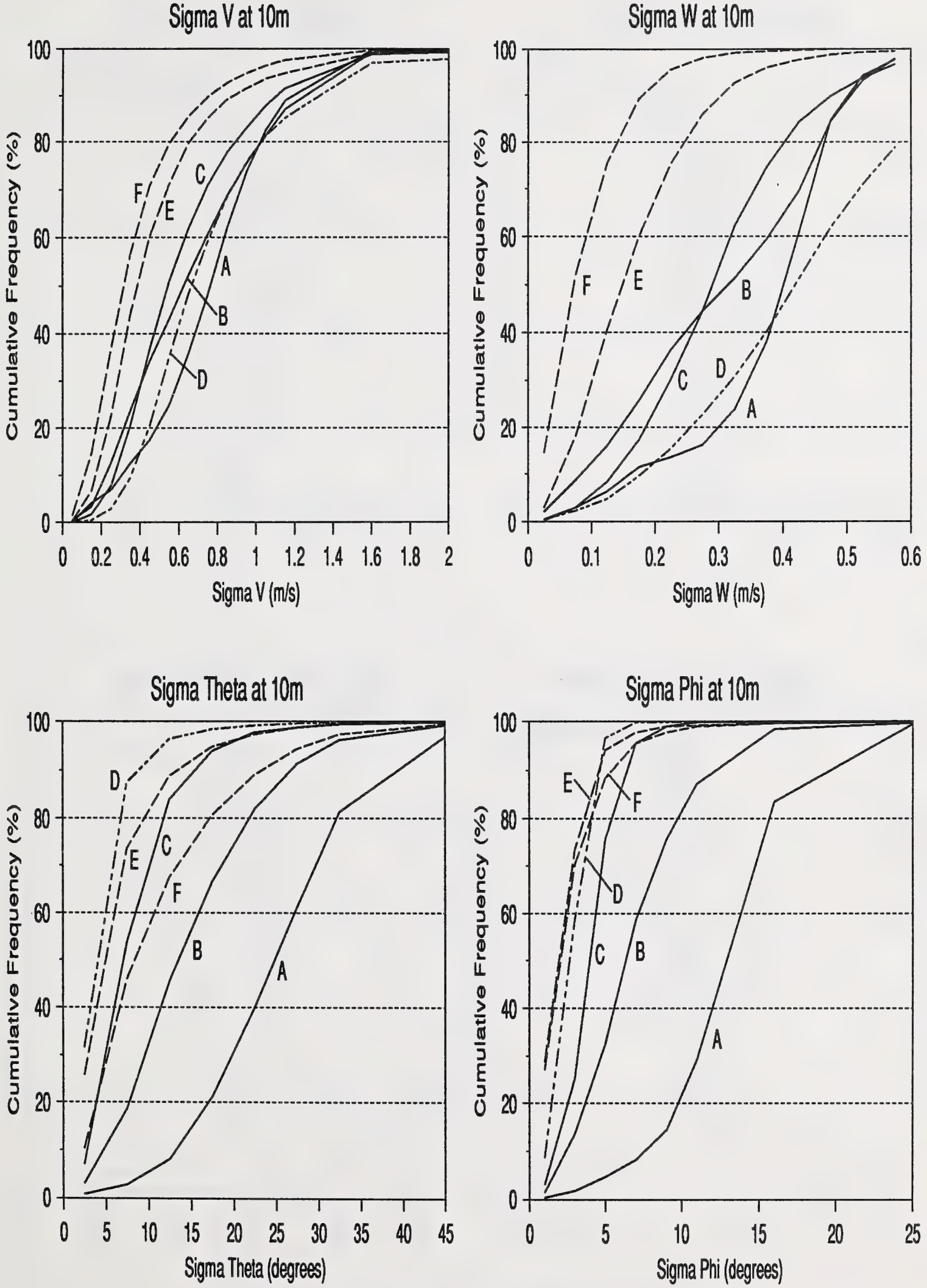
Sigma V at 10m

Sigma W at 10m

Sigma Theta at 10m

Sigma Phi at 10m

Figure 8.35 Bowen *et al*

Cumulative Frequency Distribution of σ_V, σ_W, σ_θ, σ_ϕ as a Function of the Bowen *et al* PG Stability Class.

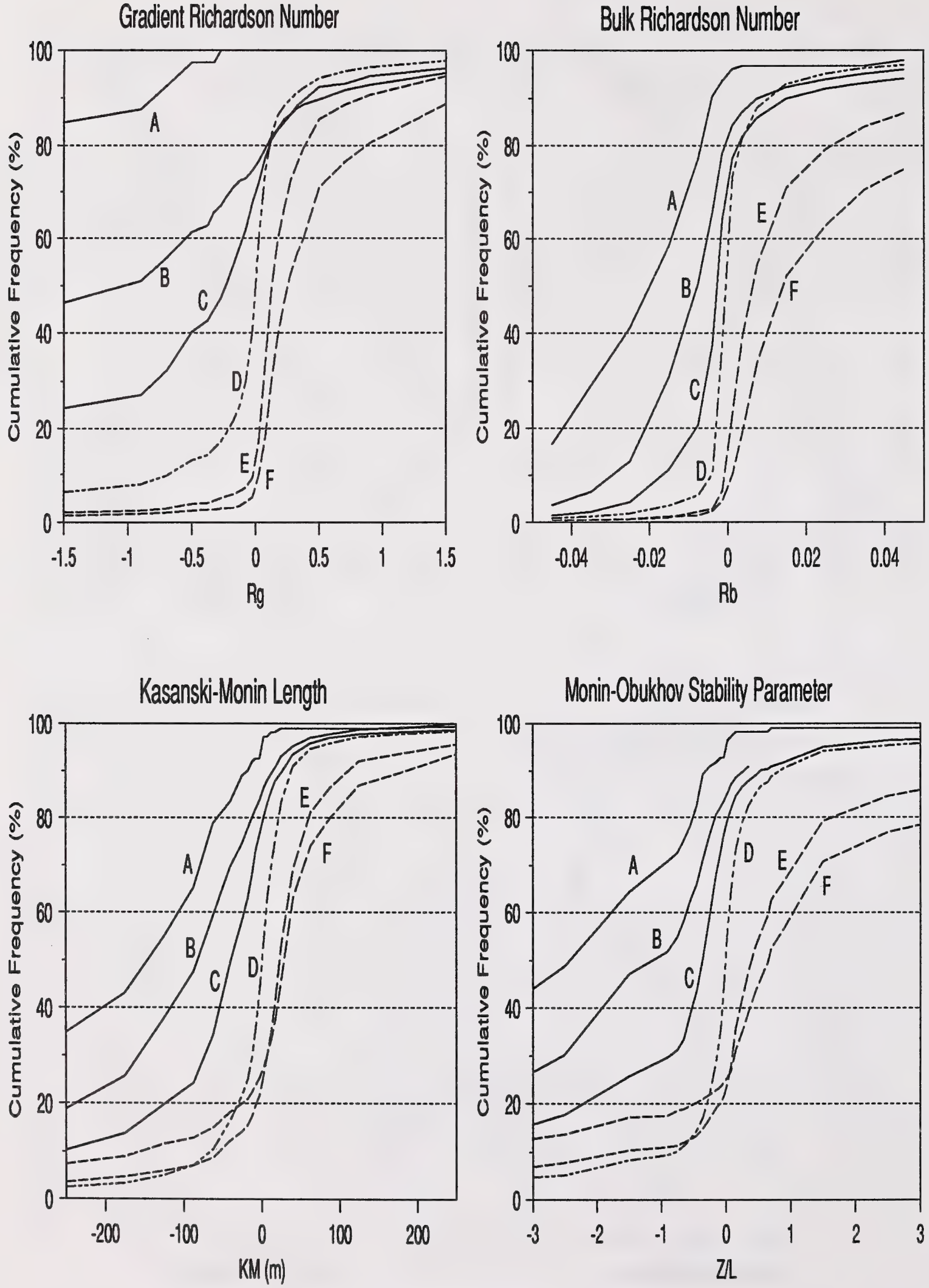

Gradient Richardson Number

Bulk Richardson Number

Kasanski-Monin Length

Monin-Obukhov Stability Parameter

Figure 8.36 STAR

Cumulative Frequency Distribution of R_g, R_b, Z/L and KM as a Function of the STAR PG Stability Class.

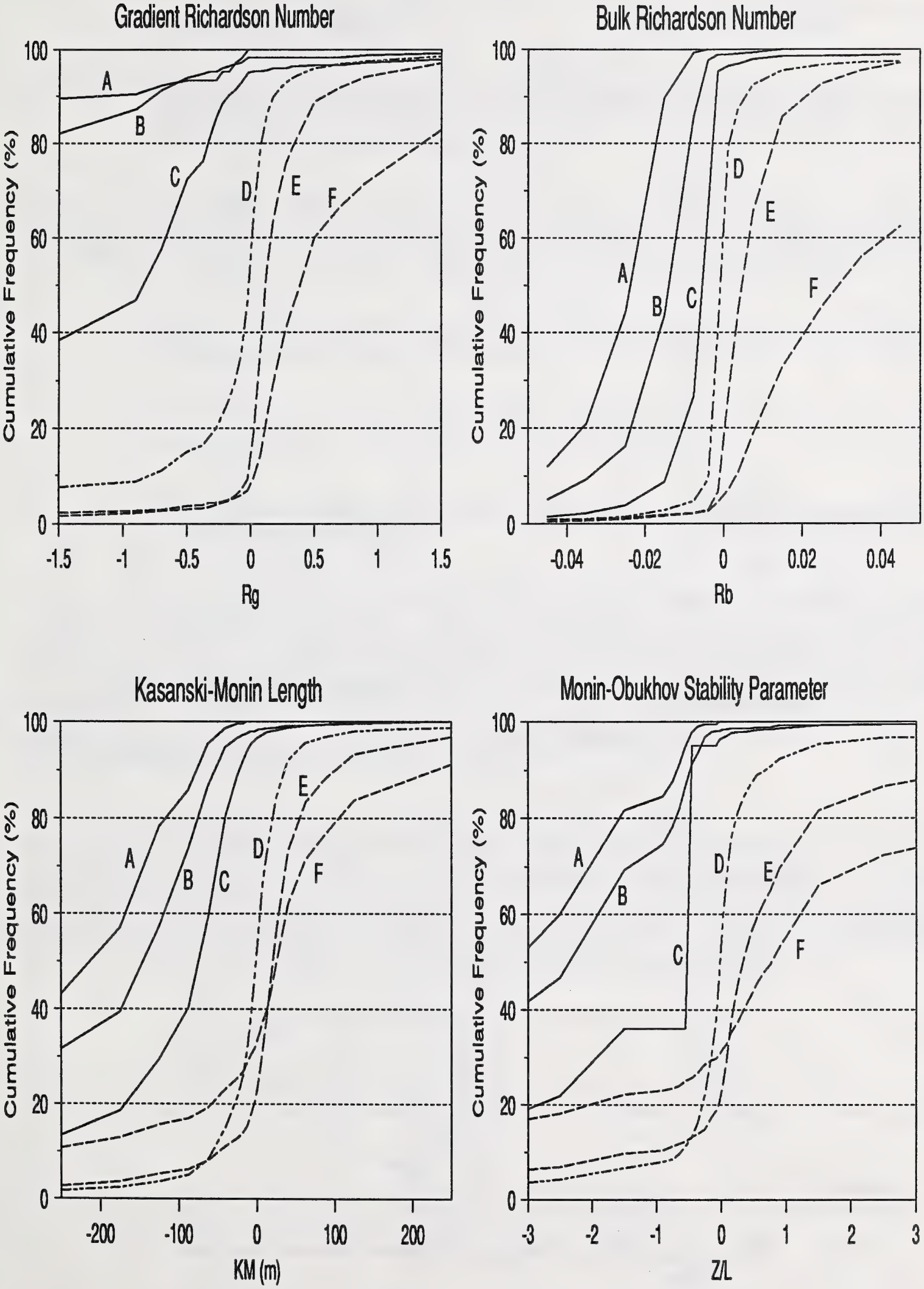
Gradient Richardson Number

Bulk Richardson Number

Kasanski-Monin Length

Monin-Obukhov Stability Parameter

Figure 8.36 Williamson and Krenmayer

Cumulative Frequency Distribution of R_g, R_b, Z/L and KM as a Function of the Williamson and Krenmayer PG Stability Class.

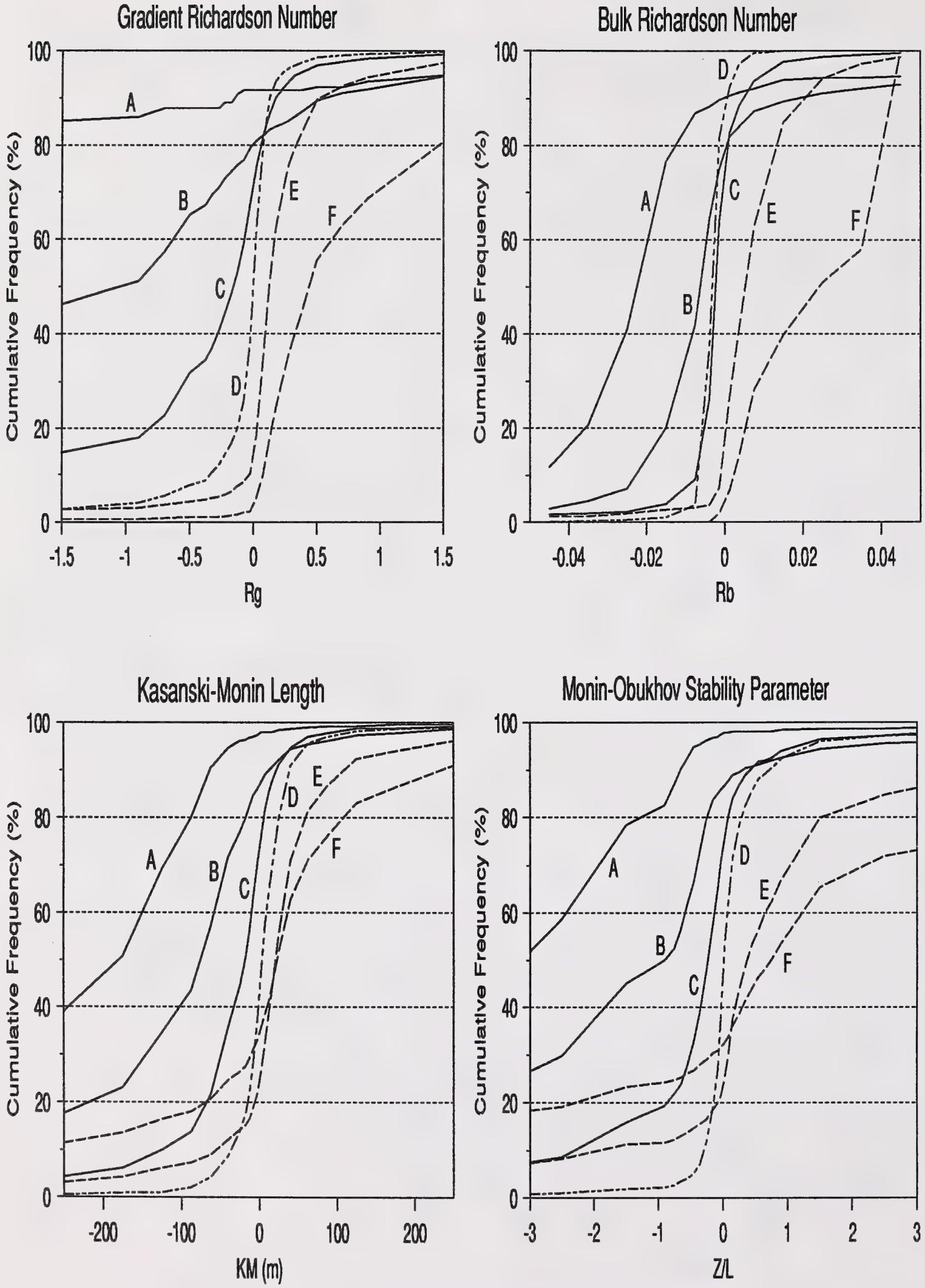
Gradient Richardson Number

Bulk Richardson Number

Kasanski-Monin Length

Monin-Obukhov Stability Parameter

Figure 8.36 Bowen *et al*

Cumulative Frequency Distribution of R_g, R_b, Z/L and KM as a Function of the Bowen PG *et al* Stability Class.

- The Monin-Obukhov stability parameter (*Z/L*) method shows good delineation for all stability classes.

- The Kazanski-Monin Length (*KM*) method shows good delineation for unstable and neutral conditions (Classes A through D). The method does not delineate the two stable classes (E and F) very well.

The Gradient Richardson Number, the bulk Richardson Number and the Monin-Obukhov stability parameter appear to provide a reasonable delineation of PG stability classes. In summary, conclusions concerning the delineation of the PG classes are as follows:

- Individually, one given meteorological parameter is generally not sufficient to estimate the occurrence of PG classes.

- The PG classes do not clearly delineate observed turbulence levels in the atmosphere.

- The selected stability indications have varying degrees of success in the prediction of the PG class.

The information presented in this section can be used to provide the basis for alternate methods of delineating the PG class when such a classification scheme is required by regulating models. Any differences between the selected stability parameters and a given PG class may be as much the fault of the PG class scheme as the limited ability of that parameter.

8.5.3 Stability Class Based on σ_θ andσ_ϕ

Selected meteorological parameters and stability indicators have been used to determine an appropriate PG class. Since it is intuitively believed that the turbulence intensities (σ_θ andσ_ϕ) are directly related to the spread of a plume, it is useful to evaluate the ability of selected stability indicators to delineate turbulence intensity classes. Specifically, turbulence intensity classes were arbitrarily defined by the following ranges (degrees):

Class	σ_θ	σ_ϕ
1	0 to 4	0 to 2
2	4 to 6	2 to 3
3	6 to 8	3 to 4
4	8 to 10	4 to 5
5	10 to 14	5 to 6
6	14+	6+

The selected stability indicators include Gradient Richardson Number (R_g), Monin-Obukhov stability parameter (*Z/L*) and the Kazanski-Monin Length (*KM*). The cumulative frequency distribution method given was used to evaluate the delineation ability. The results for σ_θ are presented in Figure 8.37 as a function of R_g, *Z/L* and *KM*. The results indicate:

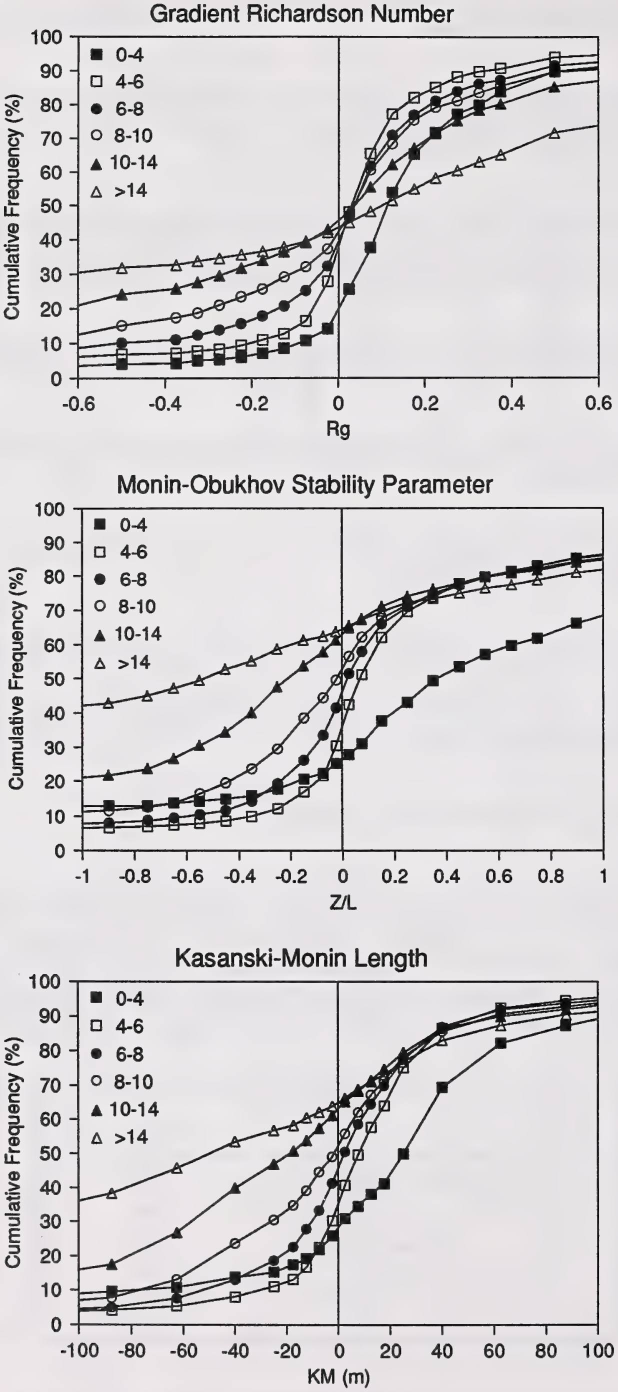

Figure 8.37

Cumulative Frequency Distribution of R_g, Z/L and KM for Selected σ_θ Classes.

- The R_g method fails to delineate the σ_θ classes.
- The Z/L method provides an orderly separation of σ_θ classes.
- The KM method also results in an orderly separation of σ_θ classes.

The median Z/L and KM distributions provide and orderly separation of the specified σ_θ classes. The shallow slopes associated with the large σ_θ values indicate that large σ_θ values can be associated with stable as well as unstable conditions.

The results for σ_ϕ are presented in Figure 8.38 as a function of R_g, Z/L and KM. The results indicate:

- The R_g method provides an orderly separation of σ_ϕ classes.
- The Z/L method also provides an orderly separation of σ_ϕ classes.
- The KM method results are similar to the Z/L method results except for σ_ϕ values less than 4 degrees.

The good delineation for σ_ϕ values is comforting and suggests that selected stability parameters can be used to delineate σ_ϕ classes. The Gradient Richardson Number appears to be qualitatively the best stability indicator.

8.5.4 Observed Heat Flux

The alternate meteorological preprocessors discussed at the introduction of Section 8.5 are based on heat flux. The sensible heat flux, H_o, is the heat directly resulting on the temperature change of the air. If the heat flux is positive, heat is being transferred to the air and the air heats up producing unstable or convective conditions. If the heat flux is negative, the air cools down producing stable conditions.

Two methods have been used to estimate the sensible heat flux. The first is based on the eddy correlation method in which:

$$H_o = -C_{p_a} \rho_a \overline{W'T'}$$

This method has been used in this report and $\overline{W'T'}$ values were based on the sonic anemometer measurements. The reported accuracy of this method is ±10% although the uncertainty may be larger for stable conditions (Strimaitis *et al* 1980).

An alternative method which has been used by various investigators is based on the energy budget method. The heat balance at the surface of the earth is given by:

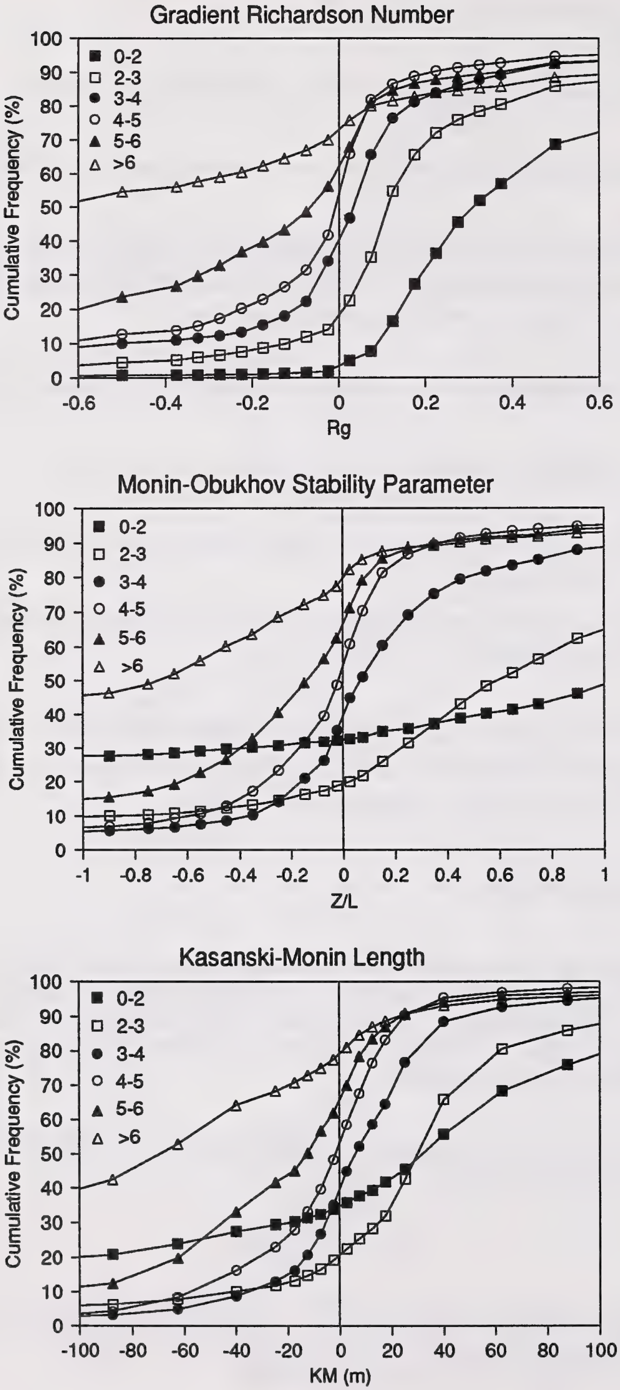

Figure 8.38

Cumulative Frequency Distribution of R_g, Z/L and KM for Selected σ_ϕ Classes.

$$Q_{net} = H_o + LE + G$$

where Q_{net} = net all wave radiation received by the ground,
H_o = sensible heat flux,
LE = latent heat flux which is the equivalent heat exchange that occurs from the evaporation or condensation of water at the surface, and
G = ground heat flux which results in a temperature change to the ground.

The heat flux estimated from the budget method is given by:

$$H_o = Q_{net} - LE - G$$

The uncertainty of this method has been quoted as ±20% (Strimaitis *et al* 1980). For the Field Measurement Program Q_{net} and G were measured directly using the net pyradiometer and soil heat flux plates, respectively. The latent heat was not measured and had to be modelled. Table 8.10 outlines a method for estimating the latent heat flux (*LE*).

Figure 8.39 shows the median net radiation, soil heat flux and latent heat flux as a function of time of day for the winter and summer seasons. The latent heat flux is shown for dry grass ($\alpha = 0.5$) and a wet grass ($\alpha = 1.0$) surfaces. There are a number of features respecting the curves in the figure.

- The soil heat flux for the summer is about 10% of the net radiation. This is consistent with the assumption incorporated into the preprocessor METPRO (Paine 1988).

- The net radiation at night is relatively constant for the two seasons shown ($Q_{net} \approx$-40 to -50 W/m^2). This is consistent with values measured by others (van Ulden and Holtslag 1985).

- The net radiation during the day is much different for the two seasons due to solar elevation. The median peak winter and summer values are 45 and 350 MW/m^3, respectively.

- For wet grass surfaces, the latent heat can be up to 70% of the net radiation for the summer months. For dry grass surfaces, the percentages falls to 35%.

The diurnal variation and magnitude of the various energy fluxes for the summer months are consistent with those reported by others (van Ulden and Holtslag 1985). Some uncertainty in the winter values is expected because the sublimation process would replace the evaporation processes which were assumed in the estimation of the latent heat.

Figure 8.40 compares the heat fluxes calculated using the eddy correlation method ($H_o = C_{pa} \rho_a \overline{W'T'}$) with those calculated using the energy budget method ($H_o = Q_{(net)} - LE - G$). The eddy correlation method was based on the four sonic anemometers located at heights of 4, 10, 16 and 25 m. The eddy budget methods show the

Table 8.10

Method for Determining Latent Heat Flux.

From Holtslag and van Ulden (1983), the latent heat flux (*LE*) can be estimated from:

$$LE = \alpha\left[\frac{1}{1+(\gamma/S)}(Q_{net}-G)+20\right]$$

where $\alpha =$ empirical surface moisture factor
($\alpha = 0$ for bare dry soil;
$\alpha = 0.5$ for a dry grass surface;
$\alpha = 1.0$ for a wet grass surface)

$\gamma = C_p/\lambda$
$C_p =$ specific heat of air at constant pressure (997 J/(kg K))
$\lambda =$ latent heat of water vaporization ($2.5 \cdot 10^6$ J/kg)

$Q_{net} =$ net radiation flux (W/m^2)

$G =$ ground heat flux (W/m^2)

$S = \partial e_s/\partial T$ (Pa/K)
$e_s =$ saturation vapour pressure (Pa)

The slope factor *S* can be calculated from the Clausius Clapeyron equation:

$$S = \frac{\partial e_s}{\partial T} = \frac{\lambda e_s}{R_v T}$$

where $T =$ ambient temperature (K)
$R_v =$ specific gas constant for water vapour (461 J/(kg K))
$e_s =$ saturation vapour pressure (Pa)

The saturation vapour pressure can be estimated from Magnus' formula:

$$e_s = 100[10^{(-2937.4/T - 4.9283\log T + 23.5518)}]$$

The above relationships are applicable to the evaporation (liquid to gas phase) rather than sublimination (solid to gas phase) process. The sublimination process, which can be significant in the Calgary area during chinook conditions, was not considered for this evaluation.

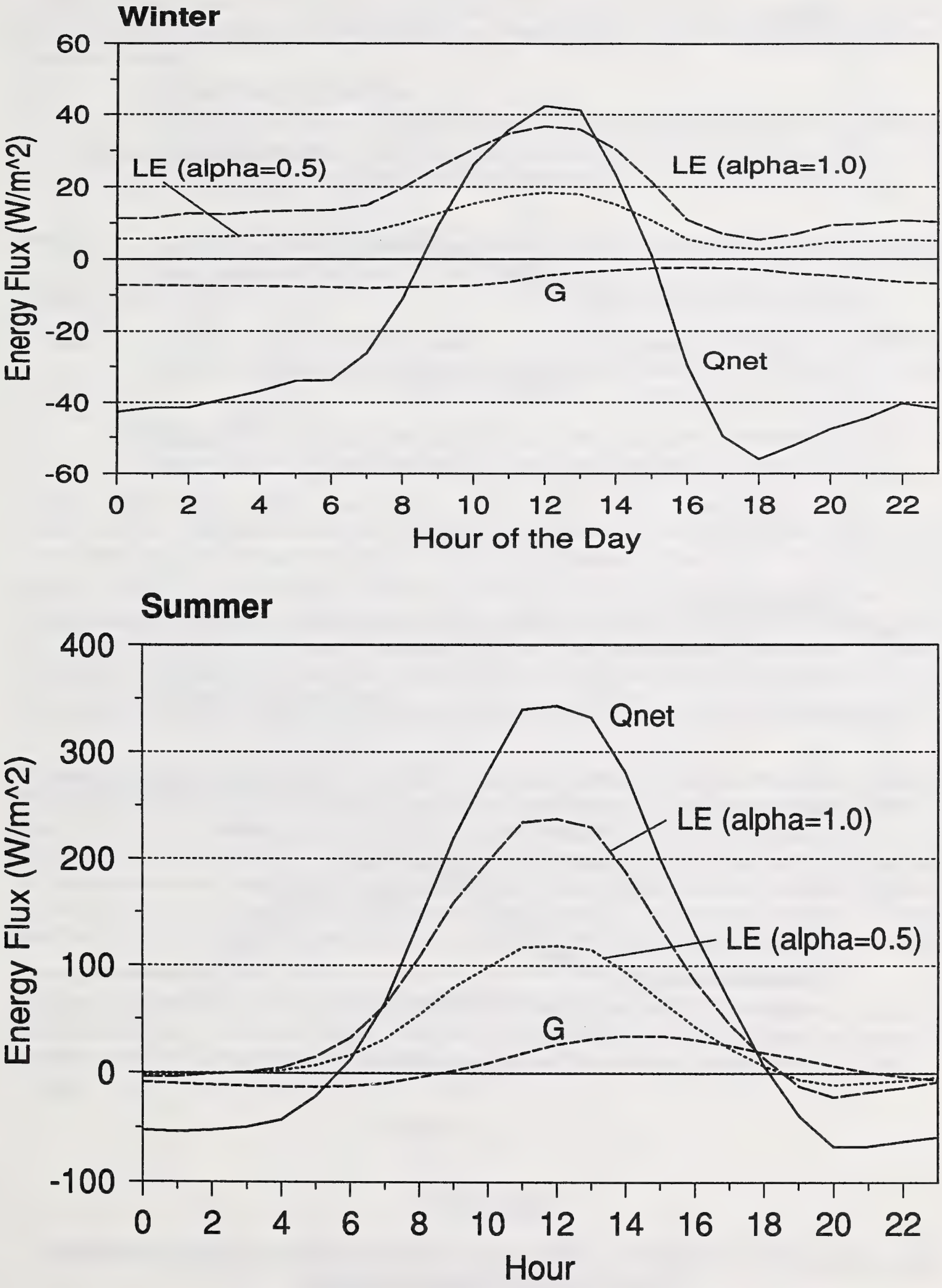

Figure 8.39

Median Observed Net Radiation (Q_{net}) Soil Heat Flux (*G*) and Calculated Latent Heat Flux (LE) for Wet Grass ($\alpha = 1.0$) and Dry Grass ($\alpha = 0.5$).

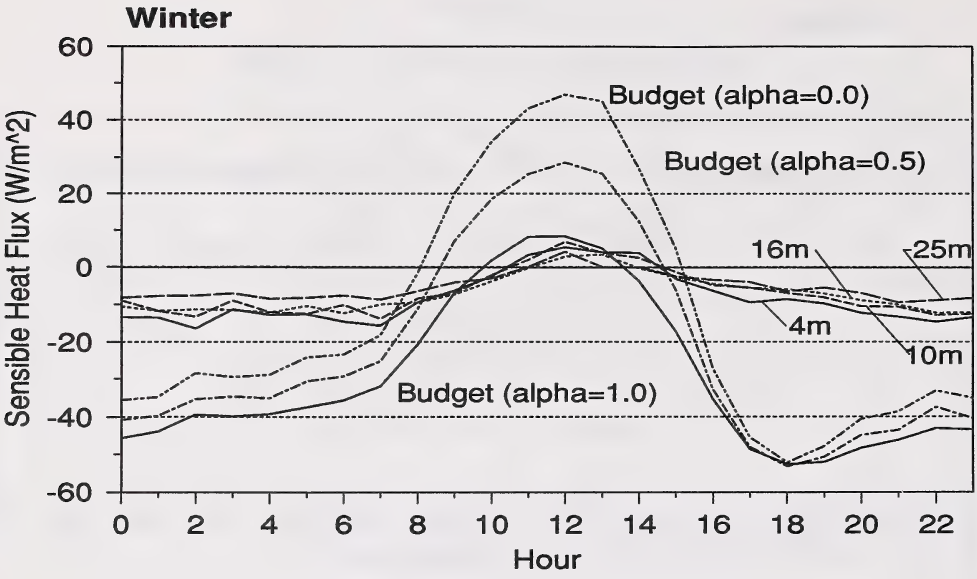

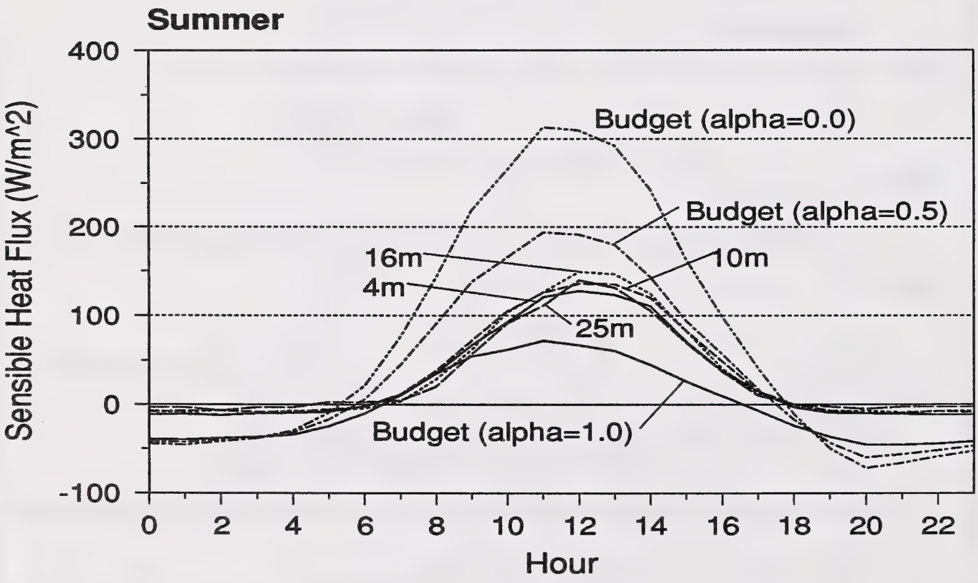

Figure 8.40

Comparison of the Sensible Heat Flux (H_o) Calculated from the Eddy Correlation and the Energy Budget Methods.

results for wet grass ($\alpha = 1.0$), dry grass ($\alpha = 0.5$) and dry bare soil ($\alpha = 0.0$). The results are shown for the winter and summer seasons. Based on the results in the figure, the following points are noted:

- During the night-time hours, the heat fluxes computed from the eddy correlation methods are much smaller in magnitude (H_o = -10 to -15 W/m^2) than those computed from the energy budget method (H_o = -30 to -50 W/m^2).

- For both seasons, the heat flux values derived from the eddy correlation method are essentially the same for all levels.

- For the winter day-time hours, the best agreement between the heat fluxes derived from the two methods is based on a value for α of 1.0 (a wet surface).

- For the summer day-time hours, the best agreement between the heat fluxes derived from the two methods is based on a value for α of about 0.75.

There is some indication that the magnitude of the heat flux values derived from the eddy correlation method are underestimated. As was discussed in Section 5.3.4, the heat flux is based on $\overline{W'T'}$, where the temperature fluctuation (T) is based on the sonic anemometer temperature. The sonic temperature can be subject to cross-wind contamination (Section 5.3.3) and may have difficulty in reflecting the true temperature fluctuation under low turbulence conditions. There was a possible factor which resulted in the difference between the determination of stable/unstable conditions using $\overline{W'T'}$ and $\partial\theta/\partial Z$ (Section 8.32).

Figure 8.41 shows the median heat flux computed from the eddy correlation method as a function of the heat flux computed from the budget method. For the estimation of the latent heat flux used in the budget method, the values assumed for α are 1.0 and 0.75 for winter and summer, respectively. The ideal agreement for the two methods could fall along the 1:1 slope shown in the figure. For positive heat fluxes, there is some sense of agreement between the two methods. For the negative heat fluxes, it is clear that the eddy correlation method limits the magnitude whereas the budget method allows fairly large negative values.

The heat fluxes derived from the budget method were compared statistically to the heat flux derived from the 10 m sonic data. Selected values assumed for the surface moisture factor (α) were 0, 0.5, 0.75 and 1.00. The regression coefficients are given below:

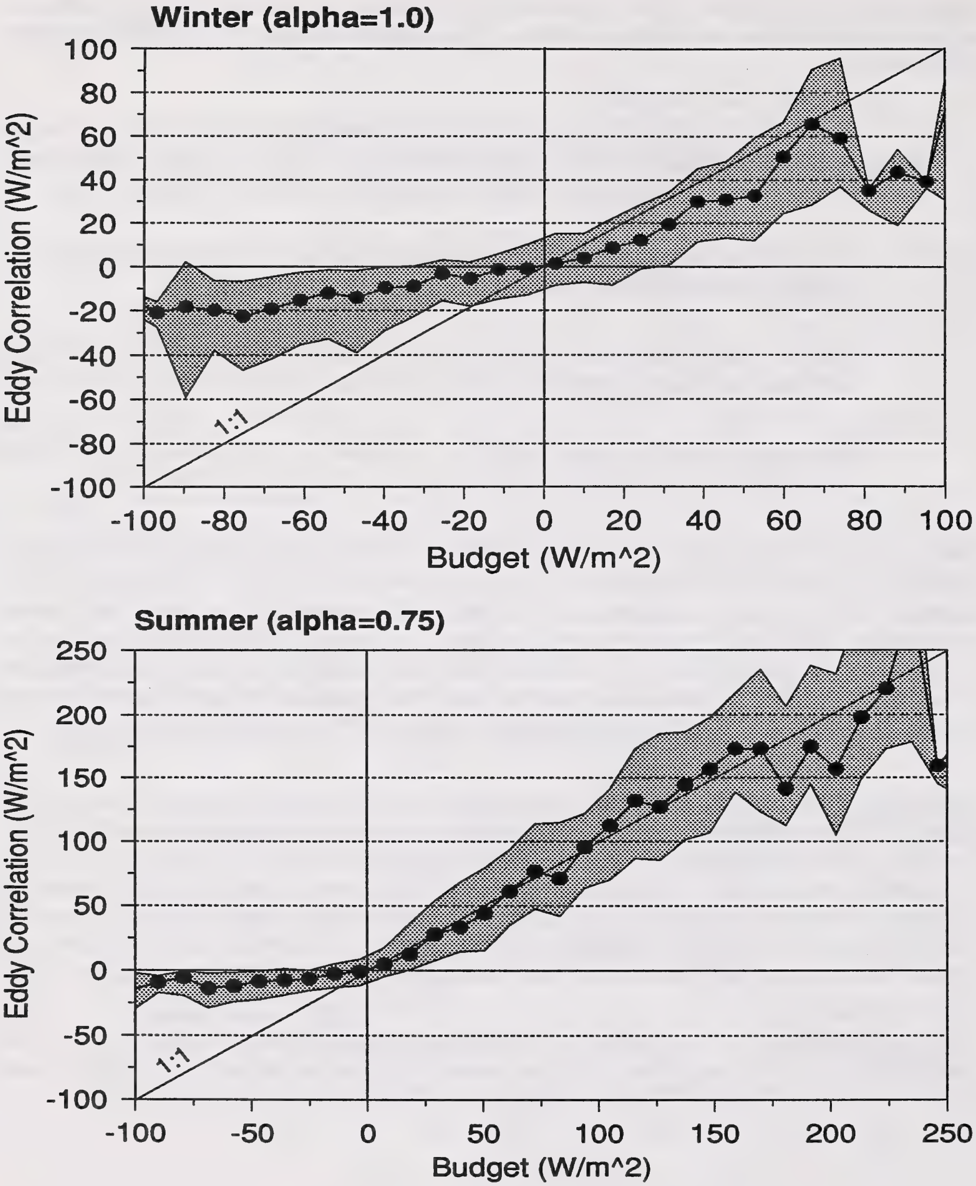

Figure 8.41

Comparison of the Heat Fluxes Predicted Using the Eddy Correlation and the Budget Methods.

	Slope	Intercept	Correlation Coefficient
Winter			
$\alpha = 0.0$	0.968	-5.3	0.51
$\alpha = 0.5$	0.738	-15.3	0.49
$\alpha = 0.75$	0.623	-20.4	0.48
$\alpha = 1.00$	0.507	-25.4	0.45
Summer			
$\alpha = 0.0$	1.609	10.8	0.82
$\alpha = 0.5$	1.050	-4.2	0.82
$\alpha = 0.75$	0.796	-1.5	0.77
$\alpha = 1.00$	0.491	-19.3	0.77

The best agreements are based on the assumption of a dry surface ($\alpha = 0$) for winter and dry grass surface ($\alpha = 0.5$) for summer. The scatter plots for these cases are shown in Figure 8.42. The basis for the best agreement considers both positive and negative heat flux values. If only positive values are considered, then the best qualitative agreement appears to be for $\alpha = 1.0$ and $\alpha = 0.75$ for winter and summer conditions, respectively (Figure 8.43).

It must be kept in mind that these discussions regarding the budget method should be regarded as a first order estimate that no attempt was made to identify the latent heat term on a short-term basis. In practice, the surface wetness factor would change on a monthly or even a daily basis. This could produce some of the scatter in the comparison between the two methods.

8.5.5 Predicted Heat Flux

The heat flux at the earth's surface may be assumed to be proportional to the net solar radiation with a correction factor for long-wave radiation loss from the ground (Scire *et al* 1984):

$$H_o = \alpha Q_{net} + H_L$$

where:

H_o = surface heat flux (W/m^2)

α = reduction factor due to surface reflectivity
= 0.00 if there is snow cover
= 0.35 otherwise

Q_{net} = net short wave solar radiation (W/m^2)

H_L = long wave heat flux from the surface (W/m^2).

The incoming solar radiation can be expressed as:

Winter

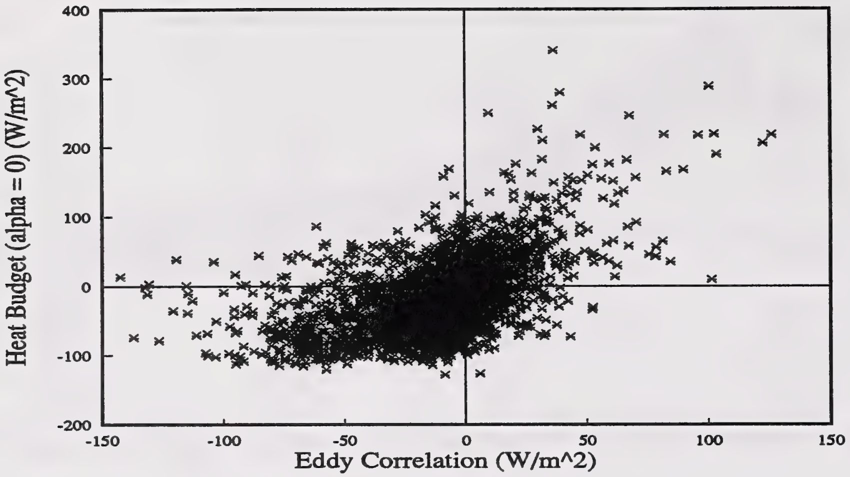

Summer

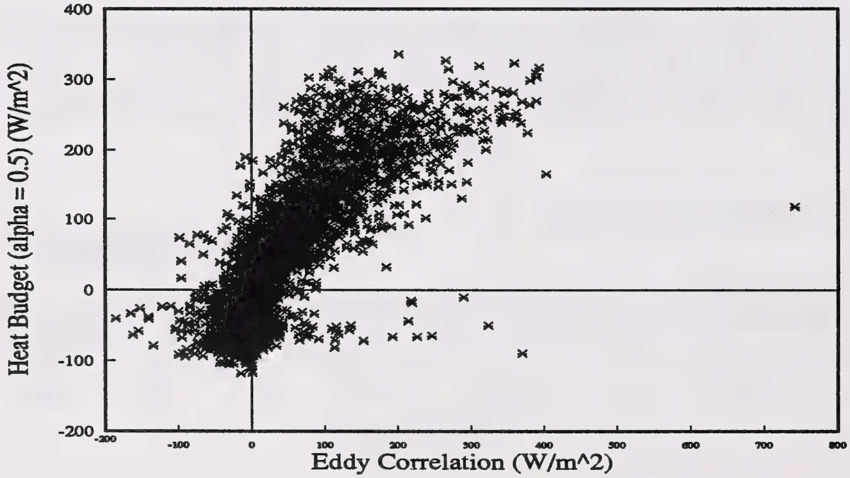

Figure 8.42

Selected Scatterplots Comparing the Energy Budget and Eddy Correlation Methods for Estimating Heat Flux.

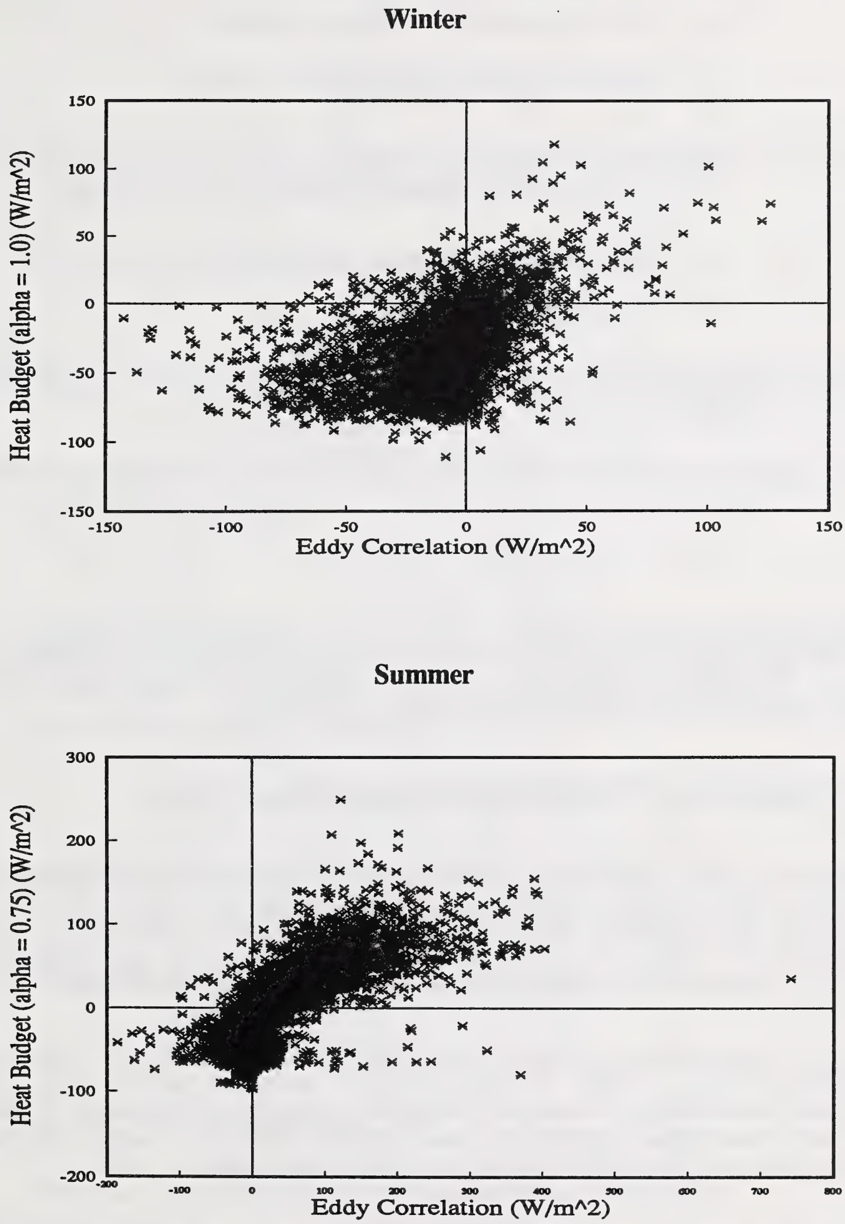

Figure 8.43

Selected Scatterplots Comparing the Energy Budget and Eddy Correlation Methods for Estimating Heat Flux.

$Q_{net} = 950\,\beta \sin\phi$ between sunrise and sunset and

$Q_{net} = 0$ between sunrise and sunset.

where: $\beta =$ reduction factor due to cloud cover
$= 1 - 0.001\,(9.54C - 0.0807C^2 - 0.000473C^3 + 0.0000110C^4$

$\phi =$ solar elevation angle above the horizon
$C =$ cloud cover in percent.

The cloud cover reduction factor (β was determined from a curve fit to data reported by Scire *et al* (1984) and Maul (1980).

The long-wave heat flux loss from the surface can be estimated from Scire *et al*, 1984):

$$H_L = 0.24(112.5 - C)$$

Sunrise and sunset times and the solar elevation angle can be estimated from the latitude and longitude of the site, the time zone standard longitude, the time of the day and the time of the year (Table 8.11). Hourly values of the snow cover can be estimated from the hourly snowing indicator and the daily snow depth values (Table 8.12).

8.5.6 Comparison of Predicted and Observed Heat Fluxes

The Scire *et al* (1980) relationships were used to predict the heat flux using Calgary airport observations. The frequency distribution of the predicted heat flux values were then compared to the frequency distribution based on the Field Measurement Program observations. The latter were based on both the eddy correlation and energy budget approaches. The results were subdivided into the winter and summer periods.

The airport observations are based on observations taken on the hour and were taken as representing an hourly average. For the purposes of comparison, the half-hourly average Field Measurement Program values were averaged to produce hourly averages. For the case of the Field Measurement Program, the data represent a true hourly average. In contrast, the airport data only represents "near instantaneous" values once every hour.

Table 8.13 compares the mean, medians and extremes associated with the predicted and Field Measurement Program based heat fluxes. For the winter period, the 95 and 5 percentile sonic based heat flux values agree most closely with the energy budget method for $\alpha = 1.0$. For the summer period, the 95 percentile sonic value agrees most closely with the energy budget method fee $\alpha = 0.5$; for the 5 percentile value, the agreement corresponds to $\alpha = 1.0$.

Table 8.11

Calculation of Solar Related Parameters

Solar Elevation Angle ϕ

(1) The sine of the solar elevation angle is given by:

$$\sin\tilde{\phi} = \cos\delta\cos\tilde{\tau}\cos L_T + \sin\delta\sin L_T$$

where:
L_T = latitude of site (e.g. 51° for Calgary) (degrees)
$\tilde{\tau}$ = hour angle (radian)
δ = solar declination (radian)

(2) The hour angle is given by:

$$\tilde{\tau} = \frac{\pi}{12}\left[t - 12 + \frac{(L_{ST} - L_O)}{15}\right]$$

where:
L_{ST} = time zone standard longitude (e.g. 105° for MST) (degrees)
L_O = longitude of site (e.g. 114° for Calgary) (degrees)

(3) The solar declination is expressed as:

$$\delta = \tan^{-1}\left[0.4348\sin\left(\frac{\pi(D-78)}{180}\right)\right]$$

where D = Julian day of the year (1 to 365)

Sunrise and Sunset Times

(1) The sunrise (t_{RISE}) and sunset (t_{SET}) times are:

$$t_{RISE} = t_N - \frac{12}{\pi}\cos^{-1}(-\tan\delta\tan L_T)$$

$$t_{SET} = t_N - \frac{12}{\pi}\cos^{-1}(-\tan\delta\tan L_T)$$

(2) where t_N = local standard noon time in decimal hours given by:

$$t_N = 12 - \left[\frac{L_{ST} - L_O}{15}\right]$$

The estimation of the above solar related parameters ignores the "Equation of Time" correction factor (Abell, 1969). This correction factor is a function of time of year and can amount to ± 15 minutes correction in the above calculated sunset and sunrise times. This correction factor is not viewed as being significant for the purposes of estimating H_O.

Table 8.12

The Determination of Hourly Snow Cover

The Atmospheric Environment Service (AES) Digital Archive contains information as to whether it is snowing during a given hour and the depth of snow on the ground for each day. With these data, it is possible to construct an algorithm for making a reasonable decision about hourly snow cover. Based on the daily observations of snow on the ground for a given day and for the previous day, four possibilities exist:

(1) The given day has snow on the ground, but the previous day did not.
(2) The given day has snow on the ground, and so did the previous day.
(3) The given day has no snow on the ground, but the previous day did.
(4) The given day has no snow on the ground, nor did the previous day.

Cases (2) and (4) are easiest to handle. If two consecutive days have snow on the ground, then it is reasonable to assume that there is snow cover for every hour of the second day. On the other hand, if two consecutive days have no snow on the ground, then it may be assumed that there is no snow cover for every hour of the second day.

Case (1) requires additional information to assess hourly snow cover. By referring to the hourly meteorological records, it is possible to find the hour during the given day when it first begins to snow. Before that time, no snow cover is assumed for every hour on the given day; after that time, snow cover is assumed for every hour on the given day.

Case (3) also requires reference to the hourly records. At some time on the given day, the snow on the ground must melt, and this time is assumed to be the hour on the given day when the maximum ambient temperature occurs. Before that hour, snow cover is assumed for every hour on the given day.

Table 8.13

Comparison of Observed and Predicted Heat Fluxes.

Winter (N = 4032)	Maximum	Mean	Minimum	95%	Median	5%
Observed						
Sonic (10m)	126	-11	-143	37	-6	-75
Budget ($\alpha = 1.0$)	118	-30	-111	34	-31	-79
Budget ($\alpha = 0.75$)	173	-27	-115	51	-27	-82
Budget ($\alpha = 0.50$)	229	-23	-119	65	-23	-88
Budget ($\alpha = 0.0$)	341	-15	-127	97	-16	-98
Predicted	187	-7	-27	79	-15	-27

Summer (N = 4986)	Maximum	Mean	Minimum	95%	Median	5%
Observed						
Sonic (10m)	741	36	-186	242	4	-51
Budget ($\alpha = 1.0$)	249	-1	-96	107	-19	-68
Budget ($\alpha = 0.75$)	273	16	-106	182	-13	-73
Budget ($\alpha = 0.50$)	336	34	-118	261	- 8	-80
Budget ($\alpha = 0.0$)	528	69	-144	417	3	-98
Predicted	267	47	-27	219	13	-27

Figure 8.44 compares the winter and summer heat flux distributions. Distributions are shown for the predicted heat fluxes and the Field Measurement Program heat fluxes based on the eddy correlation and energy budget methods. The results in the figures indicate the following:

- The predicted minimum heat flux value of -27 W/m^2 is clearly evident for both seasons. The observed minimum heat flux values are less than the -27 W/m^2.

- The eddy correlation method indicates the most frequent heat fluxes in the range of -15 to 30 W/m^2 for both seasons. This is somewhat consistent with the predicted values.

- Qualitatively the observed and predicted distributions are more similar during the summer period rather than during the winter period. This is expected due to the increased range during the summer period.

It appears that the -27 W/m^2 minimum cut-off associated with the predicted methods needs to be reassessed.

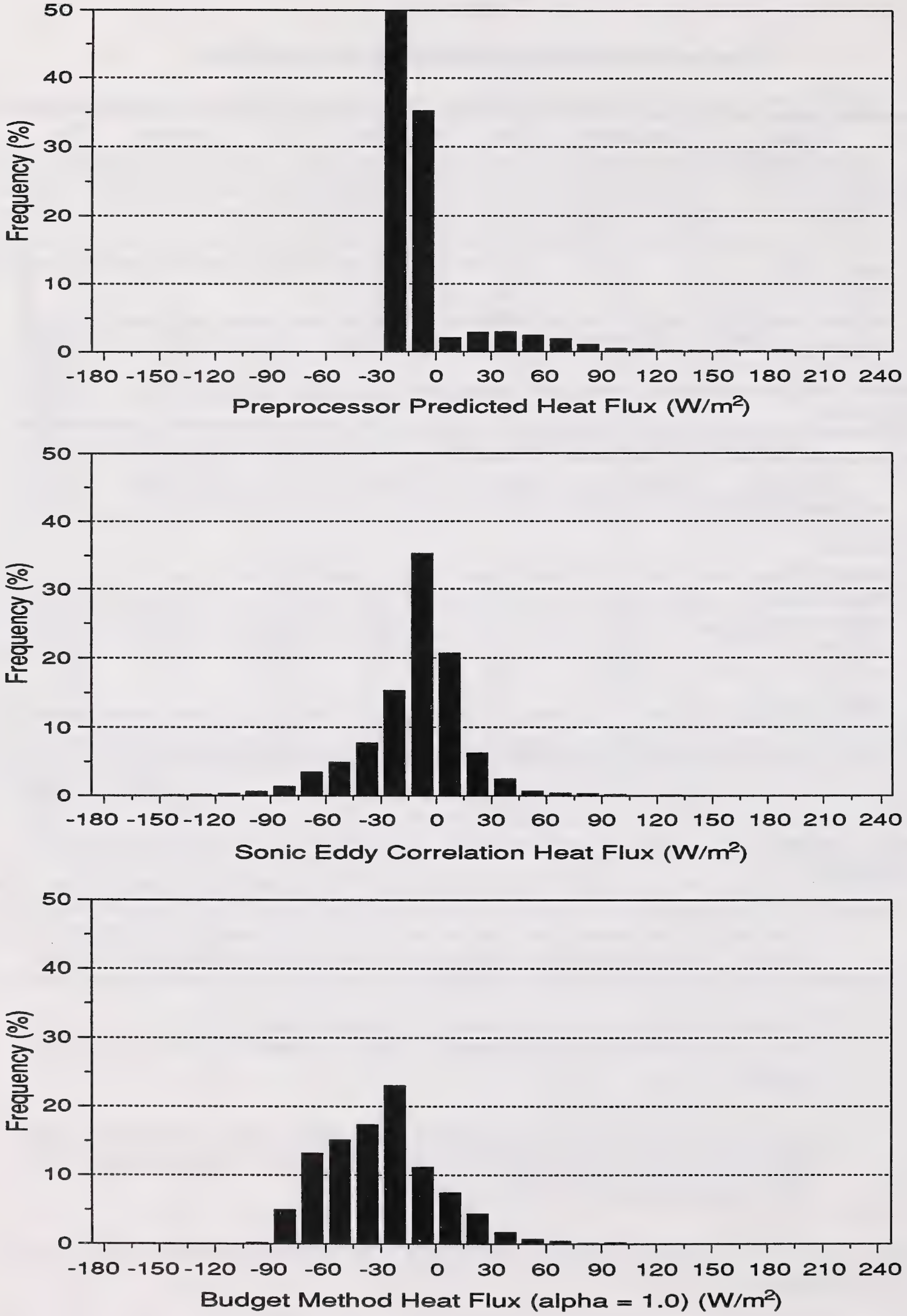

Figure 8.44 Winter

Winter Heat Flux Frequency Distributions.

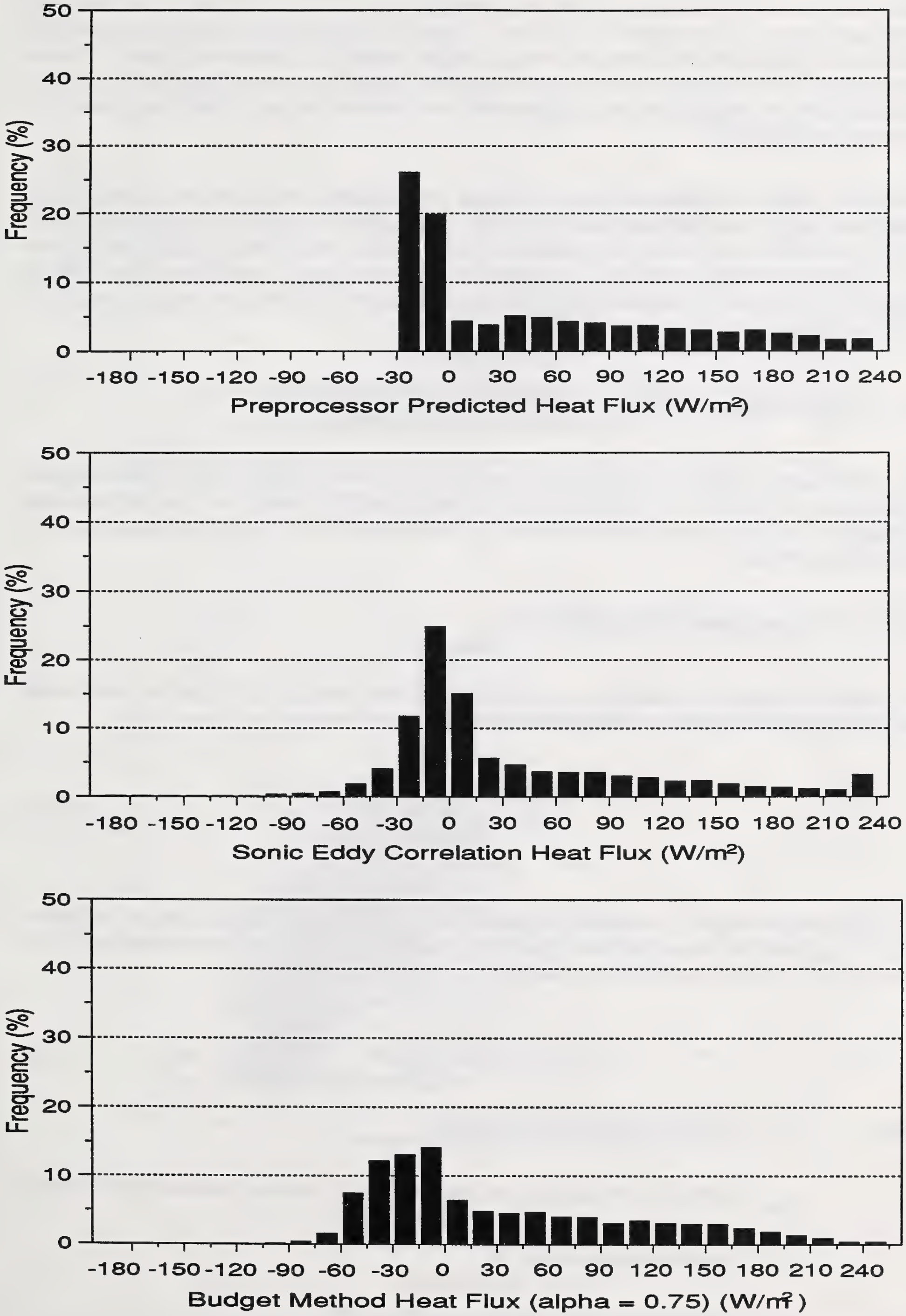

Figure 8.44 Summer

Summer Heat Flux Frequency Distributions.

Figure 8.45 shows scatter plots of the predicted heat fluxes as a function of the observed values based on the eddy correlation method. Figure 8.46 shows the scatter plots based on the observed values derived from the energy budget method. Qualitatively, there is better agreement with the summer rather than the winter values. For positive heat fluxes, there is a tendency for the predictions to be larger than the observed values. This is supported by the values in Table 8.13.

In summer, there is significant scatter between the predicted and observed values. This scatter however is not unexpected since the degree of scatter is similar to the scatter between the eddy correlation and energy budget heat flux determination methods. Additional scatter is to be expected based on the use of airport versus on-site data. The observations tend to support the adoption of a minimum heat flux value at night. The predicted minimum of -27 W/m^2, however, is not supported by the observations.

8.5.7 Preprocessor Predictions of *U** and *L*

The estimation of *U** and *L* from the heat flux (H_o) varies from one meteorological preprocessor to another. The following formulations are based on the preprocessor developed by Alp *et al* 1987 and are generally representative of the formulations used by other preprocessors.

8.5.7.1 Preprocessor Formulations

For neutral atmospheric conditions, the surface friction velocity (*U**) can be determined from the logarithmic wind profile relationship:

$$U* = \frac{kU_{REF}}{l_n\left(\frac{Z_{REF}}{Z_o}\right)} \tag{8.1}$$

The only meteorological parameter required is the wind speed (U_{REF}) at some reference height (U_{REF}) and the site aerodynamic surface roughness. The von Karman constant (*k*) is given by 0.4. The Monin-Obukhov Length (L) can be estimated from:

$$L = \frac{-\rho_a C_{pa} T_a U*^3}{kgH_o} \tag{8.2}$$

where

ρ_a = density of ambient air (*kg*/m^3)

ρ_{pa} = specific heat capacity of ambient air at constant pressure (997 J/*kg* K)

T_a = ambient temperature (K)

g = acceleration due to gravity (9.81 g/m^3)

H_o = surface heat flux (W/m^2)

Winter

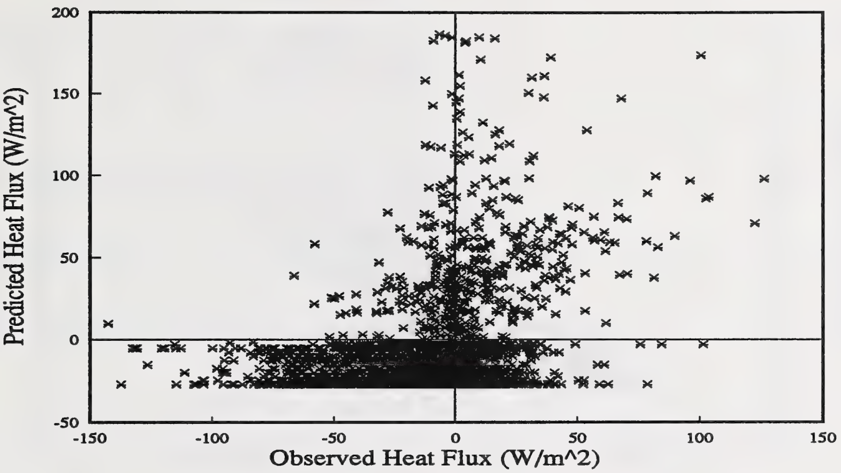

Summer

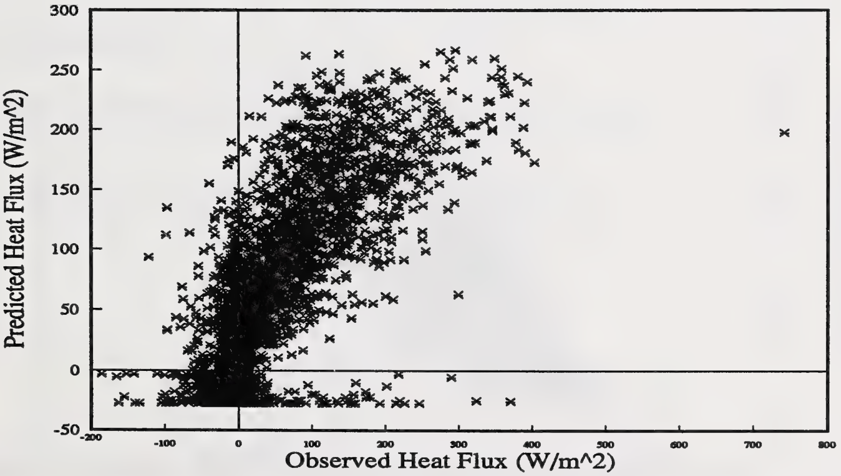

Figure 8.45

Scatter Plot of Predicted and Observed Heat Fluxes Where the Observed is based on the Eddy Correlation Method.

Winter

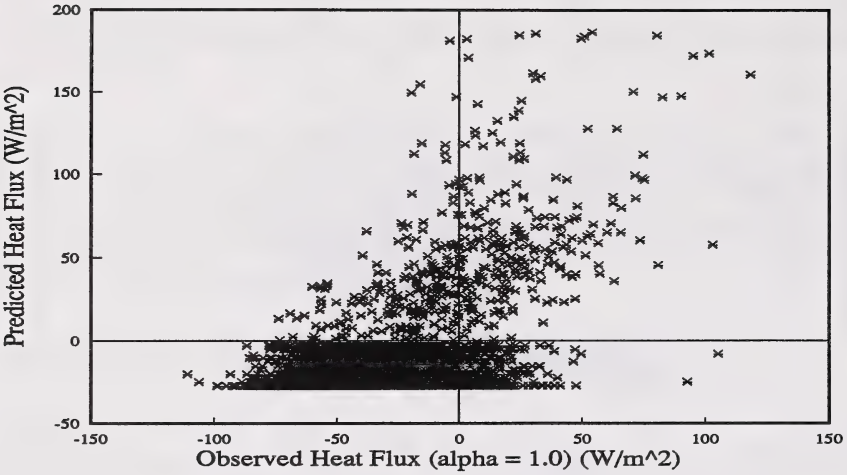

Summer

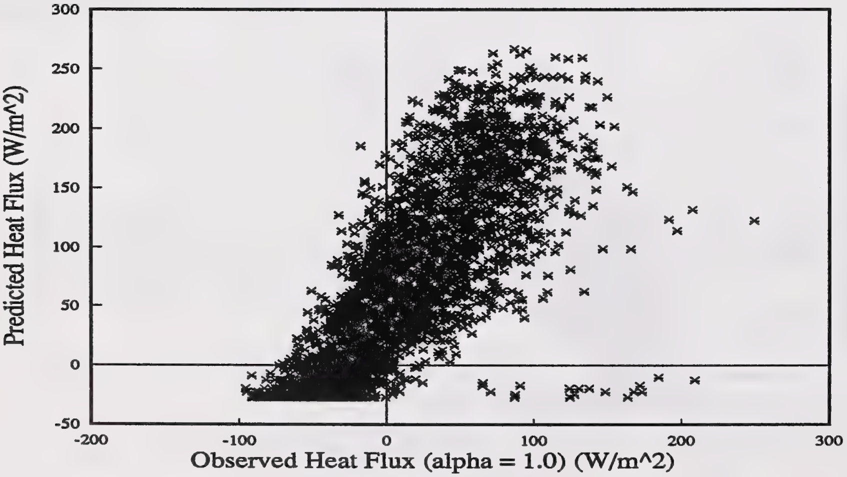

Figure 8.46

Scatter Plot of Predicted and Observed Heat Fluxes Where the Observed is based on the Energy Budget Method.

For stable and unstable conditions, a modified version of the logarithmic profile can be used to estimate the function velocity:

$$U^* = \frac{kU_{REF}}{\ln\left(\frac{Z_{REF}}{Z_O}\right) - \psi\left(\frac{Z_{REF}}{L}\right)} \tag{8.3}$$

where $\psi(Z_{REF}/L)$ is a stability dependent paramater.

Stable conditions

For stable conditions, the stability parameter is estimated from:

$$\psi\left(\frac{Z_{REF}}{L}\right) = -4.7\left(\frac{Z_{REF}}{L}\right) \tag{8.8}$$

Equation 8.3 can be combined with Equation 8.2 to produce a cubic equation for U^* which may be solved for the largest real root. For cases when no real root exists for U^*, the approach taken in Table 8.14 can be adopted. This approach leads to a minimum value for U^* which implies that a certain level of turbulence is always observed in a stable boundary layer.

Unstable conditions

For unstable conditions, the stability parameter is estimated from:

$$\psi\left(\frac{Z_{REF}}{L}\right) = 2\ln\left(\frac{1+\bar{q}}{2}\right) + \ln\left(\frac{1+\bar{q}^2}{2}\right) - 2\tan^{-1}(\bar{q}) + \frac{\pi}{2} \tag{8.9}$$

where:

$$\bar{q} = \left(1 - 15\frac{Z_{REF}}{L}\right)^{1/4} \tag{8.10}$$

For unstable conditions, the Monin-Obukhov length can be estimated from:

$$L = -\frac{\rho_A C_{PA} \overline{T}_A U^{*3}}{gkH_O R_a T_a} \tag{8.11}$$

where $\overline{T}_A$ is the average temperature in the convective boundary layer which can be estimated from:

Table 8.14

Solution for *L* and *U** for Stable Conditions.

In strongly stable conditions, no solutions for U^* and L exist when:

$$\frac{Z_{REF}}{L} > \frac{1}{2(4.7)} \ln\left(\frac{Z_{REF}}{Z_O}\right) \qquad (8.4)$$

which is equivalent to:

$$U_{REF} < \frac{3}{k}\left[-\frac{4.7 Z_{REF}\, g\, k H_O R_A}{4 C_{PA} P_A} \ln^2\left(\frac{Z_{REF}}{Z_O}\right)\right]^{1/3} \qquad (8.5)$$

If the inequality in equation 3.25 is satisfied, then (Z_{REF}/L) is set equal to the right side of the above inequality. Substituting this value into the expression for U^* yields:

$$U^* = \frac{2}{3} \frac{k U_{REF}}{\ln\left(\frac{Z_{REF}}{Z_O}\right)} \qquad (8.6)$$

and:

$$L = \frac{2(4.7) Z_{REF}}{\ln\left(\frac{Z_{REF}}{Z_O}\right)} \qquad (8.7)$$

This approach involves setting minimum limits for the values U^* and L. For example, if $Z_{REF} = 10$ m and $Z_O = 0.1$ m, then the corresponding value for L is 20.4 m. For a wind speed, $U_{REF} = 1$ m/s, this value of L corresponds to a minimum value for U^* of 0.058 m/s. The existence of these minimum values imply that a minimum level of turbulence always exists in the stable boundary layer.

$$\overline{T}_A = 0.5(2T_A - 0.0098Z_i) \tag{8.12}$$

and R_A is the particular gas constant for air (287 J/(*kg* K) and Z_i is the depth of the convective mixing layer given by

$$Z_i = \frac{2}{C_{PA}\rho_A[T_A(t) - T_A(\min)]}\int_{t_o}^{t} H_O dt \tag{8.13}$$

where T_A (t) is the ambient temperature (k) at time (t) between sunrise and sunset and T_A (min) is the minimum ambient temperature after summer (k). In the estimation of hourly values of Z_i, the following rules specified by Benkley and Schulman (1979) are applied:

- $Z_i = 0.0$ between sunrise and the time of the minimum temperature which normally occurs after sunrise. If the temperature continues to drop throughout the day, then $Z_i = 0.0$ for that day.

- Transient decreases of Z_i during the day are not allowed.

- The maximum value of Z_i is associated with the maximum temperature during the day (T_A(max)). Z_i is not allowed to increase between the time corresponding to T_A(max) and sunset.

- Transition from daytime Z_i(max) to night-time $Z_i = 0.0$ occurs when $T_A = T_A(\max) - 0.25\ [(T_A(\max) - T_A(\min)]$.

The mixing layer height Z_i is not allowed to approach zero; a lower limit of 50 m has been selected. Values for L and U^* under unstable conditions can be solved by the approach given in Table 8.15.

Table 8.15

Solution for L and U^* for Unstable Conditions.

The calculation of L and U^* is iterative in nature and can be solved through the adoption of the following procedure:

(1) Assume a value for the stability function $\Psi(Z_{REF}/L)$ of zero.

(2) Calculate a value for the friction velocity U^* (Equation 8.1).

(3) Calculate a value for the Monin-Obukhov length L (Equation 8.11).

(4) Calculate a value for the term $\tilde{q}$ (Equation 8.10).

(5) Calculate a new value for the stability function $\Psi(Z_{REF}/L)$ (Equation 8.9).

(6) Calculate a new value for the friction velocity U^* (Equation 8.1).

(7) If the difference between the new value for U^* and the previous value for U^* is less than 0.1 percent proceed to Step (8). If the difference is greater than 0.1 percent then go back to Step (3).

(8) The most recent value U^* is the selected value for U^*, this value is used to calculate a value for L.

8.5.7.2 Comparison Between Predicted and Observed U^*

In order to provide a first stage evaluation of the previously described preprocessor formulations, median diurnal variations of the friction velocity (U^*) were estimated and compared to the observed values. Only data from the months of November 1988 (winter) and May 1989 (summer) were evaluated. The observed values are based on the 10 m sonic anemometer level wind data ($U^* = (\overline{U'W'})^{1/2}$).

Prior to effecting a full comparison of the preprocessor predicted values, a limited evaluation was conducted for neutral conditions ($\psi(Z/L) = 0$ and for extremely stable conditions (where U^* = 2/3 the neutral value (Table 8.15)).

Neutral Predictions

Figure 8.47 compares the observed U^* values with those predicted assuming neutral conditions (Equation 8.1). The predicted values are based on the median 10 m level wind speeds ($Z_{REF} = 9.87$ m) and for these values of Z_o (0.1, 1 and 10 cm). For November and May, the estimated surface roughness values were 0.9 and 0.8 cm, respectively. These estimated values are based on 10 m level wind data.

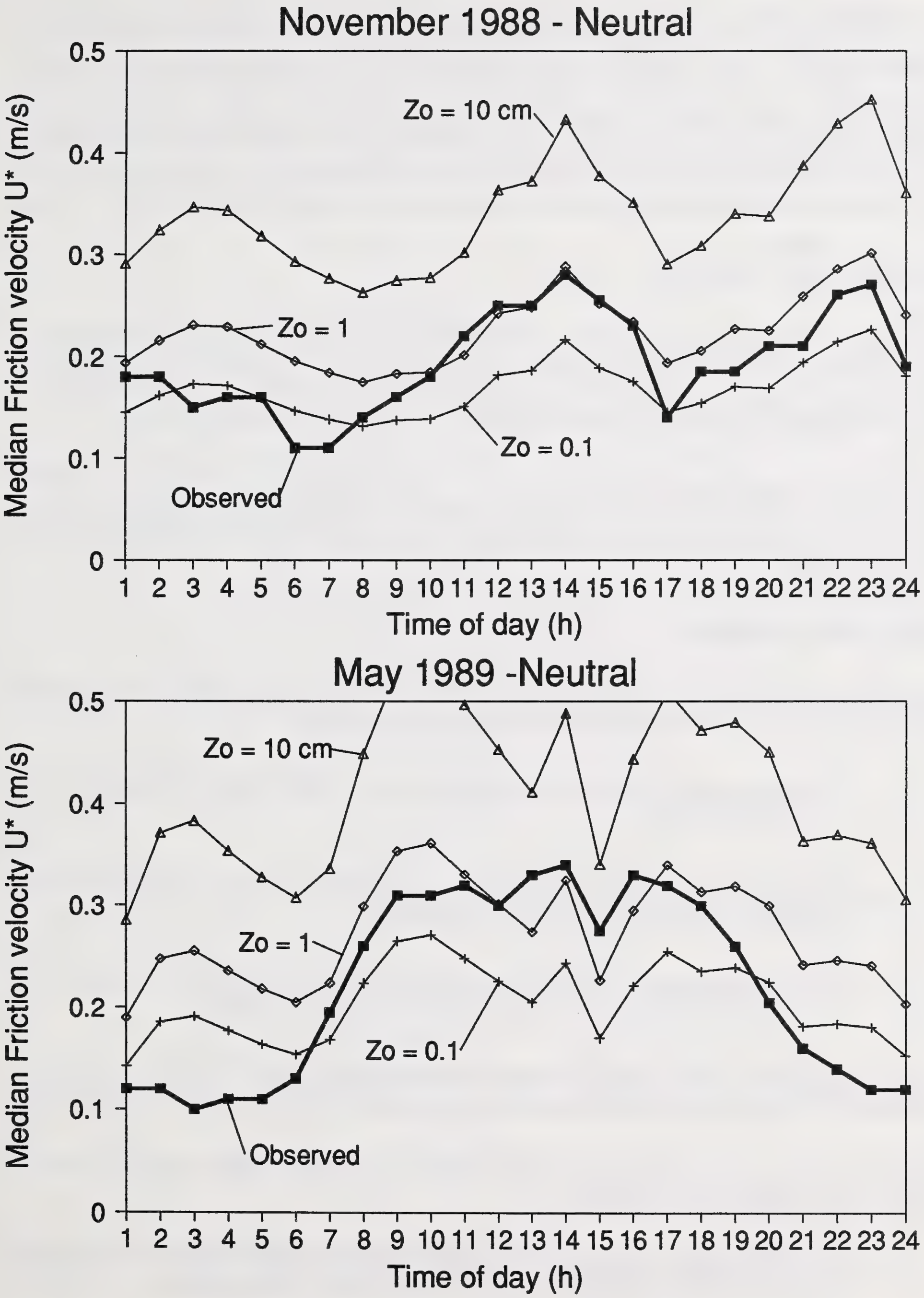

Figure 8.47

Comparison of Median Observed and Neutral Predicted *U Values.**

The predicted values would be expected to underestimate U^* during day-time conditions and overestimate U^* during night-time conditions because of the effect of the stability parameter $\psi(Z/L)$. From Figure 8.47, it appears that the best agreement occurs for predicted values based on a Z_o value of 1 cm. During November day-time conditions, the agreement is very close indicating that unstable conditions may not be important. In contrast, the predicted May day-time values for $Z_o = 1$ cm fall below the observed line indicating the effect of the unstable $\psi(Z/L)$ term. In both months, the predicted night-time values for $Z_o = 1$ cm are greater than the observed line indicating the effect of the stable $\psi(Z/L)$ term.

Extreme Stable Conditions

Figure 8.48 compares the observed U^* values with those predicted assuming the stable limit for U^*. The limit for U^* under extremely stable conditions is 2/3 times the corresponding value for neutral conditions (Equation 8.1). The predicted values are based on median 10 m level wind speeds ($Z_{REF} = 9.87$ m) and for these values of Z_o (0.1, 1 and 10 cm).

The predicted night-time values based on $Z_o = 1$ cm provide better agreement with the observed night-time values than the corresponding values did for neutral conditions (Figure 8.47). For both months, the predicted day-time values based on $Z_o = 1$ cm are less than the observed values.

Preprocessor Predictions

The full meteorological preprocessor formulations were used to estimate the diurnal variation of U^*. Predicted values were based on the following:

- The airport derived heat fluxes as per Scire *et al* 1984 (Section 8.5.5) and airport wind speed values.
- The 10 m sonic anemometer heat fluxes based on the 10 m values of $\overline{W'T'}$ (Section 8.5.4) and on-site 10 m level wind speeds.
- The heat fluxes based on the energy budget method for a surface wetness factor of $\alpha = 1.0$ (Section 8.5.4) and on-site 10 m level wind speeds.

The evaluation was conducted for a surface roughness factor of $Z_o = 10$ cm. As was seen in Figure 8.47, this should overestimate the friction velocity U^* by a factor of about 1.5.

Figure 8.49 compares the predicted and observed diurnal variation of the median U^* values. These results in the figure indicate:

- For November, the agreement between predicted and observed values appears to be the best for predicted values based on airport observations.
- For November, the use of on-site heat flux and wind speed values tend to be less than the observed values. For a $Z_o = 1$ cm, these predictions would have been less.

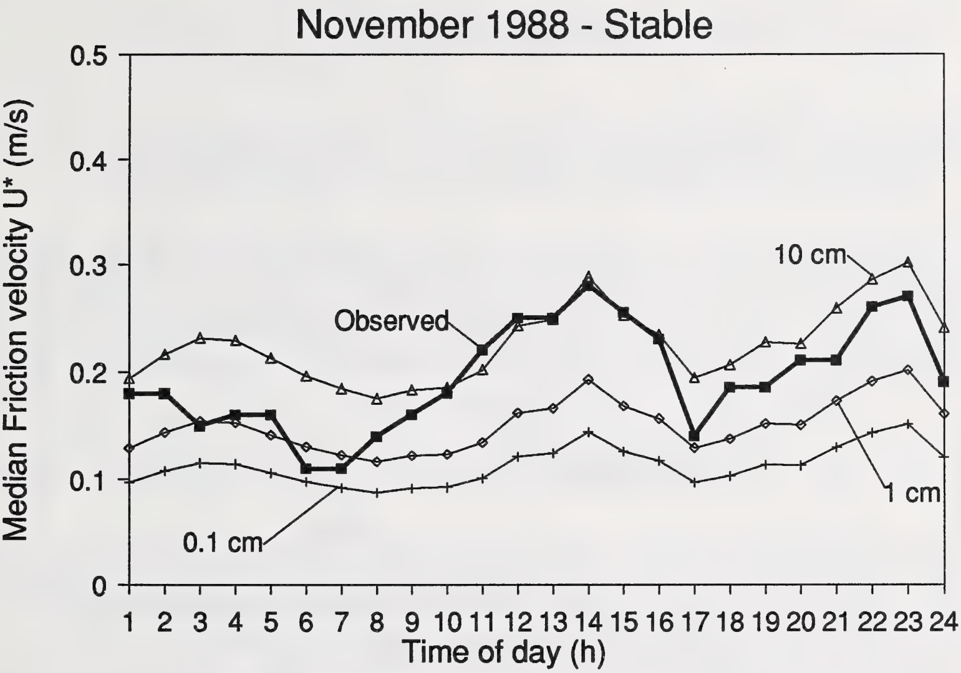

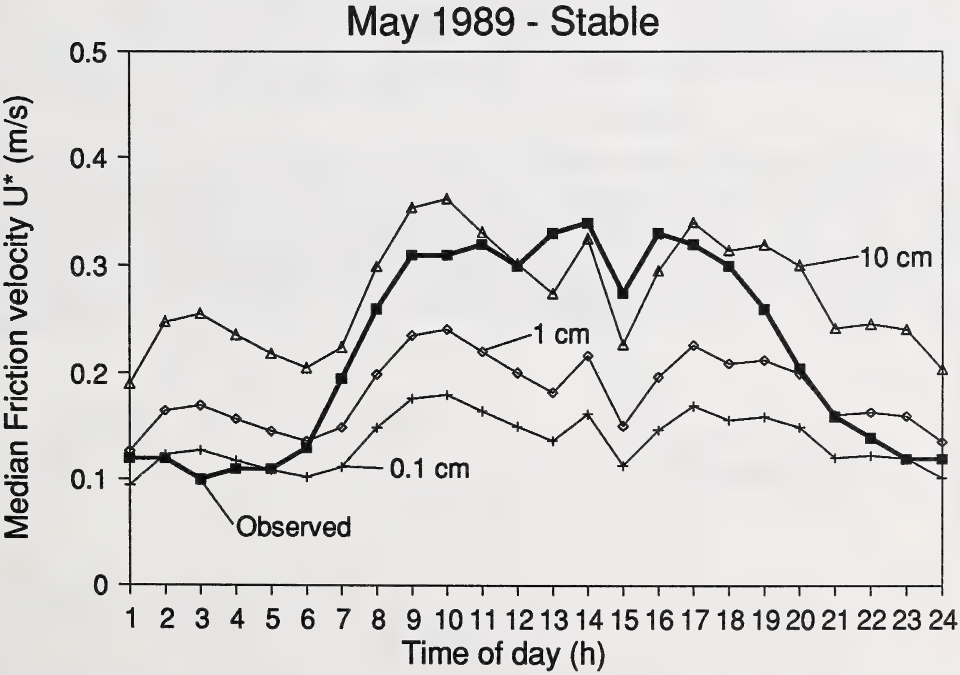

Figure 8.48

Comparison of Median Observed and Extremely Stable Predicted *U Values.**

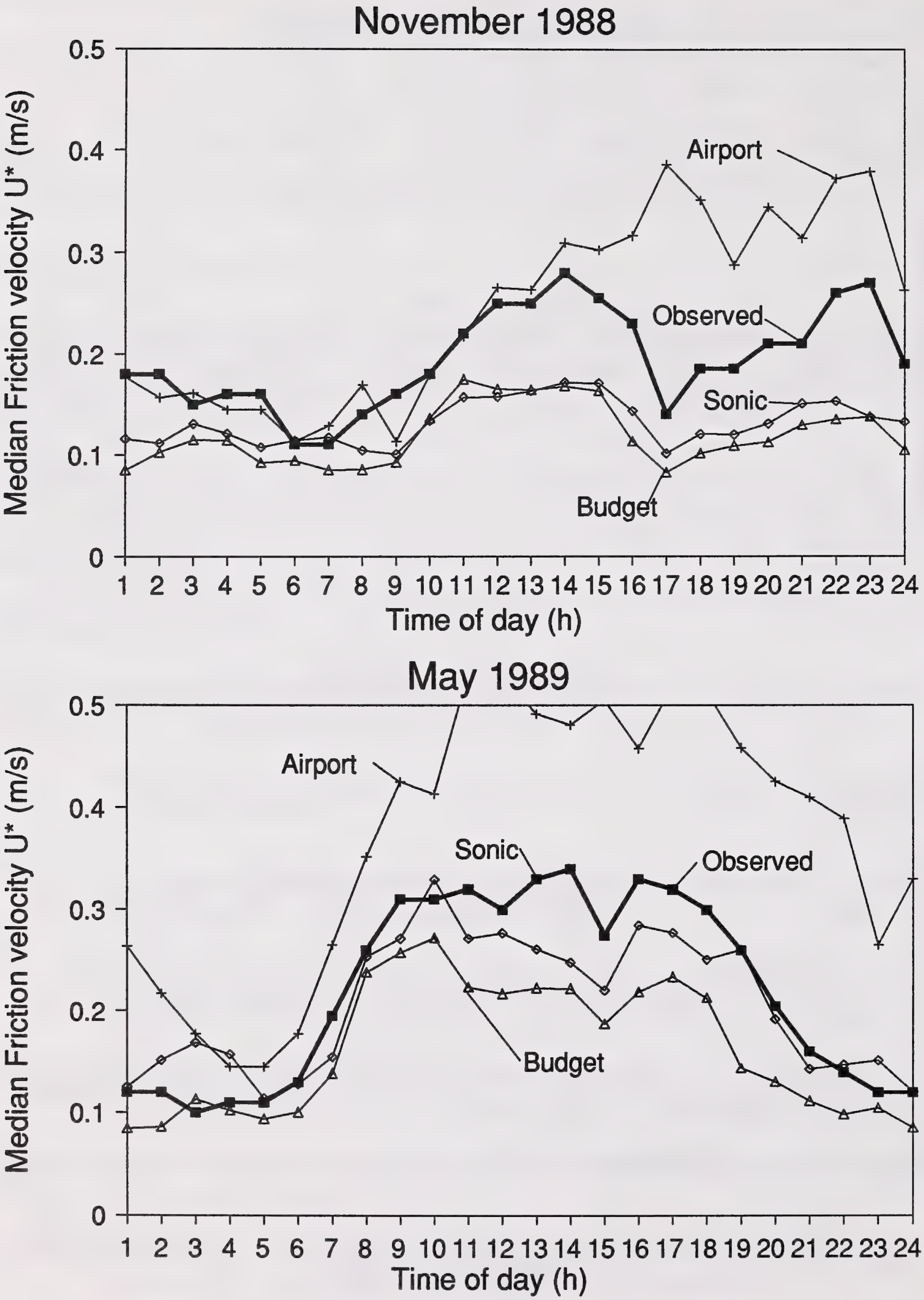

Figure 8.49

Comparison of Selected Predicted Values of U^* with Those Observed (Predicted Values Assume Z_o - 10 cm).

- For May, the use of airport heat flux and wind speed overpredicts the observed values. For a $Z_o = 1$ cm, the agreement between airport results and observations is expected to improve.

- For May, the use of on-site heat flux and wind speed values tend to be less than the observed values. For a $Z_o = 1$ cm, these predictions would have been less. The agreement for on-site May data appears to be better than for November.

The better agreement for predictions based on the airport data is somewhat unexpected. It is not immediately clear if this agreement is fortuitous, if competing effects provide a better end result or if there are problems with the preprocessor logic and/or code. It is surprising that the predicted median values based on on-site data (Figure 8.49) are less than those given for the extremely stable cases (Figure 8.48). These discrepancies warrant further investigation.

8.5.7.3 Comparison Between Predicted and Observed *Z/L*

Once U^* is evaluated, the Monin-Obukhov length L can be readily computed for neutral conditions. For stable and unstable conditions, L and U^* are evaluated simultaneously. The full meteorological preprocessor formulations were used to estimate the diurnal variation of L as well as U^*. Again, the evaluation was conducted for a surface roughness of Z_o of 10 cm rather than 1 cm. This evaluation should result in an overestimation for U^* and L of about 1.5 and 3.4, respectively (for near neutral conditions). For the purposes of discussion, the Monin-Obukhov values are expressed in terms of the Monin-Obukhov stability parameter Z/L. Therefore, if L is overestimated by a factor of 3.4, then the predicted Z/L value should be about 30% of the expected values.

Figure 8.50 compares the predicted and observed diurnal variation of the Monin-Obukhov stability parameter Z/L. The predicted values show the same general agreement for all except the evening hours when the airport values are much less than the other predictions. The maximum predicted Z/L value of 0.48 is a product of the stable cut-off limit. For both months, the same type of diurnal variation is shown for the observed and predicted values. For November, the predicted extreme values exceed those observed while for May, the opposite effect is found.

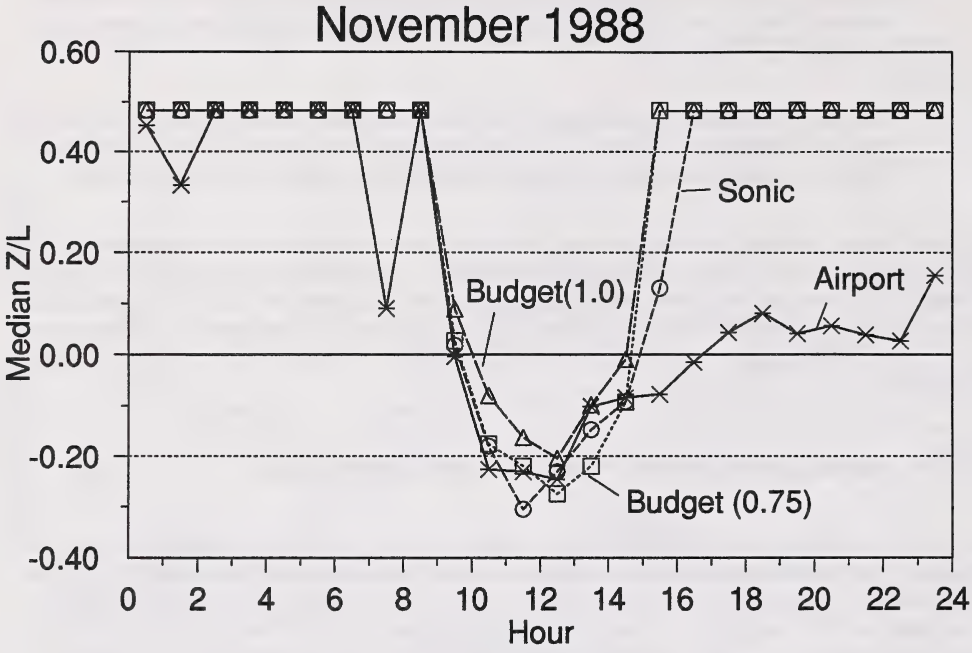

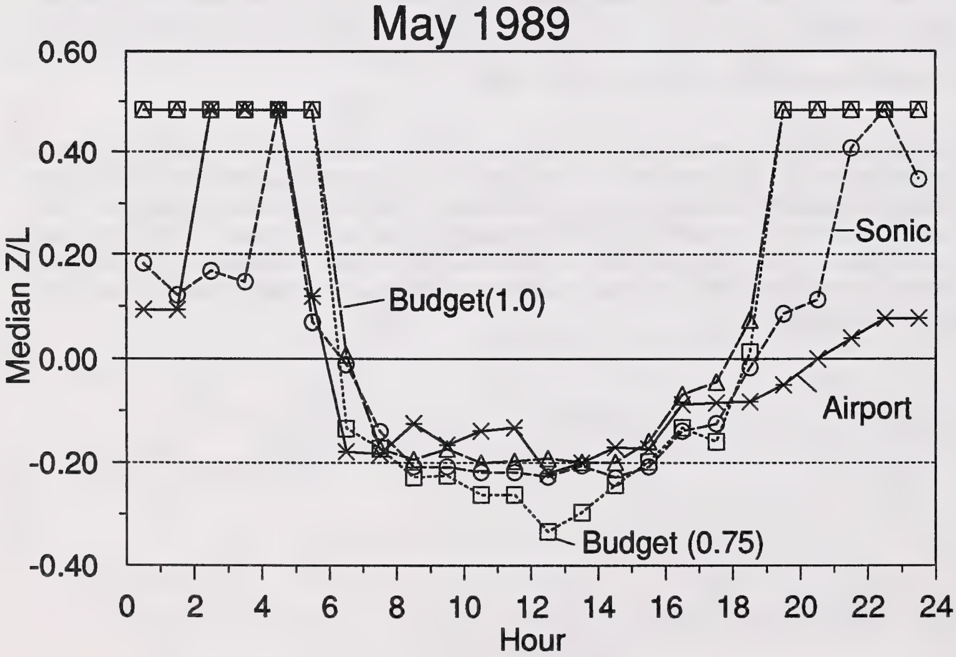

Figure 8.50

Comparison of Selected Predicted Values of *Z/L* with those Observed (Predicted Values Assume Z_o = 10 cm).

8.6 Spatial Representativeness

Mean values of selected meteorological parameters from observation stations in the vicinity of the Field Measured site were compared. The locations of the stations from where concurrent meteorological data were available are shown in Figure 8.51. The selected stations for comparison include:

- Field Measurement Program Site,
- Calgary International Airport,
- Crossfield Sour Gas Processing Plant, and
- Balzac Sour Gas Processing Plant.

Detailed descriptions of the off-site data collection were presented in Section 5.2. The Field Measurement Program and the Calgary International Airport data comparison included:

- Pressure,
- Temperature (2 m levels at both sites),
- Relative humidity (2 m levels at both sites),
- Wind speed (10 m levels at both sites), and
- Wind direction (10 m levels at both sites).

The comparison of the Crossfield and Balzac meteorological data were limited to wind speed and wind direction. The Balzac gas processing plant is serviced by two air quality monitoring trailers which measure wind speed and wind direction at 10 m level. The Crossfield gas processing plant is serviced by a tower with wind instruments at the 15 and 30 m levels.

In effecting a comparison, it is important to note that data collected at different sites represent different averaging periods. For example, reported hourly pressure, temperature and relative humidity observations at the airport are in effect instantaneous values on the hour. The wind speed and direction data are two-minute average values on the hour. The Crossfield and Balzac wind data are hourly averages. For the purposes of this comparison, three-minute average Field Measurement Program data on the hour were used.

The comparison was performed for the six-month period October 1988 to March 1989. The comparisons were based on basic statistics and frequency distributions. No formal statistical comparisons providing a quantitative measure of agreement between the sites were calculated. The comparison between the sites is more qualitative than quantitative.

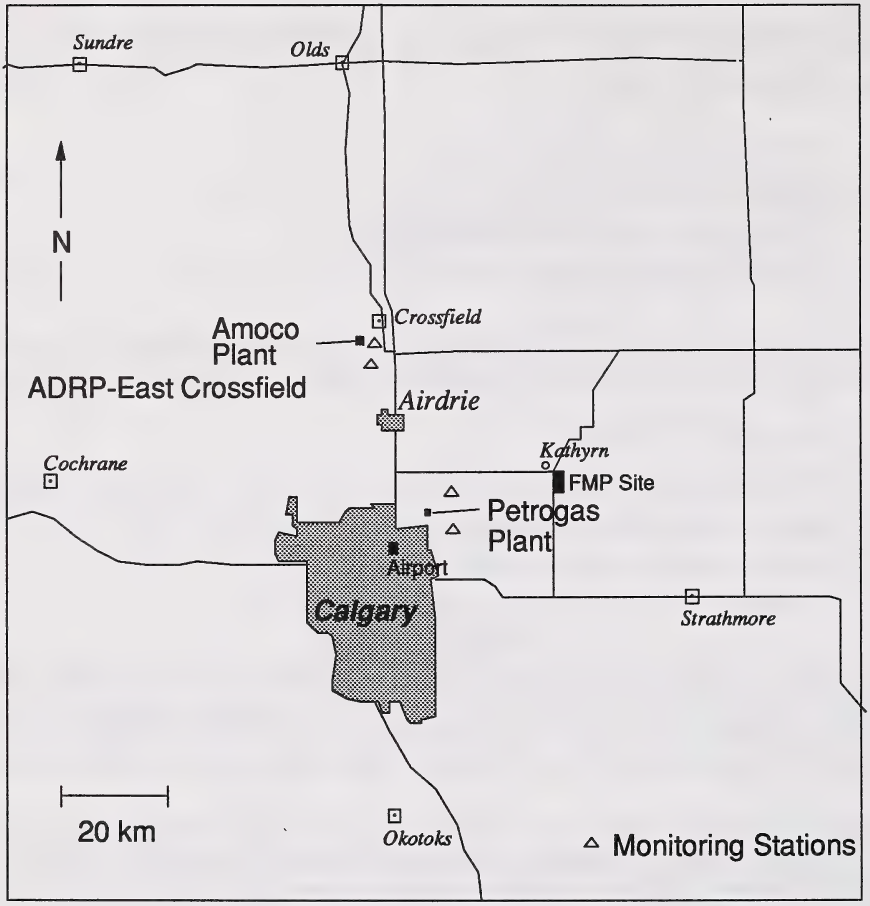

Figure 8.51

Location of Meteorological Data Stations in the Northeast Calgary Area.

8.6.1 Pressure

The basic statistics concerning atmosphere pressure (kPa) are as follows:

Pressure (kPa)	Calgary Airport	Field Measurement Program
Minimum	86.1	83.8
Mean	89.0	88.8
Maximum	91.6	91.7
Standard Deviation	0.9	1.2

The mean values differ by 0.2 kPa. This agreement is expected in spite of the elevation difference of 110 m (1.2 kPa) since a concurrent airport pressure measurement was used to calibrate the Field Measurement Program pressure sensor. No adjustments in the calibration were made for elevation differences between the airport and the Field Measurement Program site.

Figure 8.52 compares the frequency distributions of the pressure observations from the two locations. The similarity between the mean values and the frequency distributions suggests that the pressure observations at both sites were similar.

8.6.2 Temperature

The basic statistics concerning ambient temperature (°C) are as follows:

Temperature (°C)	Calgary Airport	Field Measurement Program
Minimum	-35.5	-35.4
Mean	-6.2	-6.9
Maximum	20.8	20.6
Standard Deviation	10.1	9.2

The mean and extreme distribution of temperature observations from the two locations agree to within 0.7 °C.

Figure 8.53 compares the frequency distribution of temperature observations from the two locations. The similarity between the mean values and the frequency distributions suggests that the temperature observations at both sites were similar.

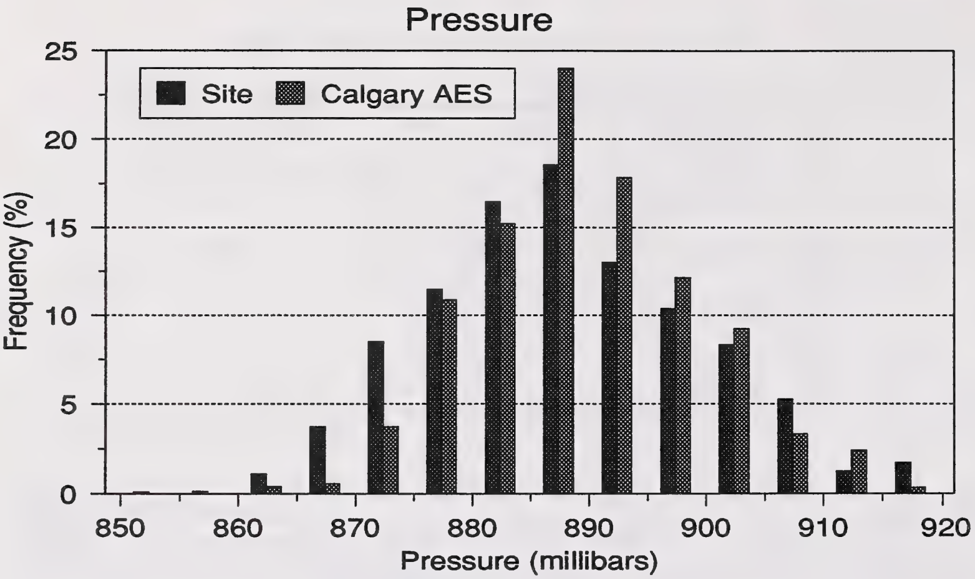

Figure 8.52

Frequency Distribution of Pressure Observed at the Kathyrn Site and Calgary Airport.

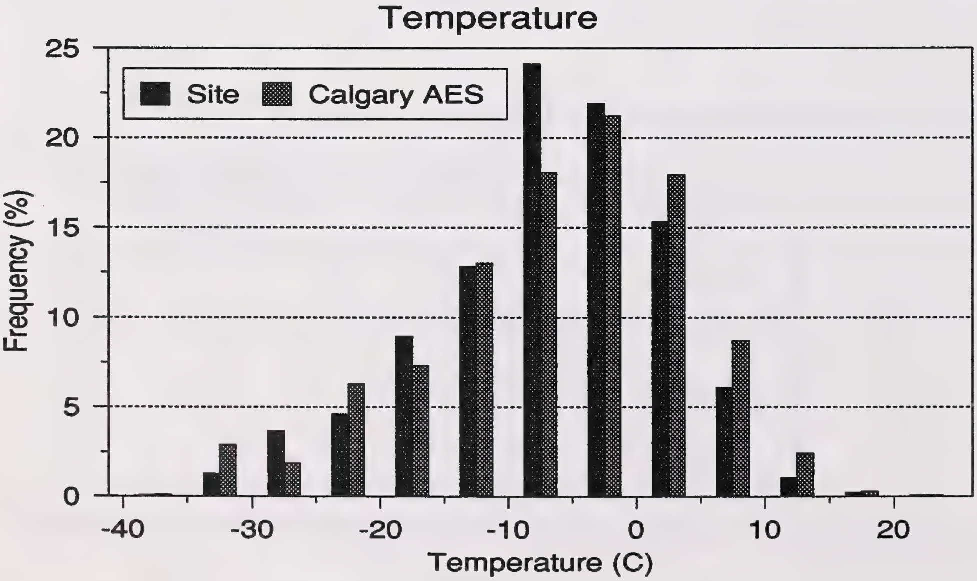

Figure 8.53

Frequency Distribution of Temperature Observed at the Kathyrn Site and Calgary Airport.

8.6.3 Relative Humidity

The basic statistics concerning relative humidity (%) are as follows:

Relative Humidity (%)	Calgary Airport	Field Measurement Program
Minimum	11.0	16.7
Mean	67.0	74.1
Maximum	95.0	99.6
Standard Deviation	16.9	16.9

The relative humidity measurements at the Field Measurement site are consistently larger than those observed at the airport. At this stage, it is not clear whether this observed difference was real or instrument dependent. For example, commercial relative humidity sensors (such as was used at the Field Measurement site) can lose accuracy at low temperatures.

Figure 8.54 compares the frequency distribution of relative humidity observations from the two locations. The bias to larger values at the Field Measurement site relative to the airport is evident from the frequency distribution. The bias suggests that if relative humidity measurements are critical for a particular monitoring program, that a suitable relative humidity probe should be selected.

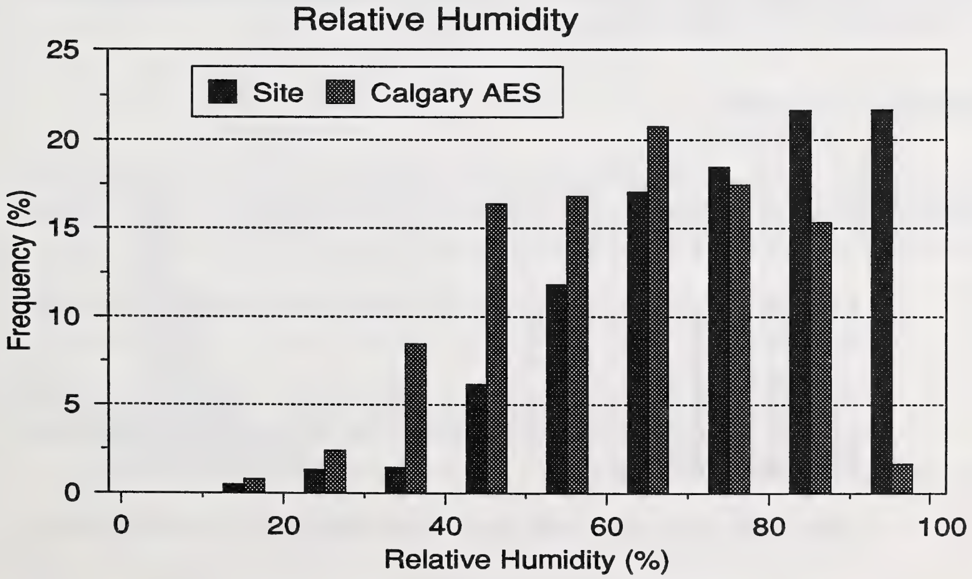

Figure 8.54

Frequency Distribution of Relative Humidity Observed at the Kathyrn Site and Calgary Airport.

8.6.4 Wind Speed

The basic statistics concerning wind speed (m/s) are as follows:

Wind Speed (m/s)	Calgary Airport	Field Measurement Program	Balzac #2 (10 m)	Balzac #3 (10 m)	Crossfield (15 m)	Crossfield (30 m)
Minimum	0.0	0.0	0.0	0.0	0.0	0.0
Mean	3.7	4.2	3.6	3.2	2.9	5.2
Maximum	15.8	18.4	12.5	14.2	13.1	19.2
Standard Deviation	2.9	2.4	2.2	2.5	1.9	2.8

In the above table, the Airport and Field Measurement values represent two and three-minute averages, respectively, while the gas plant observations represent hourly averages. The smallest and largest mean values were observed at Crossfield (15 and 30 m levels, respectively).

Figure 8.55 compares the frequency distributions of wind speed observations at the six locations. The frequency distribution observed at the Field Measurement site and the gas plant stations is relatively smooth. This is in contrast to that observed at the airport. In particular, the airport frequency distribution at low wind speeds is irregular due to the relatively high starting threshold of airport anemometers and because of the way the low wind speed data are handled. Since many air quality concerns focus on low wind speeds, the use of airport wind speed data may not be appropriate.

8.6.5 Wind Direction

Due to the circular nature of wind direction, basic statistics are not given. Instead the wind direction frequency distribution at the six locations are presented in Figure 8.56. The winds are categorized according to an 8-point compass. The figure indicates the following:

- At all sites, the least frequent winds were from the east-northeast and southeast directions.
- The Crossfield frequency distributions for the two levels are somewhat different, perhaps indicating the distortion of air flow at the lower level due to building obstructions.
- The two Balzac stations indicate that westerly winds occur most frequently.
- Calgary Airport indicates that northerly and southerly winds occur most frequently. This may be due to the influence of Nose Hill and the Nose Hill Creek valley to the west of the airport.

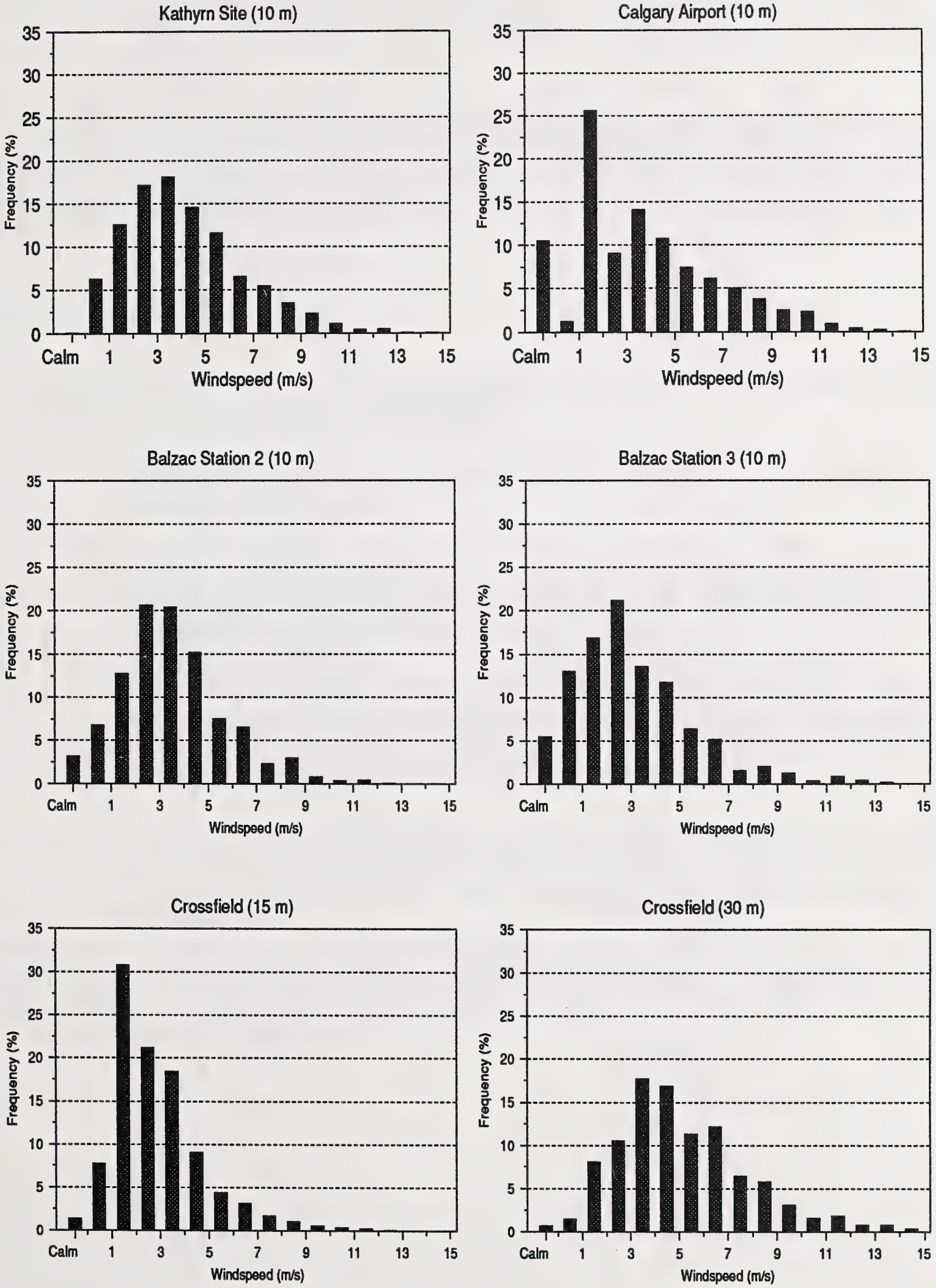

Figure 8.55

Frequency Distributions of Wind Speed Observed Concurrent With the Field Measurement Program.

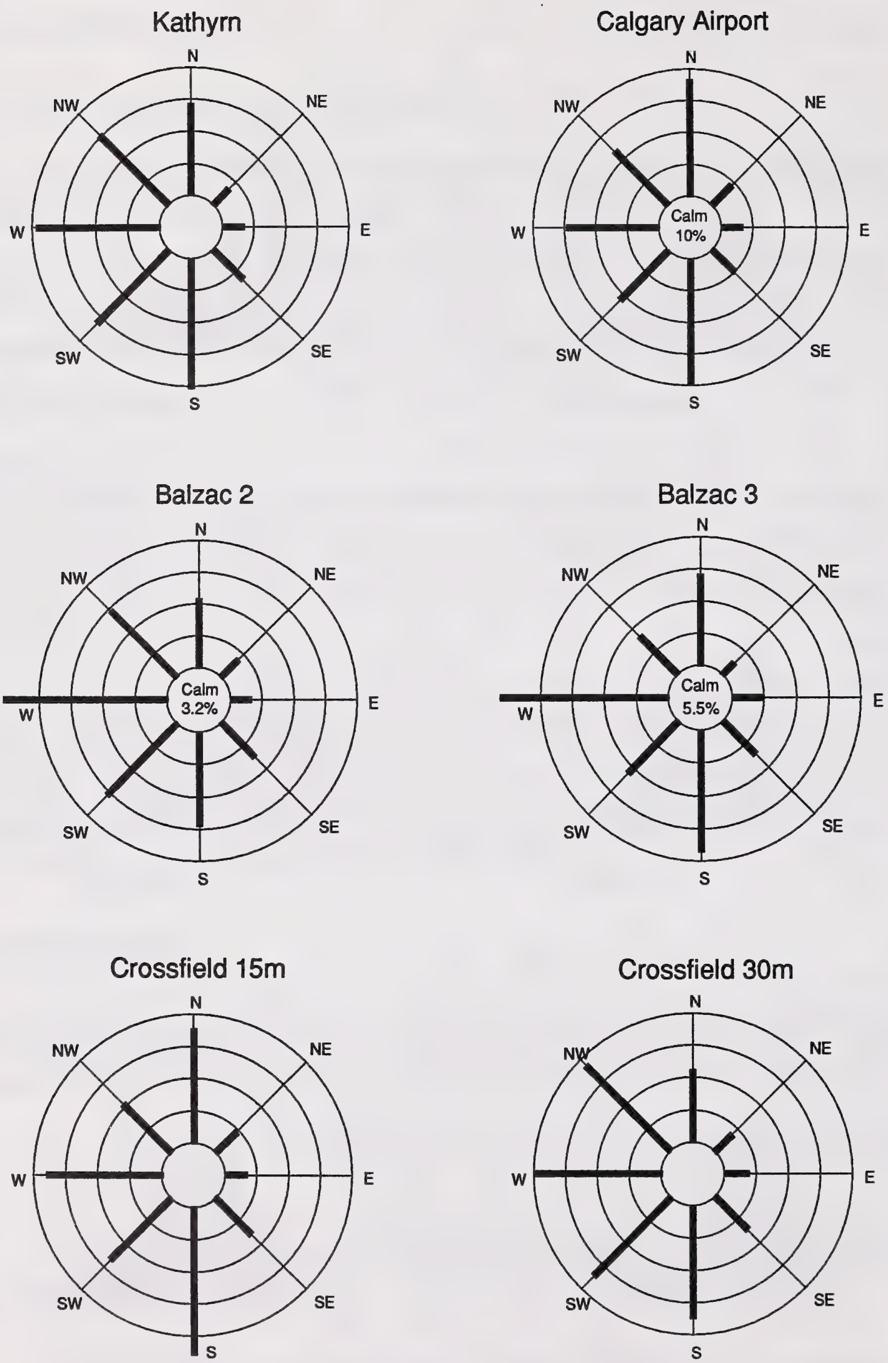

Figure 8.56

Frequency Distributions of Wind Direction Observed Concurrent With the Field Measurement Program.

- At the Field Measurement Program site, the wind directions are nearly uniformly distributed over the northerly through westerly to southerly directions.

The differences in the wind direction frequency distributions presented in the figure indicate care has to be taken when extrapolating wind direction data from one area to another. For areas with major terrain features, this conclusion is obvious, but the results in the figure indicate that this conclusion is also valid for the relatively flat to rolling terrain in the Calgary area.

8.6.6 Comments

The comparison of selected concurrent meteorological observations from different locations north and east of Calgary indicate the following:

- Pressure and temperature observations were relatively constant over the distance scales considered.

- Relative humidity observations are probably relatively constant over the distance scales considered. The differences that were observed are likely due to instrumentation difficulties at low temperatures.

- Care has to be taken in the extrapolation of airport wind speed values due to AES observation and reporting procedures for low wind speeds. Observation height and surface roughness differences also have to be considered when extrapolating wind speed data from one location to another.

- Care has to be also taken when extrapolating wind direction data from one location to another. This conclusion is not only valid for areas with major terrain features, but also for the relatively flat to rolling terrain in the Calgary area.

The qualitative comparison presented in this section supports the preference for site-specific wind speed and direction data over the extrapolation of off-site data to the study area. The extrapolation of off-site meteorological observations such as pressure, temperature and relative humidity is of less concern.

8.7 Averaging Time

Concentrations downwind from a source decrease with increasing averaging time mainly because of increased crosswind plume spread (σ_y) which results from an increased meander of wind direction. The latter can be related to the standard deviation of the wind direction (σ_θ) which is related to σ_y. The power law formula has been used to account for effects of averaging time on concentrations, plume spreads and atmospheric turbulence (i.e. σ_θ) through the empirical relationship:

$$\frac{\sigma_1}{\sigma_2}=\left(\frac{t_1}{t_2}\right)^{p} \quad \text{or} \quad \frac{\chi_1}{\chi_2}=\left(\frac{t_1}{t_2}\right)^{-p} \tag{8.30}$$

The subscripts refer to averaging periods t_1 and t_2 and the exponent (p) has been found to vary with the time period range under consideration, atmospheric stability and height above the surface (Slade 1968).

The relationship given by Equation 8.30 appears to be valid for concentration variations under relatively uniform atmospheric conditions. This condition can usually be met with time periods up to 2 or 3 hours. Additionally, the equation assumes that the concentrations are relatively near the plume centreline. Notwithstanding the previous comments, the equation has been applied to concentration data for averaging times up to one year (Herman 1980).

A range of p values have been reported in the literature and have been used in various plume dispersion models. The following summarizes some of these results.

- The Alberta Environment (1988) plume dispersion models assume a constant value for p of 0.2 for all atmospheric stability classes. The adoption of this general value is recommended by Slade (1968).

- Hanna *et al* (1982) support the use of p=0.2 for time periods between 3 and 60 minutes and p=0.25 to 0.30 for time periods between 1 and 100 hours.

- Turner (1970) recommends the use of p=0.17 to 0.20 for averaging periods of less than 2 hours.

- Cramer (1959) used a value for p of 0.2 for averaging periods ranging from 3 seconds to 10 minutes.

- The Texas Episodic Model (TEM8) allows p to vary as a function of atmospheric stability class (Texas Air Control Board 1979):

Stability Class	A	B	C	D	E	F
Exponent p	0.675	0.55	0.425	0.3	0.175	0.175

- Singer (1961) indicated that p is a function of atmospheric stability for averaging times of 100 minutes or less.

Stability	Very Unstable	Neutral
Exponent p	0.65	0.35

The values for p presented above range from 0.17 to 0.675 depending on atmospheric stability. A general value for p of 0.2 has been frequently used.

8.7.1 Field Measurement Program Results

During the tracer release and sampling field tests, 279 hourly blocks of high frequency wind data from the 10 and 25 m sonic anemometers were collected. The nominal sampling rate for the sonic data was 10 Hz; this resulted in 36 000 wind measurements for each one-hour block. Values of the along-wind (σ_U), crosswind (σ_V and σ_θ) and vertical (σ_W and σ_ϕ) turbulence were estimated for selected time periods. Table 8.16 indicates the averaging period, the number of averaging periods in a one-hour data block and the number of samples per averaging period. The data were subdivided into two time periods: short (1 to 180 seconds) and long (3 to 60 minutes).

Table 8.16

Averaging Periods Used to Evaluate the Power Law Exponent *p*.

Averaging Period	Number of Averaging Periods in One Hour	Nominal Number of Samples per Averaging Period
Short-Term (1 to 180 seconds)		
1 second	3 600	10
5	720	50
10	360	100
30	120	300
60	60	600
120	30	1 200
180	20	1 800
Long-term (3 to 60 minutes)		
3	20	1 800
5	12	3 000
10	6	6 000
15	4	9 000
30	2	18 000
60	1	36 000

The average $\overline{\sigma}$ was calculated for each averaging period within a one-hour data block. For example, the three-minute (180 seconds) average σ was calculated from:

$$\overline{\sigma_{(180)}} = \frac{\sum_{n=1}^{20} \sigma_N(180)}{20} \qquad (8.31)$$

Following this, the average power law exponent $\overline{p}$ for each one-hour block was calculated by comparing the σ from each time period (t_i) to the three-minute value from the relationship:

$$\overline{p} = \frac{\ln\{\overline{\sigma(t_i)}/\overline{\sigma(180)}\}}{\ln(t_i/180)} \tag{8.32}$$

where:
t_i = averaging period (s)
$\overline{\sigma(t_i)}$ = average σ for averaging period t_i
$\overline{\sigma(180)}$ = average σ for 3-minute averaging period.

Table 8.17 summarizes the results of the evaluation which have been subdivided by time period and by height. For the along wind (σ_U) and crosswind (σ_V and σ_θ) components, the average exponent p ranges between 0.2 and 0.3. For the vertical (σ_W and σ_ϕ) components, the exponents p are typically in the 0.04 and 0.06 range. The smaller value of p for the vertical component indicates the relative insensitivity to averaging period.

Table 8.17

Average Values of the Power Law Exponent (*p*) Based upon 10 Hz 10 and 25 m Wind Data.

Short-Time Period (1 second to 180 seconds)

Component	10 m	25 m
σ_U	0.20 ± 0.12 [(a)]	0.23 ± 0.12
σ_V	0.19 ± 0.14	0.25 ± 0.14
σ_θ	0.19 ± 0.14	0.21 ± 0.15
σ_W	0.06 ± 0.04	0.09 ± 0.06
σ_ϕ	0.06 ± 0.06	0.06 ± 0.10

Long-Time Period (3 minutes to 60 minutes)

Component	10 m	25 m
σ_U	0.26 ± 0.17	0.31 ± 0.18
σ_V	0.27 ± 0.18	0.30 ± 0.18
σ_θ	0.22 ± 0.19	0.29 ± 0.19
σ_W	0.04 ± 0.04	0.06 ± 0.07
σ_ϕ	0.03 ± 0.08	0.05 ± 0.07

(a) mean and standard deviation about the mean.

Figure 8.57 shows the median values of $\overline{p}$ as calculated from Equation 8.32 for each averaging period under consideration. For the purposes of presentation, the 10 and 25 m level data were grouped together. The relative flatness of the curves in both figures indicate a general insensitivity of the p value to time periods ranging from 1 second to 60 minutes. The exception to the above generalization is the apparent sensitivity of σ_U (and σ_ϕ) for t_i less than 10 seconds.

Figure 8.58 shows the median values of p for σ_ϕ as a function of σ_ϕ, a measure of atmospheric stability. For the short-term case with σ_ϕ values less than 10 degrees, the average median exponent is 0.07. For the long-term case, the corresponding exponent is 0.03. The exponent values appear to be relatively invariant with σ_ϕ except for large values of σ_ϕ. The variability for large σ_ϕ can be attributed to a small number of samples and to uncertainties associated with small wind speeds. For the purposes of scaling σ_ϕ according to averaging period, it appears that the assumption of $p=0$, that is σ_ϕ is invariant with time, has been confirmed for neutral and stable atmospheric conditions.

Figure 8.59 shows the median values of p for σ_θ. For both cases, there appears to be considerable variability as a function of σ_ϕ indicating the lack of a clearly defined trend. The average median values of the exponents for short and long-term cases are 0.19 and 0.28, respectively. For the purposes of scaling σ_θ according to averaging period, it appears that 0.2 can be used for time periods less than 3 minutes and 0.3 can be used for time periods between 3 and 60 minutes. This conclusion is valid only for neutral and stable atmospheres. The values are consistent with those reported in the literature for neutral conditions.

8.7.2 Comments

Average power law exponent values (p) to estimate turbulence sigmas (σ_U, σ_V, σ_θ, σ_W, and σ_ϕ) for averaging periods (t_i) ranging from 1 second to 60 minutes from three-minute average sigmas were computed. The results can be summarized as:

- For the along wind (σ_U) and crosswind (σ_V and σ_θ) components, the average p values were between 0.2 and 0.3. This is consistent with what is reported in the literature for the crosswind components. The p values were found to be insensitive to averaging period.

- For the vertical (σ_W and σ_ϕ) components, the small p values (0.04 to 0.06) indicate that the vertical component is insensitive to averaging period. The p values were insensitive to averaging period for t_i greater than 10 seconds. For t_i less than 10 seconds, median values of p approaching 0.1 were found.

- There does not appear to be any systematic variation of the exponent p for σ_ϕ and σ_θ variations as a function of stability for neutral and stable conditions.

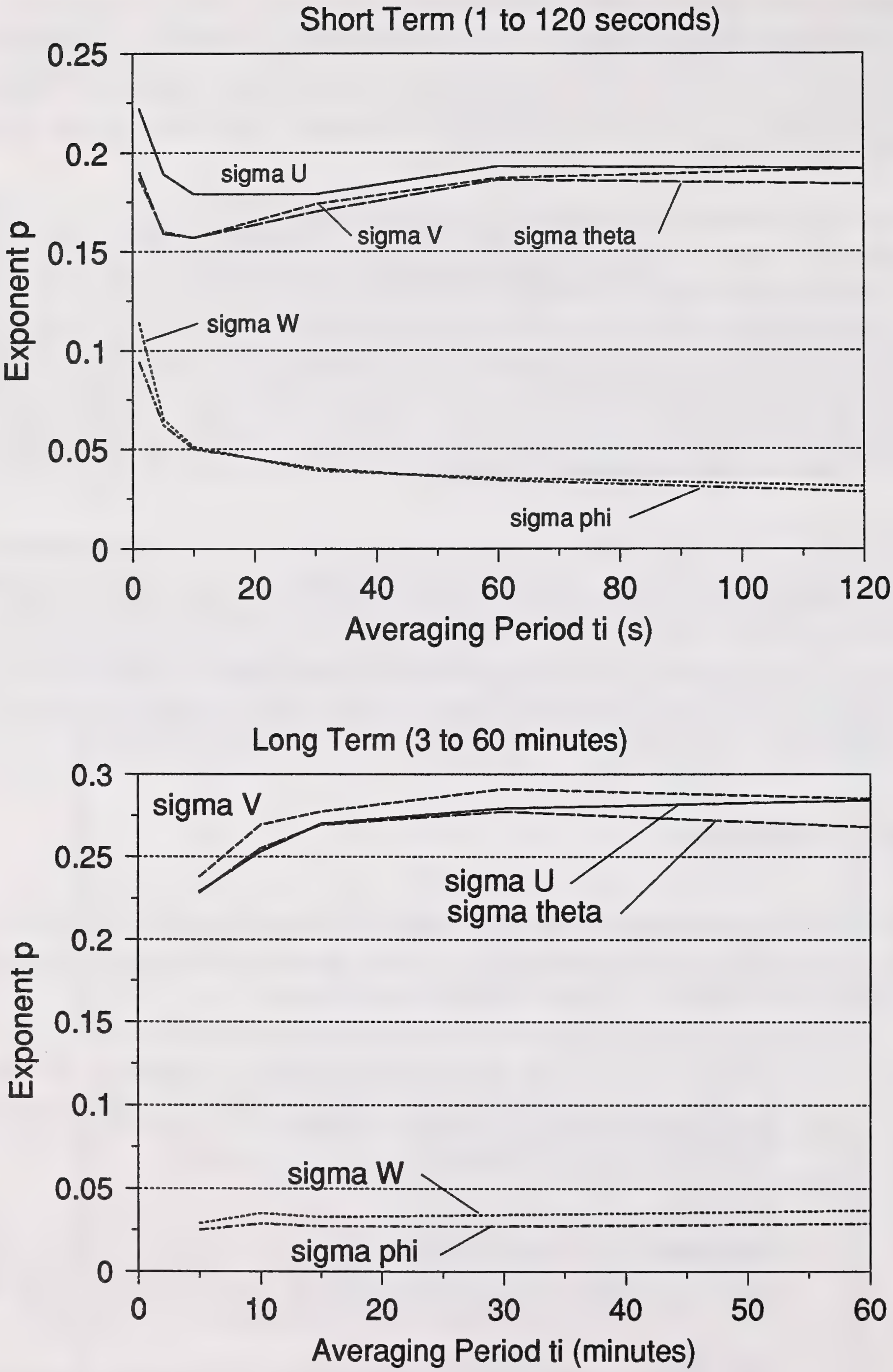

Figure 8.57

Median Values of the Exponent *p* for t_i values.

Short Term (1 to 120 seconds)

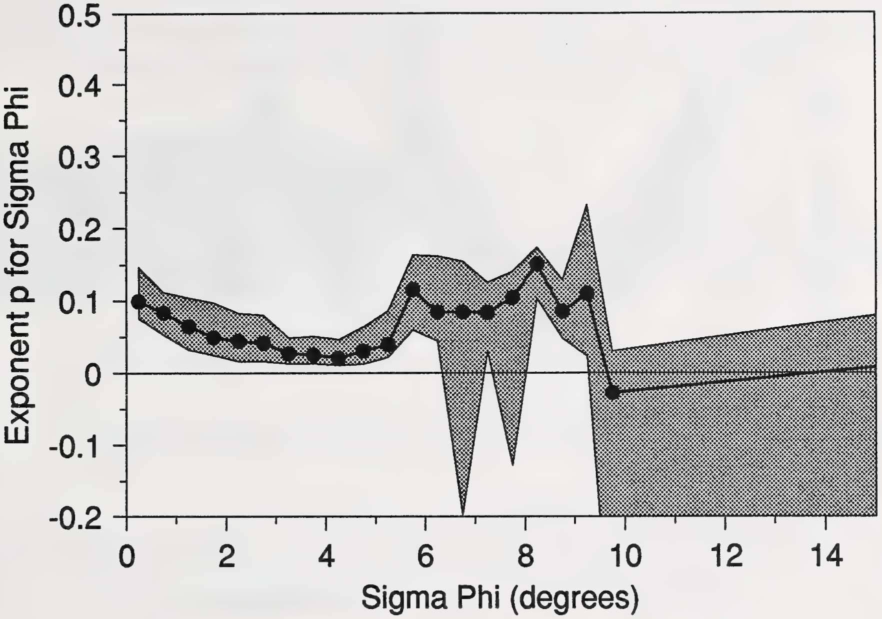

Long Term (3 to 60 minutes)

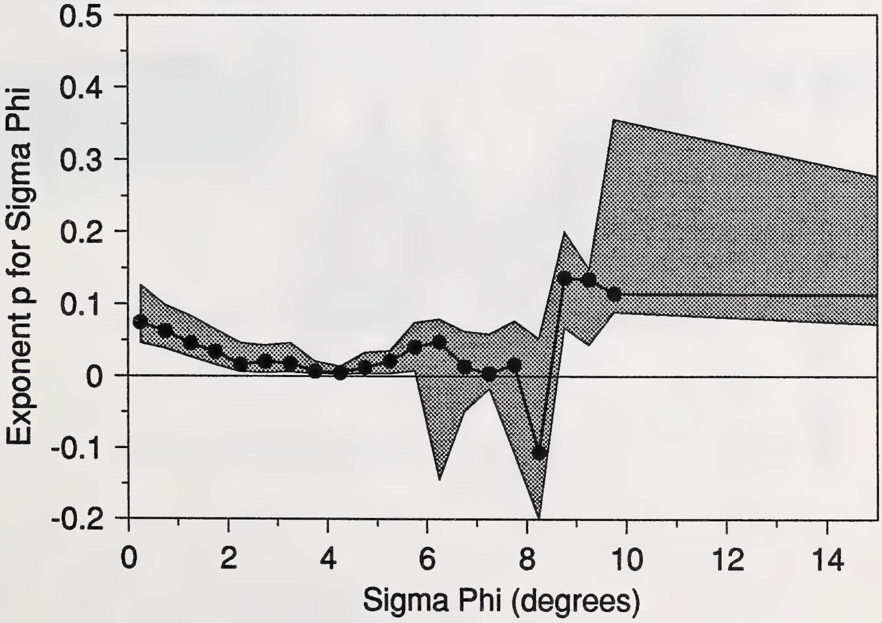

Figure 8.58

Median Values of the Power Exponent for the Vertical Wind Variation σ_ϕ (short and long term) as a Function of Atmospheric Turbulence σ_ϕ. The Shaded Envelope Indicates the 25% and 75% Quartile Limits.

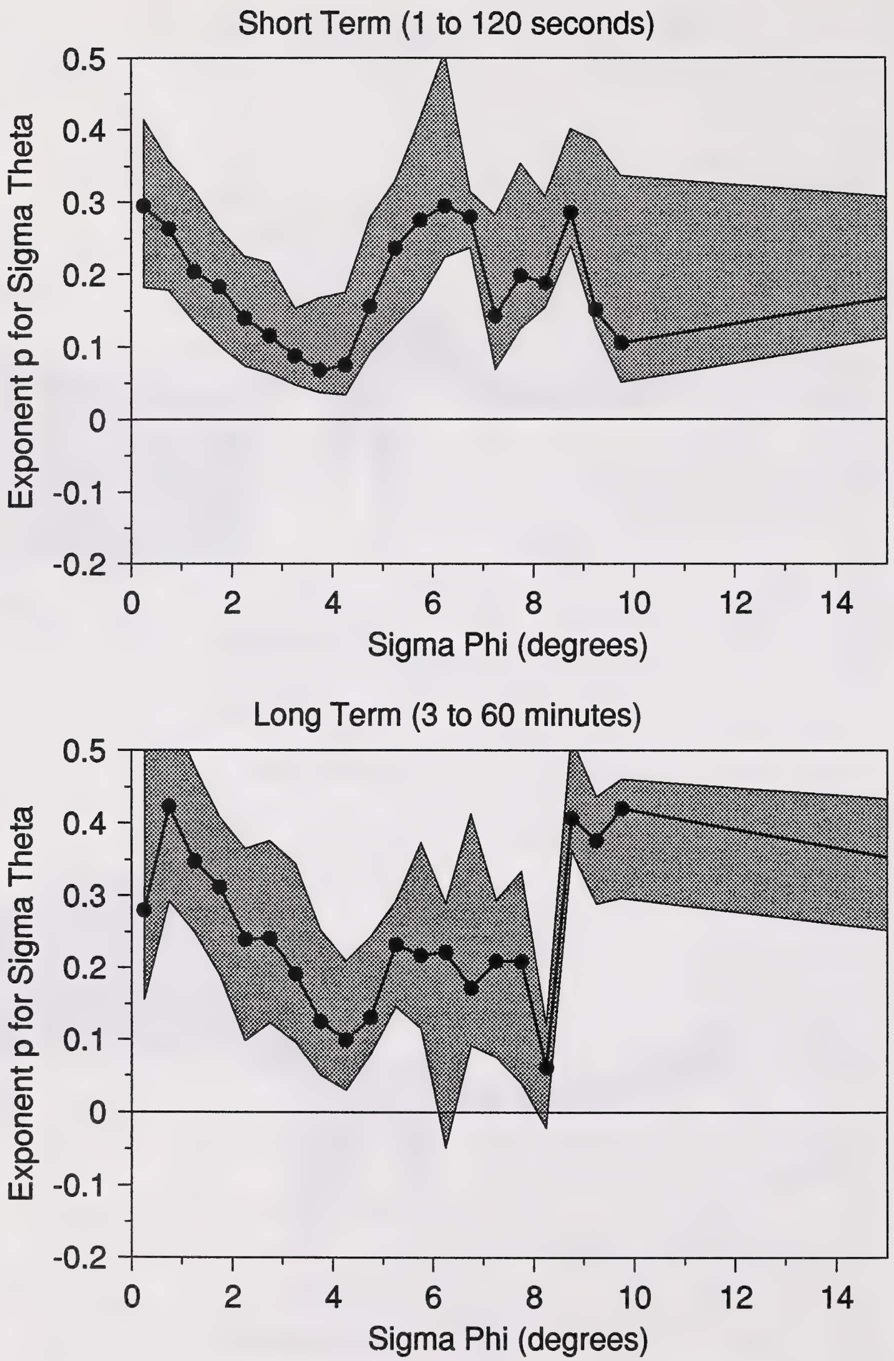

Short Term (1 to 120 seconds)

Long Term (3 to 60 minutes)

Figure 8.59

Median Values of the Power Exponent for the Horizontal Wind Variation σ_θ (short and long term) as a Function of Atmospheric Turbulence σ_ϕ. The Shaded Envelope Indicates the 25% and 75% Quartile Limits.

In conclusion, a power law exponent of 0.2 can be used to extrapolate σ_θ values from the three-minute values to shorter time periods. The exponent of 0.3 can be used to extrapolate σ_θ values from the three-minute values to longer time periods (up to 60 minutes). For most purposes, the vertical component σ_ϕ can be assumed to be independent of time.

8.8 Anemometer Comparison

Wind measurements obtained with Gill UVW propeller anemometers were compared to those obtained with sonic anemometers. The Field Measurement Program observations allowed the following comparisons to be undertaken:

- Kaijo-Denki sonic anemometer and the Gill UVW (both located at 10 m).
- Applied Technologies sonic anemometer and the Gill UVW (both located at 25 m).

The wind speed (U), wind direction (θ), standard deviation of the wind direction (σ_θ). Standard deviation of the vertical wind (σ_W and σ_ϕ) measurements at each level were compared. The comparison used three-minute average wind data.

8.8.1 Comparison Statistics

To facilitate the comparison between the two types of anemometers, the following performance statistics were used:

- Sample bias:

$$B = \frac{1}{N} \sum_{i=1}^{N} D_i \tag{8.33}$$

- Absolute precision or standard deviation of the difference:

$$S = \left(\frac{1}{N} \sum_{i=1}^{N} [D_i - \overline{B}]^2 \right)^{1/2} \tag{8.34}$$

- Relative error as a percentage of the reference:

$$P = 100 \left(\frac{S}{\overline{R}} \right) \tag{8.35}$$

where:
$D_i = Y_i - R_i$
N = number of observations
Y_i = observation for Gill UVW
R_i = observation for sonic anemometer
$\overline{R}$ = mean value of R_i from N observations.

These performance statistics have been used by others to compare wind measurement systems (Kaimal *et al* 1984, Chintawongvanich *et al* 1989). The first study focussed on tower based in situ anemometers while the second compared in situ sensors with remote sensors. Both these studies also used a comparison statistic called comparability and defined by:

$$C = \frac{1}{N}\sum_{i=}^{N}[1(Y_i - R_i)^2]^{1/2} \tag{8.36}$$

For the purposes of comparison, the comparability (C) is approximately equal to the standard deviation of the difference (S). For this reason, the comparability numbers are not shown as part of this comparison.

The comparison data set excluded wind directions through the tower. For the 10 m level, only wind directions which were within the 120° angle of acceptance for the Kaijo-Denki anemometer were considered. Care was taken to ensure misleading values were not generated for the wind direction analysis when winds were from the north. The comparison data set consisted of three-minute average values of U, θ, σ_θ, σ_W and σ_ϕ. The comparison statistics for all parameters are presented as a function of the sonic anemometer wind speed for that height.

8.8.2 Wind Speed

The comparison statistics relating to wind speed measurements for both levels are shown in Figure 8.60. The average Kaimal *et al* (1984) values are shown for the purposes of comparison and are referred to as NOAA (National Oceanic and Atmospheric Administration) on the figure.

Several conclusions can be drawn from the figure. The most interesting are the large bias, absolute precision and relative precision values for high wind speeds ($U > 13$ m/s). Additionally:

- Sample bias is relatively uniform with increasing wind speed ($U < 10$ m/s). Up to this wind speed, the absolute values of the bias are similar to the NOAA values.

- Absolute precision increases slowly with increasing wind speed for the 10 m level and is relatively uniform for the 25 m level. The 25 m values are larger than the corresponding 10 m values.

- The relative precision increases to the order of 50% for low wind speeds. For the 10 m level, the relative precision is typically 10 to 12% over the 2 to 15 m/s range.

Excluding the high wind speed data, the bias for the 25 m level was less than that for the 10 m level. The precision performance statistics, however, suggest better agreement between the sensors at the 10 m level than at the 25 m level.

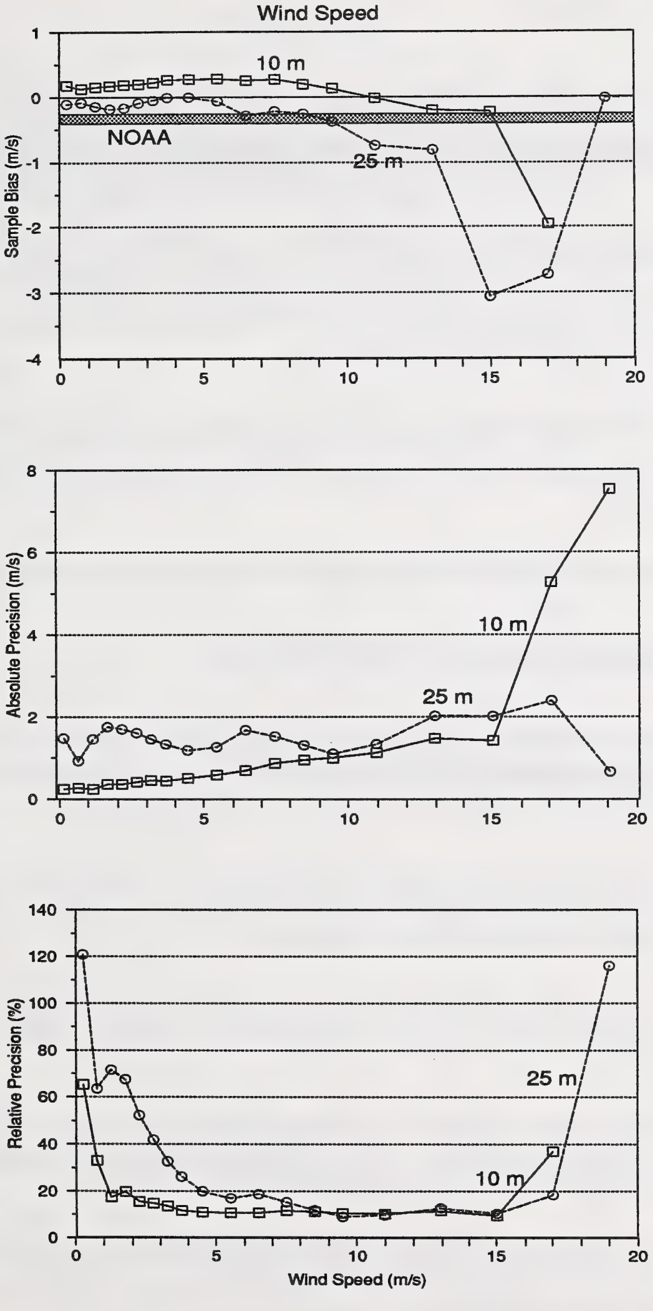

Figure 8.60

Wind Speed Plots of Bias, Absolute Precision and Relative precision for 10 and 25 m levels.

8.8.3 Wind Direction

The comparison statistics relating to wind direction measurements for both levels are shown in Figure 8.61. Due to circular nature of wind direction data, the relative precision is not relevant and, as a consequence, is not shown. Again, larger values occur for high wind speeds ($U > 15$ m/s). Specific comments with respect to wind direction are:

- For the 10 m level, the sample bias is a relatively uniform 2.0 to 2.5 degrees. This is likely due to differences in wind direction sensor alignment. For 10 m level wind speeds under 1.0 m/s, a large bias was observed. This is likely due to the starting threshold of the UVW propellors. The sample bias for the 25 m level indicates poorer agreement.

- Large absolute precision values were observed for small 10 m level wind speeds ($U < 1.0$ m/s). These precision values are about double the comparability values observed for the NOAA study. Precision values at the 25 m level were much larger.

The comparison statistics indicate better agreement at the 10 m level than at the 25 m level.

8.8.4 Standard Deviation of Wind Direction

The comparison statistics relating to the standard deviation of the wind direction (σ_θ or "sigma theta") are presented in Figure 8.62. Again, large values occur for high wind speeds ($U > 15$ m/s). Specific comments with respect to σ_θ values are:

- The sample bias is relatively uniform up to 15 m/s for the 25 m level. For the 10 m level, the bias increases for very low wind speeds ($U < 1$ m/s). Bias values are typically about 2 degrees.

- The absolute precision is relatively uniform over the range from 2 to 15 m/s for the 10 m level. At low wind speeds, the precision values increase for both levels.

- The relative precision is typically ±50% at the 10 m level for wind speeds between 2 and 10 m/s. For wind speeds less than 7 m/s, much larger relative precision values were observed for the 25 m level.

The precision and sample bias numbers shown in the figure are within the ranges provided in the NOAA study. Typical relative precision numbers for the Chinawongvanich *et al* (1989) study were about 100%.

8.8.5 Standard Deviation of Vertical Wind Speed

The comparison statistics relating to the standard deviation of the wind direction (σ_W or "sigma W") are presented in Figure 8.63. Specific comments with respect to σ_W values are:

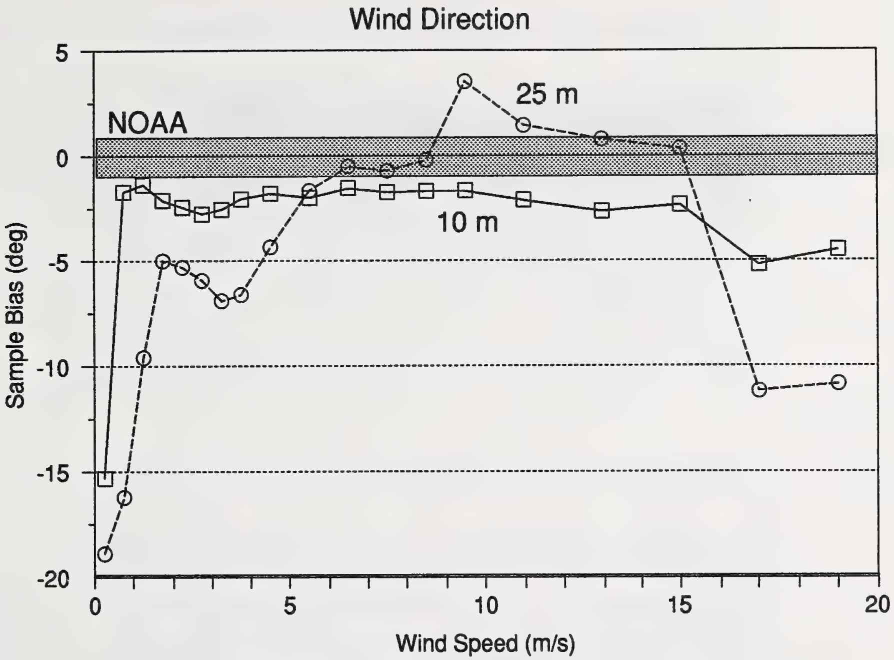

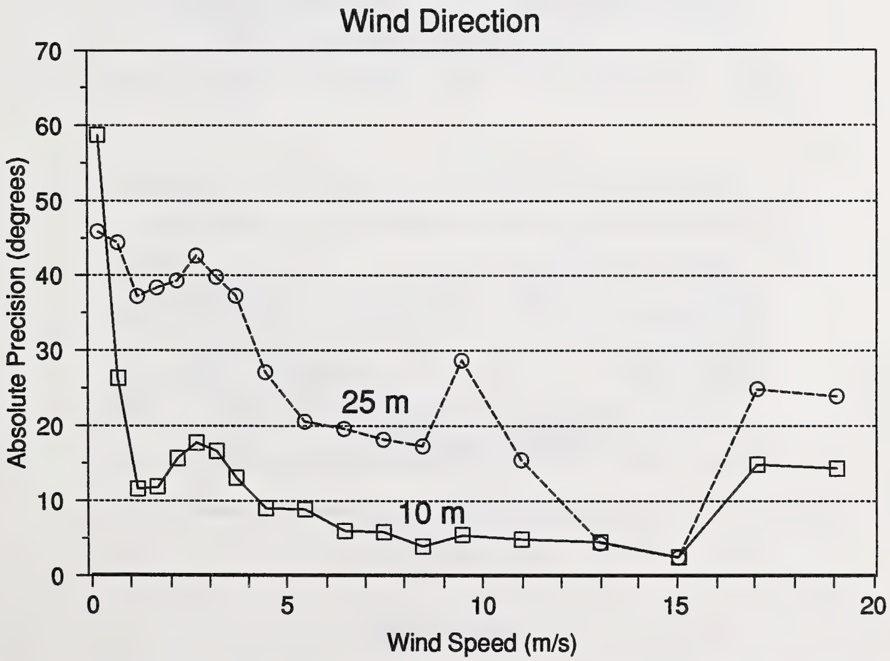

Figure 8.61

Wind Direction Plots of Bias and Absolute Precision for 10 and 25 m levels.

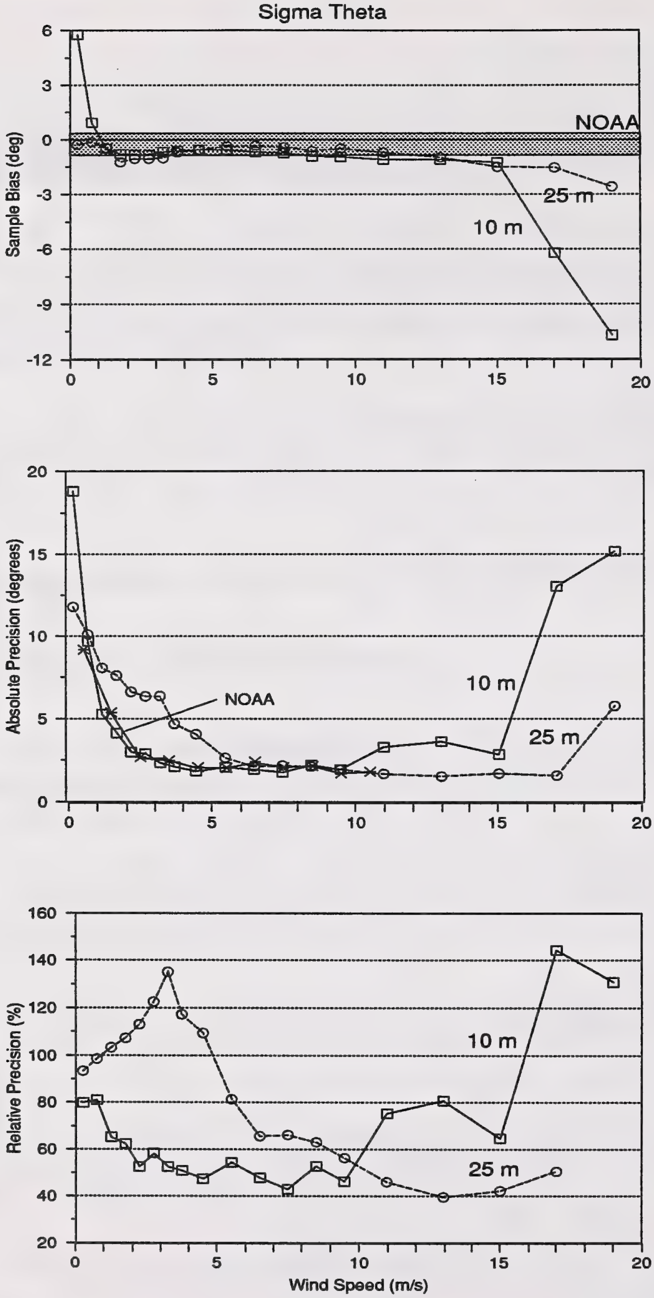

Figure 8.62

Sigma Theta Plots of Bias, Absolute Precision and Relative precision for 10 and 25 m levels.

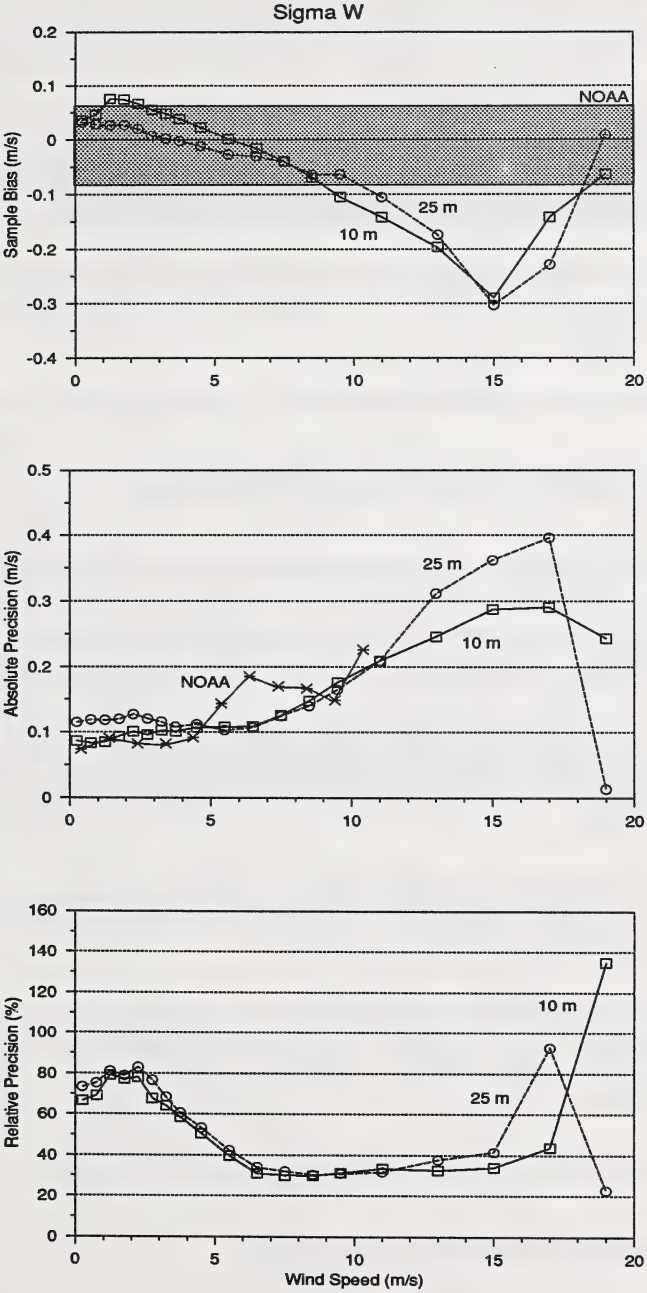

Figure 8.63

Sigma W Plots of Bias, Absolute Precision and Relative precision for 10 and 25 m levels.

- The sample bias is minimum for wind speeds of around 5 m/s. For larger wind speeds, the magnitude of the bias increases linearly with increasing wind speed. This may be due to alignment departures from vertical and/or the non-cosine response of the propellors.

- The absolute precision also increases linearly with increasing wind speed. The NOAA study observed the same magnitude with the comparability. For wind speeds less than 6 m/s, the precision values are typically 0.1 m/s.

- The relative precision indicates uncertainties of 30 to 40% for wind speed ranges from 5 to 15 m/s. For lower wind speeds, the relative precision values increase to 80%.

There is relatively little difference between the comparison statistics for the two levels.

8.8.6 Standard Deviation of Vertical Wind Angle

The comparison statistics relating to the standard deviation of the vertical elevation angle (σ_ϕ or "sigma phi") are presented in Figure 8.64. As σ_ϕ is calculated from σ_W/U, the statistical comparison will reflect uncertainties in the estimation of both σ_W and U. Large deviations from any systematic trends are observed for $U > 13$ m/s. The results in the figure indicate:

- The sample bias is the smallest over the wind speed range 4 to 10 m/s. For smaller wind speeds, the bias can increase to 1 to 2 m/s. The magnitude of the bias for these smaller wind speeds is similar to that observed for the NOAA study.

- The absolute precision is relatively uniform (1 degree) over the 5 to 15 m/s wind speed range for the 10 m level. The precision for both levels increases significantly with low wind speeds.

- The 10 m relative precision indicates uncertainties of about 40% for wind speed ranges from 5 to 15 m/s. For lower wind speeds, the 10 m relative precision values increase to 80%. The relative precision values are larger for the 25 m level.

There was better agreement at the 10 m level than at the 25 m level.

8.8.7 Turbulence Frequency Distribution

In Section 8.4.2, frequency distributions for σ_θ and σ_ϕ were shown for the 10 m Kaijo-Denki sonic anemometer. To evaluate the effectiveness of the UVW anemometer in measuring turbulence levels, similar plots based on the 10 m UVW anemometer were prepared and compared to those from the Kaijo-Denki instrument. Specifically, frequency distributions were prepared from 30-minute average data from the winter period (October 1988 to March 1989) and from 3-minute average data for December 1988.

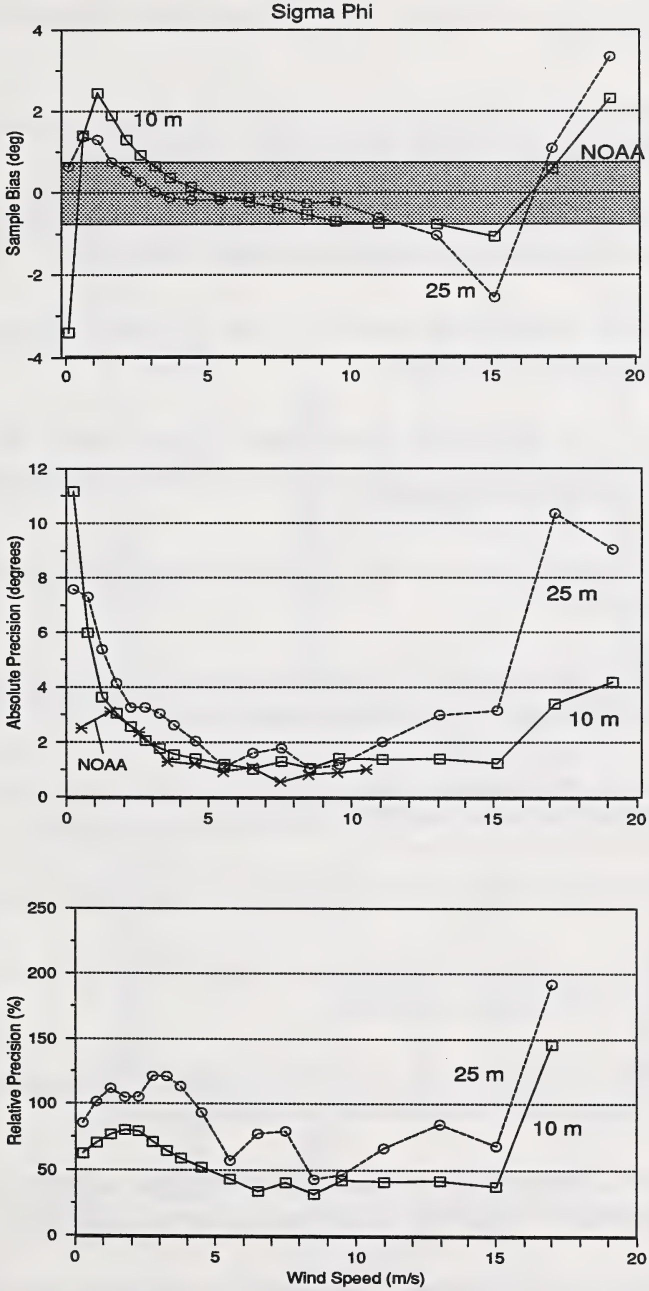

Figure 8.64

Sigma Phi Plots of Bias, Absolute Precision and Relative precision for 10 and 25 m levels.

Figure 8.65 shows the comparisons for σ_W. The conclusions which can be drawn from the figures are as follows:

- For σ_W values less than 0.2 m/s, the UVW instrument will underestimate the frequency of occurrence of the vertical turbulence levels.
- For σ_W values between 0.2 and 0.5 m/s, the UVW instrument will overestimate the frequency of occurrence of the vertical disturbance.
- For σ_W values greater than 0.5 m/s, the two instruments should read similar frequencies of occurrence.
- The UVW anemometer records zero σ_W values which likely coincide with conditions when the vertical propeller is not turning due to either low wind speeds or frosting of the propeller.

Figure 8.66 shows the comparisons for σ_ϕ. The conclusions which can be drawn from the figure are as follows:

- For σ_ϕ values less than 3°, the UVW instrument will underestimate the frequency of occurrence of the vertical turbulence intensity.
- For σ_ϕ values greater than 4°, the UVW instrument will overestimate the frequency of occurrence of the vertical turbulence intensity.
- The UVW anemometer will record zero σ_ϕ values since zero σ_W are recorded.

Figure 8.67 shows the frequency distribution comparisons for σ_θ. The conclusions which can be drawn from the figure are as follows:

- For σ_θ values less than 4°, the UVW anemometer will overestimate the frequency of occurrence of the crosswind turbulence intensity.
- For σ_θ values between 4° and 6°, the UVW anemometer will underestimate the frequency of occurrence of the crosswind turbulence intensity.
- For σ_θ values larger than 7°, both instruments should read similar frequencies.
- The agreement between the three-minute values appears to be better than that for the 30-minute values.

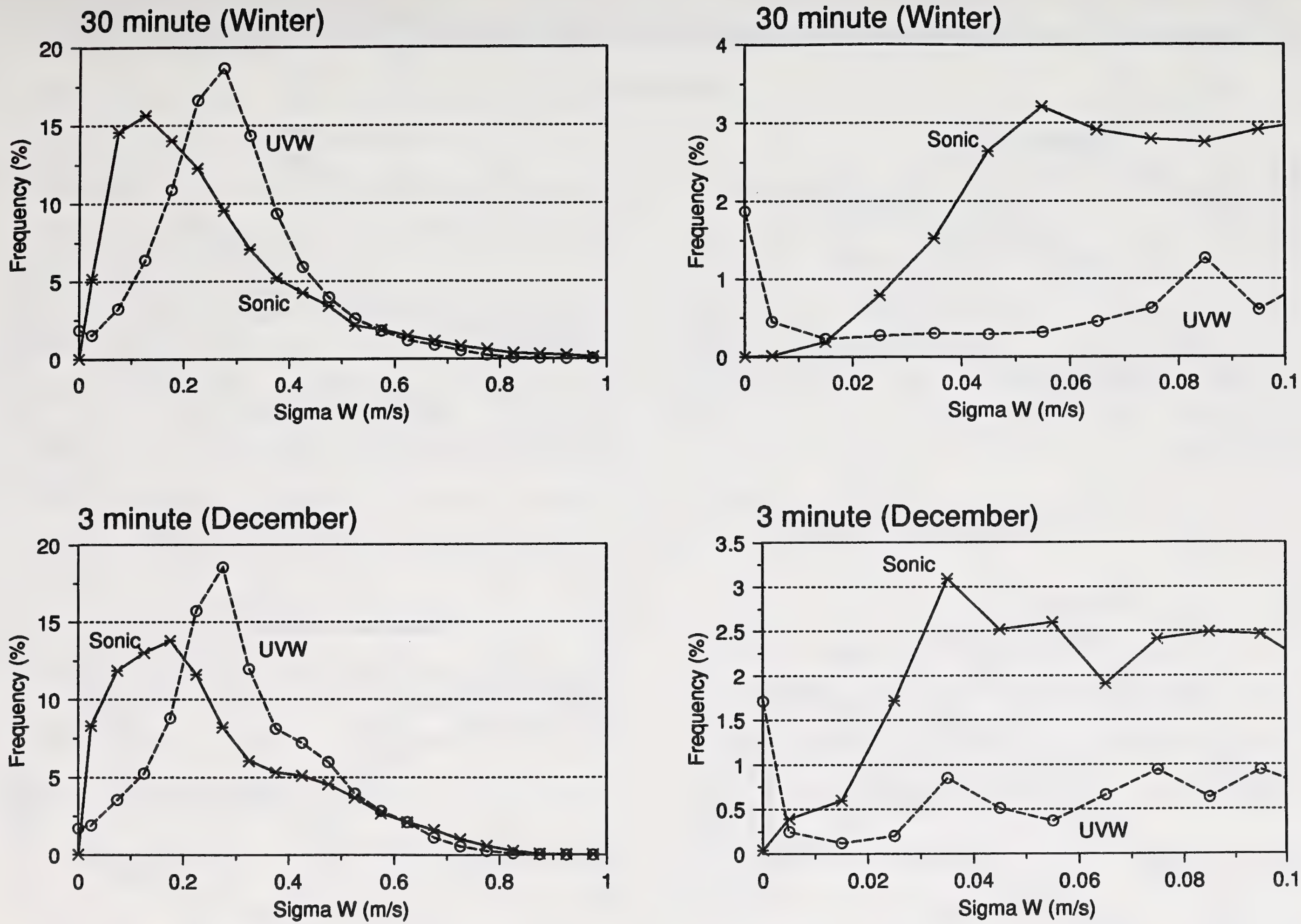

Figure 8.65

Comparison of the σ_W Frequency Distributions for the 10 m Kaijo-Denki Sonic and Gill UVW Anemometers.

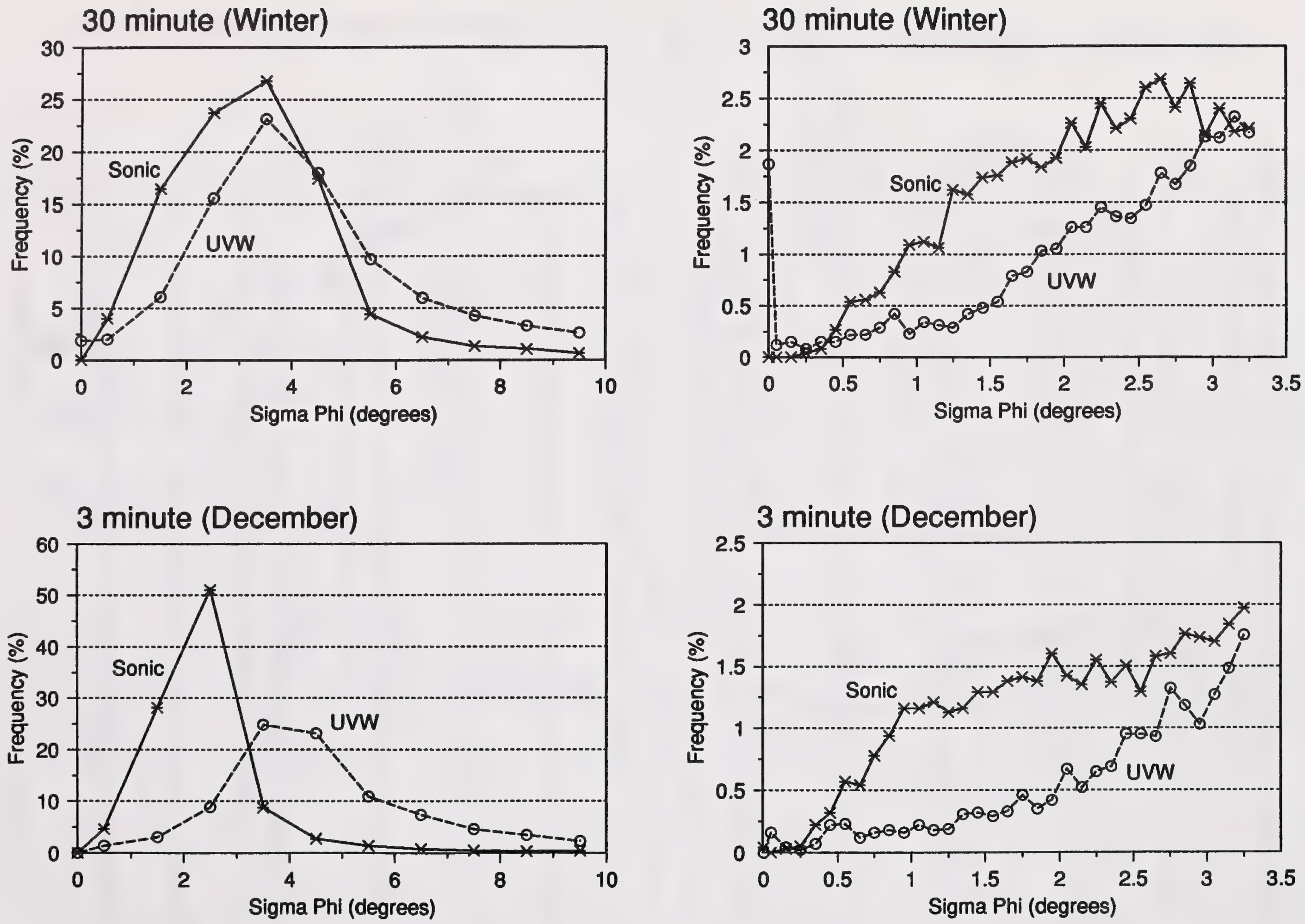

Figure 8.66

Comparison of the σ_ϕ Frequency Distributions for the 10 m Kaijo-Denki Sonic and Gill UVW Anemometers.

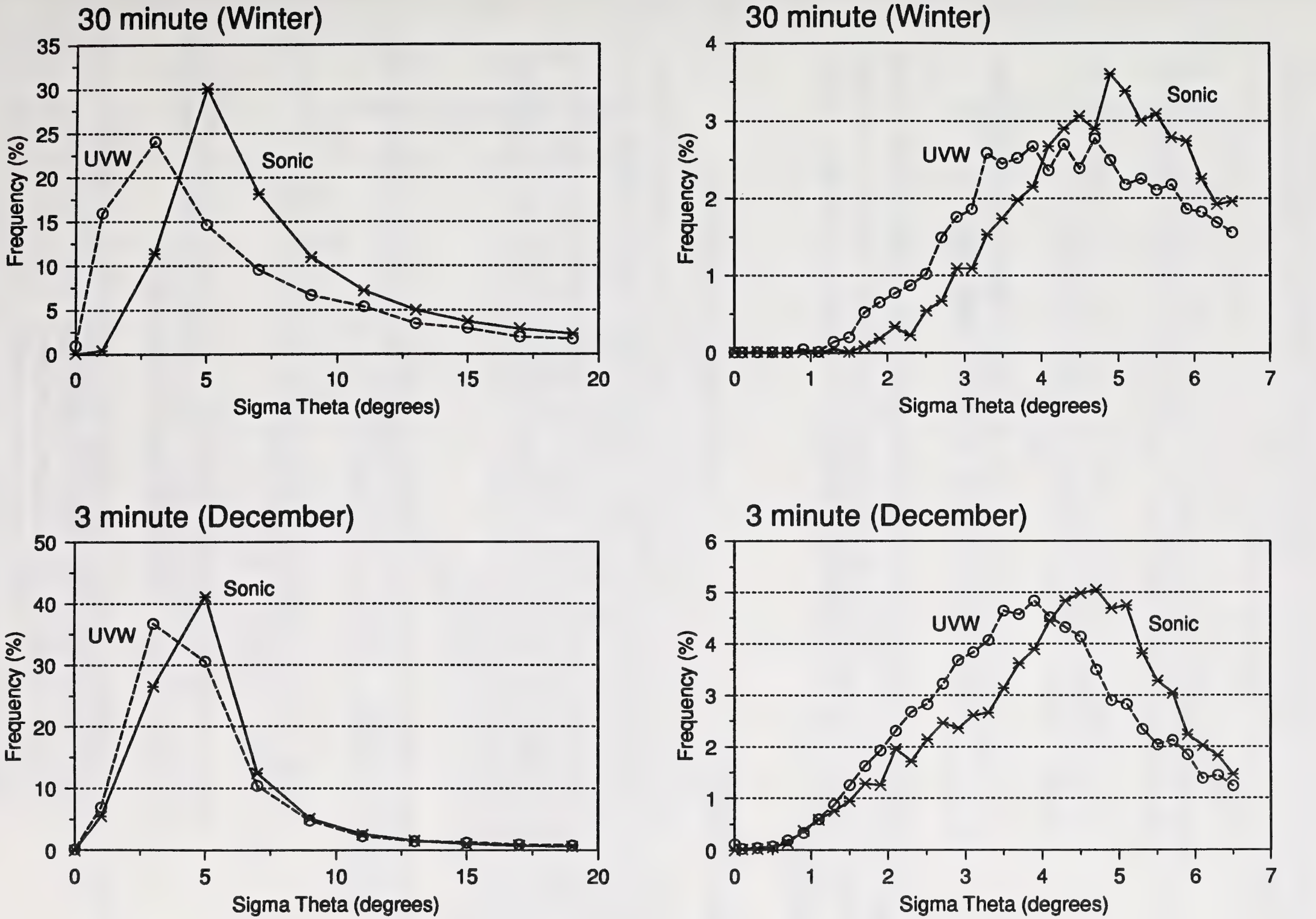

Figure 8.67

Comparison of the σ_θ Frequency Distributions for the 10 m Kaijo-Denki Sonic and Gill UVW Anemometers.

In addition, the median σ_W, σ_ϕ and σ_θ values were plotted as a function of the 10 m wind speed (sonic) for the two anemometer systems. The median values and wind speeds are based on 30-minute averages from the winter period and on 3-minute averages for the month of December 1988. The results are presented in Figure 8.68 to 8.70. The conclusions which can be drawn from these figures are as follows:

- For wind speed values less than 6 m/s, the UVW anemometer tends to overestimate the vertical turbulence (σ_W) and vertical turbulence intensity (σ_ϕ).

- For the 30-minute σ_θ values, the UVW anemometer tends to overestimate the crosswind turbulence intensity for wind speeds less than 2 m/s.

- For the crosswind turbulence intensity (σ_θ), there is better agreement between the two anemometer systems than for the vertical component.

In general, the UVW anemometer is better at estimating the crosswind (σ_θ) than the vertical components (σ_W or σ_ϕ) components under low turbulence conditions. The above conclusions are based on the sonic anemometer as providing true estimates of turbulence in the atmosphere.

8.8.8 Comments

The NOAA anemometer comparison study was a carefully controlled test carried out over a three-week period in September 1982. The wind data were carefully edited to remove spurious values that resulted from instrument malfunction, line noise, birds and rain. In contrast, the Field Measurement Program data used for this evaluation were collected over a six-month period centered on a winter season. For this reason, greater scatter can be expected for the Field Measurement Program comparison statistics when they are compared to the NOAA study. Even though a greater scatter was observed, similar trends with wind speed were observed for both studies.

The comparison statistics implicitly assume that the sonic anemometer at each level was the reference instrument. It should be noted that spurious results can be attributed to both the sonic and the UVW anemometers. Specifically:

- During the winter when the relative humidity is relatively high, a build-up of hoarfrost occurred on both instruments.

- This frost build-up obviously degraded the UVW propellor response and in the extreme caused the propellor to stop turning. The associated freeze-thaw cycle would also interfere with the free rotation of the propellers.

- The frost build-up on the transducers also resulted in spurious wind speed measurements from the Applied Technologies sonic anemometers. In particular, anomalous high wind speed values would occur before the unit would report missing data. In some cases, these anomalous values were obvious while in others there was no clear indication that a degradation of the data had occurred.

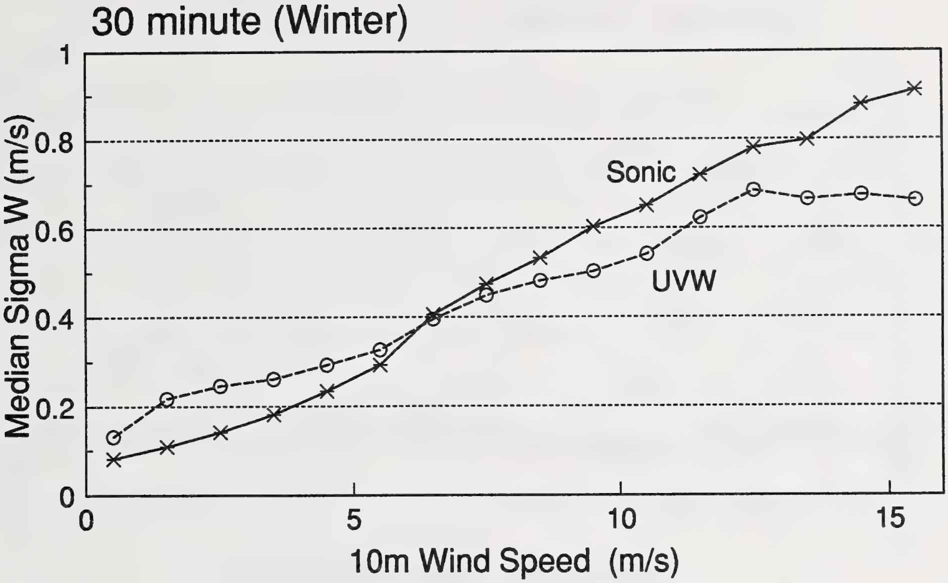

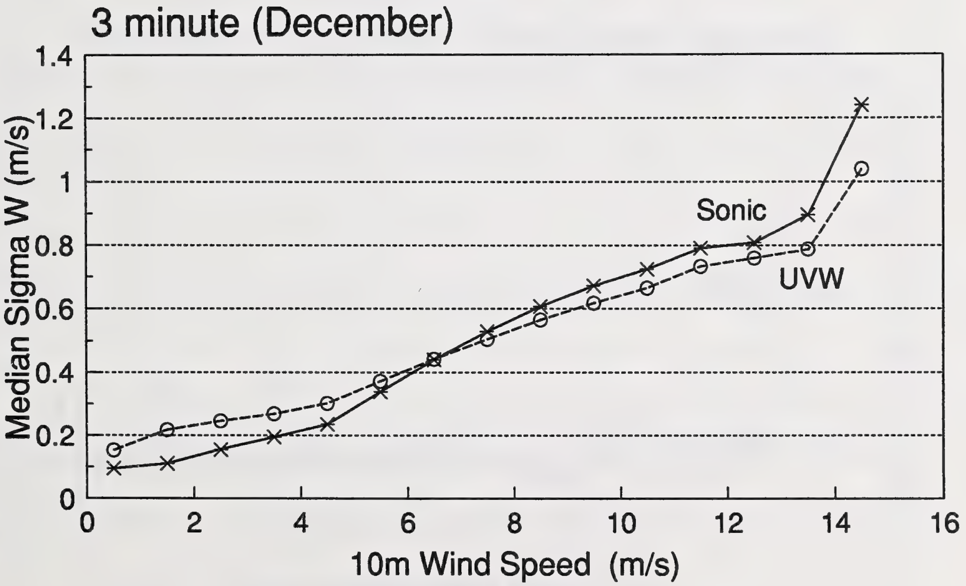

Figure 8.68

Comparison of Median σ_W Values for the 10 m Kaijo-Denki Sonic and Gill UVW Anemometers Versus Wind Speed.

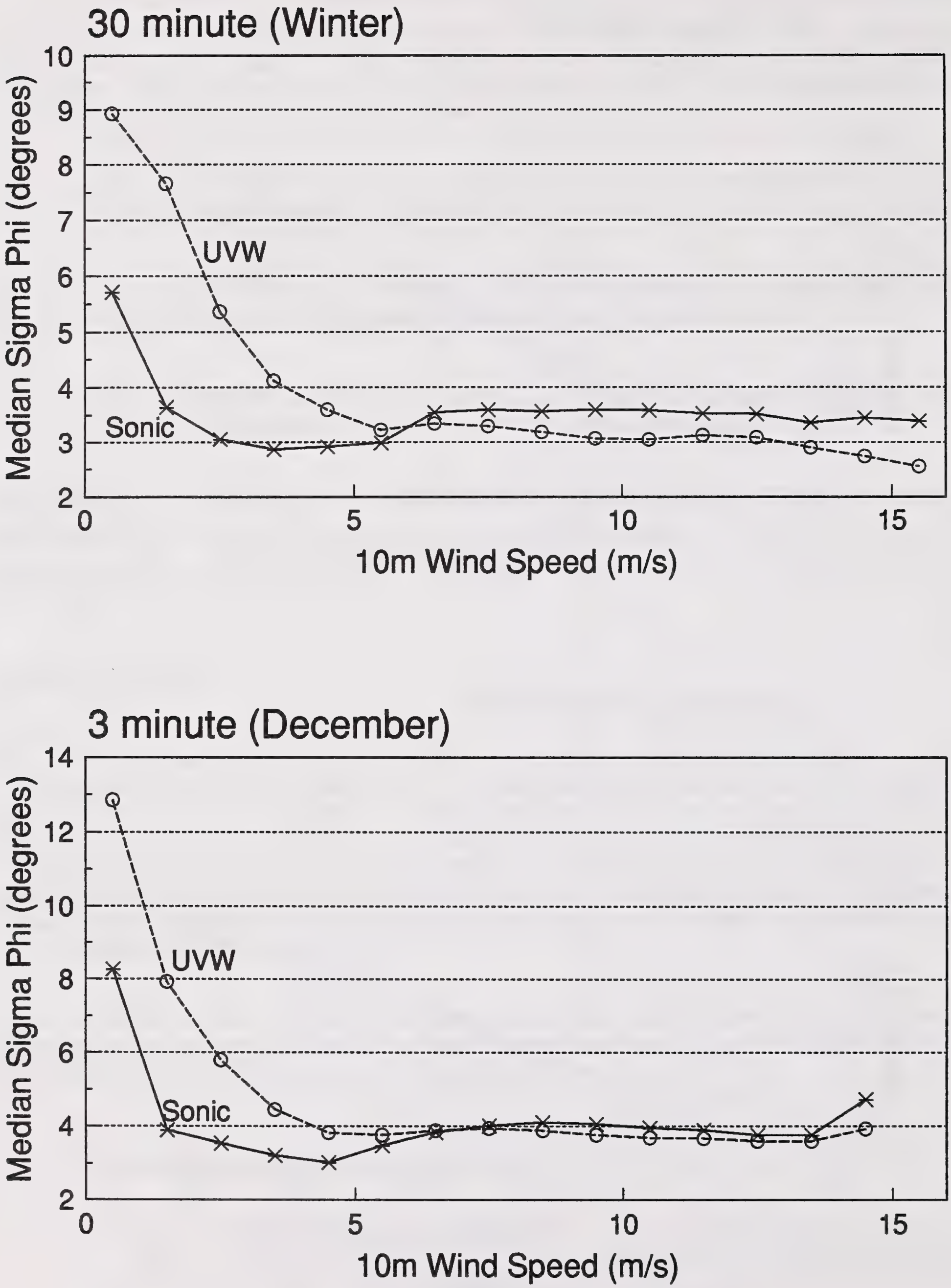

Figure 8.69

Comparison of Median σ_ϕ Values for the 10 m Kaijo-Denki Sonic and Gill UVW Anemometers Versus Wind Speed.

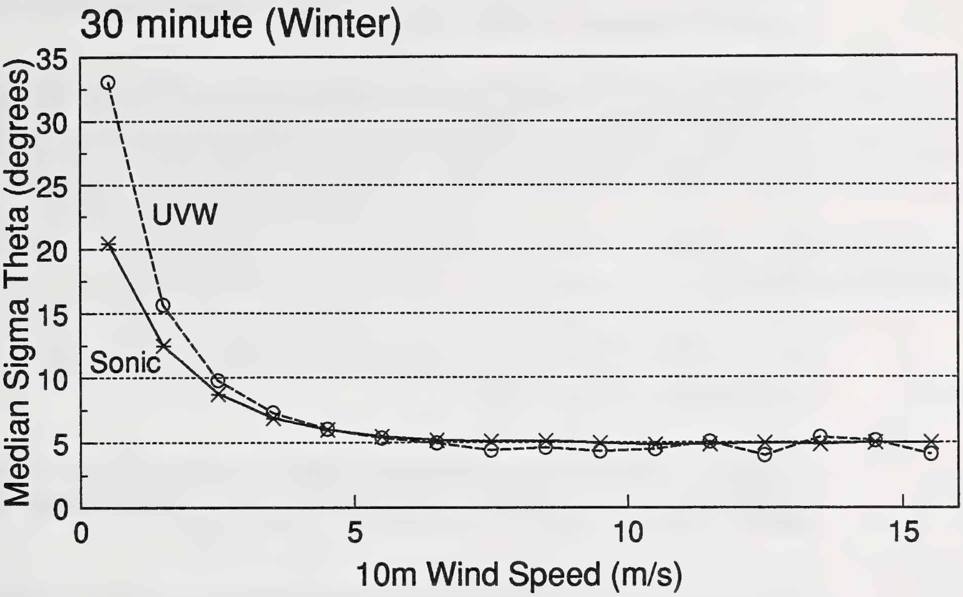

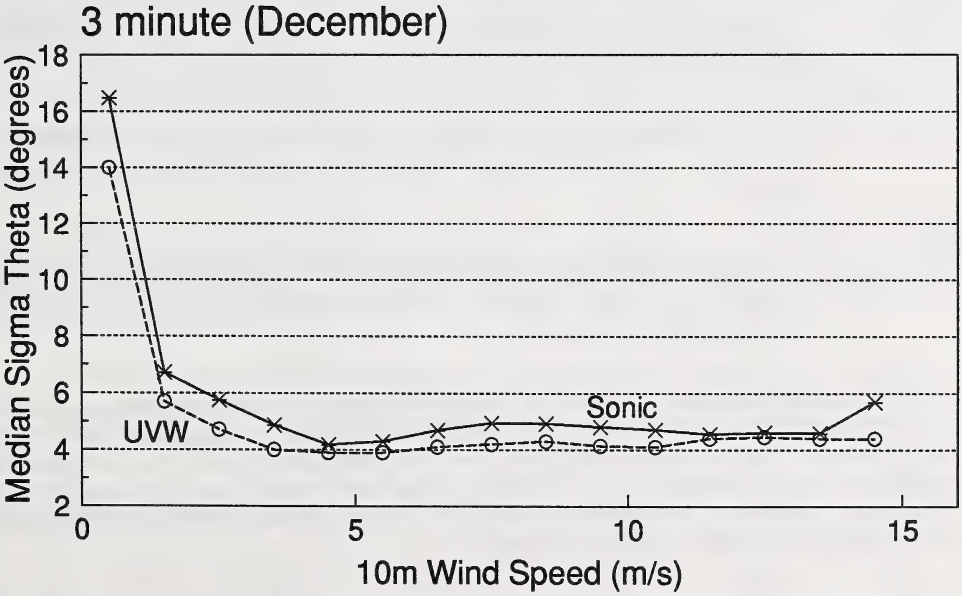

Figure 8.70

Comparison of Median σ_θ Values for the 10 m Kaijo-Denki Sonic and Gill UVW Anemometers Versus Wind Speed.

- There was no obvious evidence that the frost build-up on the Kaijo-Denki transducers degraded the wind measurements.

- The 10 m wind sensors were better maintained than the 25 m ones during the study due to the proximity to the ground. For example, when the tower and all instruments were covered in frost, the maintenance technician was more likely to clear the frost build-up from the lower sensors than the upper sensors.

With the above comments in mind, the following general conclusions based on the 10 m level data can be made:

- UVW anemometers should be able to produce reliable wind speed estimates up to 15 m/s. The scatter is typically 0.3 m/s at low wind speeds and 1 m/s at wind speeds of 10 m/s.

- Large wind direction measurement uncertainties (45 degrees) from the UVW anemometer can be expected for wind speeds less than 1 m/s. For larger wind speeds, the scatter is typically in the 5 to 15 degree range.

- Wind direction bias measurements indicate an uncertainty of 2 to 3 degrees in the alignment of the anemometers.

- In the 3 to 15 m/s wind speed range, the UVW anemometer can be used to estimate σ_θ to within 3 degrees. For wind speeds less than 1 m/s, the scatter can be typically 10 degrees.

- The UVW anemometer can estimate σ_W to within 0.1 m/s for wind speeds less than 6 m/s. σ_W values less than 0.1 m/s occur about 25% of the time (Figure 8.27).

- In the 3 to 15 m/s wind speed range, the UVW anemometer can be used to estimate σ_ϕ to within 2 degrees. For wind speeds less than 1 m/s, the scatter can be typically 6 degrees.

The above conclusions are based on new sonic anemometers that were purchased specifically for this study and on "like-new" UVW anemometers which were on loan from Alberta Environment. The latter were only used for short-term studies and new high sensitivity propellors were installed for this study. Larger uncertainties can be expected from compliance monitoring wind measurements due to the longer exposure of the anemometers between calibration and maintenance periods.

8.9 Mixing Height

The depth of the mixing layer can have a significant effect on the dispersion of plumes. Plumes that are trapped within the mixing layer can produce larger ground-level concentrations than those that disperse above the mixing layer. The mixing layer can be produced by mechanical wind shear and by convective mechanisms. Wind shear mechanisms are important for stable boundary layers and high wind speed conditions. Convective mixing is important during the day.

Several models have been used to predict mixing heights with varying degrees of success. For neutral conditions, the depth of the mechanically mixed layer is given by:

$$h_l = \frac{0.2U*}{f} \tag{8.37}$$

For stable conditions, the Zilitinkevich (1972) relationship has been used:

$$h_l = 0.4\left(\frac{U*L}{f}\right)^{1/2} \tag{8.38}$$

The prediction of mixing layer depths (especially for stable conditions) is far from an exact science. In addition, the estimation of mixing heights from acoustic sounder records or from temperature profiles is also associated with considerable uncertainty (Hanna *et al* 1985). In spite of these limitations, the mixing layer relationships given in Equations 8.37 and 8.38 were applied to the Field Measurement Program observations. The predicted values were based on the one-half hour average non-drainage file for periods when $\partial\theta/\partial Z$ and $\overline{W'T'}$ agreed on the simultaneous occurrence of stable conditions.

The predictions using Equations 8.37 and 8.38 were compared to the acoustic sounder records which provided a continuous estimate of mixing layer depths at the Field Measurement Program site. The overall minimum, mean and maximum observed and predicted mixing heights are:

Case	Minimum	Mean	Maximum
Observed	15	151	580
Predicted (Neutral)	0	429	1509
Predicted (Stable)	0	96	2347

The mean predicted stable value is in best agreement with the mean observed value. The median observed and predicted values were then plotted as functions of time of day, wind speed (10 m level) and stability indication (Z/L).

Figure 8.71 shows the observed and predicted mixing height dependence on these variables. The results from the figure indicate:

- **Hour of day**. The median observed values are relatively insensitive to time of day. The median predicted values (for both neutral and stable) show a slight increase during the middle of the day. The median neutral predictions are larger than the observed values while the median stable values tend to be about one-half the observed values.

- **Wind Speed**. The observed median mixing depths are essentially independent of wind speed. For low wind speeds, the median predicted stable values are much less than the median observed values. For most wind speeds, the median predicted neutral values are much larger than the median observed values.

- **Stability Indicator (Z/L).** The median observed mixing depth is relatively independent of stability. Both the median predicted neutral and stable mixing depths decrease with increasing stability. The predicted neutral values are much larger than the observed values. The predicted stable values are much smaller than the observed values for $Z/L > 1$.

In summary, this review of mixing height data suggest that either Equations 8.37 and 8.38 are poor predictive models or that the interpretation of mixing height data from the acoustic sounder provides a poor indication of mixing depth. Poor agreement between predicted and observed values have been reported by others (Hanna *et al* 1985). This disagreement can result from:

- Disagreement in the literature on a consistent method to define nocturnal mixing heights,

- Inability of acoustic sounder to resolve shallow mixing layers well ($Z < 50$ m), and,

- Acoustic sounder uncertainties of up to ± 30 m in the height measurement.

The latter two factors may be partially overcome by using an acoustic sounder in a research mode rather than an operational mode. To further evaluate the predictive capability of the stable mixing height relationship the tethersonde wind profiles were assessed. The mixing height can be determined from the height of the nocturnal low-level jet (Hanna *et al* 1985). As was seen in Figure 8.17, the height of this low-level jet can be in the 10 to 20 m range. The median predicted depth for large Z/L is in this range (Figure 8.71).

Mixing heights were obtained from the tethersonde wind profiles. The mixing depths were taken as the height of low-level wind speed maxima. A total of 13 wind profiles were obtained from the tethersonde data set. The observed mixing heights, concurrent U^* and L values and predicted neutral and stable values are shown in Table 8.18

On the average, the predicted neutral values are nearly an order of magnitude larger than the observed values. In contrast, the mean observed mixing height is equal to the mean predicted value for stable conditions. There is, however, considerable scatter for the individual observed and predicted stable pairs. Some of the large scatter may be due to uncertainties in L and U^* under very stable conditions.

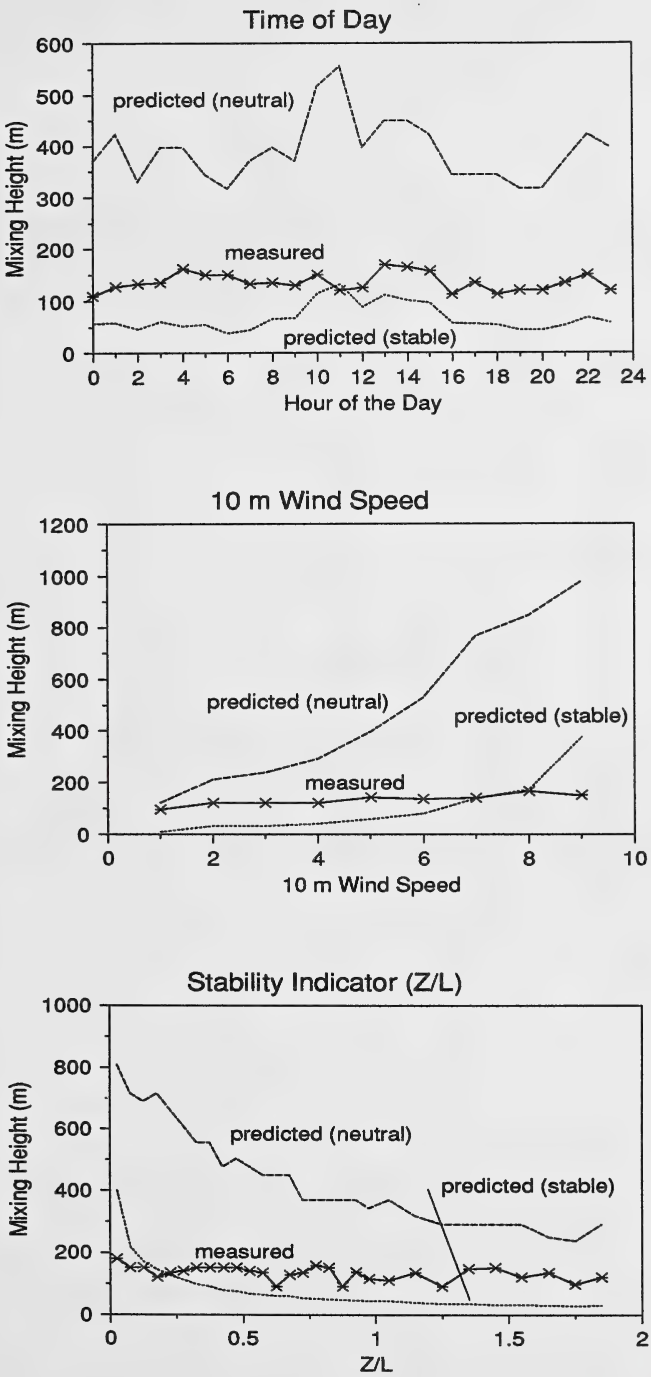

Figure 8.71

Median Observed and Predicted Mixing Heights as a Function of Time of Day, Wind Speed and Stability Indicator.

While the results presented in Table 8.18 cannot be viewed as a validation of the stable plume rise model, it does provide support that the model can predict values that are in the same order as those observed.

Table 8.18

Comparison of Predicted and Observed Mixing Height Values. Observed Values are Defined as the Height of the Low Level Wind Maximum. Predicted Levels are for Neutral and Stable Conditions.

Case	U^* (m/s)	L (m)	Z_i Observed (m)	Z_i Predicted (Neutral) (m)	Z_i Predicted (Stable) (m)
1	0.03	0.4	30	79	4
2	0.01	0.1	25	26	1
3	0.09	12.5	15	238	40
4	0.02	2.0	25	53	7
5	0.09	8.9	60	238	34
6	0.08	3.1	20	212	19
7	0.07	7.1	20	185	27
8	0.22	88.1	40	582	165
9	0.04	1.5	30	106	9
10	0.11	6.5	40	291	32
11	0.08	13.0	40	212	38
12	0.06	0.7	25	159	8
13	0.08	1.4	20	212	13
Mean	0.08	11.2	30	200	30

9 Comments

A large effort was made by the project team to collect and analyse concurrent SF_6 source, ambient SF_6 concentration and meteorological data to describe atmospheric transport and dispersion processes under low wind speed stable atmospheric conditions. Additional effort was undertaken to gain an understanding and confidence level in meteorological measurements and atmospheric turbulence processes. The objective of Volume 1 and the associated appendices (Volumes 2 and 3) is to document the approaches that were used to collect the data and present the results obtained from a review of the data. As the data set resulting from the Field Measurement Program is significant and may be of further use to other investigators in the future, special attention was given to this documentation.

The initial results of the analysis presented in this volume focussed on reviewing all the data, rather than the review of case studies. The adopted approach has the advantages of providing an overview of the important processes and a degree of understanding of the significant features of these processes. The danger in the analysis of any meteorological data set which addresses a wide range of conditions, is that significant and infrequently occurring processes may be hidden by the averaging processes. Detailed case studies which carefully screen the data set to isolate selected behavior characteristics can overcome these limitations. The analysis presented in this volume did not focus on the case study approach.

In an effort to provide concluding remarks for this analysis, the individual program objectives identified in Section 1 have been revisited. In particular, the objectives are re-stated and comments regarding the findings for that particular objective are stated.

9.1 Tracer Study Comments

Five objectives for the tracer component of the Field Measurement Program were identified in Section 1.4.1 of the report. The analyses which responded to these objectives were presented in Section 7.

Objective 1: ***Determine the appropriateness of the Gaussian plume approximation in describing the cross-wind concentration profile in the plume.***

A total of 846 individual plume traverses were collected at downwind distances of 700, 1 400 and 2 100 m and were associated with elevated and surface releases. In many cases, the observed concentration profiles were virtually indistinguishable from a Gaussian distribution, while in others, the observed profiles were skewed or even bimodal. These latter profiles, as a consequence, cannot be regarded as Gaussian. For the 846 cross-wind profiles, the mean skewness and kurtosis coefficients of 0.06 and 2.94 respectively, indicate that on the average, the cross-wind profile can be adequately represented by a Gaussian distribution.

For individual profiles which do not follow a Gaussian profile, a more detailed individual case study analysis would be required to determine the cause. For example, a skewed distribution could result if the wind direction is changing systematically as the traverse is being carried out. Variable wind direction shear with height may also result in bimodal concentration profiles.

While the more detailed case study approach may help resolve the departures from a Gaussian profile, the findings may be of limited practical use in terms of the application to our understanding of dispersion processes and subsequent modelling of these processes.

Objective 2: Identify the meteorological conditions which resulted in the smallest cross-wind plume spreads.

During the collection of the traverse data, the 10 m level mean wind speeds were typically in the 2 to 3 m/s range with minimum values less than 0.5 m/s and maximum values in the 7 to 9 m/s range. About 16% of the traverses were associated with 10 m level wind speeds less than 2 m/s. Vertical atmospheric turbulence (σ_ϕ) levels were 3 to 4 degrees with minimum values of less than 1 degree. Horizontal atmospheric turbulence (σ_θ) levels were typically in the 6 to 10 degree range with minimum values between 1 and 2 degrees. The mean vertical temperature gradients over the 10 to 2 m layer were about 0.2 K/m (2 K/100 m) with maximum values up to 1 K/m (100 K/100 m).

At 700 m, there were 15 traverses associated with instantaneous plume spreads (σ_{yi}) less than 10 m. These minimum values were consistent with those found by other investigators. The smallest (σ_{yi}) values were associated with mean 10 m level wind speeds of 2.4 m/s, vertical turbulence (σ_ϕ) of 1.6 degrees, horizontal turbulence (σ_θ) of 2.2 degrees and a vertical temperature gradient of 26 K/100 m.

At 1 400 m, there were 21 traverses that were associated with instantaneous plume spreads (σ_{yi}) that were less than 20 m. The minimum values were consistent with those found by other investigators. The smallest σ_{yi} values were associated with mean 10 m level wind speeds of 3.5 m/s, vertical turbulence (σ_ϕ) of 2.4 degrees, horizontal turbulence (σ_θ) of 7 degrees and a vertical temperature gradient of 14 K/100 m.

What appears to be significant is that, on the average, the smallest plume spread values were **not** necessarily associated with the lowest wind speed condition ($U < 1$ m/s), the smallest vertical turbulence ($\sigma_\phi < 1$ degree), the smallest horizontal turbulence ($\sigma_\theta < 2$ degrees) or with the strongest temperature gradients ($\partial T/\partial Z > 50$ K/100 m). This finding was contrary to the expectation that the smallest plume spreads would be associated with the lowest wind speed and turbulence conditions.

Furthermore, the minimum σ_{yi} values were not associated with the largest χ/Q values. A large χ/Q value indicates minimum dilution whereas a small χ/Q value indicates large dilution. The largest χ/Q values were associated with mean 10 m level wind speeds of 3.8 to 3.9 m/s, vertical turbulence (σ_ϕ) values of 1.9 to 2.3 degrees, horizontal turbulence (σ_θ) of 3.3 to 3.4 degrees and temperature gradients over the 10 and 2 m layer of about 20 K/100 m. The largest χ/Q values were associated with surface releases at the downwind distance of 700 m.

There may be merit in examining the individual traverses, which result in minimum σ_{yi} values and maximum χ/Q values on a case-by-case basis. In particular, stationary non-turbulent conditions should be isolated. A systematic wind direction shift during a traverse could also result in a small σ_{yi} value if the wind direction is turning into the traverse direction. In contrast, if the wind direction is turning in the same direction as the traverse direction, then the σ_{yi} could be overestimated.

As part of this objective, vertical plume spreads σ_{zi} were estimated from the fitted Gaussian cross-wind profiles. Only traverses associated with surface releases were evaluated. The minimum estimated σ_{zi} values were in the range found by others. ($\sigma_{zi} < 5$ m at 700 and 1 400 m). In certain cases, relatively large σ_{zi} values were estimated ($\sigma_{zi} > 20$ m). These large values may indicate some of the limitations associated with assuming a vertical Gaussian profile. Further case study evaluations could be undertaken to investigate other vertical concentration distributions (i.e. exponential).

Objective 3: ***Compare observed instantaneous and time-averaged cross-wind plume spreads with predicted values.***

Instantaneous Plume Spreads

The observed instantaneous cross-wind plume spreads (σ_{yi}) were compared to model predictions for the same. One set of predictions assumed that only turbulence contributed to the cross-wind spread while another set of predictions assumed that the wind direction variation (shear) with height enhanced the plume spread. The inclusion of the wind shear enhancement term was based on wind direction variations in the 4 to 10 m layer. In particular, the wind shear in this layer exceeded 10 degrees for about 30% of the traverses.

The comparison between the predicted and observed instantaneous plume spreads resulted in considerable scatter. For certain source configuration (elevated, ground), receptor distance (700 m, 1 400 m) combinations, there was evidence that the wind shear enhancement term increased the agreement between predicted and observed results while for other combinations, there was evidence that the addition of the wind shear enhancement term decreased the agreement. The overall best agreement was without the wind shear enhancement term where typically 60 to 70% of the predictions were within a factor of two.

To further evaluate the predictive capability of the σ_{yi} models, a case study approach should be used. In particular, traverses that are characterized by relatively stationary and horizontally homogeneous wind and turbulence conditions should be evaluated. This can be accomplished to some extent by screening the data set to select periods when a series of individual traverse profiles are relatively uniform with time and are also accompanied by a relatively uniform wind direction.

Time-averaged Plume Spreads

In addition to the evaluation of instantaneous cross-wind spreads (σ_{yi}), time-averaged cross-wind spreads (σ_{yc}) were derived from a sequence of individual instantaneous profiles. A total of 173 nominal 1/2 half hour and 83 nominal 1 hour average cross-wind spreads were derived from the data. The 1/2 hour average σ_{yc} values were, on the average, about 3.9 times the instantaneous σ_{yi} values. Similarly, the 1 hour average σ_{yc} values were, on the average, about 4.6 times the instantaneous σ_{yi} values.

Like the instantaneous values, the predicted σ_{yc} values were compared to corresponding predictions for σ_{yc}. Again the predictions were based on the exclusion and inclusion of a wind direction shear enhancement term. Draxler's surface and elevated functions for the non-dimensional term f_y were used in the predictions. Only 1/2 hourly values were predicted.

The comparison between the predicted and observed time-averaged plume spreads also resulted in considerable scatter. The predicted time-averaged plume spreads (σ_{yc}) were typically within a factor of two about 60 to 75% of the time. The time-averaged observations and predictions generally tend to have better agreement when the wind direction shear term is not included. As an exception, the addition of the wind direction shear term increased the agreement for the 700 m traverses associated with the surface releases.

Objective 4: ***Determine the peak-to-mean concentration ratios for the stationary concentration data.***

The analysis undertaken for the stationary SF_6 concentration data obtained from the Field Measurement Program was limited to a determination of peak-to-mean ratios. The results were based on 439 1/2 hour periods and 5 271 3-minute periods during which non-zero stationary SF_6 concentration data were collected. The results indicate the following:

- Instantaneous peak to 30-minute mean ratios are in the 3 to 7 range.
- Instantaneous peak to 3-minute mean ratios are in the 1 to 3 range.

These results are typical of those found in other studies. The analysis of the Field Measurement Program stationary SF_6 concentration data is currently being carried out as a separate study. These additional analyses include a determination of intermittency, conditional statistics and turbulence spectra.

Objective 5: ***Compare observed SF_6 centreline concentrations with those predicted using a simple Gaussian dispersion model.***

A simple Gaussian plume model was used to predict plume centreline SF_6 concentrations for the elevated and ground releases. For the elevated releases, plume rise was estimated using momentum plume rise relationships. Five different plume spread relationships which ranged from maximum to minimum use of on-site data were used.

- Option 1
  σ_{yi} = observed value (Moment Method)
  σ_{zi} = predicted
- Option 2
  σ_{yi} = observed value (Concentration Maximum Method)
  σ_{zi} = predicted
- Option 3
  σ_{yi} = predicted (no wind shear)
  σ_{zi} = predicted

- Option 4
  σ_{yi} = predicted (with wind shear)
  σ_{zi} = predicted
- Option 5
  σ_y = 3-minute Alberta Environment
  σ_z = 3-minute Alberta Environment

To compare predictions and observations, a number of different performance measures were selected. The selected measures were based on those used by others for the purposes of model evaluation.

The results of the comparison indicate the following:

- Option 4 provided the poorest performance when the overall data set was evaluated. Wind shear increased the predicted σ_{yi}, which decreased the predicted SF_6 concentration and led to a general concentration underprediction.

- When the overall data set was used, Options 1, 2, 3 and 5 generally resulted in 40 to 50% of the predictions being within a factor of two.

- When only stable, low wind speed conditions were considered for elevated releases, then Option 4 performed better than the other options.

- An unpaired data analysis for Option 5 prediction indicated that the model overpredicts the largest concentration values for surface releases and underpredicts the largest concentration values for elevated releases.

To fully evaluate when the simple Gaussian model predictions are in agreement and to determine reasons for any disagreement is beyond the scope of the Field Measurement Program. Like the comparison between predicted and observed σ_y values, there may be merit in pursuing the concentration predictions on a case study basis in order to evaluate model performance under stationary, homogeneous conditions.

9.2 Meteorological Study Comments

Eight objectives for the meteorology component were identified in Section 1.4.2 of this report. The analyses which responded to these objectives were presented in Section 8.

Objective 1: ***Prepare a climatological summary for the field measurement site based on 1 year of meteorological data.***

A 1 year climatology for the field measurement site was prepared. The selected climatological parameters which were presented include observed temperature (2 m), wind speed (10 m), lateral turbulence intensity (σ_θ) (10 m) and vertical turbulence intensity (σ_ϕ) (10 m). In addition, derived parameters such as heat flux (H_o), friction velocity (U^*), gradient Richardson Number (R_g) and Monin-Obukhov stability parameter (Z/L) were also presented. An overview of the 1/2 hour average data indicated:

- Temperatures ranged from -35.8 to 31.9°C.
- Median wind speeds increased with height from 3 m/s at 4 m to 5.3 m/s at 25 m.
- Median σ_θ and σ_ϕ values decrease with increasing height during the night. During the day, σ_θ values tend to either remain constant or decrease with increasing height. During the day, σ_ϕ values tend to remain constant or increase with increasing height.
- During the night, the median value of H_o and Z/L tended to be negative, while values of R_g tended to be positive. The Z/L parameter indicated stable conditions occurred about 56% of the time; in contrast the R_g parameter indicated stable conditions occurred about 67% of the time.

The objective of the tracer program was to collect concentration data during low wind speed, stable conditions. Wind speeds at 10 m were less than 2 m/s about 16% of the time during October, November and December. Similarly, stable conditions were estimated to occur 70 to 80% of the time while testing during these months.

Objective 2 ***Evaluate atmospheric boundary layer parameters which have been used to describe turbulence and dispersion processes.***

Mathematical relationships have been developed to describe wind, temperature and turbulence levels and profiles in the atmosphere. Many fundamental relationships that describe atmospheric behaviour have been derived from data, which have been carefully screened to isolate selected behaviour characteristics.

The Field Measurement Program review tested these relationships against the whole data set. The review of the boundary layer relationships resulted in the following findings:

- Drainage wind flow conditions over the study area were observed about 4% of the time. The slope of the terrain and the tower is about 1.0%.
- The primary indicators of stable and unstable conditions in the atmosphere are either $\overline{W'T'}$ or $\partial\theta/\partial Z$. These indicators were in agreement about 79% of the time. It is suspected that $\overline{W'T'}$ based on sonic temperature fluctuations may not be reliable for periods accompanied by small turbulence levels.

- The Field Measurement Program showed qualitative agreement for the expected inter-relationships between the R_g, R_f and Z/L stability parameters.

- The Field Measurement Program data supports the use of the log-linear wind speed profile for all stability conditions. The Businger-Dyer expression for $\psi(Z/L)$ under unstable conditions agreed with observations. For stable conditions, the Van Ulden and Holtslag relationship for $\psi(Z/L)$ gave much better agreement for $Z > L$ than the normally used $\psi(Z/L) = -5\ (Z/L)$.

- The normalized wind standard deviations (σ_u/U^*, σ_v/U^* and σ_w/U^*) under mechanically dominated turbulence conditions are consistent with the findings of others.

- Median σ_θ values tend to decrease with increasing height for all stability conditions. Median σ_ϕ values increase with increasing height for unstable conditions. This finding indicates that σ_θ and σ_ϕ values obtained from one level have to be carefully extrapolated when used to describe plume spreads at a different level.

Generally, the analysis of the data collected during the Field Measurement Program is in agreement with the findings of others and as such supports the mathematical relationships which were used to describe the behaviour of the atmospheric surface layer.

Objective 3 Determine the occurrence and duration of low wind speed and low turbulence conditions in the atmosphere.

Low Wind Speed Conditions

An analysis of the Field Measurement Program 10 m level wind data indicated that about 17.5% of the 1/2 hour average wind speeds were less that 2 m/s. The ADRP data indicated that about 20.3% of hourly average wind speeds were less than 2 m/s. An analysis of Calgary International Airport data found that about 19% of the wind speeds were less than 15 m/s.

The Field Measurement Program indicated that the occurrence of wind speeds less than 2 m/s under stable conditions occurred about 10.5% of the time. The ADRP data also indicated the joint occurrence of wind speeds less than 2 m/s and stable conditions about 9.6% of the time.

The Field Measurement Program indicated that 1/2 hourly average speeds less than 2 m/s may persist for up to 3 hours about 1% of the time.

Low Turbulence Levels

The frequency distributions of the wind fluctuations σ_u, σ_v, σ_w, σ_θ and σ_ϕ were determined to evaluate minimum turbulence levels in the atmosphere. Both 3-minute and 30-minute average data were used.

There was some indication that the minimum 30-minute average σ_u and σ_v could be measured and that these values are: σ_u (minimum) ≅ 0.075 m/s and σ_v (minimum) ≅ 0.060 m/s. Similarly, σ_θ (minimum) ≅ 1.5 degrees and σ_ϕ (minimum) ≅ 0.2 degrees. For the 3-minute average σ_θ, it was found that σ_θ (minimum) ≅ 0.5 degrees. Due to instrument noise, it was not possible to define a minimum value for σ_w (3 or 30-minute average) or to define a minimum for σ_ϕ (3-minute).

The wind fluctuations were plotted as a function of wind speed. As the wind speed approached zero, the behaviour of the median values of the wind fluctuations were as follows:

- σ_u approached 0.25 to 0.35 m/s values.
- σ_v approached 0.20 to 0.35 m/s values.
- σ_w approached 0.09 to 0.17 m/s values.

These ranges are dependent on the averaging period and the season. When σ_θ and σ_ϕ were plotted as functions of wind speed, the following behaviour for the median values were found:

- σ_θ values tend to remain nearly constant for wind speeds greater than 4 m/s.
- σ_ϕ values tend to remain constant for wind speeds greater than 3 m/s.
- σ_θ and σ_ϕ values increase significantly for wind speeds less than 3 m/s.

In normally used Gaussian plume models, the dispersive capability of the atmosphere is proportional to the product $\sigma_\theta \sigma_\phi U$. Large values of this product results in large dilution. A small value for this product would result in minimal dilution. This product tends to take on a minimal winter value in the wind speed range of 3 to 4 m/s indicating that these wind speed conditions are associated with the "worst case" meteorology (Figure 9.1). The summer curve shows a minimum value at a wind speed of 0.5 and 3 m/s. In both of these cases, the product term is larger than the winter minimum value. The largest normalized concentrations and smallest cross-wind plume spreads observed during the tracer study were associated with wind speeds in the 3 to 4 m/s range.

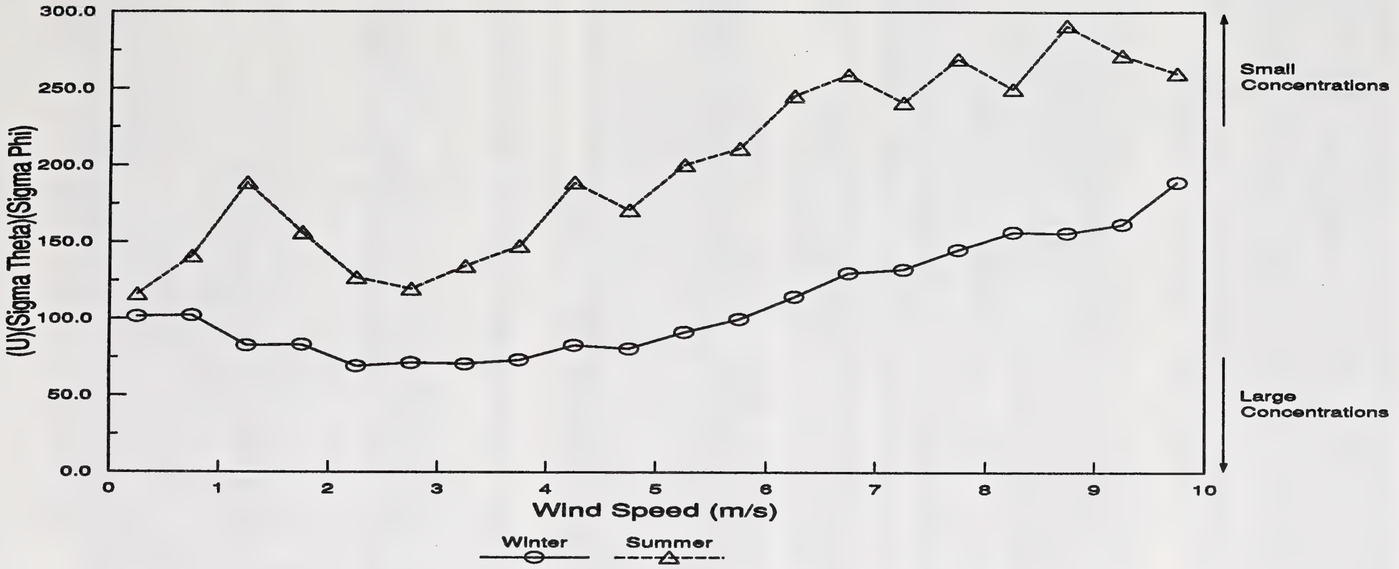

Figure 9.1

Median Value of the Product ($U\ \sigma_\theta\ \sigma_\phi$) as a Function of Wind Speed. The Product has the Units (Degrees ^{2}m/s).

Objective 4 Evaluate various meteorological preprocessor schemes to classify atmospheric turbulence.

The STAR meteorological preprocessor uses routine airport meteorological observations to determine the Pasquill-Gifford (PG) stability cases. The PG classification scheme along with the STAR preprocessor is one of the most common approaches used by regulatory models to determine atmospheric dispersion. Alternate methods to determine the PG class from on-site data have been used. In the Field Measurement Program evaluation, the STAR approach and two alternate approaches based on on-site data agreed on the PG stability class 50% of the time. The STAR and the on-site approaches agreed within ± one stability class about 90% of the time.

Selected observed and derived meteorological parameters were reviewed to determine their ability to delineate the PG classes based on Calgary International Airport and Field Measurement Program on-site meteorological data. Some parameters performed well in terms of their ability to separate stable and unstable conditions but did not perform well in terms of distinguishing between individual PG classes. Generally: the selected individual meteorological parameters were not sufficient to estimate the occurrence of a given PG class; the PG classes were not clearly delineated by direct measurements of atmospheric turbulence and selected stability indications had varying degrees of success. For arbitrary stability classes based on σ_θ and σ_ϕ, it was found that selected stability indicators could be used to delineate σ_ϕ classes. The findings suggest that σ_ϕ rather than σ_θ is a better indication of atmospheric stability classes.

Alternate meteorological preprocessors attempt to classify turbulence as a continuous variable and are based on estimates of heat flux. The eddy correlation and energy budget methods were used to estimate the heat flux. The comparison between the two methods indicate that:

- In the Calgary area, which is generally regarded as dry, the latent heat term appears to be important in winter as well as summer.
- The two methods appear to provide better agreement during the day when the heat fluxes are positive.
- During the night, the eddy correlation method tends to underestimate the magnitude of the heat flux with respect to the energy budget method.

The observed heat flux estimates were compared to these predicted using an alternate meteorological preprocessor. There was considerable scatter between the observed and predicted values. While there was some qualitative agreement, it is apparent that the minimum predicted heat flux value of -27 W/m^2 needs to be reviewed. The meteorological preprocessor was further used to estimate the friction velocity ($U*$) and the Monin-Obukhov length (L). The predicted diurnal variation of $U*$ is in agreement with the neutral and stable limits of the preprocessor. The full preprocessor predictions, however, did not provide a similar level of agreement. Similar discrepencies were noted for Z/L. It is not clear if this is due to problems with the algorithms or the computer code. Further investigation is warranted.

Objective 5 ***Determine the spatial representativeness of meteorological observations in the vicinity of the Field Measurement Program site.***

Selected meteorological parameters measured at the field measurement site were compared to concurrent parameters measured at Calgary International Airport (24 km to the southwest), Crossfield Gas Processing Plant (32 to the northwest) and the Balzac Gas Processing Plant (16 km to the west). The intervening terrain can generally be regarded as flat to slightly rolling and treeless. The results of the comparison indicated that:

- Pressure, temperature and relative humidity observations were relatively constant over the distance scales considered.
- Care has to be taken when using and extrapolating airport wind observations to other areas due to the AES observation and reporting procedures which can limit the usefulness of the wind data. Differences in observation heights and surface roughnesses have to be accounted for when extrapolating wind speed data from one location to another.

The findings generally support the collection of site specific wind data rather than extrapolating wind data from one site to another.

Objective 6 ***Review the empirical relationship to convert atmospheric turbulence from one averaging period to other time periods.***

An empirical power law relationship is frequently used to extrapolate atmospheric turbulence measurements and ambient concentrations from one averaging period to another. Various studies have suggested power law exponents ranging from 0.175 to 0.675. The high frequency wind data collected at the 10 and 25 m levels were analysed to confirm the exponent values found by others. The results confirmed that the vertical components (σ_w and σ_θ) can be assumed to be independent of averaging time. For the lateral components (σ_u σ_v and σ_θ), the exponents were found to range from 0.19 to 0.31 with standard deviation values of ranging from 0.12 to 0.19.

There was an indication that the power law relationship generally holds for averaging periods less than 3 minutes. The best value for the exponent in these cases was about 0.2. For averaging periods ranging from 3 minutes to 60 minutes, the best value for the exponent was about 0.3. Given the scatter about these values, it concluded that there is limited basis for departing from the Alberta Environment exponent value of 0.2.

Objective 7 ***Compare the wind speed and turbulence measurements obtained from a sonic anemometer system with those obtained from a conventional propellor anemometer system.***

The sonic anemometer system is a high sensitivity fast response instrument. In contrast, the propeller anemometer system threshold and response time is limited by frictional and inertial effects. On the other hand, the conventional anemometer system requires less support hardware and is less expensive than its sonic counterpart.

Operational problems associated with the anemometers during the Field Measurement Program were as follows:

- During the winter, the build-up of hoarfrost on the propeller anemometer degraded the propeller response and in the extreme prevented the propeller from turning.
- The same build-up of frost on the Applied Technologies sonic anemometer would produce anomalous high wind speed data before the unit reported missing data. There was no evidence that frost degraded the Kaijo-Denki sonic anemometer results.
- During the summer, high wind speeds and/or hail can cause severe damage to the sensitive propellers used on the propeller anemometer. As a consequence, these propellers were replaced with less sensitive propellers to reduce instrument down-time.
- During the summer, the power supply for two of the Applied Technologies sonic anemometers failed. This may have resulted from the very high electronic box enclosure temperatures (~50°C).

With the above in mind, the following conclusions regarding the capability of the propeller anemometer can be made:

- For wind speeds less than 1 m/s, the wind speed uncertainty is typically 0.3 m/s. At 10 m/s, the uncertainty is about 1 m/s.
- For wind speeds less than 1 m/s, the wind direction uncertainty can be as large as 45 degrees. For larger wind speeds, the uncertainty is typically in the 5 to 15 degrees range.
- A wind direction bias of 2 to 3 degrees may be associated with the relative alignment of the anemometers with respect to true north.
- For wind speeds between 3 and 15 m/s, the uncertainty in σ_θ is about 3 degrees. There is a shift in the σ_θ frequency distribution which results in the propeller anemometer overestimating the frequency of low σ_θ values.
- For wind speeds between 3 and 15 m/s, the uncertainty in σ_ϕ is about 2 degrees. The propeller anemometer will underestimate the frequency of low σ_θ values. The main difference between the two systems are for wind speeds less than 3 m/s.

In summary, the largest departures between the two systems measurements are at very low wind speeds ($U_{10} < 1$ m/s). For mean wind speed, wind direction and standard deviation of the wind direction (σ_θ), the propeller anemometer appears to provide reasonable results when compared to the sonic anemometer. There will be some uncertainty in the measurements obtained from propeller type instruments and this uncertainty can increase at low wind speeds.

The largest uncertainty in using a propeller instrument is in the measurement of the vertical wind components (σ_w and σ_ϕ). This is unfortunate since σ_ϕ was found to correlate better with PG class than σ_θ. The use of a propeller anemometer may be a limitation for σ_ϕ values less than 3 degrees. If low turbulence measurements are required, a sonic anemometer is preferred. If only a propeller anemometer is used, the limitations of the instrument, depending upon the application, should be accounted for.

Objective 8 Compare observed mixing height data with selected analytical relationships for predicting the mixing depth.

Limited mixing height data were obtained from the acoustic sounder echo interpretations and from tethersonde wind speed profiles. The agreement between the acoustic sounder and predicted values was poor. It was not clear from this study whether this was due to poor predictive models or limitations of the acoustic sounder to resolve shallow mixing depths.

When the limited number (13) of tethersonde profile derived mixing height values were compared to stable predicted values of the boundary layer height, reasonable agreement was obtained. However, given the scatter in individual data pairs, this agreement may have been fortuitous. The scatter may have also resulted from the uncertainty in estimating $\overline{W'T'}$ (and hence U^* and L) in very stable conditions.

9.3 Application to GASCON2

As discussed in the introduction of this report, the purpose of the Field Measurement Program was to collect tracer and meteorological data which could be used to help evaluate the GASCON2 dispersion model. The following main items were viewed to have a direct relevance to the GASCON2 model formulations and assumptions.

Heat Flux

- The GASCON2 model relies on the heat flux (H_o) as an input to determine U^* and L values. There may be some limitations in obtaining site specific heat flux measurements under very stable conditions. For some applications of GASCON2, site specific H_o measurements may not be required. For example, representative H_o values can be selected to run the model in a screening mode. Two alternate methods can be used to measure heat flux:

    - Eddy flux method ($\overline{W'T'}$) where T' is obtained from fast response temperature sensor,

    - Energy budget method where net radiation and some indication of surface wetness are measured.

Failing this, a meteorological preprocessor can be used to estimate heat flux from more readily available data. The formulations presented in the GASCON2 report should be reviewed to allow latent heat flux to be incorporated and allow for heat flux values less than -27 W/m^2.

Very Stable Conditions

- The formulations to determine both L and U^* from the heat flux are encoded into the meteorological preprocessor as well as in the model GASCON2. As was seen in the evaluation, there were differences between preprocessor predicted and observed U^* and L values. This may in part be due to the limitation in the heat flux but may also be due to the limited range of application for $\psi(Z/L) = -5(\psi/L)$ under stable conditions. An alternate form of $\psi(Z/L)$ was presented and was shown to better describe the observed wind profiles in stable conditions:

$$\psi(Z/L) = -17\left[1 - \exp\left\{-0.29\left(\frac{Z}{L}\right)\right\}\right]$$

This revised $\psi(Z/L)$ relationship should provide more realistic estimates of U^* and L and should be incorporated into GASCON2.

Site Specific Turbulence Data

- The GASCON2 model allows the user to specify lateral and vertical turbulence values (σ_v and σ_w, respectively). As was shown in this analysis, these values can vary with height and stability. It is, therefore, important that the observation height matches the expected plume height or that appropriate adjustments to the observed σ_v and σ_w values be made prior to input to the model. The model uses 30-minute average σ_v values.

The limitations of the wind instrument should be reviewed when analysing the site specific turbulence data. The most uncertainty will be with the vertical components (σ_w and σ_ϕ). As was seen in the comparison between the two types of anemometer systems, the largest uncertainties were associated with low wind speed conditions. Given that the worst case meteorology is no longer associated with these conditions, the degree of concern regarding measurement sensitivity may be decreased.

Worst Case Meteorological Conditions

- Prior to this study, the low wind speed stable atmospheric condition was viewed by some as being the meteorological condition which produced the largest ambient concentrations. The Field Measurement Program suggests that the worst conditions are associated with wind speeds between 2 and 4 m/s.

Model Uncertainty

- The simple Gaussian model indicated that at best about 50% of the concentration predictions were within a factor of two. A review of the instantaneous and time-averaged plume cross-wind spreads (σ_{yi} and σ_{yc}, respectively) indicated that the predicted σ_{yi} and σ_{yc} values were typically within a factor of two anywhere from 60 to 75% of the time. The high end represents the elevated releases and the low end represents the surface releases. On this basis, the best that GASCON2 can be expected to predict is within a factor of two 60 to 75% of the time.

These comments are applicable to other dispersion models as well as to the GASCON2 model.

10 BIBLIOGRAPHY

Abell, G., 1969. Exploration of the Universe, Second Edition, Holt, Rinehart and Winston.

Atmospheric Environment Service (AES). 1983. Documentation for the Digital Archive of Canadian Climatological Data Identified by Element. Canadian Climate Centre, Downsview, Ontario.

Alberta Environment. 1988. User's Manual for Alberta Environment Dispersion Models. Standards and Approvals Division, Air Quality Branch, Edmonton, Alberta.

Alberta Municipal Affairs. 1986. Advisory Land Use Planning Notes on the Pipeline-Urban Encroachment Problem.

Alberta Petroleum Industry-Government Environmental Committee (APIGEC). 1978. H_2S Isopleth Prediction. Phase I: Model Sensitivity Study.

Alberta Petroleum Industry-Government Environmental Committee (APIGEC). 1979. H_2S Isopleth Prediction. Phase II. Pipe Burst Study.

Alberta Petroleum Industry-Government Sour Gas Environmental Committee (APIGEC). 1974. A Report by the Alberta Petroleum Industry-Government Sour Gas Environmental Committee on Guidelines for Urban Development in Relation to the Sour Gas Industry.

Alberta Public Safety Services. 1985. Government of Alberta Emergency Response Plan for a Sour Gas Release.

Alp E., Huget, R. G., Davies, M. J. E. and Lam, L. 1987. Estimating Downwind Concentrations Resulting From Uncontrolled Sour Gas Releases. Draft. Prepared for the Energy Resources Conservation Board by Concord Scientific Corporation. Report No. CSC.J970.1.

Barr, D., 1988. Report on H_2S Toxicity. Alberta Community and Occupational Health.

Bowen, B. M., Dewart, J. M. and Chen, A. I. 1983. Stability Class Determination: A Comparison for one site. Sixth Symposium on Turbulence and Diffusion, March 22 to 25, 1983. Boston, Massachusetts. American Meteorological Society, pp. 211-214.

Brenner, R. and Lamb, B., 1985. A Fast Response Continuous Analyser for Halogenated Atmospheric Tracers. J. Atmos. Ocean. Tech., 21, 582-589.

Briggs, G. A., 1988. Analysis of Diffusion Field Experiments. Lectures on Air Pollution Modelling. Editors A. Venkatram and J. C. Wyngaard. American Meteorologist Society, pp 63-117.

Canadian Petroleum Association. 1987. Guidelines for Preparation of Sour Gas Emergency Response Plans.

Carson, D.J. and Richards, P.J.R., 1978. Modelling Surface Turbulent Fluxes in Stable Conditions. Boundary Layer Meteorology, 14:67-81.

Chintawongvanich, P., Olsen, R. and Biltoft, C. A., 1989. Intercomparison of Wind Measurements from Two Acoustic Doppler Sodar, a Laser Doppler Lidar and in-situ Sensors. JAOT 6, pp. 785-797.

Cox, W.M., 1988. Protocol for Determining the Best Performing Model, EPA, August 1988. U.S. EPA Office of Air Quality Planning and Standards.

Cramer, H.E., 1959. Engineering Estimates of Atmospheric Disposal Capacity. American Industrial Hygiene Association Journal, 20:183-189.

Davies 1986. Plume Visualization Techniques Prepared for Alberta Environment by Concord Scientific Corporation, pp. 27.

Davison, D. S. and Leavitt, E. D., 1979. Analysis and AOSERP Plume Sigma Data. Prep. for the Alberta Oil Sands Environmental Research Program by Intera Environmental Consultants Ltd., AOSERP Report 63, pp. 251.

Dietz R. N. and Senum, G. I., 1986. Capabilities, Needs and Applications of Gaseous Tracers in Atmospheric Tracer Technology and Applications. Edited by J. H. Heihen. Noyes Publications, New Jersey.

Draxler, R. R., 1976. Determination of Atmospheric Diffusion Parameters, Atmospheric Environment, 10:99-105.

Energy Resources Conservation Board. 1988. Enerfax 7 - Keeping Back From Energy Developments.

Energy Resources Conservation Board. August 1988, September 1988 and February 1988. Field Measurement Program Newsletters. An Update for Residents of the Kathyrn and Keoma Areas.

Energy Resources Conservation Board. D 84-9. Lodgepole Blowout Report.

Energy Resources Conservation Board. December 1988. News Release. Field Measurement Program.

Energy Resources Conservation Board. June 1986, October 1986 and February 1987. Northeast Sour Gas News. Prepared for the Residents of the Municipal District of Rocky View and Northeast Calgary.

Energy Resources Conservation Board. 1986. Enerfax 6 - All About Critical Sour Wells.

Energy Resources Conservation Board (ERCB). 1979. Atwell *et al.* Risk Assessment of Sour Gas Facilities.

Energy Resources Conservation Board (ERCB). ID 79-2, ID 87-2, IL 88-9, and IL 88-9 Amendment. Interim Directives and Informational Letters on Sour Well Licensing and Drilling with Amendments to July 1988.

Energy Resources Conservation Board (ERCB). ID 79-2, ID 81-3. Interim Directive on Sour Pipelines and Plants.

Gill, G. C., 1975. Development and Use of the Gill UVW Anemometer. Boundary Layer Meteorology, 8:475-495.

Golder, D., 1972. Relations Among Stability Parameters in the Surface Layer. Boundary Layer Meteorology, 3:47-58.

Halitsky, J., 1960. Single Camera Measurement of Smoke Plume Ints of Air and Water Pollution, 185-198.

Hanna, S. R., Briggs, G. A. and Hosken Jr., R. P. 1982. Hardbook on Atmospheric Diffusion. NTIS Document DE82-002045.

Hanna, S. R., 1983. Lateral Turbulence Intensity and Plume During Stable Conditions. Journal of Climatology & Applied Meteorology 22, 1424-1430.

Hanna, S. R., 1985. Development and Application of a Simple Method for Evaluating Air Quality Models Health and Environmental Affairs Department, API Publication No. 4409, January 1985.

Haugen, D. A., 1973. Workshop on Micrometeorology. American Meteorological Society.

Heiken, J. H., 1986. Atmospheric Tracer Technology and Applications. Noyes Publication, pp. 368.

Herman, M. N., 1980. Estimating Long-term Ground Level Concentrations of SO_2 from Short Term Peak Data. Journal of the Air Pollution Control Association, 30:676-678.

Hicks, B. B., 1976. Wind Profile Relationships from the "Wangara" Experiment. Quarterly Journal of the Royal Meteorological Society, 102:535-551.

Hicks, B. B., 1978. Some Limitations of Dimensional Analysis and Power Laws. Boundary Layer Meteorology, 14:567-569.

Hicks, B. B., 1981. An Examination of Turbulence Statistics in the Surface Boundary Layer. Boundary Layer Meteorology, 21:389-402.

Holtslag, A. A. M. and van Ulden, A. P., 1983. A Simple Scheme for Daytime Estimates of Surface Fluxes from Routine Weather. Journal of Climate and Applied Meteorology, 22:517-529.

Horst, T. W., 1979. Lagrangian Similarity Modelling of Vertical Diffusion from a Ground Level Source, Journal of Applied Meteorology, 18:733-740.

Irwin, J. S., 1983. Estimating Plume Dispersion - A Comparison of Several Sigma Schemes. Journal of Applied Meteorology, 22:92-114.

Islitzer, N. F. and Slade, D. H., 1968. Meteorology and Atomic Energy Chapter 4. Diffusion and Transport Experiments. In Meteorology and Atomic Energy 1968 Edited by D. H. Slade. pp. 117-188. Available for NTIS as Document TID-24190.

Kaimal, J. C., Gaynor, J. E., Finklestein, P. L., Graves, M. E., and Lockhart, T. J. 1984. A Field Comparison of in-situ Meteorological Sensors. NOAA/ERL Wave Propagation Laboratory Report Number 6.

Kaimal, J. C., 1969. Measurement of Momentum and Heat Flux Variations in the Surface Boundary Layer. Radio Science, 4:1147-1153.

Kaimal, J.C., 1988. The Atmospheric Boundary Layer - Its Structure and Measurement Lecture Notes. NOAA/ERL/Wave Propagation Laboratory.

Kondo, J., Kanechika, O. and Yasuda, N., 1978. Heat and Momentum Transfers Under Strong Stability in the Atmospheric Surface Layer. Journal of Atmospheric Surface Layer. Journal of Atmospheric Sciences, 35:1012-1021.

Leahey, D. M., Hansen, M. C. and Schroeder, M. B., June 1988. An Analysis of Wind Fluctuation Statistics Collected Under Stable Atmospheric Conditions at Three Sites in Alberta, Canada. Journal of Applied Meteorology, Volume 27, No. 6.

Legge, A. H., 1988. The Acid Deposition Research Program Biophysical Research. The Present and Potential Effects of Acidic and Acidifying Air Pollutants on Alberta's Environment. Critical Point 1. Final Report.

Lenschow, D. H., 1984. Introduction in Probing the Atmospheric Boundary Layer, Meteorological Society 1 to 4.

Lumley, J. L. and Panofsky, H. A., 1964. The Structure of Atmospheric Turbulence. Wiley-Interscience, New York.

Merry, M. and Panofsky, H. A., 1976. Statistics of Vertical Motion over Land and Water. Quarterly Journal of the Royal Meteorological Society, 102:255-260.

Mortensen, N. G., Larsen, S. E., Troen, I. and Mikkelsen, T., 1987. Two Years Worth of Turbulence Data Recorded by a Sonic Anemometer-Based Data Acquisition System. Sixth Symposium Meteorological Observations and Instrumentation. Jan. 12-16, 1987. New Orleans, La. American Meteorological Society, 393-396.

Nieuwstadt, F. T. M., 1981. The Steady State Height and Resistance Laws of the Nocturnal Boundary Layer: Theory Compared with Cabauw Observations. Boundary Layer Meteorology, 20:3-17.

Ontario Ministry of the Environment (OME). 1987. Appendix H Air Pollution - General Regulation, Modelling Proposals.

Paine, R. J., 1988. User's Guide to the CTDM (Complex Terrain Dispersion Model) Meteorological Preprocessor (METPRO) Program. Prepared for the U.S. Environmental Protection Agency. NTIS Report PB88-16202.

Panofsky, H. A. and Dutton, J. A., 1984. Atmosphere Turbulence: Models and Methods for Engineering Applications. John Wiley & Sons, Toronto, pp. 397.

Pasquill, F., 1960. The Estimation of the Dispersion of Windborne Material Meteorological Magazine, 90:31-49.

Peterson, H. G., 1989. An Investigation of Concentration Fluctuations and the Development of a Meandering Plume Model.

Plume Rise, Briggs, G. A., Prepared for Nuclear Safety Information Center, 1969.

Plume Rise Predictions, Briggs, G. A., 1975. Chapter 3, Lectures on Air Pollution and Environmental Impact Analyses. American Meteorological Society.

Sage Institute of Canada Inc. 1985. Northeast Calgary Sour Gas Task Force Final Narrative Report.

Scire, J. S., Lurmann, F. W., Bass, A. and Hanna, S. R., 1984. User's Guide to the MESOPUFF II Model and Related Preprocessor Programs. Prepared by Environmental Research and Technology for the U.S. Environmental Protection Agency. NTIS Report PB84-181775.

Sedefian, L. and Bennent, E., 1980. A Comparison of Turbulence Classification Schemes. Atmospheric Environment, 14:741-750.

Singer, I. A., 1961. The relationship Between Peak and Mean Concentrations. Journal of the Air Pollution Control Association, 11:336-341.

Smith, F. B., 1965. The Role of Wind Shear in Horizontal Diffusion of Ambient Particles. Quarterly Journal of the Royal Meteorological Society, 91:318-329.

Standards and Approvals, 1989. Guidelines for Atmospheric Dispersion Modelling in Alberta. Alberta Environment, Edmonton, Alberta.

Strimatis, D., Hoffnagle, G. and Bass, A., 1980. On-site Meteorological Instrumentation Requirements to Characterize Diffusion from Point Sources - A Workshop Prepared by Environmental Research and Technology for Environmental Protection Agency. Contract No. 68-02-3282.

Sutherland, R. A., Hansen, F. V. and Bach, W. D., 1986. A Quantitative Method for Estimating Pasquill Class From Wind Speed and Sensible Heat Flux Density. Boundary Layer Meteorology 37, 357-369.

Texas Air Control Board 1979. Texas Episodic Model Users Guide. Report EPA/DF 80/007c (NTIS Number PB 80 227 572.

Turner, D. B., 1970, Workbook of Atmospheric Dispersion Estimates. Public Health Service, 999-AP-26. (NTIS Number PB-191-482). pp. 84.

Turner, D. B., 1964. A Diffusion Model for an Urban Area. Journal of Applied Meteorology, 3:87-91.

U.S. Nuclear Regulatory Commission (N.R.C.) 1972. Safety Guide 23 On-site Meteorological Program.

van Ulden, A. P. and Holtslag, A. A. M., 1985. Estimation of Atmospheric Boundary Layer Parameters for Diffusion Applications. Journal of Climatology & Applied Meteorology, 24:1196-1207.

Webb, E. K., 1970. Profile Relationships: The Log-linear Range and Extension to Strong Stability. Quarterly Journal of Royal Meteorological Society, 96:67-90.

Williamson, H. J. and Krenmayer, R. R., 1980. Analysis of the Relationship between Turner's Stability Classifications of Wind Speed and Direct Measurements of Net Radiation. Second Joint Conference on Applications of Air Pollution Meteorology. March 24 to 27, 1980. New Orleans, La. American Meteorological Society, 777-780.

Zilitinkevich, S. S., 1972. On the Determination of the Height of the Ekman Boundary Layer. Boundary Layer Meteorology, 3:141-145.

11 SYMBOL GLOSSARY

Symbol		Section
a	Constant used in Alberta Environment estimation of σ_Y	7.3.2
B	Sample bias for anemometers	8.8.1
b	Constant used in Alberta Environment estimation of σ_Z	7.3.2
C	Concentration (ppt)	4.6.1
C	Comparability of anemometers	8.8.1
$\overline{C}$	Mean concentration (ppt)	4.6.2
C_1	Cosine correction for U_{mu} for Gill anemometers	5.3.2
C_2	Cosine correction for V_{mu} for Gill anemometers	5.3.2
C_3	Cosine correction for W_{mu} for Gill anemometers	5.3.2
C_{50}	50th percentile of concentration (ppt)	4.6.2
C_{99}	99th percentile of concentration (ppt)	4.6.2
C_a	Constant in power law relationship	4.6.3
C_b	Exponent in power law relationship	4.6.3
C_j	Concentration at location y_i on arc (ppt)	4.6.1
C_m	Maximum concentration (ppt)	4.6.1
$\overline{C_m}$	Conditional mean concentration (ppt)	4.6.2
C_o	Observed concentration (ppt)	4.6.1
C_p	Predicted concentration with the estimated σ_y, $\overline{y}$ and C_m (ppt)	4.6.1
C_p	Specific heat capacity at constant pressure (J/kg K)	5.3.3
$\int C\,dy$	Cross-wind integrated concentration (ppt m)	4.5.2
c	Exponent used in Alberta Environment estimation of σ_Z	7.3.2
D	Difference between observations from Gill and sonic anemometers	8.8.1
d	Distance from source to arc (m)	6.1.1
d	Residual or difference	7.3.3
$\overline{d}$	Bias or mean of the difference	7.3.3
ECD	Electron capture detector	3.2.1
F_m	Momentum flux (m^4/s^2)	3.4.2
FMD	Flow meter display (cm^3/min)	Table 3.1
f	Equation 8.37 and 8.38	8.9
f_y	Universal function	7.1.5

g	acceleration due to gravity (m/s^2)	3.4.2
H	Plume height above ground level (m)	3.4.2
H	Heat flux (W/m^2)	5.3.3
H	Plume height (m)	7.2.2.1
H_L	Long wave heat flux loss (W/m^2)	8.5.5
H_o	Heat flux (W/m^2)	5.1.3
h_I	Depth of the mechanically mixed layer (m)	8.9
h_s	Source height (m)	3.4.2
h_s	Fan height (m)	7.2.2.1
I	Plume intermittency (fraction)	4.6.2
I.D.	Inside diameter	4.2.2
I_p	Conditional concentration fluctuation intensity (%)	4.6.2
i	Concentration fluctuation intensity (%)	4.5.2
i_y	Lateral turbulence intensity	8.2.3
i_z	Vertical turbulence intensity	8.2.4
KM	Kasanski-Monin length (m)	7.1.5.4
k	von Karman constant (0.4)	5.3.3
L	Monin-Obukhov length (m)	5.1.3
M	SF_6 mass flow rate (g/min)	Table 3.1
M	Dimensionless mean square error	7.3.3
MSE	Mean square error	7.3.3
MW	Molecular mass (kg/kmole)	5.3.3
M	Cumulative SF_6 mass (g)	Table 3.1
O	Observed plume rise from slide measurements (m)	3.4.3
O.D.	Outside diameter	3.3.1
$\overline{O}$	Mean observed value	7.3.3
P	Predicted plume rise (m)	3.4.3
P	Relative precision (%)	8.8.1
$\overline{P}$	Mean predicted value	7.3.3
ΔP	Pressure differential (Pa)	3.3.3
ΔP_{avg}	Average pressure difference (Pa)	3.3.3
ΔP_p	Pressure differential between impact and local static pressures (Pa)	3.3.3
p	Exponent used in power law formula to convert values from one time average to another	8.7
$\overline{p}$	Average power law exponent	8.7.1
ppt	Parts per trillion ($1 \cdot 10^{-12}$)	

Q	SF_6 release rate (m^3/s)	7.2.2.1
Q_c	Cumulative SF_6 volume (cm^3 @ 0 °C and 101.3 kPa)	Table 3.1
Q_{net}	Net radiation (W/m^2)	8.4.1
Q_{in}	Incoming solar radiation (W/m^2)	8.5.2
R	Ratio used to determine cosine correction factors for Gill anemometers	5.3.2
$\overline{R}$	Mean value of R_i from N observations	8.8.1
RH	Relative Humidity	Table 5.1
R_b	Bulk Richardson number	5.3.4
R_f	Richardson Flux number	5.3.4
R_g	Richardson Gradient number	5.3.4
R_i	Observation for sonic anemometer	8.8.1
R_s	Radius of the exit for the jet (m)	3.4.2
R_s	Fan diameter (m)	7.2.2.1
R_u	Universal gas constant (8314 J/kmole K)	5.3.3
r	Correlation coefficient	7.3.3
S	Stability parameter used for estimating plume rise in stable conditions (s^{-2})	3.4.2
S	Low wind speed correction factor for Gill anemometers	Table 5.1
S	Stability parameter used in equation 7.4	7.2.2.1
S	Absolute precision or standard deviation of the difference between the two types of anemometers	8.8.1
$\overline{S}$	Mean wind speed (m/s)	5.1.3
S_d^2	Variance of the difference	7.3.3
T	Temperature (K)	
T	Ambient temperature (K)	3.4.2
$\overline{T}$	temperature (K)	5.3.3
T'	True temperature fluctuations	5.3.3
T'_s	Sonic temperature fluctuations	5.3.3
T^*	Scaling temperature used in equation 8.18 (K)	8.3.6
T_m	Measured temperature (K)	5.1.3
t	Specified averaging period	7.1.3
t_a	Average time for a traverse (hr:min:sec)	6.1.1
t_f	Finish time for a traverse (hr:min:sec)	6.1.1
t_i	Averaging period (s)	8.7.1
t_s	Start time for a traverse (hr:min:sec)	6.1.1

t_{wl}	Vertical integral time scale	7.1.4
t_{vl}	Crosswind integral time scale	7.1.4
Δt	3 minute time block (180 seconds)	6.1.1
U	Wind speed (m/s)	3.4.2
$U*$	Friction Velocity (m/s)	5.1.3
U_{mu}	Uncorrected measured along-wind vector (m/s)	5.3.2
$\overline{U_m}$	Measured along-wind vector (m/s)	5.3.1
VDC	Direct current voltage (V)	Table 3.1
V_i	4 or 10 m average wind speed (m/s)	6.1.1
V_{mu}	Uncorrected measured cross-wind vector (m/s)	5.3.2
V_{mom}	Average momentum velocity (m/s)	3.3.3
$\overline{V_m}$	Measured cross-wind vector (m/s)	5.3.1
V_p	Velocity at point p (m/s)	3.3.3
V_s	Exit velocity of the jet (m/s)	3.4.2
V_s	Fan exit velocity (m/s)	7.2.2.1
WDE	Wind shear direction enhancement	7.1.4.2
W_{mu}	Uncorrected measured vertical-wind vector (m/s)	5.3.2
$\overline{W_m}$	Measured vertical-wind vector (m/s)	5.3.2
x	Used in Businger-Dyer expression. As defined in equation 8.15	8.3.5
$\overline{x(30)}$	30 minute average of parameter x, where x can be any parameter for which a 3 minute average was calculated	5.3.4
Y_i	Plume centroid position from a single plume traverse	7.1.5
Y_i	Observation from Gill UVW anemometer	8.8.1
$\overline{Y}$	Average centroid position of N plume traverses	7.1.5
$\overline{y}$	Location of plume centerline on arc (m)	4.6.1
y_{16}	16th percentile of $\int C dy$	4.6.1
y_{50}	50th percentile of $\int C dy$	4.6.1
y_{84}	84th percentile of $\int C dy$	4.6.1
y_j	Location on arc where concentration C_i occurs (m)	4.6.1
y_m	Location of Cmax using concentration maximum method (m)	4.5.1
Z	Height of measurement (m)	5.3.3
Z_o	Surface roughness (cm)	5.5
ΔZ	Wind direction difference over the vertical layer	7.1.4

$\overline{Z/L}$	Stability parameter	5.3.3
$\frac{\partial\theta}{\partial Z}$	Vertical potential temperature gradient (K/m)	5.3.3
$\frac{\partial U}{\partial Z}$	Vertical wind speed gradient ({m/s}/m)	5.3.3
$\frac{\partial T}{\partial Z}$	Vertical temperature gradient (K/m)	3.4.2

Chemical Symbol	
$CaCl_2$	Calcium chloride
C_2Cl_6	Hexachloroethane
H_2	Hydrogen
H_2S	Hydrogen sulphide
N_2	Nitrogen
O_2	Oxygen
PVC	Poly vinyl chloride
KNO_3	Potassium nitrate
SF_6	Sulphur hexaflouride
$ZnCl_2$	Zinc chloride
ZnO	Zinc oxide

Subscripts

U	Natural wind coordinate, along-wind component
V	Natural wind coordinate, cross-wind component
W	Natural wind coordinate, vertical-wind component
4	4 m level
10	10 m level
16	16 m level
25	25 m level

Greek		Section
α	Wind direction difference over vertical layer.	7.1.4
β	Ratio of Lagrian to Eulerian time scales.	7.1.4
Γ	Adiabatic temperature gradient (K/m)	3.4.2
γ	Peak (99%) to mean ratio	4.6.2
ε	Fractional error	6.2.2
$\overline{\theta}$	Mean wind direction	5.1.3
$\overline{\theta_c}$	Correction angle for anemometers to convert to conventional coordinates (°)	5.3.1
θ_{CAT}	Correction angle for Applied Technologies anemometers (°)	5.3.1
θ_{CKD}	Correction angle for Kaijo Denki anemometer (°)	5.3.1
ρ	Density of air (kg/m^3)	3.3.3
ρ_a	Density of the ambient air (kg/m^3)	3.4.2
ρ_s	Density of the plume (kg/m^3)	3.4.2
σ_y	Standard deviation of the plume in the cross-wind direction (m)	4.6.1
σ_c	Standard deviation of concentration (ppt)	4.6.2
σ_U^2	Variance of along-wind component (m^2/s^2)	5.3.3
σ_V	Standard deviation of cross-wind component (m)	5.3.3
σ_V^2	Variance of cross-wind component (m^2/s^2)	5.3.3
σ_W	Standard deviation of vertical-wind component (m)	5.3.3
σ_W^2	Variance of vertical-wind component (m^2/s^2)	5.3.3
σ_θ	Standard deviation of wind direction (°)	5.3.3
σ_{Y_i}	Individual plume sigma from a single plume traverse	7.1.3
$\sigma_{Y_c}(t)$	Composite plume sigma from N plume traverses	7.1.3
σ_ϕ	Standard deviation of vertical wind angle.	5.3.3
$\sigma_{y_i}(s)$	Wind shear term in wind direction shear enhancement factor	7.1.4.2
$\sigma_{y_i}(t)$	Turbulence term in wind direction shear enhancement factor	7.1.4.2

σ_z	Vertical plume standard deviation (m)	7.2.2.1
σ_U	Standard deviation of along-wind component (m)	8.3.7
$\overline{\sigma}$	Average standard deviation for a given averaging period	8.7.1
$\overline{\sigma(t_i)}$	Average σ for averaging period t_i	8.7.1
$\overline{\sigma(180)}$	Average σ for 3 minute averaging period	8.7.1
ϕ_m	Normalized wind shear	8.3.4
ϕ_H	Normalized thermal stratification	8.3.6
χ	Concentration in generic gaussian model (ppt)	7.3.1
χ_{CWI}	Crosswind integrated concentration	7.1.4
$\psi\left(\frac{Z}{L}\right)$	Stability parameter for wind profile	8.3.5

σ_z	Vertical plume standard deviation (m)	7.2.2.1
σ_x	Standard deviation of along-wind component (m)	8.3.7
σ	Average standard deviation for a given averaging period	8.7.1
$\overline{\sigma(t_i)}$	Average σ for averaging period t_i	8.7.1
$\overline{\sigma(3\,\mathrm{min})}$	Average σ for 3 minute averaging period	8.7.1
ϕ_m	Normalized wind shear	8.3.4
ϕ_h	Normalized thermal stratification	8.3.6
χ	Concentration in generic gaussian model (ppt)	7.5.1
χ_{CW}	Crosswind integrated concentration	7.1.4
$\psi\left(\frac{z}{L}\right)$	Stability parameter for wind profile	8.3.5

N.L.C. - B.N.C.
3 3286 10253890 3